

NASA

Earth Resources
A Continuing
Bibliography
with Indexes

NASA SP-7041 (61)
April 1989

National Aeronautics and
Space Administration

es Earth Resource
s Earth Resource
Earth Resources
th Resources Ea
Resources Earth
Resources Earth
resources Earth D

ACCESSION NUMBER RANGES

Accession numbers cited in this Supplement fall within the following ranges.

STAR (N-10000 Series) N89-10001 — N89-15070

IAA (A-10000 Series) A89-10001 — A89-20750

EARTH RESOURCES

A CONTINUING BIBLIOGRAPHY WITH INDEXES

Issue 61

A selection of annotated references to unclassified reports and journal articles that were introduced into the NASA scientific and technical information system and announced between January 1 and March 31 in

- *Scientific and Technical Aerospace Reports (STAR)*
- *International Aerospace Abstracts (IAA).*



National Aeronautics and Space Administration
Office of Management
Scientific and Technical Information Division
Washington, DC

1989

This supplement is available from the National Technical Information Service (NTIS), Springfield, Virginia 22161, price code A08.

INTRODUCTION

The technical literature described in this continuing bibliography may be helpful to researchers in numerous disciplines such as agriculture and forestry, geography and cartography, geology and mining, oceanography and fishing, environmental control, and many others. Until recently it was impossible for anyone to examine more than a minute fraction of the Earth's surface continuously. Now vast areas can be observed synoptically, and changes noted in both the Earth's lands and waters, by sensing instrumentation on orbiting spacecraft or on aircraft.

This literature survey lists 606 reports, articles, and other documents announced between January 1 and March 31, 1989 in *Scientific and Technical Aerospace Reports (STAR)*, and *International Aerospace Abstracts (IAA)*.

The coverage includes documents related to the identification and evaluation by means of sensors in spacecraft and aircraft of vegetation, minerals, and other natural resources, and the techniques and potentialities of surveying and keeping up-to-date inventories of such riches. It encompasses studies of such natural phenomena as earthquakes, volcanoes, ocean currents, and magnetic fields; and such cultural phenomena as cities, transportation networks, and irrigation systems. Descriptions of the components and use of remote sensing and geophysical instrumentation, their subsystems, observational procedures, signature and analyses and interpretive techniques for gathering data are also included. All reports generated under NASA's Earth Resources Survey Program for the time period covered in this bibliography are also included. The bibliography does not contain citations to documents dealing mainly with satellites or satellite equipment used in navigation or communication systems, nor with instrumentation not used aboard aerospace vehicles.

The selected items are grouped in nine categories. These are listed in the Table of Contents with notes regarding the scope of each category. These categories were especially chosen for this publication, and differ from those found in *STAR* and *IAA*.

Each entry consists of a standard bibliographic citation accompanied by an abstract. The citations include the original accession numbers from the respective announcement journals.

Under each of the nine categories, the entries are presented in one of two groups that appear in the following order:

- IAA* entries identified by accession number series A89-10,000 in ascending accession number order;

- STAR* entries identified by accession number series N89-10,000 in ascending accession number order.

After the abstract section, there are seven indexes:

- subject, personal author, corporate source, foreign technology, contract number, report/ accession number, and accession number.

TABLE OF CONTENTS

	Page
Category 01 Agriculture and Forestry	1
Includes crop forecasts, crop signature analysis, soil identification, disease detection, harvest estimates, range resources, timber inventory, forest fire detection, and wildlife migration patterns.	
Category 02 Environmental Changes and Cultural Resources	22
Includes land use analysis, urban and metropolitan studies, environmental impact, air and water pollution, geographic information systems, and geographic analysis.	
Category 03 Geodesy and Cartography	25
Includes mapping and topography.	
Category 04 Geology and Mineral Resources	29
Includes mineral deposits, petroleum deposits, spectral properties of rocks, geological exploration, and lithology.	
Category 05 Oceanography and Marine Resources	35
Includes sea-surface temperature, ocean bottom surveying imagery, drift rates, sea ice and icebergs, sea state, fish location.	
Category 06 Hydrology and Water Management	56
Includes snow cover and water runoff in rivers and glaciers, saline intrusion, drainage analysis, geomorphology of river basins, land uses, and estuarine studies.	
Category 07 Data Processing and Distribution Systems	63
Includes film processing, computer technology, satellite and aircraft hardware, and imagery.	
Category 08 Instrumentation and Sensors	73
Includes data acquisition and camera systems and remote sensors.	
Category 09 General	89
Includes economic analysis.	
Subject Index	A-1
Personal Author Index	B-1
Corporate Source Index	C-1
Foreign Technology Index	D-1
Contract Number Index	E-1
Report Number Index	F-1
Accession Number Index	G-1

TYPICAL REPORT CITATION AND ABSTRACT

NASA SPONSORED
 ↓
 ON MICROFICHE

ACCESSION NUMBER → **N89-14479*** # Kansas Univ. Center for Research, Inc., Lawrence. ← **CORPORATE SOURCE**
 Radar Systems and Remote Sensing Lab.

TITLE → **INVESTIGATION OF RADAR BACKSCATTERING FROM SECOND-YEAR SEA ICE**

AUTHORS → GUANG-TSAI LEI, RICHARD K. MOORE, and S. P. GOGINENI

PUBLICATION DATE → Feb. 1988 67 p

CONTRACT NUMBERS → (Contract NASA ORDER W-16712; N00014-85-K-0200)

REPORT NUMBERS → (NASA-CR-180986; NAS 1.26:180986; RSL-TR-3311-7) Avail:

AVAILABILITY SOURCE → NTIS HC A04/MF A01 CSCL 08L ← **COSATI CODE**

The scattering properties of second-year ice were studied in an experiment at Mould Bay in April 1983. Radar backscattering measurements were made at frequencies of 5.2, 9.6, 13.6, and 16.6 GHz for vertical polarization, horizontal polarization and cross polarizations, with incidence angles ranging from 15 to 70 deg. The results indicate that the second-year ice scattering characteristics were different from first-year ice and also different from multiyear ice. The fading properties of radar signals were studied and compared with experimental data. The influence of snow cover on sea ice can be evaluated by accounting for the increase in the number of independent samples from snow volume with respect to that for bare ice surface. A technique for calculating the snow depth was established by this principle and a reasonable agreement has been observed. It appears that this is a usable way to measure depth in snow or other snow-like media using radar.

Author

TYPICAL JOURNAL ARTICLE CITATION AND ABSTRACT

NASA SPONSORED
 ↓
 ON MICROFICHE

ACCESSION NUMBER → **A89-12756*** # Michigan State Univ., East Lansing.

TITLE → **EVALUATING LANDSAT CLASSIFICATION ACCURACY FROM FOREST COVER-TYPE MAPS**

AUTHOR → W. D. HUDSON (Michigan State University, East Lansing) ← **AUTHOR'S AFFILIATION**

JOURNAL TITLE → Canadian Journal of Remote Sensing (ISSN 0008-2821), vol. 13,

PUBLICATION DATE → July 1987, p. 39-42. refs

CONTRACT NUMBER → (Contract NGL-23-004-083)

The use of complete enumeration in the form of photointerpreted forest cover-type maps to evaluate the accuracy of Landsat classifications was compared with assessments made directly from the aerial photography. A computerized, geographic information system was utilized to compare the Landsat classifications with the cover-type maps on a pixel-by-pixel basis. Error maps of pixels which were similarly misclassified by a variety of algorithms contained a larger number of errors than were verified from the aerial photography. For the two test sites studied, only 67 and 52 percent of the pixels which were originally considered to be in error were substantiated as being in error. Discrepancies between the two results were primarily caused by definitional differences between the cover-type maps and the Landsat classifications, especially with regard to minimum-type size and crown closure estimates of forest land.

C.D.

EARTH RESOURCES

A Continuing Bibliography (Issue 61)

APRIL 1989

01

AGRICULTURE AND FORESTRY

Includes crop forecasts, crop signature analysis, soil identification, disease detection, harvest estimates, range resources, timber inventory, forest fire detection, and wildlife migration patterns.

A89-10325* Wisconsin Univ., Madison.

ESTIMATION OF FOREST CANOPY CHARACTERISTICS AND NITROGEN CYCLING USING IMAGING SPECTROMETRY

CAROL A. WESSMAN, JOHN D. ABER (Wisconsin, University, Madison), and DAVID L. PETERSON (NASA, Ames Research Center, Moffett Field, CA) IN: Imaging spectroscopy II; Proceedings of the Meeting, San Diego, CA, Aug. 20, 21, 1987. Bellingham, WA, Society of Photo-Optical Instrumentation Engineers, 1988, p. 114-118. Research supported by the University of Wisconsin. refs

(Contract NCA2-28; NSF BSR-83-17531)

Canopy lignin concentration is strongly related to annual rates of nitrogen mineralization in a series of Wisconsin forest ecosystems. High spectral resolution Airborne Imaging Spectrometer (AIS) data were acquired over these forests to investigate the potential of remotely estimating canopy lignin content. Analysis of the data using a derivative transformation and correlative techniques suggests that lignin or a closely associated cellular constituent is influential in canopy reflectance. Spatial distributions of percent canopy lignin and annual rates of nitrogen mineralization for Blackhawk Island, WI, have been estimated from a mosaic of AIS imagery. Author

A89-10946#

LAND AND FOREST COVER INFORMATION FROM AERIAL VIDEO

J. VLCEK, D. KING, and X. YUAN (Toronto, University, Canada) IN: International Symposium on Remote Sensing of Environment, 21st, Ann Arbor, MI, Oct. 26-30, 1987, Proceedings. Volume 1. Ann Arbor, MI, Environmental Research Institute of Michigan, 1987, p. 319-326. Research supported by the Department of Energy, Mines and Resources, Ontario Ministry of Environment and NSERC. refs

The potential role of multispectral video sensing in forestry applications is discussed. A 4-camera video sensor is described, and its calibration and performance tests are reviewed. Three studies using the sensor are presented: spectral classification of land cover, change detection relating to cut-over, natural regeneration, and road construction, and the development of an aerial maple dieback index based on narrow-band video imagery. Also discussed is the possibility of future research using video for terrain mapping. R.B.

A89-10948#

THE APPLICATION OF REMOTE SENSING FOR DROUGHT EARLY WARNING IN AFRICA

GARY E. JOHNSON, CLARENCE M. SAKAMOTO, SHARON K. LEDUC, and SUSAN L. CALLIS (NOAA, Climatic Applications Branch; Missouri-Columbia, University, Columbia) IN: International Symposium on Remote Sensing of Environment, 21st, Ann Arbor,

MI, Oct. 26-30, 1987, Proceedings. Volume 1. Ann Arbor, MI, Environmental Research Institute of Michigan, 1987, p. 361-379. Research supported by the Agency for International Development. refs

(Contract NOAA-NA-87AAHRA076)

The use of remote sensing data, especially AVHRR imagery, for early warning of drought in northern Africa is reviewed. Composited color coordinate images and derived normalized-difference vegetation-index values plotted as a smoothed time series are used in the program. Meteosat data are being used of precipitation analysis, and the relationship between precipitation and mapped outgoing longwave radiation data is being evaluated. Prospects for future developments in drought early warning are considered. R.B.

A89-10950#

SURFACE ENERGY FLUX MEASUREMENTS AND REFLECTANCE FACTORS USING SATELLITE-, AIRCRAFT-, AND GROUND-BASED INSTRUMENTATION

ROBERT J. REGINATO (USDA, Water Conservation Laboratory, Phoenix, AZ) IN: International Symposium on Remote Sensing of Environment, 21st, Ann Arbor, MI, Oct. 26-30, 1987, Proceedings. Volume 1. Ann Arbor, MI, Environmental Research Institute of Michigan, 1987, p. 393-399. refs

A week-long experiment in June, 1987 to determine energy flux (latent heat and sensible heat) and spectral reflectance distributions spatially and temporally over several agricultural fields is presented. The energy fluxes were estimated using four ground-level Bowen ratio systems, four eddy correlation units, a tethered balloon radiosonde system, four-band and eight-band radiometers, and appropriate micrometeorological data. SPOT data and airborne radiometric data were also used. The experiment is described in detail, and some preliminary results are presented. R.B.

A89-10951#

SATELLITE DATA ANALYSIS FOR INVENTORYING CROPS GROWN IN A COMPLEX, SMALL-FIELD ENVIRONMENT

W. R. PHILIPSON, W. D. PHILPOT, S. W. BUECHEL, and M. TABERNER (Cornell University, Ithaca, NY) IN: International Symposium on Remote Sensing of Environment, 21st, Ann Arbor, MI, Oct. 26-30, 1987, Proceedings. Volume 1. Ann Arbor, MI, Environmental Research Institute of Michigan, 1987, p. 401-408. refs

A multifaceted investigation is examining whether the cost-effectiveness of crop surveys in an environmentally complex state such as New York can be improved through incorporation of satellite-derived information. Emphasis has been placed on Landsat Thematic Mapper (TM) data for identifying specific crops (vegetables, fruit-tree orchards, vineyards) and for assessing the effect of regional variation on a statewide inventory. For crop identification, spectral information has been found crucial but not always adequate without spatial information. Even when spectral information is adequate, regional variation can alter the classification process. Results to date have been promising. Author

A89-10952#

SOIL EROSION STUDY USING AN AIRBORNE LASER PROFILER

JERRY C. RITCHIE, T. J. JACKSON (USDA, Hydrology Laboratory, Beltsville, MD), J. WHITE (Photoscience, Inc., Gaithersburg, MD), and L. LESCHACK (Trident Arctic Exploration, Ltd., Calgary, Canada) IN: International Symposium on Remote Sensing of Environment, 21st, Ann Arbor, MI, Oct. 26-30, 1987, Proceedings. Volume 1. Ann Arbor, MI, Environmental Research Institute of Michigan, 1987, p. 409-421. refs

The use of a laser profiler mounted on an aircraft for measuring ground surface elevations over simulated concentrated flow gullies is evaluated to determine if this technique could be used to monitor and quantify the amount of soil loss from erosion. Analysis of data collected at altitudes of 50, 100, and 200 m using moving-average filters indicates the location, depth, and cross section of the simulated gullies. The gullies were 20-70 cm wide and 10-30 cm deep. It is suggested that airborne laser profiling can be used to detect and monitor gullies caused by concentrated flow erosion. The development of algorithms to quantify the amount of soil loss from the laser profiler data is discussed. R.B.

A89-10953*# Pennsylvania State Univ., University Park. INFRARED TEMPERATURE MEASUREMENTS OVER BARE SOIL AND VEGETATION - A HAPEX PERSPECTIVE

TOBY N. CARLSON, EILEEN M. PERRY (Pennsylvania State University, University Park), and ODILE TACONET (Centre de Recherches en Physique de l'Environnement Terrestre et Planetaire, Issy-les-Moulineaux, France) IN: International Symposium on Remote Sensing of Environment, 21st, Ann Arbor, MI, Oct. 26-30, 1987, Proceedings. Volume 1. Ann Arbor, MI, Environmental Research Institute of Michigan, 1987, p. 423-429. refs

(Contract NAG5-919)

Preliminary analyses of aircraft and ground measurements made in France during the HAPEX experiment show that horizontal radiometric surface temperature variations, as viewed by aircraft, can reflect the vertical profile of soil moisture (soil versus root zone) because of horizontal variations in vegetation density. Analyses based on one day's data show that, although horizontal variations in soil moisture were small, the vertical differences between a dry surface and a wet root zone were large. Horizontal temperature differences between bare soil, corn and oats reflect differences in the fractional vegetation cover, as seen by the radiometer. On the other hand, these horizontal variations in radiometric surface temperature seem to reflect real horizontal variations in surface turbulent energy fluxes. Author

A89-10956# REGIONAL AND GLOBAL FIRE DETECTION USING AVHRR DATA

GEORGE STEPHENS and MICHAEL MATSON (NOAA, National Environmental Satellite Data and Information Service, Washington, DC) IN: International Symposium on Remote Sensing of Environment, 21st, Ann Arbor, MI, Oct. 26-30, 1987, Proceedings. Volume 1. Ann Arbor, MI, Environmental Research Institute of Michigan, 1987, p. 447-457. refs

Case studies in Mexico, Brazil, Mozambique, the Soviet Union, the Western U.S., and China are analyzed to evaluate the use of the 3.8-micron channel of the AVHRR on the NOAA polar-orbiting satellites for detecting fires. The methodology used for fire detection and the NOAA satellites are described. Examples of temperature data and AVHRR imagery in which fires have been detected are presented. It is concluded that the use of AVHRR data makes it possible to monitor fire activity in any part of the world. R.B.

A89-10960# REMOTE SENSING AND GEOGRAPHIC INFORMATION SYSTEMS FOR AGRICULTURAL STATISTICS-GATHERING AND AGRICULTURAL MONITORING IN MOROCCO

WILL D. SWEARINGEN, THOMAS BUDGE, RAUL CAMPOS-MARQUETTI, GAR CLARKE (New Mexico, University, Albuquerque), and ABDELKADER ESSAJI (Ministry of Agriculture and Agrarian Reform, Rabat, Morocco) IN: International Symposium on Remote Sensing of Environment, 21st, Ann Arbor,

MI, Oct. 26-30, 1987, Proceedings. Volume 1. Ann Arbor, MI, Environmental Research Institute of Michigan, 1987, p. 507-512.

A89-10970*# National Aeronautics and Space Administration. Ames Research Center, Moffett Field, CA. OPERATIONAL USE OF LANDSAT DATA FOR TIMBER INVENTORY

CURTIS V. PRICE (NASA, Ames Research Center; TGS Technology, Inc., Moffett Field, CA) and HARRY L. BOWLIN (USDA, Forest Service, San Francisco, CA) IN: International Symposium on Remote Sensing of Environment, 21st, Ann Arbor, MI, Oct. 26-30, 1987, Proceedings. Volume 1. Ann Arbor, MI, Environmental Research Institute of Michigan, 1987, p. 629-639. refs

(Contract NAS2-12494)

Landsat TM data, digital elevation model (DEM) data, and field observations were used to generate a timber type/structure and land-cover strata map of the Sequoia National Forest in California, U.S. and to create a classification data set. The spectral classes were identified as 32 information classes of land cover or timber type and structure. DEM data were used for the determination of major timber species types by topographic regions of natural occurrence. The results suggest that, for inventories over large areas, traditional per-pixel classifiers are not appropriate for TM-resolution data sets over spatially complex regions such as forest lands; either resolution must be degraded, or more context-dependent classifiers, such as the ECHO classifier described by Landgrebe (1979), must be used. I.S.

A89-10973# THE CHARACTER OF REFLECTIVE SPECTRUM OF WINTER WHEAT AND THE PRINCIPLE OF ITS YIELD ESTIMATION WITH REMOTE SENSING METHOD

XIRU XU, XIACHONG ZHU, KUNQING XIE, and JICHENG CHENG (Beijing University, People's Republic of China) IN: International Symposium on Remote Sensing of Environment, 21st, Ann Arbor, MI, Oct. 26-30, 1987, Proceedings. Volume 2. Ann Arbor, MI, Environmental Research Institute of Michigan, 1987, p. 685-690. refs

The experimental results which came out of controllable sample fields are analyzed. It is shown that the spectral parameters are highly related with three basic factors which determine the yield of winter wheat (the number of ears, the number of grains and the grain weight). Through analyzing data, a simple explanation of why it is possible to estimate winter wheat yield using remote sensing is given, its advantage over other methods such as multifactor statistical method is discussed. Author

A89-10974# A STUDY OF ESTIMATION OF WINTER WHEAT YIELD FOR LARGE AREA USING REMOTE SENSING METHOD

XIRU XU, XIAOHONG ZHU, JICHENG CHENG, KUNQING XIE, ZHENG WANG (Beijing University, People's Republic of China) et al. IN: International Symposium on Remote Sensing of Environment, 21st, Ann Arbor, MI, Oct. 26-30, 1987, Proceedings. Volume 2. Ann Arbor, MI, Environmental Research Institute of Michigan, 1987, p. 691-694.

This paper briefly states the results of an estimation of winter wheat yield and its sowed area in whole Henan province, China, in 1986. The results are inspiring. The statistical correlative coefficient is 0.922 for the sowed area of winter wheat in the whole province between the number calculated and the number published. The statistical correlative coefficient for yield of whole province is 0.982 between the number published and the number estimated by the formula. The need to work out a rigorous method to extract useful information from a mixed pixel is noted. It may push forward the application of remote sensing in monitoring the environment. Author

A89-10975# EVAPOTRANSPIRATION MONITORED FROM SATELLITES AS AN INDICATION OF SHIFT AND IMPACT OF VEGETATION CHANGE

CHANSHEG HE, KYLE KITTLESAN, and JON BARTHOLIC

(Michigan State University, East Lansing) IN: International Symposium on Remote Sensing of Environment, 21st, Ann Arbor, MI, Oct. 26-30, 1987, Proceedings. Volume 2. Ann Arbor, MI, Environmental Research Institute of Michigan, 1987, p. 695-708. refs

Lysimeter data and sensitivity analyses were compared with computed results to test two evapotranspiration models. The models used NOAA-9, Landsat MSS, and ground weather station data to estimate hourly evapotranspiration values for an area in Michigan. These values were combined with statewide land-cover data to assess the impact of man-made modifications on the surface temperature, reflectance, and heat and vapor fluxes. It was found that modifications could lead to daytime temperature increases of 10-13 degrees. Reflectance as a function of land use was found to vary as much as 10 percent. Between agricultural and natural forested or wetland areas, the differences in net radiation and evapotranspiration flux densities were found to be as much as 13 cal/sq cm/hr and 10 cal/sq cm/hr, respectively.

R.B.

A89-10977*# Jet Propulsion Lab., California Inst. of Tech., Pasadena.

REFLECTANCE CHARACTERISTICS OF DRY PLANT MATERIALS

CHRISTOPHER D. ELVIDGE (California Institute of Technology, Jet Propulsion Laboratory, Pasadena) IN: International Symposium on Remote Sensing of Environment, 21st, Ann Arbor, MI, Oct. 26-30, 1987, Proceedings. Volume 2. Ann Arbor, MI, Environmental Research Institute of Michigan, 1987, p. 721-733. refs

Chlorophyll and water obscure the absorption features of all other leaf constituents in the spectra of green leaves. The predominant near-IR and thermal IR spectral features of dry plant materials originate from lignin, cellulose, and hemicellulose. These compounds account for 80 to 98 percent of the dry weight in most plant materials.

Author

A89-10979#

THE DEVELOPMENT OF A STANDARDIZED GRASSLAND LANDSAT MSS INFORMATION DATA BASE

B. TURNER (Council for Scientific and Industrial Research, National Physical Research Laboratory, Pretoria, Republic of South Africa) IN: International Symposium on Remote Sensing of Environment, 21st, Ann Arbor, MI, Oct. 26-30, 1987, Proceedings. Volume 2. Ann Arbor, MI, Environmental Research Institute of Michigan, 1987, p. 757-766. refs

The development of an information data base to quantify the spectral and physical properties of grassland near the Vaal Dam in South Africa is discussed. The data base contains Landsat MSS data from 1980 and 1981 and ground reference data. The ground reference data include soil color, species composition, height, seed height, and percentage cover for three field samples in periods coinciding with satellite overpasses. Vegetation indices, the vegetation ratio, and the normalized vegetation index have been determined for the test sites. It is suggested that the data set can be used to study grassland and environmental conditions, and to generate grassland calendars and spectral atlases of grassland species.

R.B.

A89-10980#

BACKSCATTERING COEFFICIENT OF RICE CROPS AND RICE FIELDS BY AN X-BAND SCATTEROMETER

TAKESHI SUITZ, SHIN YOSHIKADO, TAKASHI KUROSU, TOSHIKI KOZU, and TOSHIHIKO UMEHARA (Ministry of Posts and Telecommunications, Radio Research Laboratories, Tokyo, Japan) IN: International Symposium on Remote Sensing of Environment, 21st, Ann Arbor, MI, Oct. 26-30, 1987, Proceedings. Volume 2. Ann Arbor, MI, Environmental Research Institute of Michigan, 1987, p. 767-773.

An experiment to measure microwave backscattering coefficients of rice crops and rice fields was made at X-band using a FM-CW radar. This paper discusses mainly two different kinds of experimental results. The first result shows the temporal variation of the measured backscattering coefficients of rice crops

in the same field just before dawn till afternoon. The second result shows an analysis on the fading characteristics of received power caused by the movement of the scatterometer on the rail, or caused by the movement of vegetation by wind at the fixed observed area.

Author

A89-10985#

AUTOMATIC CONTROL POINT DETERMINATION FOR IMAGE REGISTRATION USING TEXTURE ANALYSIS METHODS

XIAOPING YUAN and DON JAYASINGHE (Toronto, University, Canada) IN: International Symposium on Remote Sensing of Environment, 21st, Ann Arbor, MI, Oct. 26-30, 1987, Proceedings. Volume 2. Ann Arbor, MI, Environmental Research Institute of Michigan, 1987, p. 815-824. Research supported by the Canadian Forestry Service, Department of Energy, Mines and Resources, and NSERC. refs

Methods for the automatic determination of ground control points (GCPs) in registration of two digital forest images are evaluated. The cross-correlation method for spectral pattern matching and the texture measures method for spatial pattern matching are compared. The texture was represented by a spatial gray-level dependence method and calculated by contrast, entropy, and angular second moment. Data were normalized and compressed by a preprocessing technique. The two methods were compared by calculating location errors of the GCPs under eight testing conditions. It is shown that the texture method is superior to the cross-correlation method when there are large rotational and scale differences between the two images. However, when there are only translational differences between the images, the cross-correlation method gives a much better location accuracy.

R.B.

A89-10987#

DETECTION OF FOREST DAMAGE ON WHITEFACE MOUNTAIN, NEW YORK, USING LANDSAT THEMATIC MAPPER DATA

NANCY J. DEFEO, BARRETT N. ROCK, and JAMES E. VOGELMANN (New Hampshire, University, Durham) IN: International Symposium on Remote Sensing of Environment, 21st, Ann Arbor, MI, Oct. 26-30, 1987, Proceedings. Volume 2. Ann Arbor, MI, Environmental Research Institute of Michigan, 1987, p. 835-842. refs

A89-10989#

LANDSAT TM AND MSS DIGITAL DATA COMPARISON - IMPERIAL VALLEY

BARRY HAACK and SUSAN JAMPOLER (George Mason University, Fairfax, VA) IN: International Symposium on Remote Sensing of Environment, 21st, Ann Arbor, MI, Oct. 26-30, 1987, Proceedings. Volume 2. Ann Arbor, MI, Environmental Research Institute of Michigan, 1987, p. 853-861. refs

A89-10993#

MONITORING VEGETATION INDEX AND BIOMASS PRODUCTION IN SOUTHERN GREENLAND BASED ON NOAA-AVHRR DATA

BIRGER HANSEN and HENRIK SOEGAARD (Copenhagen, University, Denmark) IN: International Symposium on Remote Sensing of Environment, 21st, Ann Arbor, MI, Oct. 26-30, 1987, Proceedings. Volume 2. Ann Arbor, MI, Environmental Research Institute of Michigan, 1987, p. 883-892. Research supported by the Rumudvalget and Ministry for Greenland. refs

A89-11000#

EVALUATION OF A MULTISPECTRAL LINEAR ARRAY SENSOR FOR ASSESSING JUVENILE STAND CONDITIONS

I. D. KNEPECK (Dendron Resource Surveys, Ltd., Ottawa, Canada) and F. J. AHERN (Canada Centre for Remote Sensing, Ottawa) IN: International Symposium on Remote Sensing of Environment, 21st, Ann Arbor, MI, Oct. 26-30, 1987, Proceedings. Volume 2. Ann Arbor, MI, Environmental Research Institute of Michigan, 1987, p. 955-969. refs

MEIS-II pushbroom scanner data at 1- and 3.5-m resolution

are compared with conventional 1:10,000 normal color photography for assessing regeneration conditions in young conifer plantations in British Columbia. It is shown that MEIS-II data can separate the regenerating stands into meaningful conifer density classes and brush density classes. The MEIS-II data are able to detect regeneration at lower conifer densities than the color photography. The MEIS-II data also provide better separation into density classes and are more sensitive to brush competition. R.B.

A89-11002# REGIONAL VARIATION AND CROP SEPARABILITY IN A THEMATIC MAPPER BASED CROP INVENTORY OF NEW YORK STATE

S. W. BUECHEL, W. R. PHILIPSON, and W. D. PHILPOT (Cornell University, Ithaca, NY) IN: International Symposium on Remote Sensing of Environment, 21st, Ann Arbor, MI, Oct. 26-30, 1987, Proceedings. Volume 2. Ann Arbor, MI, Environmental Research Institute of Michigan, 1987, p. 983-991. Research supported by Cornell University and USDA. refs

A89-11004# EFFECT OF SOIL ROUGHNESS ON SAR IMAGES OF HARVESTED AGRICULTURAL FIELDS

JOSEF CIHLAR (Canada Centre for Remote Sensing, Ottawa) IN: International Symposium on Remote Sensing of Environment, 21st, Ann Arbor, MI, Oct. 26-30, 1987, Proceedings. Volume 2. Ann Arbor, MI, Environmental Research Institute of Michigan, 1987, p. 1005-1021. refs

The relative importance of field surface characteristics that cause difference in radar return from harvested agricultural fields is assessed. X- and L-band, HH-polarized SAR images of three sites in Saskatchewan, Canada were analyzed. It was found that the soil surface roughness had the dominant effect on SAR image tones. Row orientation, row spacing, and ridge height were shown to be most closely related to variations in tone, while the weights of these parameters depend on frequency. It was found that cultivation operations can cause large and rapid changes in the appearance of a field on SAR images. R.B.

A89-11007# ACREAGE AND YIELD DETERMINATION - 1987 KANSAS WINTER WHEAT

NORMAN D. LEPPERT (Federal Crop Insurance Corp., Program Planning, Evaluation and Appeal Div., Washington, DC) IN: International Symposium on Remote Sensing of Environment, 21st, Ann Arbor, MI, Oct. 26-30, 1987, Proceedings. Volume 2. Ann Arbor, MI, Environmental Research Institute of Michigan, 1987, p. 1041-1046.

The capabilities of SPOT, NOAA-9 AVHRR, Landsat TM, MSS, and aerial photography to aid in the determination of crop conditions, acreage, and yield for the 1987 winter wheat crop in Kansas are evaluated. The wheat crop has been monitored throughout the growing season with preharvest appraisals, field reviews after harvest, and actual harvested yields by unit. The acreage per unit was determined and compared with remote sensing data. The methods used in the experiment are described in detail, and the plans for analyzing the data are given. R.B.

A89-11008# SPECTRAL AND SPATIAL CHARACTERISATION OF ORCHARDS IN NEW YORK STATE USING THEMATIC MAPPER IMAGERY

M. J. TABERNER, W. D. PHILPOT, and W. R. PHILIPSON (Cornell University, Ithaca, NY) IN: International Symposium on Remote Sensing of Environment, 21st, Ann Arbor, MI, Oct. 26-30, 1987, Proceedings. Volume 2. Ann Arbor, MI, Environmental Research Institute of Michigan, 1987, p. 1061-1072. Research supported by Cornell University and USDA. refs

A89-11009*# Pennsylvania State Univ., University Park. COMPARISON OF REMOTE MEASUREMENTS OF INFRARED SURFACE TEMPERATURES AND MICROWAVE SOIL MOISTURE

EILEEN M. PERRY and TOBY N. CARLSON (Pennsylvania State University, University Park) IN: International Symposium on Remote Sensing of Environment, 21st, Ann Arbor, MI, Oct. 26-30, 1987, Proceedings. Volume 2. Ann Arbor, MI, Environmental Research Institute of Michigan, 1987, p. 1073-1079. refs (Contract NAG5-919)

Scatterometric measurements of active microwave soil water content and radiometric measurements of thermal IR surface temperatures were made simultaneously from an aircraft flying 400 m over an agricultural region of France after harvesting. The surface temperatures were used to determine soil moisture availability estimates according to the Carlson (1986) model. Surface temperature or soil moisture availability and microwave soil moisture were correlated. The standard error in the IR temperature and soil moisture availability due to influences other than soil moisture is found to be + or - 2 C. The standard deviation of the temperature/moisture availability is greater than this standard error. It is shown that correlations between soil water content and moisture availability improve with increasing spatial or temporal variance in the measure surface temperatures. R.B.

A89-11011# THE USE OF FRACTAL GEOMETRY TO IDENTIFY RANGES OF SCALE-INVARIANCE IN DIGITAL REMOTELY SENSED DATA

M. J. MACLENNAN and P. J. HOWARTH (Waterloo, University, Canada) IN: International Symposium on Remote Sensing of Environment, 21st, Ann Arbor, MI, Oct. 26-30, 1987, Proceedings. Volume 2. Ann Arbor, MI, Environmental Research Institute of Michigan, 1987, p. 1089-1092. refs (Contract NSERC-A-0766)

Natural land cover surfaces may sometimes display what is known as statistical self-similarity over specific intervals of spatial scale. Such patterns can be characterized by what is known as a fractal dimension. The identification of characteristic scale ranges may be useful to reveal scales at which different processes in the scene operate and manifest their structure. It is shown how the fractal dimension can be computed from the surface semivariogram of a digital image. An airborne multispectral scanner image of a forest scene is examined using this method. Limitations of this approach and possibilities for future work are also discussed. Author

A89-11012*# Jet Propulsion Lab., California Inst. of Tech., Pasadena.

RELATIVE WATER CONTENT OF SPRUCE NEEDLES DETERMINED BY THE LEAF WATER CONTENT INDEX

E. RAYMOND HUNT, JR., SAM K. S. WONG, and BARRETT N. ROCK (California Institute of Technology, Jet Propulsion Laboratory, Pasadena) IN: International Symposium on Remote Sensing of Environment, 21st, Ann Arbor, MI, Oct. 26-30, 1987, Proceedings. Volume 2. Ann Arbor, MI, Environmental Research Institute of Michigan, 1987, p. 1093-1100. refs

Leaf relative water content (RWC) is defined as the volume of water in a leaf divided by the volume at full turgor. Using reflectance factors of wavelengths 0.83 micron and 1.6 microns, a Leaf Water Content Index (LWCI) was derived from the Lambert-Beer Law such that LWCI should equal RWC; LWCI was equal to RWC for *Picea pungens*, *Picea rubens*, *Liquidambar styraciflua*, and *Quercus agrifolia*. Algebraic manipulation shows that $R(1.6)/R(0.83)$ termed the Moisture Stress Index (MSI), is near-linearly correlated to RWC and to the Equivalent Water Thickness (EWT). Five species tested so far had the same relationship between MSI and EWT, but EWT is not a measure of plant water status. Author

A89-12261 DIRECTIONAL EFFECTS ON SCENE COMPLEXITY IN OBLIQUE THERMAL IMAGERY AND PHOTOGRAPHS OF A DECIDUOUS FOREST

LEE K. BALICK and EDWIN L. DOAK (EG & G Energy Measurements, Inc., Las Vegas, NV) Applied Optics (ISSN 0003-6935), vol. 27, Oct. 1, 1988, p. 3978-3987. Army-supported

research. refs
(Contract DE-AC08-83NV-10282)

A89-12354

ESTIMATION OF MULTIPLE REFLECTION AND LOWEST ORDER ADJACENCY EFFECTS ON REMOTELY-SENSED DATA

S. M. SINGH (NERC; Reading, University, England) International Journal of Remote Sensing (ISSN 0143-1161), vol. 9, Sept. 1988, p. 1433-1450. refs
(Contract NERC-F60/G6/12)

The lowest-order adjacency effect and the effect of multiple reflections between the ground and the atmosphere on the AVHRR channel 1 and channel 2 reflectances and on the normalized difference vegetation index (NDVI) are examined. The global irradiances calculated from theoretical and experimental empirical relations are compared. The effect of multiple reflection on each channel reflectance is found to be about 1-2 percent. It is shown that the multiple reflection and lowest-order adjacency effects can be ignored for the NDVI, but not when using reflectances. Also, the variations of global solar irradiance with the solar zenith angle are presented. R.B.

A89-12355

THE EFFECTS OF BARK BEETLE STRESS ON THE FOLIAR SPECTRAL REFLECTANCE OF LODGEPOLE PINE

F. J. AHERN (Canada Centre for Remote Sensing, Ottawa) International Journal of Remote Sensing (ISSN 0143-1161), vol. 9, Sept. 1988, p. 1451-1468. refs

Results are presented from a study to determine the sequence of changes which occur in the foliar reflectance properties of lodgepole pine trees being attacked by mountain pine beetles. Data for the study included spectrometry at wavelengths 360-1050 nm, foliage samples, and bore holes. The spectral reflectance data analysis included visual inspection of spectral reflectance curves of foliage from trees with obvious color changes and a factor analysis of the data from unattacked and attacked trees with no discernible color differences. The changes observed are described and the implications of the study for remote sensing are discussed. It is found that six spectral bands should be considered for detecting incipient pine beetle stress. Three of these bands (400-450 nm, 667-686 nm, and 800-850 nm) serve as reference bands to correct for atmospheric and illumination effects. The other bands (690-1050 nm, 690-730 nm, and 770-1050 nm) represent regions where significant differences between the reflectance of foliage from attacked and unattacked trees were observed. R.B.

A89-12356

ESTIMATING THE DISTRIBUTION OF GRAZING AND PATTERNS OF CATTLE MOVEMENT IN A LARGE ARID ZONE PADDOCK

G. PICKUP and V. H. CHEWINGS (CSIRO, Div. of Wildlife and Ecology, Alice Springs, Australia) International Journal of Remote Sensing (ISSN 0143-1161), vol. 9, Sept. 1988, p. 1469-1490. refs

A method is presented for modeling the distribution of grazing and for generating the pattern of movement by cattle in a large paddock in central Australia for a particular configuration of watering points, fence lines, and vegetation types. The method uses Landsat MSS data and a cattle distribution model which is based on the convection-diffusion equation and relates the number of animals grazing to distance from water and preference for particular vegetation types. Background changes in MSS band 5 over time are separated from those due to grazing. The band 5 grazing effects provide a surrogate measure of grazing intensity and are used to estimate preferences for different vegetation types and to calibrate the animal distribution models. It is found that the patterns of movement derived from Landsat band 5 data are very similar to those determined from observed cattle distributions. R.B.

A89-12756*# Michigan State Univ., East Lansing.

EVALUATING LANDSAT CLASSIFICATION ACCURACY FROM FOREST COVER-TYPE MAPS

W. D. HUDSON (Michigan State University, East Lansing) Canadian Journal of Remote Sensing (ISSN 0008-2821), vol. 13, July 1987, p. 39-42. refs
(Contract NGL-23-004-083)

The use of complete enumeration in the form of photointerpreted forest cover-type maps to evaluate the accuracy of Landsat classifications was compared with assessments made directly from the aerial photography. A computerized, geographic information system was utilized to compare the Landsat classifications with the cover-type maps on a pixel-by-pixel basis. Error maps of pixels which were similarly misclassified by a variety of algorithms contained a larger number of errors than were verified from the aerial photography. For the two test sites studied, only 67 and 52 percent of the pixels which were originally considered to be in error were substantiated as being in error. Discrepancies between the two results were primarily caused by definitional differences between the cover-type maps and the Landsat classifications, especially with regard to minimum-type size and crown closure estimates of forest land. C.D.

A89-12874

THE USE OF SPECTRAL REFLECTANCE CHARACTERISTICS FOR THE ESTIMATION OF THE WHEAT CROP STATE

R. KANTCHEVA (B'lgarska Akademiia na Naukite, Institut za Kosmicheski Izsledvanii, Sofia, Bulgaria) Bolgarskaia Akademiia Nauk, Doklady (ISSN 0366-8681), vol. 41, no. 8, 1988, p. 69-71. refs

Remote-sensing techniques for crop-status evaluation are discussed, with a focus on the results of ground-based spectral reflectance measurements at 400-800 nm. Useful correlations are established between reflectance and crop coverage index and overground phytomass. T.K.

A89-13670#

COMPUTATIONAL DESIGN AND EFFICIENCY OPTIMIZATION OF AGRICULTURAL AIRPLANES

ROLF STAUFENBIEL, THOMAS SCHERER (Aachen, Rheinisch-Westfaelische Technische Hochschule, Federal Republic of Germany), and ISTVAN STEIGER (Budapesti Muszaki Egyetem, Budapest, Hungary) IN: ICAS, Congress, 16th, Jerusalem, Israel, Aug. 28-Sept. 2, 1988, Proceedings. Volume 2. Washington, DC, American Institute of Aeronautics and Astronautics, Inc., 1988, p. 1664-1676. DFG-supported research. refs

This paper presents a simulation program for optimizing the parameters of the spraying system and the configuration of agricultural aircraft, which yields higher accuracy in calculated spraying distribution, as well as other improvements, in comparison with existing methods. The method incorporates new techniques for describing the roll-up process of the wing wake and the flow characteristics of the propeller slipstream and uses a new statistical method for describing the influence of wind fields and turbulence. Using this simulation program, it was demonstrated that, by installing winglets in the aircraft design, not only aircraft performance but also spray efficiency can be improved. This winglet configuration, in combination with optimized spray nozzle arrangements, was tested in flight tests using an aircraft of the PZL M-18 Dromader type; good agreement was obtained between flight test results and simulation results. I.S.

A89-14009

SPOT SATELLITE DATA FOR PATTERN RECOGNITION ON THE NORTH AMERICAN TALL-GRASS PRAIRIE LONG-TERM ECOLOGICAL RESEARCH SITE

M. DUANE NELLIS and JOHN M. BRIGGS (Kansas State University, Manhattan) Geocarto International (ISSN 1010-6049), vol. 3, Sept. 1988, p. 37-40.
(Contract NSF BSR-85-14327)

Data of a tall-grass prairie in Kansas are briefly discussed. A SPOT image taken on May 1, 1987 as part of the Long-Term

Ecological Research project is presented and the major classes of land cover as determined from the image are given. The analytic procedures used in the project are examined. R.B.

A89-14010**A COMPARATIVE EVALUATION OF USE OF LANDSAT MSS FCC AND MKF-6M PHOTOGRAPHS FOR FOREST TYPE DELINEATION**

N. V. MADHAVAN UNNI, S. P. S. KUSHWAHA (National Remote Sensing Agency, Hyderabad, India), A. C. KESHAVAMURTHY, and S. K. KANGEYAM (Karnataka State, Forest Department, Bangalore, India) *Geocarto International* (ISSN 1010-6049), vol. 3, Sept. 1988, p. 41-52.

MKF-6M photographs of India from the Salyut-7 mission are evaluated and their use in forest type delineation and mapping is compared with Landsat MSS data. It is found that evergreen, semievergreen, moist and dry deciduous, degraded forest, and scrub vegetation may be differentiated and mapped using both black and white and false color composites of MKF-6M data and false color composites of Landsat MSS data. The advantages and disadvantages of both types of data are discussed. It is suggested that the improvement in the spectral resolution of MKF-6M data over Landsat MSS does not have significant influence in differentiating more forest categories, although it makes it easier to delineate precise boundaries of the categories. Also, compared to Landsat MSS data, the MKF-6M data lacks geometrical fidelity unless a correction is applied to the data. R.B.

A89-14089**FOREST MAPPING ACCURACIES ARE IMPROVED USING A SUPERVISED NONPARAMETRIC CLASSIFIER WITH SPOT DATA**

ANDREW K. SKIDMORE and BRIAN J. TURNER (Australian National University, Canberra, Australia) *Photogrammetric Engineering and Remote Sensing* (ISSN 0099-1112), vol. 54, Oct. 1988, p. 1415-1421. refs

A new supervised nonparametric classifier produces an image showing the empirical probability of correct classification for a pixel as well as a thematic image. This allows an analyst to visually locate those parts of the image where classification success can be improved. The algorithm was tested using SPOT XS data over a forest plantation in southeast Australia. The classifier produced thematic maps of higher accuracy than those from conventional supervised classifiers. Author

A89-14090**SIMPLIFIED FOREST INVENTORY USING LARGE-SCALE 70-MM PHOTOGRAPHY AND TARIF TABLES**

DAVID P. PAINE and RICHARD J. MCCADDEN (Oregon State University, Corvallis) *Photogrammetric Engineering and Remote Sensing* (ISSN 0099-1112), vol. 54, Oct. 1988, p. 1423-1427. Research supported by the Oregon Forest Research Laboratory and Coastal Oregon Productivity Enhancement Program. refs

An approach to large-scale 70-mm aerial photo forest inventory, including stand and stock tables, has been developed to eliminate the need for specialized equipment such as stereo plotters, laser altimeters, and tilt indicators. The approach requires limited field work to establish a proper tarif access number and a stem to crown diameter relationship. Tarif volume tables are used to eliminate the need for photo measurement of tree heights for volume estimates. Tests using 153 photo plots of three sampling designs produced results that were within + or - 5 percent of the mean volume per acre obtained from ground inventory. It was found that stand and stock tables were accurate for all but the smaller diameter classes. R.B.

A89-15493**A SIMPLE METHOD FOR ESTIMATING MONTHLY MEAN ALBEDO OF LAND SURFACES FROM AVHRR DATA**

GEORGE GUTMAN (Maryland, University, College Park) *Journal of Applied Meteorology* (ISSN 0894-8763), vol. 27, Sept. 1988, p. 973-988. refs

A method for deriving the monthly mean clear-sky planetary

albedo from NOAA-9 AVHRR visible and NIR data is presented. The results of the method are compared with those obtained using the minimum albedo method. It is found that the minimum albedo method may lead to an underestimation of monthly values because of the angular variation in clear-sky observed albedos. Also, the derived surface albedos are compared with those reported in climatological studies based on ground observations. R.B.

A89-15918* California Univ., Santa Barbara.**INVERTIBLE CANOPY REFLECTANCE MODELING OF VEGETATION STRUCTURE IN SEMIARID WOODLAND**

JANET FRANKLIN (California, University, Santa Barbara) and ALAN H. STRAHLER (Hunter College, New York) *IEEE Transactions on Geoscience and Remote Sensing* (ISSN 0196-2892), vol. 26, Nov. 1988, p. 809-825. refs

(Contract NAGW-788; NGT-05-010-804; NAGW-735)

The Li-Strahler canopy reflectance model, driven by Landsat Thematic Mapper (TM) data, provided regional estimates of tree size and density in two bioclimatic zones in West Africa. This model exploits tree geometry in an inversion technique to predict average tree size and density from reflectance data using a few simple parameters measured in the field (spatial pattern, shape, and size distribution of trees) and in the imagery (spectral signatures of scene components). The model was tested in sparse woodland and wooded grassland in the Sahelian and Sudanian bioclimatic zones in West Africa. I.E.

A89-16061* Environmental Research Inst. of Michigan, Ann Arbor.**THE PROSPECTS FOR DETECTING SPECTRAL SHIFTS DUE TO SATELLITE SENSOR AGING**

G. SUITS, W. MALILA, and T. WELLER (Michigan, Environmental Research Institute, Ann Arbor) *Remote Sensing of Environment* (ISSN 0034-4257), vol. 26, Oct. 1988, p. 17-29. refs (Contract NAS5-29356)

Along with responsivity changes due to sensor aging, there may be concurrent spectral changes. A field-measurement approach for detecting postlaunch spectral changes is described. For illustration, one hypothetical model of change (spectral band shift) is explored through simulation for five satellite sensors. Two different types of natural terrain - vegetation and bare soil - are used as test targets. Author

A89-16062**SENSOR BAND SELECTION FOR DETECTING CURRENT DEFOLIATION CAUSED BY THE SPRUCE BUDWORM**

D. G. LECKIE (Canadian Forestry Service, Petawawa National Forestry Institute, Chalk River, Canada), P. M. TEILLET (Canada Centre for Remote Sensing, Ottawa, Canada), D. P. OSTAFF (Canadian Forestry Service, Fredericton, Canada), and G. FEDOSEJEVS (Intera Technologies, Ltd., Ottawa, Canada) *Remote Sensing of Environment* (ISSN 0034-4257), vol. 26, Oct. 1988, p. 31-50. refs

Ground-based spectral data for single crowns of balsam fir trees with varying degrees of current defoliation caused by spruce budworm feeding are analyzed. Wavelength bands suitable for discriminating different levels of damage symptoms are defined and compared with wavelength bands available with various airborne and satellite sensors. It is found that the most effective bands for determining damage caused by the spruce budworm are 2030-2210, 660-670, 1560-1620, and 770-790 nm. R.B.

A89-17282**NEAR SURFACE SOIL MOISTURE ESTIMATION FROM MICROWAVE MEASUREMENTS**

L. BRUCKLER, P. STENGEL (Institut National de la Recherche Agronomique, Montfavet, France), and H. WITONO (Bogor Agricultural University, Indonesia) *Remote Sensing of Environment* (ISSN 0034-4257), vol. 26, Nov. 1988, p. 101-121. refs

Soil moisture, water potential, and bulk density measurements were performed on a 0.4 ha bare field (27.2 pct clay, 61.7 pct fine and coarse loam). Backscattering coefficients were measured with 4.5 GHz frequency, HH polarization and 15-20 deg incidence

angle microwave sensor configuration. The data exhibited satisfactory regression lines between the backscattering coefficient and the volumetric water content calculated over arbitrary soil depths. In addition, a statistical procedure for predicting the mean and standard deviation of volumetric water content profiles from the soil surface to the microwave penetration depth is presented.

R.B.

A89-17283* National Aeronautics and Space Administration. Ames Research Center, Moffett Field, CA.

PREDICTION OF LEAF CHEMISTRY BY THE USE OF VISIBLE AND NEAR INFRARED REFLECTANCE SPECTROSCOPY

DON H. CARD, DAVID L. PETERSON, PAMELA A. MATSON (NASA, Ames Research Center, Moffett Field, CA), and JOHN D. ABER (New Hampshire, University, Durham) Remote Sensing of Environment (ISSN 0034-4257), vol. 26, Nov. 1988, p. 123-147. refs

The chemical content of dry, ground leaf material sampled from deciduous and conifer tree species from sites in Alaska, Wisconsin, and California was estimated using visible and shortwave IR spectroscopy. Seven chemical components - sugar, starch, protein, cellulose, total chlorophyll, lignin, and total nitrogen - were analyzed by wet chemical methods and their concentrations regressed against log 1/rho and first and second differences of log 1/rho (where rho is measured reflectance) at wavelengths selected by stepwise regression. Predictions of chemical concentrations based on cross validation suggest that this technique may be useful for extracting vegetation canopy biochemical information by remote sensing.

Author

A89-17284

AN AIRBORNE GAMMA RAY SNOW SURVEY OF A FOREST COVERED AREA WITH A DEEP SNOWPACK

J. E. GLYNN, P. B. HOLMAN, R. L. GRASTY (Geological Survey of Canada, Ottawa), and T. R. CARROLL (NOAA, National Weather Service, Minneapolis, MN) Remote Sensing of Environment (ISSN 0034-4257), vol. 26, Nov. 1988, p. 149-160. Research supported by the Department of the Environment of Canada and NOAA. refs

Problems arising from the airborne gamma ray measurement of snow water equivalent over a forest covered deep snowpack are examined. The principal sources of error are believed to be due to the radioactivity in the biomass and to variability in the snow cover. A theoretical model is developed to correct the airborne measurements for these sources of error. The application of the theory to data collected over the St. John River Basin, located in the eastern part of Canada and the United States, is found to significantly improve the airborne results.

Author

A89-17286

RELATIONSHIP BETWEEN DISCOLORATION AND HISTOLOGICAL CHANGES IN LEAVES OF TREES AFFECTED BY FOREST DECLINE

ENAMUL HOQUE, PETER J. S. HUTZLER, and HARALD K. SEIDLITZ (Gesellschaft fuer Strahlen- und Umweltforschung mbH, Neuherberg, Federal Republic of Germany) Remote Sensing of Environment (ISSN 0034-4257), vol. 26, Nov. 1988, p. 171-184. refs

The relationship between discoloration and histological changes induced by forest decline in leaves of Norway spruce and beech is analyzed. Discoloration of leaves by various degrees of damage is quantitatively measured by high resolution reflection spectroscopy. The cell structure of leaves is determined from microscopic images of histological cuts. Major significant changes in spectral reflectance as shown by t-value maxima are observed in the visible, but not in the near IR region. The related cellular changes are hypertrophy of chloroplasts, reduction of chloroplast number, and formation of large isodiametrical hypodermal cells.

Author

A89-17399

MONITORING WOOD STORK FORAGING HABITAT USING REMOTE SENSING AND GEOGRAPHIC INFORMATION SYSTEMS

MICHAEL E. HODGSON (Colorado, University, Boulder), JOHN R. JENSEN (South Carolina, University, Columbia), HALKARD E. MACKAY, JR., and MALCOLM C. COULTER (Du Pont de Nemours Savannah River Ecology Laboratory, Aiken, SC) Photogrammetric Engineering and Remote Sensing (ISSN 0099-1112), vol. 54, Nov. 1988, p. 1601-1607. refs

(Contract DE-AC09-76SR-00819; DE-AC09-76SR-00001)

Wetland habitats suitable for foraging by the Wood Stork were inventoried and analyzed using remotely sensed imagery, digital image processing, and geographic information system (GIS) techniques. Maps of foraging habitats were created from Landsat TM imagery, one for a 'wet' year and one for a 'dry' year. Change detection, proximity to the Wood Stork Colony, and size of foraging site analyses were performed on the maps using GIS algorithms to obtain quantitative foraging habitat statistics. Results of the analyses indicate a 47 percent reduction in foraging cover during the 'dry' year.

Author

A89-17683#

NEW SPOT GENERATION

M. ARNAUD (CNES, Toulouse, France) IAF, International Astronautical Congress, 39th, Bangalore, India, Oct. 8-15, 1988. 6 p.

(IAF PAPER 88-117)

The SPOT 2 and 3 remote sensing satellites will have improved resolution over the currently operating SPOT 1 through the addition of a new mid-IR band and an optical payload, designated 'Vegetation', which is characterized by a wide field of view and high radiometric resolution. Vegetation will be employed in global monitoring of both land vegetation and oceanic productivity. The two new SPOT satellites will also possess a longer service life capability than SPOT 1. An experimental optical link will be used between SPOT in LEO and a GEO satellite; the data will be relayed to be ground via conventional radio link.

O.C.

A89-17686#

THE IMAGE DETECTION SUBASSEMBLY FOR THE SPOT 4 'VEGETATION' INSTRUMENT

A. JUVIGNY, R. SERRADEIL (Societe Anonyme d'Etudes et Realisations Nucleaires, Limeil-Brevannes, France), J. P. DURPAIRE (CNES, Toulouse, France), and L. LE BOURLOUT (Aerospatiale, Cannes, France) IAF, International Astronautical Congress, 39th, Bangalore, India, Oct. 8-15, 1988. 6 p.

(IAF PAPER 88-121)

The SPOT 4 mission objectives are reviewed, focusing on the vegetation package to monitor vegetation on a global scale to forecast yields and improve environmental studies. The imaging instrument, data processing unit, onboard management unit and image data telemetry unit of the package are discussed. The mechanical design, thermal control, and electronics system are also considered. The performance of the package is examined, including geometric image quality, spectral response, radiometric resolution, and the contrast transfer function.

R.B.

A89-17692#

COMPARISON OF SPOT, TM AND MSS DATA FOR AGRICULTURAL LAND-USE MAPPING IN GUJARAT (INDIA)

BALDEV SAHAI, V. K. DADHWAL, and M. CHAKRABORTY (ISRO, Space Applications Centre, Ahmedabad, India) IAF, International Astronautical Congress, 39th, Bangalore, India, Oct. 8-15, 1988. 9 p. refs

(IAF PAPER 88-139)

A comparison was made between the spectral gradients, information content, redundancy, and land-cover mapping capabilities of SPOT, TM, and MSS for agricultural land-use mapping in Gujarat (India). It is found that intraclass variability is less in SPOT than in TM while statistical class separability is higher in SPOT. The advantage of the high spatial resolution of SPOT is demonstrated.

K.K.

A89-17693#

STATUS AND PERSPECTIVES OF VEGETATION MONITORING BY REMOTE SENSING

R. BACKHAUS, H. SAX, and K. WANDERS (DFVLR, Cologne, Federal Republic of Germany) IAF, International Astronautical Congress, 39th, Bangalore, India, Oct. 8-15, 1988. 12 p. (IAF PAPER 88-140)

The application of space based observation systems to vegetation monitoring is reviewed and compared with the observational requirements resulting from the ecological and economical impact of vegetational changes. The remote sensing systems which can be used to monitor vegetation are evaluated. Projects which have used remote sensing for woodland inventories, forest management, agricultural management, and landuse, landcover, and ecological mapping are listed. Research topics which might make use of remote sensing technology in the future are considered. R.B.

A89-17701*# National Aeronautics and Space Administration. Goddard Space Flight Center, Greenbelt, MD.

GLOBAL LAND-SURFACE PRIMARY PRODUCTIVITY BASED UPON NIMBUS-7 37 GHZ DATA

B. J. CHOUDHURY (NASA, Goddard Space Flight Center, Greenbelt, MD) IAF, International Astronautical Congress, 39th, Bangalore, India, Oct. 8-15, 1988. 3 p. NASA-supported research. refs

(IAF PAPER 88-159)

Accumulation and renewal of organic matter as quantified through net primary productivity (NPP) is considered a very major function of the biosphere, and its estimation is crucial in understanding the carbon cycle. A physically-based model relating NPP to the difference of vertically and horizontally polarized brightness temperatures (Delta T) observed at 37 GHz frequency of the scanning multichannel microwave radiometer on board the Nimbus-7 satellite is used for fitting areally averaged values of NPP and Delta T for five biomes. The land-surface NPP within 80 deg N to 55 deg S is then calculated using the Delta T data and compared with other estimates. Author

A89-18709

THE EFFECT OF AGROMETEOROLOGICAL CONDITIONS ON THE CHARACTERISTICS OF SPACE RADAR IMAGERY OF AGRICULTURAL REGIONS IN WINTER [VLIANIE AGROMETEOROLOGICHESKIKH USLOVII NA KHARAKTERISTIKI KOSMICHESKIKH RADIOIZOBRAZHENII SEL'SKOKHOZIAISTVENNYKH REGIONOV V ZIMNII PERIOD]

A. P. PICHUGIN, N. E. ZHURAVEL', and D. M. BYCHKOV (Khar'kovskii Gosudarstvennyi Universitet, Kharkov, Ukrainian SSR) Issledovanie Zemli iz Kosmosa (ISSN 0205-9614), July-Aug. 1988, p. 58-65. In Russian. refs

The effect of winter precipitation on the intensity of radar echoes from the earth-surface was investigated. The characteristics of radar images obtained from agricultural regions in the southern Ukraine and the meteorological data were quantitatively correlated with the conditions of the soil in these regions. The values of surface reflectance obtained from frozen and warm soils exposed to rainfall were found to be significantly different. The results showed that space radar imagery can be used for the determination of the spatial distribution of soil-surface moisture on large territories. I.S.

A89-20629* Illinois Univ., Urbana.

MAPPING DOMINANT VEGETATION COMMUNITIES IN THE COLORADO ROCKY MOUNTAIN FRONT RANGE WITH LANDSAT THEMATIC MAPPER AND DIGITAL TERRAIN DATA

THOMAS D. FRANK (Illinois, University, Urbana) Photogrammetric Engineering and Remote Sensing (ISSN 0099-1112), vol. 54, Dec. 1988, p. 1727-1734. refs (Contract NAS5-28781)

A89-20630

SHUTTERED CAMERA - AERIAL COLOR VIDEO IMAGING IN THE VISIBLE AND NEAR INFRARED

TUOMAS HAME and MARKKU RANTASUO (Technical Research Centre of Finland, Espoo) Photogrammetric Engineering and Remote Sensing (ISSN 0099-1112), vol. 54, Dec. 1988, p. 1735-1738. Research sponsored by the Finnish National Fund for Research and Development and Technical Research Centre of Finland. refs

Video imaging equipment which is suitable for large scale forestry surveys from light aircraft is discussed. Two camera systems were developed: an oblique system for forest surveys and a vertical system for general forest inventory and mapping. The systems include a digitizing module capable of producing multichannel imagery from a color composite for use in numerical processing and interpretation. Tests for forest regions in Finland show that, although several improvements to the system are needed, it has potential for use in detailed forest damage and treatment surveys. R.B.

A89-20702

RADIOMETRIC MEASUREMENTS AND CROP YIELD FORECASTING - SOME OBSERVATIONS OVER MILLET AND SORGHUM EXPERIMENTAL PLOTS IN MALI

ETIENNE BARTHOLOME (CEC, Joint Research Centre, Ispra, Italy) (European Association of Remote Sensing Laboratories, Annual Symposium on European Remote Sensing Needs in the 1990s, Noordwijkerhout, Netherlands, May 4-8, 1987) International Journal of Remote Sensing (ISSN 0143-1161), vol. 9, Oct.-Nov. 1988, p. 1539-1552. refs

A89-20703

SOME RESULTS OF MICROWAVE REMOTE SENSING RESEARCH IN THE NETHERLANDS WITH A VIEW TO LAND APPLICATIONS IN THE 1990S

L. KRUL (Delft, Technische Hogeschool, Netherlands) (European Association of Remote Sensing Laboratories, Annual Symposium on European Remote Sensing Needs in the 1990s, Noordwijkerhout, Netherlands, May 4-8, 1987) International Journal of Remote Sensing (ISSN 0143-1161), vol. 9, Oct.-Nov. 1988, p. 1553-1563. refs

A89-20704

LOWEST ORDER CORRECTION FOR SOLAR ZENITH ANGLE TO GLOBAL VEGETATION INDEX (GVI) DATA

S. M. SINGH (NERC, Unit for Thematic Information Systems, Reading, England) (European Association of Remote Sensing Laboratories, Annual Symposium on European Remote Sensing Needs in the 1990s, Noordwijkerhout, Netherlands, May 4-8, 1987) International Journal of Remote Sensing (ISSN 0143-1161), vol. 9, Oct.-Nov. 1988, p. 1565-1572. refs (Contract NERC-F60/G6/12)

The variability of vegetation indices with the solar zenith angle is discussed. An inversion technique is summarized in which raw values of the normalized difference vegetation indices (NDVI) for a variety of surface-cover types are simulated as a function of solar zenith angle. The relationship between a change in NDVI and solar zenith angle is used to correct global vegetation index data from NOAA polar orbiting satellites. R.B.

A89-20705

REGIONAL LAND COVER AND AGRICULTURAL AREA STATISTICS AND MAPPING IN THE DEPARTEMENT ARDECHE, FRANCE, BY USE OF THEMATIC MAPPER DATA

JOACHIM HILL and JACQUES MEGIER (CEC, Joint Research Centre, Ispra, Italy) (European Association of Remote Sensing Laboratories, Annual Symposium on European Remote Sensing Needs in the 1990s, Noordwijkerhout, Netherlands, May 4-8, 1987) International Journal of Remote Sensing (ISSN 0143-1161), vol. 9, Oct.-Nov. 1988, p. 1573-1595. refs

A89-20706

FOREST CLASSIFICATION BY PRINCIPAL COMPONENT ANALYSES OF TM DATA

C. CONESE, G. MARACCHI, F. MIGLIETTA, F. MASELLI (CNR, Istituto di Analisi Ambientale e Telerilevamento Applicati

all'Agricoltura, Florence, Italy), and V. M. SACCO (CNR, Istituto di Ricerca sulle Onde Elettromagnetiche, Florence, Italy) (European Association of Remote Sensing Laboratories, Annual Symposium on European Remote Sensing Needs in the 1990s, Noordwijkerhout, Netherlands, May 4-8, 1987) International Journal of Remote Sensing (ISSN 0143-1161), vol. 9, Oct.-Nov. 1988, p. 1597-1612. refs

A method of variance decomposition of TM data using principal component analyses is applied to the problem of discriminating the spectral response of woody areas distributed over hills and mountains. The method is tested using two TM images of a forested area in the Trentino region of Italy. The low quality and quantity of ground information in the research lead to an overestimation of the classification accuracy evaluated by a final confusion matrix.

R.B.

A89-20724

AERIAL PHOTOGRAPHY FOR BIOMASS ASSESSMENT IN THE INTERTIDAL ZONE

C. MEULSTEE, H. T. C. VAN STOKKOM (Rijkswaterstaat, Delft, Netherlands), and P. H. NIENHUIS (Delta Institute for Hydrobiological Research, Yerseke, Netherlands) (European Association of Remote Sensing Laboratories, Annual Symposium on European Remote Sensing Needs in the 1990s, Noordwijkerhout, Netherlands, May 4-8, 1987) International Journal of Remote Sensing (ISSN 0143-1161), vol. 9, Oct.-Nov. 1988, p. 1859-1867. refs

A method for quantitative biomass assessment of macrophytes growing at intertidal mudflats was developed using aerial false-color photography. A verification of the method has been carried out and the method has been applied over a vast area (400 sq km). The method is based on a direct relationship between color densities and field biomass at a number of sample plots. It appeared that the bidirectional reflectance properties of the macrophytes play a minor role, probably because of the flat character of the intertidal area and the small thickness of the macrophyte layer. It is concluded that the method is highly reliable and very well applicable over extended areas.

Author

N89-10305# European Space Agency, Paris (France).

PROCEEDINGS OF THE 4TH INTERNATIONAL COLLOQUIUM ON SPECTRAL SIGNATURES IN REMOTE SENSING

T. D. GUYENNE, ed. and J. J. HUNT, ed. Apr. 1988 535 p Partly in ENGLISH and FRENCH Proceedings held in Aussois, France, 18-22 Jan. 1988; sponsored in cooperation with Inst. National de la Recherche Agronomique, Montfavet, France, CNES, Toulouse, France, CNRS, Verrieres-le-Buisson, France, and ESA, Paris, France

(ESA-SP-287; ISSN-0379-6566; ETN-88-93044) Avail: NTIS HC A23/MF A01; ESA Publications Division, ESTEC, Noordwijk, Netherlands 80 Dutch guilders

Radar signatures of vegetation; microwave interaction with sea surface; models of spectral response of natural surfaces; emission of natural surfaces in the thermal infrared; laser active remote sensing; high spectral resolution; spectral characteristics of natural surfaces (MOMS program); and large scientific remote sensing programs were discussed.

ESA

N89-10306# Institut National de la Recherche Agronomique, Avignon (France). Station de Bioclimatologie.

EXTRACTING SOIL AND VEGETATION CHARACTERISTICS FROM MICROWAVE REMOTE SENSING DATA [EXTRACTION DES CARACTERISTIQUES DU SOL ET DE LA VEGETATION A PARTIR DE DONNEES DE TELEDETECTION HYPERFREQUENCES]

L. PREVOT, I. CHAMPION, and G. GUYOT /In ESA, Proceedings of the 4th International Colloquium on Spectral Signatures in Remote Sensing p 7-12 Apr. 1988 In FRENCH

Avail: NTIS HC A23/MF A01; ESA Publications Division, ESTEC, Noordwijk, Netherlands 80 Dutch guilders

Models for direct interpretation of active microwave remote sensing signals from under vegetation canopies are reviewed and

the problem of introducing characteristic vegetation variables in semi-empirical water drop type models is discussed. The feasibility of operational inversion of these models is assessed, taking into account sensor accuracy and parameter variations from one crop to another. Use of the models to invert the data is shown to be possible, although limits to the technique are indicated. ESA

N89-10307# Karlsruhe Univ. (Germany, F.R.).

COHERENT POLARIMETRIC SIGNATURES OF CONIFEROUS TREES: A SURVEY

D. KAEHNY, S. RIEGGER, G. SCHOENE, and W. WIESBECK /In ESA, Proceedings of the 4th International Colloquium on Spectral Signatures in Remote Sensing p 13-18 Apr. 1988

(Contract JRC-3106-86-12-ED-ISP-D)

Avail: NTIS HC A23/MF A01; ESA Publications Division, ESTEC, Noordwijk, Netherlands 80 Dutch guilders

The state of the art in polarimetric signatures, their inherent ideas, and typical experimental results for coniferous tree parts are reviewed. Special types of signatures are evaluated for straight twigs of picea abies (spruce tree) and abies alba (silver fir) trees. Characteristics, resulting from the measurements, are discussed and interpreted. The radar cross section matrix is shown to reveal typical characteristics for similar parts of trees. ESA

N89-10308# Institut National de la Recherche Agronomique, Montfavet (France).

MEASURING IN-SITU SOIL SURFACE ROUGHNESS USING A LASER PROFILOMETER

P. BERTUZZI and J. M. CAUSSIGNAC (Ecole Nationale des Ponts et Chaussees, Paris, France) /In ESA, Proceedings of the 4th International Colloquium on Spectral Signatures in Remote Sensing p 19-24 Apr. 1988 Prepared in cooperation with Laboratoire Central des Ponts et Chaussees, Paris (France)

Avail: NTIS HC A23/MF A01; ESA Publications Division, ESTEC, Noordwijk, Netherlands 80 Dutch guilders

An optical technique for measuring field roughness characteristics of soil using a laser profilometer is described. The method is based on the defect-of-focus of a laser light beam. Laboratory and field tests were carried out in order to improve the method for field use and to compare the technique with a reference method. The technique is considerably quicker, and causes no disturbance to soil. The degree of resolution and accuracy are satisfactory. ESA

N89-10309# Centre for Agrobiological Research, Wageningen (Netherlands).

MICROWAVE BACKSCATTER FROM BEETS, PEAS AND POTATOES THROUGHOUT THE GROWING SEASON

B. A. M. BOUMAN /In ESA, Proceedings of the 4th International Colloquium on Spectral Signatures in Remote Sensing p 25-30 Apr. 1988 Sponsored by Begeleidingscommissie Remote Sensing, Delft, The Netherlands

Avail: NTIS HC A23/MF A01; ESA Publications Division, ESTEC, Noordwijk, Netherlands 80 Dutch guilders

The X-band radar backscatter from beet, peas, and potatoes was analyzed in relation to crop growth, to changes in canopy morphology, and to meteorological data. The cloud model for microwave backscatter from vegetation is used to describe the backscatter during the growing season. The results for 1 yr are used to predict the backscatter in another year at another location. The general trend in X-band microwave backscatter from these crops can be fairly well described by the model. However large erratic fluctuations in the observed microwave backscatter remain unexplained. These are probably due to instantaneous changes in canopy geometry which can be caused by meteorological conditions. ESA

N89-10310# Institut National de la Recherche Agronomique, Montfavet (France). Station de Bioclimatologie.

COMPLEMENTARY OF MICROWAVE AND OPTICAL RANGE IN THE CHARACTERIZATION OF CROPS BY REMOTE SENSING [COMPLEMENTARITE DES HYPERFREQUENCES ET DU DOMAINE OPTIQUE DANS LA CARACTERISATION DES CULTURES PAR TELEDETECTION]

I. CHAMPION, L. PREVOT, G. RONDEAUX, F. BARET, and G. GUYOT /in ESA, Proceedings of the 4th International Colloquium on Spectral Signatures in Remote Sensing p 31-36 Apr. 1988 In FRENCH

Avail: NTIS HC A23/MF A01; ESA Publications Division, ESTEC, Noordwijk, Netherlands 80 Dutch guilders

The possibility of using the SPOT optical (red and near infrared) and microwave (C and X) bands in a complementary manner for crop characterization was studied using data acquired for winter wheat over a 2 yr period. Simplified models of reflectance and backscatter in which the main variables are leaf area index and surface soil moisture are used to compare the sensitivity of each spectral band. Estimation accuracy for one variable when the uncertainty for the other is known is evaluated. The domain in which model inversion is also possible is defined for four measurement configurations (SPOT XS2 and XS3 and bands C and X). It is shown that leaf area index can be estimated with acceptable accuracy in an index range from 0.6 to 3 in the red channel, 1.25 to 6 in the near infrared, and from 2.5 in the X-band. Soil moisture is measured well in C-band. Strategies for using the measurements to complement each other, e.g., replacing optical sensors with X-band in cloudy conditions, are suggested. ESA

N89-10317# State Univ. of New York, Binghamton.

A PERSPECTIVE ON VEGETATION CANOPY REFLECTANCE MODELS

N. S. GOEL /in ESA, Proceedings of the 4th International Colloquium on Spectral Signatures in Remote Sensing p 77-85 Apr. 1988

Avail: NTIS HC A23/MF A01; ESA Publications Division, ESTEC, Noordwijk, Netherlands 80 Dutch guilders

Factors which affect the spectral signature of or reflectance from a vegetation canopy are delineated. Canopy reflectance models which attempt to incorporate these factors are reviewed. A technique for estimating important biophysical parameters like leaf area index, leaf angle distribution, and canopy architecture, through inversion of these models is reviewed. ESA

N89-10319# Institut National de la Recherche Agronomique, Montfavet (France). Station de Bioclimatologie.

SPECTRAL PROFILE AND BIOMASS ESTIMATION [PROFIL SPECTRAL ET ESTIMATION DE LA BIOMASSE]

F. BARET, G. GUYOT, J. M. TERES, and D. RIGAL /in ESA, Proceedings of the 4th International Colloquium on Spectral Signatures in Remote Sensing p 93-98 Apr. 1988 In FRENCH

Avail: NTIS HC A23/MF A01; ESA Publications Division, ESTEC, Noordwijk, Netherlands 80 Dutch guilders

A procedure to estimate biomass production of a crop from the proportion of photosynthetic active energy (PAR) absorbed by the canopy (Sigma i) is outlined. It is shown that Sigma i is functionally linked to the radiometric response of the crop, and an analytic method to estimate it is outlined. It explicitly accounts for factors such as Sun position, canopy structure, and soil optical properties normally treated implicitly. Its use requires the inversion of reflectance models in order to deduce canopy parameters from radiometric data. These parameters can be input to a PAR absorptance model to estimate Sigma i. The data obtained can be used in a canopy function model to estimate crop yield. ESA

N89-10321# Centre d'Etude Spatiale des Rayonnements, Toulouse (France).

RETRIEVING VEGETATION AND SOIL PARAMETERS FROM RADAR MEASUREMENTS

ALPHONSE LETOAN and T LETOAN /in ESA, Proceedings of the 4th International Colloquium on Spectral Signatures in Remote

Sensing p 105-111 Apr. 1988

Avail: NTIS HC A23/MF A01; ESA Publications Division, ESTEC, Noordwijk, Netherlands 80 Dutch guilders

An approach for inverting radar measurements into soil and vegetation volumetric moisture content is presented. The approach consists in using a theoretical model (Eom and Fung, 1984) to simulate the radar responses to a wide range of vegetation and soil parameters. The simulated data are used in a sensitivity study to determine the validity conditions for inversion; and to derive fitting parameters of a semi-empirical model selected for inversion. The results obtained on soybean canopies at C-band and 20 deg of incidence are presented. Inversion is shown to be possible. ESA

N89-10322# Institut National de la Recherche Agronomique, Montfavet (France). Station de Bioclimatologie.

A SIMPLIFIED VEGETATION CANOPY REFLECTANCE AND ABSORPTION MODEL [UN MODELE SIMPLIFIE DE REFLECTANCE ET D'ABSORPTANCE D'UN COUVERT VEGETAL]

F. BARET /in ESA, Proceedings of the 4th International Colloquium on Spectral Signatures in Remote Sensing p 113-120 Apr. 1988 In FRENCH

Avail: NTIS HC A23/MF A01; ESA Publications Division, ESTEC, Noordwijk, Netherlands 80 Dutch guilders

A model giving vegetation canopy reflectance and diffuse transmittance and reflectance for vertical view angles is outlined. It is based on a Beer's law type formalism. It takes explicitly into account characteristic canopy parameters and the optical properties of its elements, as well as Sun position. The model correctly reproduces data obtained from the Suits model, on which it was adjusted. The simplified formalism facilitates inversion and allows a clear interpretation of canopy spectral response in terms of amplitude and rate of variation of reflectance (or transmittance) as a function of the leaf area index. It also allows spectral reflectance in different spectral domains to be linked, and linking of reflectance to absorptance. ESA

N89-10323# Institut National de la Recherche Agronomique, Thiverval-Grignon (France). Station de Bioclimatologie et Teledetection.

POTENTIAL NUMBER OF WINTER WHEAT EARS ESTIMATION USING RADIOMETRY TECHNIQUES AT AN EARLY STAGE

P. BOISSARD, J.-G. POINTEL, P. LETERME, and O. BUISSON /in ESA, Proceedings of the 4th International Colloquium on Spectral Signatures in Remote Sensing p 121-124 Apr. 1988 In FRENCH; ENGLISH summary

Avail: NTIS HC A23/MF A01; ESA Publications Division, ESTEC, Noordwijk, Netherlands 80 Dutch guilders

Agronomical studies showed that it is possible to estimate the potential number of winter wheat ears from dry biomass measurement at an early stage. The potential number of ears is reached without any stress condition (light excepted) and provides one of the yield components. Using radiometric measurements in SPOT bands, it is shown that dry biomass can be estimated in a range 0 to 200 g/sqm with r sq coefficient = 0.87 (+ or - 40 g/sqm at 95 percent confidence interval, corresponding to + or - 100 ears in the middle range of potential curves). Use of normalized difference to calculate a vegetation index must be discussed because this index is sensitive to incoming radiation variations. ESA

N89-10324# Institut National de la Recherche Agronomique, Montfavet (France). Station de Bioclimatologie.

INTRODUCING SPECTRAL DATA INTO A PLANT PROCESS MODEL FOR IMPROVING ITS PREDICTION ABILITY

R. DELECOLLE and M. GUERIF /in ESA, Proceedings of the 4th International Colloquium on Spectral Signatures in Remote Sensing p 125-127 Apr. 1988

Avail: NTIS HC A23/MF A01; ESA Publications Division, ESTEC, Noordwijk, Netherlands 80 Dutch guilders

The feasibility of using vegetation index values from spectral

data as inputs to AFRCWHEAT, a wheat simulation model, is studied. This is done by using an independent submodel of leaf area index (LAI) evolution which is iteratively corrected for each new LAI value estimated by normalized difference, and resuming the global simulation from sowing time. The prediction error is greatly decreased by the method, but the bias remains important. Constraining assumptions still remain like the robustness of the simulated development scale, which rules partitioning of assimilates and growth of vegetative organs. ESA

N89-10325# Los Alamos National Lab., NM. Theoretical Div.
THE ANGULAR REFLECTANCE SIGNATURE OF THE CANOPY HOT SPOT IN THE OPTICAL REGIME

S. A. W. GERSTL /in ESA, Proceedings of the 4th International Colloquium on Spectral Signatures in Remote Sensing p 129-132 Apr. 1988

Avail: NTIS HC A23/MF A01; ESA Publications Division, ESTEC, Noordwijk, Netherlands 80 Dutch guilders

It is shown from experimental data and by modeling that the canopy hot spot angular reflectance signature carries information about plant stand architecture that is often more distinctive for different plant species than their spectral signatures. Model results show that the angular width of the hot spot reflectance distribution is highly correlated with the leaf size and canopy height. Atmospheric radiative transfer calculations indicate that such angular signatures are invariant to atmospheric perturbations. Thus, the hot spot of plant canopies is recognized as an angular reflectance signature that carries information about the plant stand architecture which may be useful for instant crop identification from off-nadir satellite measurements. ESA

N89-10326*# State Univ. of New York, Binghamton.
A MODEL FOR RADIATIVE TRANSFER IN HETEROGENEOUS THREE-DIMENSIONAL CANOPIES

N. S. GOEL and T. GRIER /in ESA, Proceedings of the 4th International Colloquium on Spectral Signatures in Remote Sensing p 133-136 Apr. 1988 Sponsored by NASA

Avail: NTIS HC A23/MF A01; ESA Publications Division, ESTEC, Noordwijk, Netherlands 80 Dutch guilders CSCL 02F

A model, dubbed TRIM, for the interaction of electromagnetic radiation with inhomogeneous vegetation canopies is presented. It is based on the four flux theory for homogeneous canopies. The canopy is assumed to consist of ellipsoidal subcanopies located on the ground at periodic intervals. The model is inverted with field measured data for reflectance from corn canopies in the near infrared region. It is shown that TRIM correctly identifies the architecture of the canopy (homogeneous or row canopy, percentage of ground cover) and gives a good estimate of leaf area index. ESA

N89-10327# Institut National de la Recherche Agronomique, Montfavet (France).

BIOMASS AND WHEAT CROP YIELD ESTIMATION FROM SPOT VEGETATIVE INDEXES [ESTIMATION DE LA BIOMASSE DU RENDEMENT DE CULTURES DE BLE DUR A PARTIR DES INDICES DE VEGETATION SPOT]

M. GUERIF, R. DELECOLLE, X. GU, J. P. GUINOT, M. JAPPIOT, and S. STEINMETZ /in ESA, Proceedings of the 4th International Colloquium on Spectral Signatures in Remote Sensing p 137-141 Apr. 1988 In FRENCH Sponsored by the Conseil General de la Region P.A.C.A., France

Avail: NTIS HC A23/MF A01; ESA Publications Division, ESTEC, Noordwijk, Netherlands 80 Dutch guilders

A two stage method for regional estimation of wheat crop yield from data is presented. Biomass is estimated from vegetative index using an extremely simplified formalism derived from models of the interaction of radiation with vegetation canopy and photosynthesis. Crop yield or its components are estimated from the biomass. The model was validated over a dozen plots, and improvements are suggested. The difficulty of treating the great variety of crop situations found at regional level is stressed. ESA

N89-10328# Centre National d'Etudes Spatiales, Toulouse (France).

SPECTRAL CHARACTERIZATION OF FOREST TARGETS IN MOUNTAINOUS ZONES ON THEMATIC MAPPER IMAGES [CARACTERISATION SPECTRALE DE CIBLES FORESTIERES EN ZONE DE MONTAGE SUR DES DONNEES DU THEMATIC MAPPER]

C. LEPRIEUR, J.-M. DURAND, and J.-L. PEYRON /in ESA, Proceedings of the 4th International Colloquium on Spectral Signatures in Remote Sensing p 143-146 Apr. 1988 In FRENCH

Avail: NTIS HC A23/MF A01; ESA Publications Division, ESTEC, Noordwijk, Netherlands 80 Dutch guilders

Analysis and representation of the evolution of the LANDSAT Thematic Mapper signal of forests were used to characterize the variability of the responses. The forests are representative of relief conditions in temperate European regions. The proportion of the variability explained by the nature of the target and that induced by modification of acquisition geometry are quantified for each spectral domain. Directional effects proper to each forest species are shown. It is concluded that the signal is relatively little dependent on observation conditions. The greatest part of signal variability is linked to thematic texture. ESA

N89-10329# Southampton Univ. (England). Dept. of Geography.

A SIMPLIFIED REFLECTANCE MODEL FOR SHRUB CANOPIES

E. J. MILTON and E. M. ROLLIN /in ESA, Proceedings of the 4th International Colloquium on Spectral Signatures in Remote Sensing p 147-150 Apr. 1988

Avail: NTIS HC A23/MF A01; ESA Publications Division, ESTEC, Noordwijk, Netherlands 80 Dutch guilders

A simplified descriptive model of the angular reflectance of shrub canopies based on data from a spectroradiometer is presented. The directional reflectance observed at the solar zenith angle for a range of azimuth angles is discussed. A marked minimum in reflectance relative to nadir when viewing up-Sun and a localized peak (in visible wavelengths especially), when viewing down-Sun are both features characteristic of the heather (*Calluna vulgaris*) canopies studied. These relationships are encapsulated in a simple graphic device: that of an imaginary landscape. This is seen as a necessary first step towards an analytical model for shrub canopies. ESA

N89-10332# Institut National de la Recherche Agronomique, Thiverval-Grignon (France). Station de Bioclimatologie.

ESTIMATION OF THE INTERCEPTION EFFICIENCY OF AN ALFALFA CANOPY FROM A VEGETATIVE INDEX [ESTIMATION DE L'EFFICIENCE DE L'INTERCEPTION D'UN COUVERT DE LUZERNE A PARTIR D'UN INDICE DE VEGETATION]

J. M. ALLIRAND, M. CHARTIER, and G. GOSSE /in ESA, Proceedings of the 4th International Colloquium on Spectral Signatures in Remote Sensing p 163-166 Apr. 1988 In FRENCH

Avail: NTIS HC A23/MF A01; ESA Publications Division, ESTEC, Noordwijk, Netherlands 80 Dutch guilders

It is shown that the interception efficiency of an alfalfa canopy, needed to estimate yield, can be estimated from a combination of visible and near infrared reflectances obtained with sensors with a semi-hemispherical field of view, commonly used in agronomy. The obtained relationship depends essentially on soil optical properties. ESA

N89-10333# Institut National de la Recherche Agronomique, Thiverval-Grignon (France). Station de Bioclimatologie.

RELATION BETWEEN SUGAR BEET CROP YIELD AND VEGETATIVE INDEXES CALCULATED FROM LANDSAT MSS IMAGES [RELATION ENTRE LE RENDEMENT DE CULTURES DE BETTERAVE A SUCRE ET DES INDICES DE VEGETATION CALCULES A PARTIR D'IMAGES LANDSAT MSS]

B. ANDRIEU and J. CANEILL /in ESA, Proceedings of the 4th

International Colloquium on Spectral Signatures in Remote Sensing p 167-170 Apr. 1988 In FRENCH Sponsored by CNES/CNRS, France

Avail: NTIS HC A23/MF A01; ESA Publications Division, ESTEC, Noordwijk, Netherlands 80 Dutch guilders

Images from LANDSAT MSS were used to calculate radiometric growth indexes for 42 sugar beet parcels on July 31 and Sept. 4, and soil radiance index on Jan. 1. Yield was estimated on the ground by geometric weighing at the end of October. The proportion of yield variance explained by radiometric indexes depends mainly on the number of pixels which could be taken into account for the radiometric characterization of the parcels. A bilinear regression using the growth index in September and the radiance index in January enables 86 percent of the variance in sugar yield to be explained for parcels containing at least 8 pure pixels. ESA

N89-10334# Sheffield Univ. (England). Dept. of Geography.

DEVELOPING A RADIOMETRIC LEAF AREA INDEX

P. J. CURRAN and N. W. WARDLEY /In ESA, Proceedings of the 4th International Colloquium on Spectral Signatures in Remote Sensing p 171-173 Apr. 1988 Sponsored by the Natural Environment Research Council, London, England

Avail: NTIS HC A23/MF A01; ESA Publications Division, ESTEC, Noordwijk, Netherlands 80 Dutch guilders

A measure of vegetation amount that is sensitive to canopy geometry was developed. This measure, termed the radiometric leaf area index (RLAI), comprises measurements of LAI, leaf inclination or curvature and the area of the canopy visible to the sensor. The RLAI was evaluated on simulated data and proves to be sensitive to canopy geometry. ESA

N89-10336# Groupement Scientifique de Teledetection de Strasbourg (France).

ATTEMPT AT ABSOLUTE DETERMINATION OF SPECTRAL SIGNATURES OF BARE SOILS IN THE THERMAL INFRARED, IN EMISSION AND REFLECTION [ESSAI DE DETERMINATION ABSOLUE DES SIGNATURES SPECTRALES DE SOLS NUS DANS L'INFRAROUGE THERMIQUE, EN EMISSION ET EN REFLEXION]

F. NERRY, J. LABED, and M. P. STOLL /In ESA, Proceedings of the 4th International Colloquium on Spectral Signatures in Remote Sensing p 185-188 Apr. 1988 In FRENCH Sponsored by CNES, France

Avail: NTIS HC A23/MF A01; ESA Publications Division, ESTEC, Noordwijk, Netherlands 80 Dutch guilders

An autocalibration based method for estimating spectral emissivity signatures, without radiation temperature measurements, and without any a priori hypothesis, is discussed. Relative accuracy is + or - 0.6 percent. Measurement of spectral signatures in reflection confirm the emission results. Natural materials, minerals, and cultivated soils illustrate the measurement possibilities. ESA

N89-10342# Bonn Univ. (Germany, F.R.). Inst. fuer Pflanzenbau.

SPECTRAL REFLECTANCE OF SUGAR BEET AND WINTER WHEAT CANOPIES IN THE VISIBLE AND INFRARED DURING GROWTH

K. DOCKTER, J. SCHELLBERG, W. KUEHBAUCH, C. VONRUESTEN, U. TEMPELMANN, and G. KUPFER /In ESA, Proceedings of the 4th International Colloquium on Spectral Signatures in Remote Sensing p 211-216 Apr. 1988

Avail: NTIS HC A23/MF A01; ESA Publications Division, ESTEC, Noordwijk, Netherlands 80 Dutch guilders

The spectral reflectivity of differently managed sugar beet and winter wheat crops was investigated during growth. Simultaneously plants were analyzed for parameters relevant to yield. Meteorological data were recorded to explain the effect of illumination conditions (e.g., cloudiness). Qualitative comparisons indicate typical relationships between plant parameters (leaf vitality, water stress and fungi impact, leaf inclination angle) and spectral response. Results of a plant model (hot spot, distribution and number of leaves) are presented. ESA

N89-10343# Valencia Univ. (Spain). Remote Sensing Group. **A THEORETICAL MODEL FOR INTERPRETING REMOTELY SENSED THERMAL INFRARED MEASUREMENTS OBTAINED OVER AGRICULTURAL AREAS**

J. A. SOBRINO, V. CASELLES, and F. BECKER (Groupement Scientifique de Teledetection de Strasbourg, France) /In ESA, Proceedings of the 4th International Colloquium on Spectral Signatures in Remote Sensing p 217-220 Apr. 1988 (Contract CAICYT-A-172/85)

Avail: NTIS HC A23/MF A01; ESA Publications Division, ESTEC, Noordwijk, Netherlands 80 Dutch guilders

A theoretical model to interpret remotely sensed thermal infrared measurements carried out over agricultural areas cultivated in rows was developed. Factors which take part in the definition of the effective emissivity and temperature (observation height, viewing angle, type of soil, dimensions and separation of vegetation) are analyzed. The model was validated in a citrus orchard during three typical nights of radiative cooling (clear sky and calmed wind). The model performs to an accuracy of 1 percent. ESA

N89-10348# Karlsruhe Univ. (Germany, F.R.). Inst. of Botany.

CHANGES IN THE CHLOROPHYLL FLUORESCENCE SPECTRA DURING THE KAUSKY INDUCTION KINETICS

H. K. LICHTENTHALER and C. BUSCHMANN /In ESA, Proceedings of the 4th International Colloquium on Spectral Signatures in Remote Sensing p 245-250 Apr. 1988

Avail: NTIS HC A23/MF A01; ESA Publications Division, ESTEC, Noordwijk, Netherlands 80 Dutch guilders

An optical multichannel analyzer was used to screen the in situ chlorophyll fluorescence signatures of vegetation. It permits the fast registration of fluorescence spectra during the Kautsky induction kinetic. From the digitized data the induction kinetics at any given wavelength-range can be traced and the ratio F690/F735 and the Rfd-values determined. Though the ratio F690/F735 changes during the fluorescence induction kinetics, the changes are small compared to the differences between leaves of different chlorophyll content and different photosynthetic activity of stressed or damaged plants. Results demonstrate that the ratio F690/F735 is a very suitable fluorescence parameter to develop an airborne system for the remote sensing of chlorophyll fluorescence of terrestrial plants. ESA

N89-10349# Karlsruhe Univ. (Germany, F.R.). Inst. of Botany.

CHLOROPHYLL FLUORESCENCE SPECTRA OF LEAVES AS INDUCED BY BLUE LIGHT AND RED LASER LIGHT

H. K. LICHTENTHALER and U. RINDERLE /In ESA, Proceedings of the 4th International Colloquium on Spectral Signatures in Remote Sensing p 251-254 Apr. 1988 Sponsored by the Joint Research Center of the European Communities, Ispra, Italy

Avail: NTIS HC A23/MF A01; ESA Publications Division, ESTEC, Noordwijk, Netherlands 80 Dutch guilders

The dependence of the chlorophyll-fluorescence emission spectra of green plant tissue (leaves, needles) on the wavelength of the excitation light was determined and the differences in the spectra were quantified by the fluorescence ratio F690/F735. The differences in the ratio F690/F735, which can be taken as indicator of stress to plants, using either blue (470 + or - 30 nm) or red excitation light (620 + or - 20 nm or He/Ne-laser 632.8 nm) are listed for leaves with different chlorophyll content and photosynthetic activity. The application of the ratio F690/F735 in detecting stress to terrestrial vegetation via remote sensing of laser-induced chlorophyll fluorescence is discussed. ESA

N89-10350# Kisarazu National Coll. of Technology (Japan). Faculty of Engineering.

LASER-INDUCED FLUORESCENCE ON IN-VIVO CHLOROPHYLL OF A RICE PLANT: A TECHNIQUE FOR THE REMOTE DETECTION OF PLANT GROWTH

K. TAKAHASHI, T. NAKAMURA, Y. EMORI, and A. KIMURA (Chiba Univ., Japan) /In ESA, Proceedings of the 4th International Colloquium on Spectral Signatures in Remote Sensing p 255-258 Apr. 1988

Avail: NTIS HC A23/MF A01; ESA Publications Division, ESTEC, Noordwijk, Netherlands 80 Dutch guilders

The laser-induced fluorescence (LIF) of a rice plant is evaluated as a means of remotely detecting leaf color and estimating plant growth. The leaf color is influenced by quantity of chlorophyll contained in the leaf. Fluorescence intensity of in-vivo chlorophyll is changed by the amount of fertilizer used. Leaf color was measured in a rice field using a color scale. There are differences in its observation owing to the observer's individual character. In the LIF system, the fluorescence spectra of in-vivo chlorophyll are excited with a nitrogen laser emitting at 337.1 nm. By detecting changes in fluorescence intensity at 684 nm and 740 nm concerned with photosynthesis, rice plant growth is estimated. ESA

N89-10351# Paris XI Univ., Orsay (France). Lab. pour l'Utilisation du Rayonnement Electromagnetique.

TECHNIQUES FOR REMOTE SENSING OF LIFE SPAN AND QUANTUM YIELD OF CHLOROPHYLL FLUORESCENCE IN VIVO [TECHNIQUES POUR LA TELEDETECTION DE LA DUREE DE VIE ET DU RENDEMENT QUANTIQUE DE LA FLUORESCENCE DE LA CHLOROPHYLLE IN VIVO]

I. MOYA, Y. GOULAS, and J. M. BRIANTIS /In ESA, Proceedings of the 4th International Colloquium on Spectral Signatures in Remote Sensing p 259-262 Apr. 1988 In FRENCH

Avail: NTIS HC A23/MF A01; ESA Publications Division, ESTEC, Noordwijk, Netherlands 80 Dutch guilders

Use of laser induced fluorescence for remote sensing of chlorophyll from flying platforms is discussed. By refining the sensing it may be possible to attain the average life span of the fluorescence. Laboratory measurements under widely varying conditions show that the average life span is in proportion to the quantum yield of the fluorescence. Quantum yield can be used to predict the physiological state of chlorophylls, but it is inaccessible to direct measurement. Measurement techniques which could be adapted to remote sensing are presented, including photon counting, phase fluorimetry, and ultrarapid oscilloscope. ESA

N89-10354# Institut National de la Recherche Agronomique, Montfavet (France). Station de Bioclimatologie.

USE OF HIGH SPECTRAL RESOLUTION TO FOLLOW THE STATE OF VEGETATION CANOPIES [UTILISATION DE LA HAUTE RESOLUTION SPECTRALE POUR SUIVRE L'ETAT DES COUVERTS VEGETAUX]

G. GUYOT and F. BARET /In ESA, Proceedings of the 4th International Colloquium on Spectral Signatures in Remote Sensing p 279-286 Apr. 1988 In FRENCH

Avail: NTIS HC A23/MF A01; ESA Publications Division, ESTEC, Noordwijk, Netherlands 80 Dutch guilders

The action mechanisms of factors which control the movement of the wavelength of a point of inflection λ_i of the reflectance curve of vegetation between the red and near infrared regions are analyzed at leaf and vegetation canopy scales. Variations of λ_i seem to carry the same type of information as the combination of measurements in wide spectral bands (normalized difference, ND). However the introduction of atmospheric effects in satellite measurements reveals that the value of λ_i is much less dependent on atmospheric conditions than ND. Thus a set of four or five narrow spectral bands is proposed to determine λ_i from satellite measurements in order to determine and follow the state of vegetation canopies. ESA

N89-10355# Institute for Image Processing Computer Mapping, Graz (Austria).

STRESS DETECTION IN MIXED CONIFEROUS-BROADLEAVED FORESTS FROM AIRBORNE IMAGING SPECTROMETER (AIS) DATA

C. BANNINGER /In ESA, Proceedings of the 4th International Colloquium on Spectral Signatures in Remote Sensing p 287-290 Apr. 1988

Avail: NTIS HC A23/MF A01; ESA Publications Division, ESTEC, Noordwijk, Netherlands 80 Dutch guilders

The spectral response of forests was examined. Airborne imaging spectrometer data acquired from a metal-stressed

spruce-broadleaved forest display changes in absorption features in the near to shortwave infrared region that coincide with canopy leaf tannin and starch absorption bands. These features, however, are often subdued or masked by the influence of stronger atmospheric water and carbon dioxide absorption bands present in this wavelength region, which must be removed to delineate or enhance the subtle leaf chemistry absorption features. ESA

N89-10358# Nottingham Univ. (England). Dept. of Geography. **HIGH SPECTRAL RESOLUTION INDICES FOR MONITORING CROP GROWTH AND CHLOROSIS**

T. H. DEMETRIADES-SHAH and M. D. STEVEN /In ESA, Proceedings of the 4th International Colloquium on Spectral Signatures in Remote Sensing p 299-302 Apr. 1988 (Contract NERC-GST/02/124)

Avail: NTIS HC A23/MF A01; ESA Publications Division, ESTEC, Noordwijk, Netherlands 80 Dutch guilders

Spectral reflectance of sugar beet in the 400 to 1100 nm region was examined in relation to chlorosis inducing stresses. Spectral indices to predict crop growth and condition unambiguously were tested. Canopy growth variables are most correlated with the first derivative at 940 nm and chlorosis with the second derivative at 636 nm although other derivative indices are also promising. Conventional near-infrared/red based indices and the wavelength of maximum slope of canopy reflectance (the red edge) proposed as an index for monitoring chlorosis are not found to be as good for monitoring stressed vegetation. ESA

N89-10359# Deutsche Forschungs- und Versuchsanstalt fuer Luft- und Raumfahrt, Oberpfaffenhofen (West Germany). Inst. of Optoelectronics.

OPTIMIZATION FOR CLASSIFICATION OF FOREST DAMAGE CLASSES

G. KRITIKOS, R. MUELLER, and P. REINARTZ /In ESA, Proceedings of the 4th International Colloquium on Spectral Signatures in Remote Sensing p 303-309 Apr. 1988

Avail: NTIS HC A23/MF A01; ESA Publications Division, ESTEC, Noordwijk, Netherlands 80 Dutch guilders

Using airborne scanner data of forest stands from different flight altitudes, damage classes are classified. In order to improve classification accuracy, the scanner data can be preprocessed due to the viewing angle dependence of the reflected signal using an empirical correction method. The damage classes have a natural overlap in their signatures. The calculation of the separability of the classes with the Jeffries-Matusita measure allows the optimization of channel and training area selections. Derived features can be checked for their information content in a classification. ESA

N89-10363# Institut Francais de Recherche pour l'Exploitation de la Mer, Brest (France).

COMPARATIVE ANALYSIS OF SPECTRAL RESPONSE IN THE OPTICAL DOMAIN OF TARGETS IN A TROPICAL SWAMP AT VARIOUS SPECTRAL AND SPATIAL RESOLUTIONS [ANALYSE COMPARATIVE DES REPONSES SPECTRALES DANS LE DOMAINE OPTIQUE DES CIBLES D'UN MARAIS TROPICAL A DIVERSES RESOLUTIONS SPATIALES ET SPECTRALES]

L. LOUBERSAC, M. VIOLIER, and C. LEMASSON (ENSAIA, Nancy, France) /In ESA, Proceedings of the 4th International Colloquium on Spectral Signatures in Remote Sensing p 323-327 Apr. 1988 In FRENCH; ENGLISH summary

Avail: NTIS HC A23/MF A01; ESA Publications Division, ESTEC, Noordwijk, Netherlands 80 Dutch guilders

Spectral signatures of the same tropical salt marsh targets, acquired on the ground (Sept. 20, 1986) and from altitude (helicopter survey Sept. 17, 1986) with 3 look angles are compared to the SPOT HRV data of Sept. 18, 1986 and correlated to physical properties of the barren salt flats. Observations give coherent results but on dense vegetation the satellite response appears underestimated; on barren flats, it appears overestimated. An atmospheric environmental effect explanation is proposed.

Significant correlations between vegetation and brightness indexes and humidity and organic matter content of soils are found. ESA

N89-10367# Laval Univ. (Quebec). Dept. des Sciences Geodesiques et de Teledetection.

TEXTURE ANALYSIS IN FOREST AREAS: HIGH SPECTRAL RESOLUTION SYNTHETIC APERTURE RADAR DATA [ANALYSE TEXTURALE EN MILIEU FORESTIER: DONNEES RADAR A OUVERTURE SYNTHETIQUE DE HAUTE RESOLUTION SPATIALE]

R. LANDRY, G. EDWARDS, K. P. B. THOMSON, and P. GILBERT /In ESA, Proceedings of the 4th International Colloquium on Spectral Signatures in Remote Sensing p 341-345 Apr. 1988 In FRENCH

Avail: NTIS HC A23/MF A01; ESA Publications Division, ESTEC, Noordwijk, Netherlands 80 Dutch guilders

Visual interpretation (spectral aspect) of SAR images of forests, supported by terrain data, is described. It is concluded that radar imagery can aid in planning clearings, in mapping roads, and in evaluating the density of vertical twigs and first leaves in clearing areas. The methodology and results of a quantitative analysis of the texture (spatial aspect) are summarized. It is concluded that texture enables covers that would otherwise be confounded to be distinguished. ESA

N89-10368# Institut National de la Recherche Agronomique, Thiverval-Grignon (France). Station de Bioclimatologie.

ESTIMATION OF LEAF SPECTRA FROM MEASUREMENTS IN WIDE SPECTRAL BANDS [ESTIMATION DE SPECTRES DE FEUILLES A PARTIR DE MESURES DANS DES BANDES SPECTRALES LARGES]

B. ANDRIEU, F. BARET, J. SCHELLBERG, and U. RINDERLE (Karlsruhe Univ., West Germany) /In ESA, Proceedings of the 4th International Colloquium on Spectral Signatures in Remote Sensing p 351-356 Apr. 1988 In FRENCH

Avail: NTIS HC A23/MF A01; ESA Publications Division, ESTEC, Noordwijk, Netherlands 80 Dutch guilders

A simple reflectance model to simulate leaf spectra from chlorophyll concentration and infrared reflectance level is proposed. A derived model which only takes into account chlorophyll concentration enables leaf reflectance in the wide bands of a densitometer to be simulated. The inversion of the latter model gives precise estimates of chlorophyll concentration which can be used to reconstruct the complete reflectance spectrum of the leaf. Tests on wheat show that a rapid, but fine, characterization of the optical properties of canopy elements using a simple densitometer is possible. ESA

N89-10369# Institut National de la Recherche Agronomique, Thiverval-Grignon (France). Lab. de Pedologie.

MODELING OF SOIL COLOR BY REMOTE SENSING [MODELISATION DE LA COULEUR DES SOLS PAR TELEDTECTION]

D. COURAULT, M.-C. GIRARD, and R. ESCADAFAL (Office de la Recherche Scientifique et Technique, Bondy, France) /In ESA, Proceedings of the 4th International Colloquium on Spectral Signatures in Remote Sensing p 357-362 Apr. 1988 In FRENCH; ENGLISH summary

Avail: NTIS HC A23/MF A01; ESA Publications Division, ESTEC, Noordwijk, Netherlands 80 Dutch guilders

Eighty-four very different soil samples were characterized in the laboratory with: reflectance curves from 350 to 2000 nm recorded with a spectrophotometer; physical and chemical analysis; and color from Munsell soil chart. Different types of curve shapes were related to the main constituents of the studied samples. Using colorimetric concepts, soil spectral characteristics were modeled from Munsell color. It is shown that the reflectance curve of a soil sample can be predicted from converting its Munsell coordinates into the trichromatic system RGB. The low occurrence of materism for soils allows the relation between spectral reflectance and color to be inverted. ESA

N89-10370# Ecole Polytechnique Federale de Lausanne (Switzerland). Inst. for Agricultural Engineering.

THE NORMALIZATION OF A SOIL BRIGHTNESS INDEX FOR THE STUDY OF CHANGES IN SOIL CONDITIONS

R. CALOZ, B. ABEDNEGO, and C. COLLET (Fribourg Univ., Switzerland) /In ESA, Proceedings of the 4th International Colloquium on Spectral Signatures in Remote Sensing p 363-366 Apr. 1988

Avail: NTIS HC A23/MF A01; ESA Publications Division, ESTEC, Noordwijk, Netherlands 80 Dutch guilders

A methodology for comparing soil surface characteristics from remotely sensed data acquired from orbital remote sensing systems at different dates is proposed. It is based on the normalization of the soil line index or soil brightness index computed from red and infrared band information. The normalization removes the influence of changes in illumination and atmospheric conditions as well as in detector system characteristics. Normalized index values can therefore be utilized to study changes in soil surface conditions throughout time. ESA

N89-10373# Valencia Univ. (Spain). Dept. de Termodinamica.

SPECTRAL SIGNATURE OF CITRUS FRUITS AND ITS EVOLUTION: IDENTIFICATION OF THE VEGETATIVE INDEX OF LEAST TEMPORAL VARIATION [SIGNATURE SPECTRALE DES AGRUMES ET SON EVOLUTION: IDENTIFICATION D'INDEX DE VEGETATION DE MOINDRE VARIATION TEMPORELLE]

D. SEGARRA, A. GILABERT, S. GANDIA, and J. MELIA /In ESA, Proceedings of the 4th International Colloquium on Spectral Signatures in Remote Sensing p 377-382 Apr. 1988 In FRENCH

(Contract CAICYT-A-172/85)

Avail: NTIS HC A23/MF A01; ESA Publications Division, ESTEC, Noordwijk, Netherlands 80 Dutch guilders

Images from LANDSAT 5 were used to monitor the evolution of the spectral signature of a citrus fruit growing area during a winter period. Results show that there is no seasonal spectral signature for citrus fruits, the variability within one season being as great as that between seasons, and there are significant differences in reflectance from one plot to another, depending on vegetation cover. A method to detect zones affected by frost and to assess the impact was developed. It is based on a multitemporal analysis of the vegetative index before and after the frost. ESA

N89-10374# Musee Royal de l'Afrique Centrale, Tervuren (Belgium).

ROCK AND SOIL DISCRIMINATION IN NATURAL TROPICAL CONDITIONS USING A SPOT-CALIBRATED RADIOMETER

J. LAVREAU, J. P. RUDANT (Paris VI Univ., France), and PHILIPPE TREFOIS /In ESA, Proceedings of the 4th International Colloquium on Spectral Signatures in Remote Sensing p 383-386 Apr. 1988

Avail: NTIS HC A23/MF A01; ESA Publications Division, ESTEC, Noordwijk, Netherlands 80 Dutch guilders

A radiometry survey was executed in the western Tanzanian Karema area bordering lake Tanganyika. Spectral values in the SPOT bands were statistically analyzed. A discriminant analysis on different data sets concludes at the discriminability of the vegetal from the mineral objects, whereas the recognition of the soils, defined according to subsurface lithology, is usually less effective. A principal component and a cluster analysis of different groups shows the importance of non or less lithology-related parameters. A set of soils was submitted to a chemical analysis and a wide-range spectroradiometry. The analysis of the correlation matrix between chemical and spectral variables reveals that a better geochemical discrimination of the soils can be achieved when a greater number of spectral bands is taken into account. ESA

N89-10376# Sherbrooke Univ. (Quebec). Centre d'Applications et de Recherches en Teledetection.

DISCRIMINATION OF ZONES OF HIGH WATER EROSION RISK USING SPOT IMAGES [DISTINCTION DES ZONES A HAUT RISQUE D'EROSION HYDRIQUE A L'AIDE D'IMAGES SPOT]

S. PERRAS, D. BARIL, A. PESANT (Agriculture Canada, Lennoxville, Quebec), and F. BONN *In* ESA, Proceedings of the 4th International Colloquium on Spectral Signatures in Remote Sensing p 393-397 Apr. 1988 *In* FRENCH Sponsored in cooperation with the Centre des Recherches et des Services Agricoles, Quebec, Canada

(Contract DOSSIER-3B1-68400260-002)

Avail: NTIS HC A23/MF A01; ESA Publications Division, ESTEC, Noordwijk, Netherlands 80 Dutch guilders

Erosion risk of an arable farming area was assessed using SPOT imagery, a digitized pedological map, and soil erodability measurements. The potential of the SPOT images to discriminate between different soil series was examined. The SPOT images are incapable of classifying soil types. The digitized pedological map was superimposed on land use images to give bare soil area for each type of soil. These data, along with the rate of erodability, enable the quantity of soil eroded in the region to be estimated. ESA

N89-10378*# Jet Propulsion Lab., California Inst. of Tech., Pasadena.

MONITORING SEASONAL VARIATIONS OF SOIL MOISTURE AND VEGETATION COVER USING SATELLITE MICROWAVE RADIOMETRY

Y. H. KERR and E. G. NJOKU *In* ESA, Proceedings of the 4th International Colloquium on Spectral Signatures in Remote Sensing p 403-406 Apr. 1988 Sponsored by NASA

Avail: NTIS HC A23/MF A01; ESA Publications Division, ESTEC, Noordwijk, Netherlands 80 Dutch guilders CSDL 02F

The NIMBUS-7 scanning multichannel microwave radiometer measured brightness temperatures at 5 frequencies (6.6, 10.7, 18, 21, 37 GHz), all dual-polarized with a 50 deg incidence angle over Africa since 1978. A 3 yr data set is being processed (1983 to 1985), and a theoretical model was developed, allowing investigation of the microwave emissivity of land features in the frequency range 6.6 to 37 GHz and of the extent to which vegetation and roughness can be determined in order to improve the soil moisture estimation. ESA

N89-10387# Joint Research Centre of the European Communities, Ispra (Italy).

AGRISAR'86: CONTRIBUTING TO SIGNATURE RESEARCH

A. J. SIEBER *In* ESA, Proceedings of the 4th International Colloquium on Spectral Signatures in Remote Sensing p 459-462 Apr. 1988

Avail: NTIS HC A23/MF A01; ESA Publications Division, ESTEC, Noordwijk, Netherlands 80 Dutch guilders

Results of the evaluation of AGRISAR'86 image data are discussed as far as they may be used for signature research in microwave remote sensing. It is pointed out that such an airborne campaign includes too many problems to result in signatures based on physically meaningful model assumptions about the electromagnetic wave, target interaction. It is recommended first to undertake a dedicated calibration experiment and then a project for the investigation of the radar signatures of selected objects. ESA

N89-10389# Centre National de Recherches Meteorologiques, Toulouse (France).

A STUDY OF THE VEGETATION COVER WITH AVHRR DURING HAPEX-MOBILHY

T. PHULPIN and J. P. JULLIEN *In* ESA, Proceedings of the 4th International Colloquium on Spectral Signatures in Remote Sensing p 469-472 Apr. 1988

Avail: NTIS HC A23/MF A01; ESA Publications Division, ESTEC, Noordwijk, Netherlands 80 Dutch guilders

The LANDSAT AVHRR vegetation index images were used to

map the dominant vegetation types and study the vegetation state in the South-West of France. It is shown that artifacts due to haze, precipitations, or difference of anisotropy between AVHRR channels 1 and 2 could falsify the interpretation of the temporal variations of NDVI in terms of phenologic evolution. A compositing procedure allowing to keep a high time sampling rate is proposed. ESA

N89-10395*# Michigan State Univ., East Lansing. Center for Remote Sensing.

USE OF REMOTE SENSING FOR LAND USE POLICY

FORMULATION Final Report, Jan. 1985 - May 1987

1987 101 p

(Contract NGL-23-004-083)

(NASA-CR-183148; NAS 1.26:183148) Avail: NTIS HC A06/MF A01 CSDL 08B

The overall objectives and strategies of the Center for Remote Sensing remain to provide a center for excellence for multidisciplinary scientific expertise to address land-related global habitability and earth observing systems scientific issues. Specific research projects that were underway during the final contract period include: digital classification of coniferous forest types in Michigan's northern lower peninsula; a physiographic ecosystem approach to remote classification and mapping; land surface change detection and inventory; analysis of radiant temperature data; and development of methodologies to assess possible impacts of man's changes of land surface on meteorological parameters. Significant progress in each of the five project areas has occurred. Summaries on each of the projects are provided. Author

N89-10396# Instituto de Pesquisas Espaciais, Sao Jose dos Campos (Brazil).

IDENTIFYING THE REFORESTED AREAS UTILIZING THE SPOT SATELLITE DATA

PEDRO HERNANDEZFILHO Jul. 1988 13 p *In* PORTUGUESE; ENGLISH summary Presented at the 69th Congresso Florestal Estadual, Nova Prata, Brazil, 24 Sep. 1988 Submitted for publication

(INPE-4624-PRE/1343) Avail: NTIS HC A03/MF A01

The objective of this work is to evaluate the application of the SPOT satellite data to the assessment of reforested areas. The study area (4,000 ha) is localized at the municipality of Mogi-Guaçu in the state of Sao Paulo, Brazil, and is reforested by *Pinus elliotii*, *P. taeda*, *P. patula*, *P. oocarpa*, *P. caribee* (Campininha fram of the Forestry Institute of the state of Sao Paulo), and *Eucalyptus grandis* and *E. saligna* (Santa Terezinha Park - Champion Paper and Cellulose). The utilized image is the one acquired by the multispectral mode XS (714-374), 15 June 1986 hard copy, color composite 3, 2, 1, at the scale of 1:100,000. The procedure for visual interpretation of the image considered classical features of conventional photointerpretation such as tone, photographic texture, and shape, in order to identify the reforested areas. The mapped classes are *Pinus-1* (*P. elliotii*, *P. oocarpa*), *Pinus-2* (*P. taeda*, *P. caribee*, *P. patula*) and *Euca* (*Eucalyptus* spp) and the overall classification accuracy reached circa 90 percent. The obtained results reveal that the SPOT images are very useful to the characterization and mapping of reforested areas. Author

N89-10400# Instituto de Pesquisas Espaciais, Sao Jose dos Campos (Brazil).

THE TRANSFORMED VEGETATION INDEX (TVI) FOR ESTIMATION OF BRAZILIAN CERRADO'S PHYTOMASS

JOAO ROBERTO DOSSANTOS, ATTILIO ANTONIO DISPERATI, ANTONIO JOSE DEARAUJO, and ROBERTO TUYOSHI HOSAKAWA (Universidade Federal de Parana, Curitiba, Brazil) Jun. 1988 11 p Presented at the Remote Sensing Workshop on Vegetation Indices and Their Interpretation, Nottingham, England, 25 May 1988

(INPE-4603-PRE/1326) Avail: NTIS HC A03/MF A01

The main objective of this study is to make an analysis of the relationship between the cerrado's foliar phytomass and the vegetation indices (TVI sub 4,3 and TVI sub 5,3) obtained by the

Thematic Mapper/LANDSAT-5. The ground and remote sensing data were gathered in three selected areas: Roncador Ecological Reserve-IBGE, Experimental Station of Brazilia University-UnB, and CPAC/EMBRAPA Station, located at the central region of Brazil. The linear ($y = a + bx$) and exponential ($y = ae^{bx}$) were used to analyze the functional relationship between each of the vegetation indices (x) and cerrado's phytomass (y). From the results it can be inferred that the exponential regression model shows a better fit compared to the linear one although a significant difference was not obtained. Also, the results showed better performance of the TVI sub 4,3 to fit the cerrado's phytomass (dry weight). It explained 62 percent of the variation in the dependent variable (y). This study is part of the large project that is being carried out by INPE and CPAC/EMBRAPA, of the test the TM/LANDSAT data capability for phytomass estimation of the cerrado in order to support future monitoring of this ecosystem.

Author

N89-10402# Instituto de Pesquisas Espaciais, Sao Jose dos Campos (Brazil).

NATION-WIDE FOREST MAPPING AND TIMBER VOLUME ESTIMATION USING LANDSAT-5 TM IMAGERY

RENE ANTONIO NOVAES, DAVID CHUNG LIANG LEE, PEDRO HERNANDEZFILHO, ARMANDO PACHECODOSSANTOS, and FLAVIO JORGE PONZONI Aug. 1988 33 p Presented at the Simposio Latino-Americano de Sensoriamento Remoto, 7th Reunion Plenaria SELPER, Bogota, Colombia, 16-20 Nov. 1987 (INPE-4643-PRE/1354) Avail: NTIS HC A03/MF A01

The project described was supported by the United Nations Industrial Development Organization (UNIDO). The main objective of this project was to obtain basic forest information for development, promotion, and utilization of alternative sources of energy based on the use of the country's natural resources. A methodology is described which used LANDSAT TM data as a first segment of a two-stage sampling plan designed to produce typical forest information for the plantations and to map forest areas in Uruguay. From this project it can be concluded that the total forest area is about 3 percent of the total land area in Uruguay. The plantation forest, which has high productivity of woods, is about 23.7 percent of total forested areas. The overall interpretation and mapping accuracies were 90.6 and 83.3 percent, respectively. The total stand timber volume of pine and eucalypt plantation was estimated at 3,539,418.15 cubic meters and 24,231,118.83 cubic meters, respectively. From all the results obtained the project would conclude that LANDSAT-5 TM imagery, at a scale of 1:100,000, served well as the primary source of data from forest area mapping and timber inventory over a nation-wide level.

Author

N89-10404# Deutsche Forschungs- und Versuchsanstalt fuer Luft- und Raumfahrt, Oberpfaffenhofen (West Germany). Abteilung Fernerkundung.

APPLICATIONS OF LANDSAT (TM AND MSS) DATA FOR AN ESTIMATION OF RANGELAND CONDITIONS IN SEMIARID AND ARID AREAS OF NORTHERN KENYA

CHRISTOPH DREISER Dec. 1987 119 p In GERMAN; ENGLISH summary Original contains color illustrations (DFVLR-FB-88-18; ISSN-0171-1342; ETN-88-93185; AD-B126126L) Avail: NTIS HC A06/MF A01; DFVLR, VB-PL-DO, 90 60 58, 5000 Cologne, Fed. Republic of Germany, 66 Deutsche marks

Digital multispectral data are analyzed to prove the applicability of LANDSAT 5 sensors, Thematic Mapper (TM) and Multispectral Scanner (MSS), to recognize variations of sparse vegetation coverage. The research area is a dwarf-shrub semidesert in Northern Kenya (Marsabit District). The size of the scene is 1024 x 1024 pixels. Data were acquired in the dry season. Perpendicular vegetation index is used for tracing training areas. A maximum likelihood classification of TM channels, 3, 4, 5, and 7 gives acceptable results. Compared with the classification of MSS data, TM classification leads to much more exact results. Classification results are processed further to estimate the actual rangeland potential.

ESA

N89-11292*# California Univ., Santa Barbara. Dept. of Geography.

IMPROVEMENT AND EXTENSION OF A RADAR FOREST BACKSCATTERING MODEL Annual Report

DAVID S. SIMONETT and YONG WANG 20 Sep. 1988 38 p (Contract NAG5-1010) (NASA-CR-183259; NAS 1.26:183259) Avail: NTIS HC A03/MF A01 CSCL 02F

Research to-date has focused on modeling development and programming based on model components proposed during the past several months and research progress made by the Simonett team. The model components and programs (in C language under UNIX) finished to date are summarized. These model components may help explain the contributions of various vegetation structural components to the attenuation and backscattering of vegetated surfaces to extract useful data concerning forest stands and their underlying surfaces for both the seawater-on and seawater-off.

Author

N89-11294# Instituto de Pesquisas Espaciais, Sao Jose dos Campos (Brazil).

TECHNIQUE FOR OBTAINING AGRICULTURAL PROPERTY BOUNDARIES THROUGH SATELLITE IMAGERY, CERTIFIED TO CONTROL AND ACCOMPANY AGRICULTURAL ACTIVITY [TECNICA PARA OBTEN LIMI TES DE PROPRIEDADES AGRICOLAS SOBRE IMAGENS DE SATELITE, VISANDO CONTROLAR E ACOMPANHAR A ATIVIDADE AGRICOLA]

VALDETE DUARTE Aug. 1988 11 p In PORTUGUESE; ENGLISH summary Presented at the Enserplan-National Meeting of Remote Sensing Applied to Municipal Planning, Campos do Jordao, Oct. 1987 (INPE-4640-PRE/1351) Avail: NTIS HC A03/MF A01

This work is part of a project named Fiscalizacao de Propriedades Agricolas por Satelite (FISATE). The survey of the rural credit for properties with wheat crops in the Assis county in the Sao Paulo State is presented. The following materials were utilized: aerial photographs at the 1:35,000 scale; photomosaic at the 1:100,000; and IBGE topographic charts at the 1:250,000 and 1:50,000 scales. One Banco de Brasil clerk from the Assis agency, was trained on aerial photography handling to be able to make property cadaster from the available photographs. The agricultural properties boundaries outlined on the aerial photographs were transferred to the cartographic maps at the 1:50,000 scale using the KARTOFLEX equipment. From this cartographic map the properties boundaries as well as some features such as rivers, roads, and cities, were extracted to be used as reference points on the satellite data. This information was reduced to 1:100,000 scale map on a transparent film to be compatible to the satellite images. The final product is a transparency in a lithographic film containing the agricultural properties boundaries. This transparency was overlaid on the satellite images and allowed to locate perfectly the agricultural properties. Hence, the wheat plantations were identified and their areal extent evaluated through the satellite images.

Author

N89-11296*# Michigan Univ., Ann Arbor. Radiation Lab.

EFFECT OF CURVATURE ON THE BACKSCATTERING FROM LEAVES

K. SARABANDI, T. B. A. SENIOR, and F. T. ULABY 1988 36 p (Contract NAG5-480) (NASA-CR-183326; NAS 1.26:183326) Avail: NTIS HC A03/MF A01 CSCL 20F

Using a model previously developed for the backscattering cross section of a planar leaf at X-band frequencies and above, the effect of leaf curvature is examined. For normal incidence on a rectangular section of a leaf curved in one and two dimensions, an integral expression for the backscattered field is evaluated numerically and by a stationary phase approximation, leading to a simple analytical expression for the cross section reduction produced by the curvature. Numerical results based on the two methods are virtually identical, and in excellent agreement with

measured data for rectangular sections of coleus leaves applied to the surfaces of styrofoam cylinders and spheres of different radii. Author

N89-11297# Instituto de Pesquisas Espaciais, Sao Jose dos Campos (Brazil).

SPECTRAL STUDIES OF THREE OXISOLS AND A ULTISOL OF BRAZIL

ANTONIO ROBERTO FORMAGGIO and JOSE CARLOS NEVESEPIPHANIO Aug. 1988 24 p In PORTUGUESE; ENGLISH summary Presented at the 2nd Latin American Symposium on Remote Sensors, Bogota, Columbia, 16-20 Nov. 1987

(INPE-4644-PRE/1355) Avail: NTIS HC A03/MF A01

The correlation was verified between spectral behavior of three Oxisols and one Ultisol from Sao Paulo State (Brazil) with their following characteristics: iron oxides and organic matter contents, particle size, colour, surface conditions, cation exchange capacity and parent material. The data was collected in three spectral levels: laboratory, field and satellite. For the first two levels, data were collected between 400 and 1100 nm with a spectroradiometer and a hand held radiometer, respectively. For the satellite level (MSS and TM-LANDSAT) it was used the Multispectral Imagery Analyser - Image 100 with data from compatible computer tapes (CCTs). The physical and chemical parameters were highly correlated with the spectral behavior of the four soil types. In one of the two study areas, where the parent material is argillic (clay) it was observed a type of spectral discrimination between the soils; and where the parent material originate sandy pedological substrate it was observed another type of discrimination between studied soils. These results show the importance of parent material and soil texture as influencing parameters of the soil spectral behavior. Also, clear indications of the inference potential from soil properties related with iron oxides due strong absorption occurred mainly at near infrared for the soils originated from eruptive basic rocks. Author

N89-11324# Instituto de Pesquisas Espaciais, Sao Jose dos Campos (Brazil).

CIR AERIAL PHOTOGRAPHY APPLIED TO THE EVALUATION OF THE AIR POLLUTION IMPACT IN A TROPICAL FOREST: THE CASE OF CUBATAO, BRAZIL

DALTON DEMORISSONVALERIANO and FLAVIO JORGE PONZONI Aug. 1988 11 p

(INPE-4651-PRE/1358) Avail: NTIS HC A03/MF A01

A 1:25,000 color infrared survey was used to map and evaluate the extent of the damage caused by air pollution originated from Cubatao city's industrial plant on the Tropical Forest covering the Serra do Mar mountain range in southeastern Brazilian coast. The survey covered an area of 240 sq km and encompasses a heavily damaged drainage basin and a preserved one. One primary forest and four secondary types were identified in the preserved area by means of their tonal and textural characteristics. Four types of damaged forest covers were discriminated in the polluted valley on the basis of the density and size of the remnant trees. DBH and tree height field measurements of these cover types reveal that the degradation process of the Tropical Forest takes place as a progressive elimination of the larger trees. Although the proliferation of smaller plants follows this process, the impact of the air pollution in the forest favors the occurrence of landslide in the rainy season. Author

N89-11368*# Nebraska Univ., Lincoln. Inst. of Agriculture and Natural Resources.

COMPARISON OF MEASURED AND MODELED RADIATION, HEAT AND WATER VAPOR FLUXES: FIFE PILOT STUDY Final Technical Report, 1 Apr. 1985 - 31 Dec. 1987

BLAINE L. BLAD, SHASHI B. VERMA, KENNETH G. HUBBARD, PATRICK STARKS, CYNTHIA HAYS, JOHN M. NORMAN, and ELIZABETH WALTERSHEA Oct. 1988 88 p

(Contract NAG5-561)

(NASA-CR-183304; NAS 1.26:183304; CAMAC-PR-87-7) Avail: NTIS HC A05/MF A01 CSCL 04B

The primary objectives of the 1985 study were to test the feasibility of using radio frequency receivers to collect data from automated weather stations and to evaluate the use of the data collected by the automated weather stations for modeling the fluxes of latent heat, sensible heat, and radiation over wheat. The model Cupid was used to calculate these fluxes which were compared with fluxes of these entities measured using micrometeorological techniques. The primary objectives of the 1986 study were to measure and model reflected and emitted radiation streams at a few locations within the First International Satellite Land-Surface Climatology Project Field Experiment (FIFE) site and to compare modeled and measured latent heat and sensible heat fluxes from the prairie vegetation. Author

N89-12106# Instituto de Pesquisas Espaciais, Sao Jose dos Campos (Brazil).

AN AGRICULTURAL CROP YIELD MODEL BY SATELLITE: A SIMULATION [UMODELO DE PRODUTIVIDADE AGRICOLA POR SATELITE: UMA SIMULACAO]

FAUSTO CARLOSDEALMEIDA, CORINA DACOSTA-FREITASANASSE, and THELMA KRUG Aug. 1988 25 p In PORTUGUESE; ENGLISH summary Presented at the 2nd Latin American Symposium of Remote Sensing, Bogota, Columbia, 16-20 November 1987

(INPE-4639-PRE/1350) Avail: NTIS HC A03/MF A01

Variables derived from rainfall and sunshine are used in a crop yield model called the Method of Critical Periods proposed by Celaschi and Almeida and developed by Celaschi, aiming at the estimation of crop yields using satellite data. These variables, which can be extracted from environmental satellites, are simulated from conventional meteorological data gathered at the surface. The variables derived from rainfall are of the dummy type associated with the incidence of rainfall beyond a threshold value, while the variable derived from sunshine hours is weighted by calk of rainfall, expressing the tendency for water stress. The model was tested for corn in the State of Sao Paulo, Brazil. The results are compared with those obtained by the conventional method employing temperature and rainfall and with the officially reported data for the state of Sao Paulo. Author

N89-12107# Instituto de Pesquisas Espaciais, Sao Jose dos Campos (Brazil).

DIGITAL PROCESSING APPLIED TO VEGETATION [PROCESSAMENTO DIGITAL APLICADO A VEGETACAO]

FLAVIO JORGE PONZONI and VITOR CELSODECARVALHO Sep. 1988 25 p In PORTUGUESE; ENGLISH summary (INPE-4695-MD/036) Avail: NTIS HC A03/MF A01

The main digital processing techniques of satellite imagery applied to the study of vegetation cover are presented in order to guide agricultural professionals interested in remote sensing studies. Research works concerned with these techniques are also presented. Author

N89-12108# Instituto de Pesquisas Espaciais, Sao Jose dos Campos (Brazil).

METHOD OF VISUAL ANALYSIS OF REMOTE SENSING DATA-VEGETATION [METODOLOGIA DA ANALISE VISUAL DE DADOS DE SENSORIAMENTO REMOTO-VEGETACAO]

PEDRO HERNANDEZFILHO Sep. 1988 25 p In PORTUGUESE; ENGLISH summary

(INPE-4696-MD/037) Avail: NTIS HC A03/MF A01

A methodology for visual analysis of remote sensing data is presented as applied to vegetative cover through the classical photointerpretation approach, i.e., tone, texture and form. Examples of vegetative targets and respective patterns in LANDSAT spectral imagery are shown. Some examples of vegetation cover, such as cerrado, young and old eucalyptus reforestation, burnt and reforested areas are shown in TM-3, TM-4 and TM-5 imagery. Author

N89-12109# Instituto de Pesquisas Espaciais, Sao Jose dos Campos (Brazil).

INTERACTION OF SOLAR RADIATION WITH VEGETATION

DALTON MORISSONVALERIANO Sep. 1988 35 p
(INPE-4697-MD/038) Avail: NTIS HC A03/MF A01

The acquisition of information about vegetation canopies by remote sensing has important applications in the fields of vegetation science, agronomy, geobotany, etc. The correct interpretation of this data from the reflected radiance measured by remote sensors demands knowledge of the interaction mechanisms of the electromagnetic radiation from a leaf as well as from the totality of elements that comprise the vegetation canopy. Some of the basic concepts of vegetation relevant to the understanding of the processes that determine the behavior of its spectral reflectance are discussed. Some methodological approaches to the study of these processes are also presented. Author

N89-12110# Instituto de Pesquisas Espaciais, Sao Jose dos Campos (Brazil).

CROP SEPARATION ANALYSIS THROUGH SPOT AND TM DIGITAL DATA [SEPARABILIDADE DE CULTURAS ATRAVES DA ANALISE DIGITAL DE DADOS SPOT E TM]

GETULIO TEIXEIRABATISTA, SHERRY CHOU CHEN, ANTONIO TEBALDITARDIN, and JEAN FRANCOIS DALLEMAND Aug. 1988 15 p In PORTUGUESE; ENGLISH summary Presented at the 2nd Simposio Latino Americano de Sensoriamento Remoto, Bogota, Colombia, 16-20 Nov. 1987
(INPE-4641-PRE/1352) Avail: NTIS HC A03/MF A01

The objective of this paper was to evaluate SPOT and TM data for spectral discrimination of coffee, wheat, sugar cane, and pasture in the Northwest of Parana State. The test site comprises a SPOT scene of approximately 60X60 km. Fifteen fields were analyzed for each crop. Field information such as variety, planting date, phenological stage, row space, planting direction, percent soil cover, etc., was obtained. Wheat was originally considered as two classes according to its growth stage. Data were analyzed using one SPOT scene (5.3 deg off nadir, east viewing) acquired on July, 10, 1986, and one TM scene from August 2, 1986. J-M distance was calculated taking into account several classes and band combinations from both SPOT/HRV and LANDSAT-TM data. The best TM band combination for crop discrimination was determined. Separability analysis of crops using SPOT and TM images is presented. Author

N89-12951*# National Aeronautics and Space Administration. Goddard Space Flight Center, Greenbelt, MD.

MODELLING OF SAR POLARISATION PHASE DIFFERENCE FROM TREES

TSAN MO (Computer Sciences Corp., Beltsville, Md.) and J. R. WANG In ESA, Proceedings of the 1988 International Geoscience and Remote Sensing Symposium (IGARSS 1988) on Remote Sensing: Moving Towards the 21st Century, Volume 1 p 55-58 Aug. 1988

Avail: NTIS HC A99/MF E03; ESA Publications Div., ESTEC, Noordwijk, Netherlands, 120 US dollars or 250 Dutch guilders CSCL 02F

The data for polarization phase difference Delta Phi between the HH- and VV-polarized backscattered waves from tree-covered fields were obtained with an airborne synthetic aperture radar at 1.225 GHz. The mean values over tree-covered fields were derived from the images of the phase difference and were examined as a function of incident beam angle from 15 to 55 deg. A theoretical model for simulating these data, based on the electromagnetic wave scatterings from the tree trunk and its branches, both of which are assumed as very long dielectric cylinders was developed. The radius and direction of a tree branch are taken as random variables and are chosen by a Monte Carlo method to encounter the incident waves in producing the scattering events. The Monte Carlo simulated results are in good agreement with the observations within experimental uncertainty. ESA

N89-12962# Leeds Univ. (England). School of Geography. **MODELLING LAND RESOURCES WITHIN A PILOT GEOGRAPHICAL INFORMATION SYSTEM**

J. HOGG In ESA, Proceedings of the 1988 International

Geoscience and Remote Sensing Symposium (IGARSS 1988) on Remote Sensing: Moving Towards the 21st Century, Volume 1 p 101-105 Aug. 1988

Avail: NTIS HC A99/MF E03; ESA Publications Div., ESTEC, Noordwijk, Netherlands, 120 US dollars or 250 Dutch guilders

A pilot geographical information system (GIS) for regional evaluation of land resources is outlined and its scope for modeling is considered in the context of remote sensing of upland vegetation in northern England. The pilot GIS uses a proprietary relational database management system to handle objects abstracted from a spatial database or supplied by users. The spatial database is made up of binary square images encoded and held as linear quadrees. To illustrate how the pilot GIS is used, spatial and aspatial data are analyzed to identify homogeneous land units for resource management and planning. Different strategies for modeling land resources within such units are outlined using geographic data from digital maps, LANDSAT TM, and climatic records. ESA

N89-12967# Leeds Univ. (England). School of Geography. **ANALYSIS OF POTATO CROP DISTRIBUTION USING REMOTELY SENSED AND ENVIRONMENTAL DATA IN A PILOT GEOGRAPHICAL INFORMATION SYSTEM**

N. STUART, J. HOGG, G. G. WRIGHT, and J. G. MORRICE (MacAulay Land Use Research Inst., Aberdeen, Scotland) In ESA, Proceedings of the 1988 International Geoscience and Remote Sensing Symposium (IGARSS 1988) on Remote Sensing: Moving Towards the 21st Century, Volume 1 p 119-124 Aug. 1988

Avail: NTIS HC A99/MF E03; ESA Publications Div., ESTEC, Noordwijk, Netherlands, 120 US dollars or 250 Dutch guilders

Use of geographic information systems (GIS) to predict production of potato crops in Scotland is described. To quantify the extent to which the crop may be subject to drought stress, soil types and soil water deficits in the potato growing areas were studied. In the light of results obtained using raster images, the potential of a pilot GIS is assessed for the inventory and analysis of the potato crop distribution. Spatial and statistical analyses are used to describe and measure associations between the presence of crop and a range of environmental conditions. These relationships can be explored interactively, used to describe and explain crop distribution, and as the basis of predictive models of crop suitability or drought risk. ESA

N89-12986# Karlsruhe Univ. (Germany, F.R.). Inst. fuer Photogrammetrie und Fernerkundung.

LARGE AREA TM LAND COVER CLASSIFICATION OF MITTLERER OBERRHEIN COUNTY, SOUTHWEST GERMANY, AND ITS USE FOR REGIONAL PLANNING AND CROP SURVEYS

C. SCHMULLIUS In ESA, Proceedings of the 1988 International Geoscience and Remote Sensing Symposium (IGARSS 1988) on Remote Sensing: Moving Towards the 21st Century, Volume 1 p 207-210 Aug. 1988

Avail: NTIS HC A99/MF E03; ESA Publications Div., ESTEC, Noordwijk, Netherlands, 120 US dollars or 250 Dutch guilders

The spectral problems of classifying a whole, geographically very heterogenic county were investigated. A map is presented and its use for regional planning and crop surveys discussed. The influence of three distinctive natural regions on the phenological situation of six different crop types is demonstrated. Diagrams show how the dynamics of crop development differ due to varying locations. Differences in reflections of one crop type in several training sites are illustrated in histograms. Classification results are compared to official land inventory statistics. It is concluded that the classification is of little use for such a large area, but the mapping possibilities are interesting. ESA

N89-12988# Kingston Polytechnic, Kingston-Upon-Thames (England). School of Geography.

THE DETECTION OF UNIMPROVED GRASSLAND IN BERKSHIRE USING A BINARY DECISION TREE APPROACH

N. M. TRODD and A. J. MORTON (Imperial Coll. of Science and

Technology, London, England) In ESA, Proceedings of the 1988 International Geoscience and Remote Sensing Symposium (IGARSS 1988) on Remote Sensing: Moving Towards the 21st Century, Volume 1 p 213-214 Aug. 1988

Avail: NTIS HC A99/MF E03; ESA Publications Div., ESTEC, Noordwijk, Netherlands, 120 US dollars or 250 Dutch guilders

In order to detect unimproved grassland, a binary discard decision tree method of classification was used to target this land cover. The flexibility of the algorithm allowed multitemporal LANDSAT-TM data to be incorporated into the best practical method. Per-field criteria show more promise than per-pixel to discriminate unimproved from improved grassland. The results are compatible with, but do not mimic, existing ecological survey procedures and should enhance a regional detection strategy.

ESA

N89-12990# Kingston Polytechnic, Kingston-Upon-Thames (England). School of Geography.

CROP CLASSIFICATION WITH MULTI-TEMPORAL X-BAND SAR DATA

G. M. FOODY, P. J. CURRAN, G. B. GROOM, and D. C. MUNRO (Hawaii Univ., Manoa.) In ESA, Proceedings of the 1988 International Geoscience and Remote Sensing Symposium (IGARSS 1988) on Remote Sensing: Moving Towards the 21st Century, Volume 1 p 217-220 Aug. 1988

Avail: NTIS HC A99/MF E03; ESA Publications Div., ESTEC, Noordwijk, Netherlands, 120 US dollars or 250 Dutch guilders

Multitemporal X-band HH polarized synthetic aperture radar data were used to classify crop type. Prior to the classification, the influence of non-crop variables on crop separability were evaluated. While the influence of the soil moisture content was unimportant, the data sets had to be radiometrically corrected and intercalibrated. A per-field classification of these data enables the 3 main crop types of the test site to be classified with accuracies approaching 90 percent when the complete multitemporal data set acquired four data is used. Comparable levels of accuracy can, however, be obtained from the use of data recorded on only two of the four dates.

ESA

N89-12991# Rothamsted Experimental Station, Harpenden (England).

SPATIAL RESOLUTION FOR REMOTE SENSING OF FOREST PLANTATIONS

P. M. ATKINSON and F. M. DANSON (Sheffield Univ., England) In ESA, Proceedings of the 1988 International Geoscience and Remote Sensing Symposium (IGARSS 1988) on Remote Sensing: Moving Towards the 21st Century, Volume 1 p 221-223 Aug. 1988 Sponsored by the Natural Environment Research Council, London, United Kingdom

Avail: NTIS HC A99/MF E03; ESA Publications Div., ESTEC, Noordwijk, Netherlands, 120 US dollars or 250 Dutch guilders

The optimum spatial resolution for the collection of remotely sensed data of forest plantations was determined by modeling the spatial dependence in high resolution airborne multispectral scanner (MSS) data. It is shown that spatial dependence is present in coniferous and oak plantations and that the range is related to the stand age and species. Three methodologies for determining the optimum spatial resolution using the semivariance at lag one ($\gamma(h=1)$ max) are discussed. The method provides an approximation of this statistic but where it is possible to estimate ($h=1$)max by degrading the image a sound and tractable estimate of the optimum resolution is obtained. Further work is required to investigate the precision of estimates obtained by regularization of the semi-variogram.

ESA

N89-13002# Sheffield Univ. (England). Dept. of Geography.
RELATIONSHIPS BETWEEN THE NITROGEN CONTENT OF GRASS AND REFLECTANCE

S. E. PLUMMER In ESA, Proceedings of the 1988 International Geoscience and Remote Sensing Symposium (IGARSS 1988) on Remote Sensing: Moving Towards the 21st Century, Volume 1 p 265-267 Aug. 1988

Avail: NTIS HC A99/MF E03; ESA Publications Div., ESTEC, Noordwijk, Netherlands, 120 US dollars or 250 Dutch guilders

The results of an experiment to test the hypothesized negative relationship between green reflectance and leaf nitrogen content and the positive relationship between near infrared reflectance and leaf nitrogen content under field conditions are reported. It is concluded that neither relationship holds unless the effect of canopy geometry is suppressed in visible wavelengths and the effect of biomass is suppressed in near infrared wavelengths.

ESA

N89-13003# Joint Research Centre of the European Communities, Ispra (Italy).

SMALL FORMAT AIR PHOTO FROM ULTRAHIGH AIRCRAFT AS AN AID FOR DATA COLLECTION OF AGRICULTURAL STATISTICS IN SAHELIAN COUNTRIES

E. BARTHOLOME, J.-M. GREGOIRE, and R. ZEYEN In ESA, Proceedings of the 1988 International Geoscience and Remote Sensing Symposium (IGARSS 1988) on Remote Sensing: Moving Towards the 21st Century, Volume 1 p 269-270 Aug. 1988

Avail: NTIS HC A99/MF E03; ESA Publications Div., ESTEC, Noordwijk, Netherlands, 120 US dollars or 250 Dutch guilders

An experiment was carried out in Mali to assess the feasibility in Sahelian conditions of 70 mm air photography for field mapping of ground segments to be used for the crop statistics and crop surface assessment. It is found that the ultralight aircraft is an efficient tool for air photography at the local or subregional level. Accurate field mapping can be achieved if the photos are made during the growing season. Black and white film and scales smaller than 1/15000 are sufficient. Such a procedure could be applied on an operational basis without major difficulty. For crop classification, 1/5000 infrared photos are required. They allow only the recognition of major crop types, which is sufficient for production forecasting, not for agricultural statistics. The operational use of this technique is difficult because of the special film processing involved, and the manpower required for the data analysis.

ESA

N89-13050# Research Inst. for Soil Science and Agricultural Chemistry, Budapest (Turkey).

AGROECOLOGICAL INFORMATION CONTENT OF SPOT DATA

F. CSILLAG, G. BUTTNER (FOMI Remote Sensing Center, Budapest, Hungary), and I. JUHASZ In ESA, Proceedings of the 1988 International Geoscience and Remote Sensing Symposium (IGARSS 1988) on Remote Sensing: Moving Towards the 21st Century, Volume 1 p 465-470 Aug. 1988 Sponsored by the Ministry of Agriculture, Budapest, Hungary and Spot Image, Toulouse, France

Avail: NTIS HC A99/MF E03; ESA Publications Div., ESTEC, Noordwijk, Netherlands, 120 US dollars or 250 Dutch guilders

Four SPOT scenes acquired over Hungary are evaluated in terms of their potential use for agroecological mapping. Extremely variable soil conditions characteristic of the study area are found to be limiting factors of crop growth. In-field heterogeneities were mapped based on bi-temporal (spring and summer) data using soil brightness and normalized vegetation index. They were field checked and identified as well as on color infrared aerial photography.

ESA

N89-13051# Edinburgh Univ. (Scotland). Dept. of Geography.
EVALUATION OF LANDSAT TM AND SPOT IMAGERY FOR AGRICULTURAL LAND USE PLANNING IN LESS DEVELOPED COUNTRIES

J. R. WHEELER, C. JARVIS, A. J. B. MITCHELL, R. B. KING, and R. J. WHITE In ESA, Proceedings of the 1988 International Geoscience and Remote Sensing Symposium (IGARSS 1988) on Remote Sensing: Moving Towards the 21st Century, Volume 1 p 471-472 Aug. 1988

Avail: NTIS HC A99/MF E03; ESA Publications Div., ESTEC, Noordwijk, Netherlands, 120 US dollars or 250 Dutch guilders

Imagery from SPOT and LANDSAT-TM were acquired for a part of Tabora Region (Tanzania) to investigate the value of both types of imagery for interpreting areas of agricultural potential,

current land use, vegetation, cultural features, and clarity and ease of interpretation. Satellite imagery with ground resolution of 20 to 30 m at a scale of 1:50,000 is shown to be extremely useful for land use planners in less developed countries. It provides a means of rapidly appraising areas of cultivation, eroded areas and likely sources of erosion, natural vegetation, and areas with potential for increased population. The main advantages of satellite imagery compared with aerial photography are synopsis and provision of up to date information. ESA

N89-13055# Stockholm Univ. (Sweden). Dept. of Physical Geography.

LANDSAT THEMATIC MAPPING (TM) AND SPOT HRV FOR SURVEY MAPPING OF BEDROCK OUTCROPS

B. LUNDEN and K. WESTER *In* ESA, Proceedings of the 1988 International Geoscience and Remote Sensing Symposium (IGARSS 1988) on Remote Sensing: Moving Towards the 21st Century, Volume 1 p 483-484 Aug. 1988

Avail: NTIS HC A99/MF E03; ESA Publications Div., ESTEC, Noordwijk, Netherlands, 120 US dollars or 250 Dutch guilders

It is shown that LANDSAT TM and SPOT HRV provide good possibilities for mapping of bedrock outcrop areas to be presented on the Swedish topographical map on the scale of 1:50,000. The classification errors can be reduced by the use of a slicing procedure on the training data, and by combining the automatic classification with a subsequent manual improvement. ESA

N89-13057# Aston Univ., Birmingham (England). Remote Sensing Unit.

AN EVALUATION OF SATELLITE IMAGERY, LANDSAT THEMATIC MAPPER AND SPOT-1 HRV, FOR GRASSLAND INVENTORY IN THE UK

J. MCGUIRE and W. G. COLLINS *In* ESA, Proceedings of the 1988 International Geoscience and Remote Sensing Symposium (IGARSS 1988) on Remote Sensing: Moving Towards the 21st Century, Volume 1 p 489-491 Aug. 1988

Avail: NTIS HC A99/MF E03; ESA Publications Div., ESTEC, Noordwijk, Netherlands, 120 US dollars or 250 Dutch guilders

Grassland classification and mapping using the spectral discrimination properties of LANDSAT Thematic Mapper (TM) and SPOT-1 HRV data, as a basis for the production of grassland cover maps is discussed. From such derived maps, the extent, distribution, and general quality of lowland grassland types can be surveyed, providing an information system capable of creating landcover/grassland maps, quickly and inexpensively, as an aid to environmental, agroecological, and ecological planning and for monitoring change. Classifications are evaluated with the assistance of detailed field survey vegetation maps. The use of temporal and spatial features for classification are investigated and the spectral characteristics of different grassland types analyzed. ESA

N89-13077# Scott, Wilson, Kirkpatrick and Partners, Basingstoke (England).

COTTON AREA MAPPING USING MULTITEMPORAL SATELLITE DATA INTEGRATED WITHIN A GEOGRAPHICAL INFORMATION SYSTEM APPLIED TO A COTTON BOLL WEEVIL CONTROL PROGRAMME IN PARAGUAY

B. J. DENORE, T. E. BEAUMONT, J. PENDER, D. G. CAMPION, B. R. CRITCHLEY, and L. R. M. MARENGO (Ministry of Agriculture and Livestock, Asuncion, Paraguay) *In* ESA, Proceedings of the 1988 International Geoscience and Remote Sensing Symposium (IGARSS 1988) on Remote Sensing: Moving Towards the 21st Century, Volume 1 p 581-582 Aug. 1988

Avail: NTIS HC A99/MF E03; ESA Publications Div., ESTEC, Noordwijk, Netherlands, 120 US dollars or 250 Dutch guilders

An attempt to map the distribution of cotton using satellite imagery in a pest control program is described. Image classification is performed using GIST, a system incorporating image processing, digital mapping, and a relational database. If resulting cotton maps are accurate a program of pest control can be undertaken, which will involve creating a cotton free buffer zone. The location and implementation of a buffer zone depends on many factors including

socioeconomic conditions. The biogeography of the boll weevil, the feasibility of monitoring the spread of the pest, and the cotton distribution can be incorporated into GIST to assist in formulating an integrated control program. ESA

N89-13079# Goettingen Univ. (Germany, F.R.). Inst. fuer Forsteinrichtung.

BUILDING A MONITORING SYSTEM BASED ON SATELLITE DATA TO DETECT VEGETATION AND LAND USE CHANGES IN A SUBTROPICAL REGION OF MEXICO

J. SCHNURR *In* ESA, Proceedings of the 1988 International Geoscience and Remote Sensing Symposium (IGARSS 1988) on Remote Sensing: Moving Towards the 21st Century, Volume 1 p 587-588 Aug. 1988 Sponsored by the Deutsche Forschungsgemeinschaft, Bonn, Fed. Republic of Germany

Avail: NTIS HC A99/MF E03; ESA Publications Div., ESTEC, Noordwijk, Netherlands, 120 US dollars or 250 Dutch guilders

A project was carried out in an area in Mexico typical of subtropical regions to compare different satellite systems as to classification accuracy for subtropical vegetation types; for a multitemporal analysis (1973 - 1986) to build up a monitoring system for such an area based on satellite data only; and to develop software. The resulting maps and tables demonstrate the potential of satellite data for change detection in extensively used subtropical areas. The images were analyzed by applying a classification method based on discriminant analysis in combination with a global F-test, which provides a measure to describe the separability of training areas. ESA

N89-13080# Instituto de Pesquisas Espaciais, Sao Jose dos Campos (Brazil).

MICROWAVE REMOTE SENSING AT THE INSTITUTE FOR SPACE RESEARCH (INPE) BRAZIL: CONCEPTS AND FUTURE PROSPECTS OF SOIL MOISTURE STUDIES

H. J. H. KUX and J. V. SOARES *In* ESA, Proceedings of the 1988 International Geoscience and Remote Sensing Symposium (IGARSS 1988) on Remote Sensing: Moving Towards the 21st Century, Volume 1 p 591-593 Aug. 1988

Avail: NTIS HC A99/MF E03; ESA Publications Div., ESTEC, Noordwijk, Netherlands, 120 US dollars or 250 Dutch guilders

Experience in microwave remote sensing, applied specifically to soil moisture studies, including the main concepts and prospects for future research is summarized. In the approach proposed, information derived from ground truth, airborne and orbital data, as well as meteorological data, are important inputs. ESA

N89-13083*# National Aeronautics and Space Administration. Goddard Space Flight Center, Greenbelt, MD.

THE DERIVATION OF SUB-CANOPY SURFACE TERRAIN MODELS OF COASTAL FORESTS USING SYNTHETIC APERTURE RADAR

M. L. IMHOFF and D. B. GESCH (Science Applications Research, Lanham, Md.) *In* ESA, Proceedings of the 1988 International Geoscience and Remote Sensing Symposium (IGARSS 1988) on Remote Sensing: Moving Towards the 21st Century, Volume 1 p 613-617 Aug. 1988 Sponsored by the Overseas Development Administration, Surrey, United Kingdom

Avail: NTIS HC A99/MF E03; ESA Publications Div., ESTEC, Noordwijk, Netherlands, 120 US dollars or 250 Dutch guilders

Radar data acquired by the Shuttle Imaging Radar-B mission covering a portion of the Mouths of the Ganges forests were used to create a terrain model for use in determining tidal flow and eventual nutrient transport from the forest to the marine habitat. Results show that good digital topographic terrain models of wet coastal forests can be generated using multiple sets of L-band SAR and ancillary tide elevation data. The dominance of the interaction phenomenon in the radar backscatter of flooded forests can be used to create sub-canopy inundation maps which when merged with tide surface data can be used to generate reasonable topographic models. Ideally models could be improved by using multiple sets of data at a constant incidence angle over the total tide range. The optimal angle for the SAR depends upon the characteristics of the forest. The range of 46 to 57 deg seems

applicable to the 12.5 m tall closed canopy in this example. Such models can be an extremely valuable tool for studying and mapping the mangal ecosystem. ESA

N89-13084# Joint Research Centre of the European Communities, Ispra (Italy).

THE CLASSIFICATION OF SEMI-NATURAL VEGETATION FROM LANDSAT THEMATIC MAPPER IMAGERY: A USER'S PERSPECTIVE

A. S. BELWARD, J. C. TAYLOR, M. J. STUTTARD, E. SIGNAL, J. MATHEWS (Nature Conservancy Council, London, England), and D. CURTIS /n ESA, Proceedings of the 1988 International Geoscience and Remote Sensing Symposium (IGARSS 1988) on Remote Sensing: Moving Towards the 21st Century, Volume 1 p 621-622 Aug. 1988

Avail: NTIS HC A99/MF E03; ESA Publications Div., ESTEC, Noordwijk, Netherlands, 120 US dollars or 250 Dutch guilders

An unsupervised maximum likelihood classification of LANDSAT Thematic Mapper imagery is found to provide the basis for a thematic map of broad habitat types over an area of complex seminatural vegetation. The cover categories to be mapped must be selected such that they have spectral homogeneity in addition to ecological significance. The use of photographic prints of satellite imagery in the field is found to be invaluable in this respect. Where cover categories are selected on the basis of ecological divisions alone, results are shown to be poor. ESA

N89-13085# Deutsche Forschungs- und Versuchsanstalt fuer Luft- und Raumfahrt, Oberpfaffenhofen (West Germany).

SPECTRAL CHARACTERIZATION OF FOREST DAMAGE IN BEECH, OAK AND PINE STANDS

W. KIRCHHOF, S. GUTTMANN, M. SCHRAMM, I. ZWENGER, and M. LAMBERTY (Forstamt, Frankfurt, West Germany) /n ESA, Proceedings of the 1988 International Geoscience and Remote Sensing Symposium (IGARSS 1988) on Remote Sensing: Moving Towards the 21st Century, Volume 1 p 623-624 Aug. 1988

Avail: NTIS HC A99/MF E03; ESA Publications Div., ESTEC, Noordwijk, Netherlands, 120 US dollars or 250 Dutch guilders

Multispectral scanner data were gathered at 2000 and 4000 m flight altitudes over a test site to serve as data basis for the development of operational methods for the detection, classification, and mapping of forest disease in larger areas of Germany. In the visible, near IR and short wave IR region, radiance values of beech and oak decrease with increasing damage level. The spectral behavior of pine is nonuniform and influenced by understory vegetation, except one dense homogenous stand. It shows yellowing of foliage in the visible, which could not be measured for deciduous leaves; decreasing reflectance in the near IR; and slight rise in the short wave IR for the damaged class. Experience suggests important influence of secondary effects mainly caused by loss of biomass, increase of shadow areas, background, and understory vegetation. ESA

N89-13088*# Wyoming Univ., Laramie. Dept. of Botany.

BIOGEOCHEMICAL PROCESSES IN SAGEBRUSH STEPPE: INTERACTIONS OF TERRAIN, VEGETATION AND CHEMICAL CYCLES Final Technical Report, 1 Jun. 1985 - 29 Feb. 1988

WILLIAM A. REINERS 1988 8 p

(Contract NAG2-355)

(NASA-CR-181486; NAS 1.26:181486) Avail: NTIS HC A02/MF A01 CSCL 02C

Publications, manuscripts in various stages of progress, presentations made at scientific meetings, and undergraduate honor thesis and one Ph.D. dissertation are contained. B.G.

N89-13091*# Massachusetts Inst. of Tech., Cambridge. Lab. for Water Resources and Hydrodynamics.

THE STRUCTURE OF RED-INFRARED SCATTERGRAMS OF SEMIVEGETATED LANDSCAPES

MICHAEL F. JASINSKI and PETER S. EAGLESON 25 Nov. 1988 46 p Submitted for publication

(Contract NAG5-510)

(NASA-CR-183385; NAS 1.26:183385) Avail: NTIS HC A03/MF A01 CSCL 02F

A physically based linear stochastic geometric canopy soil reflectance model is presented for characterizing spatial variability of semivegetated landscapes at subpixel and regional scales. Landscapes are conceptualized as stochastic geometric surfaces, incorporating not only the variability in geometric elements, but also the variability in vegetation and soil background reflectance which can be important in some scenes. The model is used to investigate several possible mechanisms which contribute to the often observed characteristic triangular shape of red-infrared scattergrams of semivegetated landscapes. Scattergrams of simulated and semivegetated scenes are analyzed with respect to the scales of the satellite pixel and subpixel components. Analysis of actual aerial radiometric data of a pecan orchard is presented in comparison with ground observations as preliminary confirmation of the theoretical results. Author

N89-13821*# Columbia Univ., New York, NY. Dept. of Geography.

DEVELOPMENT OF A GROUND HYDROLOGY MODEL SUITABLE FOR GLOBAL CLIMATE MODELING USING SOIL MORPHOLOGY AND VEGETATION COVER, AND AN EVALUATION OF REMOTELY SENSED INFORMATION Final Technical Report, 1 Jan. 1984 - 31 May 1988

L. ZOBLER and R. LEWIS 26 Oct. 1988 5 p

(Contract NCC5-32)

(NASA-CR-180463; NAS 1.26:180463) Avail: NTIS HC A02/MF A01 CSCL 08H

The long-term purpose was to contribute to scientific understanding of the role of the planet's land surfaces in modulating the flows of energy and matter which influence the climate, and to quantify and monitor human-induced changes to the land environment that may affect global climate. Highlights of the effort include the following: production of geo-coded, digitized World Soil Data file for use with the Goddard Institute for Space Studies (GISS) climate model; contribution to the development of a numerical physically-based model of ground hydrology; and assessment of the utility of remote sensing for providing data on hydrologically significant land surface variables. Author

N89-13823*# Massachusetts Inst. of Tech., Cambridge. Dept. of Civil Engineering.

USE OF LANDSAT IMAGES OF VEGETATION COVER TO ESTIMATE EFFECTIVE HYDRAULIC PROPERTIES OF SOILS Final Technical Report, 1 Aug. - 30 Sep. 1988

PETER S. EAGLESON and MICHAEL F. JASINSKI 23 Nov. 1988 10 p

(Contract NAG5-510)

(NASA-CR-183384; NAS 1.26:183384) Avail: NTIS HC A02/MF A01 CSCL 02F

The estimation of the spatially variable surface moisture and heat fluxes of natural, semivegetated landscapes is difficult due to the highly random nature of the vegetation (e.g., plant species, density, and stress) and the soil (e.g., moisture content, and soil hydraulic conductivity). The solution to that problem lies, in part, in the use of satellite remotely sensed data, and in the preparation of those data in terms of the physical properties of the plant and soil. The work was focused on the development and testing of a stochastic geometric canopy-soil reflectance model, which can be applied to the physically-based interpretation of LANDSAT images. The model conceptualizes the landscape as a stochastic surface with bulk plant and soil reflective properties. The model is particularly suited for regional scale investigations where the quantification of the bulk landscape properties, such as fractional vegetation cover, is important on a pixel by pixel basis. A summary of the theoretical analysis and the preliminary testing of the model with actual aerial radiometric data is provided. Author

N89-13824*# National Aeronautics and Space Administration. Ames Research Center, Moffett Field, CA.

THE CALIFORNIA COOPERATIVE REMOTE SENSING PROJECT Final Report

CHRISTINE A. HLAVKA and EDWIN J. SHEFFNER (TGS Technology, Inc., Moffett Field, Calif.) Jul. 1988 96 p (NASA-TM-100073; A-88105; NAS 1.15:100073) Avail: NTIS HC A05/MF A01 CSCL 08B

The USDA, the California Department of Water Resources (CDWR), the Remote Sensing Research Program of the University of California (UCB) and NASA have completed a 4-yr cooperative project on the use of remote sensing in monitoring California agriculture. This report is a summary of the project and the final report of NASA's contribution to it. The cooperators developed procedures that combined the use of LANDSAT Multispectral Scanner imagery and digital data with good ground survey data for area estimation and mapping of the major crops in California. An inventory of the Central Valley was conducted as an operational test of the procedures. The satellite and survey data were acquired by USDA and UCB and processed by CDWR and NASA. The inventory was completed on schedule, thus demonstrating the plausibility of the approach, although further development of the data processing system is necessary before it can be used efficiently in an operational environment. Author

N89-14608# Environmental Protection Agency, Corvallis, OR. Environmental Research Lab.

ANALYSIS OF CROP LOSS FOR ALTERNATIVE OZONE EXPOSURE INDICES

DAVID T. TINGEY, WILLIAM E. HOGSETT, and E. HENRY LEE (Northrop Services, Inc., Corvallis, Oreg.) May 1988 15 p (PB88-214788; EPA-600/D-88-118) Avail: NTIS HC A03/MF A01 CSCL 13B

Defining the appropriate exposure index that best relates plant response to exposure necessitates a consideration of the underlying biological basis for the response and a method for characterizing the temporal variations in pollutant occurrence. Although no single index was deemed best (in all cases) for relating O₃ exposure to plant response, the top-performing exposure indices were those that: (1) cumulate the hourly O₃ concentrations over time, (2) emphasize concentrations of 0.06 ppm and higher either by continuous sigmoid weights or by discrete (0 or 1) weights of the threshold indices. The best index gave greater weight to exposures occurring 20 to 40 days before harvest. When assessing the impact of O₃ on plant growth, these findings illustrate the importance of exposure duration, the importance of repeated peaks, and the time of increased plant sensitivity. GRA

N89-14637*# Kansas State Univ., Manhattan. Div. of Biology.

THE INFLUENCE OF GRAZING ON LAND SURFACE CLIMATOLOGICAL VARIABLES Semiannual Report

T. R. SEASTEDT and M. I. DYER (Biosphere Research, Inc., Lenoir City, TN.) 28 Oct. 1988 53 p (Contract NAG5-897) (NASA-CR-183308; NAS 1.26:183308) Avail: NTIS HC A04/MF A01 CSCL 04B

Research accomplishments in empirical measurements, laboratory analyses, data analyses, and modeling are summarized. Publications are listed. Presentations made during the funding period are also listed. B.G.

ENVIRONMENTAL CHANGES AND CULTURAL RESOURCES

Includes land use analysis, urban and metropolitan studies, environmental impact, air and water pollution, geographic information systems, and geographic analysis.

A89-10926

INTERNATIONAL SYMPOSIUM ON REMOTE SENSING OF ENVIRONMENT, 21ST, UNIVERSITY OF MICHIGAN, ANN ARBOR, OCT. 26-30, 1987, PROCEEDINGS. VOLUMES 1 & 2

Symposium organized by the Environmental Research Institute of Michigan; Sponsored by the Canada Centre for Remote Sensing, Environmental Research Institute of Michigan, NASA, et al. Ann Arbor, MI, Environmental Research Institute of Michigan, 1987, p. Vol. 1, 692 p.; vol. 2, 468 p. For individual items see A89-10927 to A89-11017.

Papers on remote sensors, data systems, and scientific investigations related to land, open ocean, ice, atmosphere, and climate research are presented. Topics include the High-Resolution Imaging Spectrometer for NASA's Earth Observing System; the future of remote sensing techniques; airborne electrooptical imaging; airborne stereo line imager data; a helicopter-borne scatterometer; SAR image data compression; international remote-sensing satellites; Radarsat; the integration of remote sensing and geographic information systems; the Argos system; TM data screening; surveillance radar; the use of microwave radiometry in hydrology; and the use of Landsat, AVHRR, and SPOT data in environmental studies. Research using remote-sensing techniques is presented, covering topics such as the measurement of currents, intense and tornadic thunderstorms, suspended sediments in estuaries, calculating land and forest cover, flash flood potential, sea-level variations, agricultural monitoring, fire detection, analysis of marine shallow water-bottom features, detection of human-induced environmental change, crop yield estimation, the composition of volcanic rocks, ice surveillance, snow-cover mapping, road detection, surface wind-speed measurements, and mineral exploration. R.B.

A89-10927#

ON-BOARD PROCESSING AND NATIONAL EARTH OBSERVATIONS CENTERS

JOHN H. MCELROY (Texas, University, Arlington) IN: International Symposium on Remote Sensing of Environment, 21st, Ann Arbor, MI, Oct. 26-30, 1987, Proceedings. Volume 1. Ann Arbor, MI, Environmental Research Institute of Michigan, 1987, p. 5-21. refs

The creation of an international joint venture to pursue a comprehensive program in earth observations, known as Envirosat-International, is proposed. The organization is based on the international organizations for telecommunications and maritime satellite users. It is also proposed that centralized facilities, called national earth observations centers, be created around the world to serve as focal points for research and operations and as connection points for investigations located at distant institutions. It is suggested that, because of advances in pattern recognition and on-board processing, these centralized facilities will be needed to handle additional signals transmitted to the ground. R.B.

A89-10957#

ENHANCEMENTS TO THE ARGOS SYSTEM - PRESENTED AT THE TWENTY-FIRST INTERNATIONAL SYMPOSIUM ON REMOTE SENSING OF ENVIRONMENT, ANN ARBOR, MICHIGAN, OCTOBER 26-30, 1987

DAVID D. CLARK (Service ARGOS, Inc., Seattle, Washington) IN: International Symposium on Remote Sensing of Environment, 21st, Ann Arbor, MI, Oct. 26-30, 1987, Proceedings. Volume 1. Ann Arbor, MI, Environmental Research Institute of Michigan, 1987, p. 461-468.

Improvements made to the ARGOS system during 1986 and 1987 will have a significant, favorable impact on all system users. The new United States Global Processing Center (USGPC), located in Landover, Maryland, became fully operational in April 1987. Better delays on global coverage are now possible due to both shorter transmission time between NOAA and the USGPC, and improved hardware and software within both NOAA and ARGOS. The global reliability of the system has been improved through operation of two redundant computer centers. Additional enhancements offer new services to users. Author

A89-10959#

INTEGRATING REMOTELY SENSED DATA INTO PC-BASED GEOGRAPHIC INFORMATION SYSTEMS

CHARLES PARSON (Bemidji State University, MN), PAUL A. TESSAR, LESLIE W. MAKI, and MICHAEL BAKER (Minnesota Land Management Information Center, Saint Paul) IN: International Symposium on Remote Sensing of Environment, 21st, Ann Arbor, MI, Oct. 26-30, 1987, Proceedings. Volume 1. Ann Arbor, MI, Environmental Research Institute of Michigan, 1987, p. 495-506.

Technical issues involved in the integration of remotely sensed data into geographic information system (GIS) data bases are discussed. The differences between vector-based and raster-based systems, the problem of observational and resampling errors, the choice between personal computers and super minicomputers for GIS, and software options are examined. Examples are presented in which grouse and moose habitats are successfully identified through the integration Landsat TM data with conventional ground inventory using personal computers. R.B.

A89-10982#

LAND COVER CHANGE DETECTION WITH THEMATIC MAPPER SPECTRAL TEXTURAL DATA AT THE RURAL-URBAN FRINGE

TUNG FUNG and ELLSWORTH LEDREW (Waterloo, University, Canada) IN: International Symposium on Remote Sensing of Environment, 21st, Ann Arbor, MI, Oct. 26-30, 1987, Proceedings. Volume 2. Ann Arbor, MI, Environmental Research Institute of Michigan, 1987, p. 783-789. refs

The purpose of this research is to detect rural to urban land cover changes at the urban fringe of the cities of Kitchener-Waterloo, Ontario, Canada, with TM spectral and textural data. The textural features used include the standard deviation from first order statistics, a Laplacian filter, and inverse difference moment from grey level cooccurrence probabilities. Edge density images can be extracted from these images. Urban and rural land covers can be differentiated from them, but errors occur as some of the rural land covers may have textures similar to the urban land covers. By combining the spectral (thresholded TM 3 and differenced TM 3 images) and textural data, changes from rural land to construction sites can be identified and isolated from all other land covers. Author

A89-10997#

AUTOMATIC ROAD DETECTION ON LANDSAT 4 TM IMAGES

JEZCHING TON, ANIL K. JAIN, WILLIAM R. ENSLIN, and WILLIAM D. HUDSON (Michigan State University, East Lansing) IN: International Symposium on Remote Sensing of Environment, 21st, Ann Arbor, MI, Oct. 26-30, 1987, Proceedings. Volume 2. Ann Arbor, MI, Environmental Research Institute of Michigan, 1987, p. 925-937. refs

A conceptually parallel road detection method using Landsat-4 TM images is proposed and tested for an area in Michigan. The method consists of two phases: low-level road detection and high-level road labeling. In the low-level phase, a road sharpening operator calculates a magnitude and direction value for each pixel. Then, a parallel road following algorithm is implemented at selected seed pixels. In the high-level phase, more global information is used to classify roads into different levels. Experimental results from several images show that the method can detect roads reasonably well in the low-level phase and is useful for detecting potential oil/gas pads. In the high-level phase, however, only major roads are labeled. R.B.

A89-11730

REAL-TIME ENVIRONMENT MONITORING USING DATA FROM METEOSAT AND NOAA IMAGING SATELLITES

H. A. VAN INGEN SCHENAU and J. C. VENEMA (Nationaal Lucht-en Ruimtevaartlaboratorium, Amsterdam, Netherlands) IN: Digital image processing and visual communications technologies in meteorology; Proceedings of the Meeting, Cambridge, MA, Oct. 27, 28, 1987. Bellingham, WA, Society of Photo-Optical Instrumentation Engineers, 1987, p. 18-22. Research supported by the Netherlands Ministry of Foreign Affairs and UN. refs

An operational remote sensing system is described which supports the environment monitoring using the multisensor-multitemporal data acquired by the geostationary and polar orbiting weather satellites. The information derived from the satellite images are maps on a continental scale with data on the estimated rainfall, the vegetation index (NDVI), and for experimental use, with data on the soil water available for crops. The operational system, called ARTEMIS, will meet the information requirements of the FAO monitoring programs in the areas of food and feed security and plant protection. Author

A89-15050

AEROSPACE MONITORING OF ECOSYSTEM DYNAMICS AND ECOLOGICAL PROGNOSIS

B. V. VINOGRADOV (AN SSSR, Institut Evoliutsionnoi Morfologii i Ekologii Zhivotnykh, Moscow, USSR) Photogrammetria (ISSN 0031-8663), vol. 43, Sept. 1988, p. 1-16. refs

The paper presents Soviet experience with aerospace monitoring of ecosystem dynamics based on a comparison of repeated aerial and/or space images. The dynamics of single ecosystems are described by linear or, more commonly, nonlinear exponential or parabolic functions. The dynamics of simple two-component ecosystems are described by the interrelation of 'reserve' vs. 'resource' trends. The dynamics of composite ecosystems are represented by transition matrices and graphs of transition probabilities, using Markovian chains. Provided the areal dimensions and identification accuracy are sufficient, a normative long-term forecast may be calculated for 5-20 years ahead. Author

A89-17678#

REMOTE SENSING STRATEGIES FOR GLOBAL RESOURCE EXPLORATION AND ENVIRONMENTAL MANAGEMENT

FREDERICK B. HENDERSON, III (Geosat Committee, Inc., Norman, OK) IAF, International Astronautical Congress, 39th, Bangalore, India, Oct. 8-15, 1988. 23 p. refs (IAF PAPER 88-103)

International land and ocean satellite remote sensing systems are reviewed and the possible future developments for remote sensing systems are discussed. Data access, distribution, and integration of existing systems, geographic information systems, and airborne remote sensing are considered. Plans for launching civil land and ocean remote sensing satellites in the 1990s are outlined. The economic potential and commercialization of satellite remote sensing and the role of remote sensing in the development of global resources are examined. R.B.

A89-17702#

COMPLEX EXPERIMENT ON THE INVESTIGATION OF THE ATMOSPHERE POLLUTION USING SPACE, AIRCRAFT AND GROUND INFORMATION

IU. NOVIKOV (GK SSSR po Gidrometeorologii i Kontroliu Prirodnoi Sredy, Laboratorii Monitoringa Prirodnoi Sredy i Klimata, Moscow, USSR) and B. SOBISHEK (Hydrometeorologicky Ustav, Prague, Czechoslovakia) IAF, International Astronautical Congress, 39th, Bangalore, India, Oct. 8-15, 1988. 4 p. (IAF PAPER 88-161)

N89-10413# Instituto de Pesquisas Espaciais, Sao Jose dos Campos (Brazil).

ENVIRONMENTAL IMPACT OF THE URBAN GROWTH ON THE WESTERN SAO PAULO METROPOLITAN AREA

CELINA FORESTI Aug. 1988 11 p Presented at the 16th

Congress of International Society for Photogrammetry and Remote Sensing, Kyoto, Japan, 1-10 Jul. 1988 Submitted for publication (INPE-4670-PRE/1370) Avail: NTIS HC A03/MF A01

Satellite-borne remote sensing data are useful for urban environment analysis owing to their improved spatial, spectral, and radiometric resolution. The present study assesses the environmental impact of urban growth on the Western Sao Paulo Metropolitan Area from 1975 to 1985. Multidate digital data from MSS/LANDSAT, TM/LANDSAT, and HRV-SPOT were registered and urban structure changes within that period were detected. Color composite photographs of TM band 5, 3, and 4 were applied to map the urban land use for new urban areas. The HRV-SPOT panchromatic data, digitally enlarged to the scale of 1:10,000 were applied to urban structure mapping and environmental monitoring. Ground truth data collection and helicopter-borne data collection were used to complement the remote sensed data. Several environment degradation levels were determined and compared to the Physical Aptitude for Urban Settlement Chart. The results showed that environmental impacts are more related to the pattern of urban settlement than to the physiographic features. Vegetative cover proved to be the most important key, indicating environmental change as far as orbital remote sensing is concerned. Soil erosion is caused by the removal of vegetative cover, but the erosion rates are controlled by the different patterns of land use. Author

N89-10676# Instituto de Pesquisas Espaciais, Sao Jose dos Campos (Brazil).

A GENERAL DATA MODEL FOR GEOGRAPHIC INFORMATION SYSTEMS

GUARACI JOSE ERTHAL, GILBERTO CAMARANETO, and DIOGENES SALASALVES May 1988 11 p Presented at the 16th Congress of International Society for Photogrammetry and Remote Sensing, Kyoto, Japan, 1-10 Jul. 1988 Submitted for publication (INPE-4560-PRE/1301) Avail: NTIS HC A03/MF A01

Recently, a major trend in Geographic Information Systems (GIS) is integrating remote sensing data in such an environment. This work presents a GIS to be used in remote sensing applications, together with an image processing system, enabling satellite imagery to be combined with thematic maps, DTMs, and tabular data. In designing an integrated system, vector and raster data must be treated on a common data base. In order to overcome such diversities, the design relied on abstract data types. The data base uses a geo-relational model. Author

N89-12958*# National Aeronautics and Space Administration. Goddard Space Flight Center, Greenbelt, MD.

REQUIREMENTS FOR ONGOING DEVELOPMENT OF THE PILOT LAND DATA SYSTEM (PLDS)

S. W. WHARTON and J. A. NEWCOMER (ST Systems Corp., Lanham, Md.) In ESA, Proceedings of the 1988 International Geoscience and Remote Sensing Symposium (IGARSS 1988) on Remote Sensing: Moving Towards the 21st Century, Volume 1 p 85-88 Aug. 1988 Sponsored by NASA, Washington D.C. Avail: NTIS HC A99/MF E03; ESA Publications Div., ESTEC, Noordwijk, Netherlands, 120 US dollars or 250 Dutch guilders CSDL 05B

The Pilot Land Data System being developed to address the information processing needs of the NASA land sciences research community is presented. The objective of the pilot program is to establish a limited-scale, distributed information system for the archival, location, transfer, integration, and manipulation of data across multiple sites connected by a high-speed communications network. Functional capabilities required for users to create, access, and maintain local and distributed data bases containing various types of data in support of land sciences research are summarized. ESA

N89-12959# Reading Univ. (England). NERC Unit for Thematic Information Systems.

THE USE OF REMOTE SENSING IN CONJUNCTION WITH GEOGRAPHIC INFORMATION SYSTEMS FOR LOCAL PLANNING

N. A. QUARMBY, J. L. CUSHNIE, and J. SMITH (National Remote Sensing Centre, Farnborough, England) In ESA, Proceedings of the 1988 International Geoscience and Remote Sensing Symposium (IGARSS 1988) on Remote Sensing: Moving Towards the 21st Century, Volume 1 p 89-92 Aug. 1988 (Contract NERC-F60/G6/12)

Avail: NTIS HC A99/MF E03; ESA Publications Div., ESTEC, Noordwijk, Netherlands, 120 US dollars or 250 Dutch guilders

The use of remote sensing and other types of geographic information for local planning purposes is discussed. Perspective views, combining remotely sensed data and digital elevation data, are a useful tool in the decision-making process for housing land supply. Weighting, overlay, and dilation operations were performed on digitized information showing environmental constraints and communication networks to illustrate the ability of a geographic information system to provide alternative solutions to the problem of assessing the potential impact of new housing developments. ESA

N89-12960# Katholieke Universiteit te Leuven (Belgium). Lab. for Land Management.

AN INTEGRATED REMOTE SENSING APPROACH FOR REGIONAL AGROSTATISTICS AND LAND MONITORING

M. ROCKAERTS, W. DEVOS, H. PEETERS, H. EERENS, and P. GOMBEER In ESA, Proceedings of the 1988 International Geoscience and Remote Sensing Symposium (IGARSS 1988) on Remote Sensing: Moving Towards the 21st Century, Volume 1 p 93-96 Aug. 1988

Avail: NTIS HC A99/MF E03; ESA Publications Div., ESTEC, Noordwijk, Netherlands, 120 US dollars or 250 Dutch guilders

Nine satellite images of six different recording dates were merged after radiometric recalibration and geometrical correction to the Belgian Lambert cartographic projection. This multitemporal dataset was classified with a decision tree incorporating single channel level-slicing, different vegetation-indices, and a minimum distance classification algorithm, all based on the recalibrated digital values. Fourteen terrain-classes are distinguished including 10 crops, deciduous and coniferous forest, waterbodies, and urbanization. The classification proves to be in accordance with the data gathered by the National Institute of Statistics. ESA

N89-12964# Edinburgh Univ. (Scotland). Dept. of Geography.

INTEGRATING REMOTE SENSING DATA INTO A GEOGRAPHICAL INFORMATION SYSTEM: A FOUNDATION FOR RURAL LAND USE STRATEGIES: NATURE CONSERVANCY COUNCIL PROJECT

R. HEALEY, P. DOWIE, A. MOWLE, and J. HOLBROOK (Natural Environment Research Council, Edinburgh, Scotland) In ESA, Proceedings of the 1988 International Geoscience and Remote Sensing Symposium (IGARSS 1988) on Remote Sensing: Moving Towards the 21st Century, Volume 1 p 111-112 Aug. 1988 Avail: NTIS HC A99/MF E03; ESA Publications Div., ESTEC, Noordwijk, Netherlands, 120 US dollars or 250 Dutch guilders

The development of a geographic information system, and approaches to the integration of digital cartographic and remote sensing data to support this process, are described. Data from available map sources, as well as detailed field survey, combined with LANDSAT TM imagery allow different land use classifications to be assessed at different scales. The possible effects of alternative policies for resolving conflicts of interest in rural development can be examined, including specific problems such as the impact of designating areas as sites of special scientific interest. ESA

N89-12966# Reading Univ. (England).

AN INTERNATIONAL APPROACH TO GIS BASED ON REMOTE SENSING AND TERRAIN CLASSIFICATION

C. W. MITCHELL In ESA, Proceedings of the 1988 International Geoscience and Remote Sensing Symposium (IGARSS 1988) on Remote Sensing: Moving Towards the 21st Century, Volume 1 p 117-118 Aug. 1988

Avail: NTIS HC A99/MF E03; ESA Publications Div., ESTEC, Noordwijk, Netherlands, 120 US dollars or 250 Dutch guilders

Geographic information systems (GIS) which emphasize environmental data based on remote sensing are discussed. The use of terrain units, recognizable on remotely sensed imagery, as a framework offers a number of advantages, including ready comprehensibility, economy, applicability to different disciplines, mapping scales and technological levels, a capability for self-refinement, and a recognition of analogs between different areas. The UK, the Middle East, and North Africa provide examples of the method. An outline design for linked national and international GIS is proposed. ESA

N89-12987# Liege Univ. (Belgium). Dept. of Geography.
**TOWARDS AN URBAN LAND-USE CLASSIFICATION USING
 TEXTURAL AND MORPHOLOGICAL CRITERIA**

Y. BAUDOT, I. NADASDI, and J.-P. DONNAY / In ESA, Proceedings of the 1988 International Geoscience and Remote Sensing Symposium (IGARSS 1988) on Remote Sensing: Moving Towards the 21st Century, Volume 1 p 211-212 Aug. 1988
 Avail: NTIS HC A99/MF E03; ESA Publications Div., ESTEC, Noordwijk, Netherlands, 120 US dollars or 250 Dutch guilders

The use of satellite data to provide land use maps suitable for urban planners is discussed. Spatial resolutions of civilian satellites are not adapted to the complexity of urban milieu. A land use does not correspond to a specific spectral signature; thus a classification of land uses cannot be reached only by means of radiometric information, but requires morphological and topological elements, in a way inspired by the processes involved in visual interpretation of aerial photographs. ESA

N89-13058# National Remote Sensing Centre, Farnborough (England).

**MONITORING URBAN CHANGE FROM LANDSAT TM AND
 SPOT SATELLITE IMAGERY BY IMAGE DIFFERENCING**

G. H. GRIFFITHS / In ESA, Proceedings of the 1988 International Geoscience and Remote Sensing Symposium (IGARSS 1988) on Remote Sensing: Moving Towards the 21st Century, Volume 1 p 493-497 Aug. 1988
 Avail: NTIS HC A99/MF E03; ESA Publications Div., ESTEC, Noordwijk, Netherlands, 120 US dollars or 250 Dutch guilders

It is shown that visual interpretation of satellite imagery is the most accurate technique for detecting urban change. This would particularly be the case if enhanced SPOT imagery combining the spectral information of the multispectral channels (XS) and the spatial information of the panchromatic channels was available for both image dates. However, at county, regional, and national scales a more automated technique is required to provide a unified record of the distribution of urban change at specified time intervals. This can be achieved by using a modified form of image differencing in which unwanted agricultural change is differentiated from the urban change of interest by using the variance of the SPOT panchromatic channel as a textural discriminator. In this way it is possible to discriminate between areas of reflectance change on the difference image that display a high variance and correspond to urban land, and areas of reflectance change with low variance which are generally nonurban. ESA

N89-14942# Sandia National Labs., Albuquerque, NM. Applied Mechanics Div.

DOE/DOD ENVIRONMENTAL DATA BANK

C. A. DAVIDSON 1988 6 p Presented at the 59th Shock and Vibration Symposium, Albuquerque, NM, 18 Oct. 1988 (Contract DE-AC04-76DP-00789) (DE88-015262; SAND-88-1429C; CONF-881076-5) Avail: NTIS HC A02/MF A01

The purpose of this paper is to describe an engineering analysis support activity which involves the collection, analysis, storage, and retrieval of technical environmental information. This information is at the disposal of system and component analysts for use in formulating initial conditions, forcing functions and performance requirements for numerous hardware application evaluations. This paper will describe the Engineering Environmental Data Bank system which provides this information service to many

Sandia Laboratories' technical analysis efforts and other qualified programs. Its structure and data sources will be summarized.

DOE

03

GEODESY AND CARTOGRAPHY

Includes mapping and topography.

A89-13757* National Aeronautics and Space Administration. Goddard Space Flight Center, Greenbelt, MD.

THE CRUSTAL DYNAMICS PROJECT

ROBERT J. COATES (NASA, Goddard Space Flight Center, Greenbelt, MD) IN: The impact of VLBI on astrophysics and geophysics; Proceedings of the 129th IAU Symposium, Cambridge, MA, May 10-15, 1987. Dordrecht, Kluwer Academic Publishers, 1988, p. 337, 338.

The Crustal Dynamics Project has been developing, deploying, and operating very-long-baseline interferometry (VLBI) systems and satellite laser ranging (SLR) systems for highly accurate geodetic measurements of global plate motion, plate stability, regional crustal deformation, and earth rotation/polar motion. Over the past 10 years, the measurement accuracies of these systems have been improved by a factor of 10 to the cm level. Plans are to continue these developments to reach mm level accuracies. The present deployment of the VLBI systems is primarily in the Northern Hemisphere. This network has produced measurements of the relative plate motion between the North American, Eurasian, and Pacific plates; the stability of the same plates; and the regional deformation at the North American/Pacific plate boundary in California and Alaska. Author

A89-13759* National Aeronautics and Space Administration. Goddard Space Flight Center, Greenbelt, MD.

**GEODESY BY RADIO INTERFEROMETRY - DETERMINATION
 OF VECTOR MOTIONS FOR SITES IN THE WESTERN UNITED
 STATES**

DAVID GORDON (NASA, Goddard Space Flight Center; Science Applications Research, Greenbelt, MD) IN: The impact of VLBI on astrophysics and geophysics; Proceedings of the 129th IAU Symposium, Cambridge, MA, May 10-15, 1987. Dordrecht, Kluwer Academic Publishers, 1988, p. 355, 356.

The use of VLBI to study plate tectonic motion, plate boundary deformation, earth dynamics, and the crustal motions in the western U.S. is discussed. Results from dual frequency (S and X band) mobile VLBI experiments between October 1982 and February 1987 are presented. It is suggested that significant northwest motion is occurring well east of the San Andreas fault. R.B.

A89-13760

**NASA/CRUSTAL DYNAMICS PROJECT GEODETIC DATA
 ANALYSIS**

W. E. HIMWICH (Interferometrics, Inc., Vienna, VA) IN: The impact of VLBI on astrophysics and geophysics; Proceedings of the 129th IAU Symposium, Cambridge, MA, May 10-15, 1987. Dordrecht, Kluwer Academic Publishers, 1988, p. 357, 358.

The VLBI group in NASA's Crustal Dynamics Project (CDP) maintains an integrated system for analyzing geodetic VLBI data. This system includes: CALC, calibration programs, SOLVE, GLOBL, and the Data Base System. CALC is the program which contains the models used to calculate the theoretical delay. SOLVE is used to analyze single experiments. GLOBL is used to analyze large groups of experiments. The Data Base System is a self-documenting data storage system used to pass data between programs and archive the data. Kalman filtering is being investigated for operational use in geodetic data analysis.

Author

A89-13761* Jet Propulsion Lab., California Inst. of Tech., Pasadena.

DISTRIBUTION OF RELATIVE PLATE MOTION ALONG THE PACIFIC-NORTH AMERICAN PLATE BOUNDARY DETERMINED FROM MOBILE VLBI MEASUREMENTS

P. M. KROGER, G. A. LYZENGA, K. S. WALLACE, and J. M. DAVIDSON (California Institute of Technology, Jet Propulsion Laboratory, Pasadena) IN: The impact of VLBI on astrophysics and geophysics; Proceedings of the 129th IAU Symposium, Cambridge, MA, May 10-15, 1987. Dordrecht, Kluwer Academic Publishers, 1988, p. 365, 366.

A89-13762* Harvard-Smithsonian Center for Astrophysics, Cambridge, MA.

VLBI GEODESY - 2 PARTS-PER-BILLION PRECISION IN LENGTH DETERMINATIONS FOR TRANSCONTINENTAL BASELINES

J. L. DAVIS, T. A. HERRING, and I. I. SHAPIRO (Harvard-Smithsonian Center for Astrophysics, Cambridge, MA) IN: The impact of VLBI on astrophysics and geophysics; Proceedings of the 129th IAU Symposium, Cambridge, MA, May 10-15, 1987. Dordrecht, Kluwer Academic Publishers, 1988, p. 367, 368. refs (Contract NAG5-538; NSF EAR-83-06380; NSF EAR-86-18989; F19628-86-K-0025)

VLBI was to make twenty-two independent measurements, between September 1984 and December 1986, of the length of the 3900-km baseline between the Mojave site in California and the Haystack/Westford site in Massachusetts. These experiments differ from the typical geodetic VLBI experiments in that a large fraction of observations is obtained at elevation angles between 4 and 10 deg. Data from these low elevation angles allow the vertical coordinate of site position, and hence the baseline length, to be estimated with greater precision. For the sixteen experiments processed thus far, the weighted root-mean-square scatter of the estimates of the baseline length is 8 mm. Author

A89-13764* Harvard-Smithsonian Center for Astrophysics, Cambridge, MA.

VLBI STUDIES OF THE NUTATIONS OF THE EARTH

T. A. HERRING (Harvard-Smithsonian Center for Astrophysics, Cambridge, MA) IN: The impact of VLBI on astrophysics and geophysics; Proceedings of the 129th IAU Symposium, Cambridge, MA, May 10-15, 1987. Dordrecht, Kluwer Academic Publishers, 1988, p. 371-375. refs (Contract NAG5-538; NSF EAR-83-06380; NSF EAR-86-18989; F19628-86-K-0025)

The analysis of six years of VLBI data has yielded corrections to the coefficients of the seven largest terms in the IAU 1980 nutation series with periods of one year or less, with accuracies approaching the truncation error of this nutation series (0.1 mas). This paper examines the methods used to extract the nutation information from the VLBI data, the calculation of the uncertainties of the resultant corrections to the nutation-series coefficients, and current research on the earth's nutations. B.J.

A89-17945

TIME SERIES OF EUROPEAN BASELINES DETERMINED WITH LAGEOS

A. CAPORALI (Padova, Università, Padua, Italy), A. CENCI, M. FERMI, and F. PALUTAN (Telespazio S.p.A., Rome, Italy) Nuovo Cimento C, Serie 1 (ISSN 0390-5551), vol. 11 C, May-June 1988, p. 273-286. CNR-supported research. refs

Results of the analysis of laser ranging data consisting in the repeated determination of baselines across Europe are presented. Time series of selected baselines and the results of a calibration experiment aimed to determine possible system biases among three key laser stations are included. The time period covered is September 1983 - February 1986. No statistically significant change in the length of baselines is visible, but the repeatability of successive estimates of most baselines is good enough to justify the idea that crustal motion in the Mediterranean basin of the order of few cm/y, if present, should be reliably detected in few

years of repeated measurements, assuming the present density and quality of the laser ranging data. Author

A89-20200

GEOPHYSICAL INTERPRETATION OF THE MAGNETIC ANOMALIES OF CHINA DERIVED FROM MAGSAT DATA

J. ARKANI-HAMED, S. K. ZHAO, and D. W. STRANGWAY (British Columbia, University, Vancouver, Canada) Geophysical Journal (ISSN 0952-4592), vol. 95, Nov. 1988, p. 347-359. refs (Contract NSERC-A-2037)

Magnetometer satellite (Magsat) data are used to construct a regional magnetic anomaly map of China. It is found that short wavelength (less than or equal to 540 km) features are dominated by noncrustal noise. The magnetic anomaly map, derived on the basis of the covariant harmonics of the two sets with wavelengths in the range of 540-2300 km, presents the crustal magnetic anomalies of China at a satellite altitude of about 400 km. K.K.

N89-10303# Dornier-Werke G.m.b.H., Friedrichshafen (Germany, F.R.).

SOLID EARTH MISSION STUDY. VOLUME 2: TECHNICAL REPORT Final Report

R. BENZ, H. FAULKS, P. G. HARDTKE, R. KLEIN, M. LANGEMANN, U. DENSKAT, C. ETIENNE, P. PEYROT, A. BERNARD, A. CIAMPOLINI (Aeritalia S.p.A., Turin, Italy) et al. Paris, France ESA Nov. 1987 387 p Prepared in cooperation with Matra Espace, Toulouse, France; ONERA, Paris, France; Aeritalia SpA, Turin, Italy; Fokker BV, Amsterdam, The Netherlands; BAe, Bristol, United Kingdom; LABEN Space Instrumentation and Systems, Milan, Italy (Contract ESTEC-7149/87-NL-JS) (ESA-CR(P)-2626-VOL-2; ETN-88-93153) Avail: NTIS HC A17/MF A01

The Applications and Research Involving Space Techniques Observing The Earth field from Low Earth Satellite (ARISTOTELES) mission is introduced. The ARISTOTELES studies include gravity field measurements, magnetic field measurements, and geokinematics. Gravity anomalies are to be determined with better than 5 mGal accuracy at 100 km spatial resolution by a gravity gradiometer (GRADIO) made with a three axis assembly of microaccelerometers (design goal 0.001 EU accuracy). The satellite is to be launched by Ariane with ERS-2. A dawn-dusk orbit at 220 km is suggested. The most critical point is accommodation of GRADIO, but this is not insurmountable. Technical aspects of the mission are presented. ESA

N89-10397# Dornier-Werke G.m.b.H., Friedrichshafen (Germany, F.R.).

SOLID EARTH MISSION STUDY. VOLUME 1: EXECUTIVE SUMMARY Final Report

R. BENZ, H. FAULKS, P. G. HARDTKE, R. KLEIN, M. LANGEMANN, U. DENSKAT, C. ETIENNE, P. PEYROT, A. BERNARD, A. CIAMPOLINI (Aeritalia S.p.A., Turin, Italy) et al. Paris, France ESA Nov. 1987 71 p Prepared in cooperation with Matra Espace, Toulouse, France; ONERA, Paris, France; Aeritalia SpA, Turin, Italy; Fokker BV, Amsterdam, The Netherlands; BAe, Bristol, United Kingdom; LABEN Space Instrumentation and Systems, Milan, Italy (Contract ESTEC-7149/87-NL-JS) (ESA-CR(P)-2626-VOL-1; ETN-88-93152) Avail: NTIS HC A04/MF A01

The Applications and Research Involving Space Techniques Observing The Earth field from Low Earth Satellite (ARISTOTELES) mission is introduced. The ARISTOTELES studies include gravity field measurements, magnetic field measurements, and geokinematics. Gravity anomalies are to be determined with better than 5 mGal accuracy at 100 km spatial resolution by a gravity gradiometer (GRADIO) made with a three axis assembly of microaccelerometers (design goal 0.001 EU accuracy). The satellite is to be launched by Ariane with ERS-2. A dawn-dusk orbit at 220 km is suggested. The most critical point is accommodation of GRADIO, but this is not insurmountable. A summary is presented of the planned mission. ESA

N89-10399# Dornier-Werke G.m.b.H., Friedrichshafen (Germany, F.R.).

SOLID EARTH MISSION STUDY. VOLUME 3: PROGRAM PLANNING REPORT Final Report

R. BENZ, H. FAULKS, P. G. HARDTKE, R. KLEIN, M. LANGEMANN, U. DENSKAT, C. ETIENNE, P. PEYROT, A. BERNARD, A. CIAMPOLINI (Aeritalia S.p.A., Turin, Italy) et al. Paris, France ESA Nov. 1987 54 p Prepared in cooperation with Matra Espace, Toulouse, France; ONERA, Paris, France; Aeritalia SpA, Turin, Italy; Fokker BV, Amsterdam, The Netherlands; BAe, Bristol, United Kingdom; LABEN Space Instrumentation and Systems, Milan, Italy

(Contract ESTEC-7149/87-NL-JS)

(ESA-CR(P)-2626-VOL-3; ETN-88-93154) Avail: NTIS HC A04/MF A01

The Applications and Research Involving Space Techniques Observing the Earth field from Low Earth Satellite mission program planning is outlined. ESA

N89-10886# Army Engineer Topographic Labs., Fort Belvoir, VA.

CONTINUOUS DEFORMATION MONITORING WITH GPS

STEPHEN R. DELOACH 12 Apr. 1988 39 p Presented at the ASCE Specialty Conference, Nashville, Tenn., 11-14 May 1988 (AD-A196447; ETL-R-138) Avail: NTIS HC A03/MF A01 CSCL 13B

The U.S. Army Corps of Engineers makes extensive use of modern instrumentation for measuring the behavior of large structures. One of these instrumentation programs is high precision geodetic surveying which provides a reliable measure of displacement as a function of time. Typically, accuracies of 5 to 10 mm can be achieved. Final accuracy of the displacement is a function of many factors, including: network geometry, field procedures, survey crew experience, and equipment. Unfortunately, the high precision geodetic survey is labor intensive, time consuming and rather expensive. For this reason, surveys are made infrequently, or sometimes not at all unless there is a suspicion of structural distress. The NAVSTAR Global Positioning System has the potential to be used in an automatic mode to continuously monitor structural deformations. During the next few months, a system will be developed to operate such a system. It will then be installed at the USACE Corps of Engineers Dworshak Dam in Idaho for demonstration. Testing of presently owned government GPS equipment indicates the system will detect movements of about 6 mm in three dimensions if reference points and object points are within a few kilometers of each other.

GRA

N89-11615# Stanford Linear Accelerator Center, CA.

INTEGRATED DATABASE APPROACH FOR GEODETIC APPLICATIONS

ROBERT RULAND and DETLEV RULAND (Wuerzburg Univ., West Germany) Nov. 1987 20 p Presented at the 4th International Working Conference on Statistical and Scientific Database Management, Rome, Italy, 21 Jun. 1988

(Contract DE-AC03-76SF-00515)

(DE88-012726; SU-SLAC-PUB-4474; CONF-8806166-2) Avail: NTIS HC A03/MF A01

Geodetic measurements even of a defined project produce a vast amount of heterogeneous data. The analysis of these data used to be time-and-manpower consuming and only focused on subsets of the data. This paper demonstrates how an integrated database system will provide an immediate standardized and easy access to the entire information support data management, and, consequently, streamline the analysis. DOE

N89-12097*# Ohio State Univ., Columbus.

PRESENTATIONS BY PARTICIPANTS (EDITED AND CONDENSED)

R. R. B. VONFRESE /In Naval Ocean Research and Development Activity, Geomagnetic Autonomous Shuttle-Launched Probe Workshop p 13-21 Jun. 1987

(Contract NAGW-736; NSF DPP-83-13071)

Avail: NTIS HC A04/MF A01 CSCL 08G

The utility of Geomagnetic Autonomous Shuttle-Launched Probe (GASP) for studying the earth's crust can be characterized in terms of lithospheric contributions by past satellite programs. In contrast to the POGO and MAGSAT satellites, GASP will orbit at a lower elevation to provide better resolved lithospheric magnetic anomalies for more detailed and improved geologic analysis. In the geological representation of satellite magnetic anomaly data, two current approaches can serve the analysis of GASP observations. When global scale coverage is available, spherical harmonic expansions of the observations may be utilized. When satellite elevation data is used, a useful and efficient approach is to determine the physical properties of an array of point equivalent sources by least squares matrix inversion of the observations, which will closely duplicate the observed field. An important preliminary step in the representation of satellite magnetic observations by either approach, is to register the data at constant elevation over uniform intervals of latitude and longitude. Further applications of GASP are discussed. Author

N89-12098# Newcastle Univ. (England).

WORKING GROUP REPORTS SUBMITTED BY GROUP CHAIRMEN FOLLOWING WORKSHOP

FRANK J. LEWES /In Naval Ocean Research and Development Activity, Geomagnetic Autonomous Shuttle-Launched Probe Workshop p 41 Jun. 1987

Avail: NTIS HC A04/MF A01 CSCL 08D

The scientific problems are described in the document, Magnetic Field Explorer, (Dec. 1985). To address these problems the orbit should be near polar; a sampling rate of one sample every 15 secs would give adequate spatial resolution for the core field. Two days of good vector data in magnetically quiet conditions would be sufficient. Even if only scalar (intensity) data were available, this would be a vast improvement on Project MAGNET, but it is not clear how good a field model could be produced. It is likely that GASP will measure only the intensity and not the direction of the geomagnetic field, and this leads to significant problems in using such measurements to estimate a model of the main field. Possible magnetometer options were discussed. Three-component fluxgate magnetometers might be the simplest, but previous experience of unpredictable baseline shifts suggests three component fluxgate. Some form of backup is strongly recommended. Suggestions are given. Author

N89-12099# National Geophysical Data Center, Boulder, CO.

WORKING GROUP ON STUDIES OF THE LITHOSPHERE: RECOMMENDATIONS

DAVID HASTINGS /In Naval Ocean Research and Development Activity, Geomagnetic Autonomous Shuttle-Launched Probe Workshop p 42 Jun. 1987

Avail: NTIS HC A04/MF A01 CSCL 08D

A summary is presented on the conclusions of the working group concerned with studies of the lithosphere. Listed and briefly discussed are specific benefits of Geomagnetic Autonomous Shuttle-Launched Probe (GASP) to crustal anomaly modeling. The specific goals of the group are listed along with the specifications for the missions and recommendations for processing the acquired data. Data archiving, documentation, and availability is also briefly discussed. E.R.

N89-12100# Brown Univ., Providence, RI.

CONTRIBUTIONS TO THE GASP WORKSHOP PROCEEDINGS (NOT PRESENTED ORALLY)

JOHN F. HERMANCE /In Naval Ocean Research and Development Activity, Geomagnetic Autonomous Shuttle-Launched Probe Workshop p 43-46 Jun. 1987

Avail: NTIS HC A04/MF A01 CSCL 08B

The earth's magnetic field at satellite altitudes not only has contributions from the earth's core and static magnetization in the lithosphere, but also from external electric current systems in the lithosphere and magnetosphere, along with induced electric currents flowing in the conducting earth. The author in 1982

assessed these last two conditions, the external time varying fields and their associated internal counterparts, which are electromagnetically induced. The group recommends a follow-on mission to MAGSAT for a better understanding of the internal/external field coupling problem. By doing so, the time base of the primary data set is extended. And by flying this mission during all local times, a unique opportunity is obtained to discriminate between the sources of the external field contribution, i.e., both the effects of ionospheric current systems and magnetospheric current systems can be studied. E.R.

**N89-12101# Geological Survey, Dover, DE.
SIMULATION OF A SPINNING SPACECRAFT
MAGNETOMETER**

Z. WANG and J. C. CAIN /In Naval Ocean Research and Development Activity, Geomagnetic Autonomous Shuttle-Launched Probe Workshop p 47-51 Jun. 1987
Avail: NTIS HC A04/MF A01 CSCL 22B

In a companion report, A Study of Accuracy Enhancement in Satellite Magnetic Modeling, it is shown that the maximum fitting error in scalar field modeling could be dramatically reduced to a level of 140 nT in component field, or of the order of 0.2 degrees in declination, when a small quantity of vector data within some 10 degrees of the dip equator was added. A promising option to acquire the desired vector data is to employ the proposed spinning magnetometer system, a simpler and less costly device than the oriented spacecraft concept. One aspect of the spinning satellite idea is demonstrated. The preliminary results of the simulation studies prove optimistic, though further work needs to be done to detail its feasibility. Author

**N89-12102# Geological Survey, Dover, DE.
A STUDY OF ACCURACY ENHANCEMENT IN SATELLITE
MAGNETIC MODELING**

Z. WANG and J. C. CAIN /In Naval Ocean Research and Development Activity, Geomagnetic Autonomous Shuttle-Launched Probe Workshop p 52-58 Jun. 1987
Avail: NTIS HC A04/MF A01 CSCL 08G

The purpose of this study was to examine geomagnetic field modeling options for the Geomagnetic Autonomous Shuttle-Launched Probe (GASP) project as presently conceived for mapping requirements, and to suggest ways that the product could be improved with little added expense. The assumption made is that GASP will collect data for a period of 6 to 10 days of the total scalar field of the earth in a near-polar orbit from low altitude. Future enhancements for obtaining a small amount of vector data in limited regions will also be addressed either with GASP in a spinning mode, or in a larger spacecraft. The addition of surface data will be investigated using observatory annual means. The first phase of the study involves the use of MAGSAT scalar and vector data. The second phase involves a combination of scalar satellite and surface data. The third phase involves determining whether a spinning spacecraft could make observation of the field perpendicular to the earth's rotation axis and that the axis and phase of the spin could be determined from the magnetic field observations. Author

**N89-12103# Colorado Univ., Boulder.
SATELLITE MEASUREMENTS REQUIRED FOR DEEP-EARTH
GEOPHYSICS**

EDWARD R. BENTON /In Naval Ocean Research and Development Activity, Geomagnetic Autonomous Shuttle-Launched Probe Workshop p 59-60 Jun. 1987
Avail: NTIS HC A04/MF A01 CSCL 08G

Three major scientific issues arising within the less accessible, deeper parts of the earth can be phrased as the following questions: (1) What is the vertical profile of horizontally averaged electrical conductivity in the lower mantle (below the depths available to magnetotelluric sounding); (2) What is the intensity and pattern of the geomagnetic field (especially the vertical component) at the core-mantle boundary; and (3) What are the patterns of horizontal fluid motion in the outer core just beneath the core-mantle boundary. Answers to the first two questions are prerequisite to

the thorough understanding of the geodynamo, that can only be started with an answer to question 3. Yet traditionally mantle conductivity is ignored in the downward extrapolation of surface magnetic measurements to the core-mantle boundary. The questions and some possible answers are briefly discussed.

Author

**N89-12982*# National Aeronautics and Space Administration.
Goddard Space Flight Center, Greenbelt, MD.**

**GEODYNAMICS LASER RANGING SYSTEM: PERFORMANCE
SIMULATIONS AND DEVELOPMENT OF THE EOS FACILITY**
S. C. COHEN /In ESA, Proceedings of the 1988 International Geoscience and Remote Sensing Symposium (IGARSS 1988) on Remote Sensing: Moving Towards the 21st Century, Volume 1 p 187-189 Aug. 1988
Avail: NTIS HC A99/MF E03; ESA Publications Div., ESTEC, Noordwijk, Netherlands, 120 US dollars or 250 Dutch guilders CSCL 20E

The NASA Geodynamics Laser Ranging System is a spaceborne multicolor laser ranger to be used for studying regional and local scale crustal movements and will provide a capability for height profiling of ice-sheets, land terrains, cloud-tops, and other surfaces. Ranging measurements to retroreflector targets will produce intersite distances and relative heights with subcentimeter accuracy over baselines up to several hundred kilometers long. Arrays containing up to a few hundred targets can be surveyed nearly simultaneously. Altimetric profiling can be performed with spatial resolution of 80m and vertical accuracy of 10cm with the latter depending on the roughness and slope of the terrain. ESA

**N89-13054# University Coll., London (England). Dept. of
Geography.**

**THE DIFFERENTIAL RECTIFICATION OF SPOT HRV
PANCHROMATIC AND MULTISPECTRAL IMAGERY USING A
DIGITAL ELEVATION MODEL**

S. KAY /In ESA, Proceedings of the 1988 International Geoscience and Remote Sensing Symposium (IGARSS 1988) on Remote Sensing: Moving Towards the 21st Century, Volume 1 p 479-481 Aug. 1988 Sponsored by the Natural Environment Research Council, London, United Kingdom
Avail: NTIS HC A99/MF E03; ESA Publications Div., ESTEC, Noordwijk, Netherlands, 120 US dollars or 250 Dutch guilders

For SPOT image differential rectification, a semi-automated method, utilizing a parametric solution and a digital terrain model, is described. Elevation point interpolation and radiometric resampling are achieved by bilinear interpolation. Two panchromatic subscenes were processed. Geometric rectification is achieved reliably and quickly. Similar results are expected for multispectral data. ESA

**N89-14485# Technische Hogeschool, Delft (Netherlands).
Faculty of Geodesy.**

**ON THE CONNECTION OF GEODETIC POINT FIELDS IN
RESEAU EUROPEAN TRIGONOMETRIQUE (RETRIG) AND
RELATED TESTS FOR MODEL ERRORS Thesis**

ANTON J. M. KOSTERS 1988 105 p
(ETN-89-93327) Avail: NTIS HC A06/MF A01

A general view of connection problems in geodesy is presented, with worked out practical examples from the adjustment of the European Triangulation RETRIG. The problems studied include combining two RETRIG blocks, using their common points, and combining satellite derived coordinates with terrestrial ellipsoidal coordinates. Attention is given to the use of two- and three-dimensional statistical tests on station coordinates and to the use of substitute covariance matrices for coordinates. Computing results are presented. ESA

**N89-14487# Technische Hogeschool, Delft (Netherlands). Dept.
of Geodesy.**

**ON THE CONNECTION OF DIGITIZED MAPS TO A UNIFORM
COORDINATE SYSTEM. A SPECIAL CASE OF THE GEODETIC
CONNECTION PROBLEM Thesis**

FRANK KENSELAAR Nov. 1987 103 p
(B8821602; ETN-89-93330) Avail: NTIS HC A06/MF A01

Delft theory is used for the connection of geodetic point fields. The transformation between two coordinate systems is determined by a least squares solution from a set of connection points. A stochastic model is described, as well as the algorithm for an iterative solution. An analytical solution for the connection with a similarity or affine transformation is also given. The formulas of the reliability of the connection are discussed. A designed configuration can be analyzed using these formulas. ESA

N89-14492# Technische Hogeschool, Delft (Netherlands). Dept. of Geodesy.

A STUDY ON LEAST-SQUARES PREDICTION AND COLLOCATION Thesis

R. P. VANETTEN Mar. 1988 107 p
(ETN-89-93336) Avail: NTIS HC A99/MF E11

Collocation is defined as the extension of geodesy least squares prediction to the case of multiple observation types and a collocation method is described using data from geostatistics and mining. It is shown that the procedure is not much different from familiar methods, although the generalized variances do show interesting qualities. Practical aspects of least squares collocation are examined including computation of degree variances, problems with the full covariance matrix, and hypothesis testing. Prediction results which confirm the potential of the method are presented. ESA

N89-14493# Technische Hogeschool, Delft (Netherlands). Faculty of Geodesy.

VERY LONG BASELINE INTERFEROMETRY (VLBI): RELATIVITY AND GEODESY Thesis [VLBI: RELATIVITEIT EN GEODESIE]

LEENDERT BOER May 1988 95 p In DUTCH; ENGLISH summary
(ETN-89-93337) Avail: NTIS HC A05/MF A01

Relativistic effects to be taken into account in geodetic VLBI measurements are discussed. The delay of a radio signal is derived in a barycentric system which is then transformed via a Lorentz transformation into a terrestrial system in order to relate it with geodetic VLBI measurements. The relativistic deflection of radio waves is derived in the gravitational fields of the Sun, the planets and the Earth, and is found to be strongly related to the value of the so-called gravitational deflection parameter gamma. A model was developed to estimate the gamma parameter and was implemented. It is shown that VLBI is a suitable method to test the general theory of relativity via this parameter. ESA

N89-14624*# California Inst. of Tech., Pasadena.
DETERMINATION OF CONVERGENCE RATES ACROSS THE VENTURA BASIN, SOUTHERN CALIFORNIA, USING GPS AND HISTORICAL TRIANGULATION

ANDREA DONNELLAN, BRADFORD H. HAGER, and SHAWN LARSEN 1988 14 p
(Contract NAG5-842)
(NASA-CR-183014; NAS 1.26:183014) Avail: NTIS HC A03/MF A01 CSCL 08G

Comparison of angles from historical triangulation observations dating as far back as 1932 with Global Positions System (GPS) measurements taken in 1987 indicates that rapid convergence may be taking place on decade timescales in the central and eastern part of the Ventura basin, an east-west trending trough bounded by thrust faults. Changes in angles over this time were analyzed using Prescott's modified Frank's method and in terms of a model which assumes that the regions to the north and south of the basin are rigid blocks undergoing relative motion. For the two block model, inversion of the observed angle changes over the last 28 years for the relative motion vector leads to north-south convergence across the basin of 30 + or - 5 mm/yr, with a left lateral component of 10 + or - 1 mm/yr in the Fillmore-Santa Paula area in the central part of the basin. The modified Frank's method yields strain rates of approximately 2 microrad/yr in both the east and central parts of the basin for

measurements spanning the 1971 San Fernando earthquake. Assuming no east-west strain yields north-south compression of approximately 3.5 + or - .2 cm/yr. Comparison of triangulation data prior to the earthquake shows no strain outside the margin of error. The convergence rates determined by geodetic techniques are consistent with geologic observations in the area. Such large geodetic deformation rates, with no apparent near-surface creep on the major thrust, can be understood if these faults become subhorizontal at relatively shallow depths and if the subhorizontal portions of the faults are creeping. An alternative explanation of the large displacement rates might be that the pumping of oil in the vicinity of the benchmarks caused large horizontal motions, although it is unlikely that meter scale horizontal motions are due to oil withdrawal. These and other hypotheses are evaluated to better constrain the tectonics of this active region. Author

04

GEOLOGY AND MINERAL RESOURCES

Includes mineral deposits, petroleum deposits, spectral properties of rocks, geological exploration, and lithology.

A89-10326

EXTRACTING SPECTRAL INFORMATION FROM IMAGING SPECTROMETER DATA - A CASE HISTORY FROM THE NORTHERN GRAPEVINE MOUNTAINS, NEVADA/CALIFORNIA

FRED A. KRUSE (Cooperative Institute for Research in Environmental Sciences, Boulder, CO) IN: Imaging spectroscopy II; Proceedings of the Meeting, San Diego, CA, Aug. 20, 21, 1987. Bellingham, WA, Society of Photo-Optical Instrumentation Engineers, 1988, p. 119-128. USGS-supported research. refs

A89-10967#

SINO-AMERICAN COOPERATIVE STUDIES ON APPLICATIONS OF REMOTE SENSING TO SURVEYING AND MAPPING

DONALD T. LAUER (USGS, EROS Data Center, Sioux Falls, SD) and LIANGCAI CHU (National Bureau of Surveying and Mapping, Research Institute of Surveying and Mapping, Beijing, People's Republic of China) IN: International Symposium on Remote Sensing of Environment, 21st, Ann Arbor, MI, Oct. 26-30, 1987, Proceedings. Volume 1. Ann Arbor, MI, Environmental Research Institute of Michigan, 1987, p. 591-595.

The cooperation program initiated in April 1985 between the U.S. Geological Survey of the United States of America and the National Bureau of Surveying and Mapping of the People's Republic of China is described. The program will promote technical and scientific cooperation in the photogrammetry, remote sensing, cartography, and geographic information systems. The cooperative studies will use remotely sensed data from Landsat and SPOT for making image maps, thematic maps, and map revisions on scales of 1:50,000, 1:100,000, and 1:250,000 of the Ningxiang area in Hunan Province, China, and the Black Hills area in the state of South Dakota, U.S. To date, Chinese and American scientists have digitally processed Landsat TM data acquired over the Black Hills area and carried out radiometric calibrations, destripping, control point selection, geometric registration, resampling, selection, classification, and product generation. I.S.

A89-10976#

SIR-B VIEW OF THE JABAL HADN LINEAMENT AND ITS GROUNDWATER IMPLICATIONS

GRAYDON LENNIS BERLIN (Northern Arizona University, Flagstaff; King Abdulaziz Center for Science and Technology, Riyadh, Saudi Arabia), KAMEL M. SHEIKHO, and ABDULLAH H. AL-NASER (King Abdulaziz Center for Science and Technology, Riyadh, Saudi Arabia) IN: International Symposium on Remote Sensing of Environment, 21st, Ann Arbor, MI, Oct. 26-30, 1987, Proceedings. Volume 2. Ann Arbor, MI, Environmental Research Institute of Michigan, 1987, p. 709-719. refs

04 GEOLOGY AND MINERAL RESOURCES

SIR-B radar imagery of the shield terrain of the Jabal Hadn region in north-central Saudi Arabia clearly defines a 32-5-km long lineament that field study suggests is the trace of a dip-slip fault of precambrian age. The Jabal Hadn lineament coincides with a relatively straight and narrow valley that is cut in an assemblage of several different types of crystalline rock. Tonal image enhancement of the lineament was facilitated by a lack of backscatter response from the valley's specular surface, versus a strong backscatter response from bounding topographic foreslopes. Field observations indicate that the valley system could be acting as an aquiclude in influencing the movement and distribution of groundwater in the local region. Author

A89-10988#

DESERT VARNISH ON VOLCANIC ROCKS OF THE BASIN AND RANGE PROVINCE - COMPOSITION, MORPHOLOGY, DISTRIBUTION, ORIGIN AND INFLUENCE ON LANDSAT IMAGERY

D. M. SPATZ, J. V. TARANIK, and L. C. HSU (Nevada, University, Reno) IN: International Symposium on Remote Sensing of Environment, 21st, Ann Arbor, MI, Oct. 26-30, 1987, Proceedings. Volume 2. Ann Arbor, MI, Environmental Research Institute of Michigan, 1987, p. 843-852. refs

A89-11017#

A USEFUL MODEL IN MINERAL EXPLORATION WITH REMOTELY SENSED DATA

PIN QING WANG (Center for Remote Sensing in Geology, Beijing, People's Republic of China) IN: International Symposium on Remote Sensing of Environment, 21st, Ann Arbor, MI, Oct. 26-30, 1987, Proceedings. Volume 2. Ann Arbor, MI, Environmental Research Institute of Michigan, 1987, p. 1145-1152. refs

The paper presents a useful model for mineral exploration at a regional scale with the help of geostatistics and information from remotely sensed data, both on the linear structure and the lithologic spectral signature, for which one may quantitatively evaluate and predict mineral deposit distributions. General binomial distribution function and the concept of regionalized variable were used for the geological factors in one or two dimension domains. Author

A89-12290* Lamont-Doherty Geological Observatory, Palisades, NY.

SOMALI BASIN, CHAIN RIDGE, AND ORIGIN OF THE NORTHERN SOMALI BASIN GRAVITY AND GEOID LOW

JAMES R. COCHRAN (Lamont-Doherty Geological Observatory, Palisades, NY) Journal of Geophysical Research (ISSN 0148-0227), vol. 93, Oct. 10, 1988, p. 11985-12008. Navy-supported research. refs (Contract NAG5-881)

Geophysical data are used to investigate the origin of the Northern Somali Basin and its relationship to surrounding tectonic elements. The results show the Northern Somali Basin to be the third of a series of oceanic basins separated by long transform faults created during movement between East and West Gondwanaland. The flexure resulting from differential subsidence across Chain Ridge along with the difference in lithospheric thermal structure on either side of it can account for the amplitude and shape of the observed geoid step and gravity anomalies across Chain Ridge. It is suggested that the geoid and gravity low over the Northern Somali Basin may result from the superposition of a continental edge effect anomaly and the fracture zone edge effect anomaly. R.R.

A89-12292

MAGNETIC MINERALOGY IN AN ARCHEAN CRUSTAL CROSS SECTION - IMPLICATIONS FOR CRUSTAL MAGNETIZATION

PETER N. SHIVE and DAVID M. FOUNTAIN (Wyoming, University, Laramie) Journal of Geophysical Research (ISSN 0148-0227), vol. 93, Oct. 10, 1988, p. 12177-12186. refs (Contract NSF EAR-85-07061; NSF EAR-84-18350)

A traverse across Precambrian rocks from the Kapuskasing uplift in Ontario provided 31 samples from a crustal cross section

that is now exposed at the surface. About half the samples are dominantly paramagnetic. Magnetite, accompanied in a few samples by minor amounts of pyrrhotite, is the only significant magnetic mineral in the other half; magnetic susceptibilities of these samples are constant between room temperature and about 540 C, above which temperature they drop rapidly to zero. Magnetic susceptibility does not depend on rock type, apparent original depth in the crust, or degree of metamorphism. The average induced magnetization of the most magnetic units in this section is less than 1 A/m, which is much lower than the source requirements for the deep crust deduced from aeromagnetic and satellite magnetometer surveys. Author

A89-12358

DETECTION OF CIRCULAR GEOLOGICAL FEATURES USING THE HOUGH TRANSFORM

A. M. CROSS (NERC; Reading, University, England) International Journal of Remote Sensing (ISSN 0143-1161), vol. 9, Sept. 1988, p. 1519-1528. refs (Contract NERC-F60/G6/12)

The Hough transform is a technique commonly used in the field of computer vision for detecting lines and shapes in digital imagery. The application of this method to the detection of circular geological structures in Landsat Multispectral Scanner imagery is described. The method was successful in identifying most of those features apparent to the human analyst, in addition to a number of errors of commission. It is proposed that the error rate is tolerable for this particular application. Author

A89-14008

GEOLOGICAL MAPPING AND MINERAL EXPLORATION IN EASTERN NOVA SCOTIA UTILIZING AIRBORNE AND SPACEBORNE MULTISENSOR DATA

W. P. JONES and M. S. AKHAVI (College of Geographic Sciences, Lawrencetown, Canada) Geocarto International (ISSN 1010-6049), vol. 3, Sept. 1988, p. 31-36. Research supported by the Department of Energy, Mines, and Resources. refs

A89-14011

IMAGE ANALYSIS TECHNIQUES FOR THE INTERPRETATION OF AIRPHOTO LINEAMENTS - PETROLEUM EXPLORATION, EROMANGA BASIN, AUSTRALIA

GEOFFREY R. TAYLOR (New South Wales, University, Kensington, Australia) Geocarto International (ISSN 1010-6049), vol. 3, Sept. 1988, p. 53-60. refs

A89-15915* Jet Propulsion Lab., California Inst. of Tech., Pasadena.

RADAR POLARIMETRY - ANALYSIS TOOLS AND APPLICATIONS

DIANE L. EVANS, TOM G. FARR, JAKOB J. VAN ZYL, and HOWARD A. ZEBKER (California Institute of Technology, Jet Propulsion Laboratory, Pasadena) IEEE Transactions on Geoscience and Remote Sensing (ISSN 0196-2892), vol. 26, Nov. 1988, p. 774-789. refs

The authors have developed several techniques to analyze polarimetric radar data from the NASA/JPL airborne SAR for earth science applications. The techniques determine the heterogeneity of scatterers with subregions, optimize the return power from these areas, and identify probable scattering mechanisms for each pixel in a radar image. These techniques are applied to the discrimination and characterization of geologic surfaces and vegetation cover, and it is found that their utility varies depending on the terrain type. It is concluded that there are several classes of problems amenable to single-frequency polarimetric data analysis, including characterization of surface roughness and vegetation structure, and estimation of vegetation density. Polarimetric radar remote sensing can thus be a useful tool for monitoring a set of earth science parameters. I.E.

A89-17694#

PROJECT VASUNDHARA - MULTI-THEME INTEGRATION OF SATELLITE REMOTE SENSING AND GEOLOGICAL DATA FOR REGIONAL LEVEL MINERAL PROGNOSTICS

T. S. SESHADRI, M. PONNUSWAMY, V. SUBRAHMANYAM, R. K. CHOUDHARY, T. V. RAMACHANDRAN (Geological Survey of India, Bangalore, India) et al. IAF, International Astronautical Congress, 39th, Bangalore, India, Oct. 8-15, 1988. 9 p. (IAF PAPER 88-145)

A three-year collaborative program called Project Vasundhara has been launched in India with the aim of identifying and mapping regional lithostratigraphic, structural, and geoenvironmental guides to mineral localization and adopting geostatistical guides to assess mineral prognostics. The program also aims to develop computer overlay techniques and a geographic information system data base for presenting thematic data, developing a methodology for multilevel, multitheme data integration, and delineating potential target areas for mineral research. The availability of geoscientific data using satellite imagery is reviewed, and the rationale for using an approach integrating remote sensing data with geological data is described. The project methodology is summarized and delineation of regional targets for mineral search is examined for the various geological regions of India. C.D.

A89-18705

THE ROLE OF LINEAR AND RING FEATURES IN HYDROGEOLOGY [O GIDROGEOLOGICHESKOI ROLI LINEINYKH I KOL'TSEVYKH STRUKTUR]

F. SH. AMIRKHANOVA and A. K. GLUKH (Gosudarstvennyi Nauchno-Issledovatel'skii i Proizvodstvennyi Tsentr Priroda, USSR) Issledovanie Zemli iz Kosmosa (ISSN 0205-9614), July-Aug. 1988, p. 31-35. In Russian. refs

This paper discusses the significance of the linear and the ring structures observed on remote photographs for the evaluation of the direction of the movement of underground streams. A map of lineaments and ring structures was analyzed, in parallel with a landscape map of Uzbekistan, and the tectonic features identified by interpretation of remote images were compared with those found on a hydrogeological map constructed by traditional methods. It was found that tectonic distortions such as faults, regional fault zones, and ring structures identifiable on remote images can be correlated with different hydrogeological features. I.S.

A89-18706

RECOGNITION OF SEISMICALLY HAZARDOUS FAULT DISLOCATIONS IN SPACE IMAGES OF THE DUSHANBE DEPRESSION [OPYT VYIAVLENIIA NA KOSMICHESKIIH SNIMKAKH SEISMOOPASNYKH RAZRYVNYKH NARUSHENII V DUSHANBINSKOM PROGIBE]

IU. N. PIL'GUI and A. K. GAIKOVA (Nauchno-Proizvodstvennoe Ob'edinenie Tadzhikaerokosmogeodeziia, Dushanbe, Tadzhik SSR) Issledovanie Zemli iz Kosmosa (ISSN 0205-9614), July-Aug. 1988, p. 36-40. In Russian. refs

A89-18707

ENGINEERING EVALUATION OF MOUNTAIN TOPOGRAPHY EXODYNAMICS FROM REMOTELY SENSED DATA [INZHENERNAIA OTSENKA EKZODINAMIKI GORNOGO REL'EFA PO DANNYM S'EMKI IZ KOSMOSA]

A. L. REVZON, A. P. BGATOV, A. I. BOGDANOV, and A. M. BOGDANOV (Vsesoiuznyi Nauchno-Issledovatel'skii Institut Transportnogo Stroitel'stva, Moscow, USSR) Issledovanie Zemli iz Kosmosa (ISSN 0205-9614), July-Aug. 1988, p. 41-48. In Russian.

This paper describes a computer-aided thematic mapping method based on remotely sensed data and engineering calculations. It is shown that large-scale remotely sensed data can be used to analyze the exodynamics of various elements of mountain topography, such as rock-fall niches, landslide bodies, collapse trails, mud-flow beds, and debris cones. The method can be used to account for exogenous dynamic processes in planning railway and highway construction projects in mountainous areas. I.S.

A89-19838* Lunar and Planetary Inst., Houston, TX.

LANDSAT THEMATIC MAPPER OBSERVATIONS OF DEBRIS AVALANCHE DEPOSITS IN THE CENTRAL ANDES

P. W. FRANCIS and G. L. WELLS (Lunar and Planetary Institute, Houston, TX) Bulletin of Volcanology (ISSN 0258-8988), vol. 50, 1988, p. 258-278. refs

(Contract NAS5-28759; NASW-4066; NAGW-1167)

Remote sensing with the Landsat Thematic Mapper of debris avalanche deposits in the Central Andes between 18 and 27 deg S revealed, for the first time, the presence of 28 breached volcanic cones and 11 major volcanic debris avalanche deposits, several of which cover areas in excess of 100 sq km. It is concluded that such avalanche deposits are normal products of the evolution of large composite volcanoes, comparable with lava and pyroclastic flow deposits. A statistical survey of 578 composite volcanoes in the same area indicated that a majority of cones which achieve edifice heights between 2000 and 3000 m may undergo sector collapse. The paper describes morphological criteria for identifying breached composite cones and volcanic debris avalanches using orbital images. I.S.

A89-20628

REMOTE SENSING OF LATERIZED ARCHAEAN GREENSTONE TERRAIN - MARSHALL POOL AREA, NORTHEASTERN YILGARN BLOCK, WESTERN AUSTRALIA

S. A. DRURY and G. A. HUNT (Open University, Milton Keynes, England) Photogrammetric Engineering and Remote Sensing (ISSN 0099-1112), vol. 54, Dec. 1988, p. 1717-1725. refs

(Contract NERC-GS/T/02/125)

Airborne multispectral image data were tested over an intractable terrain of deeply lateritized Archaean basic and ultrabasic igneous rocks in Australia. The data are equivalent to those available from the Landsat-5 TM. The use of likely spectral features in weathered rocks and lateritic soils to select combinations of bands and interband ratios to display in color is discussed. Also, ways of overcoming the high interband correlations which produce muted color images are considered. Geological maps from the images are compared with conventional maps. R.B.

A89-20709

MINERAL EXPLORATION ALONG THE AQABA-LEVANT STRUCTURE BY USE OF TM-DATA - CONCEPTS, PROCESSING AND RESULTS

H. KAUFMANN (Karlsruhe, Universitaet, Federal Republic of Germany) (European Association of Remote Sensing Laboratories, Annual Symposium on European Remote Sensing Needs in the 1990s, Noordwijkerhout, Netherlands, May 4-8, 1987) International Journal of Remote Sensing (ISSN 0143-1161), vol. 9, Oct.-Nov. 1988, p. 1639-1658. DFG-supported research. refs

The capabilities and limitations of spaceborne TM data and associated image processing techniques for mineral exploration in the area along the Aqaba-Levant structure in Jordan are evaluated. Different approaches involving ratioing, principal component analysis, and IHS-decorrelation processing are used to enhance the diagnostic features associated with hydrothermally altered areas. It is found that ratio and principal components approaches often fail to clearly accentuate diagnostic features. It is shown that decorrelated and filtered color composites of TM bands 1, 4, and 7 are successful for delineation of known and unknown mineralizations by the presence of alteration guide minerals such as iron oxides and phyllosilicates. R.B.

A89-20710

USE OF LANDSAT AND SEASAT DATA AS A TOOL IN KINEMATIC ANALYSIS - THE TUNISIAN ATLAS

C. M. MARINO and A. TIBALDI (Milano, Universita, Milan, Italy) (European Association of Remote Sensing Laboratories, Annual Symposium on European Remote Sensing Needs in the 1990s, Noordwijkerhout, Netherlands, May 4-8, 1987) International Journal of Remote Sensing (ISSN 0143-1161), vol. 9, Oct.-Nov. 1988, p. 1659-1673. refs

Brittle and plastic deformations of the Tunisian Atlas were studied using Landsat data, Seasat SAR data and field surveys.

Locations of structural stations were guided by detailed analysis of images and computer compatible tapes. Digital processing and enlargements at scales of 1:100,000 and 1:200,000 allowed the recognition of several fault displacements and strata dips, followed by field checks. This paper presents an original and complete structural map of the Tunisian Atlas. Four principal deformational phases, developed from the Palaeogene to the Holocene, have been recognized and discussed. Stress field evolution is presented and compared with plate tectonic knowledge of the Western Mediterranean Basin.

Author

N89-10313# Paris VI Univ. (France).

EVALUATION OF VARAN DATA IN GEOLOGY AND GEOMORPHOLOGY IN THE SOUTHEAST OF FRANCE [EVALUATION DES DONNEES VARAN EN GEOLOGIE ET EN GEOMORPHOLOGIE SUR LE SUD-EST DE LA FRANCE]

J. P. RUDANT, B. CERVELLE, J. CHOROWICZ, P. DURAND, P. KAMOUN, S. LOUAHALA, L. POLIDORI, S. RIAZANOFF, A. SIMONIN, and I. TANNOUS (Paris VII Univ., France) In ESA, Proceedings of the 4th International Colloquium on Spectral Signatures in Remote Sensing p 47-50 Apr. 1988 In FRENCH
 Avail: NTIS HC A23/MF A01; ESA Publications Division, ESTEC, Noordwijk, Netherlands 80 Dutch guilders

The utility of synthetic aperture radar imagery for geology and geomorphology was assessed using the VARAN airborne system. Filtering, pattern recognition, multisource data superpositioning, and stereoscopy are discussed. Image interpretation and digital terrain models are considered. Advantages of the technique over traditional aerial photography and spaceborne imagery are shown.

ESA

N89-10337# Iceland Univ., Reykjavik. Lab. for Information Technology and Signal Processing.

STRENGTHS AND SHORTCOMINGS IN AIRBORNE THEMATIC MAPPER (ATM) TECHNOLOGY AS APPLIED TO VOLCANIC AND GEOTHERMAL AREAS IN ICELAND

S. BJORNSSON and K. ARNASON (Technische Univ., Munich, West Germany) In ESA, Proceedings of the 4th International Colloquium on Spectral Signatures in Remote Sensing p 189-191 Apr. 1988

Avail: NTIS HC A23/MF A01; ESA Publications Division, ESTEC, Noordwijk, Netherlands 80 Dutch guilders

Experiments with an airborne thermal scanner of conventional design were conducted to test the applicability of airborne thematic mappers to geothermal research in Iceland. Results from two thermal areas which show strengths and shortcomings of the method as commonly applied are presented. The technology provides much better global data on the spatial distribution of surface temperatures than any other previously obtained. Sites of convective thermal output inside geothermal areas are readily discernible because of their relatively high temperatures, but in areas where heat conduction plays a primary role, subtle temperature differences can not be differentiated, in particular on surface materials with varying emissivities. Due to lack of radiometric resolution, discrimination of slight temperature variations especially in regions of low to moderate temperatures is insufficient. The result of the observations led to the development of an improved thermal scanner in the 8 to 14 micron wavelength range.

ESA

N89-10360# Paris VI Univ. (France). Lab. de Mineralogie-Cristallographie.

USEFULNESS OF HIGH SPECTRAL RESOLUTION RADIOMETRY FOR GEOLOGICAL MAPPING IN THE MEDITERRANEAN REGION [INTERET DE LA RADIOMETRIE A HAUTE RESOLUTION SPECTRALE POUR LA CARTOGRAPHIE GEOLOGIQUE EN REGION MEDITERRANEENE]

S. LOUAHALA, B. CERVELLE, J. CHOROWICZ, J.-P. RUDANT, and J.-Y. SCANVIC (Bureau de Recherches Geologiques et Minieres, Orleans, France) In ESA, Proceedings of the 4th International Colloquium on Spectral Signatures in Remote Sensing p 311-314 Apr. 1988 In FRENCH

Avail: NTIS HC A23/MF A01; ESA Publications Division, ESTEC, Noordwijk, Netherlands 80 Dutch guilders

Absorbance spectra between 470 and 910 nm were acquired on the ground, using a spectroradiometer, for 30 different lithologies representing 8 types representative of the Mediterranean area. Their form is mainly decided by the presence on the surface of iron in the form of oxide and chlorophyll micro-organisms on the surface of the rocks. The study shows that natural geological surfaces in the Mediterranean region have important spectral variations over short distances. Information contained in the ground spectra of these surfaces are only extremely roughly correlated with the underlying lithology. In favorable cases, positioning in the 540 to 600 nm band can restore the most important ferrous contrasts. Spectral resolution less than 20 nm does not improve discrimination between the rocks studied for such surfaces.

ESA

N89-10362# Paris VI Univ. (France). Lab. Mineralogie-Cristallographie.

CHARACTERIZATION OF ROCKS BY VISIBLE AND INFRARED HIGH SPECTRAL RESOLUTION TERRAIN SPECTROSCOPY [CARACTERISATION DES ROCHES PAR SPECTROMETRIE DE TERRAIN A HAUTE RESOLUTION SPECTRALE VISIBLE ET INFRAROUGE PROCHE]

B. CERVELLE, J. CHOROWICZ, J.-P. RUDANT, G. TAMAIN, and E. M. ALEM (Mohammed V Univ., Rabat, Morocco) In ESA, Proceedings of the 4th International Colloquium on Spectral Signatures in Remote Sensing p 319-322 Apr. 1988 In FRENCH

Avail: NTIS HC A23/MF A01; ESA Publications Division, ESTEC, Noordwijk, Netherlands 80 Dutch guilders

Two spectral signatures were derived from the analysis of 200 high spectral resolution spectra at 500 and 900 nm of rocky terrain in an arid region: those of ferrous iron and those of an acid/base character of the rocks. They are represented by indexes for the SPOT bands. However, surface alterations and roughness mask the fine spectral characteristics of the underlying lithology. Processing of SPOT data, given their geometrical quality, does nonetheless discriminate between and outline with precision, the various rock faces; spectral signatures appear to be amplified by morphological signatures. The case of remote sensing of heavenly bodies with no atmosphere, little subject to alteration, but bombarded by meteorites and cosmic rays is quoted.

ESA

N89-10366*# National Aeronautics and Space Administration. Goddard Space Flight Center, Greenbelt, MD.

THE BASIS FOR THE SPECTRAL BEHAVIOUR OF SILICATES IN THE THERMAL INFRARED AND APPLICATIONS TO REMOTE SENSING

L. S. WALTER and J. W. SALISBURY (Geological Survey, Reston, Va.) In ESA, Proceedings of the 4th International Colloquium on Spectral Signatures in Remote Sensing p 337-340 Apr. 1988
 Avail: NTIS HC A23/MF A01; ESA Publications Division, ESTEC, Noordwijk, Netherlands 80 Dutch guilders CSCL 02F

Variations in the thermal infrared (TIR) spectral response of silicate rocks is related to changes in the structures and divalent cation contents of the minerals which form the rocks. These considerations lead to a chemical parameter, SCFM, which reflects mineral structures, rock types, and their spectra. The parameter is the ratio of silica to the abundance of depolymerizing cations, defined as $SCFM = SiO_2 / (SiO_2 + CaO + MgO + FeO)$. Parameter SCFM is therefore proposed for use in TIR remote sensing of igneous rocks. It is also demonstrated that two or three broad bands are sufficient for distinguishing among major rock types and the system noise has little effect on the quality of the results. These factors can be traded off against improved spatial resolution in instrument design.

ESA

N89-10377*# National Aeronautics and Space Administration. Lyndon B. Johnson Space Center, Houston, TX.

EMITTED SHORT WAVELENGTH INFRARED RADIATION FOR DETECTION AND MONITORING OF VOLCANIC ACTIVITY

D. A. ROTHERY, P. W. FRANCIS (Open Univ., Milton, England), and C. A. WOOD In ESA, Proceedings of the 4th International

Colloquium on Spectral Signatures in Remote Sensing p 399-402
Apr. 1988

(Contract NASW-4066)

Avail: NTIS HC A23/MF A01; ESA Publications Division, ESTEC, Noordwijk, Netherlands 80 Dutch guilders CSDL 02F

Thematic Mapper images from LANDSAT were used to monitor volcanoes. Achievements include: (1) the discovery of a magmatic precursor to the 16 Sept. 1986 eruption of Lascar, northern Chile, on images from Mar. and July 1985 and of continuing fumarolic activity after the eruption; (2) the detection of unreported major changes in the distribution of lava lakes on Erta Ale, Ethiopia; and (3) the mapping of a halo of still-hot spatter surrounding a vent on Mount Erebus, Antarctica, on an image acquired 5 min after a minor eruption otherwise known only from seismic records. A spaceborne short wavelength infrared sensor for observing hot phenomena of volcanoes is proposed. A polar orbit is suggested.
ESA

N89-10380# Phillips Petroleum Co., Bartlesville, OK.

THE RESULTS OF THE GEOSAT MOMS SUBCOMMITTEE'S DATA EVALUATION: PERFORMANCE AND APPLICABILITY OF THE MOMS-1 SENSOR FOR EXPLORATION GEOLOGY

G. I. BALLEW and F. B. HENDERSON, III (Geosat Committee, Inc., Norman, Okla.) /n ESA, Proceedings of the 4th International Colloquium on Spectral Signatures in Remote Sensing p 413-423
Apr. 1988

Avail: NTIS HC A23/MF A01; ESA Publications Division, ESTEC, Noordwijk, Netherlands 80 Dutch guilders

Digital imagery from 14 sites in Africa, Asia, Australia, and South America acquired by the MOMS-01 sensor on Space Shuttle flight STS-4 (41-B) in February 1984 was analyzed to determine suitability for hydrocarbon energy and mineral exploration by comparison with geological maps and other satellite data. The MOMS two-band spectral data and 20m resolution display many geological and vegetation features discernable on LANDSAT and SPOT data. The MOMS limitations include striping, limited gray shades, non-map geometry, and large data size. On balance, MOMS provides high resolution data useful for international energy and mineral exploration.
ESA

N89-10382# Paris VI Univ. (France). Dept. de Geotectonique. THE USE OF MOMS-1 DATA FOR GEOLOGICAL MAPPING OF THE ASWA LINEAMENT (EAST AFRICAN RIFT)

J. CHOROWICZ, M. GUEZLANE, J.-P. RUDANT, and G. VIDAL /n ESA, Proceedings of the 4th International Colloquium on Spectral Signatures in Remote Sensing p 431-434 Apr. 1988

Avail: NTIS HC A23/MF A01; ESA Publications Division, ESTEC, Noordwijk, Netherlands 80 Dutch guilders

The MOMS-01 characteristics (20 m ground resolution, two spectral bands, the yellow band expressing the drainage pattern, the infrared one giving geomorphology, and synoptic view) were exploited to produce a geological map of the large Aswa lineament zone. This zone appears to be a Late Proterozoic NW-SE fault zone due to the wrapping of the Mozambiquian belt around the Tanzanian shield. Frontal and lateral ramps developed in the belt were reworked respectively as normal and transcurrent faults of the East African Rift, responsible for virgation of the Gregory Rift. The NE trending fault direction expressed in the Archean basement, resulted in the Nyanza graben formation.
ESA

N89-10383# Dundee Univ. (Scotland). Dept. of Applied Physics and Electronic and Manufacturing Engineering.

MOMS-1 DATA FOR BATHYMETRIC AND GEOLOGICAL STUDIES

A. K. SARAF, A. P. CRACKNELL, and M. IBRAHIM /n ESA, Proceedings of the 4th International Colloquium on Spectral Signatures in Remote Sensing p 435-438 Apr. 1988

Avail: NTIS HC A23/MF A01; ESA Publications Division, ESTEC, Noordwijk, Netherlands 80 Dutch guilders

The MOMS data from the Shuttle flights STS-7 and STS-11 were used to investigate water depths in the Red Sea and for geological studies in Burma, respectively. For the Red Sea an exponential relationship between pixel intensity and water depth

is obtained but the root-mean-square deviation of the fit of the data to control points is 3.7 m which is far too large for operational bathymetric work. The main reason for this is the low sensitivity of the instrument for the typical intensities received from the water. The data for Burma are useful for structural mapping but for lithological mapping the spectral response of rocks is less sensitive.
ESA

N89-10384# Open Univ., Milton (England). Dept. of Earth Sciences.

MOMS-1 USED SYNERGISTICALLY WITH LANDSAT TM

D. A. ROTHERY /n ESA, Proceedings of the 4th International Colloquium on Spectral Signatures in Remote Sensing p 439-442
Apr. 1988

Avail: NTIS HC A23/MF A01; ESA Publications Division, ESTEC, Noordwijk, Netherlands 80 Dutch guilders

It is shown how the best attributes of MOMS-01 imagery and LANDSAT TM can be combined to make an optimized image. For many geological applications, the important information within an image can be considered as comprising textural and spectral components. Because of the non-sun-synchronous orbit of the Space Shuttle, MOMS-01 acquired many images during low solar elevation which shows up topographic textural features very well. The TM records much more spectral information than MOMS-01, which can be emphasized by decorrelation stretching and related techniques. By modulating three enhanced TM channels by one of the MOMS-01 channels, a color composite can be produced which combines the spectral advantages of TM with the textural detail recorded by MOMS-01.
ESA

N89-10385# Technische Univ., Munich (Germany, F.R.). Inst. for General and Applied Geology.

COMPARATIVE GEOLOGICAL EVOLUTION OF DIFFERENT REMOTE SENSING DATA OF THE HOGGAR MOUNTAINS (ALGERIA)

F. JASKOLLA and M. RAST (European Space Agency. European Space Research and Technology Center, ESTEC, Noordwijk, Netherlands) /n ESA, Proceedings of the 4th International Colloquium on Spectral Signatures in Remote Sensing p 443-450
Apr. 1988

Avail: NTIS HC A23/MF A01; ESA Publications Division, ESTEC, Noordwijk, Netherlands 80 Dutch guilders

The suitability for geological mapping of spaceborne remote sensing data (LANDSAT-5 TM, MOMS-01, Metric Camera and SIR-A) of the Hoggar Mountains (Algeria) was assessed. The optoelectronic MOMS-01 data prove their suitability for the task. Qualitative differences with comparable LANDSAT TM bands are not significant. Additional data are of great importance, especially the availability of stereoscopic data for geological applications. They can provide information which can not be collected by multispectral scanning systems. Radar data offer distinct improvements especially in sand covered areas; however, the question must be put if the information gain is in relation to the enormous costs of a required multifrequency/multipolarization radar system.
ESA

N89-10386# Technische Univ., Munich (Germany, F.R.). Inst. for General and Applied Geology.

DIGITAL ANALYSIS OF MOMS-1, LANDSAT TM, AND SPOT DATA OF THE NAKURU AREA (KENYA)

J. HENKEL, U. TERHALLE, and J. ZILGER /n ESA, Proceedings of the 4th International Colloquium on Spectral Signatures in Remote Sensing p 451-456 Apr. 1988

Avail: NTIS HC A23/MF A01; ESA Publications Division, ESTEC, Noordwijk, Netherlands 80 Dutch guilders

Data from MOMS were compared with LANDSAT TM and SPOT for geoscientific thematic mapping. When operating in gain level 1, MOMS has a lower dynamic range than TM; switched to gain position 2, the dynamic ranges are comparable. The infrared band of MOMS-01, which was out of focus during the first mission, then tried to be corrected during the refurbishment, still is slightly out of focus; in processings where the visible channel is included, the overall detectability is not reduced, because it is controlled by

the highest resolving data set of the product. The radiometric correction procedures, though improved for the STS-11/41-B flight by introducing preflight calibration tables in dependence of the saturation (steps of 5 percent starting from 0 to 100 percent), still leaves sensor invariances, in flight and across flight direction; gray value variations are between 1 and 2. The optoelectronic concept provides for a high geometric accuracy. In terms of the SPOT/TM comparison, the spectral range presently available for optoelectronic systems (VIS to NIR) is not utilized optimally for applications, for geologic as for those of renewable resources.

ESA

N89-10401*# National Aeronautics and Space Administration, Washington, DC.

SAPPING FEATURES OF THE COLORADO PLATEAU: A COMPARATIVE PLANETARY GEOLOGY FIELD GUIDE

ALAN D. HOWARD, ed., R. CRAIG KOCHER, ed., and HENRY E. HOLT, ed. (Geological Survey, Flagstaff, Ariz.) 1987 115 p Original contains color illustrations (Contract NSG-7572)

(NASA-SP-491; NAS 1.21:491; LC-87-15305) Avail: NTIS HC A06/MF A01; also available SOD HC \$6.00 as 003-000-01027-3 CSDL 08H

This book is an attempt to determine geomorphic criteria to be used to distinguish between channels formed predominantly by sapping and seepage erosion and those formed principally by surface runoff processes. The geologic nature of the Colorado Plateau has resulted in geomorphic features that show similarities to some areas on Mars, especially certain valley networks within thick sandstone formations. Where spring sapping is an effective process, the valleys that develop are unique in terms of their morphology and network pattern.

Author

N89-12950*# Jet Propulsion Lab., California Inst. of Tech., Pasadena.

INFERENCE OF GEOLOGIC SURFACE PARAMETERS FROM POLARIMETRIC RADAR OBSERVATIONS AND MODEL INVERSION

JAKOB J. VANZYL, P. C. DUBOIS, H. A. ZEBKER, and T. G. FARR /In ESA, Proceedings of the 1988 International Geoscience and Remote Sensing Symposium (IGARSS 1988) on Remote Sensing: Moving Towards the 21st Century, Volume 1 p 51-52 Aug. 1988

Avail: NTIS HC A99/MF E03; ESA Publications Div., ESTEC, Noordwijk, Netherlands, 120 US dollars or 250 Dutch guilders CSDL 08G

The results of inferring geologic parameters such as rms surface height, correlation length, and dielectric constant of rough surfaces by fitting observed polarization signatures with those predicted by the second order Rice model are discussed. The inferred results are compared to measured values of rms height and correlation length. The rms height values inferred are in good agreement with in situ measurements. The inferred correlation lengths generally do not agree with measured values. The results allow the separation of the effects of surface roughness and dielectric constant on the overall backscatter from rough surfaces.

ESA

N89-13022# Griffiths Remote Sensing, London (England). **THE RELATIVITY UTILITY OF LANDSAT MSS AND SIR-A IMAGERY IN RECONNAISSANCE GEOLOGICAL MAPPING IN NORTHERN SUDAN**

P. S. GRIFFITHS /In ESA, Proceedings of the 1988 International Geoscience and Remote Sensing Symposium (IGARSS 1988) on Remote Sensing: Moving Towards the 21st Century, Volume 1 p 359-362 Aug. 1988

Avail: NTIS HC A99/MF E03; ESA Publications Div., ESTEC, Noordwijk, Netherlands, 120 US dollars or 250 Dutch guilders

Reconnaissance geological mapping for mineral exploration of crystalline basement in the Sudanese Nubian Desert was carried out by interpretation of LANDSAT MSS, LANDSAT RBV, and SIR-A imagery, helped by a field-check. Radar and simply-enhanced MSS imagery are compared. Although the SIR-A data provide the greater density of structural information, both image types give a similar

overall impression of rock-unit variation, structure and geological history. Since reconnaissance work normally demands acquisition by the simplest means of a broad range of geological information, it is concluded that the required result could be obtained using MSS imagery alone, although the interpretation of other image types raises confidence in the result.

ESA

N89-13023# Open Univ., Milton (England). Dept. of Earth Sciences.

A REGIONAL TECTONIC STUDY OF NE AND E AFRICA AND ITS IMPLICATION FOR MINERAL EXPLORATION: A SYNOPSIS VIEW FROM SATELLITE IMAGERY

S. M. BEHRE /In ESA, Proceedings of the 1988 International Geoscience and Remote Sensing Symposium (IGARSS 1988) on Remote Sensing: Moving Towards the 21st Century, Volume 1 p 363-366 Aug. 1988

Avail: NTIS HC A99/MF E03; ESA Publications Div., ESTEC, Noordwijk, Netherlands, 120 US dollars or 250 Dutch guilders

The regional tectonic framework of NE and E Africa was established, based on a study of published maps and reports, fieldwork, and remote sensing data. The major lineaments identified in the Horn of Africa are 010 + or - 10 deg., 055 to 065 deg. and 145 to 165 deg. The earliest conjugate fractures are N-S and NW-SE trending. A later deformation episode produced NE-SW lineaments but also reactivated NW-SE trending lineaments. These lineaments extended histories from the late Proterozoic to the Tertiary and were reactivated repeatedly during the breakup of Gondwanaland. They controlled ore deposits, basin sedimentation and subsequently controlled the evolution of the East African Rift system. Tectonic and metallogenic evolution of the NE Sudan-Eritrea region is cited as a case study.

ESA

N89-13024# Reading Univ. (England). NERC Unit for Thematic Informations Systems.

MAPPING THE DISTRIBUTION AND ABUNDANCE OF LITHOLOGICAL UNITS AND SURFACE MINERALOGIES AT JABAL SA'ID, SAUDI ARABIA: AN APPLICATION OF SPECTRAL MIXTURE MODELLING

N. DRAKE, S. MACKIN, T. J. MUNDAY, J. SETTLE, and A. AL-SARI (Durham Univ., England) /In ESA, Proceedings of the 1988 International Geoscience and Remote Sensing Symposium (IGARSS 1988) on Remote Sensing: Moving Towards the 21st Century, Volume 1 p 367-368 Aug. 1988

Avail: NTIS HC A99/MF E03; ESA Publications Div., ESTEC, Noordwijk, Netherlands, 120 US dollars or 250 Dutch guilders

The spatial distribution of various lithologies, and in particular the abundance of particular surface mineralogies relating to the alteration found around Jabal Sa'id (Saudi Arabia), were examined and compared using data acquired by LANDSAT TM and an airborne multispectral scanner. These systems provide information on the spatial distributions of certain mineralogies based upon the strength and position of spectral absorption features located in the wavelength region 0.4 to 2.4 micrometer. In the study area, observed absorptions are due primarily to the presence of iron (hematite and limonite) and various phyllosilicates (chlorite, sericite). Airborne and LANDSAT data agree.

ESA

N89-13025# Open Univ., Milton (England). Dept. of Earth Sciences.

THE NEED FOR VOLCANO MONITORING AND THE ABILITY TO DETECT ACTIVITY USING EMITTED SHORT WAVELENGTH INFRARED

D. A. ROTHERY /In ESA, Proceedings of the 1988 International Geoscience and Remote Sensing Symposium (IGARSS 1988) on Remote Sensing: Moving Towards the 21st Century, Volume 1 p 369-372 Aug. 1988

Avail: NTIS HC A99/MF E03; ESA Publications Div., ESTEC, Noordwijk, Netherlands, 120 US dollars or 250 Dutch guilders

It is argued that remote sensing in the short wavelength infrared (SWIR) has the potential for providing a great deal of information about activity at volcanoes, by virtue of the radiation emitted by hot surfaces. This can be used to give warning of imminent eruptions, monitor their progress, and model volcanic processes.

The LANDSAT TM is the only operational instrument which returns suitable data. This is particularly valuable because it incorporates two SWIR bands enabling constraints to be put on the sub-pixel structure of the image. Current orbital thermal infrared imagery (e.g., AVHRR, TM band 6) cannot resolve most volcanic thermal anomalies because the pixel size is too coarse. Moreover, the gains of operational thermal infrared sensors make them unsuitable for measuring volcanic temperatures. ESA

N89-13026# Sheffield Univ. (England). Dept. of Geography.
**IMPROVING THE ACCESSIBILITY OF SPATIALLY
 REFERENCED GEOLOGICAL INFORMATION**

S. M. BLACK *In* ESA, Proceedings of the 1988 International Geoscience and Remote Sensing Symposium (IGARSS 1988) on Remote Sensing: Moving Towards the 21st Century, Volume 1 p 373-374 Aug. 1988

Avail: NTIS HC A99/MF E03; ESA Publications Div., ESTEC, Noordwijk, Netherlands, 120 US dollars or 250 Dutch guilders

The structure and operation of an idealized data integration and analysis system is outlined. It is based on an advanced micro or minicomputer and embodies aspects of graphics/image processing and geographic information systems (GIS) technology within a desktop environment. The aim of the system is to improve the accessibility of spatially referenced information for geological research and application on a local and regional level. However, the system's operational capabilities and structures are equally applicable in other areas of Earth science and nonrelated fields. ESA

N89-13027# Dundee Univ. (Scotland). Dept. of Applied Physics and Electronic and Mfg. Engineering.

**THE INTERPRETATION OF ICELANDIC TUNDRA FEATURES
 FROM LANDSAT-MSS DATA**

R. A. VAUGHAN and P. O. VAUGHAN (Imperial Coll. of Science and Technology, London, England) *In* ESA, Proceedings of the 1988 International Geoscience and Remote Sensing Symposium (IGARSS 1988) on Remote Sensing: Moving Towards the 21st Century, Volume 1 p 375-376 Aug. 1988

Avail: NTIS HC A99/MF E03; ESA Publications Div., ESTEC, Noordwijk, Netherlands, 120 US dollars or 250 Dutch guilders

A multidisciplinary expedition to Iceland collected summer ground truth data from the area east of the Vatnajökull ice-cap. Geological and geomorphological features within this area were identified on the ground and using air photographs, and correlated with LANDSAT MSS imagery. Because of the very low percentage of vegetation cover, exposed rock surfaces, gravel plains, and large (over 200 m high) scree slopes can be identified on such imagery. These features are particularly well-defined on principal component color composites, although attempts at meaningful classification are not successful due to poor discrimination in feature space and high correlation between bands. ESA

N89-13087# Geological Survey of Britain, Nottingham.
**APPLICATIONS OF REMOTE SENSING FOR GEOLOGICAL
 MAPPING IN EASTERN EGYPT**

E. A. OCONNOR and A. J. W. MCDONALD *In* ESA, Proceedings of the 1988 International Geoscience and Remote Sensing Symposium (IGARSS 1988) on Remote Sensing: Moving Towards the 21st Century, Volume 1 p 631-632 Aug. 1988

Avail: NTIS HC A99/MF E03; ESA Publications Div., ESTEC, Noordwijk, Netherlands, 120 US dollars or 250 Dutch guilders

Results from a mapping project illustrate the relative contributions from multivariate remote sensing data sets to structural and lithological discrimination in a tectonically-mixed terrain of a hyper-arid climatic zone. Structural and morphological detail are well served by air and space photography depending on map-scale requirements. Shuttle-borne radar fulfils a similar role but can yield additional information in areas veneered by thin sand sheets, e.g., dykes in degraded granite plutons. The LANDSAT MSS data is widely available at modest cost and provides an efficient means of producing scalimetrically-accurate image interpreted geological and topographical maps. When more highly detailed lithological extraction is required for mineral exploration

and groundwater assessment, the wider infrared wavebands and improved pixel resolution of the LANDSAT TM is an indispensable and cost-effective data base. ESA

N89-13093# Alaska Univ., Fairbanks. Petroleum Development Lab.

DEVELOPMENT OF ALASKAN GAS HYDRATE RESOURCES

Annual Report, Oct. 1986 - Sep. 1987

G. D. SHARMA, V. A. KAMATH, S. P. GODBOLE, S. L. PATIL, SURESH G. PARANJPE, PRALHAD MUTALIK, and MEHRDAD NADEM Oct. 1987 223 p

(Contract DE-FG21-86FE-61114)

(DE88-010270; DOE/FE-61114/2608) Avail: NTIS HC A10/MF A01

Solid ice-like mixtures of natural gas and water in the form of natural gas hydrated have been found immobilized in the rocks beneath the permafrost in Arctic basins and in muds under the deep water along the American continental margins, in the North Sea and several other locations around the world. It is estimated that the arctic areas of the United States may contain as much as 500 trillion SCF of natural gas in the form of gas hydrates (Lewin and Associates, 1983). While the U.S. Arctic gas hydrate resources may have enormous potential and represent long term future source of natural gas, the recovery of this resource from reservoir frozen with gas hydrates has not been commercialized yet. Continuing study and research is essential to develop technologies which will enable a detailed characterization and assessment of this alternative natural gas resource, so that development of cost effective extraction technology. This study presents a state-of-the-art review of the various aspects related to gas hydrates. Reviews on gas hydrated have been published earlier by Byk and Fomina (1968) and Makogen (1981). Since then, many articles have been published on different aspects of gas hydrates. An attempt has been made in this review to provide a more complete and up-to-date information of gas hydrate literature. DOE

N89-14477# National Academy of Sciences - National Research Council, Washington, DC. Commission on Physical Sciences, Mathematics and Resources.

GEOLOGIC MAPPING IN THE US GEOLOGICAL SURVEY

1987 34 p

(Contract DI-14-08-0001-A-0468)

(PB88-223870) Avail: NTIS HC A03/MF A01 CSCL 08B

The Subcommittee on Geologic Mapping of the Committee Advisory to the U.S. Geological Survey (USGS) was convened to determine the status and extent of the geologic mapping program and activities of the USGS. Three meetings were held with representatives of the USGS office of Regal Geology, Mineral Resources, Energy and Marine Geology, and Earthquakes, Volcanoes, and Engineering. Programs covered included geologic framework and synthesis, Cooperative Geologic Mapping Program, regional geology branch programs, Isotope Geology Program, wilderness, GEODAT, statehich and critical materials, land administered by the Bureau of Land Management, coal resources, marine geology and the Pacific and Atlantic, oil and gas resources, energy and minerals, volcanic hazards and geology, engineering seismology and geology, engineering geology and tectonism, and igneous and geothermal processes. GRA

OCEANOGRAPHY AND MARINE RESOURCES

Includes sea-surface temperature, ocean bottom surveying imagery, drift rates, sea ice and icebergs, sea state, fish location.

A89-10930#

**OVERVIEW OF OCEANIC MICROWAVE REMOTE SENSING
 FROM SPACE**

CALVIN T. SWIFT (Massachusetts, University, Amherst) IN: International Symposium on Remote Sensing of Environment, 21st, Ann Arbor, MI, Oct. 26-30, 1987, Proceedings. Volume 1. Ann Arbor, MI, Environmental Research Institute of Michigan, 1987, p. 49-53. refs

The use of microwave sensors for satellite observations of the open ocean and sea ice is reviewed. Tables of the European and U.S. radar altimeters, scatterometers, SARs, and microwave radiometers used in space are presented. Prospects for future development in satellite observations are considered. R.B.

A89-10931# Bergen Univ. (Norway).

MIZEX '87 - OVERVIEW OF THE WINTER MARGINAL ICE ZONE EXPERIMENT IN THE GREENLAND AND BARENTS SEAS

OLA M. JOHANNESSEN, TOR I. OLAUSSEN, STEIN SANDVEN, JOHNNY A. JOHANNESSEN (Bergen, Universitetet, Norway), ROBERT A. SHUCHMAN (Michigan, Environmental Research Institute, Ann Arbor) et al. IN: International Symposium on Remote Sensing of Environment, 21st, Ann Arbor, MI, Oct. 26-30, 1987, Proceedings. Volume 1. Ann Arbor, MI, Environmental Research Institute of Michigan, 1987, p. 55-74. Research supported by the Norges Teknisk-Naturvitenskapelige Forskningsrad, U.S. Navy, NASA, et al. refs

SAR and in situ data were combined to study the winter marginal ice zone conditions in the Greenland and Barents Seas in 1987 as part of the ESA prelaunch ERS-1 Seasonal Ice Zone Experiment. Topics of the experiment include oceanography, meteorology, ice characterization, ice and snow properties, ambient noise studies, and biology. Systems of strong ice jets with cyclonic and anticyclonic vortex pairs shooting out of the shelf were observed along the shelf-break. Other findings include information on wave propagation into the ice pack, identification of ice types such as grease, new, first, and multiyear, the observation of convective 'chimneys' off the ice edge extending through the main pycnocline. It is suggested that the SAR data provide an excellent base for studies of ice kinematics, which are essential for ice modeling. R.B.

A89-10942*# Massachusetts Univ., Amherst.

PASSIVE MICROWAVE REMOTE SENSING OF SALINITY IN COASTAL ZONES

CALVIN T. SWIFT (Massachusetts, University, Amherst), HANS-JUERGEN C. BLUME, and BRUCE M. KENDALL (NASA, Langley Research Center, Hampton, VA) IN: International Symposium on Remote Sensing of Environment, 21st, Ann Arbor, MI, Oct. 26-30, 1987, Proceedings. Volume 1. Ann Arbor, MI, Environmental Research Institute of Michigan, 1987, p. 241-252. refs

The theory of measuring coastal-zone salinity from airborne microwave radiometers is developed. The theory, as presented, shows that precision measurements of salinity favor the lower microwave frequencies. To this end, L- and S-Band systems were built, and the flight results have shown that accuracies of at least one part per thousand were achieved. The aircraft results focus on flights conducted over the Chesapeake Bay and the mouth of the Savanna River off the Georgia Coast. This paper presents no new work, but rather summarizes the capabilities of the remote sensing technique. Author

A89-10947#

DOES A SAR RESPOND TO BOTH PHASE SPEED AND ORBITAL VELOCITY IN OCEAN SENSING?

R. K. RANEY and P. W. VACHON (Radarsat, Ottawa, Canada) IN: International Symposium on Remote Sensing of Environment, 21st, Ann Arbor, MI, Oct. 26-30, 1987, Proceedings. Volume 1. Ann Arbor, MI, Environmental Research Institute of Michigan, 1987, p. 327-346. refs

A method for improving the apparent wave contrast when processing airborne SAR imagery of ocean waves is examined. By changing the focus adjustment in proportion to one half of the phase velocity of the dominant wave, the apparent wave contrast of experimental data is improved. However, this focus response

cannot be predicted theoretically, based on the coherently sensible velocity of the individual scatters, which is equal to the orbital velocity of the waves. This problem is discussed in detail, and new processing ideas which do not depend on details of the surface scattering are presented. It is suggested that processing by compensation of each of the looks for feature movement is better than processing by focus adjustment. R.B.

A89-10954#

THE SEAWIFS SENSOR FOR LANDSAT-6

LOREN M. WOODY (Santa Barbara Research Center, Goleta, CA) IN: International Symposium on Remote Sensing of Environment, 21st, Ann Arbor, MI, Oct. 26-30, 1987, Proceedings. Volume 1. Ann Arbor, MI, Environmental Research Institute of Michigan, 1987, p. 431-436.

The sea-viewing wide-field sensor (Seawifs), designed for ocean color and sea surface temperature remote sensing on Landsat-6, is discussed. The sensor is based on the Coastal Zone Color Scanner which was flown on Nimbus-7. The sensor requirements, concept, and performance are discussed, and the Seawifs system is described and illustrated. At 443 nm, the Seawifs sensor achieves a polarization sensitivity of less than 1.4 percent in all bands at all scan angles. The system consists of the scanner, the electronics module, a data switcher, data recorders, and four transmitters and two antennas for local and global area coverage output. The Seawifs weighs about 143 pounds and has a power consumption of about 185 W when operating. R.B.

A89-10961#

SEA LEVEL VARIATIONS IN THE TROPICAL PACIFIC DURING 1985-87 DERIVED FROM GEOSAT ALTIMETRY

ROBERT E. CHENEY and LAURY MILLER (NOAA, National Ocean Service, Rockville, MD) IN: International Symposium on Remote Sensing of Environment, 21st, Ann Arbor, MI, Oct. 26-30, 1987, Proceedings. Volume 1. Ann Arbor, MI, Environmental Research Institute of Michigan, 1987, p. 513-520. refs

The GEOSAT altimeter, launched in 1985, has provided more than 2 years of precise (2-3 cm), global observations of sea level. These data have proven to be especially useful in the tropical Pacific, where changes in sea level can be related to fluctuations in the large-scale wind field. Sea level time series and anomaly maps derived from GEOSAT have provided a dramatic look at the 1986-87 El Nino. Author

A89-10962#

IMPROVEMENTS IN THE MARINE GRAVITY FIELD FROM GEOSAT/ERM

DAVID C. MCADOO (NOAA, National Ocean Service, Rockville, MD) and DAVID T. SANDWELL (Texas, University, Austin) IN: International Symposium on Remote Sensing of Environment, 21st, Ann Arbor, MI, Oct. 26-30, 1987, Proceedings. Volume 1. Ann Arbor, MI, Environmental Research Institute of Michigan, 1987, p. 521-529.

The Geosat Exact Repeat Mission (ERM) makes observations of sea-surface topography to study the marine gravity field. Data obtained in 1987 for the southern oceans around Antarctica show uncharted fracture zones, seamounts, and other features. It is shown that when several repeat tracks of ERM data are stacked, the effects of oceanographic mesoscale variability are reduced and the precision of along-track gravity improves to the 1 mgal level (excluding wavelengths shorter than 35 km). R.B.

A89-10964#

OPERATIONAL ENVIRONMENTAL INSTRUMENTATION PROPOSED BY NOAA AND THE INTERNATIONAL COMMUNITY FOR THE NASA AND ESA POLAR ORBITING PLATFORMS

BRUCE H. NEEDHAM (NOAA, Washington, DC) IN: International Symposium on Remote Sensing of Environment, 21st, Ann Arbor, MI, Oct. 26-30, 1987, Proceedings. Volume 1. Ann Arbor, MI, Environmental Research Institute of Michigan, 1987, p. 551-559.

In the mid-1990's the National Aeronautics and Space Administration (NASA) and the European Space Agency (ESA) each

plan to launch serviceable polar orbiting platforms as part of the International Space Station program. The National Oceanic and Atmospheric Administration (NOAA) is planning to utilize the NASA and ESA polar orbiting platforms to carry its' operational instruments for environmental remote sensing as a follow-on to the NOAA K, L, M series of operational polar orbiting satellites. Author

A89-10971#**EVOLUTION OF THE HELICOPTER-BORNE SCATTEROMETER**

ROBERT G. ONSTOTT and ROBERT A. SHUCHMAN (Michigan, Environmental Research Institute, Ann Arbor) IN: International Symposium on Remote Sensing of Environment, 21st, Ann Arbor, MI, Oct. 26-30, 1987, Proceedings. Volume 1. Ann Arbor, MI, Environmental Research Institute of Michigan, 1987, p. 657-665. refs

This paper describes the characteristics of a multifrequency multipolarization helicopter-borne scatterometer system, Heloscat II, designed for the measurement of the backscatter coefficients of Arctic sea-ice. The Heloscat is based on the proven application of FM-CW radar. It includes three radar front ends (each containing a two-channel homodyne receiver), two parabolic dish center-fed antennas, a radar altimeter, a remote controlled solid-state color video system, an electronically controlled antenna positioning system, radar control and processing circuitry, a 24-channel data acquisition system, and a dc-to-dc converter-based power supply system. The Helostat system provides the ability to make detailed local measurements, be transported rapidly to remote locations, make large area surveys, adapt to special measurement situations, and quickly gather very large numbers of spatial measurements in scenes that change rapidly. Block diagrams of the system are included. I.S.

A89-10972#**STUDY OF MONITORING SEA ICE USING AN AIRBORNE MICROWAVE RADIOMETER SYSTEM**

XUYAN TENG, RENYU ZHAO, JUNRONG ZHANG, and DIANCHEN ZHANG (Chinese Academy of Sciences, Changchun Institute of Geography, People's Republic of China) IN: International Symposium on Remote Sensing of Environment, 21st, Ann Arbor, MI, Oct. 26-30, 1987, Proceedings. Volume 2. Ann Arbor, MI, Environmental Research Institute of Michigan, 1987, p. 675-684.

An airborne microwave radiometer system was used to monitor sea ice in the Bohai Sea between 1985 and 1987. A microprocessor was used to identify ice types from false-color microwave radiometric imagery. The relationship between the emissivity and the thickness of ice is discussed. The regression equations for brightness temperature versus thickness are given. The average emissivity of the sea was found to be about 0.85. It is suggested that the difference between this and the emissivity of polar ice-caps (0.95) is due to the increase of water content and volume scatter. R.B.

A89-10981#**ANALYSES OF MARINE SHALLOW WATER-BOTTOM FEATURES USING THE LANDSAT THEMATIC MAPPER, SPOT, AND THE LARGE FORMAT CAMERA**

MATTHEW HERIC (Autometric, Inc., Alexandria, VA) IN: International Symposium on Remote Sensing of Environment, 21st, Ann Arbor, MI, Oct. 26-30, 1987, Proceedings. Volume 2. Ann Arbor, MI, Environmental Research Institute of Michigan, 1987, p. 775-782. refs

Large Format Camera photography and Landsat TM and SPOT imagery of the Florida Keys have been analyzed and compared to a NOAA 1:80,000 nautical chart to delineate shallow water-bottom features. A restricted unsupervised classification on the soft copy and a photogrammetric analysis of the hard copy were performed for each data set. The spectral characteristics of the data sets were used to chart bathymetric information. Comparison of mutual transect measurements has shown that each of the data sets provided accurate imagery. R.B.

A89-10990#**SPOT BATHYMETRIC IMAGE FOR ARCHEOLOGICAL INVESTIGATIONS**

KENNETH P. FERGUSON, FRED J. TANIS, and WILLIAM A. TYLER (Michigan, Environmental Research Institute, Ann Arbor) IN: International Symposium on Remote Sensing of Environment, 21st, Ann Arbor, MI, Oct. 26-30, 1987, Proceedings. Volume 2. Ann Arbor, MI, Environmental Research Institute of Michigan, 1987, p. 863-866. refs

Imagery from the first two multispectral bands of the SPOT system were used to determine ocean depths for an archeological study of the area surrounding Bassas da India in the Mozambique Channel of the Indian Ocean. It was found that the observed radiance depends on water depth, atmospheric attenuation, bottom type, and the amount of material suspended in the water. The shallow-water-depth algorithm was used to transform the raw digital number values into estimated water depths in meters, based on the exponential attenuation of light with water depth. A false-color composite and a bathymetric image were produced at 1:25,000 scale. Observations of the area showed that the estimated depths reported on the bathymetric image were reasonable. R.B.

A89-10991#**SURVEILLANCE RADAR, A NEW TOOL FOR ICE SURVEILLANCE**

P. RUDKIN and H. T. RIPLEY (Atlantic Airways, Ltd., Saint John's, Canada) IN: International Symposium on Remote Sensing of Environment, 21st, Ann Arbor, MI, Oct. 26-30, 1987, Proceedings. Volume 2. Ann Arbor, MI, Environmental Research Institute of Michigan, 1987, p. 867-874.

Surveillance radar capable of detecting small targets is being used to detect small icebergs to improve the safety of oil exploration off the eastern coast of Canada. Tests of the radar show that it has a typical detection range of 25-30 nmi for a 2 x 2-m target and 35-40 nmi for a 10 x 10-m target. The radar system is described, including the radar, navigation system, video tape recorder, and computer systems. It is suggested that this provides better results than side-looking airborne radars used in ice surveillance. R.B.

A89-10994#**PREDICTION OF MESOSCALE OCEAN CIRCULATION IN THE NORWEGIAN COASTAL CURRENT**

JOHNNY ANDRE JOHANNESSEN (Bergen, Universitetet, Norway) and MOTO IKEDA (Bedford Institute of Oceanography, Dartmouth, Canada) IN: International Symposium on Remote Sensing of Environment, 21st, Ann Arbor, MI, Oct. 26-30, 1987, Proceedings. Volume 2. Ann Arbor, MI, Environmental Research Institute of Michigan, 1987, p. 893-905. Research supported by the Norges Teknisk-Naturvitenskapelige Forskningsrad, Universitetet i Bergen, Statoil, et al. refs

NOAA satellite IR images are used to study the Norwegian coastal current system, showing that the dominant features are mesoscale (50-100-km) eddies. The eddies were located, and an optimal ship survey was outlined using near-real-time analysis. The correlation between the surface thermal distribution and interior structure is documented, and the three-dimensional oceanic and velocity structure of the eddies is obtained. A quasi-geostrophic two-layer numerical model is used to simulate the mesoscale ocean circulation of the current. The simulation cannot be tested or modified, because IR images are not available on a regular basis due to frequent cloud cover. It is suggested that the SAR and radar altimeter of the planned ERS-1 satellite may provide the data necessary to test the model. R.B.

A89-10995#**THE PRACTICE AND UNDERSTANDING OF USING AERIAL REMOTE SENSING IN THE INVESTIGATION OF COASTAL ZONE**

GAN-CHENG CHEN (State Oceanic Administration, Hangzhou, People's Republic of China) IN: International Symposium on Remote Sensing of Environment, 21st, Ann Arbor, MI, Oct. 26-30, 1987, Proceedings. Volume 2. Ann Arbor, MI, Environmental Research Institute of Michigan, 1987, p. 909-916. refs

Four missions between 1979 and 1984 which used aerial remote sensing to examine Chinese coastal zones are reviewed. Panchromatic aerial photography, multiband scanner digital tape, large-format color IR photography, and large-format multiband photography were used for research including the study of near-shore marine pollution; the measurement of beach areas; near-shore bathymetry; and the classification of surface sediment, landforms, vegetation, and land use. The data obtained in these studies are outlined, and several remote sensing techniques are evaluated. It is suggested that aerial remote sensing is better than conventional investigation techniques. Color aerial photography is found to have particular advantages, including convenience and high sensitivity and resolution. R.B.

A89-11001# REMOTE MEASUREMENTS OF DIATOMS CHLOROPHYLL-A IN THE NORI FARM

KAZUYA SAITO, SEIJIRO HAYAKAWA, TATSUO HAYAKAWA, and KIICHI HIRONO (Asia Air Survey Co., Ltd., Atsugi, Japan) IN: International Symposium on Remote Sensing of Environment, 21st, Ann Arbor, MI, Oct. 26-30, 1987, Proceedings. Volume 2. Ann Arbor, MI, Environmental Research Institute of Michigan, 1987, p. 971-980. refs

A method is presented to quantitatively evaluate chlorophyll-a concentration using remote measurements of the Ariake Sea, which contains an abundance of Nori. Data were collected from boats, aircraft, and Landsat. The application of remote sensing data to fisheries research is discussed, and results of experiments to determine the quality of Nori are presented. A preliminary analysis suggested a dependence of suspended solid on surface reflection coefficients. Airborne MSS data show a correlation between single-band data and chlorophyll-a concentration. Water-quality maps of Landsat TM and airborne MSS data were found to be similar. In an attempt to find the degree of Nori color change, airborne MSS data suggested that it is possible to estimate Nori quality. R.B.

A89-11005# SAR AND VISIBLE REMOTE SENSING OF THE TAOER RIVER COASTAL ZONE AT BOHAI BAY

BAIDE XU and XINGWEI SHA (State Oceanic Administration, Hangzhou, People's Republic of China) IN: International Symposium on Remote Sensing of Environment, 21st, Ann Arbor, MI, Oct. 26-30, 1987, Proceedings. Volume 2. Ann Arbor, MI, Environmental Research Institute of Michigan, 1987, p. 1023-1029.

A89-11143* California Univ., La Jolla. GEOSAT CROSSOVER ANALYSIS IN THE TROPICAL PACIFIC. I - CONSTRAINED SINUSOIDAL CROSSOVER ADJUSTMENT

CHANG-KOU TAI (California, University, La Jolla) Journal of Geophysical Research (ISSN 0148-0227), vol. 93, Sept. 15, 1988, p. 10621-10629. Previously announced in STAR as N88-15285. refs
(Contract NSF OCE-86-07962; NAGW-808; N00014-86-K-0752)

A new method (constrained sinusoidal crossover adjustment) for removing the orbit error in satellite altimetry is tested (using crossovers accumulated in the first 91 days of the Geosat non-repeat era in the tropical Pacific) and found to have excellent qualities. Two features distinguish the new method from the conventional bias-and-tilt crossover adjustment. First, a sine wave (with wavelength equaling the circumference of the Earth) is used to represent the orbit error for each satellite revolution, instead of the bias-and-tilt (and curvature, if necessary) approach for each segment of the satellite ground track. Secondly, the indeterminacy of the adjustment process is removed by a simple constraint minimizing the amplitudes of the sine waves, rather than by fixing selected tracks. Overall the new method is more accurate, more efficient, and much less cumbersome than the old. The idea of restricting the crossover adjustment to crossovers between tracks that are less than certain days apart in order to preserve the large-scale long-term oceanic variability is also tested with

inconclusive results because the orbit error was unusually nonstationary in the initial 91 days of the GEOSAT mission.

Author

A89-11145*# National Aeronautics and Space Administration, Goddard Space Flight Center, Greenbelt, MD.

VARIATIONS IN THE ARCTIC, ANTARCTIC, AND GLOBAL SEA ICE COVERS DURING 1978-1987 AS OBSERVED WITH THE NIMBUS 7 SCANNING MULTICHANNEL MICROWAVE RADIOMETER

PER GLOERSEN (NASA, Goddard Space Flight Center, Greenbelt, MD) and WILLIAM J. CAMPBELL (USGS; University of Puget Sound, Tacoma, WA) Journal of Geophysical Research (ISSN 0148-0227), vol. 93, Sept. 15, 1988, p. 10666-10674. refs

A89-11148 A THREE-DIMENSIONAL COUPLED ICE-OCEAN MODEL OF COASTAL CIRCULATION

MOTOYOSHI IKEDA (Bedford Institute of Oceanography, Dartmouth, Canada) Journal of Geophysical Research (ISSN 0148-0227), vol. 93, Sept. 15, 1988, p. 10731-10748. refs

The role of ocean circulation on the formation of sea ice and on its distribution along the east coasts of North America and Greenland is examined using a three-dimensional coupled ice-ocean model of coastal circulation with idealized northerly wind stress and atmospheric cooling. The results suggest that wind-driven time-dependent ocean circulation may be as important for ice redistribution as is ice movement directly driven by the air-ice stress. The oceanic circulation also affects heat transport, playing an important role in producing a narrow ice band along the east coast of the continent. I.S.

A89-11149 OPTICAL MODELING OF THE UPPER OCEAN IN RELATION TO ITS BIOGENOUS MATTER CONTENT (CASE I WATERS)

ANDRE MOREL (Paris VI, Universite, Villefranche-sur-Mer, France) Journal of Geophysical Research (ISSN 0148-0227), vol. 93, Sept. 15, 1988, p. 10749-10768. CNRS-supported research. refs

The optical behavior of oceanic case I waters is interpreted in terms of chlorophyll-related pigment concentration. Chlorophyll-like pigment concentration was used as an index to quantify the algal material (living and detrital), and the statistical relationships between this index and the depth of the euphotic layer, the spectral values of the attenuation coefficient for downwelling irradiance, and the scattering coefficient were determined and used to develop a pigment-dependent optical model. The model makes it possible to predict the propagation of the visible radiant energy within the ocean or the backscattered radiation from the upper layer as a function of the local phytoplanktonic content. I.S.

A89-11150 COMPARISON OF NIMBUS 7 SCANNING MULTICHANNEL MICROWAVE RADIOMETER RADIANCE AND DERIVED SEA ICE CONCENTRATIONS WITH LANDSAT IMAGERY FOR THE NORTH WATER AREA OF BAFFIN BAY

KONRAD STEFFEN and JAMES A. MASLANIK (Cooperative Institute for Research in Environmental Sciences, Boulder, CO) Journal of Geophysical Research (ISSN 0148-0227), vol. 93, Sept. 15, 1988, p. 10769-10781. refs
(Contract NSF DPP-85-20883)

A89-11158 MODELING OF THE DYNAMIC SEA SURFACE WITH SATELLITE ALTIMETER SIGNALS

ERNST W. SCHWIDERSKI (U.S. Navy, Naval Surface Warfare Center, Dahlgren, VA) IN: Developments in theoretical and applied mechanics. Volume 14; Proceedings of the Fourteenth Southeastern Conference on Theoretical and Applied Mechanics, Biloxi, MS, Apr. 18, 19, 1988. University, MS, University of Mississippi, 1988, p. 121-128. NOAA-Navy-sponsored research. refs

New well-designed multiple-effects models were developed for

a unified decomposition of the altimeter signals of the dynamic sea height into all their major contributions. These include high-resolution and precision models of the geoid or mean-sea surface, geocentric and/or ocean tides, mesoscale dynamic ocean variations, and residual large-scale ocean variations. The unified double-effects model accounts for some 13,000 altimeter signals over a 200 x 200 km area with a lateral 10 x 10 km resolution and an absolute minimum rms error of just 6 cm. K.K.

A89-11225**ATMOSPHERIC ABSORPTION IN THE VAS SPLIT-WINDOW CHANNELS**

IAN J. BARTON (CSIRO, Div. of Atmospheric Research, Mordialloc, Australia) *Journal of Applied Meteorology* (ISSN 0894-8763), vol. 27, Aug. 1988, p. 965-969. refs

Empirical algorithms have been developed for obtaining measurements of sea surface temperature and precipitable water amount in the lower troposphere from VISSR Atmospheric Sounder (VAS) split-window channels at 10-12.5 and 12.6-12.8 microns. The differential absorption coefficients for these VAS channels produced by Chesters et al. (1987) are used in a spectral band model to improve the match between empirical and theoretical sea surface temperature algorithms. It is suggested that the absorption coefficient of a dry atmosphere in the 12.7 micron channel should be less than that for the 10-12.5 micron channel. However, the differential absorption coefficient, (12.7 microns minus 10-12.5 microns) should be increased. R.B.

A89-11424**A COMPARISON OF REDUCTION METHODS FOR SATELLITE ALTIMETRY DATA**

P. A. M. BERRY (Leicester, University, England), A. J. MEADOWS (Loughborough University of Technology, England), T. D. ALLAN (Institute of Oceanographic Sciences, Wormley, England), and J. G. OLLIVER (Oxford University, England) *Geophysical Journal* (ISSN 0952-4592), vol. 95, Oct. 1988, p. 63-68. refs (Contract SERC-SG/D/08464)

This paper gives a comparison of crossing-arc techniques for reduction of test grids of satellite altimetry data. For this study, Seasat data was selected for two areas: the eastern Mediterranean, an area which incorporates considerable variation in sea-floor topography, and part of the North Atlantic. Three implementations of crossover-point and repeat-arc methods were considered, and evaluated for accuracy and speed of implementation. The sample geoids produced were found to contain significant differences, indicating that choice of reduction method can be an important criterion for consideration in such analyses. Author

A89-12124#**MARINE REMOTE SENSING AND INTERNATIONAL LAW**

WILLIAM E. MOUNTS IN: Colloquium on the Law of Outer Space, 30th, Brighton, England, Oct. 10-17, 1987, Proceedings. Washington, DC, American Institute of Aeronautics and Astronautics, 1988, p. 350-360. refs

Satellite remote sensing of the oceans is considered from a legal perspective, with a focus on the contrasting provisions of the Principles on Remote Sensing adopted by COPUOS in 1986 and the UN Convention on the Law of the Sea (UNCLOS). The applications of satellite technology to oceanography, marine biology, sea transport, and marine communication are reviewed, and the treaties and conventions applicable are listed and characterized in detail. The main discrepancy between space and sea law is found to be in the treatment of marine exploration in territorial waters: the COPUOS Principles permit satellite remote sensing of marine resources without prior consent from anyone, while UNCLOS prohibits ship or airborne remote sensing of marine resources without the explicit consent of the nation holding territorial rights. T.K.

A89-12156**JOINT CANADA-U.S. OCEAN WAVE INVESTIGATION PROJECT - AN OVERVIEW OF THE GEORGIA STRAIT EXPERIMENT**

B. A. HUGHES and T. W. DAWSON (Defence Research Establishment Pacific, Victoria, Canada) *Journal of Geophysical Research* (ISSN 0148-0227), vol. 93, Oct. 15, 1988, p. 12219-12234. DND-Navy-DARPA-supported research. refs

This paper presents an overview of the Georgia Strait Experiment (Joint Canada-U.S. Ocean Wave Investigation Project), 1983, which was initiated to obtain measurements of surface wave modulations induced by natural and ship-generated internal waves, identify radar backscattering mechanisms as a function of incidence angle and surface wave conditions, to obtain calibrated SAR images of internal waves at X and L band for different radar angles, and to investigate SAR imagery mechanisms for Kelvin wakes. The paper providing the list of participants, detailed descriptions of measurement techniques, and major results obtained and describes the conditions encountered in the three operating areas. The paper also includes hitherto unpublished tables of time periods showing possible atmospheric thermal boundary layer instabilities. I.S.

A89-12157**MICROWAVE SCATTERING FROM INTERNAL WAVE MODULATED SURFACE WAVES - A SHIPBOARD REAL APERTURE COHERENT RADAR STUDY IN THE GEORGIA STRAIT EXPERIMENT**

D. S. W. KWONG, B. M. LAKE, and H. RUNGALDIER (TRW, Inc., TRW Space and Technology Group, Redondo Beach, CA) *Journal of Geophysical Research* (ISSN 0148-0227), vol. 93, Oct. 15, 1988, p. 12235-12248. DARPA-supported research. refs

A89-12158**MODULATION OF RADAR BACKSCATTER FROM THE OCEAN BY A VARIABLE SURFACE CURRENT**

E. A. CAPONI, D. R. CRAWFORD, H. C. YUEN (TRW, Inc., TRW Space and Technology Group, Redondo Beach, CA), and P. G. SAFFMAN (California Institute of Technology, Pasadena) *Journal of Geophysical Research* (ISSN 0148-0227), vol. 93, Oct. 15, 1988, p. 12249-12263. refs

Model calculations of surface wave and radar cross section modulations induced by a surface currents were compared with field measurements made with SAR (X and L bands), real aperture radar (X band), and CCD video camera during the Joint Canada-U.S. Ocean Wave Investigation Project. Results indicated that many existing wind relaxation models underpredict the hydrodynamic effect of the current; among several models used, the one proposed by Snyder et al. (1981) yielded the best agreement with data. A theoretical model based on simple Bragg scattering and wind relaxation predicted modulations measurable at X band to be an order of magnitude or more smaller than those measurable at L band, in disagreement with observations, which show that the modulation magnitudes at X and L bands are similar. When the effects of long surface waves was accounted for, the discrepancy between measurements and calculations at high radar frequency was reduced (but not eliminated). I.S.

A89-12160**COMPARISON OF JOINT CANADA-U.S. OCEAN WAVE INVESTIGATION PROJECT SYNTHETIC APERTURE RADAR DATA WITH INTERNAL WAVE OBSERVATIONS AND MODELING RESULTS**

R. A. SHUCHMAN, E. S. KASISCHKE (Michigan, Environmental Research Institute, Ann Arbor), D. R. LYZENGA (Michigan, Environmental Research Institute, Ann Arbor; Delaware, University, Newark), B. M. LAKE (TRW, Inc., TRW Space and Technology Group, Redondo Beach, CA), B. A. HUGHES (Defence Research Establishment Pacific, Victoria, Canada) et al. *Journal of Geophysical Research* (ISSN 0148-0227), vol. 93, Oct. 15, 1988, p. 12283-12291. DND-DARPA-supported research. refs (Contract N00014-81-C-0692)

The L-band and X-band SAR images of internal waves were compared with in situ measurements of surface currents and surface wave spectral perturbations obtained during the Joint Canada-U.S. Ocean Wave Investigation Project. The comparison for the L band showed agreement between predicted and observed perturbations to within about a factor of 2, but the agreement for

the X band was much less satisfactory. Simultaneous X-band and L-band SAR images showed comparable internal wave modulations. I.S.

A89-12162

AN OVERVIEW OF THE SAR INTERNAL WAVE SIGNATURE EXPERIMENT

R. F. GASPAROVIC, J. R. APEL (Johns Hopkins University, Laurel, MD), and E. S. KASISCHKE (Michigan, Environmental Research Institute, Ann Arbor) *Journal of Geophysical Research* (ISSN 0148-0227), vol. 93, Oct. 15, 1988, p. 12304-12316. Navy-supported research. refs

This paper analyzes the data obtained during the SAR Internal Wave Signature Experiment, conducted in the New York Bight in the late summer and early fall of 1984, to investigate the possibilities of SAR imaging of oceanic internal waves. The results obtained on the surface-wave modulations are compared with the results of calculations that were carried out using hydrodynamic theories for the interaction of surface waves and currents, and theories for radar imaging of internal wave surface manifestations. Excellent agreement was found between measured and calculated surface wave modulations at wavelengths from 20 to 100 cm, as well as between the calculated SAR intensity modulations and the observed modulations at both the X and the L bands. Internal wave signatures in SAR images at X and L band were found to have comparable magnitudes. I.S.

A89-12163*# National Aeronautics and Space Administration. Goddard Space Flight Center, Greenbelt, MD.

ANALYSIS OF NONLINEAR INTERNAL WAVES IN THE NEW YORK BIGHT

ANTONY K. LIU (NASA, Goddard Space Flight Center, Greenbelt, MD) *Journal of Geophysical Research* (ISSN 0148-0227), vol. 93, Oct. 15, 1988, p. 12317-12329. refs
(Contract N00014-83-C-0724)

An analysis of the nonlinear-internal-wave evolution in the New York Bight was performed on the basis of current meter mooring data obtained in the New York Bight during the SAR Internal Wave Signature Experiment (SARSEX). The solitary wave theory was extended to include dissipation and shoaling effects, and a series of numerical experiments were performed by solving the wave evolution equation, with waveforms observed in the SARSEX area as initial conditions. The results of calculations demonstrate that the relative balance of dissipation and shoaling effects is crucial to the detailed evolution of internal wave packets. From an observed initial wave packet at the upstream mooring, the numerical evolution simulation agreed reasonably well with the measurements at the distant mooring for the leading two large solitons. I.S.

A89-12164

MEASUREMENTS OF SURFACE WAVE MODULATIONS FROM INTERNAL WAVES DURING THE SAR INTERNAL WAVE SIGNATURE EXPERIMENT

B. L. GOTWOLS and R. E. STERNER, II (Johns Hopkins University, Laurel, MD) *Journal of Geophysical Research* (ISSN 0148-0227), vol. 93, Oct. 15, 1988, p. 12330-12338. Navy-sponsored research. refs

This paper presents the results of a laser slope meter readings and the video images of surface waves occurring in the presence of large internal wave induced currents, that were recorded from a research vessel during the SAR Internal Wave Signature Experiment. The measurements presented clearly show the presence of correlations between increases and decreases in wave slope spectral density and internal waves; it is shown that the largest internal wave surface currents and gradients produce the largest spectral modulations. The increased roughness was found to occur forward of the peak internal wave displacement. I.S.

A89-12165

A COMPARISON OF MEASURED SURFACE WAVE SPECTRAL MODULATIONS WITH PREDICTIONS FROM A WAVE-CURRENT INTERACTION MODEL

D. R. THOMPSON, B. L. GOTWOLS, and R. E. STERNER, II (Johns Hopkins University, Laurel, MD) *Journal of Geophysical Research* (ISSN 0148-0227), vol. 93, Oct. 15, 1988, p. 12339-12343. Navy-sponsored research. refs

Predictions from a wave-current interaction model based on a wave action balance equation are compared with measured surface-wave modulations induced by internal waves. The comparison involves relative modulations of the surface-wave spectrum at wavelengths ranging from 0.2 to 1.0 m for wind speeds of 3.5 and 7 m/s. Good agreement is found between measurements and predictions for interactions with eight internal waves in two wave packets encountered during the Synthetic Aperture Radar Internal Wave Signature Experiment. Author

A89-12166

FULL-SPECTRUM MODELING OF SYNTHETIC APERTURE RADAR INTERNAL WAVE SIGNATURES

DAVID R. LYZENGA and JOHN R. BENNETT (Michigan, Environmental Research Institute, Ann Arbor) *Journal of Geophysical Research* (ISSN 0148-0227), vol. 93, Oct. 15, 1988, p. 12345-12354. refs
(Contract N00014-81-C-0692)

This paper presents an integrated hydrodynamic-electromagnetic model for full-spectrum modeling of SAR internal wave signatures, which combines a full-spectrum numerical solution of the wave action equation with a two-scale SAR model. The combined model was applied to two test cases that were observed during recent SAR Internal Wave Signature Experiment. Results indicate that, in some cases, such as light winds, using vertical polarization, and at larger incidence angles, the longwave effects on the backscatter are negligible. In other cases, such as at X band under moderate wind conditions or when the radar look direction is perpendicular to the internal wave propagation direction, these effects can be very important. In such cases, a significant variation in radar backscatter may be predicted by the composite model, even though little or no variation is predicted by a simple Bragg model. I.S.

A89-12167

CONTRAST RATIOS OF INTERNAL WAVES IN SYNTHETIC APERTURE RADAR IMAGERY - A COMPARISON OF SAR INTERNAL WAVE SIGNATURE EXPERIMENT OBSERVATIONS WITH THEORY

ERIC S. KASISCHKE, DAVID R. LYZENGA, ROBERT A. SHUCHMAN, and CHRISTOPHER C. WACKERMAN (Michigan, Environmental Research Institute, Ann Arbor) *Journal of Geophysical Research* (ISSN 0148-0227), vol. 93, Oct. 15, 1988, p. 12355-12369. refs
(Contract N00014-81-C-0692)

This paper discusses three aspects of SAR Internal Wave Signature Experiment investigations: (1) methods to quantify the internal wave signatures on SAR imagery, which account for the natural variability within the internal waves; (2) the use of the Lyzenga and Bennett (1988) theoretical model to explore the expected trends in the SAR-observed internal wave signatures as a function of radar frequency, incidence angle, and look direction and of wind speed; and (3) the comparison of the model-derived and the SAR-observed trends. The results showed that the model underpredicts the SAR-observed modulations, especially for the azimuth-traveling internal wave case. I.S.

A89-12171*# Army Cold Regions Research and Engineering Lab., Hanover, NH.

NUMERICAL SIMULATIONS OF THE PROFILE PROPERTIES OF UNDEFORMED FIRST-YEAR SEA ICE DURING THE GROWTH SEASON

G. F. N. COX and W. F. WEEKS (U.S. Army, Cold Regions Research and Engineering Laboratory, Hanover, NH) *Journal of Geophysical Research* (ISSN 0148-0227), vol. 93, Oct. 15, 1988, p. 12449-12460. Navy-supported research. refs
(Contract NAGW-1051)

A model is presented for estimating salinity profiles for the first-year sea ice during the growth season, in which ice growth

equations were coupled with salt entrapment and brine drainage relations to obtain the relationship between the initial ice salinity and the ice-growth velocity and seawater salinity, as well as the subsequent drainage of brine from the ice. The results obtained were found to be in reasonable agreement with field observations in that they showed characteristic C-shaped profiles similar to natural profiles. The average ice salinity values were also in reasonable agreement with field data. The predicted ice property profiles give composite plate properties that are significantly different from bulk property estimates that would result by assuming that sea ice could be represented as a homogeneous plate. I.S.

A89-12172**A NUMERICAL STUDY OF MESOSCALE OCEAN EDDY INTERACTION WITH A MARGINAL ICE ZONE**

DAVID C. SMITH, IV, ARLENE A. BIRD (U.S. Naval Postgraduate School, Monterey, CA), and W. PAUL BUDGELL (Institute of Ocean Sciences, Sidney, Canada) *Journal of Geophysical Research* (ISSN 0148-0227), vol. 93, Oct. 15, 1988, p. 12461-12473. refs (Contract N00014-85-C-0055)

The interaction of isolated mesoscale ocean eddies with a free-drift marginal ice zone was investigated using a two-layer nonlinear primitive equation ocean model coupled with a free-drift ice model. It is shown that, in the absence of winds, the ice equilibrates rapidly to the ocean eddy velocity, resulting in radial ice motion. With along-the-ice-edge winds of about 10 m/s, the ice responds largely to the wind and, to a lesser extent, to the ocean eddy. Under ice, the ocean eddy can be rapidly eroded by wind-driven ice motion. These findings are compared with observations made in 1983 and 1984 during the marginal ice zone experiments. I.S.

A89-12173**SYNTHETIC APERTURE RADAR IMAGING OF OCEAN WAVES FROM AN AIRBORNE PLATFORM - FOCUS AND TRACKING ISSUES**

R. K. RANEY (Radarsat Project Office, Ottawa, Canada) and P. W. VACHON (Canada Centre for Remote Sensing, Ottawa) *Journal of Geophysical Research* (ISSN 0148-0227), vol. 93, Oct. 15, 1988, p. 12475-12486. refs

This paper addresses the aspects of focus and tracking in the process of SAR imaging of ocean waves from an airborne platform. It is demonstrated that there is a direct relationship between focus and wave phase velocity, through purely noncoherent consequences of the SAR response to the translating reflectivity density envelope of the wave field. It is also shown that the orbital velocity affects the phase of the received signal, leading to velocity bunching, and is scaled by the ratio of sensor altitude to sensor velocity. It is suggested that better performance can be obtained by compensating individual looks for wave movement before look summation, while using nominal perfect focus. I.S.

A89-12174* University of Southern California, Los Angeles.**PHYTOPLANKTON STANDING CROPS WITHIN AN ANTARCTIC ICE EDGE ASSESSED BY SATELLITE REMOTE SENSING**

C. W. SULLIVAN (Southern California, University, Los Angeles, CA), C. R. MCCLAIN, J. C. COMISO (NASA, Goddard Space Flight Center, Greenbelt, MD), and W. O. SMITH, JR. (Tennessee, University, Knoxville) *Journal of Geophysical Research* (ISSN 0148-0227), vol. 93, Oct. 15, 1988, p. 12487-12498. NASA-supported research. refs

(Contract NSF DPP-82-18752; NSF DPP-87-13916; NSF DPP-82-18758; NSF DPP-84-20213)

The dynamic interactions between the pack-ice recession and the occurrence of ice blooms of phytoplankton in waters of the marginal ice zone within an Antarctic ice edge were investigated using CZCS and SMMR imageries from the Nimbus 7 satellite (September 16-December 17, 1983), together with in situ measurements of pigments and sea ice concentration carried out from November 7 to December 2. A substantial amount of spatial variability in pigment concentration was observed to occur along the ice edge in the Weddell Sea. The relationships among light,

ice distribution, and vertical stability and their effects on observed spatial variations in phytoplankton biomass are discussed. The results of this investigation suggest that the retreat of ice provides an input of significant volumes of meltwater which creates vertical stability for a period necessary to permit growth and accumulation of phytoplankton. I.S.

A89-12203#**THE DEVELOPMENT OF TROPICAL CYCLONES IN THE NORTH-WEST OF AUSTRALIA**

I. J. FOSTER and T. J. LYONS (Murdoch University, Australia) *Royal Meteorological Society, Quarterly Journal* (ISSN 0035-9009), vol. 114, July 1988, pt. B, p. 1187-1199. Research supported by the Australian Research Grants Scheme and Australian Marine Science and Technology Advisory Committee. refs

Conventional and satellite observations have been used to construct case studies of developing and nondeveloping tropical depression in the northwest region of Australia during the 1979/80 and 1980/81 cyclone seasons. It is shown that enhanced low-level winds can occur during the lifetime of nondeveloping disturbances and are not exclusively associated with cyclogenesis. Both types of systems were found to possess lower-level cyclonic circulations and an overlapping was observed, such that nondeveloping storms could have stronger circulations than some developing storms. At upper levels, development was associated with the subtropical ridge over the surface position of the disturbance. The ridge tended to be southwards of nondevelopers. The model of cyclone development is supported by calculations of area-averaged vorticity at 850 and 200 mb. The features are consistent with both classes of disturbance existing within the monsoon shearline. R.B.

A89-12209#**A DUAL-SATELLITE ALGORITHM FOR DERIVING SEA SURFACE TEMPERATURE**

ANU DUDHIA (Oxford University, England) *Royal Meteorological Society, Quarterly Journal* (ISSN 0035-9009), vol. 114, July 1988, pt. B, p. 1305-1319. refs

The conventional multichannel sea surface temperature algorithms for NOAA-7 AVHRR/2 data have been extended to include data from the Meteosat-2 IR1 (11-micron) channel. This extension provides a combination of multichannel and dual-angle techniques for determining the atmospheric correction. The algorithms were derived from results of transmission calculations on a number of temperature/humidity profiles and were tested under pseudooperational conditions against ship measurements. It is concluded that the technique is feasible although because of uncertainties in the Meteosat radiances caused by residual cloud contamination, the additional data are given only a low weight in the algorithms and the influence on retrieved sea surface temperature is small. R.B.

A89-12260*# National Aeronautics and Space Administration. Wallops Flight Facility, Wallops Island, VA.**AIRBORNE LIDAR DETECTION OF SUBSURFACE OCEANIC SCATTERING LAYERS**

FRANK E. HOGE, C. WAYNE WRIGHT, WILLIAM B. KRABILL (NASA, Wallops Flight Center, Wallops Island, VA), RODNEY R. BUNTZEN, GARY D. GILBERT (U.S. Naval Ocean Systems Center, San Diego, CA) et al. *Applied Optics* (ISSN 0003-6935), vol. 27, Oct. 1, 1988, p. 3969-3977. refs

The airborne lidar detection and cross-sectional mapping of submerged oceanic scattering layers are reported. The field experiment was conducted in the Atlantic Ocean southeast of Assateague Island, VA. NASA's Airborne Oceanographic Lidar was operated in the bathymetric mode to acquire on-wavelength 532-nm depth-resolved backscatter signals from shelf/slope waters. Unwanted laser pulse reflection from the air-water interface was minimized by spatial filtering and off-nadir operation. The presence of thermal stratification over the shelf was verified by the deployment of airborne expendable bathythermographs. Optical beam transmission measurements acquired from a surface truthing vessel indicated the presence of a layer of turbid water near the sea floor over the inner portion of the shelf. Author

A89-12645* Texas Univ., Austin.

ORBIT DETERMINATION REQUIREMENTS FOR TOPEX

B. D. TAPLEY and J. C. RIES (Texas, University, Austin) IN: Astrodynamics 1987; Proceedings of the AAS/AIAA Astrodynamics Conference, Kalispell, MT, Aug. 10-13, 1987. Part 1. San Diego, CA, Univelt, Inc., 1988, p. 321-338. refs
(Contract JPL-956689)
(AAS PAPER 87-429)

The orbit determination requirements for the Ocean Topography Experiment (Topex/Poseidon) are discussed. A radial orbit accuracy of 13 cm for a period of three to five years is required for the mission. The factors which limit the orbit accuracy for the geopotential, the solar radiation pressure, and the atmospheric drag model are examined. Also, the effects introduced by variations with aspect angle in the spacecraft area-to-mass ratio are considered. R.B.

A89-12776

CONFERENCE ON SATELLITE METEOROLOGY AND OCEANOGRAPHY, 3RD, ANAHEIM, CA, FEB. 1-5, 1988, PREPRINTS

Conference sponsored by the American Meteorological Society. Boston, MA, American Meteorological Society, 1988, 519 p. For individual items see A89-12777 to A89-12865, A89-12867 to A89-12871.

The present conference on satellite remote sensing technologies for meteorology and oceanography discusses advancements in the fields of temperature retrieval, water vapor retrieval, multiple-parameter studies, radiation budget studies, forecasting and analysis of weather, oceanographic applications of remote sensing, prospective developments of satellite remote sensing systems, rainfall observations, the detection of clouds and their parameters, and ocean-atmosphere interface-related sensing. The satellite sensors discussed encompass microwave radiometry, VISSR, microwave sounding, wide field-of-view radiometry, multispectral imagery, stereoscopic image pairs, high resolution interferometric sounding, IR sea surface temperature mappers, Doppler lidar, IR rain sensors, AVHRR, wide-swath radar altimetry, SMMR, and X-band scatterometers. O.C.

A89-12779

RETRIEVAL OF AIR SURFACE TEMPERATURES OVER OCEANS FROM SATELLITE RADIANCE MEASUREMENTS USING STRATIFICATION TECHNIQUES

LARRY M. MCMILLIN (NOAA, Satellite Research Laboratory, Washington, DC) IN: Conference on Satellite Meteorology and Oceanography, 3rd, Anaheim, CA, Feb. 1-5, 1988, Preprints. Boston, MA, American Meteorological Society, 1988, p. 10-12. refs

Atmospheric measurements of the National Environmental Satellite, Data, and Information Service are currently made with the TIROS Operational Vertical Temperature Sounder. It is noted that, with this sounder's filter instruments, sufficient resolution for such features as surface inversions is difficult to obtain. Attention is presently given to calculation results for the covariance matrix of TIROS' channels 4-8, 10-15, and 22. Coefficients of the eigenvectors associated with the four largest eigenvalues were calculated for the dependent data set, and the maxima and minima for each is used to determine the range. Each eigenvector range was then divided into groups whose mean brightness temperature values were calculated. O.C.

A89-12792* Washington Univ., Seattle.

AN EXAMPLE OF ESTIMATES OF PRECIPITABLE WATER DERIVED FROM NIMBUS-7 SMMR SATELLITE MEASUREMENTS AND FGGE UPPER AIR DATA

DOUGLAS K. MILLER (Washington, University, Seattle) and DAYTON G. VINCENT (Purdue University, West Lafayette, IN) IN: Conference on Satellite Meteorology and Oceanography, 3rd, Anaheim, CA, Feb. 1-5, 1988, Preprints. Boston, MA, American Meteorological Society, 1988, p. 70-73. refs
(Contract NAS8-35187; NAS8-37127)

A sample of results from the Scanning Multichannel Microwave

Radiometer (SMMR) instrument aboard the Nimbus-7 satellite is compared with those obtained from analyses of First GARP Global Experiment Level III-b data collected over the South Pacific on January 10-18, 1979, when the South Pacific Convergence Zone and its accompanying cloud band were quasi-stationary features of this ocean's circulation. It is found that the patterns of Goddard Laboratory for Atmospheres precipitable water values compare well with patterns of the SMMR brightness temperature differences. O.C.

A89-12798

REMOTE SENSING OF SURFACE AIR TEMPERATURE AND HUMIDITY OVER OCEANIC AREAS WITH APPLICATION TO CLIMATOLOGY AND WEATHER PREDICTION

LOUIS GARAND (Department of the Environment, Atmospheric Environment Service, Dorval, Canada) IN: Conference on Satellite Meteorology and Oceanography, 3rd, Anaheim, CA, Feb. 1-5, 1988, Preprints. Boston, MA, American Meteorological Society, 1988, p. 95-99. refs

Cloud classification is evaluated as a basis for the determination of surface air temperature and humidity over oceans, using the dew point depression as a humidity variable and assuming that a given class of clouds may be associated with a significant deviation of the variable from climatology. A major asset of the present classifier is its ability to recognize mesoscale cellular patterns that are known to be associated with large cold temperature anomalies. The humidity retrievals are found to be useful for cloud classes associated with a mean relative humidity lower than 68 or greater than 80 percent. O.C.

A89-12823

SATELLITE DIAGNOSIS OF TROPICAL CYCLONES

RAYMOND M. ZEHR (Cooperative Institute for Research in the Atmosphere, Fort Collins, CO) IN: Conference on Satellite Meteorology and Oceanography, 3rd, Anaheim, CA, Feb. 1-5, 1988, Preprints. Boston, MA, American Meteorological Society, 1988, p. 241-246. refs
(Contract NOAA-NA-85RAH05045; NOAA-NA-84AAH00020; NOAA-NA-84AAD00017)

Preliminary results are presented from a study to improve intensity estimates of tropical cyclones. Data from U.S. Air Force reconnaissance flights in the western Pacific and three-hourly Geostationary Meteorological Satellite (GMS) data at 10 km resolution were compiled to analyze 48 tropical storms and typhoons during 1983-1984. Time series plots of cloud areas were derived from the IR GMS data for the entire life cycle of each tropical cyclone. The plots are used to illustrate objective satellite diagnosis for tropical cyclone intensity changes, size and outer core winds, and tropical cyclone genesis. R.B.

A89-12835* National Aeronautics and Space Administration, Marshall Space Flight Center, Huntsville, AL.

THUNDERSTORM ICE INDUCED BRIGHTNESS TEMPERATURE DEPRESSIONS AT 18, 37, AND 92 GHZ DURING COHMEX AND THEIR IMPLICATIONS FOR SATELLITE PRECIPITATION RETRIEVALS

ROBBIE E. HOOD and ROY W. SPENCER (NASA, Marshall Space Flight Center, Huntsville, AL) IN: Conference on Satellite Meteorology and Oceanography, 3rd, Anaheim, CA, Feb. 1-5, 1988, Preprints. Boston, MA, American Meteorological Society, 1988, p. 303-308. refs

Measurements of thunderstorm ice scattering at 18, 37, and 92 GHz, and with high spatial and temporal resolution from the Cooperative Huntsville Meteorological Experiment (Cohmex) are discussed. The Cohmex experiment consisted of ground-based, airborne, and satellite experiments in June and July, 1986. The rainfall rates from the experiment are compared with other measurements and the implications of the results for satellite precipitation retrievals are examined. R.B.

A89-12836**COMPARISON OF WEATHER RADAR AND SATELLITE-BASED PASSIVE MICROWAVE OBSERVATIONS OF RAINFALL OVER LAND AND OCEANS**

RALPH R. FERRARO, JOSEPH V. FIORE (Research and Data Systems Corp., Lanham, MD), and JOHN C. ALISHOUSE (NOAA, National Environmental Satellite, Data, and Information Service, Washington, DC) IN: Conference on Satellite Meteorology and Oceanography, 3rd, Anaheim, CA, Feb. 1-5, 1988, Preprints. Boston, MA, American Meteorological Society, 1988, p. 309-314. refs

Algorithms are developed for the retrieval of rainrates over land and ocean using matchups between weather radar observations and coincident passive microwave measurements. The results are compared to those from visible and IR techniques. It is suggested that the microwave technique responds directly to the column of rain, while the visible and IR techniques can only indirectly determine the presence and intensity of rain. R.B.

A89-12837* Nebraska Univ., Lincoln.**A PILOT STUDY TO DETERMINE RELATIONSHIPS BETWEEN NORTH PACIFIC PRECIPITATION FROM NIMBUS-7****SCANNING MULTICHANNEL MICROWAVE RADIOMETER DATA AND ASSOCIATED ATMOSPHERIC CONDITIONS**

MARK R. ANDERSON (Nebraska, University, Lincoln) and JOHN O. ROADS (California, University, La Jolla) IN: Conference on Satellite Meteorology and Oceanography, 3rd, Anaheim, CA, Feb. 1-5, 1988, Preprints. Boston, MA, American Meteorological Society, 1988, p. 315-318. Research supported by the University of California. refs

(Contract NAG2-36)

Relationships between the large scale field and the location of cyclone tracks are found by deriving monthly precipitation positions in the North Pacific. The precipitation locations are determined from Nimbus-7 SMMR data for the winter seasons 1978-1979 and 1979-1980. These locations are compared to the large scale atmospheric conditions. R.B.

A89-12855**EVALUATION OF 3.7 MICRON SPLIT WINDOWS FOR ESTIMATING SURFACE TEMPERATURE**

DAVID S. CROSBY (American University; NOAA, Satellite Research Laboratory, Washington, DC), LARRY M. MCMILLIN, and JOHN C. ALISHOUSE (NOAA, Satellite Research Laboratory, Washington, DC) IN: Conference on Satellite Meteorology and Oceanography, 3rd, Anaheim, CA, Feb. 1-5, 1988, Preprints. Boston, MA, American Meteorological Society, 1988, p. 406-409. refs

The accuracy obtained by using a split window wavelength pair in the 3.7 micron region for the estimation of SSTs was compared with the accuracy of split windows in the 11-micron region, using simulated SST data for various combinations of 3.7-micron and 11-micron split windows. The results showed that a combination of both split windows provided a complementary set of measurements. The 11-micron pair provided accurate SSTs in polar and midlatitude regions under all lighting conditions, while the 3.7-micron pair provided the best results in the tropics, compensating for the major limitation of the 11-micron pair due to the high atmospheric absorption frequently experienced in tropical areas. I.S.

A89-12856**EOF ANALYSIS OF AVHRR AND CZCS IMAGERY**

GARY S. E. LAGERLOEF (Science Applications International Corp., Bellevue, WA) IN: Conference on Satellite Meteorology and Oceanography, 3rd, Anaheim, CA, Feb. 1-5, 1988, Preprints. Boston, MA, American Meteorological Society, 1988, p. 410-415. Research supported by the U.S. Department of the Interior and Science Applications International Corp. refs

(Contract N00014-87-M-0057)

The empirical orthogonal function (EOF) analysis of AVHRR and CZCS imagery of the central California shelf and the Santa Barbara Channel region off southern California was used to decompose the space-time distributed oceanographic and

meteorological data into modes ranked by their temporal variance. It is shown that the spatial variance EOF decomposition is useful for studying quasi-permanent patterns such as fronts, eddies, or cross-shelf jets found in the satellite imagery. Used in conjunction with temporal variance EOF analysis, considerably more useful information can be gained on the modes of spatial and temporal variability than by use of either technique alone. I.S.

A89-12857**NIMBUS-7 SMMR DERIVED SEA-ICE CONCENTRATIONS OVER ANTARCTICA**

RALPH R. FERRARO, EUGENE R. MAJOR (Research and Data Systems Corp., Lanham, MD), JANE D'AGUANNO, and J. D. TARPLEY (NOAA, National Environmental Satellite, Data, and Information Service, Washington, DC) IN: Conference on Satellite Meteorology and Oceanography, 3rd, Anaheim, CA, Feb. 1-5, 1988, Preprints. Boston, MA, American Meteorological Society, 1988, p. 416-420. refs

The sea-ice behavior in the Eltanin Bay region of the Bellingshausen Sea, western Antarctica was investigated using clear-scene AVHRR channel-2 measurements to derive sea-ice concentrations, and Nimbus-7 SMMR passive microwave measurements at 18 and 37 GHz to derive depolarized brightness temperatures. Linear regressions were performed to derive relationships between the microwave brightness temperatures and ice concentrations. The ice-concentration retrieval algorithms derived will be used for the Advanced Microwave Sounding Unit to be flown aboard the upcoming NOAA-K,L,M satellites scheduled for launch in the 1990s. I.S.

A89-12858**MODELLING OF SURFACE WAVES AND SEA STATE-DEPENDENT WIND STRESS FOR THE NORTHEAST PACIFIC OCEAN USING SEASAT SCATTEROMETER DATA**

H. C. GRABER, K. A. KELLY, R. C. BEARDSLEY (Woods Hole Oceanographic Institution, MA), and S. HASSELMANN (Max-Planck-Institut fuer Meteorologie, Hamburg, Federal Republic of Germany) IN: Conference on Satellite Meteorology and Oceanography, 3rd, Anaheim, CA, Feb. 1-5, 1988, Preprints. Boston, MA, American Meteorological Society, 1988, p. 421-424. refs

Monthly averages of wind stress and significant wave height estimated from Seasat altimeter data (Atlas et al., 1987) are compared with fields computed from the global hindcast study of the third generation ocean wave prediction model (Hasselmann et al., 1987). It is suggested that regional models with spatial resolution of 100 or 50 km are better suited to study wave and wind fields. Also, the importance of including the sea state in calculation of the surface wind stress is assessed. R.B.

A89-12871**INFLUENCE OF SEA SURFACE TEMPERATURE ON INTRA- AND INTER-ANNUAL VARIATIONS OF ITCZ**

JAIME M. DANIELS (ST Systems Corp., Lanham, MD) and ANANDU D. VERNEKAR (Maryland, University, College Park) IN: Conference on Satellite Meteorology and Oceanography, 3rd, Anaheim, CA, Feb. 1-5, 1988, Preprints. Boston, MA, American Meteorological Society, 1988, p. J61-J64. refs

OLR (outgoing long-wave radiation) data derived from measurements made by the NOAA polar-orbiting satellites were used to estimate intraannual and interannual variations of the monthly mean position and intensity of the ITCZ (intertropical convergence zone). These variations are compared with corresponding variations of the sea surface temperature (SST) to assess the role of the SST in maintaining the ITCZ position and intensity. B.J.

A89-13300**THE REGISTRATION OF THE SURFACE EFFECTS OF INTERNAL OCEAN WAVES USING MICROWAVE RADIOMETRY [REGISTRATSIIA POVERKHNOSTNYKH PROIAVLENIY VNUSTRENNIKH VOLN V OKEANE METODAMI SVCH-RADIOMETRII]**

S. I. GAIDANSKII, V. E. GERSHENZON, and V. K. GROMOV (AN SSSR, Institut Kosmicheskikh Issledovani, Moscow, USSR) Akademii Nauk SSSR, Izvestia, Fizika Atmosfery i Okeana (ISSN 0002-3515), vol. 24, Sept. 1988, p. 1000-1005. In Russian. refs

The brightness temperature of the surface of the northern Pacific Ocean was measured using a multifrequency set of microwave radiometers with wavelengths of 0.8, 2, 8, and 18 cm. The variations in brightness temperature due to the intense generation of subsurface waves are examined. R.B.

A89-13758* Massachusetts Inst. of Tech., Cambridge.
BEYOND PLATE TECTONICS - LOOKING AT PLATE DEFORMATION WITH SPACE GEODESY

THOMAS H. JORDAN (MIT, Cambridge, MA) and J. BERNARD MINSTER (California, University, La Jolla) IN: The impact of VLBI on astrophysics and geophysics; Proceedings of the 129th IAU Symposium, Cambridge, MA, May 10-15, 1987. Dordrecht, Kluwer Academic Publishers, 1988, p. 341-350. refs (Contract NAG5-459; NAS5-28572)

The requirements that must be met by space-geodetic systems in order to constrain the horizontal secular motions associated with the geological deformation of the earth's surface are explored. It is suggested that in order to improve existing plate-motion models, the tangential components of relative velocities on interplate baselines must be resolved to an accuracy of less than 3 mm/yr. Results indicate that measuring the velocities between crustal blocks to + or - 5 mm/yr on 100-km to 1000-km scales can produce geologically significant constraints on the integrated deformation rates across continental plate-boundary zones such as the western United States. R.R.

A89-13958
A PRELIMINARY MODEL FOR GEOSAT ALTIMETER DATA ERRORS

A. RICHARD LESCHACK and RICHARD V. SAILOR (Analytic Sciences Corp., Reading, MA) Geophysical Research Letters (ISSN 0094-8276), vol. 15, Oct. 1988, p. 1203-1206. Research supported by Johns Hopkins University. refs

The nongeoidal component of Geosat altimeter data is studied in terms of its spatial frequency. Noise power spectral densities (PSDs) are derived from Geosat altimeter data segments of nearly collinear repeat tracks. The difference time series are analyzed using autoregressive modeling techniques. An average noise PSD, obtained from eight independent repeat-track PSDs, is closely fitted by a first-order Markov model with a white-noise floor. The Geosat average noise PSD is compared with analogous spectra derived for GEOS-3 and Seasat. It is found that the Geosat noise PSD is generally the same as the Seasat noise spectrum at wavelengths greater than about 100 km, but has a lower noise level at shorter wavelengths. R.B.

A89-15116
THE FRENCH SPACE OCEANOGRAPHY PROGRAM [LE PROGRAMME FRANCAIS D'OCEANOGRAPHIE SPATIALE]

J.-L. FELLOUS (CNES, Toulouse, France) and B. VOITURIEZ (Institut Francais de Recherche pour l'Exploitation de la Mer, Paris, France) L'Aeronautique et l'Astronautique (ISSN 0001-9275), no. 131, 1988, p. 21-25. In French.

The French program for applying space technology to the study of the oceans and their role in climate and climate change is described. Special attention is given to the Topex/Poseidon program for the precise global measurement of topography and the ocean's surface and circulation, the passive microwave radiometer ATSR/M flown aboard ERS 1, and the large-swath medium-resolution radiometer, Vegetation, to be flown aboard the SPOT 4 satellite. Ocean data archiving and processing projects and international programs for the study of the evolution of planetary systems (including the Tropical Ocean and Global Atmosphere program and the World Ocean Circulation experiment) are discussed. R.R.

A89-15495
A COMPARISON OF SATELLITE AND EMPIRICAL FORMULA TECHNIQUES FOR ESTIMATING INSOLATION OVER THE OCEANS

ROBERT FROUIN, CATHERINE GAUTIER (California, University, La Jolla), KRISTINA B. KATSAROS, and RICHARD J. LIND (Washington, University, Seattle) Journal of Applied Meteorology (ISSN 0894-8763), vol. 27, Sept. 1988, p. 1016-1023. refs (Contract N00014-80-C-0440; N00014-84-C-0111)

Surface insolation data from the Mixed Layer Dynamics Experiment are used to compare the satellite technique of Gautier et al. (1980) and five commonly referenced empirical formulas for estimating the daily insolation over the oceans. It is found that the satellite technique is superior to all of the empirical formula techniques, having a 0.97 correlation coefficient, a 12.0 W/sq m standard error of estimate, and a -4.9 W/sq m bias error. The satellite technique is able to account for water vapor, ozone, and dust amount variations in the atmosphere and can monitor large extents of ocean quasi-instantaneously. R.B.

A89-15923
MICROWAVE EMISSION AND REFLECTION FROM THE WIND-ROUGHENED SEA SURFACE AT 6.7 AND 18.6 GHZ

YASUNORI SASAKI, ICHIO ASANUMA, KEI MUNEYAMA (Japan Marine Science and Technology Center, Dept. of Marine Research and Development, Yokosuka), GEN'ICHI NAITO (National Research Center for Disaster Prevention, Hiratsuka, Japan), and TSUTOMU SUZUKI (University of Electro-Communications, Tokyo, Japan) IEEE Transactions on Geoscience and Remote Sensing (ISSN 0196-2892), vol. 26, Nov. 1988, p. 860-868. refs

Microwave radiometric observations were made with specially designed microwave radiometers at 6.7 and 18.6 GHz, and results compared with those of other investigators, over the frequency range of 1-40 GHz. Dependences of sea surface emission and reflection on wind speed, frequency, incidence angle, and polarization type are discussed in detail, following discussions of the reflective processes of sky radiation and error estimation in the retrieval of mainlobe-averaged brightness temperature. The wind speed sensitivity of brightness temperature, emissivity, and reflectivity is formulated with respect to frequency and incidence angle in each polarization. The brightness temperature, emissivity, and reflectivity at arbitrary wind speed are derived employing this formulation. Based on the results obtained it is suggested that the 10-19-GHz band may be optimal for satellite microwave radiometer observations of sea-surface wind. I.E.

A89-16976* Jet Propulsion Lab., California Inst. of Tech., Pasadena.

TOWER OCEAN WAVE AND RADAR DEPENDENCE EXPERIMENT - AN OVERVIEW

O. H. SHEMDIN (California Institute of Technology, Jet Propulsion Laboratory, Pasadena) Journal of Geophysical Research (ISSN 0148-0227), vol. 93, Nov. 15, 1988, p. 13829-13836. Navy-supported research. refs

The Tower Ocean Wave and Radar Dependence experiment was conducted between October 1984 and January 1986 to study the mechanisms involved in the SAR imaging of the ocean surface. Measurements obtained included in situ capillary and short gravity waves, long surface waves and internal waves, ambient current and detailed meteorological measurements, and stereophotography. None of the hypotheses on SAR imaging of long surface waves considered are able to explain all of the present SAR observations. R.R.

A89-16977* Jet Propulsion Lab., California Inst. of Tech., Pasadena.

THEORY FOR SYNTHETIC APERTURE RADAR IMAGING OF THE OCEAN SURFACE - WITH APPLICATION TO THE TOWER OCEAN WAVE AND RADAR DEPENDENCE EXPERIMENT ON FOCUS, RESOLUTION, AND WAVE HEIGHT SPECTRA

DAYALAN P. KASILINGAM (Ocean Research and Engineering, Pasadena CA) and OMAR H. SHEMDIN (California Institute of

Technology, Jet Propulsion Laboratory, Pasadena) Journal of Geophysical Research (ISSN 0148-0227), vol. 93, Nov. 15, 1988, p. 13837-13848. refs

A one-dimensional model for simulating azimuthal SAR imaging of the ocean surface is developed which can admit both the 'distributed surface' and 'velocity bunching' approaches. Computer simulations demonstrate that the time-dependent modulation patterns due to the radar cross section variation and the velocity bunching effects provide optimum focusing around half the phase velocity of the long wave. The results indicate that in the Tower Ocean Wave and Radar Dependence experiment, SAR imaging at L band is approximately linear. R.R.

A89-16978

MULTIFOCUS PROCESSING OF L BAND SYNTHETIC APERTURE RADAR IMAGES OF OCEAN WAVES OBTAINED DURING THE TOWER OCEAN WAVE AND RADAR DEPENDENCE EXPERIMENT

E. K. TAJIRIAN (Ocean Research and Engineering, Pasadena, CA) Journal of Geophysical Research (ISSN 0148-0227), vol. 93, Nov. 15, 1988, p. 13849-13857. refs

As part of the Tower Ocean Wave and Radar Dependence experiment objectives, the mechanisms of SAR imaging of ocean waves are investigated using L band SAR data over the Naval Ocean Systems Center tower. This paper provides experimental evidence needed to validate the differing hypotheses. Various processing methods are investigated to generate spectra with large degrees of freedom. The results show that waves traveling in the aircraft direction are most detectable at focus settings in the range 10.0-15.0 m/s, which is consistent with the Marine Remote Sensing Experiment observations reported by Jain and Shemdin (1983). Waves traveling in the direction opposite to the aircraft are most detectable at settings equal to -5.0 to -15.0 m/s. The SAR imaging system acts as a low-pass filter with the peak of the ocean wave height spectrum occurring at higher wave numbers compared with the peak in the SAR image spectrum. Author

A89-16979

AN ANALYTIC REPRESENTATION OF THE SYNTHETIC APERTURE RADAR IMAGE SPECTRUM FOR OCEAN WAVES

DAVID R. LYZENGA (Delaware, University, Newark) Journal of Geophysical Research (ISSN 0148-0227), vol. 93, Nov. 15, 1988, p. 13859-13865. Navy-sponsored research. refs

An analytic expression is derived for the spectrum of a synthetic aperture radar image in terms of the surface reflectivity covariance function. It is shown that within the severe constraints imposed by the short integration time, the third (temporal) dimension of the spectrum can be extracted by varying the processor focus parameter. The results also illustrate the dependence of the image spectrum on the scene coherence time, as well as various nonlinear effects associated with the velocity bunching mechanism. Example calculations are presented for two cases corresponding to data sets collected during the Tower Ocean Wave and Radar Dependence Experiment. Author

A89-16981* Jet Propulsion Lab., California Inst. of Tech., Pasadena.

COMPARISON OF MEASURED AND PREDICTED SEA SURFACE SPECTRA OF SHORT WAVES

O. H. SHEMDIN (California Institute of Technology, Jet Propulsion Laboratory, Pasadena) and P. A. HWANG (Ocean Research and Engineering, Pasadena, CA) Journal of Geophysical Research (ISSN 0148-0227), vol. 93, Nov. 15, 1988, p. 13883-13890. refs

Reliable sea surface slope time series, using a laser optical receiver system deployed on a wave follower, are analyzed to yield slope frequency spectra of the ocean surface up to 300 Hz. The results show significant differences when compared with the Pierson and Stacy (1973) model. An empirical model is proposed in this paper that is consistent with the observed slope spectra. The newly proposed model is compared with other more recently advanced shortwave spectral models. Author

A89-16982* Jet Propulsion Lab., California Inst. of Tech., Pasadena.

DIRECTIONAL MEASUREMENT OF SHORT OCEAN WAVES WITH STEREOPHOTOGRAPHY

OMAR H. SHEMDIN (California Institute of Technology, Jet Propulsion Laboratory, Pasadena), H. MINH TRAN (Ocean Research and Engineering, Pasadena, CA), and S. C. WU (USGS, Flagstaff, AZ) Journal of Geophysical Research (ISSN 0148-0227), vol. 93, Nov. 15, 1988, p. 13891-13901. Navy-sponsored research. refs

Stereophotographs of the sea surface, acquired during the Tower Ocean Wave and Radar Dependence experiment are analyzed to yield directional wave height spectra of short surface waves in the 6-80-cm range. The omnidirectional wave height spectra are found to deviate from the k exp -4 distribution, where k is the wave number. The stereo data processing errors are found to be within ± 5 percent. The omnidirectional spectra yield 514 deg of freedom for 30-cm-long waves. The directional distribution of short waves is processed with a directional resolution of 30 deg, so as to yield 72 deg of freedom for 30-cm-long waves. The directional distributions show peaks that are aligned with the wind and swell directions. It is found that dynamically relevant measurements can be obtained with stereophotography, after removal of the mean surface associated with long waves. Author

A89-16983* Jet Propulsion Lab., California Inst. of Tech., Pasadena.

THE DEPENDENCE OF SEA SURFACE SLOPE ON ATMOSPHERIC STABILITY AND SWELL CONDITIONS

PAUL A. HWANG (Ocean Research and Engineering, Pasadena, CA) and OMAR H. SHEMDIN (California Institute of Technology, Jet Propulsion Laboratory, Pasadena) Journal of Geophysical Research (ISSN 0148-0227), vol. 93, Nov. 15, 1988, p. 13903-13912. refs
(Contract N00014-86-C-0303)

A tower-mounted optical device is used to measure the two-orthogonal components of the sea surface slope. The results indicate that an unstable stratification at the air-sea interface tends to enhance the surface roughness. The presence of a long ocean swell system steers the primary direction of shortwave propagation away from wind direction, and may increase or reduce the mean square slope of the sea surface. Author

A89-16984

WIND STRESS MEASUREMENTS DURING THE TOWER OCEAN WAVE AND RADAR DEPENDENCE EXPERIMENT

G. L. GEERNAERT (U.S. Navy, Naval Research Laboratory, Washington, DC), K. L. DAVIDSON (U.S. Naval Postgraduate School, Monterey, CA), S. E. LARSEN, and T. MIKKELSEN (Forsogsanlaeg Riso, Roskilde, Denmark) Journal of Geophysical Research (ISSN 0148-0227), vol. 93, Nov. 15, 1988, p. 13913-13923. Navy-sponsored research. refs

During the Tower Ocean Wave and Radar Dependence experiment, near-continuous measurements of the wind drag were conducted using the dissipation technique. An intercomparison between these measurements and direct stress magnitudes using a sonic anemometer was performed over three days of the experiment. The results indicated that the dissipation technique results compared well with the directly determined values when conditions were steady and neutral; otherwise, the dissipation method performed poorly. When neutrally stratified data were used, the drag coefficient exhibited a systematic dependence on both surface tension and wave age. Author

A89-16986#

ACOUSTIC DOPPLER CURRENT PROFILING IN THE EQUATORIAL PACIFIC IN 1984

DOUG WILSON (NOAA, Atlantic Oceanographic and Meteorological Laboratory, Miami, FL) and ANTS LEETMAA (NOAA, Climate Analysis Center, Washington, DC) Journal of Geophysical Research (ISSN 0148-0227), vol. 93, Nov. 15, 1988, p. 13947-13966. NOAA-supported research. refs

Hydrographic data and acoustic Doppler current profiles obtained in the equatorial Pacific during 1984 are used to study seasonal changes in the temperature and velocity fields. On the equator between April and November the current changed from eastward to westward, the equatorial undercurrent transport (EUC) decreased, the equatorial zonal pressure gradient increased, and the depth of the mixed layer and the EUC core deepened. Results obtained include Reynolds stresses due to the waves, heat and momentum flux estimates, and details of the vertical phase structure. R.R.

A89-16987

OBSERVING THE SEASONAL VARIABILITY IN THE TROPICAL ATLANTIC FROM ALTIMETRY

YVES MENARD (CNES, Groupe de Recherches de Geodesie Spatiale, Toulouse, France) Journal of Geophysical Research (ISSN 0148-0227), vol. 93, Nov. 15, 1988, p. 13967-13978. NOAA-CNES-supported research. refs

Sea level heights measured by GEOS 3 and Seasat altimeters are used to investigate the strong wind-driven seasonal cycle of the tropical Atlantic circulation. Maps reveal a large annual signal in the western side of the basin where the north equatorial countercurrent and south equatorial current are predominant. The maps are found to agree well with those obtained previously using hydrographic data. R.R.

A89-16989

COASTALLY TRAPPED WAVES IN THE PRESENCE OF A SHELF EDGE DENSITY FRONT

SAVITHRI NARAYANAN (Newfoundland, Memorial University, Saint John's, Canada) and IAN WEBSTER (CSIRO, Centre for Environmental Mechanics, Canberra, Australia) Journal of Geophysical Research (ISSN 0148-0227), vol. 93, Nov. 15, 1988, p. 14025-14031. Research supported by the Memorial University of Newfoundland. refs

A model for determining the stability and propagation characteristics of coastally trapped waves is applied to the Sagilek Bank on the Labrador Shelf in order to investigate the ice edge undulations noted in NOAA 5 satellite images. It is shown that the instability is suppressed by the bottom slope if the entire shelf slope is below the front. The presence of a density front on a continental shelf is found to result in either the restriction or the elimination of the backward propagation of energy on the shelf, and thus has a significant effect on the energy propagation along the shelf. R.R.

A89-16990* Massachusetts Inst. of Tech., Cambridge.

CORRELATION FUNCTION STUDY FOR SEA ICE

F. C. LIN, J. A. KONG, R. T. SHIN (MIT, Cambridge, MA), A. J. GOW, and S. A. ARNONE (U.S. Army, Cold Regions Research and Engineering Laboratory, Hanover, NH) Journal of Geophysical Research (ISSN 0148-0227), vol. 93, Nov. 15, 1988, p. 14055-14063. refs
(Contract N00014-83-K-0258; NSF ECS-85-04381; NAG5-270)

For active and passive microwave remote sensing of sea ice, a correlation function of exponential form is extracted from the photograph of a horizontal thin section taken from a sample of artificially grown saline ice that closely resembled Arctic congelation sea ice. It is found that the extracted correlation lengths are consistent with the published average size of brine pockets. With the application of strong fluctuation theory and the bilocal approximation, the effective permittivity tensor is derived in the low-frequency limit for an unbounded uniaxial random medium with two-phase mixtures. Using the extracted correlation lengths, the effective permittivity tensor is computed as a function of fractional volume of brine inclusions and compared with in situ measurements at 4.8 and 9.5 GHz. Author

A89-16991#

EVALUATION OF PRELIMINARY EXPERIMENTS ASSIMILATING SEASAT SIGNIFICANT WAVE HEIGHTS INTO A SPECTRAL WAVE MODEL

DINORAH C. ESTEVA (NOAA, Ocean Products Center, Washington, DC) Journal of Geophysical Research (ISSN 0148-0227), vol. 93, Nov. 15, 1988, p. 14099-14105. refs

The assimilation of significant wave heights (SWHs) from the Seasat altimeter into the National Oceanic and Atmospheric Administration Ocean Wave global spectral model is considered. Forecasts of SWH from each assimilation run and from hindcasts (with no assimilation) are compared to the corresponding Seasat SWH estimate from subsequent satellite passes. The best results were obtained by employing a three-hour assimilation frequency with simple replacement and by scaling the forecasted spectrum with the observed SWH. R.R.

A89-16992*

Jet Propulsion Lab., California Inst. of Tech., Pasadena.

ALTIMETRY FOR NON-GAUSSIAN OCEANS - HEIGHT BIASES AND ESTIMATION OF PARAMETERS

ERNESTO RODRIGUEZ (California Institute of Technology, Jet Propulsion Laboratory, Pasadena) Journal of Geophysical Research (ISSN 0148-0227), vol. 93, Nov. 15, 1988, p. 14107-14120. refs

The effects of a non-Gaussian ocean on satellite altimetry parameter estimation are discussed. The first part of this paper shows how non-Gaussian ocean parameters affect height estimation for satellites of the Seasat/Geosat/TOPEX type. In the second part, the estimation of the altimeter tracker bias and the non-Gaussian ocean parameters from the altimeter return signal is studied. A new convolution model that facilitates the deconvolution of the ocean surface specular point probability density function is introduced. Next, it is argued that it is not feasible in practice to estimate the electromagnetic bias from noisy altimeter returns. It is then shown that the least squares estimation of the surface parameters in the log-frequency domain has several advantages overestimating parameters in the time domain. The maximum likelihood estimation equations for the estimation of the waveform parameters are derived, and their solution is discussed. Author

A89-17695#

APPLICATION OF SATELLITE DATA FOR MONITORING DEGRADATION OF TIDAL WETLANDS OF THE GULF OF KACHCHH, WESTERN INDIA

SHAILESH NAYAK, ANJALI PANDEYA, M. C. GUPTA (ISRO, Space Applications Centre, Ahmedabad, India), C. R. TRIVEDI, K. N. PRASAD (Gujarat Fisheries and Aquatic Sciences Research Institute, Okha, India) et al. IAF, International Astronautical Congress, 39th, Bangalore, India, Oct. 8-15, 1988. 9 p. refs
(IAF PAPER 88-146)

A89-17698#

SATELLITE PHASING PROBLEMS FOR OCEAN AND ATMOSPHERIC STUDIES

SYLVIANE DAILLET-ROCHETTE (CNES, Toulouse, France) IAF, International Astronautical Congress, 39th, Bangalore, India, Oct. 8-15, 1988. 6 p.
(IAF PAPER 88-152)

Numerical techniques for optimizing the orbital phase of a satellite are described and demonstrated, with a focus on atmospheric and oceanographical remote-sensing missions. A geometrical approach based on the altitude and inclination of a family of orbits is employed, and particular attention is given to the wavelengths and periodicity of the phenomena to be observed and the desired repetition and local timing of the tracking pattern. Results of optimization for daily coverage, long-term coverage, an orbit phased to observe a particular point at constant intervals, subcycle phasing, and observation of periodic phenomena are presented in extensive graphs and briefly characterized. T.K.

A89-17700#

ROLE OF ABSORBED SOLAR RADIATION ON INDIAN OCEAN SURFACE TEMPERATURE - A CASE STUDY USING SATELLITE DATA

M. M. ALI (ISRO, Space Applications Centre, Ahmedabad, India)

IAF, International Astronautical Congress, 39th, Bangalore, India, Oct. 8-15, 1988. 5 p.
(IAF PAPER 88-155)

The effect of absorbed solar radiation at the ocean surface on the variation of SST in the Indian Ocean was investigated using MONEX-79 data. The values of absorbed solar radiation at the ocean surface were estimated from the cloud amount and the planetary value of the absorbed solar radiation obtained from the TIROS-N operational products. The day-to-day changes in the absorbed solar radiation were correlated with changes in SST obtained from ship measurements. It was found that, in the month of May, changes in SST were in phase with changes in absorbed solar radiation. When the same regression equation was used for the months of June and July, significant departures were found between the estimated and measured values of SST, due to prominent changes in the mixed-layer depth (MLD) and wind speed after the onset of the monsoon, indicating that SST can be estimated from the absorbed solar radiation only in the absence of significant variations in the MLD and wind speed. I.S.

A89-18843

ESTIMATION OF THE VARIABILITY OF ACOUSTIC CHARACTERISTICS IN THE REGION OF FRONTAL ZONES AND MESOSCALE VORTICES USING REMOTE SENSING DATA [OTSENKA IZMENCHIVOSTI AKUSTICHESKIKH KHARAKTERISTIK V OBLASTI FRONTAL'NYKH ZON I MEZOMASSHTABNYKH VIKHREI S ISPOL'ZOVANIEM DANNYKH DISTANTSIONNOGO ZONDIROVANIYA]

V. I. IL'ICHEV, V. B. LOBANOV, and L. M. MITNIK (AN SSSR, Tikhookeanskii Okeanologicheskii Institut, Vladivostok, USSR) *Akusticheskii Zhurnal* (ISSN 0320-7919), vol. 34, Sept.-Oct. 1988, p. 857-864. In Russian. refs

For a subarctic front west of Japan, ship-monitored sound velocities at the ocean surface and at depths up to 1000 m are compared with satellite imagery based on ocean surface temperature monitoring. It is shown that satellite imagery can be used for the diagnostics of acoustic inhomogeneities of different scales, for estimating spatial sound velocity gradients, and for predicting the effect of surface vortex formation on the acoustic characteristics. V.L.

A89-20721

COMPARISON OF WAVE PARAMETERS DETERMINED FROM SLAR IMAGES AND A PITCH AND ROLL BUOY

P. HOOGEBOOM (Centrale Organisatie voor Toegepast-Natuurwetenschappelijk Onderzoek, The Hague, Netherlands), H. C. PETERS (Rijkswaterstaat, Rijswijk, Netherlands), and H. POUWELS (Nationaal Lucht- en Ruimtevaartlaboratorium, Amsterdam, Netherlands) (European Association of Remote Sensing Laboratories, Annual Symposium on European Remote Sensing Needs in the 1990s, Noordwijkerhout, Netherlands, May 4-8, 1987) *International Journal of Remote Sensing* (ISSN 0143-1161), vol. 9, Oct.-Nov. 1988, p. 1787-1796. Research sponsored by the National Remote Sensing Steering Committee of The Netherlands. refs

The nature of the data recorded by Side-Looking Airborne Radar (SLAR) and that by a pitch and roll buoy differ completely. The radar records a spatial data set at one instant in time, whereas the buoy records a time series on a given point on the sea surface. The spectrum in wave number space of the radar image is transformed to the frequency domain by using the dispersion relation for shallow water waves. With further processing, the radar derived data can be presented in the traditional form of pitch and roll buoy displays - a (relative scale) waveheight spectrum, a directional distribution and the directional spreading, all as a function of frequency. Limitations of the method and differences in the results of the sensors are discussed. Author

A89-20722

SEA SURFACE PARAMETERS INFERRED FROM METEOROLOGICAL SATELLITE DATA AT CMS, LANNION

P. LEBORGNE, J. LE VOURCH, and A. MARSOUIN (Centre de Meteorologie Spatiale, Lannion, France) (European Association

of Remote Sensing Laboratories, Annual Symposium on European Remote Sensing Needs in the 1990s, Noordwijkerhout, Netherlands, May 4-8, 1987) *International Journal of Remote Sensing* (ISSN 0143-1161), vol. 9, Oct.-Nov. 1988, p. 1819-1834. refs

The paper discusses research in the field of sea surface parameter restitution at CMS (Centre de Meteorologie Spatiale) in Lannion, France. Individual experiments are examined, including the use of an interactive image processing system for sea surface temperature (SST) analysis over the Mediterranean Sea, the use of Meteosat and AVHRR data for SST field production, the production of surface solar irradiance fields, and the survey of phytoplankton blooms with visible AVHRR data. The overall objective of the program is to retrieve small-scale characteristics of the ocean-atmosphere thermodynamics. R.B.

A89-20723

SATELLITE REMOTE SENSING AND WAVE STUDIES INTO THE 1990S

D. J. T. CARTER, P. G. CHALLENGER (NERC, Institute of Oceanographic Sciences, Wormley, England), and M. A. SROKOSZ (NERC, British National Space Centre, Farnborough, England) (European Association of Remote Sensing Laboratories, Annual Symposium on European Remote Sensing Needs in the 1990s, Noordwijkerhout, Netherlands, May 4-8, 1987) *International Journal of Remote Sensing* (ISSN 0143-1161), vol. 9, Oct.-Nov. 1988, p. 1835-1846. refs

Questions about sea surface waves which might be addressed by existing and proposed satellite remote sensing techniques are discussed. The topics considered include wave climatology, spatial and temporal variability, the joint distributions of parameters, and wave spectra. The application of remotely-sensed wave data to practical problems requiring temporal statistical information is considered. Also, issues involved in algorithm development, calibration and validation, and data banking, retrieval, and analysis are examined. It is suggested that the issue of facilities for the storage, retrieval, and analysis of data must be addressed to fully exploit the large quantity of wave data which would be provided by proposed missions. R.B.

N89-10314# Universite Catholique de Louvain (Belgium). Lab. de Telecommunications et d'Hyperfréquences.

A THREE DEGREE-OF-FREEDOM DESCRIPTION OF THE OCEAN SURFACE FOR MICROWAVE REMOTE SENSING OF WAVE HEIGHT AND WIND FRICTION VELOCITY

C. BAUFAYS, A. GUISSARD, and P. SOBIESKI In ESA, Proceedings of the 4th International Colloquium on Spectral Signatures in Remote Sensing p 55-61 Apr. 1988
Avail: NTIS HC A23/MF A01; ESA Publications Division, ESTEC, Noordwijk, Netherlands 80 Dutch guilders

A sea surface displacement spectral model which combines three components in a unique spectrum with three degrees of freedom is proposed. This spectral model is described through two internal parameters and the wind friction velocity. Comparisons are made with wind dependent models and with sea data gathered by McClain et al (1982). The application of this model for electromagnetic scattering calculation is under study, showing results nearest the reality in the parameters of propagation during a satellite-ship mobile link with grazing angles. ESA

N89-10315# Marconi Co. Ltd., Great Baddow (England).

THE USE OF THE COMPLEX CORRELATION FUNCTION IN THE RECOVERY OF OCEAN WAVE SPECTRA FROM SAR IMAGES

R. A. CORDEY and J. T. MACKLIN In ESA, Proceedings of the 4th International Colloquium on Spectral Signatures in Remote Sensing p 63-67 Apr. 1988
(Contract ESA-6878/87-HGE-I(SC))

Avail: NTIS HC A23/MF A01; ESA Publications Division, ESTEC, Noordwijk, Netherlands 80 Dutch guilders

A method to predict the wavenumber dependence of the speckle component in spectra of synthetic-aperture radar intensity images was tested using data from VARAN-S and Seasat systems.

The method uses the correlation function of the corresponding complex images and assumes that pixel statistics are Gaussian. It is expected that such a technique will be of use in the routine recovery of ocean wave height spectra from SAR imagery. Results from the Agrisar campaign with VARAN-S over land and sea are good, with speckle spectra being well matched by their predicted forms. Ocean spectra from Seasat are, however, poorly matched in their dependence on azimuth wavenumber. This is not thought to be caused by any sea surface or propagation effect but rather to be an artifact of signal processing. ESA

N89-10316# Centre National d'Etudes Spatiales, Toulouse (France).

COMPARISON BETWEEN ACTIVE AND PASSIVE MICROWAVE MEASUREMENTS OVER ANTARCTICA

F. REMY, M. ANDERSON (Scripps Institution of Oceanography, La Jolla, Calif.), and J. F. MINSTER /In ESA, Proceedings of the 4th International Colloquium on Spectral Signatures in Remote Sensing p 69-72 Apr. 1988

Avail: NTIS HC A23/MF A01; ESA Publications Division, ESTEC, Noordwijk, Netherlands 80 Dutch guilders

The effects of wind on the snow grain size derived from passive microwave radiometer data above continental ice was examined. Wind speed is provided by the power return of the Seasat altimeter measurements. The grain size is derived from the emissivity estimated from 37 GHz NIMBUS-7 radiometer. All possible interactions between the retrieved parameters are reviewed. The role of the wind on the thermal history of ice grains seems to be a dominant factor, while other effects are either insignificant or account for less than 10 percent of the emissivity variance. ESA

N89-10344# Universite Catholique de Louvain (Belgium). Lab. de Telecommunications et d'Hyperfrequences.

AN APPROXIMATIVE MODEL FOR THE MICROWAVE BRIGHTNESS TEMPERATURE SCATTERED BY A ROUGH OPEN OCEAN SURFACE

P. SOBIESKI, A. GUISSARD, and C. BAUFAYS /In ESA, Proceedings of the 4th International Colloquium on Spectral Signatures in Remote Sensing p 221-224 Apr. 1988

Avail: NTIS HC A23/MF A01; ESA Publications Division, ESTEC, Noordwijk, Netherlands 80 Dutch guilders

A modified two-scale model for scattering and emissivity calculations for the random rough sea surface is described. It produces a contracted approximated form of the radiative transfer equation including a scattering correction. This leads to a method simple and accurate enough for real-time inversion algorithms in microwave remote sensing. ESA

N89-10352# GKSS-Forschungszentrum Geesthacht (Germany, F.R.).

HIGH-RESOLUTION SPECTROSCOPY FOR REMOTE SENSING OF OCEAN AND ATMOSPHERE

R. DOEFFER, J. FISCHER, and H. GRASSL /In ESA, Proceedings of the 4th International Colloquium on Spectral Signatures in Remote Sensing p 267-272 Apr. 1988

Avail: NTIS HC A23/MF A01; ESA Publications Division, ESTEC, Noordwijk, Netherlands 80 Dutch guilders

The benefits of using narrow spectral features, like chlorophyll fluorescence for the detection of phytoplankton and oxygen A-band absorption for the retrieval of cloud heights are demonstrated. Radiative transfer calculations are used because of the advantage of a systematic analysis of possible measurement conditions. However, the results are transferable to real conditions as far as the assumptions of a plane-parallel atmosphere-cloud or atmosphere-ocean system and the optical properties used in the radiative transfer model are valid. Results show that retrieval of concentrations of water substances is improved if the Sun stimulated chlorophyll fluorescence at 685 nm is measured with a spectral resolution of at least 5 nm. Spectral absorption within the oxygen A-band in the near infrared can be used for cloud-top height detection. ESA

N89-10361# Sherbrooke Univ. (Quebec).

IMAGING SPECTROMETRY APPLIED TO THE REMOTE SENSING OF SUBMERGED SEAWEED

N. T. ONEILL, Y. GAUTHIER, E. LAMBERT (Montreal Univ., Quebec), L. HUBERT, J. M. M. DUBOIS, and H. EDEL /In ESA, Proceedings of the 4th International Colloquium on Spectral Signatures in Remote Sensing p 315-318 Apr. 1988 Sponsored by the Department of Fisheries and Oceans, Ontario, Canada

Avail: NTIS HC A23/MF A01; ESA Publications Division, ESTEC, Noordwijk, Netherlands 80 Dutch guilders

The utility of imaging spectrometry data for the remote sensing of submerged seaweed is investigated by analyzing data collected by the fluorescence line imager (FLI) and comparing these results with ground based measurements and spectral reflectance models. Radiance differences referenced to the values of the deep water radiance are computed for the FLI data and the spectral models in order to analyze the spectral influence of the water turbidity and the reflectance of the seaweed species indigenous to the region of study (*Laminaria* sp). Comparisons of ground based spectral measurements and the computations of a spectral reflectance indicate a reasonable level of agreement when the free parameters of the model (chlorophyll concentration and depth) are adjusted to obtain the best spectral fit to the measured points. A method of radiance differences was employed to enhance a broad yellow-red peak in the FLI data which is believed to be related to the presence of submerged *Laminaria* sp seaweed canopies. The model employed to simulate the airborne signal yields a spectral feature which is narrower and whose peak is shifted relative to the FLI data. This discrepancy may be related to a significant decrease in water turbidity in going from shallow to deep waters. ESA

N89-10365# Institut Francais de Recherche pour l'Exploitation de la Mer, Brest (France).

HIGH RESOLUTION RADIOMETRIC MEASUREMENT OF INTERTIDAL MICROPHYTOBENTHOS [MESURES RADIOMETRIQUES HAUTE RESOLUTION DU MICROPHYTOBENTHOS INTERTIDAL]

B. GUILLAUMONT, P. GENTIAN, and M. VIOLLIER (Centre National de la Recherche Scientifique, Roscoff, France) /In ESA, Proceedings of the 4th International Colloquium on Spectral Signatures in Remote Sensing p 333-336 Apr. 1988 In FRENCH

Avail: NTIS HC A23/MF A01; ESA Publications Division, ESTEC, Noordwijk, Netherlands 80 Dutch guilders

High resolution spectroradiometric measurements were used to show that spectral variations of the reflectance of intertidal sediments can be likened to spectrophotometric measurements of acetone extracts, a technique usually employed to estimate the microbenthic biomass. Analysis suggests that utilization of the normalized vegetative index calculated from SPOT channels should enable the importance of microflora zones to be determined. For more accurate quantitative estimates, a certain number of ground control points are necessary. ESA

N89-10371# Centre National d'Etudes Spatiales, Toulouse (France). Lab. d'Etudes et de Recherches en Teledetection Spatiale.

ESTIMATION OF PRIMARY MARINE PRODUCTION USING SPACEBORNE DATA ON OCEAN COLOR [ESTIMATION DE LA PRODUCTION PRIMAIRE MARINE A L'AIDE DE DONNEES SPATIALES DE COULEUR DE L'OCEAN]

B. BERTHELOT and P.-Y. DESCHAMPS /In ESA, Proceedings of the 4th International Colloquium on Spectral Signatures in Remote Sensing p 367-370 Apr. 1988 In FRENCH

Avail: NTIS HC A23/MF A01; ESA Publications Division, ESTEC, Noordwijk, Netherlands 80 Dutch guilders

An algorithm which directly determines the amount of photosynthetic available radiation absorbed by chlorophyll pigments from backscattered reflectance from sea water was developed. It assumes that the chemical output of the photosynthesis is known. The algorithm can be used in estimating primary marine production (PMP) from narrow or wideband satellite observations of ocean

color, and establishes a linear relationship between PMP and backscattered reflectance. The algorithm was tested using simulated data from the NIMBUS-7 coastal zone color scanner and the SPOT 4 vegetation instrument. It was compared with an algorithm that uses the determination of the concentration of chlorophyll pigments. The superiority of the developed algorithm, especially given the noisy nature of satellite data, is shown. ESA

N89-10403*# National Aeronautics and Space Administration. Lewis Research Center, Cleveland, OH.

DATA REPORT FOR THE SIPLE COAST (ANTARCTICA) PROJECT

R. A. BINDSCHADLER, S. N. STEPHENSON, E. P. ROBERTS, D. R. MACAYEAL, and D. R. LINDSTROM (Chicago Univ., Ill.) Oct. 1988 108 p
(NASA-TM-100708; NAS 1.15:100708; REPT-88B-0214) Avail: NTIS HC A06/MF A01 CSDL 08B

This report presents data collected during three field seasons of glaciological studies in the Antarctica and describes the methods employed. The region investigated covers the mouths of Ice Streams B and C (the Siple Coast) and Crary Ice Rise on the Ross Ice Shelf. Measurements included in the report are as follows: surface velocity and deformation from repeated satellite geociever positions; surface topography from optical levelling; radar sounding of ice thickness; accumulation rates; near-surface densities and temperature profiles; and mapping from aerial photography.

Author

N89-10516# National Oceanic and Atmospheric Administration, Miami, FL. Oceanographic and Meteorological Labs.

DRIFTING BUOY DATA FROM THE EQUATORIAL PACIFIC FOR THE PERIOD JANUARY 1, 1984 THROUGH MAY 31, 1985

MAYRA C. PAZOS Mar. 1988 106 p
(PB88-212824; NOAA-DR-ERL-AOML-11) Avail: NTIS HC A06/MF A01 CSDL 08C

Satellite tracked drifting buoy Oceanographic data collected in the eastern tropical Pacific Ocean during the period of 1 January 1984 through 31 May 1985 is presented. Deployment times, locations and characteristics of each buoy is detailed. Author

N89-11374# Air Force Inst. of Tech., Wright-Patterson AFB, OH.

ACTIVE MODES OF THE PACIFIC INTERTROPICAL CONVERGENCE ZONE (ITCZ) M.S. Thesis

PATRICK M. HAYES May 1988 105 p
(AD-A196406; AFIT/CI/NR-88-29) Avail: NTIS HC A06/MF A01 CSDL 04A

Satellite-observed outgoing longwave radiation (OLR) data from eight 6-month cool seasons were examined to find periods of active convection within the Pacific intertropical convergence zone (ITCZ). Descriptive statistics were used to define and describe the time-mean behavior of the Pacific ITCZ. Two seasons (76 to 77 and 82 to 83) showed distinctive El Nino-Southern Oscillation (ENSO) signatures in mean, standard deviation, and frequency distribution of OLR. Four other seasons (74 to 75, 75 to 76, 79 to 80, and 80 to 81) had normal OLR statistics. The remaining seasons preceded and followed the major 82 to 83 event and had intermediate seasonal-mean OLR fields. Time series of an index measuring convective intensity in the ITCZ were analyzed to find active convection periods. Time-longitude diagrams of intensity estimates showed how active modes develop, spread, and propagate across the Pacific. Three types of variability of the active modes were identified. The first type had small spatial scales (less than 4000 km), short temporal scales (10 to 20 day durations), and occurred mostly in the eastern Pacific. The second type had longer spatial scales (5000 to 10,000 km), short temporal scales, and was found throughout. The second type also showed evidence of propagation. The third type had large temporal scales (less than 30 days), medium spatial scales (2000 to 6000 km), and was a fixed feature. GRA

N89-12112# Naval Postgraduate School, Monterey, CA.

MARINE BOUNDARY LAYER DEPTH AND RELATIVE HUMIDITY ESTIMATES USING MULTISPECTRAL SATELLITE MEASUREMENTS M.S. Thesis

STEVEN P. SMOLINSKI Mar. 1988 81 p
(AD-A196525) Avail: NTIS HC A05/MF A01 CSDL 04B

A technique is presented to estimate surface relative humidity and boundary layer depth from multispectral satellite measurements using the AVHRR sensor on TIROS-N generation satellites. A sensitivity study quantifies the effect of a combination of input measurement errors of sea-surface temperature, optical depth and total water vapor used in the technique to produce outputs of surface relative humidity and boundary layer depth under simulated conditions and model atmospheres. Technique verification is then accomplished with satellite data compared to ship and aircraft vertical soundings and sea-surface temperature measurements. The root mean square differences between the surface relative humidity/boundary layer depth satellite-measured estimates and verified measurements are 6 percent and 75 m respectively. Finally, synoptic-scale mapping of the surface relative humidity and boundary layer depth fields based on the satellite derived estimates is accomplished with monochromatic and color enhanced satellite images. Horizontal variability of surface relative humidity and boundary layer depth on the order of kilometers can be visually detected from these images. GRA

N89-12945# GEC-Marconi Electronics Ltd., Chelmsford (England).

CONSTRAINTS ON TWO-SCALE DESCRIPTIONS OF RADAR BACKSCATTERING FROM THE SEA SURFACE USING SCATTEROMETER MODEL FUNCTIONS

J. A. CONWAY, R. A. CORDEY, and J. T. MACKLIN In ESA, Proceedings of the 1988 International Geoscience and Remote Sensing Symposium (IGARSS 1988) on Remote Sensing: Moving Towards the 21st Century, Volume 1 p 33-34 Aug. 1988
Avail: NTIS HC A99/MF E03; ESA Publications Div., ESTEC, Noordwijk, Netherlands, 120 US dollars or 250 Dutch guilders

Scatterometer model functions for Seasat and ERS-1 are used to obtain constraints on the cut-off wavenumber k_d required in the composite-surface description of radar backscattering from the sea surface. These data are inverted, neglecting specular backscatter, to obtain the short-wave spectral energy density $E(kB)$ at a particular Bragg wavenumber kB , for a wide range of values of k_d . Due to the overlap of the Seasat and ERS-1 data, a constraint on k_d can be obtained by requiring $E(kB)$ to be a power-law smoothly connecting the data sets. The value of k_d obtained is $0.3kr$ (kr being the radar wavenumber) with a weak dependence on wind speed, thus agreeing with results of other investigators. ESA

N89-12946# Naval Research Lab., Washington, DC.

SHADOWS AND WEDGES IN SCATTERING FROM THE SEA

L. B. WETZEL In ESA, Proceedings of the 1988 International Geoscience and Remote Sensing Symposium (IGARSS 1988) on Remote Sensing: Moving Towards the 21st Century, Volume 1 p 35-38 Aug. 1988

Avail: NTIS HC A99/MF E03; ESA Publications Div., ESTEC, Noordwijk, Netherlands, 120 US dollars or 250 Dutch guilders

By using simple physical optics diffraction theory to calculate the distribution of diffracted illumination over the trough of a trochoidal wave model, it was found that geometrical optics can provide a reasonable shadowing approximation only for the higher wind speeds and radar frequencies, e.g., the greater than 15kts at 10GHz. Under these conditions, the modified illumination profile implied by a threshold shadowing theory leads to a shadowing function with a sharp cut-off below 2 deg. The standard asymptotic approximations used in wedge scattering are found to be unsuitable for describing scattering from the randomly oriented features on a real sea surface. Generalizations turn out to be noncausal, and alternative theories give wrong results at intermediate angles. The failure of both wedge and Bragg scattering theories to provide a self-consistent model of sea scatter is discussed in relation to the

actual scattering structures appearing on the surface of an active sea. ESA

N89-12968# Ecole Nationale Supérieure des Telecommunications, Brest (France). Groupe Traitement d'Images.

SPECTRAL ANALYSIS OF OCEAN WAVE IMAGERY USING 2-D LINEAR PREDICTION

C. CARIOT, J.-M. BOUCHER, C. ROUX, and P. LAROUCHE (Institut Maurice Lamontagne, Mont-Joli, Quebec) /In ESA, Proceedings of the 1988 International Geoscience and Remote Sensing Symposium (IGARSS 1988) on Remote Sensing: Moving Towards the 21st Century, Volume 1 p 127-130 Aug. 1988
 Avail: NTIS HC A99/MF E03; ESA Publications Div., ESTEC, Noordwijk, Netherlands, 120 US dollars or 250 Dutch guilders

A method for spectral estimation based on 2-D linear prediction for the determination of wavelength and propagation direction of swell fields given by Seasat synthetic aperture radar (SAR) and SPOT imaging is presented. The method is shown to provide interesting results when compared to classical Fourier analysis. It allows the estimation of wavelength and propagation direction over small analysis windows (up to 400 sqm) and makes possible the analysis of nonstationary phenomena such as waves refracted by bathymetry or internal waves. ESA

N89-12969# Johns Hopkins Univ., Laurel, MD. Applied Physics Lab.

ON THE USE OF SPECKLE STATISTICS FOR THE EXTRACTION OF OCEAN WAVE SPECTRA FROM SAR IMAGERY

F. M. MONALDO /In ESA, Proceedings of the 1988 International Geoscience and Remote Sensing Symposium (IGARSS 1988) on Remote Sensing: Moving Towards the 21st Century, Volume 1 p 133-136 Aug. 1988
 Avail: NTIS HC A99/MF E03; ESA Publications Div., ESTEC, Noordwijk, Netherlands, 120 US dollars or 250 Dutch guilders

The effects of speckle noise on a synthetic aperture radar (SAR) image spectrum and the necessity for accounting for speckle noise in calibrating ocean wave height-variance spectra derived from SAR imagery are discussed. Speckle noise complicates the procedure of estimating wave slope and height variance spectra from SAR imagery. The incorrect compensation for the speckle noise floor in SAR image spectra causes errors in the total level of ocean wave height or slope-variance estimates from SAR imagery. To alleviate this problem, it is proposed that high resolution SAR ocean wave imagery be averaged to reduced speckle noise. A moderate amount of averaging leaves sufficient resolution to image typical ocean surface waves, but still very significantly reduces speckle noise and its attendant problems. ESA

N89-12970# Forut, Tromsø (Norway).

OCEAN WAVE NUMBER SPECTRA AND SPATIAL AUTOCORRELATION FUNCTIONS FROM SAR IMAGES

H. JOHNSEN, T. ELTOFT, and S. JACOBSEN (Tromsø Univ., Norway) /In ESA, Proceedings of the 1988 International Geoscience and Remote Sensing Symposium (IGARSS 1988) on Remote Sensing: Moving Towards the 21st Century, Volume 1 p 137-140 Aug. 1988
 Avail: NTIS HC A99/MF E03; ESA Publications Div., ESTEC, Noordwijk, Netherlands, 120 US dollars or 250 Dutch guilders

Optimal estimates of the directional long gravity ocean wavenumber spectra were computed from digitally processed X and L-band synthetic aperture radar (SAR) images. An unspeckled estimate of the ocean wave spectrum was obtained from the speckled image spectrum. By performing an inverse Fourier transformation on the wave spectrum, an estimate of the long gravity ocean wave autocorrelation is obtained. For near range traveling waves, the main peak of the wave spectrum is in good agreement with in-situ measured swell wavelength. The direction of propagation (azimuth angle) however, is 15 percent larger than the in-situ measured swell direction. This may be caused by the loss of azimuth resolution caused by the motion of the scatterer. In the case of azimuth traveling waves, no imaging of waves is

observed in the X or in the L-band under the present sea conditions. A combination of nonlinear imaging and loss of azimuth resolution may explain the observations. ESA

N89-12971# Canada Centre for Remote Sensing, Ottawa (Ontario). RADARSAT Project Office.

SAR-SEEN MULTIMODE WAVES IN ICE: EVIDENCE OF IMAGING NONLINEARITIES

R. K. RANEY and P. W. VACHON /In ESA, Proceedings of the 1988 International Geoscience and Remote Sensing Symposium (IGARSS 1988) on Remote Sensing: Moving Towards the 21st Century, Volume 1 p 141-144 Aug. 1988
 Avail: NTIS HC A99/MF E03; ESA Publications Div., ESTEC, Noordwijk, Netherlands, 120 US dollars or 250 Dutch guilders

A two dimensional wave field analytic model based on the synthetic aperture radar (SAR) velocity bunching mechanism that is extended to the multi-modal case and includes the effects of wave component translation between looks is discussed. Using this model, directional spectra results are presented for a bimodal sea. As significant wave height is increased, the image spectra evolve from the correct bimodal form through suppression of the correct modes to creation of a new and dominant spectral artifact propagating at approximately 90 deg to the true wave direction. The simulated wave images compare favorably to actual imagery of waves in ice from the LIMEX/LEWEX 87 EXPERIMENT using similar radar, viewing geometry, and wave parameters. It is concluded that coherence time limitation is beneficial, as it expands the effective linear domain of the SAR imaging process. ESA

N89-12972# Oceanor, Trondheim (Norway).

AN INTERCOMPARISON OF SAR AND BUOY DIRECTIONAL WAVE SPECTRA FROM THE LABRADOR SEA EXTREME WAVES EXPERIMENT (LEWEX)

H. E. KROGSTAD and R. B. OLSEN /In ESA, Proceedings of the 1988 International Geoscience and Remote Sensing Symposium (IGARSS 1988) on Remote Sensing: Moving Towards the 21st Century, Volume 1 p 147-148 Aug. 1988
 Avail: NTIS HC A99/MF E03; ESA Publications Div., ESTEC, Noordwijk, Netherlands, 120 US dollars or 250 Dutch guilders

The Labrador Sea Extreme Waves Experiment (LEWEX) provided an opportunity to compare several airborne remote sensing and in situ wave measuring instruments. Comparisons of C-band synthetic aperture radar (SAR) data with measurements from a heave/pitch/roll buoy are discussed. A method for modifying the buoy data to provide spectra which are equivalent to those expected from an ideal airborne scanning instrument is suggested. Scanning distortion is demonstrated to have a significant effect on the appearance of the spectra. Directional distributions for different wavelengths indicate a fair agreement between the two instruments. However, components in the SAR spectra are not identified in the buoy spectra. ESA

N89-12973# Johns Hopkins Univ., Laurel, MD. Applied Physics Lab.

DIRECTIONAL OCEAN WAVE SPECTRA: PROSPECTS FOR ACQUIRING A GLOBAL DATA BASE FROM SIR-C

R. C. BEAL, J. L. MACARTHUR, F. M. MONALDO, and S. F. ODEN /In ESA, Proceedings of the 1988 International Geoscience and Remote Sensing Symposium (IGARSS 1988) on Remote Sensing: Moving Towards the 21st Century, Volume 1 p 149-150 Aug. 1988
 Avail: NTIS HC A99/MF E03; ESA Publications Div., ESTEC, Noordwijk, Netherlands, 120 US dollars or 250 Dutch guilders

Use of SIR-C to collect directional ocean wave spectra over global scales is discussed. The very low shuttle range-to-velocity ratio will allow the synthetic aperture radar (SAR) to image ocean waves that are reasonably undistorted by Doppler motion blur in the azimuth direction. To take advantage of this opportunity, an experimental on-board processor which, if continually activated below 30S, will provide more than 100,000 directional spectral estimates over a 5 day interval will be implemented. This data base may be sufficiently dense in space and time (one 7 km x 7

km sample per second) to allow a fairly accurate reconstruction of a time-space history of the directional wave spectrum over the entire southern ocean. ESA

N89-12974# Johns Hopkins Univ., Laurel, MD. Applied Physics Lab.

THE LABRADOR SEA EXTREME WAVES EXPERIMENT: OBJECTIVES, STATUS AND PLANS

R. C. BEAL and T. W. GERLING /In ESA, Proceedings of the 1988 International Geoscience and Remote Sensing Symposium (IGARSS 1988) on Remote Sensing: Moving Towards the 21st Century, Volume 1 p 151-154 Aug. 1988
 Avail: NTIS HC A99/MF E03; ESA Publications Div., ESTEC, Noordwijk, Netherlands, 120 US dollars or 250 Dutch guilders

The Labrador Sea Extreme Waves Experiment (LEWEX) is an international effort to assess method of measuring and modeling the directional aspects of wind-generated ocean waves, especially their evolution in the presence of rapidly turning winds. The main data-gathering period of LEWEX occurred from 13 through 19 March 1987, and was supported by a large number of ship and aircraft-based estimates of the directional wave spectrum. Directional spectra were forecast by first, second, and third generation wave models (using their own separately determined wind fields) and will be hindcast by these same models (using a common wind field). A final consensus wind field history may be synthesized by iteration, using a consensus wave field history. ESA

N89-12975# Ministry of Posts and Telecommunications, Tokyo (Japan). Communications Research Lab.

INFERENCE OF RADIO SCATTERING PARAMETERS OF ANTARCTIC ICE SHEET USING 179 MHZ AIRBORNE RADIO ECHO SOUNDING DATA

S. URATSUKA, F. NISHIO, H. OHMAE, and S. MAE (Hokkaido Univ., Sapporo, Japan) /In ESA, Proceedings of the 1988 International Geoscience and Remote Sensing Symposium (IGARSS 1988) on Remote Sensing: Moving Towards the 21st Century, Volume 1 p 157-160 Aug. 1988
 Avail: NTIS HC A99/MF E03; ESA Publications Div., ESTEC, Noordwijk, Netherlands, 120 US dollars or 250 Dutch guilders

Characteristics of radio wave scattering of Antarctic ice sheet are inferred from the 179 MHz airborne radio echo sounding data. The A-scope data from the sounder with wide beam antennas include information on the scattering characteristics at the air/ice interface, at the inner region of the ice sheet, and at the ice/bedrock interface. These characteristics are derived from the A-scope form by using expanded radar equations. These parameters are available to survey the roughness of the air/ice interface of the ice sheet and ice/bedrock the interface, and the temperature of inner regions of the ice sheet. ESA

N89-12998*# National Aeronautics and Space Administration. Goddard Space Flight Center, Greenbelt, MD.

RAINFALL INDEX OVER OCEANS DERIVED FROM SSM/I DATA

A. T. C. CHANG and T. T. WILHEIT /In ESA, Proceedings of the 1988 International Geoscience and Remote Sensing Symposium (IGARSS 1988) on Remote Sensing: Moving Towards the 21st Century, Volume 1 p 251-252 Aug. 1988
 Avail: NTIS HC A99/MF E03; ESA Publications Div., ESTEC, Noordwijk, Netherlands, 120 US dollars or 250 Dutch guilders
 CSCL 04B

The Special Sensor Microwave/Imager radiometer on board the DMSP satellite measured microwave radiation at 19.35, 22.235, 37.0, and 85.5 GHz with a swath width of 1400 km, providing an opportunity to study global precipitation distributions. A monthly averaged rainfall index was derived using only the 19.35 GHz data. It covers the + or - 50 deg portion of the world with a 5 deg x 5 deg grid. The brightness temperature histogram is analyzed to derive the rainfall distribution. Estimates of the freezing level heights and the water vapor contents are utilized to understand the rainfall distribution better. Log normal and gamma distribution

functions are fitted to the data and the derived monthly rainfall index compares favorably with historical precipitation patterns. ESA

N89-13005# Iwate Univ., Morioka (Japan). Dept. of Computer Science.

ESTIMATION OF SEA SURFACE TEMPERATURE VIA NOAA-AVHRR SENSOR: COMPARISON WITH SEA TRUTH DATA BY FIXED BUOYS

R. YOKOYAMA and SUMIO TANBA /In ESA, Proceedings of the 1988 International Geoscience and Remote Sensing Symposium (IGARSS 1988) on Remote Sensing: Moving Towards the 21st Century, Volume 1 p 275-280 Aug. 1988
 Avail: NTIS HC A99/MF E03; ESA Publications Div., ESTEC, Noordwijk, Netherlands, 120 US dollars or 250 Dutch guilders

Brightness temperatures observed by channels 4 and 5 HRPT data of the Advanced Very High Resolution Radiometer (AVHRR) aboard NOAA-9 were compared with in situ sea surface temperature provided by fixed buoys in Mutsu bay in northern Japan. The total of 154 match-ups of the coincidence within 30 min and 3 pixels were screened out. Linear regression analysis was applied to the three grouped data sets, i.e., the total data, the daytime data and the nighttime data. The standard errors in both single and double variate regression functions are comparable (0.5C), but the maximum residues are improved in the double variate regression. ESA

N89-13030# Naval Ocean Research and Development Activity, Bay St. Louis, MS.

SOME CHARACTERISTICS OF SHORT OCEAN WAVES AS MICROWAVE SCATTERERS

P. SMITH and D. JOHNSON /In ESA, Proceedings of the 1988 International Geoscience and Remote Sensing Symposium (IGARSS 1988) on Remote Sensing: Moving Towards the 21st Century, Volume 1 p 395-396 Aug. 1988
 Avail: NTIS HC A99/MF E03; ESA Publications Div., ESTEC, Noordwijk, Netherlands, 120 US dollars or 250 Dutch guilders

In order to assess the applicability of scattering models, and to estimate the range of values for their parameters, a spar buoy equipped with 6 capacitance wave gages spaced at distances appropriate to the 100 to 10 cm scale of ocean waves was developed. Directional wave spectra derived from this data set show that 10 to 100 cm waves in the vicinity of roughness transitions propagate in the downwind direction. The directional resolution is + or - 15 deg. However the confidence limits on the spectral amplitude are not sufficiently small to determine the amplitude of the Bragg scatterers with enough precision to evaluate the relative importance of the Rice perturbation theory. An increase in the number of wires to 14 will alleviate this problem. The directional spectra derived in this manner can give useful information about the wave components present, however. ESA

N89-13031# Kansas Univ., Lawrence. Radar Systems and Remote Sensing Lab.

MODULATION OF THE RADAR BACKSCATTER FROM THE OCEAN SURFACE BY A LONG GRAVITY WAVE

J. C. HOLTZMAN, J. C. WEST, S. P. GOGINENI, and R. K. MOORE /In ESA, Proceedings of the 1988 International Geoscience and Remote Sensing Symposium (IGARSS 1988) on Remote Sensing: Moving Towards the 21st Century, Volume 1 p 397-398 Aug. 1988
 Avail: NTIS HC A99/MF E03; ESA Publications Div., ESTEC, Noordwijk, Netherlands, 120 US dollars or 250 Dutch guilders

The modulation of the scattering cross-section as a function of position on a long gravity wave is calculated from experimental data. The phase position of the signal on the long wave is determined from spectral analysis of the wave-height time series. Samples of return power from the same phase position are averaged together to reduce the effects of phase-interference (Rayleigh) fading. The resulting modulation curves suggest that hydrodynamic and aerodynamic effects are responsible for the radar cross-section modulation. Sea spikes are most common on

the front face of the wave, suggesting they are associated with wave breaking. ESA

N89-13032*# Johns Hopkins Univ., Laurel, MD. Applied Physics Lab.

ESTIMATING AIRCRAFT SAR RESPONSE CHARACTERISTICS AND APPROXIMATING OCEAN WAVE SPECTRA IN THE LABRADOR SEA

D. G. TILLEY /In ESA, Proceedings of the 1988 International Geoscience and Remote Sensing Symposium (IGARSS 1988) on Remote Sensing: Moving Towards the 21st Century, Volume 1 p 399-402 Aug. 1988 Sponsored by NASA and the ONR Avail: NTIS HC A99/MF E03; ESA Publications Div., ESTEC, Noordwijk, Netherlands, 120 US dollars or 250 Dutch guilders CSDL 171

The data processing methods employed to compute estimates of two-dimensional wave height-variance spectra from the ocean imagery obtained in the Labrador Sea by a C-band airborne SAR system are described. The SAR spectra are compared for high and low altitude geometries with large and small elevation angles. A surface contour radar and a radar ocean wave spectrometer aboard an aircraft are used to verify the surface wave spectrum. ESA

N89-13033# Canada Centre for Remote Sensing, Ottawa (Ontario). RADARSAT Project Office.

PHASE VERSUS ORBITAL VELOCITY IN SAR WAVE IMAGING: PARADOX LOST

R. K. RANEY and P. W. VACHON /In ESA, Proceedings of the 1988 International Geoscience and Remote Sensing Symposium (IGARSS 1988) on Remote Sensing: Moving Towards the 21st Century, Volume 1 p 405-406 Aug. 1988 Avail: NTIS HC A99/MF E03; ESA Publications Div., ESTEC, Noordwijk, Netherlands, 120 US dollars or 250 Dutch guilders

The focus paradox in ocean wave SAR imaging from the air is reconciled. Improved wave imagery from an airborne SAR is possible by compensating individual looks (in a multilook data set) for wave movement prior to look summation. By observing the direction of wave motion between looks, the omnipresent 180 deg ambiguity (in wave direction estimation through spectral analysis) may be resolved using only the SAR data from one pass of the sensor. (There are known methods for resolution of the directional ambiguity for a single mode sea using two opposed passes). Approximation of the required image shift by focus adjustment is not recommended because the azimuth impulse response is degraded in the process, the method by definition is tuned to only one wave component, and the resulting image shift is in the azimuthal direction only and thus not necessarily in the direction of wave propagation. For directional spectral calculations, Fourier transformation of individual looks by magnitude summation leads to better results than the normal method of Fourier transformation of the look summed wave image. These results do not depend on invocation of any particular wave imaging mechanism. ESA

N89-13034# Environmental Research Inst. of Michigan, Ann Arbor.

SAR IMAGE STATISTICS RELATED TO ATMOSPHERIC DRAG OVER SEA ICE

B. A. BURNS and A. WEGENER (Institute for Polar and Marine Research, Bremerhaven, West Germany) /In ESA, Proceedings of the 1988 International Geoscience and Remote Sensing Symposium (IGARSS 1988) on Remote Sensing: Moving Towards the 21st Century, Volume 1 p 409-412 Aug. 1988 (Contract N00014-81-C-0295)

Avail: NTIS HC A99/MF E03; ESA Publications Div., ESTEC, Noordwijk, Netherlands, 120 US dollars or 250 Dutch guilders

The possibility of using SAR data to distinguish sea ice regions with different atmospheric drag is explored. The amplitude of the radar backscatter cross section and the areal statistics derived from SAR imagery are examined. Using surface roughness data from pack ice areas it is shown that the scattering coefficients for radar wavelengths presently used are insensitive to the roughness

elements responsible for drag coefficient variations. For seasonal ice zones, where ice concentration and floe deformation contribute to atmospheric drag, statistical filters applied to 23.5 cm SAR digital image data are found to produce maps related to these quantities. ESA

N89-13035# GEC-Marconi Electronics Ltd., Chelmsford (England).

ANALYSIS OF SEASAT SAR SEA-ICE DATA FROM THE BEAUFORT SEA

K. C. PARTINGTON /In ESA, Proceedings of the 1988 International Geoscience and Remote Sensing Symposium (IGARSS 1988) on Remote Sensing: Moving Towards the 21st Century, Volume 1 p 413-416 Aug. 1988

Avail: NTIS HC A99/MF E03; ESA Publications Div., ESTEC, Noordwijk, Netherlands, 120 US dollars or 250 Dutch guilders

Seasat synthetic aperture radar imagery of the Beaufort sea is analyzed. Despite the presence of a large proportion of new ice and a limited dynamic range in the data, computationally-efficient correlation algorithms are highly successful at measuring the motion. The good performance is explained by analysis of the speckle properties of segmented regions of the image. A maximum of 7 percent of the area of the analyzed image is characterized by fully-developed speckle. ESA

N89-13036# Helsinki Univ. of Technology, Espoo (Finland). Dept. of Space Technology.

MICROWAVE DIELECTRIC PROPERTIES OF LOW-SALINITY SEA ICE

M. T. HALLIKAINEN, M. V. O. TOIKKA, and J. M. HYYPPA /In ESA, Proceedings of the 1988 International Geoscience and Remote Sensing Symposium (IGARSS 1988) on Remote Sensing: Moving Towards the 21st Century, Volume 1 p 419-420 Aug. 1988

Avail: NTIS HC A99/MF E03; ESA Publications Div., ESTEC, Noordwijk, Netherlands, 120 US dollars or 250 Dutch guilders

A waveguide transmission system was used to measure the dielectric properties of sea ice during the Bothnian Experiment in Preparation for ERS-1 Campaign in the Gulf of Bothnia, March 31 - April 3, 1987. The temperature range of the ice samples was minus 6.0 to minus 0.3 C and the salinity range 0.0 to 1.0 per mille. The dielectric properties of the sea ice are dominated by those of the brine liquid. ESA

N89-13037# Canada Centre for Remote Sensing, Ottawa (Ontario).

THE LIMEX 1987 PILOT PROJECT, LIMEX 1989 AND LONG-TERM OBJECTIVE FOR DATA COLLECTION ON THE CANADIAN EAST COAST

L. MCNUTT and R. K. RANEY /In ESA, Proceedings of the 1988 International Geoscience and Remote Sensing Symposium (IGARSS 1988) on Remote Sensing: Moving Towards the 21st Century, Volume 1 p 421-422 Aug. 1988

Avail: NTIS HC A99/MF E03; ESA Publications Div., ESTEC, Noordwijk, Netherlands, 120 US dollars or 250 Dutch guilders

The Labrador Ice Margin (LIMEX) Series to develop techniques to combine remotely sensed data with meteorological and oceanographic information into air/sea ice interaction models to predict ice and ocean conditions, both short-term and seasonally is introduced. The results obtained from LIMEX '87; the experiment planned for LIMEX '89; and the approach to be used in LIMEX '91 are described. Another followon study will be prepared for the RADARSAT Program, based on experience gained in the previous experiments. ESA

N89-13039# Environmental Research Inst. of Michigan, Ann Arbor. Radar Science Lab.

SEA ICE TYPE CLASSIFICATION OF SAR IMAGERY

C. C. WACKERMAN, R. R. JENTZ, and R. A. SHUCHMAN /In ESA, Proceedings of the 1988 International Geoscience and Remote Sensing Symposium (IGARSS 1988) on Remote Sensing: Moving Towards the 21st Century, Volume 1 p 425-428 Aug. 1988

(Contract N00014-87-C-0418; N00014-81-C-0195)

Avail: NTIS HC A99/MF E03; ESA Publications Div., ESTEC, Noordwijk, Netherlands, 120 US dollars or 250 Dutch guilders

Fully automatic algorithms were developed to produce sea ice type classification maps and sea ice concentration estimates of SAR imagery. The sea ice type classification algorithm uses local statistics to determine ice type boundaries, and the ice concentration algorithm iteratively decomposes the histogram into ice and water histograms. The algorithms were used on simulated imagery and actual SAR imagery gathered during the 1984 and 1987 Marginal Ice Zone Experiments (MIZEX). The results are compared with ground truth data gathered during MIZEX '87.

ESA

N89-13070# University of Southern California, Los Angeles.
MODEL-BASED ESTIMATION OF WIND FIELDS OVER THE OCEAN FROM WIND SCATTEROMETER MEASUREMENTS

D. G. LONG and J. M. MENDEL In ESA, Proceedings of the 1988 International Geoscience and Remote Sensing Symposium (IGARSS 1988) on Remote Sensing: Moving Towards the 21st Century, Volume 1 p 553-556 Aug. 1988

Avail: NTIS HC A99/MF E03; ESA Publications Div., ESTEC, Noordwijk, Netherlands, 120 US dollars or 250 Dutch guilders

A model-based approach to estimating the entire wind field over the swath simultaneously is described. The approach incorporates dynamical constraints provided by a mathematical model of the wind field and eliminates the dealiasing required in a traditional wind retrieval process. The approach results in more accurate wind estimates and the ability to quantify the accuracy of the resulting wind field estimates. The development of the wind field model, and a comparison of the model-based and traditional wind estimation schemes are reviewed.

ESA

N89-13073*# Jet Propulsion Lab., California Inst. of Tech., Pasadena.

PERFORMANCE OF A SCANNING PENCIL-BEAM SPACEBORNE SCATTEROMETER FOR OCEAN WIND MEASUREMENTS

R. K. MOORE (Kansas Univ. Center for Research, Inc., Lawrence.), R. G. KENNETT, and K. FUK In ESA, Proceedings of the 1988 International Geoscience and Remote Sensing Symposium (IGARSS 1988) on Remote Sensing: Moving Towards the 21st Century, Volume 1 p 563-564 Aug. 1988

Avail: NTIS HC A99/MF E03; ESA Publications Div., ESTEC, Noordwijk, Netherlands, 120 US dollars or 250 Dutch guilders

Simulation results show that a scatterometer design using two pencil beams scanning at different incidence angles measures the near-surface oceanic winds from a satellite better under most conditions than previous designs. The return signals from the ocean surface are much stronger than those from the fan beams used previously. Performance on a polar-orbiting satellite is compared with that of a fan beam spaceborne scatterometer. A wider and continuous swath is covered. The improvement in performance is higher at low wind speeds, so it is particularly suitable for measuring the low-mean-speed tropical wind fields. Performance on a low altitude tropic-orbiting platform such as the Space Station is also shown.

ESA

N89-13089 California Univ., San Diego.

MASS AND HEAT BALANCES IN THE UPPER OCEAN Ph.D. Thesis

DANIEL LARS RUDNICK 1987 114 p
Avail: Univ. Microfilms Order No. DA8804753

The mass and heat balances in the upper ocean are examined from both theoretical and observational points of view. The theoretical model investigates the conditions necessary for frontogenesis in mixed layers. The objective is to understand the roles of advection and turbulent mixing. A unified theory of frontogenesis in mixed layers is proposed. Analytical solutions of the nonlinear mass and density balances in a mixed layer are found in the Lagrangian frame for a wide class of entrainment parameterizations. These solutions show mixed-layer depth and density to be functions of particle position and separation, where

mixing is represented by an integral over time following a particle. Thus, given a knowledge of only the cross-front velocity field, the likelihood of frontal formation can be predicted. Both surface convergence and divergence in conjunction with vertical mixing can be frontogenetic. The mass and heat budgets on the northern California continental shelf between Point Arena and Point Reyes are examined using moored measurements of horizontal water velocity and temperature made during the second Coastal Ocean Dynamics Experiment (CODE-2). Dissert. Abstr.

N89-13128# Washington Univ., Seattle. Inst. for Study of Atmosphere and Ocean.

A NUMERICAL MODEL FOR THE COMPUTATION OF RADIANCE DISTRIBUTIONS IN NATURAL WATERS WITH WIND-ROUGHENED SURFACES

CURTIS D. MOBLEY and RUDOLPH W. PREISENDORFER Jan. 1988 201 p

(Contract N00014-87-K-0525)

(AD-A197207; CONTRIB-40; NOAA/PMEL-TM-75;

NOAA/PMEL-CONTRIB-813) Avail: NTIS HC A10/MF A01 CSCL 08H

The details are compiled of the derivation of a numerical procedure to determine the unpolarized radiance distribution as a function of depth, direction, and wavelength, in a natural hydrosol such as a lake or sea. The input to the model consists of the incidence radiance distribution at the air water surface, the state of randomness of the air water surface as a function of wind speed, the volume scattering and volume attenuation functions of the medium as a function of depth and wavelength, and the type of bottom boundary. The fundamental mathematical operation is the discretization over direction space of the continuous radiative transfer equation. The directionally discretized radiances, called quadaveraged radiances, are the averages over a finite set of solid angles of the directionally continuous radiance. The quadaveraged equations are azimuthally decomposed using standard Fourier analysis to obtain equations for the quadaveraged radiances are assembled from the solution reflectances and transmittances of the water body, in combination with the boundary conditions. The model has an expandable library of derived quantities that are of use in various applications of optics to natural waters, such as marine biological studies, underwater visual search tasks, remote sensing, and climatology. GRA

N89-13861*# National Aeronautics and Space Administration. Goddard Space Flight Center, Greenbelt, MD.

NASA SEA ICE AND SNOW VALIDATION PROGRAM FOR THE DMSP SSM/I: NASA DC-8 FLIGHT REPORT

D. J. CAVALIERI Sep. 1988 145 p
(NASA-TM-100706; REPT-88B0262; NAS 1.15:100706) Avail: NTIS HC A07/MF A01 CSCL 08C

In June 1987 a new microwave sensor called the Special Sensor Microwave Imager (SSM/I) was launched as part of the Defense Meteorological Satellite Program (DMSP). In recognition of the importance of this sensor to the polar research community, NASA developed a program to acquire the data, to convert the data into sea ice parameters, and finally to validate and archive both the SSM/I radiances and the derived sea ice parameters. Central to NASA's sea ice validation program was a series of SSM/I aircraft underflights with the NASA DC-8 airborne Laboratory. The mission (the Arctic '88 Sea Ice Mission) was completed in March 1988. This report summarizes the mission and includes a summary of aircraft instrumentation, coordination with participating Navy aircraft, flight objectives, flight plans, data collected, SSM/I orbits for each day during the mission, and lists several piggyback experiments supported during this mission. Author

N89-13863# Massachusetts Inst. of Tech., Cambridge.

EVALUATION OF GEOSAT (GEODETIC SATELLITE) DATA AND APPLICATION TO VARIABILITY OF THE NORTHEAST PACIFIC OCEAN M.S. Thesis

JEFFREY WILLIAM CAMPBELL Sep. 1988 161 p Prepared in cooperation with Woods Hole Oceanographic Inst., Mass. (AD-A198950) Avail: NTIS HC A08/MF A01 CSCL 08E

Part of the N.E. Pacific was studied to evaluate and use altimetric data from the Navy Geodetic Satellite GEOSAT. The zero-order accuracy of the major GEOSAT geophysical data record (GDR) channels was verified, and occasional gaps in the altimeter coverage were noted. GEOSAT's 17-day repeat orbit allowed use of collinear-track processing to create profiles of the difference between the sea surface height along a given satellite repeat, and the mean sea surface height along that repeat's groundtrack. Detrending of sea surface bias and tilt on each repeat reduced orbit and other long wavelength errors in the difference profiles. Corrections provided on the GEOSAT GDR were examined for their effects on the difference profiles of three test arcs. It was found that only the ocean tide, electromagnetic bias, and inverted barometer corrections varied enough over the arc lengths (approx. 4400 km) to have any noticeable effect on the difference profiles. Only the ocean tide correction was accurate enough to warrant using it to adjust the sea surface heights. data for the area including making the ocean tide correction, three-point block averaging successive sea surface heights, and forming the mean height profiles from 18 repeat cycles (to reduce aliasing of the M2 tidal component). A set of difference profiles for one GEOSAT arc indicated that a reasonable estimate of GEOSAT's system precision was approx. 4.5 cm (RMS). The mid wavelength range (100 to 500 km) of these profiles was found to be the only range in which oceanic mesoscale features could be separated from altimeter errors. GRA

N89-13864# Naval Ocean Research and Development Activity, Bay St. Louis, MS.

THE IMPACT OF SATELLITE INFRARED SEA SURFACE TEMPERATURES ON THE FNOC (FLEET NUMERICAL OCEANOGRAPHY CENTER) EOTS (EXPANDED OCEAN THERMAL STRUCTURE) REGIONAL GULF STREAM ANALYSIS Final Report

DOUGLAS A. MAY and JEFFREY D. HAWKINS Jul. 1988 18 p
(AD-A198965; NORDA-183) Avail: NTIS HC A03/MF A01 CSCI 08C

In July 1987, two Expanded Ocean Thermal Structure (EOTS) analysis runs were made daily at 12Z for 5 consecutive days. These runs were made offline at the FNOC for the ENOTS Gulf Stream region. All available satellite multichannel sea surface temperature (MCSST) retrievals, ship reports, and expendable bathythermograph observations were assimilated into the first analysis, with MCSSTs withheld from the second to determine satellite data impact on the analysis. Aircraft-launched expendable bathythermograph (AXBT) data from coincident Regional Energetics Experiment flights were used as independent ground truth. The analysis results and input data sets were compared to the AXBT data. This study shows that MCSST data significantly add to the accuracy of front and eddy mapping by tightening up strong frontal gradients and reducing the impact of relatively noisy ship data. The reliability, the accuracy, and the quantity of MCSSTs far exceed that of ship reports. This difference is evident in the better identification of significant oceanographic features by the satellite-aided analysis. Accuracy of regional EOTS analysis was found to be severely degraded when the only available MCSST data are over 48 hours old. GRA

N89-13865# Flow Research, Inc., Kent, WA.

AN AUTONOMOUS OCEAN INSTRUMENT PLATFORM DRIVEN VERTICALLY BY THE CURRENT Final Technical Report, Sep. 1986 - May 1988

D. C. ECHERT, E. W. GELLER, G. B. WHITE, and J. H. MORISON (Washington Univ., Seattle.) Jul. 1988 56 p
(Contract N00014-86-C-0816; N00014-85-C-0675)
(AD-A198226; FLOW-TR-448) Avail: NTIS HC A04/MF A01 CSCI 08C

This report describes the development and initial field test results of the Autonomous Ocean Profiler (AOP). The AOP is an oceanographic instrument platform for measuring profiles of physical, thermodynamic, and biological properties in the ocean. The profiler employs a hydrodynamic lift device to fly the instrument

package up and down the water column along a taut vertical cable. Because the local currents drive the platform's vertical motion, power requirements are low and, therefore, long, unattended deployments are possible. By using ARGOS and GOES satellite retrieval networks, the system can supply near real time data. The system provides profile data at very high vertical resolution in contrast to conventional buoys, which gather data only at fixed sensor depths. Because only a single set of sensors is required to cover the vertical range desired, the system is low cost and, for many applications, expendable. The initial deployment configuration is as an Arctic drifting buoy. A satellite retransmission buoy is placed on the sea ice surface with the cable suspended below the ice. Conductivity, temperature, and depth information are gathered over a depth range of 0 to 300 m. Data are internally recorded and are relayed to the surface buoy through an inductive communication link for transmission via satellite. Initial test results from Puget Sound and from an Arctic test are described. GRA

N89-14479*# Kansas Univ. Center for Research, Inc., Lawrence. Radar Systems and Remote Sensing Lab.

INVESTIGATION OF RADAR BACKSCATTERING FROM SECOND-YEAR SEA ICE

GUANG-TSAI LEI, RICHARD K. MOORE, and S. P. GOGINENI Feb. 1988 67 p

(Contract NASA ORDER W-16712; N00014-85-K-0200)
(NASA-CR-180986; NAS 1.26:180986; RSL-TR-3311-7) Avail: NTIS HC A04/MF A01 CSCI 08L

The scattering properties of second-year ice were studied in an experiment at Mould Bay in April 1983. Radar backscattering measurements were made at frequencies of 5.2, 9.6, 13.6, and 16.6 GHz for vertical polarization, horizontal polarization and cross polarizations, with incidence angles ranging from 15 to 70 deg. The results indicate that the second-year ice scattering characteristics were different from first-year ice and also different from multiyear ice. The fading properties of radar signals were studied and compared with experimental data. The influence of snow cover on sea ice can be evaluated by accounting for the increase in the number of independent samples from snow volume with respect to that for bare ice surface. A technique for calculating the snow depth was established by this principle and a reasonable agreement has been observed. It appears that this is a usable way to measure depth in snow or other snow-like media using radar. Author

N89-14484# SACLANT ASW Research Center, La Spezia (Italy). Undersea Research Center.

THE NUMERICAL SIMULATION OF INFRARED SATELLITE MEASUREMENTS OVER THE GREENLAND-ICELAND-NORWEGIAN SEA

P. J. MINNETT Jun. 1988 64 p
(AD-A198653; SACLANTCEN-SR-137) Avail: NTIS HC A04/MF A01 CSCI 08C

The accuracy with which self-calibrating satellite infrared radiometers can measure sea-surface temperature is limited by the modification of the electromagnetic radiation before it reaches the radiometer. These physical effects are described for the spectral interval of infrared wavelengths from approx 10 to approx 14 microns and the split-window expression for sea-surface temperature is derived and discussed. An accurate numerical line-by-line model of the radiative transfer through the atmosphere is presented and is used to simulate measurements of the Advanced Very High Resolution Radiometer (AVHRR/2) on the NOAA series of near-polar orbiting satellites for conditions of the region of the Greenland, Iceland and Norwegian Seas. A set of regionally optimized zenith-angle dependent coefficients for the split-window algorithm is derived and its error characteristics are discussed. While the benefit of using such coefficients is demonstrated, the errors resulting from failing to account properly for seasonal changes in this particular region are shown to be relatively small. The FORTRAN programs used for the AVHRR/2 simulations at SACLANTCEN are described in appendices. GRA

N89-14534*# Princeton Univ., NJ. Atmospheric and Ocean Sciences Program.

EVOLUTION OF POLAR STRATOSPHERIC CLOUDS DURING THE ANTARCTIC WINTER Abstract Only

V. RAMASWAMY /In NASA, Goddard Space Flight Center, Polar Ozone Workshop. Abstracts p 83-84 May 1988

Avail: NTIS HC A14/MF A01 CSCL 13B

The occurrence of Polar Stratospheric Clouds (PSCs), initially inferred from satellite measurements of solar extinction, have now also been noted by the recent scientific expeditions in the Antarctic. The presence of such clouds in the Antarctic has been postulated to play a significant role in the depletion of ozone during the transition from winter to spring. The mechanisms suggested involve both dynamical and chemical processes which, explicitly or implicitly, are associated with the ice particles constituting the PSCs. It is, thus, both timely and necessary to investigate the evolution of these clouds and ascertain the nature and magnitude of their influences on the state of the Antarctic stratosphere. To achieve these objectives, a detailed microphysical model of the processes governing the growth and sublimation of ice particles in the polar stratosphere was developed, based on the investigations of Ramaswamy and Detwiler. The present studies focus on the physical processes that occur at temperatures below those required for the onset of ice deposition from the vapor phase. Once these low temperatures are attained, the deposition of water vapor onto nucleation particles becomes extremely significant. First, the factors governing the magnitude of growth and the growth rate of ice particles at various altitudes are examined. Second, the ice phase mechanisms are examined in the context of a column model with altitudes ranging from 100 to 5 mb pressure levels. The column microphysical model was used to perform simulations of the cloud evolution, using the observed daily temperatures. The effect due to the growth of the particles on the radiation fields are also investigated using a one dimensional radiative transfer model. Specifically, the perturbations in the longwave cooling and that in the shortwave heating for the late winter/early spring time period are analyzed. Author

N89-14634*# National Aeronautics and Space Administration, Washington, DC.

SUMMARY OF ALONG-TRACK DATA FROM THE EARTH RADIATION BUDGET SATELLITE FOR SEVERAL REPRESENTATIVE OCEANIC REGIONS

DAVID R. BROOKS and MARTA A. FENN (Planning Research Corp., Hampton, Va.) Nov. 1988 216 p
(NASA-RP-1206; L-16449; NAS 1.61:1206) Avail: NTIS HC A10/MF A01 CSCL 04B

For several days in January and August 1985, the Earth Radiation Budget Satellite, a component of the Earth Radiation Budget Experiment (ERBE), was operated in an along-track scanning mode. A survey of radiance measurements taken in this mode is given for five ocean regions: the north and south Atlantic, the Arabian Sea, the western Pacific north of the Equator, and part of the Intertropical Convergence Zone. Each overflight contains information about the clear scene and three cloud categories: partly cloudy, mostly cloudy, and overcast. The data presented include the variation of longwave and shortwave radiance in each scene classification as a function of viewing zenith angle during each overflight of one of the five target regions. Several features of interest in the development of anisotropic models are evident, including the azimuthal dependence of shortwave radiance that is an essential feature of shortwave bidirectional models. The data also demonstrate that the scene classification algorithm employed by the ERBE results in scene classifications that are a function of viewing geometry. Author

N89-14652# Proudman Oceanographic Lab., Birkenhead (England).

FEASIBILITY STUDY FOR THE DEVELOPMENT OF A JOINT SURGE AND WAVE MODEL

J. WOLF, K. P. HUBBERT, and R. A. FLATHER 1988 108 p
(PB88-230917; REPT-1) Avail: NTIS HC A06/MF A01 CSCL 08C

A preliminary investigation of the interactions between surface waves and the longer period motions due to tides and surges was conducted. The aim is to study the feasibility of developing a combined model of tides, surges and waves with particular application to flood prediction. The theoretical background of the interactions between tide and surge motion and the surface waves is summarized. The modified equations for the conservation of momentum for tide and surge motion and conservation of wave spectral energy density are derived. Some calculations of the magnitude of the interaction terms were made using results of existing surge/tide and wave models. Author

N89-14653*# Miami Univ., Coral Gables, FL.

HEAT FLOW AND MAGNETIZATION IN THE OCEANIC LITHOSPHERE Ph.D. Thesis Semiannual Report, Nov. 1987 - Apr. 1988

KJELL LENNART HAYLING 1988 130 p

(Contract NAG5-414)

(NASA-CR-183346; NAS 1.26:183346) Avail: NTIS HC A07/MF A01 CSCL 08C

Two aspects of the processing and interpretation of satellite measurements of the geomagnetic field are described. One deals with the extraction of the part of the geomagnetic field that originates from sources in the earth's atmosphere. The other investigates the possibility of using the thermal state of the oceanic lithosphere to further constrain modelling and interpretation of magnetic anomalies. It is shown that some of the magnetic signal in crustal anomaly maps can be an artifact of the mathematical algorithms that have been used to separate the crustal field from the observed data. Strong magnetic anomalies can be distorted but are probably real, but weak magnetic anomalies can arise from leakage of power from short wavelengths, and will also appear in anomaly maps as repetitions of the strong crustal anomaly. The distortion and the ghost anomalies follow the magnetic dip lines in a way that is similar to actual MAGSAT anomaly fields. This phenomenon will also affect the lower degree spherical harmonic terms in the power spectrum of the crustal field. A model of the magnetic properties of the oceanic crust that has been derived from direct measurements of the rock magnetic properties of oceanic rocks is presented. The average intensity of magnetization in the oceanic crust is not strong enough to explain magnetic anomalies observed over oceanic areas. This is the case for both near surface observations (ship and aeromagnetic data) and satellite altitude observations. It is shown that magnetic sources in the part of the upper mantle that is situated above the Curie isotherm, if sufficiently strong, can produce satellite magnetic anomalies that are comparable to MAGSAT data. The method developed for the study of depth to the Curie isotherm and magnetic anomalies can also be used in inverse modelling of satellite magnetic anomalies when the model is to be adjusted with an annihilator. Author

N89-14654# Naval Ocean Research and Development Activity, Bay St. Louis, MS. Ocean Sensing and Prediction Div.

THE ROLE OF HORIZONTAL PROCESSES IN UPPER-OCEAN PREDICTION: A FORECAST SIMULATION IN THE SEA OF JAPAN Ph.D. Thesis. Final Report

JOHN M. HARDING, JR. Aug. 1988 250 p

(AD-A198827; NORDA-190) Avail: NTIS HC A11/MF A01 CSCL 08C

Present-day, operational, upper-ocean, thermal-structure forecast models consist of mixed layer models with local wind-generated horizontal and vertical advection. To extend their applicability into dynamically active regions, e.g., western boundary current regions, the next generation ocean models are envisioned to include mesoscale advection provided by high horizontal resolution circulation nowcast and, eventually, forecast models. This study considers the impact of this additional component for advection in a representative dynamic ocean region. Four experiments were performed using a modified version of an operational, upper-ocean, thermal prediction model. Each consisted of a series of daily, 72-hour-duration, upper-ocean hindcasts and was conducted for 4 weeks during the warming season in the

Sea of Japan. The first experiment used an $N \times 1$ -dimensional mixed-layer model with no horizontal and vertical advection. The 3rd, repeated the 2nd, with the addition of a fixed geostrophic component to the horizontal advection. The 4th allowed daily variation of the geostrophic component through each 3-day forecast. Statistical measures applied to the results indicated a small but statistically significant increase in forecast skill due to the addition of the nowcast mesoscale advection. GRA

N89-14655# Naval Ocean Research and Development Activity, Bay St. Louis, MS.

CHEMICAL VARIABILITY IN OCEAN FRONTAL AREAS Final Report

DENIS A. WIESENBURG and DANA A. KESTER Jul. 1988 27 p Presented at a workshop on Biological and Chemical Processes at Oceanic Fronts, Bay St. Louis, MS, 19-22 Sep. 1983 (AD-A198418; NORDA-SP-035; REPT-333; REPT-88) Avail: NTIS HC A03/MF A01 CSCL 08C

Between 19 and 22 September 1983, over 50 scientists met at the Naval Ocean Research and Development Activity (NORDA) to discuss issues related to the study of biological and chemical processes at oceanic fronts. In lieu of the publication of NORDA Report 78, this document has been printed to distribute the abstracts of the meeting. It was evident from the discussion of this workshop that rapid progress could be made in understanding chemical variability and processes at fronts, if a coordinated plan of research is pursued. The scope of the work to be done is multidisciplinary and extensive; this is a problem that would benefit greatly from a long-range, multi-investigator, coordinated study. The major components of such an investigation would include: (1) satellite and aircraft remote sensing, (2) physical characterization of the frontal system and its exchange processes, (3) measurements of chemical gradients and rates for substances participating in biological, photochemical, and solid phase processes, and (4) determination of the abundance and rates of biological activity associated with a front. It is likely that there is a wide range of frontal systems in the ocean that need to be distinguished. A coordinated investigation would provide the greatest advancement of knowledge for a given investment of resources. GRA

N89-14656# SACLANT ASW Research Center, La Spezia (Italy). Undersea Research Center.

QUALITATIVE ASPECTS OF SEISMOGRAPH/OCEAN BOTTOM INTERACTION

M. SNOEK and R. HERBER Jun. 1988 27 p (AD-A198652; SACLANTCEN-SM-206) Avail: NTIS HC A03/MF A01 CSCL 17J

The parameters affecting the coupling of the Ocean Bottom Seismometer to the ground have been studied in a controlled experiment in the large seawater test pit of the Centre Oceanologique de Bretagne, France. An outline of the experiment is presented and an attempt is made to understand the processes involved and relate them to a simple physical mechanism. Examples of sensor performance are given and basic ideas for the design of sensors in general and ground interacting elements are presented. GRA

06

HYDROLOGY AND WATER MANAGEMENT

Includes snow cover and water runoff in rivers and glaciers, saline intrusion, drainage analysis, geomorphology of river basins, land uses, and estuarine studies.

A89-10327

IMAGING SPECTROMETRY FOR WATER APPLICATIONS

N. T. O'NEILL (Sherbrooke, Universite, Canada), A. R. KALINAUSKAS (Moniteq, Ltd., Concord, Canada), G. A. BORSTAD

(G. A. Borstad Associates, Ltd., Sidney, Canada), H. EDEL (Department of Fisheries and Oceans, Ottawa, Canada), J. F. GOWER (Department of Fisheries and Oceans, Institute of Ocean Sciences, Sidney, Canada) et al. IN: Imaging spectroscopy II; Proceedings of the Meeting, San Diego, CA, Aug. 20, 21, 1987. Bellingham, WA, Society of Photo-Optical Instrumentation Engineers, 1988, p. 129-135. refs

Preliminary data acquired by the Fluorescence Line Imager (FLI) of the Canadian Department of Fisheries and Oceans over coastal and inland water scenes is analyzed with a focus on the need for imaging spectrometry in water remote sensing applications. Various examples are given wherein the information contribution of spectral images is advantageous if not essential toward solving the remote sensing inversion problem. Author

A89-10728

NIVAL-GLACIAL SYSTEMS AND THEIR MAPPING [NIVAL'NO-GLIATSIAL'NYE SISTEMY I IKH KARTOGRAFIROVANIE]

N. I. OSOKIN Moscow, VINITI, 1988, 136 p. In Russian. refs

The structure and functioning of nival-glacial systems (i.e., natural systems with the predominant role of the snow/ice cover in its matter balance) are discussed, with emphasis placed on the methods used for their investigation, of which spaceborne information is of foremost importance, and the mapping procedures. Special attention is given to the effect of human activity on the nival-glacial systems and the dangers presented by these systems in the areas of industrial and transportation activities. Glaciological mapping procedures using computer techniques for data collection, storage, processing, and mapping to investigate variations and changes in nival-glacial systems are described. Glaciological maps reflecting the glacial and nival-glacial activity on the territories of southern Siberia and Spitzbergen are presented. I.S.

A89-10934# National Oceanic and Atmospheric Administration, Fort Collins, CO.

BETTER UNDERSTANDING OF INTENSE AND TORNADIC THUNDERSTORMS THROUGH RESEARCH USING GEOSTATIONARY SATELLITE DATA

JAMES F. W. PURDOM (NOAA, Regional and Mesoscale Meteorology Branch; Colorado State University, Fort Collins) IN: International Symposium on Remote Sensing of Environment, 21st, Ann Arbor, MI, Oct. 26-30, 1987, Proceedings. Volume 1. Ann Arbor, MI, Environmental Research Institute of Michigan, 1987, p. 95-115. refs

(Contract NSF ATM-84-20980; NOAA-NA-85RAH05045; NAS8-36472)

The use of satellite data to study convective storm behavior and better understand intense and tornadic storm development is discussed. The influence of terrain and cloud cover on thunderstorm development, the life cycle and dynamics of the arc cloud line, and the difference in the thermodynamic characteristics of the air into which it advances are examined. The properties of convective-scale interaction are outlined, and the way in which severe convective storms can be isolated using satellite imagery is described. Examples of studies of severe convective and tornadic storms using GOES imagery are presented. R.B.

A89-10939#

REMOTE SENSING OF ESTUARIES - AN OVERVIEW

V. KLEMAS and M. A. HARDISKY (Delaware, University, Newark) IN: International Symposium on Remote Sensing of Environment, 21st, Ann Arbor, MI, Oct. 26-30, 1987, Proceedings. Volume 1. Ann Arbor, MI, Environmental Research Institute of Michigan, 1987, p. 183-203. refs

The application of remote sensing techniques to the study of estuaries and coastal properties is reviewed, including the mapping of coastal vegetation and land use, the assessment of wetlands biomass and productivity, and remote sensing of currents and water properties. The use of aerial film cameras for beach erosion mapping, thermal and IR scanner imagery for mapping surface water temperatures, and microwave devices for salinity and wave measurements is discussed. The use of low-cost microcomputers

for analyzing satellite imagery is considered. The importance of Landsat and SPOT imagery to estuarine investigations is examined. It is suggested that the combination of data from several satellites and aircraft is necessary to meet both spatial and temporal resolution requirements. R.B.

A89-10940# REMOTE SENSING OF SUSPENDED SEDIMENTS IN ESTUARIES USING ATMOSPHERIC AND COMPOSITIONAL CORRECTIONS TO AVHRR DATA

RICHARD P. STUMPF (NOAA, Assessment and Information Services Center, Washington, DC) IN: International Symposium on Remote Sensing of Environment, 21st, Ann Arbor, MI, Oct. 26-30, 1987, Proceedings. Volume 1. Ann Arbor, MI, Environmental Research Institute of Michigan, 1987, p. 205-222. refs

The use of AVHRR imagery to study estuaries with widths 3-4 km or larger is examined. Atmospherically corrected reflectances for the red and near-IR can be used to measure turbidity. When using a fixed physical relationship, these reflectances can be used to estimate suspended solids concentrations, having an accuracy of up to + or - 30 percent from 3 to 100 mg/l. The combined use of AVHRR and Landsat MSS data is discussed, the determination of suspended solids, and the processes of atmospheric and pigment correction are discussed. R.B.

A89-10941# LASER FLUOROSENSING OF WATER QUALITY - A REVIEW

WILLIAM D. PHILPOT and ANTHONY VODACEK (Cornell University, Ithaca, NY) IN: International Symposium on Remote Sensing of Environment, 21st, Ann Arbor, MI, Oct. 26-30, 1987, Proceedings. Volume 1. Ann Arbor, MI, Environmental Research Institute of Michigan, 1987, p. 223-240. refs

The use of laser fluorosensing, or the remote detection of a substance which fluoresces in response to excitation by laser light, to study chlorophyll and dissolved organic matter in a water column is reviewed. The process of laser fluorosensing and the use of Raman normalization to improve the reliability of relative concentration predictions are discussed. Improvements in laser and detector technology which make it possible to detect more subtle fluorescence effects, and which could lead to improved identification and quantification, are examined. R.B.

A89-10949# VALIDATION OF THE ON-SITE FLASH FLOOD POTENTIAL SYSTEM FOR NEXRAD

MARK L. WALTON, EDWARD R. JOHNSON, and ROBERT C. SHEDD (NOAA, National Weather Service, Silver Spring, MD) IN: International Symposium on Remote Sensing of Environment, 21st, Ann Arbor, MI, Oct. 26-30, 1987, Proceedings. Volume 1. Ann Arbor, MI, Environmental Research Institute of Michigan, 1987, p. 381-392. refs

A Flash Flood Potential System has been developed for use in Next Generation Weather Radar. The system, consisting of a precipitation projection procedure as well as a flash flood potential assessment procedure, has been tested on a storm in Colorado. Test results indicate that the projection procedure forecasts a one-hour precipitation accumulation with 66-83 percent of the grid points within 2.5 mm of what was observed during the forecast hour. The flash flood potential assessment procedure accurately forecasts areas where flooding did occur. In addition, use of the Flash Flood Potential System could have resulted in flash flood warnings three hours earlier than the National Weather Service warning issued during the actual storm. Author

A89-10992# THE USE OF MICROWAVE RADIOMETRY IN WATERSHED HYDROLOGY

L. CHIARANTINI (Segnalamento Marittimo ed Aereo S.p.A., Florence, Italy), S. PALOSCIA, and P. PAMPALONI (CNR, Istituto di Ricerca sulle onde Elettromagnetiche, Florence, Italy) IN: International Symposium on Remote Sensing of Environment, 21st, Ann Arbor, MI, Oct. 26-30, 1987, Proceedings. Volume 2. Ann

Arbor, MI, Environmental Research Institute of Michigan, 1987, p. 875-881. refs

Microwave radiometers at 10 and 36 GHz and a thermal IR radiometer (8-14 microns) were used to investigate soil and vegetation features of the Po Valley in northern Italy. It is found that the difference between brightness temperature at 39 GHz and that at 10 GHz measured on bare soil is much higher than the difference measured on vegetation. It is shown that the normalized temperature at 10 GHz is sensitive to surface soil moisture variations of bare soils. Different crop types are distinguished by four normalized temperature ranges at both frequencies. Hydrological models are used to show that indices obtained by combining microwave and IR data are sensitive to the total biomass covering the soil and to the water stored in plants and soils. R.B.

A89-11014# UTILIZATION OF LANDSAT DATA AND A GEOGRAPHIC INFORMATION SYSTEM (GIS) FOR IMPROVING WATERSHED MANAGEMENT IN INDIA

RAYMOND LAURIN, JOHN COLWELL (Michigan, Environmental Research Institute, Ann Arbor), SHARAFAT ALI, and DIN DAYAL DOHARE (Department of Agriculture and Cooperation, All India Soil and Land Use Survey Organization, New Delhi) IN: International Symposium on Remote Sensing of Environment, 21st, Ann Arbor, MI, Oct. 26-30, 1987, Proceedings. Volume 2. Ann Arbor, MI, Environmental Research Institute of Michigan, 1987, p. 1111-1118.

A89-12211* Centre National de Recherches Meteorologiques, Toulouse (France).

EVAPORATION OVER LAND SURFACES - FIRST RESULTS FROM HAPEX-MOBILHY SPECIAL OBSERVING PERIOD

JEAN-CLAUDE ANDRE, JEAN-PAUL GOUTORBE, PIERRE BESSEMOULIN (Centre National de Recherches Meteorologiques, Toulouse, France), ALAIN PERRIER (Institut National de Recherches Agronomiques, Grignon, France), FRANCOIS BECKER (NASA, Goddard Space Flight Center, Greenbelt, MD; Groupement Scientifique de Teledetection Spatiale, Strasbourg, France) et al. Annales Geophysicae (ISSN 0980-8752), vol. 6, Oct. 1988, p. 477-492. Research supported by Direction de la Meteorologie Nationale, Institut National de Recherches Agronomiques, USDA, et al. refs

(Contract NSF ATM-85-11196; NSF ATM-85-12535; NSF INT-85-14251; NSF ATM-86-01115; CNES-86-1285; CNRS-DRCI-86-920118; CEC-ST2J-0049-1-F; CEC-ST2J-0049-2-UK)

Preliminary results are presented from the May 7-July 15, 1986 Special Observing Period (SOP) of the HAPEX-MOBILHY program, which examines the hydrological budget and evaporation flux at the scale of a 10,000 sq km GCM grid square to determine soil moisture, surface-energy budgets, and surface hydrology. The SOP used two highly instrumented remote sensing aircraft to obtain detailed measurements of atmospheric fluxes and surface properties. It is noted that the measurements are reliable at spatially local and short time scales, as well as on the monthly time scale. The data base obtained may be used in parametrization schemes against which land-surface water budgets can be tested. O.C.

A89-12845* General Sciences Corp., Laurel, MD. COMPARISON OF SATELLITE IR RAIN ESTIMATES WITH RADAR RAIN OBSERVATIONS IN HURRICANES

K. ROBERT MORRIS (General Sciences Corp., Laurel, MD), ANDREW J. NEGRI, and ROBERT F. ADLER (NASA, Goddard Space Flight Center, Greenbelt, MD) IN: Conference on Satellite Meteorology and Oceanography, 3rd, Anaheim, CA, Feb. 1-5, 1988, Preprints. Boston, MA, American Meteorological Society, 1988, p. 358-362. refs

Radar-observed rainrates and rain areas obtained for the Hurricanes Frederic (1979), Alicia (1983), and Diana (1984) were used in conjunction with GOES IR data to examine the validity of three satellite IR rain estimation techniques: the Arkin (1983) method, the Negri-Adler-Wetzel (1984) technique, and the

convective-stratiform technique of Adler and Negri (1987). The Alicia hurricane was also monitored using the subjective manual technique of Spayd and Scofield (1984). It is shown that the success of IR techniques in identifying areas of rainfall depends on the hurricane feature being addressed. Thus, the three objective IR techniques were unable to identify the locations of radar-observed eyewall and inner band precipitation areas because of strong vertical wind shear in the eyewall and the lack of the vertical extent of stratiform precipitation beneath the central dense overcast. I.S.

A89-14022# CORRECTIONS OF SURFACE PARTICLE PROBE MEASUREMENTS FOR THE EFFECTS OF ASPIRATION

TERRY DESHLER (USBR, Auburn, CA) Journal of Atmospheric and Oceanic Technology (ISSN 0739-0572), vol. 5, Aug. 1988, p. 547-560. USBR-sponsored research. refs

Corrections of a 2D-C optical array probe with a horn-shaped aspirator are discussed. The probe has been used for surface snowfall measurements for six winter seasons in the Sierra Nevada in California. Three other methods to measure ice particle concentrations and size distributions at the ground are compared to simultaneous measurements by the aspirated 2D-C probe. It is found that the 2D-C probe routinely overestimates ice particle concentration by factors of 2.4 to 3.2. The amount of overestimation is shown to be a function of particle size and surface wind speed. R.B.

A89-17285*# National Air and Space Museum, Washington, DC.

MAPPING ABANDONED RIVER CHANNELS IN MALI THROUGH DIRECTIONAL FILTERING OF THEMATIC MAPPER DATA

P. A. JACOBBERGER (National Air and Space Museum, Washington, DC) Remote Sensing of Environment (ISSN 0034-4257), vol. 26, Nov. 1988, p. 161-170. refs (Contract NAS5-28774)

A89-17681# FUTURE MEASUREMENTS OF RAIN FROM SPACE

GERALD R. NORTH (Texas A & M University, College Station) IAF, International Astronautical Congress, 39th, Bangalore, India, Oct. 8-15, 1988. 10 p. refs (IAF PAPER 88-112)

Methods for measuring rain rates from space are discussed and several planned missions to provide rainfall data are reviewed. Techniques for making rain measurements include the IR radiation to space method (Arkin, 1979), the use of microwave radiometers, and the use of cross track scanning active microwave devices (radars). Missions proposed for studying rainfall include the Tropical Rainfall Measuring Mission (Simpson et al., 1988 and Okamoto, 1988) and payloads for the Space Station, including Tropical Rain Mapping Radar, passive microwave radiometer, and visual/IR radiometers. R.B.

A89-17688# DESIGN OF A SPACEBORNE RAIN MAPPING RADAR

N. KAROUCHE (CNES, Toulouse, France), P. AMAYENC, and M. MARZOUG (Centre de Recherches en Physique de l'Environnement Terrestre et Planetaire, Issy-les-Moulineaux, France) IAF, International Astronautical Congress, 39th, Bangalore, India, Oct. 8-15, 1988. 7 p. refs (IAF PAPER 88-124)

The proposed Best project to measure tropical rainfall is discussed. The mission would combine simultaneous measurements by active and passive sensors and integrate this information with visible and IR data from other satellites. The mission objectives, rain radar parameters, and mission configuration are examined. Candidate instruments for the basic payload include a multichannel microwave radiometer, a rain mapping radar, and a non-scanning Doppler lidar. R.B.

A89-17697#

OBSERVATION OF PRECIPITATION USING GMS IMAGERY

LAI-CHEN CHIEN (Academia Sinica, Institute of Physics, Taipei, Republic of China) IAF, International Astronautical Congress, 39th, Bangalore, India, Oct. 8-15, 1988. 11 p. refs (IAF PAPER 88-151)

Geostationary Meteorology Satellite (GMS) infrared data, hourly rainfall data, and conventional observations were used to study the mesoscale convective system (MCS) during the Taiwan Area Mesoscale Experiment (TAMEX) occurring over Taiwan and its vicinity during June 24 and 25, 1987. The MCS cloud system, the rainfall distribution, and the relationship between satellite data and rainfall are analyzed, and the synoptic situation of the MCS formation, intensification, and dissipation is studied. The results show that the convergence produced by the surface front and 850-700 mb short wave trough coupled with the diffluence at 300-200 mb were favorable conditions for the formation and organization of the MCS. The distribution of the MCS cloud top blackbody temperature pattern is found to have a very intimate relationship with the rainfall distribution. C.D.

A89-17873#

PRISM B (PREDICTION OF THE INDIAN SUMMER MONSOON - BELLEVUE)

ISABELLE AMILHAT, LAYLA DARWISH, VALERIE DUTTO, BENEDICTE HAUDECOEUR, CAROLINE MARCHAND (Lycee Bellevue, Toulouse, France) et al. IAF, International Astronautical Congress, 39th, Bangalore, India, Oct. 8-15, 1988. 9 p. Research supported by Association Aeronautique et Astronautique de France, CNES, France Telecom, et al. (IAF PAPER ST-88-02)

The PRISM-B instrument for the prediction of the Indian summer monsoon on the SPOT 4 platform in a 30 deg inclination circular low orbit is discussed. The PRISM-B instrument, which is based on a DIAL concept, is described. The economical impact of the monsoon, the monsoon mechanism, and the PRISM-B mission specifications are examined. R.B.

A89-18708

THE POTENTIAL OF USING REMOTELY SENSED INFORMATION FOR STUDYING THE CONTAMINATION AND EUTROPHICATION OF LAKE SYSTEMS [VOZMOZHNOSTI ISPOL'ZOVANIYA KOSMICHESKOI INFORMATSII DLIA IZUCHENIYA PROTSESSOV ZAGRIAZNENIYA I EVTRIFIROVANIYA OZERNYKH SISTEM]

K. IA. KONDRAT'EV, V. V. BRUK, G. V. DRUZHININ, L. K. EGOROV, I. I. MALYKHINA (AN SSSR, Institut Ozerovedeniia, Leningrad, USSR; Vsesoiuznyi Nauchno-Issledovatel'skii Institut po Okhrane Vod, Kharkov, Ukrainian SSR) et al. Issledovanie Zemli iz Kosmosa (ISSN 0205-9614), July-Aug. 1988, p. 49-57. In Russian. refs

This paper presents the results of an investigation of the eutrophication and the contamination of Ladoga lake, which was conducted on the basis of in situ and remotely sensed data. Significant correlations were established for both of these conditions with the indicators of the lake's water quality, such as temperature, Secchi-disk transparency, electrical conductivity, suspended-matter concentration, chlorophyll content, and total phosphorus. Equations were developed by bivariate and multiple linear regressions between the above indicators and optical characteristics of space imagery. I.S.

A89-18711

ESTIMATING CONCENTRATIONS OF OPTICALLY ACTIVE COMPONENTS FROM THE REMOTELY SENSED SPECTRAL RADIANCE OF A WATER SURFACE [OTSENKA KONTSENTRATSII OPTICHESKII AKTIVNYKH SOSTAVLIAUSHCHIKH PO DISTANTSIONNYM IZMERENIYAM SPEKTRAL'NOI IARKOSTI VODNOI POVERKHNOSTI]

T. FARAGO (Kozponti Meteorologiai Intezet, Budapest, Hungary) Issledovanie Zemli iz Kosmosa (ISSN 0205-9614), July-Aug. 1988, p. 77-83. In Russian. refs

This paper describes a bidirectional approach to the radiative

transfer equation for the estimation of hydrological parameters of a water area. An algorithm is developed for the estimation of optically active components from the values of the spectral radiance of the water surface. The algorithm is used to obtain the distribution of chlorophyll in a bay of Ladoga Lake, and the chlorophyll distribution profiles are compared with data obtained by in situ measurements. I.S.

A89-18712

THE EFFECT OF SNOW PARAMETER VARIATIONS ON THE THERMAL MICROWAVE EMISSION OF THE SOIL-SNOW-ATMOSPHERE SYSTEM [O VLIIANII IZMENENII PARAMETROV SNEGA NA SOBSTVENNOE RADIOTEPLOVOE IZLUCHENIE SISTEMY POCHVA-SNEG-ATMOSFERA]

V. E. GERSHENZON, A. A. GLOTOV, N. B. ERASTOVA, V. G. MIROVSKII, V. V. NIKITIN (Moskovskii Gosudarstvennyi Pedagogicheskii Institut; AN SSSR, Institut Kosmicheskikh Issledovani, Moscow, USSR) et al. Issledovanie Zemli iz Kosmosa (ISSN 0205-9614), July-Aug. 1988, p. 84-89. In Russian. refs

Snow-cover thermal emission measurements at wavelengths of in the 8, 1.5, and 0.8 cm were conducted at a station located in the vicinity of the Elbrus mountain with the purpose of investigating factors affecting the thermal microwave emission of the soil-snow-atmosphere system. Results indicate that, under conditions of constant snow-cover thickness and in the absence of melting, the major cause of changes in the thermal microwave emission characteristics of snow cover was a change in the structure of the snow layer occurring due to snow-recrystallization processes. I.S.

A89-20707

THE USE OF TM DATA FOR THE STUDY OF A MODERN DELTAIC DEPOSITIONAL SYSTEM

M. SGAVETTI and C. FERRARI (Parma, Universita, Italy) (European Association of Remote Sensing Laboratories, Annual Symposium on European Remote Sensing Needs in the 1990s, Noordwijkerhout, Netherlands, May 4-8, 1987) International Journal of Remote Sensing (ISSN 0143-1161), vol. 9, Oct.-Nov. 1988, p. 1613-1627. MPI-supported research. refs

TM data have been used to study the deltaic depositional systems of the Po and Adige rivers. The identification of sedimentary bodies that have formed in well-defined depositional environments requires the reconstruction of their morphology. To this end, several interactive processing techniques have been applied to a large volume of Thematic Mapper (TM) data relative to different spectral bands and acquisition dates. When necessary, data integration has also been made. Association of genetically related depositional elements allowed the interpretation of depositional environments and developmental stages in the study area. Author

A89-20719

THE REMOTE SENSING LOOSDRECHT LAKES PROJECT

A. G. DEKKER and E. SEYHAN (Amsterdam, Vrije Universiteit, Netherlands) (European Association of Remote Sensing Laboratories, Annual Symposium on European Remote Sensing Needs in the 1990s, Noordwijkerhout, Netherlands, May 4-8, 1987) International Journal of Remote Sensing (ISSN 0143-1161), vol. 9, Oct.-Nov. 1988, p. 1761-1773. refs

The Remote Sensing Loosdrecht Lakes to study and detect the temporal and spatial variations in water quality of lakes in the Netherlands is discussed. In the study, TM, SPOT, airborne MSS and low-altitude aerial color images are analyzed qualitatively and quantitatively. The statistical approach used to study spatial variations in water quality is described. Preliminary results of statistical image analyses are presented. R.B.

A89-20720

REGIONAL HYDROLOGICAL SYSTEMS ANALYSIS USING SATELLITE REMOTE SENSING DATA AND A GEOGRAPHICAL INFORMATION SYSTEM - APPLICATION TO GROUNDWATER MODELLING OF THE ROERMOND AREA, THE NETHERLANDS

R. ALLEWIJN (Amsterdam, Vrije Universiteit, Netherlands) (European Association of Remote Sensing Laboratories, Annual Symposium on European Remote Sensing Needs in the 1990s, Noordwijkerhout, Netherlands, May 4-8, 1987) International Journal of Remote Sensing (ISSN 0143-1161), vol. 9, Oct.-Nov. 1988, p. 1775-1785. refs

N89-10372# Grenoble-1 Univ. (France).

SATELLITE SURVEILLANCE OF ICE AND SNOW COVERED SURFACES IN THE FRENCH ALPS USING VISIBLE AND NEAR INFRARED REFLECTANCE MEASUREMENTS FROM THE SPOT AND LANDSAT THEMATIC MAPPER SENSORS [SURVEILLANCE SATELLITAIRE DES SURFACES ENGLACEES ET ENNEIGEEES DANS LES ALPES FRANCAISES PAR MESURE DE REFLECTANCES VISIBLES ET PROCHE INFRAROUGE ISSUE DES CAPTEURS SPOT ET LANDSAT THEMATIC MAPPER]

J.-P. DEDIEU and E. ELIZECHEA (Groupement pour le Developpement de la Teledetection Aerospatiale, Toulouse, France) In ESA, Proceedings of the 4th International Colloquium on Spectral Signatures in Remote Sensing p 371-375 Apr. 1988 In FRENCH

Avail: NTIS HC A23/MF A01; ESA Publications Division, ESTEC, Noordwijk, Netherlands 80 Dutch guilders

The use of satellite imagery to monitor glacier mass balance was studied. Analysis of spectral signatures of snow and ice to discriminate between firm and moving ice zones is described. The analysis is based on the utilization of specific ratios in the visible and near infrared spectral domains, sensitive to the effects of snow grain and ice crystal size. Tests show the utility of combining SPOT panchromatic and multispectral images, with the 10m ground resolution of the panchromatic images allowing comparisons with terrain measurements, and the multispectral images giving a means for fine radiometric discrimination of snow and ice particles. ESA

N89-10375# Office de la Recherche Scientifique et Technique Outre-Mer, Dakar (Senegal). Centre de Recherches Oceanographiques.

BATHYMETRY USING SPOT IMAGERY OF THE CASAMANCE (SENEGAL). FIRST RESULTS [BATHYMETRIE PAR IMAGERIE SPOT SUR LA CASAMANCE (SENEGAL). RESULTATS PRELIMINAIRES]

J. PAGES, J. CITEAU, and H. DEMARCO In ESA, Proceedings of the 4th International Colloquium on Spectral Signatures in Remote Sensing p 387-392 Apr. 1988 In FRENCH; ENGLISH summary

Avail: NTIS HC A23/MF A01; ESA Publications Division, ESTEC, Noordwijk, Netherlands 80 Dutch guilders

The bathymetry of Casamance river in Senegal was studied using SPOT images to help develop a model to predict salinity, which governs economic activities such as fishing and rice growing. Four campaigns for ground truth measurements were done with determination of the usual hydrobiological parameters. The use of a hand-borne radiometer with spectral windows identical to the 3 SPOT channels, used over various type of shallow waters, shows that the channel 3/channel 1 ratio correlates highly with chlorophyll content ($C3/C1 = K.Ln(Chl.)$) and with depth in the 0.8 to 0.02 m depth range ($C3/c1 = K.Ln(z)$). Using SPOT imagery for the end of rainy season, 4 water categories were determined: deep water (over 0.6 m), shallow water, partly emerged sludge, and land. Similarly to ground measurements results, the SPOT channel 3/channel 1 ratio was used to define semiquantitative scales of depths. On test areas bathymetry was determined by relative value. Preliminary results need to be refined, and the depth scale to be improved and extended to larger areas to take into account the shallow water areas in the salinity budget of Casamance River. ESA

N89-10388# Department of Agriculture, Beltsville, MD. Hydrology Lab.

AIRCRAFT REMOTE SENSING IN HAPEX

T. SCHMUGGE and L. JANSSEN (Wageningen Agricultural Univ., Netherlands) In ESA, Proceedings of the 4th International

Colloquium on Spectral Signatures in Remote Sensing p 463-467
Apr. 1988

Avail: NTIS HC A23/MF A01; ESA Publications Division, ESTEC, Noordwijk, Netherlands 80 Dutch guilders

A C-130 remote sensing aircraft was used in calculation of surface moisture and heat fluxes using combined aircraft observations of surface temperature and soil moisture with surface measurements of the fluxes; spatial integration of aircraft surface albedo and temperature observations for comparison with satellite data; and comparison of the fluxes estimated using the remotely sensed data with those determined from an eddy correlation aircraft. Sensors operating from the visible through the infrared into the microwave provided data over two small fresh water lakes. Thermal infrared multispectral scanner performance is discussed. The instrument can estimate surface temperature with 1 C accuracy if atmospheric effects are accounted for. ESA

N89-10390# Institut National de la Recherche Agronomique, Thiverval-Grignon (France).

A NEW METHOD FOR ESTIMATING REGIONAL EVAPORATION FROM THERMAL INFRARED SURFACE TEMPERATURE MEASUREMENTS [UNE NOUVELLE METHODE D'ESTIMATION DE L'EVAPORATION REGIONALE A PARTIR DE MESURES DE TEMPERATURE DE SURFACE DANS L'INFRAROUGE THERMIQUE]

Y. BRUNET, J. P. LAGOUARDE, and M. NUNEZ (Hobart Univ., Australia) / In ESA, Proceedings of the 4th International Colloquium on Spectral Signatures in Remote Sensing p 473-476 Apr. 1988 In FRENCH

Avail: NTIS HC A23/MF A01; ESA Publications Division, ESTEC, Noordwijk, Netherlands 80 Dutch guilders

A method to estimate evaporation at regional scale, on an hourly basis, based on a single measurement of surface temperature is presented. The algorithm is based on the coupling of a model of surface exchanges with a simple model of the planetary boundary layer. Climate data become dependent variables and the only surface parameters to be taken into account are albedo, emissivity, and roughness length. Model initialization requires radio sounding. The method is validated using three sets of micrometeorological data for dry, wet, and average conditions. ESA

N89-11102*# Applied Research Corp., Landover, MD.
A NEW RADAR TECHNIQUE FOR SATELLITE RAINFALL ALGORITHM DEVELOPMENT

ARTHUR R. JAMESON Sep. 1987 15 p

(Contract NAS5-30041)

(NASA-CR-183471; NAS 1.26:183471; ARC-R87-157) Avail: NTIS HC A03/MF A01 CSCL 171

A potential new radar parameter was investigated for measuring rainfall, namely the summation of the phase shifts at horizontal and vertical polarizations due to propagation through precipitation. The proposed radar technique has several potential advantages over other approaches because it is insensitive to the drop size distribution and to the shapes of the raindrops. Such a parameter could greatly assist the development of satellite rainfall estimation algorithms by providing comparative measurements near the ground. It could also provide hydrologically useful information for such practical applications as urban hydrology. Results of the investigation showed that the parameters can not be measured by radar. However, a closely related radar parameter, propagation differential phase shift, can be readily measured using a polarization diversity radar. It is recommended that propagation differential phase shift be further investigated and developed for radar monitoring of rainfall using a polarization agile radar. It is also recommended that a prototype multiple frequency microwave link be constructed for attenuation measurements not possible by existing radar systems. Author

N89-11293# Pennsylvania State Univ., University Park. Environmental Resources Research Inst.

REMOTE SENSING AND HYDROLOGIC MODELING OF ARID WATERSHEDS: A SCALE ANALYSIS Progress Report

1988 5 p

(Contract DE-FG02-86ER-60472)

(DE88-014625; DOE/ER-60472/02) Avail: NTIS HC A02/MF A01

The ultimate goal of this multiyear research effort is to model long-term (100 to 10,000 yrs), cut and fill cycles in arid region fluvial systems (arroyos). Historic and geologic (late Quaternary) data bases indicate that arid region fluvial systems have oscillated between periods of pronounced aggradation and degradation. This cyclic behavior has affected both water and sediment discharge from arid watersheds as well as ecosystem habitats along hillslopes and valley bottoms. One of the primary causes that has been proposed for this cyclic activity is climatic change for gradual (glacial-interglacial) and catastrophic (volcanic eruptions, el Nino) rates of climatic change on a global scale. The immediate goal of this multiyear research effort is to modify existing numeric hydrologic models (SPUR, KINEROS) which utilize as input multilayered, co-registered remotely sensed data for the prediction of surface hydrology and sediment erosion, transport and deposition in arid region watersheds. It is hypothesized that different types of co-registered, remotely sensed data including digital elevation data sets (DEDS), multispectral scanner (TM, SPOT), and thermal infrared multispectral scanner (TMS) can be used in conjunction with limited ground truth data to predict values of input parameters for numeric watershed hydrology models and thus to compute watershed hydrologic and sedimentologic characteristics. DOE

N89-12993# Rutherford High Energy Lab., Chilton (England).

CROSS-POLAR RADAR MEASUREMENTS IN ICE AND RAIN

J. F. W. GODDARD, S. M. CHERRY, and K. HOLLOWAY / In ESA, Proceedings of the 1988 International Geoscience and Remote Sensing Symposium (IGARSS 1988) on Remote Sensing: Moving Towards the 21st Century, Volume 1 p 235-236 Aug. 1988

Avail: NTIS HC A99/MF E03; ESA Publications Div., ESTEC, Noordwijk, Netherlands, 120 US dollars or 250 Dutch guilders

Linear cross-polar measurements to characterize hydrometeor types and size distributions were made using a 3 GHz radar. Different hydrometeor phases are clearly distinguished, and tight limits can be put on the degree of canting present in different conditions, by comparisons with theoretical modeling of cross-polar and copolar characteristics. ESA

N89-12997# Centre de Recherches en Physique de l'Environnement, Issy-les-Moulineaux (France).

DESIGN OF A SPACEBORNE RADAR FOR TROPICAL RAIN MAPPING AT THE CLIMATOLOGICAL SCALE

M. MARZOUQ, P. AMAYENC, and N. KAROUCHE (Centre National d'Etudes Spatiales, Toulouse, France) / In ESA, Proceedings of the 1988 International Geoscience and Remote Sensing Symposium (IGARSS 1988) on Remote Sensing: Moving Towards the 21st Century, Volume 1 p 247-248 Aug. 1988

Avail: NTIS HC A99/MF E03; ESA Publications Div., ESTEC, Noordwijk, Netherlands, 120 US dollars or 250 Dutch guilders

A high resolution spaceborne radar designed to perform rainfall rate profiling in tropical rain, from the low-inclination platform of the BEST mission project on tropical system energy budget is presented. The main characteristics and the expected performances of the nominal system (one operating frequency in Ku-band, cross-track scanning antenna beam with 1.6 km footprint size) are listed. System characteristics improvement in more sophisticated options are also mentioned. ESA

N89-13028# Reading Univ. (England). Dept. of Geography.

MONITORING PLAYAS USING THEMATIC MAPPER DATA

A. C. MILLINGTON, N. A. QUARMBY, N. DRAKE, A. J. READING, and J. R. G. TOWNSHEND / In ESA, Proceedings of the 1988 International Geoscience and Remote Sensing Symposium (IGARSS 1988) on Remote Sensing: Moving Towards the 21st Century, Volume 1 p 377-380 Aug. 1988

(Contract NERC-F60/G6/12; NERC-GT4/85/GS/85)

Avail: NTIS HC A99/MF E03; ESA Publications Div., ESTEC, Noordwijk, Netherlands, 120 US dollars or 250 Dutch guilders

Image analysis techniques were applied to multitemporal Thematic Mapper data to monitor sediment transfer processes in semi-arid Tunisia. This enabled process-domains on salt playas to be identified, and the detection of seasonal, inter-seasonal, and spatial changes in salt playas which were related to variations in sediment, salt, and moisture fluxes. Surface water and groundwater activity, and eolian processes are all identified as important sediment transfer processes. ESA

N89-13040# Zurich Univ. (Switzerland). Remote Sensing Labs. **IMPROVEMENT IN NOAA-AVHRR SNOWCOVER DETERMINATION FOR RUNOFF PREDICTION** C. FRANK, K. I. ITTEN, and K. STAENZ /In ESA, Proceedings of the 1988 International Geoscience and Remote Sensing Symposium (IGARSS 1988) on Remote Sensing: Moving Towards the 21st Century, Volume 1 p 433-435 Aug. 1988
Avail: NTIS HC A99/MF E03; ESA Publications Div., ESTEC, Noordwijk, Netherlands, 120 US dollars or 250 Dutch guilders

Computer based theme masking and specific image enhancement techniques are demonstrated for an accurate and fast determination of the snow covered area. Cloud masks and height classes from a digital elevation model combined with region masks form the basis for a principal component analysis of NOAA-AVHRR multispectral imagery for an efficient snow cover classification for runoff prediction. ESA

N89-13042# Kanazawa Univ. (Japan). Lab. of Information Science.

SNOWMELT RUNOFF ESTIMATION USING SNOW COVER EXTENT DATA AND ITS APPLICATION TO OPTIMUM CONTROL OF DAM WATER LEVEL Y. KAWATA, T. KUSAKA, and S. UENO (Kyoto Inst. of Tech., Japan) /In ESA, Proceedings of the 1988 International Geoscience and Remote Sensing Symposium (IGARSS 1988) on Remote Sensing: Moving Towards the 21st Century, Volume 1 p 439-440 Aug. 1988
Avail: NTIS HC A99/MF E03; ESA Publications Div., ESTEC, Noordwijk, Netherlands, 120 US dollars or 250 Dutch guilders

Using LANDSAT MSS data and meteorological information, the daily runoff volume in the Sai river basin (Japan) for 3 years was estimated. Simulation of streamflow based on the Martinec Snowmelt Runoff Model (SRM) has an accuracy of 90 percent in the Sai river basin. The snow-cover depletion curve may be estimated from the value of maximum snow depth in the basin. Computer simulation shows that the optimum water level of the Sai River dam can be maintained with the aid of predicted inflow by the SRM. ESA

N89-13043# Puget Sound Univ., Tacoma, WA. **POLARISATION OF PASSIVE MICROWAVE SIGNALS AS INDICATOR OF SNOW WATER EQUIVALENT** Z. F. DANES and P. L. R. DANES /In ESA, Proceedings of the 1988 International Geoscience and Remote Sensing Symposium (IGARSS 1988) on Remote Sensing: Moving Towards the 21st Century, Volume 1 p 441-442 Aug. 1988
(Contract GS-14-08-0001-A-0353)
Avail: NTIS HC A99/MF E03; ESA Publications Div., ESTEC, Noordwijk, Netherlands, 120 US dollars or 250 Dutch guilders

Difference in polarization between the 37 GHz and the 18 GHz passive microwave signals from the upper Colorado River watershed shows strong correlation with the amount of snow on the ground in areas of sparse vegetation. Under such conditions, this difference may become a measure of the snow-water equivalent. However, in wooded areas the correlation is weak if any, probably due to the large amount of energy radiated by the trees. ESA

N89-13044# Zurich Univ. (Switzerland). Remote Sensing Labs. **MONITORING OF SEASONAL SNOW COVER ON GLACIERS** H. HAEFNER and P. LAAGER /In ESA, Proceedings of the 1988 International Geoscience and Remote Sensing Symposium (IGARSS 1988) on Remote Sensing: Moving Towards the 21st

Century, Volume 1 p 443-445 Aug. 1988

Avail: NTIS HC A99/MF E03; ESA Publications Div., ESTEC, Noordwijk, Netherlands, 120 US dollars or 250 Dutch guilders

The delineation of the transient snow line on a glacier was studied for the melting period by comparing the data from an automatic camera, aerial photographs, and LANDSAT-TM images. The accuracy achieved from TM band 2 regarding the course of the snow line lies, except at a few areas of very low contrast, within 1 pixel. The highest snow line in fall and the separation of the firn line allow direct conclusions on the position of the equilibrium line. The dynamics of the melting pattern and the melting curve were established. This allows the influence of weather conditions on the seasonal snow cover and consequently on the runoff pattern to be assessed. ESA

N89-13045*# National Aeronautics and Space Administration. Goddard Space Flight Center, Greenbelt, MD.

AVERAGE AREAL WATER EQUIVALENT OF SNOW IN A MOUNTAIN BASIN USING MICROWAVE AND VISIBLE SATELLITE DATA

A. RANGO, J. MARTINEC, A. T. C. CHANG, J. L. FOSTER, and V. VANKATWIJK (Vrije Univ., Amsterdam, Netherlands) /In ESA, Proceedings of the 1988 International Geoscience and Remote Sensing Symposium (IGARSS 1988) on Remote Sensing: Moving Towards the 21st Century, Volume 1 p 447-448 Aug. 1988
Avail: NTIS HC A99/MF E03; ESA Publications Div., ESTEC, Noordwijk, Netherlands, 120 US dollars or 250 Dutch guilders

Satellite microwave data were used to evaluate the average areal water equivalent of snow cover in the mountainous Rio Grande basin of Colorado. Areal water equivalent data for the basin were obtained from contoured values of point measurements and from zonal water volume values generated by a snowmelt runoff model. Comparison of these snow water equivalent values shows the model values to consistently exceed the contoured values, probably because of the narrow elevation range in the lower part of the basin where the point measurements are concentrated. A significant relationship between the difference in microwave brightness temperatures at two different wavelengths and a basin-wide average snow water equivalent value is obtained. The average water equivalent of the snow cover in the basin was derived from differences of the microwave brightness temperatures. ESA

N89-13046# Massachusetts Univ., Amherst. Microwave Remote Sensing Lab.

MILLIMETER-WAVE BACKSCATTER MEASUREMENTS OF VARIOUS SNOW FORMS

R. M. NARAYANAN, P. M. LANGLOIS, P. W. GAISER, and R. E. MCINTOSH /In ESA, Proceedings of the 1988 International Geoscience and Remote Sensing Symposium (IGARSS 1988) on Remote Sensing: Moving Towards the 21st Century, Volume 1 p 451-452 Aug. 1988
Avail: NTIS HC A99/MF E03; ESA Publications Div., ESTEC, Noordwijk, Netherlands, 120 US dollars or 250 Dutch guilders

Normalized radar cross section measurements of various snow profiles for VV, VH, HM, and HV polarizations at 215 GHz are presented. Combined backscatter model calculations based on surface and volume scattering theory, together with shadowing corrections, agree with the measured data reasonably well. ESA

N89-13047# Georgia Inst. of Tech., Atlanta. **STATISTICS AND HIGH RESOLUTION IMAGING OF SNOWPACK AT 35 GHZ USING A MICROCOMPUTER**

J. M. TROSTEL /In ESA, Proceedings of the 1988 International Geoscience and Remote Sensing Symposium (IGARSS 1988) on Remote Sensing: Moving Towards the 21st Century, Volume 1 p 453-454 Aug. 1988
Avail: NTIS HC A99/MF E03; ESA Publications Div., ESTEC, Noordwijk, Netherlands, 120 US dollars or 250 Dutch guilders

Millimeter wave (MMW) reflectivity data from snow-covered ground was collected during the winter by two polarization-agile, frequency-stepped radars. One radar gathered data over a bandwidth of 640 MHz centered about 35 GHz and the other

gathered data over a 256 MHz bandwidth centered about 95 GHz. A microcomputer-based system, consisting of a microcomputer with two 9-track tape drives and a color printer, is being developed for use in data calibration, statistical analysis of data, and production of high resolution range and inverse synthetic aperture images from frequency-agile MMW data bases. This analysis system was used to look at snow measurement data. ESA

N89-13048# Trier Univ., Trier-Tarforst (Germany, F.R.). Dept. of Geography and Remote Sensing.

SNOW COVER TO ALTER TERRAIN SIGNATURES ON RADAR IMAGES

W. GEILE *In* ESA, Proceedings of the 1988 International Geoscience and Remote Sensing Symposium (IGARSS 1988) on Remote Sensing: Moving Towards the 21st Century, Volume 1 p 455-457 Aug. 1988

Avail: NTIS HC A99/MF E03; ESA Publications Div., ESTEC, Noordwijk, Netherlands, 120 US dollars or 250 Dutch guilders

Differences of an HH-polarized X-band airborne SAR image recorded with the terrain covered by 10 to 15 cm of dry snow compared to imagery of the same test site also recorded in winter but without snow are detailed. A drastically increased contrast between overall low returning open agricultural areas (largely irrespective of the soil surface roughness within the field pattern) and high returning textures such as forests and settlements is seen. An increased brightness and signal compression of individual target returns, strongly enhancing small targets and relief features of the smallest order such as dams or ditches on the background of a more favorable target-to-noise or target-to-clutter ratio is shown. ESA

N89-13049# Department of Agriculture, Beltsville, MD. Hydrology Lab.

MICROCOMPUTERS (PCS) FOR SNOW COVER ANALYSES USING MULTISENSOR SATELLITE DATA

M. F. BAUMGARTNER and A. RANGO *In* ESA, Proceedings of the 1988 International Geoscience and Remote Sensing Symposium (IGARSS 1988) on Remote Sensing: Moving Towards the 21st Century, Volume 1 p 459-460 Aug. 1988

Avail: NTIS HC A99/MF E03; ESA Publications Div., ESTEC, Noordwijk, Netherlands, 120 US dollars or 250 Dutch guilders

The design of a general snow cover mapping scheme which can be used in basins with different geographical characteristics is considered. Selecting the appropriate procedures, the scheme allows precise snow cover mapping taking into account topographical effect, solar illumination, and vegetation and cloud coverage. Based on tests of PC image processing systems, limitations for operational snow cover mapping on microcomputers are presented. ESA

N89-13067# Hydrological Research Inst., Pretoria (South Africa). Dept. of Water Affairs.

THE EXTRAPOLATION OF SPECTRAL SIGNATURES ILLUSTRATES LANDSATS' POTENTIAL TO DETECT WETLANDS

A. HOWMAN *In* ESA, Proceedings of the 1988 International Geoscience and Remote Sensing Symposium (IGARSS 1988) on Remote Sensing: Moving Towards the 21st Century, Volume 1 p 537-539 Aug. 1988

Avail: NTIS HC A99/MF E03; ESA Publications Div., ESTEC, Noordwijk, Netherlands, 120 US dollars or 250 Dutch guilders

Spectral signatures of a wetland area were determined using LANDSAT MSS data, hydromorphic soil information, and a pixel extraction technique. Investigations indicate that wetlands could be identified and that the same wetland signatures could be extrapolated to another part of the same image to classify similar wetland systems. ESA

N89-13822*# National Marine Fisheries Service, Miami, FL. UTILIZING REMOTE SENSING OF THEMATIC MAPPER DATA TO IMPROVE OUR UNDERSTANDING OF ESTUARINE PROCESSES AND THEIR INFLUENCE ON THE PRODUCTIVITY OF ESTUARINE-DEPENDENT FISHERIES

Semiannual Progress Report No. 5

JOAN A. BROWDER, L. NELSON MAY, JR., ALAN ROSENTHAL, ROBERT H. BAUMANN, and JAMES G. GOSSELINK (Louisiana State Univ., Baton Rouge.) 10 Jun. 1988 51 p

(NASA-CR-183409; NAS 1.26:183409) Avail: NTIS HC A04/MF A01 CSCL 08B

The continuing disintegration of the coastal marshes of Louisiana is one of the major environmental problems of the nation. The problem of marsh loss in Louisiana is relevant to fishery management because Louisiana leads the nation in landings of fishery products, and most of the landed species are dependent upon estuaries and their associated tidal marshes. In evaluating the potential effect of marshland loss on fisheries, the first two critical factors to consider are: whether land-water interface in actual disintegrating marshes is currently increasing or decreasing, and the magnitude of the change. In the present study, LANDSAT Thematic Mapper (TM) data covering specific marshes in coastal Louisiana were used to test conclusions from the Browder et al (1984) model with regard to the stage in disintegration at which maximum interface occurs; to further explore the relationship between maximum interface and the pattern of distribution of land and water suggested by the model; and to determine the direction and degree of change in land-water interface in relation to land loss in actual marshes. Author

N89-13924# Colorado State Univ., Fort Collins.

SIMULATION OF RADAR AND SURFACE MEASUREMENTS OF RAINFALL

V. CHANDRASEKAR and V. N. BRINGI *In* its Computer Science and Statistics. Proceedings of the 18th Symposium on the Interface p 183-191 26 Aug. 1987

Avail: NTIS HC A20/MF A01 CSCL 04B

Researchers considered a class of statistical simulations which are computationally intensive and amenable to implementation on a vector computer. Two totally different types of measurements, viz., radar, and surface disdrometer, measurements of rainfall were simulated. These simulations involve exponential, Poisson and gamma random deviates. The problem is a large scale one since the parameters describing the rainfall must be varied over a wide range. Thus, complete control over the physical and statistical variables was obtained. Simulations were applied to explain why the correlation is less in plots of radar measured reflectivity verses surface measured rain intensity as compared to plots when both quantities are obtained from surface instruments. Previous interpretations have ascribed this feature to physical causes. While physical factors are important when comparing radar measurements of rainfall to surface measurements of rain intensity, it is important to have a good measure of statistical variabilities before ascribing the features to physical causes alone. Author

N89-14480# Earth Satellite Corp., Chevy Chase, MD.

REMOTE SENSING TECHNOLOGIES AND SPATIAL DATA APPLICATIONS Final Research Report, 1986 - 1987

WILLIAM G. BROONER, EARL S. MERRITT, MICHAEL PLACE, ROBERT M. RAGAN, DONALD WIESNET, and MORRIS DEUTSCH (Satellite Hydrology, Inc., Vienna, VA.) Dec. 1987 154 p

(Contract DACW05-87-C-0012) (AD-A195809; RD-29) Avail: NTIS HC A08/MF A01 CSCL 17H

In the last decade, significant new tools have become available for planners, managers and scientists working in hydrologic engineering. Two new and significant tools are the widespread availability of spaceborne multi-spectral remote sensing systems, and the development of more sophisticated and less expensive micro computer work stations for both image processing and spatial data(GIS)analyses. This paper describes an evaluation of emerging remote sensing and spatial data capabilities and applications performed for the Corps of Engineers Hydrologic Engineering Center at Davis, California. It first surveys recent and planned

spaceborne remote sensing systems providing data relevant to the hydrologic community. Next, integrated digital image processing and Geographic Information Systems (GIS) available today on microcomputers for applied hydrologic analyses are reviewed. Finally, the interaction of these capabilities is examined in the context of specific hydrologic engineering and planning tasks, ranging from real-time flood forecasting, to urban watershed modeling, to snow cover, evaporation, and soil moisture estimation. GRA

N89-14636 Texas Technological Univ., Lubbock.

THE DESIGN AND PROTOCOL OF A SUMMERTIME RAINFALL ENHANCEMENT PROGRAM FOR WEST TEXAS Ph.D. Thesis

ERIC ANDREW PANI 1987 264 p

Avail: Univ. Microfilms Order No. DA8806020

Original analyses of data collected during three rainfall enhancement experiments are combined with other individual studies to assess the state of knowledge about rainfall enhancements in West Texas. The small, multiple-cell convection system is chosen for study because treating it offers the potential for significantly increasing growing-season rainfall in the region. Geostationary Operational Environmental Satellite (GOES) images are used to develop a climatology of the frequency, location, and timing of the small, multiple-cell convective system formations within 150 km of Big Spring, TX. The small, multiple-cell convective system is initiated in a moist, conditionally-unstable atmosphere by weak forcing mechanisms. Microphysical characteristics of the clouds are highly variable and lead to the conclusion that data in addition to those which already exist are needed before the precipitation process in the clouds is sufficiently understood to be altered in a verifiable manner. The relationship between rainfall rate and radar reflectivity factor in the small, multiple-cell convective system is examined considering the effects of evaporation and horizontal transport of rainfall. A field experiment is designed for sampling of the small, multiple-cell convective system with Doppler radars and instrumented aircraft. Dissert. Abstr.

07

DATA PROCESSING AND DISTRIBUTION SYSTEMS

Includes film processing, computer technology, satellite and aircraft hardware, and imagery.

A89-10611

PHOTOGRAMMETRIC WEEK, 41ST, UNIVERSITAET STUTTGART, FEDERAL REPUBLIC OF GERMANY, SEPT. 14-19, 1987, PROCEEDINGS (PHOTOGRAMMETRISCHE WOCHE, 41ST, UNIVERSITAET STUTTGART, FEDERAL REPUBLIC OF GERMANY, SEPT. 14-19, 1987, VORTRAEGE)

Photogrammetric Week sponsored by the Universitaet Stuttgart. Stuttgart, Federal Republic of Germany, Universitaet Stuttgart (Institut fuer Photogrammetrie, Schriftenreihe, No. 12), 1987, 244 p. No individual items are abstracted in this volume.

Various papers on photogrammetry are presented. The topics addressed include: multiple-image computer vision, introduction to new products P-series Planicomp/PHOCUS, performance data of the P-series Planicomp, principles of PHOCUS software, the Navstar GPS for aerial triangulation, automatic photogrammetric car-body measurement, new challenges of close-range photogrammetry, analytical close-range photogrammetry in practice, photogrammetric documentation and form-control of large components of a fusion reactor, photogrammetric deformation measurements, automatic reconstruction of simple objects using digital photogrammetry, and digital image processing using Reseau scanning. Also discussed are: digital evaluation of raster electron microscope images, towards real-time photogrammetry, production and revision of topographic maps with PHOCUS, towards expert

systems in digital mapping, digital mapping at the ordnance survey, digital photogrammetric mapping at the Dutch Cadastre service, experiences with digital mapping, studies of forest damage. C.D.

A89-10937#

RESOLUTION IMPROVEMENT BY MULTI-TEMPORAL DATA MERGING

ROBERT DYE and LYNNETTE WOOD (Michigan, Environmental Research Institute, Ann Arbor) IN: International Symposium on Remote Sensing of Environment, 21st, Ann Arbor, MI, Oct. 26-30, 1987, Proceedings. Volume 1. Ann Arbor, MI, Environmental Research Institute of Michigan, 1987, p. 163-169.

The use of multitemporal data merging for resolution enhancement of same-sensor data is evaluated. The procedure for merging two images of the same geographic area acquired at different times is described, and the possibility of combining several images is discussed. An example is presented, using the process for Landsat TM imagery of Detroit. It is suggested that the procedure could be used for change detection of a nonvarying site. R.B.

A89-10945#

THE POTENTIALS AND CHALLENGES AFFORDED BY SPOT-1 DATA

THOMAS M. LILLESAND (Wisconsin, University, Madison) IN: International Symposium on Remote Sensing of Environment, 21st, Ann Arbor, MI, Oct. 26-30, 1987, Proceedings. Volume 1. Ann Arbor, MI, Environmental Research Institute of Michigan, 1987, p. 307-316. Research supported by the University of Wisconsin and William and Flora Hewlett Foundation. refs

A program to assess the utility of SPOT-1 data for natural resource applications is examined. Images of Madison, Green Bay, and Spooner, Wisconsin were analyzed to assess the use of SPOT data for generalized land-cover mapping, preparing large-scale image maps, forest classification, and water-quality analysis. Preliminary results of the analysis are presented. Two data-processing procedures are discussed: the digital merger of SPOT 10-m panchromatic and 20-m multispectral data using intensity-hue-saturation color-space transformations, and the development of a semiautomated training-sample selector designed to reduce image-analysis times in multispectral-image classification efforts. It is found that SPOT-1 data are useful across a broad range of natural-resource applications. R.B.

A89-10958#

APPLICATIONS OF SPATIAL POSTCLASSIFICATION MODELS

EUGENE A. FOSNIGHT (TGS Technology, Inc., Sioux Falls, SD) IN: International Symposium on Remote Sensing of Environment, 21st, Ann Arbor, MI, Oct. 26-30, 1987, Proceedings. Volume 1. Ann Arbor, MI, Environmental Research Institute of Michigan, 1987, p. 469-485. refs

(Contract USGS-14-08-0001-22521)

Spatial filtering procedures for nominal grid-cell data, which incorporate spatial or neighborhood information into post-classification data models, are discussed. It is suggested that spatial postclassification reduces the complexity of data, making interpretation simpler, and reduces the number of regions to allow transfer to a vector analysis system. The processes of region labeling, region flagging, and region removal are examined. Examples of applying spatial filtering to data are presented, including data for irrigated agriculture with and without slope and soils information and high-relief forest data. R.B.

A89-10968#

APPLICATIONS OF MULTISPECTRAL VIDEO FOR NATURAL RESOURCE ASSESSMENT

J. H. EVERITT, D. E. ESCOBAR, and P. R. NIXON (USDA, Agricultural Research Service, Weslaco, TX) IN: International Symposium on Remote Sensing of Environment, 21st, Ann Arbor, MI, Oct. 26-30, 1987, Proceedings. Volume 1. Ann Arbor, MI, Environmental Research Institute of Michigan, 1987, p. 597-618. refs

The development and the application of video imaging systems

for natural resource assessment by the USDA, Weslaco, Texas are discussed. Special attention is given to three video systems: a multispectral black-and-white four-band system with visible/NIR sensitivity, a multispectral false-color system that acquires selectable three-band color composite imagery generated by an encoder and its black-and-white narrowband image components, and a black-and-white monoband system with mid-IR sensitivity. It is shown that the near-real-time imagery provided by these systems can be used to detect differences among many agricultural and rangeland resource variables such as plant species, cotton-root rot infestations, soil variations, phytomass levels, burned areas, and ant mounds. I.S.

A89-10978#**THEMATIC MAPPER DATA SCREENING AND EXTERNAL EFFECTS CORRECTION**

JULIE B. ODENWELLER and DANIEL P. RICE (Michigan, Environmental Research Institute, Ann Arbor) IN: International Symposium on Remote Sensing of Environment, 21st, Ann Arbor, MI, Oct. 26-30, 1987, Proceedings. Volume 2. Ann Arbor, MI, Environmental Research Institute of Michigan, 1987, p. 745-754. refs

A procedure to estimate and correct for haze level in a Landsat TM scene is described and demonstrated, including a means for dealing with haze that spatially varies in thickness over a large scene. A screening procedure that identifies five major scene classes is presented and is shown to be extendable from one area to another if the data are first normalized with the haze correction procedure. Author

A89-10983#**IMPROVING THE DETECTION OF HUMAN-INDUCED CHANGE IN WEST AFRICA'S SEMI-ARID ZONE USING MULTITEMPORAL LANDSAT MSS IMAGERY**

PAUL G. PILON, PHILIP J. HOWARTH (Waterloo, University, Canada), and PETER O. ADENIYI (Lagos, University, Nigeria) IN: International Symposium on Remote Sensing of Environment, 21st, Ann Arbor, MI, Oct. 26-30, 1987, Proceedings. Volume 2. Ann Arbor, MI, Environmental Research Institute of Michigan, 1987, p. 797-804. Research supported by the International Development Research Centre and NSERC. refs

A multicomponent approach is presented which combines image enhancement and multirate classifications and makes it possible to obtain information on the location and nature of both natural and human-induced change. The technique is applied to Landsat images acquired before and after construction of the Bakolori dam and reservoir in northern Nigeria to assess the impacts of the dam on downstream agricultural patterns. It is found that there has been significant degradation in flood plain areas downstream of the Bakolori dam. It is suggested that the technique could provide valuable information for environmental decision making. R.B.

A89-10984#**EDGE DETECTION AND PROCESSING OF REMOTELY SENSED DIGITAL IMAGES**

S. H. PAINE and G. D. LODWICK (Calgary, University, Canada) IN: International Symposium on Remote Sensing of Environment, 21st, Ann Arbor, MI, Oct. 26-30, 1987, Proceedings. Volume 2. Ann Arbor, MI, Environmental Research Institute of Michigan, 1987, p. 805-814. refs

An automated technique for edge extraction that has consistent logic linking the various stages of detection and formation and avoids artificial limits is presented. A wide range of operators, as well as filters and detectors in both the spatial and frequency domains, were evaluated using rate-of-change and orientation criteria. It was found that a minimum-variance filter produced the most accurate and reliable results for smoothing. The best method of edge detection was shown to be that of the derivative filters. Methods for efficiently extracting edges for both boundaries and linear features are presented. It is suggested that these methods are relatively tolerant of noise in the data and utilize a logical set of rules that can be adapted as the data dictate. R.B.

A89-10986#**GEOMETRIC CORRECTION OF SATELLITE IMAGES USING COMPOSITE TRANSFORMATION FUNCTIONS**

ARDESHIR GOSHTASBY (Kentucky, University, Lexington) IN: International Symposium on Remote Sensing of Environment, 21st, Ann Arbor, MI, Oct. 26-30, 1987, Proceedings. Volume 2. Ann Arbor, MI, Environmental Research Institute of Michigan, 1987, p. 825-834. refs

Geometric distortion in a satellite image could be due to many local factors such as sensor nonlinearity, atmospheric turbulence, and scene elevation. In this paper, a transformation function that is composed of many local transformation functions is proposed for image geometric correction. Each local function represents distortion in a small area in an image. The composite transformation function obtained in this manner can represent high degree distortions in an image and has the ability to describe the position and the amount of the distortion. Distortion at a point in an image is modeled by a polynomial and the parameters of the polynomial are determined by weighted least-squares. Distortion in an image is corrected relying more on local information than on global data to ensure that a local distortion is not spread all over the image. Author

A89-10996#**A NEW TOOL - SPOT IMAGERY FOR STUDYING RAPID MOVEMENTS**

M. STERN (Satimage, Kiruna, Sweden) IN: International Symposium on Remote Sensing of Environment, 21st, Ann Arbor, MI, Oct. 26-30, 1987, Proceedings. Volume 2. Ann Arbor, MI, Environmental Research Institute of Michigan, 1987, p. 917-924.

The possibility of using the time lag between two registrations of simultaneous SPOT images to study rapid movements is discussed. The panchromatic sensors (P mode) and multispectral sensors (XS mode) are pointed 0.529 degrees off nadir along-track, causing the time lag between registration in the two modes. Although this lag does not interfere with normal use of SPOT data, it is suggested that the rapid movement of objects could be detected by flickering the two images on a display monitor, or by subtracting one image from the other. Tests were performed on two images of New York City. It was found that the velocities of cumulus clouds and moving boats, ships, and trains could be determined from the images. Also, aircraft which were undetectable in either single image could be observed through a comparison of the two images. R.B.

A89-10998*# Science Applications Research, Lanham, MD.**ATMOSPHERIC CORRECTION OF NS-001 DATA AND EXTRACTION OF MULTIPLE ANGLE REFLECTANCE DATA SETS**

D. E. STREBEL, S. J. GOETZ (Science Applications Research, Lanham, MD), and F. G. HALL (NASA, Goddard Space Flight Center, Greenbelt, MD) IN: International Symposium on Remote Sensing of Environment, 21st, Ann Arbor, MI, Oct. 26-30, 1987, Proceedings. Volume 2. Ann Arbor, MI, Environmental Research Institute of Michigan, 1987, p. 939-948. refs (Contract NAS5-28200)

The percentage of incident solar flux reflected by a surface is a quantity of considerable interest in remote sensing studies. To calculate reflectance from remotely sensed radiance data some estimate of incident flux is needed. Since simultaneous ground-based radiometric measurements are often not available for observations by aircraft or satellite sensors, a procedure based on modeling atmospheric transmittance and scattering was developed. The primary application is to an aircraft data set collected with the NASA C-130 over the Superior National Forest, Minnesota. Atmospherically corrected multiple angle reflectance data sets and reflectance images are generated for areas of natural forest vegetation. These data and the technique may be useful for studies of the interactions of light with forested canopies. Author

A89-11003* Science Applications Research, Lanham, MD.

IMPROVEMENT OF CLOUD COVER ASSESSMENT OF LANDSAT THEMATIC MAPPER DATA

R. LUDWIG, R. KUMAR, and M. MACKIE (Science Applications Research, Lanham, MD) IN: International Symposium on Remote Sensing of Environment, 21st, Ann Arbor, MI, Oct. 26-30, 1987, Proceedings. Volume 2. Ann Arbor, MI, Environmental Research Institute of Michigan, 1987, p. 993-1004.

(Contract NAS5-28200)

Various methods for cloud cover assessment of Landsat TM data are compared and evaluated. A total of 3906 TM 241-mm black-and-white photo prints of different seasons and regions were assessed manually. These images were mostly in band 4 (0.76-0.90 microns) for daytime data and band 6 (10.4-12.5 microns) for nighttime data. The results of this manual assessment are compared to available automated and manual assessments, and the differences between results obtained by various methods are discussed. R.B.

A89-11010#

TERRAIN RELIEF AND PATTERN DESCRIPTION USING DIGITAL ELEVATION AND LANDSAT DATA

STEVEN E. FRANKLIN (Newfoundland, Memorial University, Saint John's, Canada) IN: International Symposium on Remote Sensing of Environment, 21st, Ann Arbor, MI, Oct. 26-30, 1987, Proceedings. Volume 2. Ann Arbor, MI, Environmental Research Institute of Michigan, 1987, p. 1081-1088. NSERC-supported research. refs

The use of digital elevation-model data to describe terrain relief and patterns in convexity is discussed, focusing on the integration of spectral and geomorphometric variables for landscape mapping of a National Park in Canada. It is suggested that the Landsat MSS bands for this area are highly redundant, and that the spectral/geomorphometric relationships are generally weak and can be explained in physical terms. Common patterns in MSS and geomorphometric data may be the digital equivalent of the recurring patterns in the topography, vegetation, soils and lithology mapped in the landscape approach to terrain classification. R.B.

A89-11013#

AN IMPROVED PROCEDURE FOR ANALYSIS OF CHANGE IN THEMATIC MAPPER IMAGE-PAIRS

L. A. VIRAG and J. E. COLWELL (Michigan, Environmental Research Institute, Ann Arbor) IN: International Symposium on Remote Sensing of Environment, 21st, Ann Arbor, MI, Oct. 26-30, 1987, Proceedings. Volume 2. Ann Arbor, MI, Environmental Research Institute of Michigan, 1987, p. 1101-1110.

Analysis of change has become an important use of Landsat MSS and TM data. Many of the change analysis procedures which have been implemented have been dependent on image interpretation of 'change images' prepared by color coding and combining information from two anniversary dates. The objective of this study is to demonstrate an improved method for producing color coded change images. The procedure incorporates multispectral change magnitude and direction information obtained through change vector analysis. The change product is created by appending change magnitude data to a base image and assigning colors according to the direction of change. Techniques for editing the change image are also demonstrated. Results are shown and discussed for a test area in Michigan. Author

A89-11726

DIGITAL IMAGE PROCESSING AND VISUAL COMMUNICATIONS TECHNOLOGIES IN METEOROLOGY; PROCEEDINGS OF THE MEETING, CAMBRIDGE, MA, OCT. 27, 28, 1987

PAUL JANOTA, ED. (Analytic Sciences Corp., Reading, MA) Meeting sponsored by SPIE. Bellingham, WA, Society of Photo-Optical Instrumentation Engineers (SPIE Proceedings. Volume 846), 1987, 162 p. For individual items see A89-11727 to A89-11748.

(SPIE-846)

The following topics are considered; the digital image processing of remotely sensed data, the visual communication of

meteorological phenomena, and meteorological workstation technology. Particular papers are presented on real-time environment monitoring using data from Meteosat and NOAA imaging satellites, the four-dimensional display of satellite cloud images, color-composite image processing for multispectral meteorological satellite data, and NASA's use of McIDAS technology. B.J.

A89-11727* South Dakota School of Mines and Technology, Rapid City.

CLASSIFICATION OF CLOUD FIELDS BASED ON TEXTURAL CHARACTERISTICS

R. M. WELCH, S. K. SENGUPTA, and D. W. CHEN (South Dakota School of Mines and Technology, Rapid City) IN: Digital image processing and visual communications technologies in meteorology; Proceedings of the Meeting, Cambridge, MA, Oct. 27, 28, 1987. Bellingham, WA, Society of Photo-Optical Instrumentation Engineers, 1987, p. 2-5. refs

(Contract NSF ATM-85-07918; NAG1-542)

The present study reexamines the applicability of texture-based features for automatic cloud classification using very high spatial resolution (57 m) Landsat multispectral scanner digital data. It is concluded that cloud classification can be accomplished using only a single visible channel. Author

A89-11740

METEOROLOGICAL SURFACE ANALYSIS USING PERSPECTIVE TOPOGRAPHIC MAPS

JOSEPH M. RUSSO, JOHN G. W. KELLEY, PAUL G. KNIGHT, and FREDERICK J. GADOMSKI (Pennsylvania State University, University Park) IN: Digital image processing and visual communications technologies in meteorology; Proceedings of the Meeting, Cambridge, MA, Oct. 27, 28, 1987. Bellingham, WA, Society of Photo-Optical Instrumentation Engineers, 1987, p. 86-90. refs

A computer-generated, perspective topographic map was used for meteorological surface analysis to evaluate its advantage over traditional map backgrounds. A traditional and perspective map were compared for a precipitation case study that followed the passage of a warm front in the northeastern U.S.. Two precipitation data sets were analyzed against two different map backgrounds centered on Pennsylvania. Besides its immediate three-dimensional 'feel', the perspective map delineated the surface topographical features that were coupled with the prefrontal winds to produce the orographically-lifted precipitation patterns. The computer-generated map was judged superior to the traditional map used for surface analysis, especially in the case of the mesoscale data set. Author

A89-11743

APPLICATIONS OF DIGITAL IMAGE PROCESSING TO ONGOING RESEARCH IN COMPLEX TERRAIN METEOROLOGY

JOHN M. HUBBE, C. DAVID WHITEMAN, HARLAN P. FOOTE, and L. GUY MCWETHY (Battelle Pacific Northwest Laboratories, Richland, WA) IN: Digital image processing and visual communications technologies in meteorology; Proceedings of the Meeting, Cambridge, MA, Oct. 27, 28, 1987. Bellingham, WA, Society of Photo-Optical Instrumentation Engineers, 1987, p. 107-112. refs

(Contract DE-AC06-76RL-01830)

Digital elevation models and Landsat 5 Thematic Mapper (TM) scenes constitute image resolution data over spatial domains of typical interest in complex terrain meteorology. Techniques in use and under development for applying these data to research problems are presented. Topics include decorrelation of topographic shading under direct beam illumination and investigation of nighttime surface temperature. Author

A89-12220

THE EFFECTIVE RESOLUTION ELEMENT OF LANDSAT THEMATIC MAPPER

ANDREW K. WILSON (NERC, Computer Services, Swindon,

England) International Journal of Remote Sensing (ISSN 0143-1161), vol. 9, Aug. 1988, p. 1303-1314. refs
(Contract NERC-F60/G6/03)

Two methods are used to measure the spatial resolution of the TM scanner by determining its effective resolution element (ERE). The first method, in which the TM spatial response is simulated in an analytical model, gave an ERE value of 122 m for band 4, near infrared, of the MSS. The second method, in which water bodies on a selected Landsat-5 TM scene are measured, gave a value of 75 m for band 4 of the Landsat-5 TM scene. It is suggested that the increase in the ERE over the sensor-only value is due to additional factors within the imagery such as the pixel sampling of the scene, ground segment processing, and the contribution of atmospheric effects. R.R.

A89-12221

EFFECT OF SPATIAL RESOLUTION OF THE STATISTICAL PROPERTIES OF SATELLITE IMAGES - A CASE STUDY [EFFET DE LA RESOLUTION SPATIALE SUR DES PROPRIETES STATISTIQUES DES IMAGES SATELLITES - UNE ETUDE DE CAS]

XIANG NING KONG and DANIEL VIDAL-MADJAR (Centre de Recherches en Physique de l'Environnement Terrestre et Planetaire, Issy-les-Moulineaux, France) International Journal of Remote Sensing (ISSN 0143-1161), vol. 9, Aug. 1988, p. 1315-1328. refs

Satellite images of the Beauce region of France have been analyzed in order to study the effect of resolution in using AVHRR data as a means of interpolating two MSS images. With respect to mean radiometric values, it is found that a linear transformation exists between the MSS and AVHRR data, but that this relation depends strongly on the observed scene. The effect of spatial resolution on higher-order statistical properties is investigated through the transformation of the images' texture by progressively degrading the MSS image. A scene-dependent threshold on resolution is identified below which all the statistical information disappears. R.R.

A89-12222

SEGMENTATION OF REMOTELY-SENSED IMAGES BY A SPLIT-AND-MERGE PROCESS

A. M. CROSS (NERC, Unit for Thematic Information Systems, Reading, England), D. C. MASON (Reading, University, England), and S. J. DURY (Oxford University, England) International Journal of Remote Sensing (ISSN 0143-1161), vol. 9, Aug. 1988, p. 1329-1345. refs
(Contract NERC-F60/G6/12)

An image segmentation technique is used to analyze remotely-sensed terrain images, with application to environmental monitoring. The preprocessing segmentation operation, applied prior to image classification, uses a split-and-merge technique employing a hierarchical quadtree data structure to segment images into regions of homogeneous tone and texture. Texture is determined using computed grey value difference statistics. Application of the method to sample classifications of aerial MSS data from two test sites demonstrates an increase in classification accuracy in comparison to that achievable by classifying pixels individually on the basis of their spectral signatures. R.R.

A89-12223

MODEL-BASED REMOTELY-SENSED IMAGERY INTERPRETATION

JIAN-KANG WU, DOU-SHEN CHENG, WEN-TAO WANG (University of Science and Technology of China, Hefei, People's Republic of China), and DENG-LIN CAI (Institute of Forest Inventory and Planning, Beijing, People's Republic of China) International Journal of Remote Sensing (ISSN 0143-1161), vol. 9, Aug. 1988, p. 1347-1356. refs

A model-based remotely-sensed image interpretation expert system embedded in a knowledge-based geographic information system (KBIS) is presented. The KBIS consists of four subsystems: a pictorial data base system, an image interpretation expert system, a computer-aided planning system, and a computer-aided

cartographic system. The image interpretation expert system represents ecological knowledge and other expert knowledge by frames. Its reasoning process consists of a forward reasoning based on the Bayes classification of Landsat imagery, a backward reasoning using frame knowledge and reasoning using a spatial consistency model. A forest inventory study was conducted in Shaxian county, in the southern part of China, using this expert system. The results have shown a significant improvement. Building image interpretation expert systems within knowledge-based pictorial systems is very convenient and efficient because there are well-organized data, knowledge, and procedures available.

Author

A89-12224*

National Aeronautics and Space Administration. Goddard Space Flight Center, Greenbelt, MD.

ALGORITHM FOR AUTOMATIC ATMOSPHERIC CORRECTIONS TO VISIBLE AND NEAR-IR SATELLITE IMAGERY

YORAM J. KAUFMAN (NASA, Goddard Space Flight Center, Greenbelt, MD; Technion - Israel Institute of Technology, Haifa) and CLAUDIA SENDRA International Journal of Remote Sensing (ISSN 0143-1161), vol. 9, Aug. 1988, p. 1357-1381. refs

An algorithm for automatic atmospheric correction of satellite imagery of the earth's surface is proposed which is applicable to low-resolution and high-resolution imagery of land areas. The algorithm is based on the satellite image being corrected and on the climatology of the area, and it requires that some pixels in the image correspond to dense dark vegetation as the surface cover. The algorithm is sensitive to the assumed reflectance of the dense dark vegetation, and the accuracy of the corrected surface reflectance is expected to be + or - 0.01. Using the method, aerosol optical thicknesses were derived from clear and hazy Landsat MSS images in the Washington, D.C. and Chesapeake Bay region, and the results are found to agree well with simultaneous sunphotometer ground measurements. R.R.

A89-12352

SPOT IMAGE QUALITY - TWENTY MONTHS OF EXPERIENCE

GERARD BEGNI (CNES, Toulouse, France) (Photogrammetric Society and Remote Sensing Society, Joint Meeting on Results of the Preliminary Evaluation Programme for SPOT (PEPS), London, England, Nov. 11, 1987) International Journal of Remote Sensing (ISSN 0143-1161), vol. 9, Sept. 1988, p. 1409-1414. refs

SPOT image quality is evaluated based on data from the twenty month in-flight assessment period. A quality control program was developed, which allowed changes to be made in the satellite configuration, the operational procedures, ground-based parameters, and software. The geometric image quality is evaluated, including localization accuracy, intrinsic geometry, local coherence, cartographic accuracy, multispectral and multirate registration, and elevation measurement accuracy. Radiometric image quality is assessed, including resolution performance, detector noise, detector normalization, absolute calibration, and the modulation transfer function performance. R.B.

A89-12357

THE NAVIGATION OF AVHRR IMAGERY

R. J. H. BRUSH (Dundee, University, Scotland) International Journal of Remote Sensing (ISSN 0143-1161), vol. 9, Sept. 1988, p. 1491-1502. refs

One of the difficulties encountered in dealing with AVHRR imagery is that of navigating the data with an acceptable degree of precision. This paper describes a method, based on satellite ephemeris, which allows accurately gridded hard copy images to be produced in an easily reproducible manner. Author

A89-12842

THE EVALUATION OF SIMPLE APPROACHES FOR THE DELINEATION OF RAIN AREA FROM SATELLITE IMAGERY

ANASTASIOS A. TSONIS (Wisconsin, University, Milwaukee) IN: Conference on Satellite Meteorology and Oceanography, 3rd, Anaheim, CA, Feb. 1-5, 1988, Preprints. Boston, MA, American Meteorological Society, 1988, p. 340-345. refs

This paper compares the skills of a simple approach for the estimation of mesoscale instantaneous rainfall with the results obtained using more elaborate techniques. The simplest method delineates the rain area by using a single threshold from a single visible or IR image. In the assessment made in terms of single thresholding and instantaneous rain area delineation at a spatial resolution of 4 x 4 km, it was found that very little loss of accuracy occurred when a simple approach is considered. The reason for this is that the rain delineation from visible and IR imagery is based on the fact that the clouds that will most likely precipitate are the thick (high visible responses) and the tall (high IR responses) clouds. I.S.

A89-12843

VARIATION OF SATELLITE RAIN RELATIONSHIPS IN SPACE AND TIME

PATRICK KING and TSOI-CHING YIP (Department of the Environment, Atmospheric Environment Service, Downsview, Canada) IN: Conference on Satellite Meteorology and Oceanography, 3rd, Anaheim, CA, Feb. 1-5, 1988, Preprints. Boston, MA, American Meteorological Society, 1988, p. 346-351. refs

This paper examines the characteristics of the probability of rain relationships (PORR) derived from GOES satellite data and surface and radar data. It was found that the PORRs calculated from a month's worth of data were relatively constant within a given season and changed only slightly from season to season. The PORRs varied significantly over periods of a few days; however, these day-to-day variations were not consistent enough with synoptic type to allow the construction of PORRs keyed to synoptic type. PORRs derived from radar data were quite consistent with those derived from surface data, indicating that the techniques developed by the AES RAINSAT algorithm could be used in regions where radar data are unavailable. I.S.

A89-12852

RESOLUTION DEPENDENCE IN SATELLITE IMAGERY - MULTIFRACTAL ANALYSIS

P. GABRIEL, S. LOVEJOY, and D. SCHERTZER (McGill University, Montreal, Canada) IN: Conference on Satellite Meteorology and Oceanography, 3rd, Anaheim, CA, Feb. 1-5, 1988, Preprints. Boston, MA, American Meteorological Society, 1988, p. 392-394. refs

The problem of image resolution for remote-sensing satellites is investigated theoretically, with a focus on the scale dependence of brightness fractions. Published analyses based on in situ measurements and mathematical results on scaling and fractals are applied, and numerical results for visible, IR, and radar imaging are presented in extensive graphs. Scale-invariant functions are constructed, and it is shown that many of the statistical properties of the field and their variation with scale can be described by two-parameter universality classes. T.K.

A89-12864* California Univ., La Jolla.

A SATELLITE DATA PROCESSING AND ANALYSIS SOFTWARE SYSTEM FOR EARTH'S ATMOSPHERE AND SURFACE RESEARCH

B. DEALY, C. GAUTIER, R. FROUIN, J. BATES, D. LINGNER (California, University, La Jolla) et al. IN: Conference on Satellite Meteorology and Oceanography, 3rd, Anaheim, CA, Feb. 1-5, 1988, Preprints. Boston, MA, American Meteorological Society, 1988, p. J23-J28. refs
(Contract NAGW-1141)

The OASIS (Oceanic and Atmospheric Satellite Imaging System) is a satellite data processing and analysis software system being developed by the California Space Institute (Cal Space) for support of interdisciplinary and integrated earth sciences research programs. The system's software applications are integrated under a common executive, NASA's Transportable Application Executive (TAE). In this paper, TAE and the system software and hardware are described, and specific techniques used for ingesting, processing, analyzing, and graphically displaying data from many

of the sensors presently being flown are presented. Scientific uses of these capabilities that are, or will shortly be, running under TAE at Cal Space are described. C.D.

A89-14005

A PROCEDURE FOR MODELING THE TERRAIN RELIEF BY USING DIGITIZED TOPOGRAPHIC MAPS

SERGIO VETRELLA and ANTONIO MOCCIA (Napoli, Università, Naples, Italy) Geocarto International (ISSN 1010-6049), vol. 3, Sept. 1988, p. 3-11. Research supported by Ministero della Pubblica Istruzione and CNR. refs

A procedure is presented for obtaining a digital elevation model by using digitized scattered elevation points as inputs. In the procedure, the area studied is divided into rectangular meshes, with the terrain relief for each mesh modeled by polynomial approximation. The elevation and slopes are given in a digital raster format, representing a standard format of an integrated hardware and software system for the simulation and data processing high resolution space sensors. An application of the procedure is presented, showing that the achievable accuracy depends on the mesh dimension. The introduction of elevation points from other sources, such as stereoscopes, produces results of general validity. R.B.

A89-14007

REGION EXTRACTION IN SPOT DATA

HIROICHI EGAWA and TAKASHI KUSAKA (Kanazawa Institute of Technology, Nonoichi, Japan) Geocarto International (ISSN 1010-6049), vol. 3, Sept. 1988, p. 25-30. refs

A method is presented for segmenting SPOT HRV data using color edge points to separate small regions with nearly constant color. The method uses isograms of equal distances from the boundary points between the partially enclosed regions. The small enclosed regions are separated, based on the local isogram maxima. Spectral and spatial features such as color, vegetation index, size, and shape are extracted from each region. It is shown that the method successfully characterizes typical land cover types by spectral and spatial features. R.B.

A89-14012

LOOK-UP TABLES TO CONVERT LANDSAT TM THERMAL IR DATA TO WATER SURFACE TEMPERATURES

LUIS A. BARTOLUCCI (Murray State University, KY) and MAO CHANG (Indiana State University, Terre Haute) Geocarto International (ISSN 1010-6049), vol. 3, Sept. 1988, p. 61-67. Research supported by Purdue University and Murray State University. refs

The primary aim of this paper is to provide the users of Landsat-4 and Landsat-5 TM data with a more convenient means to convert the relative digital counts of the TM thermal band into temperatures. Two conversion (calibration) look-up tables corresponding to two different periods of operation of Goddard's TM image processing system facilities, prior and after Jan. 15, 1984, are included. The procedures utilized to produce the look-up tables are briefly described. Author

A89-14088

TOPOGRAPHIC MAPPING FROM SPOT IMAGERY

D. J. GUGAN and I. J. DOWMAN (University College, London, England) Photogrammetric Engineering and Remote Sensing (ISSN 0099-1112), vol. 54, Oct. 1988, p. 1409-1414. Research supported by the Ordnance Survey and NERC. refs

The methods for map compilation from SPOT imagery are discussed, including the accuracy attainable, image content, and comparisons with other systems. A geometrical model for image restitution implemented on analytical and digital stereoplotters is examined. The model gives accuracies compatible with mapping at 1:50,000 scale with 25-m contours, obtaining about 80 percent of the information required for this scale. This figure can be reduced through image degradation during film writing. R.B.

A89-15919

COMBINING LAPLACIAN IMAGES OF DIFFERENT SPATIAL FREQUENCIES (SCALES) - IMPLICATIONS FOR REMOTE SENSING IMAGE ANALYSIS

SEAN C. AHEARN (Minnesota, University, Saint Paul) IEEE Transactions on Geoscience and Remote Sensing (ISSN 0196-2892), vol. 26, Nov. 1988, p. 826-831. refs

The author proposes a solution to the longstanding problem of how to combine the different scales of analysis in multifrequency image analysis. The premise for combining different scales of analysis is that the absolute value of the result of the difference of two Gaussian filters (DOG) will be at a maximum at different parts of an object for the DOGs passing the spatial frequencies composing those parts. Combining images derived from a DOGs passing a range of frequencies (called Laplacian images or the Laplacian pyramid) is performed by taking the maximum absolute value among the values in the Laplacian image being combined (for each pixel) to form what is called a multifrequency Laplacian image. The rationale for the development of a multifrequency Laplacian pyramid and its implications for multifrequency image analysis and remote-sensing image classification are discussed.

I.E.

A89-15920

ON THE APPLICATION OF AVERAGING MEDIAN FILTERS IN REMOTE SENSING

A. A. VASSILIOU (Mobil Dallas Research Laboratory, TX), M. BOULIANNE, and J. A. R. BLAIS (Calgary, University, Canada) IEEE Transactions on Geoscience and Remote Sensing (ISSN 0196-2892), vol. 26, Nov. 1988, p. 832-838. refs

The application of averaging median filters to remote sensing has been investigated, and the results are presented with some discussion and recommendations. Averaging median filters can be considered as a subclass of the standard median filters. For image processing purposes, a two-dimensional window is first filtered by a number of average filters, and the final result of the averaging filters is equal to the median of the central pixel value and the averaging filter results. Applications of this averaging median filter to Landsat images are presented, and the results show that the fine details are preserved while attenuating the impulsive noise. The Shannon-Wiener entropy and the maximum-entropy method of two-dimensional spectral analysis are used to assess the quality of the results. Suggestions for further research and development are included.

I.E.

A89-16063* National Aeronautics and Space Administration. Goddard Inst. for Space Studies, New York, NY.

EXTRACTION OF TOPOGRAPHY FROM SIDE-LOOKING SATELLITE SYSTEMS - A CASE STUDY WITH SPOT SIMULATION DATA

STEPHEN G. UNGAR (NASA, Goddard Institute for Space Studies, New York), CAROLYN J. MERRY, HARLAN L. MCKIM (U.S. Army, Cold Regions Research and Engineering Laboratory, Hanover, NH), RICHARD IRISH (Science Applications Research; NASA, Goddard Space Flight Center, Greenbelt, MD), and MICHAEL S. MILLER (New York City, Dept. of City Planning, NY) Remote Sensing of Environment (ISSN 0034-4257), vol. 26, Oct. 1988, p. 51-73. Army-sponsored research. refs

A simulated data set was used to evaluate techniques for extracting topography from side-looking satellite systems for an area of northwest Washington state. A negative transparency orthophotoquad was digitized at a spacing of 85 microns, resulting in an equivalent ground distance of 9.86 m between pixels and a radiometric resolution of 256 levels. A bilinear interpolation was performed on digital elevation model data to generate elevation data at a 9.86-m resolution. The nominal orbital characteristics and geometry of the SPOT satellite were convoluted with the data to produce simulated panchromatic HRV digital stereo imagery for three different orbital paths and techniques for reconstructing topographic data were developed. Analyses with the simulated HRV data and other data sets show that the method is effective.

R.B.

A89-17906

AUTOMATED SEGMENTATION OF PSEUDOINVARIANT FEATURES FROM MULTISPECTRAL IMAGERY

CARL SALVAGGIO and JOHN R. SCHOTT (Rochester Institute of Technology, NY) IN: Three-dimensional imaging and remote sensing imaging; Proceedings of the Meeting, Los Angeles, CA, Jan. 14, 15, 1988. Bellingham, WA, Society of Photo-Optical Instrumentation Engineers, 1988, p. 118-127. refs

The present automated segmentation algorithm for pseudoinvariant-feature isolation employs rate-of-change information from a thresholding process previously associated with the Volchok and Schott (1986) pseudoinvariant feature-normalization technique. The algorithm was combined with the normalization technique and applied to the six reflective bands of the Landsat TM for both urban and rural scenes. An evaluation of the normalization results' accuracy shows the combined techniques to have consistently produced normalization results whose errors are of the order of about 1-2 reflectance units for both rural and urban TM imagery.

O.C.

A89-20626

COMPARISON OF THE SPECTRAL INFORMATION CONTENT OF LANDSAT THEMATIC MAPPER AND SPOT FOR THREE DIFFERENT SITES IN THE PHOENIX, ARIZONA REGION

PAT S. CHAVEZ, JR. and JO ANN BOWELL (USGS, Flagstaff, AZ) Photogrammetric Engineering and Remote Sensing (ISSN 0099-1112), vol. 54, Dec. 1988, p. 1699-1708. refs

A89-20627

AN ENHANCED CLASSIFICATION APPROACH TO CHANGE DETECTION IN SEMI-ARID ENVIRONMENTS

PAUL G. PILON, PHILIP J. HOWARTH, RONALD A. BULLOCK (Waterloo, University, Canada), and PETER O. ADENIYI (Lagos, University, Nigeria) Photogrammetric Engineering and Remote Sensing (ISSN 0099-1112), vol. 54, Dec. 1988, p. 1709-1716. Research supported by the International Development Research Centre. refs

An enhanced classification approach which combines image enhancement to isolate change with multispectral classification to identify change dynamics has been applied to Landsat MSS images of northwestern Nigeria during the dry season. The images were taken over a nine-year period before and after construction of the Bakolori dam and reservoir. The results show evidence of land degradation in flood plain areas downstream of the dam. Comparisons with ground survey data confirm that the enhanced classification approach provides more accurate information on change by minimizing errors associated with misregistration and misclassifications. The approach also makes it possible to suppress environmental factors by separating natural and human-induced change.

R.B.

A89-20631

ON DISPLAYING MULTISPECTRAL IMAGERY

JACK BRYANT (Texas A & M University, College Station) Photogrammetric Engineering and Remote Sensing (ISSN 0099-1112), vol. 54, Dec. 1988, p. 1739-1743. refs

A method is proposed which makes it possible to display a digital image with more than three measurements per picture element on a conventional color monitor as a single image product. A transformation from a multispectral image to a displayable three band image is developed which preserves the measurement-space structure of the data. The method makes it possible to perform image processing operations such as clustering and classification on the three-band image instead of the original higher dimensional data with essentially identical results. Two examples using the process are presented.

R.B.

A89-20708

EVALUATION AND DIGITAL PROCESSING OF MULTISPECTRAL SPOT DATA

F. JASKOLLA and J. HENKEL (Arbeitsgemeinschaft der Grossforschungseinrichtungen, Munich, Federal Republic of Germany) (European Association of Remote Sensing Laboratories,

Annual Symposium on European Remote Sensing Needs in the 1990s, Noordwijkerhout, Netherlands, May 4-8, 1987) International Journal of Remote Sensing (ISSN 0143-1161), vol. 9, Oct.-Nov. 1988, p. 1629-1637. refs

The high correlation of the SPOT spectral bands S1 and S2 (green and red) was demonstrated on the basis of multispectral data of a test site in southern Algeria. It is suggested that this correlation decreases the geological possibilities by means of standard products. It is found, however, that the application of advanced image processing techniques based on the IHS color transform make it possible to present subtle spectral differences and a better differentiation of geologically relevant phenomena.

R.B.

A89-20712

TESTS OF TOPOGRAPHIC MAPPING WITH THEMATIC MAPPER IMAGES

G. TOGLIATTI, G. LECHI, and A. MORIONDO (Milano, Politecnico, Milano, Italy) (European Association of Remote Sensing Laboratories, Annual Symposium on European Remote Sensing Needs in the 1990s, Noordwijkerhout, Netherlands, May 4-8, 1987) International Journal of Remote Sensing (ISSN 0143-1161), vol. 9, Oct.-Nov. 1988, p. 1681-1686.

The potential of TM images for topographic mapping from the viewpoint of accuracy and content is discussed. From tests of a region in northern Italy using Large Format Camera images as ground truth, the accuracy of point positioning was found to be about 50 m. Due to a lack of fundamental information in the TM images, it was difficult to update or draw new 1:50,000 maps. It is suggested that TM images are not useful for topographic mapping at this scale.

R.B.

A89-20713

MULTI-POINT MATCHING ALONG VERTICAL LINES IN SPOT IMAGES

DAN ROSENHOLM (Swedish Space Corp., Solna; Kungliga Tekniska Hogskolan, Stockholm, Sweden) (European Association of Remote Sensing Laboratories, Annual Symposium on European Remote Sensing Needs in the 1990s, Noordwijkerhout, Netherlands, May 4-8, 1987) International Journal of Remote Sensing (ISSN 0143-1161), vol. 9, Oct.-Nov. 1988, p. 1687-1703. refs

A multipoint matching method using epipolar geometry with the stereoparallaxes in one of the images used as unknowns (Rosenholm, 1986, 1987) is reformulated to SPOT geometry with the elevations as unknowns. The constraints minimizing the curvature and slope of the digital elevation model measured with this method are studied. A stereo pair of SPOT images of Stockholm were used in the research. A total of 2073 points in the images were compared with heights from official 1:10,000 maps with a 5 m contour interval. For the images studied, the results provide a rms matching accuracy around 0.15-0.20 pixels.

R.B.

A89-20716

INTERPRETATION AND GEOMETRICAL ASPECTS OF THEMATIC MAPPER DATA

M. MICHAELIS (Hannover, Universitaet, Hannover, Federal Republic of Germany) (European Association of Remote Sensing Laboratories, Annual Symposium on European Remote Sensing Needs in the 1990s, Noordwijkerhout, Netherlands, May 4-8, 1987) International Journal of Remote Sensing (ISSN 0143-1161), vol. 9, Oct.-Nov. 1988, p. 1723-1737. refs

For visual analysis assisted by digital image enhancement procedures of a Thematic Mapper scene of the German Bight, a combination of the spectral channels 1-4 is suitable. Because of the extremely high correlation between channels 2 and 3 a principal component transformation is performed. This procedure enhances the interpretation possibilities especially for the recognition of structures like surface material in water. Incorporation of digitized contour lines from a marine chart and a synthetic channel derived from the lines can support the interpretation. For that reason it is necessary to rectify the scene to the Mercator projection of the

marine chart. The rectification performed by a second degree polynomial produces subpixel accuracies.

Author

A89-20717

ADVANCES IN COMPUTERIZED INFORMATION RETRIEVAL IN REMOTE SENSING

E. C. HYATT (Sheffield, University, England), J. J. COX, and W. G. COLLINS (Aston University, Birmingham, England) (European Association of Remote Sensing Laboratories, Annual Symposium on European Remote Sensing Needs in the 1990s, Noordwijkerhout, Netherlands, May 4-8, 1987) International Journal of Remote Sensing (ISSN 0143-1161), vol. 9, Oct.-Nov. 1988, p. 1739-1750.

Developments in the provision of bibliographic and factual data to the remote sensing community are reviewed. The available remote sensing data bases are evaluated. The information available is discussed, including services that outline news, legislation, space policies, commercialization, technical parameters, components, and the availability of remotely-sensed imagery. The imbalance in online accessibility between developed and developing countries is examined.

R.B.

N89-10318*# National Aeronautics and Space Administration. Goddard Space Flight Center, Greenbelt, MD.

THE SPECTRAL BIDIRECTIONAL REFLECTANCE OF SNOW

J. DOZIER, R. E. DAVIS (Sierra Nevada Aquatic Research Lab., Mammoth Lakes, Calif.), A. T. C. CHANG, and K. BROWN /In ESA, Proceedings of the 4th International Colloquium on Spectral Signatures in Remote Sensing p 87-92 Apr. 1988 Sponsored in cooperation with JPL, Calif. Inst. of Technology, Pasadena; and California Univ., Santa Barbara

Avail: NTIS HC A23/MF A01; ESA Publications Division, ESTEC, Noordwijk, Netherlands 80 Dutch guilders CSCL 02F

A radiative transfer model for the bidirectional reflectance-distribution function (BRDF) shows that snow is moderately anisotropic in the near-infrared wavelengths. Although the directional-hemispherical albedo of snow decreases as the grains become larger, the forward scattering also increases, with the result that the illumination and viewing geometry must be considered when interpreting physical properties of the surface layer of the snow pack from remote sensing data. Measurements of the BRDF for a variety of snow conditions were made throughout the winter and spring seasons with a spectroradiometer, for wavelengths from 0.38 to 1.11 microns. Coincident with these the surface grain properties were analyzed by stereological methods. The data show that Mie scattering calculations using an equivalent spherical radius match the directional-hemispherical reflectance, but the BRDF usually shows a small peak in the backscattered direction that would not occur from spherical grains. The sphere with the same surface-to-volume ratio as the ice grains is used as the equivalent sphere.

ESA

N89-10338*# National Aeronautics and Space Administration. Goddard Space Flight Center, Greenbelt, MD.

ATMOSPHERIC EFFECT REMOVAL FROM SPACE IMAGERY

HONGSUK H. KIM /In ESA, Proceedings of the 4th International Colloquium on Spectral Signatures in Remote Sensing p 193-196 Apr. 1988

Avail: NTIS HC A23/MF A01; ESA Publications Division, ESTEC, Noordwijk, Netherlands 80 Dutch guilders CSCL 02F

A method to derive a ground reflectance scene from space imagery by removing the contribution of atmospheric radiance was developed. The method utilizes a multiple scattering radiative transfer code to model the Earth-atmosphere system and converts the output into a set of quadratic coefficients which best fit the relationships between the upwelling radiance reaching the sensor and the lower boundary conditions of the ground reflectance. Pixel by pixel correction of the atmospheric effects is done by invoking these coefficients. The algorithm was applied to a number of Thematic Mapper and CZCS data to generate interesting ground scenes and was used to simulate space imagery from ground reflectance scenes.

ESA

N89-10339# Linköping Univ. (Sweden). Dept. of Electrical Engineering.

ATMOSPHERIC CORRECTION OF THERMAL INFRARED DATA FROM LANDSAT-5 FOR SURFACE TEMPERATURE ESTIMATION

S. AXELSSON and B. LUNDEN (Stockholm Univ., Sweden) / In ESA, Proceedings of the 4th International Colloquium on Spectral Signatures in Remote Sensing p 197-200 Apr. 1988 Sponsored by the Swedish Board for Space Activities, Stockholm, Sweden and the Swedish Natural Science Research Council, Stockholm, Sweden
 Avail: NTIS HC A23/MF A01; ESA Publications Division, ESTEC, Noordwijk, Netherlands 80 Dutch guilders

The information of the LANDSAT-5 thermal channel was assessed using two satellite registrations over the Stockholm area. Atmospheric corrections are predicted from a multilayer radiative transfer model, in which the temperature and water vapor attenuation of each layer is estimated from radiosonde profiles of temperature, pressure, and specific humidity. The modeling of the water vapor attenuation, which dominates in the window 10.4 to 12.5 microns includes continuum and line absorption effects. The usefulness of the correction algorithm was verified by comparing water temperatures derived from TM band 6 data with in situ measurements. Another comparison was based on the temperature of conifers, which at moderate and high wind-speed is close to the air temperature. With access to radiosonde data and an atmospheric propagation model it seems possible to use LANDSAT TM band 6 for mapping of relative and absolute temperatures of natural surfaces. ESA

N89-10340# Groupement Scientifique de Teledetection de Strasbourg (France).

MULTISPECTRAL CHARACTERIZATION OF THE SPATIAL STRUCTURE OF REMOTELY SENSED SCENES [CARACTERISATION MULTISPECTRALE DE LA STRUCTURE SPATIALE DES SCENES TELEDETECTEES]

G. RAMSTEIN and M. RAFFY / In ESA, Proceedings of the 4th International Colloquium on Spectral Signatures in Remote Sensing p 201-203 Apr. 1988 In FRENCH
 Avail: NTIS HC A23/MF A01; ESA Publications Division, ESTEC, Noordwijk, Netherlands 80 Dutch guilders

The notion of regionalized variables used in geostatistics is applied to remote sensing to analyze the spatial organization of the image. The variogram concept is reviewed and it is shown that its modeling enables the structural parameters characterizing the different textures to be defined. The evolution of the variogram in the spectral domain translates the differentiation of textures according to wavelength. Modeling of the variogram also allows an optimal choice of spectral band for a textural classification. The covariogram widens the variogram concept and synthesizes the available spectral and spatial information. These notions lead to a resampling of the image based on the stochastic behavior of a scene in different spectral bands. ESA

N89-10341# Centre National d'Etudes Spatiales, Toulouse (France).

ANALYSIS OF DIRECTIONAL EFFECTS ON NOAA AVHRR

A. BEGUE, P. Y. DESCHAMPS, A. PODAIRE, and D. TANRE (Universite des Sciences et Techniques de Lille, France) / In ESA, Proceedings of the 4th International Colloquium on Spectral Signatures in Remote Sensing p 205-209 Apr. 1988 In FRENCH; ENGLISH summary
 Avail: NTIS HC A23/MF A01; ESA Publications Division, ESTEC, Noordwijk, Netherlands 80 Dutch guilders

Using the NOAA AVHRR GAC data base for west Africa (a month of consecutive data for May 1985) and simultaneous measurements of atmospheric parameters, spectral response was analyzed according to imaging configuration (angles under which the target was viewed within a 130 deg range). This analysis was used to evaluate the importance of directional effects in raw data, extracted after sampling, on a target. The sensitivity of acquired measurements to an atmospheric correction (knowing the size

and composition of aerosols) was studied. Interpretation of the results enables the possibility of inverting the signal after correction for atmospheric effects to be considered. ESA

N89-10930# Centre National d'Etudes Spatiales, Toulouse (France).

STUDY OF THE MULTIPLEXING OF IMAGE TELEMETRY DATA FROM SPOT 4 HRVIR AND VEGETATION SENSORS [ETUDE DU MULTIPLEXAGE DES TELEMESURES IMAGE HRVIR ET VEGETATION DE SPOT 4]

M. GRONDIN 16 Oct. 1987 35 p In FRENCH; ENGLISH summary
 (CNES-87/229/CT/DRT/TIT/TR; ETN-88-93091) Avail: NTIS HC A03/MF A01

Multiplexing of HRVIR and Vegetation sensor data from SPOT 4 so as to use only 1 transmit antenna (8200 to 8310 MHz) and so as to maintain compatibility with existing SPOT ground stations is discussed. Degradations introduced by the presence onboard of an OMUX frequency multiplexer are considered. Results of software simulations of the telemetry link in terms of bit error rate degradations and carrier to interference ratios are presented. The simulations show that with the OMUX, acceptable multiplexing is achieved. For HRVIR predetection stations the present filter should be replaced by a three pole Butterworth filter. ESA

N89-11418# Instituto de Pesquisas Espaciais, Sao Jose dos Campos (Brazil).

COLOR ENHANCEMENT OF REMOTE SENSING IMAGERY USING IHS TRANSFORMATIONS AND DECORRELATION STRETCH METHODS

LUCIANO VIEIRADUTRA, PAULO ROBERTO MENESES (Brasilia Univ., Brazil), and WALDIR R. PARADELLA Jun. 1988 11 p (INPE-4559-PRE/1300) Avail: NTIS HC A03/MF A01

Two digital color image processing methods for providing color contrast stretch and improvement of visual interpretation of remote sensing imagery are presented and compared. The first methodology is based on the transformation of the image represented in RGB coordinates to perception independent IHS (intensity, hue, saturation) coordinates. In IHS space it is possible to process each component independently, therefore achieving better control over the color. Examples of such process include linear operations and hue shifts. After the color enhancement, high pass filtering operation can be performed to enhance spatial detail. The second methodology is the well known decorrelation method, where a decorrelating spectral rotation is performed, followed by a standard deviation equalization among channels and finally a rotation back to the original coordinate system. Several experiments with LANDSAT TM images were made. The results proved to be valuable and different enhancement procedures were suitable for different observations. Author

N89-12113# National Aerospace Lab., Amsterdam (Netherlands). Remote Sensing Dept.

THE POTENTIAL OF COMBINED USE OF SATELLITE DATA WITH TOPOGRAPHIC INFORMATION

F. B. VANDERLAAN 31 Aug. 1987 18 p Presented at the Willi Nordberg Symposium on Remote Sensing Towards Operational Cartographic Application, Graz, Austria, Sep. 1987 (NLR-MP-87061-U; B8815927; ETN-88-93402) Avail: NTIS HC A03/MF A01

Thematic Mapper, SPOT panchromatic, and SPOT Multispectral Scanner (MSS) imagery were investigated for their capabilities of keeping topographic maps up to date. Topographic information was digitally combined with satellite data using raster techniques. From the map line-information on roads, naming-conventions, water, and housing was used to cover a minimum part of the image and to obtain a maximum geographic reference structure in the imagery. A product with optimum characteristics was composed of a SPOT panchromatic band, a SPOT HRV infrared band, and a theme file with topographic information. The size of the file limits applications to manual procedures. Updating is limited to features of at least 4 m wide. The topographic overlay increases the user-friendliness of satellite data. Thematic information (on

land use) can be combined with satellite imagery in a similar way as carried out with linear features. This can supply a highly detailed stratification of a region in functional classes, permitting classification procedures to achieve better results. ESA

N89-12976# Scott Polar Research Inst., Cambridge (England).
TOPOGRAPHIC EFFECTS ON LIGHT SCATTERING FROM SNOW

W. G. REES and J. A. DOWDESWELL (University Coll. of Wales, Aberystwyth.) /In ESA, Proceedings of the 1988 International Geoscience and Remote Sensing Symposium (IGARSS 1988) on Remote Sensing: Moving Towards the 21st Century, Volume 1 p 161-164 Aug. 1988

Avail: NTIS HC A99/MF E03; ESA Publications Div., ESTEC, Noordwijk, Netherlands, 120 US dollars or 250 Dutch guilders

The influence of surface topography on the appearance of a LANDSAT image of a snow-covered ice surface is quantitatively assessed. The correlation of pixel brightness against surface slope (parallel to the solar azimuth) is shown to be 0.8 to 0.9. The accuracy with which this correlation allows surface slope to be deduced from the LANDSAT image is 0.5 deg. The possibility of using this correlation to deduce surface topography from a satellite image is investigated. A theoretical model was developed, and its application to the LANDSAT data gives typical errors of 100m, although when nearest-neighbor smoothing is applied this is reduced to 40m. The most likely applications of the methods, and the surface truth requirements of each of them are discussed.

ESA

N89-12985# North Carolina Univ., Raleigh.
MULTITEMPORAL RESOURCE COMPLEX ANALYSIS OF CATANIA PROVINCE, ITALY FROM LANDSAT-TM DATA

S. KHORRAM, J. BROCKHAUS, and A. GERACHI (Catania Univ., Italy) /In ESA, Proceedings of the 1988 International Geoscience and Remote Sensing Symposium (IGARSS 1988) on Remote Sensing: Moving Towards the 21st Century, Volume 1 p 201-204 Aug. 1988

Avail: NTIS HC A99/MF E03; ESA Publications Div., ESTEC, Noordwijk, Netherlands, 120 US dollars or 250 Dutch guilders

Thematic Mapper (TM) digital data were used to analyze a multiresource complex. Nineteen Anderson (USGS) Level 1, 2, and 3 land use/land cover types were studied and mapped. Spectral signatures characterizing the land use/land cover types were generated through interactive guided clustering of training sites representative of these types. Editing of the signatures resulted in 55 clusters being required to represent the 19 cover types of interest. Raw TM digital data were assigned to the land use/land cover types with a minimum distance to means classifier. The patterns seen in the classified image seem to correspond to those observed in the field.

ESA

N89-12989# National Inst. for Environmental Studies, Tsukuba (Japan).

DETECTION OF SEASONAL AND LONG-TERM CHANGES IN LAND COVER FROM MULTITEMPORAL LANDSAT MSS DATA

T. YOKOTA and Y. MATSUMOTO /In ESA, Proceedings of the 1988 International Geoscience and Remote Sensing Symposium (IGARSS 1988) on Remote Sensing: Moving Towards the 21st Century, Volume 1 p 215-216 Aug. 1988

Avail: NTIS HC A99/MF E03; ESA Publications Div., ESTEC, Noordwijk, Netherlands, 120 US dollars or 250 Dutch guilders

Procedures for detecting changes in land cover by using multitemporal LANDSAT MSS data were developed and tested, to detect seasonal changes and long-term changes in land cover. Four observation dates by LANDSAT were selected in spring and winter at an interval of 7 or 8 yr. Four bands of MSS were used for each date. The CCT values were transformed to the values comparable to spectral reflectances by using references. The change detection procedures proposed use no training data, and are preclassification methods. In one procedure spectral differences are calculated at each pixel between every two dates out of four by using a Euclidean distance norm of the four band data. From these norms the spectral changes among the four dates are

checked in every pixel, and seasonal and long-term changes are detected. The principal component procedure is also tested. Results are variable.

ESA

N89-13009# Dornier-Werke G.m.b.H., Friedrichshafen (Germany, F.R.).

PERFORMANCE MODELING AND RESULTS FOR X-SAR

D. MILLER /In ESA, Proceedings of the 1988 International Geoscience and Remote Sensing Symposium (IGARSS 1988) on Remote Sensing: Moving Towards the 21st Century, Volume 1 p 293-296 Aug. 1988

Avail: NTIS HC A99/MF E03; ESA Publications Div., ESTEC, Noordwijk, Netherlands, 120 US dollars or 250 Dutch guilders

Image performance of X-synthetic aperture radar (X-SAR) objectives are reviewed; modeling algorithms are summarized, and predicted performance results examples are given. The problems of beam pointing errors and consequent processing errors are highlighted.

ESA

N89-13029# GEC-Marconi Electronics Ltd., Chelmsford (England).

COMPLEX SAR IMAGERY AND SPECKLE FILTERING FOR ERS-1 WAVE MODE

R. A. CORDEY and J. T. MACKLIN /In ESA, Proceedings of the 1988 International Geoscience and Remote Sensing Symposium (IGARSS 1988) on Remote Sensing: Moving Towards the 21st Century, Volume 1 p 387-390 Aug. 1988

Avail: NTIS HC A99/MF E03; ESA Publications Div., ESTEC, Noordwijk, Netherlands, 120 US dollars or 250 Dutch guilders

A method to predict the wavenumber dependence of the speckle component in spectra of SAR intensity images is described. Filtering of this component is an important step in recovering wave height spectra from SAR images of the ocean, and an effective means of doing so is required for the wave mode of ERS-1. The method uses the correlation function of the corresponding complex images and was tested using airborne and spaceborne imagery obtained over land and sea. Examples of successful and unsuccessful applications of the method are shown. The successes show a great improvement in speckle filtering over previous techniques, while the failures can be explained in terms of artefacts of an individual SAR processor or too coarse a digitization of complex pixel amplitudes.

ESA

N89-13052# Universite Catholique de Louvain (Belgium). Lab. for Cartography.

COMBINING SPECTRAL AND STRUCTURAL ANALYSES TO SELECT USEFUL CARTOGRAPHIC INFORMATION FROM SPOT IMAGERY

H. WILLEMSSEN /In ESA, Proceedings of the 1988 International Geoscience and Remote Sensing Symposium (IGARSS 1988) on Remote Sensing: Moving Towards the 21st Century, Volume 1 p 473-475 Aug. 1988

Avail: NTIS HC A99/MF E03; ESA Publications Div., ESTEC, Noordwijk, Netherlands, 120 US dollars or 250 Dutch guilders

The possibilities of cartographic applications of SPOT-imagery are investigated, emphasizing spectral analysis and structural analysis. A maximum of information is achieved through combination of both approaches. Examples of applied techniques and their results are given.

ESA

N89-13053# MacDonald, Dettwiler and Associates Ltd., Richmond (British Columbia).

EXTRACTION OF DENSE DIGITAL ELEVATION MODELS FROM SPOT STEREO IMAGERY

D. S. KAUFFMAN and S. R. HAJA (Digim, 1983, Inc. Montreal, Quebec) /In ESA, Proceedings of the 1988 International Geoscience and Remote Sensing Symposium (IGARSS 1988) on Remote Sensing: Moving Towards the 21st Century, Volume 1 p 477-478 Aug. 1988

Avail: NTIS HC A99/MF E03; ESA Publications Div., ESTEC, Noordwijk, Netherlands, 120 US dollars or 250 Dutch guilders

Automatic techniques for accurately extracting dense digital elevation models from SPOT PLA data are reviewed. Digital

techniques of extracting terrain height from stereo satellite images that match or better the accuracy and throughput of traditional photogrammetric techniques exist. While digital methods develop, there are issues to resolve. They involve making sure that the cartographic specifications of the Earth's geoid are accurate, and beginning to address standard methods of storing and accessing the huge quantities of data available. ESA

N89-13056# Reading Univ. (England). Dept. of Geography.

THE PRODUCTION OF ANAGLYPHS FROM SPOT-HRV PANCHROMATIC DATA FOR GEOMORPHOLOGICAL MAPPING

P. J. STYLES *In* ESA, Proceedings of the 1988 International Geoscience and Remote Sensing Symposium (IGARSS 1988) on Remote Sensing: Moving Towards the 21st Century, Volume 1 p 485-487 Aug. 1988

(Contract NERC-CASE-GT4/86/GS/90)

Avail: NTIS HC A99/MF E03; ESA Publications Div., ESTEC, Noordwijk, Netherlands, 120 US dollars or 250 Dutch guilders

The production of geomorphological maps from nadir SPOT-HRV data is discussed. Problems arise due to the masking of topographic features by vegetation cover. Given the availability of off nadir HRV imagery, the quality of maps may be improved by the use of imagery stereo-pairs. Methods of combining of nadir imagery into stereo pairs are described, and the processing steps necessary to produce a stereo view are outlined. The improvements in interpretability that result from the use of data in this form are considered together with problems encountered in map production. ESA

N89-13060# National Inst. for Environment, Ibaraki (Japan).

EFFICIENT CLASSIFICATION OF MULTISPECTRAL IMAGES BY A BEST LINEAR DISCRIMINANT FUNCTION

Y. IKURA, T. MIZOGUCHI, and Y. YASUOKA *In* ESA, Proceedings of the 1988 International Geoscience and Remote Sensing Symposium (IGARSS 1988) on Remote Sensing: Moving Towards the 21st Century, Volume 1 p 505-508 Aug. 1988

Avail: NTIS HC A99/MF E03; ESA Publications Div., ESTEC, Noordwijk, Netherlands, 120 US dollars or 250 Dutch guilders

An algorithm for satellite imagery classification which uses best linear discrimination (BLD) as a decision rule of binary decision tree is proposed. Performance of the proposed method is shown by applying it to multispectral data of LANDSAT 5. Conventional methods (maximum likelihood, Fisher's linear discrimination, and binary decision tree) were also applied to the same data and were compared with the proposed method. The BLD method is a better classifier, although maximum likelihood can be more time efficient. ESA

N89-13061# Tokai Univ., Kanagawa (Japan). Research and Information Center.

A NEW SPATIAL CLASSIFICATION ALGORITHM FOR HIGH GROUND RESOLUTION IMAGES

ZI-JUE ZHANG, H. SHIMODA, K. FUKUE, and T. SAKATA *In* ESA, Proceedings of the 1988 International Geoscience and Remote Sensing Symposium (IGARSS 1988) on Remote Sensing: Moving Towards the 21st Century, Volume 1 p 509-512 Aug. 1988

Avail: NTIS HC A99/MF E03; ESA Publications Div., ESTEC, Noordwijk, Netherlands, 120 US dollars or 250 Dutch guilders

A landcover/use classification algorithm to increase classification accuracies for high resolution images is presented. The algorithm is based on a two stage recognition model of landcover/use. Each concept of landcover categories is defined by the component ratio of landcover elements surrounding the corresponding pixel. The classification procedure can be divided into three steps: the first step is the land cover element recognition of each pixel using a pixelwise classifier; the second step is the calculation of the component ratio of each element within local image region; the third step is the final decision for landcover categories using a minimum distance classifier. The results of experiments using TM data show that this algorithm achieves 7 percent improvements of classification accuracies. ESA

N89-13062# Kingston Polytechnic, Kingston-Upon-Thames (England). School of Geography.

CLASSIFICATION DECISION RULE MODIFICATION ON THE BASIS OF INFORMATION EXTRACTED FROM TRAINING DATA

G. M. FOODY, T. F. WOOD, and N. M. TRODD *In* ESA, Proceedings of the 1988 International Geoscience and Remote Sensing Symposium (IGARSS 1988) on Remote Sensing: Moving Towards the 21st Century, Volume 1 p 513-516 Aug. 1988

Avail: NTIS HC A99/MF E03; ESA Publications Div., ESTEC, Noordwijk, Netherlands, 120 US dollars or 250 Dutch guilders

Classification of training data to increase thematic classification accuracy is discussed. Not only does it indicate the distribution of misclassification but it can provide data which can enable the modification of classifier decision rules. This can lead to significant increases in classification accuracy. Rule modification also permits the definition of uncertainty classes which may be used to delimit transitional zones between cover-types. Rule modification and uncertainty class definition are discussed in relation to the classification of seminatural vegetation in England from LANDSAT-TM data. ESA

N89-13066# Tokai Univ., Kanagawa (Japan). Research and Information Center.

ACCURACY OF LAND COVER CLASSIFICATION OF THEMATIC MAPPER (TM) AND SPOT DATA

H. SHIMODA, K. FUKUE, R. YAMAGUCHI, ZI-JUE ZHANG, and T. SAKATA *In* ESA, Proceedings of the 1988 International Geoscience and Remote Sensing Symposium (IGARSS 1988) on Remote Sensing: Moving Towards the 21st Century, Volume 1 p 529-535 Aug. 1988

Avail: NTIS HC A99/MF E03; ESA Publications Div., ESTEC, Noordwijk, Netherlands, 120 US dollars or 250 Dutch guilders

Land cover/use classification capabilities of a conventional classifier for SPOT HRV and LANDSAT TM data were evaluated as to ground resolution, spectral resolution, and utilization of spatial feature characteristics. Accuracies of classified results were evaluated with the aid of digital land cover/use test site data. The increase of spatial resolution does not necessarily provide higher classification accuracies. This indicates that spatial information should be utilized to obtain higher accuracies. However, a simple addition of texture features to spectral features can not increase the classification accuracy. The addition of spectral bands, i.e., band 1, 5, and 7 in TM increases land cover classification accuracy. These bands greatly increase the number of discriminable categories. ESA

N89-13068# New South Wales Univ., Kensington (Australia). Center for Remote Sensing.

CHANGE DIRECTION ANALYSIS USING LANDSAT IMAGERY: A REVIEW OF METHODOLOGY

A. K. MILNE *In* ESA, Proceedings of the 1988 International Geoscience and Remote Sensing Symposium (IGARSS 1988) on Remote Sensing: Moving Towards the 21st Century, Volume 1 p 541-544 Aug. 1988

Avail: NTIS HC A99/MF E03; ESA Publications Div., ESTEC, Noordwijk, Netherlands, 120 US dollars or 250 Dutch guilders

Techniques that can be applied to LANDSAT data in order to detect changes in land surface conditions once potential sources of error introduced through variations in illumination conditions, atmospheric differences, sensor observations, and plant phenology are removed are reviewed. The development of change detection procedures suitable for use in monitoring land cover changes over an extended period of time is related to providing a routine that can be regularly and systematically applied to data collected from satellite sensors and that can be easily integrated with other information sources in order to facilitate decision making in relation to environmental management. The suitability of such a procedure needs to be assessed according to its complexity, ease of implementation, costs in terms of man hours involved, computer time, and the amount of fieldwork and ground truth information required. ESA

INSTRUMENTATION AND SENSORS

N89-13090# Instituto de Pesquisas Espaciais, Cachoeira Paulista (Brazil).

PHOTOGRAMMETRIC MODEL FOR CORRECTION OF MSS-LANDSAT IMAGERY

ANTONIO JOSE F. MACHADOESILVA Aug. 1988 15 p In PORTUGUESE; ENGLISH summary Presented at the 3rd Brazilian Symposium on Remote Sensing, Rio de Janeiro, Brazil, 28-30 Nov. 1984

(INPE-4652-PRE/1359) Avail: NTIS HC A03/MF A01

This photogrammetric model for the correction of MSS-LANDSAT imagery is based on collinearity equations. Using geodetic coordinates (latitude and longitude) it associates each point of the image to a point on the Earth's surface. Internal and external image system distortion are eliminated by the model. The resulting improved geometric image accuracy is reached (about 1 pixel) independently of the Ground Control Point (GCP). Many possibilities exist for refinement of the image using GCP, and cartographic projection images can be generated to satisfy user requirements.

Author

N89-13908# Texas Univ., Austin.

BINARY IMAGE CLASSIFICATION

CARL N. MORRIS In Colorado State Univ., Computer Science and Statistics. Proceedings of the 18th Symposium on the Interface p 71-74 26 Aug. 1987 Sponsored by NASA, Washington, D.C. (Contract NSF DMS-84-07876)

Avail: NTIS HC A20/MF A01 CSDL 09B

Motivated by the LANDSAT problem of estimating the probability of crop or geological types based on multi-channel satellite imagery data, Morris and Kostal (1983), Hill, Hinkley, Kostal, and Morris (1984), and Morris, Hinkley, and Johnston (1985) developed an empirical Bayes approach to this problem. Here, researchers return to those developments, making certain improvements and extensions, but restricting attention to the binary case of only two attributes.

Author

N89-14483# SACLANT ASW Research Center, La Spezia (Italy).

MAKE-MAP AND MEDMAP: TWO PROGRAMS FOR PLOTTING MAPS OF THE MEDITERRANEAN SEA

P. SCRIMGER and A. TRANGELED Jun. 1988 26 p (AD-A198491; SACLANTCEN-SM-207) Avail: NTIS HC A03/MF A01 CSDL 08B

Two FORTRAN computer programs MAKE-MAP and MEDMAP are described which, when used together, will plot maps of all or any portion of the Mediterranean Sea. Examples are given which show the high degree of detail provided by the 2' resolution of the database. A description of how the maps are created in MAKE-MAP program by means of intermediate landmass matrices is given, and applications of these landmass matrices are mentioned. A flow chart of the main stages of this program is given. The landmass matrix is read by MEDMAP which uses an interpolating contour routine to plot the coastline; a flow chart of the program is given. FORTRAN listings for MAKE-MAP and MEDMAP are also included.

GRA

N89-14486# Technische Hogeschool, Delft (Netherlands). Faculty of Geodesy.

PRECISION OF LINE FOLLOWING IN DIGITAL IMAGES [PRECISIE VAN LIJNVOLGING IN DIGITALE BEELDEN]

ERIK BRUEL Feb. 1988 73 p In DUTCH; ENGLISH summary (B8821610; ETN-89-93329) Avail: NTIS HC A04/MF A01

The precision of two line following methods for digital images was compared by scanning a large scale aerial color photo. A technique in three phases: smoothing, edge detection, and line following was used. The optimal combination of smoothing filter, gradient operation, and line following method was found. Dynamic programming is found to be the optimal line following method. The algorithm works faster and the visual results are much better than those of edge relaxation. The precision of both methods is nearly equal. Different smoothing filters and gradient operators do not affect the results. Because of the high quality of the aerial image, it might be possible to use simpler operators.

ESA

Includes data acquisition and camera systems and remote sensors.

A89-10311* Jet Propulsion Lab., California Inst. of Tech., Pasadena.

IMAGING SPECTROSCOPY II; PROCEEDINGS OF THE MEETING, SAN DIEGO, CA, AUG. 20, 21, 1987

GREGG VANE, ED. (California Institute of Technology, Jet Propulsion Laboratory, Pasadena) Meeting sponsored by SPIE, Bellingham, WA, Society of Photo-Optical Instrumentation Engineers (SPIE Proceedings. Volume 834), 1988, 241 p. For individual items see A89-10312 to A89-10338. (SPIE-834)

The conference presents papers on airborne imaging spectrometers, imaging spectrometry analysis, and spaceborne imaging spectrometers. Consideration is given to an imaging spectrometer for ocean and land remote sensing, an advanced solid-state array spectroradiometer, airborne visible/infrared imaging spectrometer design and performance, and a signal chain for the airborne visible/infrared imaging spectrometer. Other topics include imaging spectrometry as a tool for botanical mapping, the estimation of forest canopy characteristics and nitrogen cycling using laser spectrometry, and a continuous readout photon counting imaging detector.

K.K.

A89-10312

THE FLUORESCENCE LINE IMAGER - AN IMAGING SPECTROMETER FOR OCEAN AND LAND REMOTE SENSING

A. B. HOLLINGER, L. H. GRAY (MONITEQ, Ltd., Concord, Canada), J. F. R. GOWER (Department of Fisheries and Oceans, Institute of Ocean Sciences, Sidney, Canada), and H. R. EDEL (Department of Fisheries and Oceans, Ottawa, Canada) IN: Imaging spectroscopy II; Proceedings of the Meeting, San Diego, CA, Aug. 20, 21, 1987. Bellingham, WA, Society of Photo-Optical Instrumentation Engineers, 1988, p. 2-11.

An airborne programmable imaging spectrometer has been developed to meet the increased requirements of land and water imaging in general and for mapping of chlorophyll fluorescence in particular. This latter application gives rise to the name of the sensor which is called Fluorescence Line Imager (FLI). An imaging spectrometer provides the opportunity to examine both narrow bandwidth features in the target spectrum and to acquire high fidelity spatial images. The FLI has also been applied to hydrographic mapping, mapping of crops, forest and rangeland as well as geobotanical exploration. Distinctive spectral features which fall near atmospheric absorption lines of water and oxygen can be readily discerned and atmospheric artifacts can be avoided in the interpretation of resulting imagery.

Author

A89-10324

IMAGING SPECTROMETRY AS A TOOL FOR BOTANICAL MAPPING

J. R. MILLER, E. W. HARE (York University, North York, Canada), A. B. HOLLINGER, and D. R. STURGEON (MONITEQ, Ltd., Concord, Canada) IN: Imaging spectroscopy II; Proceedings of the Meeting, San Diego, CA, Aug. 20, 21, 1987. Bellingham, WA, Society of Photo-Optical Instrumentation Engineers, 1988, p. 108-113. NSERC-supported research. refs

During the summers of 1985 and 1986 a Programmable Multispectral Imager (PMI), also known as the Fluorescence Line Imager (FLI), has been used to collect airborne data over a number of forested targets in Canada and the U.S. The sites were selected on the basis of suspected localized vegetation stress due to possible excess metal uptake or reported regional forest decline due to suspected acid deposition damage. This paper focuses on the characteristics of the spectral/image data available from this new sensor along with results of preliminary analysis of some of

these data. Stable pixel to pixel vegetation spectral properties provide a verification of sensor calibration methods. Comparison of FLI vegetation spectra with ground-based spectra of vegetation samples show good correspondence for a variety of species studied, including spectral properties of the red edge. Author

A89-10332* Jet Propulsion Lab., California Inst. of Tech., Pasadena.

EARTH OBSERVING SYSTEM - A PLATFORM FOR IMAGING SPECTROMETERS

DEBORAH VANE (California Institute of Technology, Jet Propulsion Laboratory, Pasadena) IN: Imaging spectroscopy II; Proceedings of the Meeting, San Diego, CA, Aug. 20, 21, 1987. Bellingham, WA, Society of Photo-Optical Instrumentation Engineers, 1988, p. 176-180.

Several advanced imaging spectrometers will be deployed on the Space Station Polar Platforms as a part of the Earth Observing System (EOS) program. Two of these, the Moderate-Resolution Imaging Spectrometer (MODIS) and High-Resolution Imaging Spectrometer (HIRIS), will be provided as facility instruments, and currently are under conceptual study at the Jet Propulsion Laboratory and the Goddard Space Flight Center. Other imaging spectrometer concepts, including proposals for a thermal infrared imaging spectrometer, are expected in response to the EOS Announcement of Opportunity scheduled for release in January of 1988. Author

A89-10334* Jet Propulsion Lab., California Inst. of Tech., Pasadena.

HIGH RESOLUTION IMAGING SPECTROMETER (HIRIS)

JOSEPH M. CONLEY, MARK HERRING, and DAVID D. NORRIS (California Institute of Technology, Jet Propulsion Laboratory, Pasadena) IN: Imaging spectroscopy II; Proceedings of the Meeting, San Diego, CA, Aug. 20, 21, 1987. Bellingham, WA, Society of Photo-Optical Instrumentation Engineers, 1988, p. 188-195. refs (Contract NAS7-918)

The High Resolution Imaging Spectrometer (HIRIS), related data system, orbit, and mission operations are described. The pushbroom instrument simultaneously images the terrestrial surface in 192 spectral bands from 0.4 to 2.5 microns. The swath width is 30 km and spatial resolution is 30 m. It is planned to be launched with the Earth Observing System aboard the Space Station Polar Platform in 1995. Array detectors allow concurrent integration of the signals at 192,000 detector elements. Author

A89-10338

SEAWIFS - AN OCEAN-IMAGING SENSOR

LOREN M. WOODY and THOMAS S. PAGANO (Santa Barbara Research Center, Goleta, CA) IN: Imaging spectroscopy II; Proceedings of the Meeting, San Diego, CA, Aug. 20, 21, 1987. Bellingham, WA, Society of Photo-Optical Instrumentation Engineers, 1988, p. 229-231.

A low-cost high-performance sensor design for LEO ocean-color remote sensing is presented. This sensor meets the requirements specified by the NASA/NOAA/Eosat Sea-viewing Wide-Field-of-View Sensor (SeaWiFS) Working Group. This concept uses a rasterscan with a rotating telescope; it results in a small, lightweight, low-power, high-performance instrument. K.K.

A89-10359

FIBER-OPTIC SENSOR SYSTEMS FOR AEROSPACE APPLICATIONS

E. UDD, R. J. MICHAL, S. E. HIGLEY, J. P. THERIAULT, P. LECONG (McDonnell Douglas Astronautics Co., Huntington Beach, CA) et al. IN: Fiber optic and laser sensors V; Proceedings of the Meeting, San Diego, CA, Aug. 17-19, 1987. Bellingham, WA, Society of Photo-Optical Instrumentation Engineers, 1988, p. 162-168.

Advanced aircraft and spacecraft will require fiber-optic sensor systems to monitor the environment around the platform as well as the structural integrity of the vehicle itself. These sensors when embedded in composite or metal matrix material can also be used

to monitor the manufacturing process. Thus, this technology provides a means to sense key environmental parameters from the creation of parts, through assembly, test and flight for the life of the platform. Author

A89-10928#

HIRIS - EOS INSTRUMENT WITH HIGH SPECTRAL AND SPATIAL RESOLUTION

JEFF DOZIER (California Institute of Technology, Jet Propulsion Laboratory, Pasadena; California, University, Santa Barbara) and ALEXANDER F. H. GOETZ (Colorado, University, Boulder) IN: International Symposium on Remote Sensing of Environment, 21st, Ann Arbor, MI, Oct. 26-30, 1987, Proceedings. Volume 1. Ann Arbor, MI, Environmental Research Institute of Michigan, 1987, p. 31-39. refs

The High-Resolution Imaging Spectrometer (HIRIS) is designed for NASA's Earth Observing System (EOS). It will have 10-nm wide spectral bands from 0.4-2.5 microns at 30 m spatial resolution over a 30 km swath. The spectral resolution allows identification of many minerals in rocks and soils, important algal pigments in oceans and inland waters, spectral changes associated with plant canopy biochemistry, composition of atmospheric aerosols, and grain size of snow and contamination by absorbing impurities. The bands will have 12-bit quantization over a dynamic range suitable for bright targets, such as snow. For targets of low brightness, such as water bodies, image-motion compensation will allow gains up to a factor of 8 to increase signal-to-noise ratios. The sensor will be able to point + or - 24 deg crosstrack and +60/-30 deg downtrack. In the 824-km orbit altitude proposed for EOS, the crosstrack pointing capability will allow 4-5 views during a 16-day revisit cycle. Author

A89-10929#

ADVANCED AIRBORNE ELECTRO-OPTICAL IMAGER

S. M. TILL, R. A. NEVILLE (Canada Centre for Remote Sensing, Ottawa), D. G. LECKIE (Canadian Forestry Service, Petawawa National Forestry Institute, Chalk River, Canada), and W. M. STROME (Rem/Sense Mapping Technologies, Inc., Toronto, Canada) IN: International Symposium on Remote Sensing of Environment, 21st, Ann Arbor, MI, Oct. 26-30, 1987, Proceedings. Volume 1. Ann Arbor, MI, Environmental Research Institute of Michigan, 1987, p. 41-47. refs

The development of an operational linear array imager for forestry applications based on the technology associated with the MEIS II airborne multispectral imager is discussed. The MEIS II system and its operation are described, and the system requirements and structure of the proposed imager are examined. The imager system is being developed for forest inventory mapping, insect and disease damage assessment, inventory update, and forest sampling. The proposed imager system consists of three major components: an airborne system with multispectral imager and navigation system, a fast processor/display aboard the aircraft, and a ground processor. R.B.

A89-10932*# Massachusetts Univ., Amherst.

THE ELECTRONICALLY STEERED THINNED ARRAY RADIOMETER

C. S. RUF, A. B. TANNER (Massachusetts, University, Amherst), and D. M. LEVINE (NASA, Goddard Space Flight Center, Greenbelt, MD) IN: International Symposium on Remote Sensing of Environment, 21st, Ann Arbor, MI, Oct. 26-30, 1987, Proceedings. Volume 1. Ann Arbor, MI, Environmental Research Institute of Michigan, 1987, p. 75-84. refs

An L-band radiometer which allows global imaging of soil moisture from LEO is discussed. The system consists of an array of antennas with amplifiers, a device to cross-correlate the signals from the antennas, and a process to translate the resulting data into an image of brightness temperature over the field of view. The process is based on a Fourier transform relation that exists between the incident electric field strength as a function of incidence angle and electric fields across the aperture plane of the antenna. The system's image reconstruction technique and signal-to-noise performance are examined. R.B.

A89-10933#**A CONCEPT FOR MEASURING CURRENTS FROM GEOSTATIONARY SATELLITES**

I. POPSTEFANIJA and R. E. MCINTOSH (Massachusetts, University, Amherst) IN: International Symposium on Remote Sensing of Environment, 21st, Ann Arbor, MI, Oct. 26-30, 1987, Proceedings. Volume 1. Ann Arbor, MI, Environmental Research Institute of Michigan, 1987, p. 85-93. refs

The measurement of ocean surface currents may be possible from geostationary satellites in space using coherent dual-frequency radars. However, feasibility of this concept depends on how reliable a resonant 'Delta K peak' is observed when the cross-product power spectrum of the two microwave signals is formed. Experimental results obtained with the University of Massachusetts Stepped-Frequency Delta K radar. The radar is a frequency-agile radar, which rapidly switches between pairs of signal frequencies. Data obtained at a North Truro, Massachusetts, test site indicates that the radar can measure tidal surface currents as well as wind-driven currents. When surface winds are steady, periodic tidal current variations are observed. However, when the wind changes speed or direction there are corresponding fluctuations in the measured currents. Author

A89-10936#**ACCURACY EVALUATION OF AIRBORNE STEREO LINE IMAGER DATA**

J. R. GIBSON (Canada Centre for Remote Sensing, Ottawa) and M. A. CHAPMAN (Calgary, University, Canada) IN: International Symposium on Remote Sensing of Environment, 21st, Ann Arbor, MI, Oct. 26-30, 1987, Proceedings. Volume 1. Ann Arbor, MI, Environmental Research Institute of Michigan, 1987, p. 147-154. refs

The accuracy of the corrected imagery from a pushbroom stereo line imager is evaluated. The line imager system consists of the MIES II imaging system, an auxiliary data system, and a postflight data-processing system. The imagery and navigation data are tied to ground control points by a photogrammetric bundle adjustment to resolve low-frequency position errors. The accuracy of the correct imagery was found to be 1.5 pixels rms in position and 0.5 pixels rms in height. R.B.

A89-10943#**CLIMATE TRACKING WITH REMOTE SENSING**

WALTER G. EGAN (Lamont-Doherty Geological Observatory, Palisades, NY) and DANIEL SMILEY (Mohonk Preserve, New Paltz, NY) IN: International Symposium on Remote Sensing of Environment, 21st, Ann Arbor, MI, Oct. 26-30, 1987, Proceedings. Volume 1. Ann Arbor, MI, Environmental Research Institute of Michigan, 1987, p. 253-272. Research supported by the Mohonk Preserve. refs

Climate tracking using remote sensing is presented for the area surrounding Mohonk, NY. Historical records dating from 1896 to 1987 and photometric observations beginning in January 31, 1987 are used in the experiment. No temperature trends for the area were found, although it was found that rainfall maxima are correlated with sunspot minima, and related to the corresponding increased meridional circulation. Soil temperature measurements as a function of depth indicate that percolation of rain into the soil has a strong influence on the temperature gradient in the soil. Tables and graphs of various climate parameters are presented, including average temperatures, solar flux, optical water vapor, and precipitation. R.B.

A89-10955*# National Aeronautics and Space Administration. Goddard Space Flight Center, Greenbelt, MD.

MODIS - A GLOBAL OCEAN FACILITY FOR THE EARTH OBSERVING SYSTEM

W. L. BARNES (NASA, Goddard Space Flight Center, Greenbelt, MD) IN: International Symposium on Remote Sensing of Environment, 21st, Ann Arbor, MI, Oct. 26-30, 1987, Proceedings. Volume 1. Ann Arbor, MI, Environmental Research Institute of Michigan, 1987, p. 437-445. refs

A Moderate Resolution Imaging Spectrometer (MODIS) is being

planned as a NASA furnished facility for the Earth Observing System (Eos). This sensor will be the primary source of optical global ocean data for a ten-year period following the Eos launch in the mid-1990's. During this period, the MODIS will survey the Earth's surface continuously once every three days in over 100 spectral bands ranging from 0.4 to 14.2 micrometers at a spatial resolution of 1 kilometer. The system is to be divided into two units, MODIS-T which consists of 64 visible and near-infrared channels and which is capable of tilting to avoid specular reflectance from the ocean surface, and MODIS-N with 31-40 spectral channels including ocean color, ocean temperature and atmospheric characterization bands. The total system is anticipated to be a powerful tool for studying global ocean productivity, dynamics and long-term trends. Author

A89-10965#**GOES I-M IMAGE NAVIGATION AND REGISTRATION SYSTEM**

A. A. KAMEL and M. K. P. BHAT (Ford Aerospace and Communications Corp., Palo Alto, CA) IN: International Symposium on Remote Sensing of Environment, 21st, Ann Arbor, MI, Oct. 26-30, 1987, Proceedings. Volume 1. Ann Arbor, MI, Environmental Research Institute of Michigan, 1987, p. 561-575.

This paper summarizes the Image Navigation and Registration System employed in the next generation Geostationary Operational Environmental Satellite (GOES) system to provide near-real-time radiometric data that are accurately registered relative to a reference grid that remains valid for an extended period of several days. These features, coupled with other enhancements of the GOES I-M radiometers such as improved sensitivity, spatial resolution, scan flexibility, and pointing accuracy, are expected to improve meteorological data utilization significantly in severe local storm and tropical cyclone analysis and forecasting during the 1990s and beyond. Author

A89-10969#**RADAR APPLICATIONS IN REMOTE SENSING - AN AIRBORNE REMOTE SENSING CASE HISTORY PRESENTED AT THE TWENTY-FIRST INTERNATIONAL SYMPOSIUM ON REMOTE SENSING OF ENVIRONMENT, ANN ARBOR, MICHIGAN, OCTOBER 26-30, 1987**

BRIAN L. BULLOCK (INTERA Technologies, Ltd., Calgary, Canada) IN: International Symposium on Remote Sensing of Environment, 21st, Ann Arbor, MI, Oct. 26-30, 1987, Proceedings. Volume 1. Ann Arbor, MI, Environmental Research Institute of Michigan, 1987, p. 619-627.

This paper presents a major case study that would dispel the popular remote sensing myth that airborne data products are more costly than satellite products. It discusses the current commercial market for airborne synthetic aperture radar (SAR) data with a generalized pricing for various types of airborne data. A discussion of potential future markets for airborne SAR data is provided. The paper concludes with an estimate of real costs versus pricing for satellite data and some observations concerning the trends in the industry. Author

A89-11006#**SURFACE WINDSPEED MEASUREMENTS OVER THE OCEAN WITH A C-BAND MICROWAVE RADIOMETER**

C. T. SWIFT, A. B. TANNER (Massachusetts, University, Amherst), and P. G. BLACK (NOAA, Hurricane Research Div., Miami, FL) IN: International Symposium on Remote Sensing of Environment, 21st, Ann Arbor, MI, Oct. 26-30, 1987, Proceedings. Volume 2. Ann Arbor, MI, Environmental Research Institute of Michigan, 1987, p. 1031-1039. refs

A computer algorithm has been developed for use aboard an aircraft carrying a C-band stepped-frequency microwave radiometer to analyze the radiometer data and to provide real-time measurements of surface wind speed and rain rate. The algorithm is described, and the results of experiments testing the ability of the radiometer to perform measurements at high wind speeds are presented. The algorithm uses the radiative-transfer equation and measures wind speed accurate to within 2 m/s and rain rates accurate to within 2 mm/h. R.B.

A89-11016#

EVALUATION OF TECHNOLOGY IN THE DETECTION AND COUNTING OF SEALS

H. T. RIPLEY (Aerial Mapping and Photography, Ltd., Saint John's, Canada), I. H. NI (Department of Fisheries and Oceans, Saint John's, Canada), and B. DAWE (Nordco, Ltd., Saint John's, Canada) IN: International Symposium on Remote Sensing of Environment, 21st, Ann Arbor, MI, Oct. 26-30, 1987, Proceedings. Volume 2. Ann Arbor, MI, Environmental Research Institute of Michigan, 1987, p. 1131-1139. refs

The use of aerial UV photography to detect white-coated harp seal pups on pack ice is discussed. Medium- and large-format cameras, a variety of films, glass and quartz lenses, and low-light-level television were used in order to define the parameters needed to conduct this type of survey. The equipment used in the study is described, and recommendations are made for future surveys. It was found that the upper altitude limit doubled to 100 feet (photoscale 1:4,000) when a quartz lens was used. It is suggested that the equipment most suitable for this type of survey is a large-format mapping camera equipped with a quartz lens and a UV filter. R.B.

A89-11731

SATELLITE CLOUD IMAGE STANDARDIZATION

HOWARD J. SCHULTZ and RONALD G. ISAACS (Atmospheric and Environmental Research, Inc., Cambridge, MA) IN: Digital image processing and visual communications technologies in meteorology; Proceedings of the Meeting, Cambridge, MA, Oct. 27, 28, 1987. Bellingham, WA, Society of Photo-Optical Instrumentation Engineers, 1987, p. 23-31. refs (Contract F19628-85-C-0102)

A method is presented for transforming cloud images from one spaceborne sensor format to another. The procedure, known as Cloud Image Standardization (CIS), uses the known spatial resolution and spectral response properties of a sensor and the modeled angular scattering and emittance properties of various cloud types to derive spatial and spectral resampling relationships. The CIS system can be used to simulate cloud images of a supported sensor from cloud images of other supported sensors. The supported sensors potentially include DMSP OLS, GOES VISSR, NOAA AVHRR, and Landsat MSS and TM. Image standardization enables direct comparison of cloud images from different sensors and provides an interface applicable to the assimilation of nonstandard imagery data by specialized applications models. Since images processed by the CIS system appear to have been generated by the same sensor, there is an effective increase in the global coverage of cloud image data. Applications are presented to cloud field transformations using Landsat MSS and GOES image data. Author

A89-11742

COLOR-COMPOSITE IMAGE PROCESSING FOR MULTISPECTRAL METEOROLOGICAL SATELLITE DATA

ROBERT P. D'ENTREMONT, LARRY W. THOMASON, and JAMES T. BUNTING (USAF, Geophysics Laboratory, Hanscom AFB, MA) IN: Digital image processing and visual communications technologies in meteorology; Proceedings of the Meeting, Cambridge, MA, Oct. 27, 28, 1987. Bellingham, WA, Society of Photo-Optical Instrumentation Engineers, 1987, p. 96-106. refs (AD-A199574; AFGL-TR-88-0207)

Visible and infrared satellite imagery data are a primary source of global cloud observations. Visible channels measure reflected solar energy and are used to detect clouds and snow. Infrared channels measure emitted thermal energy and, consequently, the brightness temperatures of clouds and the earth's surface both day and night. It is sometimes difficult to interpret such imagery because of varying conditions encountered on global scales. Snow cover is often confused with clouds in visible imagery because each surface reflects sunlight well. Low clouds are frequently confused with cloudfree land and oceans in infrared imagery because their temperatures can be nearly equal. It is found that more confident discriminations can be performed between such features when DMSP Operational Linescan System (OLS), NOAA

Advanced Very High Resolution Radiometer (AVHRR), or Nimbus Scanning Multifrequency Microwave Radiometer (SMMR) data are combined into color image products. A multispectral image display technique is described that simultaneously combines several meteorological satellite images into a color image product. The technique, which has its origin in Landsat Multispectral Scanner image processing, is quick and effective, and clearly reveals many features of meteorological interest. Author

A89-12353

CANVAS - AN INTELLIGENT SYSTEM FOR COLOUR SELECTION ON CRT DISPLAYS

GRAHAM A. GILL and ANDREW D. TRIGG (NERC; Reading, University, England) International Journal of Remote Sensing (ISSN 0143-1161), vol. 9, Sept. 1988, p. 1423-1432. refs (Contract NERC-F60/G6/12)

An easy-to-use tool for the selection of colors for density-sliced and classified single band images has been developed and implemented on a proprietary image processing system. Colors may be selected interactively from a range of displayed palettes, or chosen by the system, which maximizes the apparent distinction between them through the use of a uniform color space. Author

A89-12790* Washington Univ., Seattle.

ON THE INTERPRETATION OF INTEGRATED WATER VAPOR PATTERNS IN MIDLATITUDE CYCLONES DERIVED FROM THE NIMBUS 7 SCANNING MULTICHANNEL MICROWAVE RADIOMETER

LYNN A. MCMURDIE and KRISTINA B. KATSAROS (Washington, University, Seattle) IN: Conference on Satellite Meteorology and Oceanography, 3rd, Anaheim, CA, Feb. 1-5, 1988, Preprints. Boston, MA, American Meteorological Society, 1988, p. 60-63. refs (Contract NAS8-36473)

The present exploration of methods for the interpretation of the Nimbus 7 satellite's Scanning Multichannel Microwave Radiometer (SMMR) vapor patterns and the ways in which they relate to the dynamical structure of individual midlatitude storms employs gridded meteorological data from the First GARP Global Experiment special observing period in order to calculate diagnostic quantities. SMMR patterns for a storm at a weak stage determined from the diagnostic quantities are compared with SMMR patterns for the storm at a stronger stage. A more complete interpretation of the SMMR patterns emerges from these considerations. O.C.

A89-12796

AN EXTENSION OF THE SPLIT WINDOW TECHNIQUE FOR THE RETRIEVAL OF PRECIPITABLE WATER - EXPERIMENTAL VERIFICATION

THOMAS J. KLEESPIES (USAF, Geophysics Laboratory, Hanscom AFB, MA) and LARRY M. MCMILLIN (NOAA, National Environmental Satellite, Data, and Information Service, Washington, DC) IN: Conference on Satellite Meteorology and Oceanography, 3rd, Anaheim, CA, Feb. 1-5, 1988, Preprints. Boston, MA, American Meteorological Society, 1988, p. 84-88. refs (AD-A199515; AFGL-TR-88-0237)

An account is given of the results of an extension of the 'split window' technique which permits the retrieval of precipitable water with a minimum of a priori information. The technique is applied to both AVHRR and the VISSR Atmospheric Sounder (VAS). In all cases of comparison with radiosonde transmittance ratio, the transmittance ratio was computed from collocated radiosondes using the wide-band radiative transfer model of Weinreb and Hill (1980). The correlation between the VAS transmittance ratio and that computed from collocated radiosondes is about 0.72. O.C.

A89-12810* National Oceanic and Atmospheric Administration, Fort Collins, CO.

USING SATELLITE DATA TO AID IN DIAGNOSING AND FORECASTING CONVECTIVE DEVELOPMENT AND INTENSITY ALONG ARC CLOUD LINES

JAMES F. W. PURDOM (NOAA, National Environmental Satellite, Data, and Information Service; Cooperative Institute for Research

in the Atmosphere, Fort Collins, CO) and PETER C. SINCLAIR (Colorado State University; Cooperative Institute for Research in the Atmosphere, Fort Collins) IN: Conference on Satellite Meteorology and Oceanography, 3rd, Anaheim, CA, Feb. 1-5, 1988, Preprints. Boston, MA, American Meteorological Society, 1988, p. 166-171. refs

(Contract NSF ATM-84-20980; NOAA-NA-85RAH05045; NAS8-36472)

The convective scale interactions associated with the arc cloud line are studied using GOES data. Studies of convective scale interactions are reviewed and the convective scale interaction phenomena is described. The use of satellite data in nowcasting and forecasting convective storms is discussed. R.B.

A89-12811* National Aeronautics and Space Administration. Goddard Space Flight Center, Greenbelt, MD.

ASSIMILATION OF SATELLITE SURFACE WIND SPEED DATA USING THE GLA ANALYSIS/FORECAST SYSTEM

S. C. BLOOM and R. ATLAS (NASA, Goddard Space Flight Center, Greenbelt, MD) IN: Conference on Satellite Meteorology and Oceanography, 3rd, Anaheim, CA, Feb. 1-5, 1988, Preprints. Boston, MA, American Meteorological Society, 1988, p. 172-177. refs

Research at the Goddard Laboratory for Atmospheres to evaluate methods to assign directions to both real and simulated surface wind speed data is discussed. Surface wind speed measurements are obtained from satellites, including Seasat, Nimbus-7, and Geosat. The methods include the interpolation of modeled forecast winds to the wind speed datum location, the use of surface pressures with a balance relation, and a variational analysis method. It is found that the best estimates may be obtained using a multipass approach to perform a surface analysis incorporating all conventional surface data. R.B.

A89-12816* National Aeronautics and Space Administration. Goddard Space Flight Center, Greenbelt, MD.

TROPOPAUSE ADJUSTMENT TO TROPICAL CYCLONES AS INFERRED FROM SATELLITE OZONE OBSERVATIONS

EDWARD B. RODGERS (NASA, Goddard Space Flight Center, Greenbelt, MD), JOHN STOUT, JOSEPH STERANKA (General Sciences Corp., Laurel, MD), and SIMON CHANG (U.S. Navy, Naval Research Laboratory, Washington, DC) IN: Conference on Satellite Meteorology and Oceanography, 3rd, Anaheim, CA, Feb. 1-5, 1988, Preprints. Boston, MA, American Meteorological Society, 1988, p. 197-202. refs

Data from the Total Ozone Mapping Spectrometer on the Nimbus-7 are used to map the climatological total ozone within and around tropical cyclones. A tropical cyclone numerical model is used to interpret total ozone patterns. The total ozone maps are used to diagnose storm intensity and to differentiate between intensifying and weakening tropical cyclones. The tropical cyclone intensity versus total ozone anomaly distribution is examined and examples of mapping the total ozone of tropical cyclones in the period 1979-1982 are presented. R.B.

A89-12818

THE USE OF POLAR ORBITER DATA IN TROPICAL WEATHER SYSTEM ANALYSIS

DEBRA A. LUBICH (Cooperative Institute for Research in the Atmosphere, Fort Collins, CO) and RAYMOND M. ZEHR (NOAA, Satellite Applications Laboratory, Fort Collins, CO) IN: Conference on Satellite Meteorology and Oceanography, 3rd, Anaheim, CA, Feb. 1-5, 1988, Preprints. Boston, MA, American Meteorological Society, 1988, p. 209-214. refs

(Contract NOAA-NA-85RAH05045)

The availability of satellite data for areas outside of GOES coverage is discussed and the processing and application of a data set covering the development of a tropical storm are reviewed. Measurements from geostationary and polar orbiting satellites are used in conjunction with surface and flight level information to study a storm over northern Australia in January 1987. NOAA-9 and NOAA-10 AVHRR data, TOVS, microwave sounding, and high resolution IR sounding data, and Geostationary Meteorological

Satellite (GMS) data are compared. It is found that the low spatial and high temporal resolution of the GMS data are useful for obtaining large scale circulation and weather pattern information. R.B.

A89-12819

USING THE VAS DATA UTILIZATION CENTER (VDUC) FOR THE ANALYSIS AND FORECASTING OF HEAVY RAINFALL PRODUCING MESOSCALE CONVECTIVE SYSTEMS (MCSS)

RODERICK A. SCOFIELD (NOAA, Satellite Applications Laboratory, Washington, DC) IN: Conference on Satellite Meteorology and Oceanography, 3rd, Anaheim, CA, Feb. 1-5, 1988, Preprints. Boston, MA, American Meteorological Society, 1988, p. 215-221. refs

A four stage analysis and forecast methodology for heavy convective rainfall is proposed for use with VISSR Atmospheric Sounder (VAS) data utilization center (VDUC) systems. An example using the method is presented, in which a mesoscale convective system over the central and southeastern U.S. on August 14, 1987 is analyzed. The VDOC system is used to identify and locate features in the conventional and satellite data that may initiate or focus heavy convective rainfall, to monitor the propagation and stability characteristics of the developing system, to estimate flash flood rainfall potentials, and to predict expected rainfall for a 3-hour period. It is suggested that the system may also be applied to extratropical and tropical cyclones. R.B.

A89-12828* National Aeronautics and Space Administration. Marshall Space Flight Center, Huntsville, AL.

NASA'S EARTH SCIENCE GEOSTATIONARY PLATFORM

GREGORY S. WILSON (NASA, Marshall Space Flight Center, Huntsville, AL), ROBERT J. CURRAN, and DIXON M. BUTLER (NASA, Washington, DC) IN: Conference on Satellite Meteorology and Oceanography, 3rd, Anaheim, CA, Feb. 1-5, 1988, Preprints. Boston, MA, American Meteorological Society, 1988, p. 272-277.

This paper describes the features of the NASA Earth Science Geostationary Platform (ESGP) scheduled for launch in 1998, discusses the objectives of the ESGP's steering committee, and presents a summary status report on the committee's activity. Special attention is given to the elements of the ESGP concept and requirements and to the ESGP program schedule options. A diagram of the ESGP concept is included. I.S.

A89-12829* National Aeronautics and Space Administration. Marshall Space Flight Center, Huntsville, AL.

DOPPLER LIDAR WIND MEASUREMENTS ON THE EOS - LAWS

DANIEL E. FITZJARRALD (NASA, Marshall Space Flight Center, Huntsville, AL) IN: Conference on Satellite Meteorology and Oceanography, 3rd, Anaheim, CA, Feb. 1-5, 1988, Preprints. Boston, MA, American Meteorological Society, 1988, p. 278, 279.

This paper discusses the efforts currently underway to prepare for the deployment of the Laser Atmospheric Wind Sounder (LAWS) instrument on an Earth Observing System (EOS) polar orbiter and on the Space Station. Attention is given to the measurement techniques, which include ground-based and airborne measurements in the atmosphere, and to the scientific and the technical issues being addressed. Global wind profiles obtained with the LAWS will effect dramatic improvement in numerical weather prediction and will be useful in determining the midtroposphere steering currents that are important in hurricane track forecasts. The global wind data will also provide information on large-scale atmospheric circulation and climate dynamics and on biogeochemical and hydrologic cycles. I.S.

A89-12833* National Aeronautics and Space Administration. Goddard Space Flight Center, Greenbelt, MD.

SATELLITE MICROWAVE RAINFALL SIMULATIONS WITH A THREE-DIMENSIONAL DYNAMICAL CLOUD MODEL

ROBERT F. ADLER, JOANNE SIMPSON (NASA, Goddard Space Flight Center, Greenbelt, MD), WEI-KUO TAO, N. PRASAD (General Sciences Corp., Laurel, MD), and HWA-YOUNG YEH (Caelum Research Corp., Silver Spring, MD) IN: Conference on Satellite

Meteorology and Oceanography, 3rd, Anaheim, CA, Feb. 1-5, 1988, Preprints. Boston, MA, American Meteorological Society, 1988, p. 290-295. refs

The three-dimensional, multcloud model of Tao and Soong (1986) is used to generate three-dimensional distribution of pertinent microphysical and state parameters which are used as input into a microwave radiative transfer model. The model is used to calculate upwelling radiance (brightness temperature) at microwave frequencies from 10 to 183 GHz with an ocean background. The model is used to study the relationship between simulated upwell brightness temperature and the cloud-model-generated rain rate at the surface. It is suggested that these calculations can be used to simulate satellite observed brightness temperature values and to make area-averaged rain rates. R.B.

A89-12839* National Aeronautics and Space Administration. Goddard Space Flight Center, Greenbelt, MD.

THE ADDITION OF VISIBLE CHANNEL DATA TO SATELLITE INFRARED RAIN ESTIMATION SCHEMES

ANDREW J. NEGRI and ROBERT F. ADLER (NASA, Goddard Space Flight Center, Greenbelt, MD) IN: Conference on Satellite Meteorology and Oceanography, 3rd, Anaheim, CA, Feb. 1-5, 1988, Preprints. Boston, MA, American Meteorological Society, 1988, p. 325-330. refs

The effect of adding visible channel (VIS) data to the IR data in satellite rain estimation schemes was investigated by comparing the abilities of satellite threshold schemes based on VIS, IR channel, or bispectral (VIS/IR) data to estimate convective precipitation. Using the methodology of Bellon and Austin (1986), empirical relationships between the satellite and radar data were determined for two areas: the Florida Area Cumulus Experiment (FACE) area and a 25-km area on a side centered on 26 N, 81 W, which was inclusive of the FACE area but exclusive of points within 50 km or greater than 170 km of the Miami WSR-57 radar. The results did not demonstrate an unequivocal effect of VIS data. The normalized rms error data for the three estimation schemes used in a four-day experiment are presented. I.S.

A89-12844

MID-LATITUDE EVALUATION OF SOME SATELLITE RAINFALL ESTIMATION TECHNIQUES

W. D. HOGG, A. J. HANSEN, A. NIITSOO, and V. L. POLAVARAPU (Department of the Environment, Atmospheric Environment Service, Downsview, Canada) IN: Conference on Satellite Meteorology and Oceanography, 3rd, Anaheim, CA, Feb. 1-5, 1988, Preprints. Boston, MA, American Meteorological Society, 1988, p. 352-357. refs

The accuracies of the Negri et al. (1984), Lovejoy and Austin (1979), and Barrett (1970) rainfall estimation techniques were compared using a month of satellite data to calculate the daily, weekly, and monthly precipitation totals over southern Canada. The comparison was carried out by remapping GOES, radar, and gauge data to a common latitude-longitude grid ranging from 42 to 47 deg N and 72 to 84 deg W, with a grid spacing of 0.05 deg. The correlation coefficients obtained for each satellite technique and each of the nine 3-day events were found to be all quite low, with no single technique standing out. I.S.

A89-12850

SNOW AND LOW-CLOUD DISCRIMINATION FROM MULTISPECTRAL SATELLITE MEASUREMENTS

ROBERT C. ALLEN, PHILIP A. DURKEE, and CARLYLE H. WASH (U.S. Naval Postgraduate School, Monterey, CA) IN: Conference on Satellite Meteorology and Oceanography, 3rd, Anaheim, CA, Feb. 1-5, 1988, Preprints. Boston, MA, American Meteorological Society, 1988, p. 383-387. Navy-supported research. refs

This paper presents an algorithm for discriminating among clouds, snow cover, and clear land from NOAA AVHRR multispectral imagery, utilizing channels 1, 3, and 4 (centered at 0.63, 3.7, and 11.0 microns, respectively). Specifically, channel-3 imagery is utilized in conjunction with channels 1 and 4 to improve the daylight detection of low clouds over snow. Six images were

analyzed, and the total cloud cover was verified against a total of 110 conventional surface observations, using the standard categories of clear, scattered, broken, and overcast surfaces. The algorithm identified low clouds over snow, the extent of the snow cover, and high clouds such as cirrus, producing excellent results even at very large solar zenith angles. I.S.

A89-12854

EFFECTS OF DATA RESOLUTION ON MARINE STRATIFORM CLOUD DETECTION USING AVHRR AND VISSR SATELLITE DATA

CHI-FAN SHIH, MELANIE WETZEL, and THOMAS H. VONDER HAAR (Cooperative Institute for Research in the Atmosphere, Fort Collins, CO) IN: Conference on Satellite Meteorology and Oceanography, 3rd, Anaheim, CA, Feb. 1-5, 1988, Preprints. Boston, MA, American Meteorological Society, 1988, p. 401-403. (Contract N00014-86-C-0459)

VISSR data from the GOES-6 satellite and AVHRR data from the NOAA-7 satellite were used to investigate the spatial resolution effects of the sampling procedures used by the International Satellite Cloud Climatology Project on the accuracy of stratiform cloud detection over twelve target areas chosen for subjective cloud analysis. The cloud fractions derived from visible and IR channel data from the AVHRR and VISSR data at full resolution were treated as the 'true' fractions, and these were compared with cloud fractions from the same data at reduced resolution. The results indicated that the values of cloud fraction varied with data resolution if the target areas were located in a discrete zone. For target areas located in the uniform zone, the cloud fraction results obtained from reduced-resolution data were consistent with those from full-resolution data. I.S.

A89-12859

WIND AND WIND STRESS CURL FIELDS FOR THE NORTHEAST PACIFIC OCEAN USING SATELLITE SCATTEROMETER DATA

K. A. KELLY, H. C. GRABER, and R. C. BEARDSLEY (Woods Hole Oceanographic Institution, MA) IN: Conference on Satellite Meteorology and Oceanography, 3rd, Anaheim, CA, Feb. 1-5, 1988, Preprints. Boston, MA, American Meteorological Society, 1988, p. 425-427. refs

A technique is being developed to generate maps of the wind stress and wind stress curl fields from the 96-day Seasat-A satellite scatterometer record. A synthetic data set with the wavenumber-frequency spectrum expected from scatterometer data is made from the European Center for Mediumrange Weather Forecasting model. The covariance function used for objective mapping is presented. The data are sampled using the sampling scheme of the NASA scatterometer and the orbit of Seasat for a three-day repeat cycle. Methods for minimizing errors are examined. R.B.

A89-12860

VISSR SENSOR INTRODUCED MODIFICATIONS IN THE PRESENCE OF LARGE TEMPERATURE GRADIENTS

E. V. CHERNA, G. L. AUSTIN, A. BELLON, and A. KILAMBI (McGill Radar Weather Observatory, Sainte-Anne-de-Bellevue, Canada) IN: Conference on Satellite Meteorology and Oceanography, 3rd, Anaheim, CA, Feb. 1-5, 1988, Preprints. Boston, MA, American Meteorological Society, 1988, p. J9-J13. refs

An investigation is conducted of the temperature field retrieved from GOES Visible and Infrared Spin-Scan Radiometer (VISSR) measurements for evidence of sensor-introduced modifications, in order to estimate the response time characteristic of the thermal IR channel. The response time of the VISSR is, at about 20 microsecs, rather large by comparison to the 8-microsec sampling interval; as a result, large temperature gradients are stretched over several IR pixels and modify their brightness temperature. O.C.

A89-12867

X-BAND SCATTEROMETER MEASUREMENTS AT LOW WINDS IN A WAVETANK

MARY R. KELLER and WILLIAM J. PLANT (U.S. Navy, Naval Research Laboratory, Washington, DC) IN: Conference on Satellite Meteorology and Oceanography, 3rd, Anaheim, CA, Feb. 1-5, 1988, Preprints. Boston, MA, American Meteorological Society, 1988, p. J41-J43. refs

Experimental results for radar backscatter at X-band were obtained in a wave tank in the low-wind-speed range and compared with previous model results. The Donelan and Pierson (1987) model predicted the observed sharp drop-off in cross section at low winds, but no temperature dependence was found. The Plant (1986) model did not predict this sharp roll-off, but provided good results at high winds and at low winds when small-amplitude, low-frequency long waves were present. R.R.

A89-13415

USE OF SATELLITE AND RADAR IMAGES IN OPERATIONAL PRECIPITATION NOWCASTING

S. HOWES (Logica Space and Defence Systems, Ltd., London, England) British Interplanetary Society, Journal (ISSN 0007-084X), vol. 41, Oct. 1988, p. 455-460. refs

The Frontiers system, a precipitation nowcasting system used by the UK Meteorological Office, uses Meteosat and ground-based weather radar imagery to provide quantitative precipitation forecasts for up to three hours ahead over the British Isles. Frontiers can be used to bring together remotely sensed data and terrestrial data and to generate forecasts. An advanced man-machine interface is provided, making it possible for a forecaster to interact effectively with the data. K.K.

A89-14073

OROGRAPHIC CHANNELING OF A COLD FRONT BY THE PYRENEES

KLAUS P. HOINKA and DIETRICH HEIMANN (DFVLR, Institut fuer Physik der Atmosphaere, Oberpfaffenhofen, Federal Republic of Germany) Monthly Weather Review (ISSN 0027-0644), vol. 116, Sept. 1988, p. 1817-1823. refs

The channeling effect of the Pyrenees on a cold front is illustrated using high resolution surface data. Satellite data support the analysis of the surface data and show that the surface front is trapped to a significant degree in the vicinity of the mountains. Author

A89-15870* National Aeronautics and Space Administration. Langley Research Center, Hampton, VA.

AIRBORNE AND SPACEBORNE LASERS FOR TERRESTRIAL GEOPHYSICAL SENSING; PROCEEDINGS OF THE MEETING, LOS ANGELES, CA, JAN. 14, 15, 1988

FRANK ALLARIO, ED. (NASA, Langley Research Center, Hampton, VA) Meeting sponsored by SPIE. Bellingham, WA, Society of Photo-Optical Instrumentation Engineers (SPIE Proceedings. Volume 889), 1988, 171 p. For individual items see A89-15871 to A89-15890. (SPIE-889)

The present conference on airborne and spaceborne remote sensing laser applications discusses topics in atmospheric and geophysical sciences-related sensors, lidar and DIAL component and subsystem technologies, and coherent laser experiments and semiconductor laser technologies. Attention is given to airborne lidar measurement of aerosols, a ground-based injection-locked pulsed TEA laser for wind measurements, chemical/biological agent standoff detection methods, lidars for wind shear erosion, laser tuning to selected gas absorption lines in the atmosphere, the NASA lidar-in-space technology experiment, and the Laser Atmospheric Wind Sounder. O.C.

A89-15873* National Aeronautics and Space Administration. Langley Research Center, Hampton, VA.

LIDAR ATMOSPHERIC SOUNDER AND ALTIMETRY FOR THE EARTH OBSERVING SYSTEM (EOS) SATELLITE

CHARLES V. WOERNER (NASA, Langley Research Center, Hampton, VA) IN: Airborne and spaceborne lasers for terrestrial geophysical sensing; Proceedings of the Meeting, Los Angeles,

CA, Jan. 14, 15, 1988. Bellingham, WA, Society of Photo-Optical Instrumentation Engineers, 1988, p. 29-37.

The NASA Space Station Program includes development of a polar orbiting platform as part of the Earth Observing System (EOS) Program. A lidar facility is in turn being developed for the EOS polar platforms to make atmospheric science measurements utilizing techniques of laser atmospheric backscatter (optical radar), Differential Absorption Lidar (DIAL) and altimetry. The science for this facility has been developed by the Lidar Atmospheric Sounder and Altimetry (LASA) panel for the Earth Observing System and will be addressed in an Announcement of Opportunity which will be released early in 1988 to solicit science proposals and experiment proposals for the EOS missions. Author

A89-15878*

National Aeronautics and Space Administration. Goddard Space Flight Center, Greenbelt, MD.

APPLICATIONS OF SPACEBORNE LASER RANGER ON EOS

JOHN J. DEGNAN and STEVEN C. COHEN (NASA, Goddard Space Flight Center, Greenbelt, MD) IN: Airborne and spaceborne lasers for terrestrial geophysical sensing; Proceedings of the Meeting, Los Angeles, CA, Jan. 14, 15, 1988. Bellingham, WA, Society of Photo-Optical Instrumentation Engineers, 1988, p. 77-85. refs

An account is given of the design concept and potential applications in science and engineering of the spaceborne laser ranging and altimeter apparatus employed by the Geodynamics Laser Ranging System; this is scheduled for 1997 launch as part of the multiple-satellite Earth Observing System. In the retrograding mode for geodynamics, the system will use a Nd:YAG laser's green and UV output for distance determination to ground retroreflectors. Engineering applications encompass land management and long-term ground stability studies relevant to nuclear power plant, pipeline, and aqueduct locations. O.C.

A89-15889*

National Aeronautics and Space Administration. Marshall Space Flight Center, Huntsville, AL.

LASER ATMOSPHERIC WIND SOUNDER (LAWS)

D. FITZJARRALD, J. W. BILBRO, R. BERANEK, and V. KELLER (NASA, Marshall Space Flight Center, Huntsville, AL) IN: Airborne and spaceborne lasers for terrestrial geophysical sensing; Proceedings of the Meeting, Los Angeles, CA, Jan. 14, 15, 1988. Bellingham, WA, Society of Photo-Optical Instrumentation Engineers, 1988, p. 160, 161.

A development status report is presented for the Laser Atmospheric Wind Sounder (LAWS) instrument that is to be carried by both an Earth Observing System polar-orbit satellite and the NASA manned Space Station. The wind Doppler lidar profiles thus obtained by LAWS will furnish essential information for future numerical weather prediction, large-scale atmospheric circulation and climate dynamics, and the global biogeochemical and hydrologic cycles; it will then be possible to approach the atmosphere, oceans, cryosphere, and biota as a single, coupled system. O.C.

A89-15922#

SURFACE IDENTIFICATION USING SATELLITE MICROWAVE RADIOMETERS

NORMAN C. GRODY (NOAA, Washington, DC) IEEE Transactions on Geoscience and Remote Sensing (ISSN 0196-2892), vol. 26, Nov. 1988, p. 850-859. refs

The use of satellite microwave radiometers for identifying natural surfaces is analyzed. A retrieval technique is developed by considering the related mixed-pixel problem where two or more surfaces are contained within the viewing area. At a given frequency w , the emissivity measurement $\epsilon(w)$ depends on the fractional amounts f_n and a priori emissivities $\epsilon_n(w)$ where $\epsilon(w) = \sum (\epsilon_n(w) f_n)$. In applications involving surface identification the fractional amounts act as discriminants to identify the most likely surface among the a priori candidates. In principle, the fractional amounts can be obtained using multispectral measurements of emissivity. However, due to the limited spectral characteristics of emissivity the maximum number of distinguishable

surfaces is reduced to three. The fractional amounts are derived using dual-frequency emissivity measurements and the effects of errors in measurement and a priori values are analyzed. I.E.

A89-17679#**A TYPICAL CASE OF INTEGRATED REMOTE SENSING CENTER CONCEPT - THE NAIROBI MULTIPURPOSE RECEPTION AND PROCESSING CENTER**

D. K. ANDERE (DRSRS, Nairobi, Kenya) and J.-P. ANTIKIDIS (CNES, Toulouse, France) IAF, International Astronautical Congress, 39th, Bangalore, India, Oct. 8-15, 1988. 11 p. (IAF PAPER 88-106)

The development of the Nairobi Receiving Station, a remote sensing ground receiving and processing center in East Africa is discussed. The political status of remote sensing in East Africa and the requirements of the region are discussed. Ground systems requirements for the center's data receiving and handling facilities are considered. Plans for the center include the capability of handling SPOT, Landsat, and Meteosat data. R.B.

A89-17682*# National Aeronautics and Space Administration. Goddard Space Flight Center, Greenbelt, MD.

THE EARTH OBSERVING SYSTEM

GERALD A. SOFFEN (NASA, Goddard Space Flight Center, Greenbelt, MD) IAF, International Astronautical Congress, 39th, Bangalore, India, Oct. 8-15, 1988. 9 p. (IAF PAPER 88-114)

NASA's Earth Observing System (EOS) is a prospective program for earth observation from space using various unmanned, sun-synchronous polar orbit sensor platforms in conjunction with the Space Station to conduct measurements over a period of 15 years. The most important instruments will be the Moderate-Resolution Imaging Spectrometer, the High-Resolution Imaging Spectrometer, a large-area coverage SAR, the Laser Atmospheric Wind Sounder, the Atmospheric IR Sounder, and a Geodynamics and Laser-Ranging System. O.C.

A89-17684#**THREE-DIMENSIONAL OBSERVATION BY MEANS OF TETHERED ANTENNAE**

A. MOCCIA and S. VETRELLA (Napoli, Università, Naples, Italy) IAF, International Astronautical Congress, 39th, Bangalore, India, Oct. 8-15, 1988. 14 p. Research supported by the Italian Space Agency and MPI. refs (IAF PAPER 88-118)

A digital simulation is conducted for a SAR interferometric system of novel configuration, in which two antennae are respectively held at different orbital altitudes by a main space station and a tether-connected subsatellite. The station transmits radar pulses, and both antennae receive return signals. Attention is given to a specific mission specification that illustrates the accuracy thus achievable in terrain mapping tasks, with a view to the development of future real-time space cartographic services able to operate in adverse weather and nocturnally as well as diurnally. O.C.

A89-17685#**WIDE FIELD HIGH PERFORMANCE LENSES**

JACKY JOUAN, MICHEL MARTINUZZI, N. MALLINGE, and M. COUSSOT (Matra, S.A., Toulouse, France) IAF, International Astronautical Congress, 39th, Bangalore, India, Oct. 8-15, 1988. 7 p. (IAF PAPER 88-120)

The two optical lenses presented have been developed for the Indian Remote Sensing program's LISS pushbroom-operational mode cameras. The lenses, which are of 162 and 324 mm focal lengths, furnish high optical quality over a 10-deg field that is well-adapted to the use of standard focal plane CCD detectors. The focal length, focal distance, and optical axis exhibit exceptionally high optical stability required for simultaneous image registration in four earth sensing spectral bands. Twelve such lenses have been integrated into the IRS1 satellite. O.C.

A89-17689#**INDIAN EXPERIENCE IN THE DISSEMINATION AND USE OF REMOTE SENSING DATA AND FUTURE PROSPECTS**

Y. S. RAJAN (Ministry of Science and Technology, New Delhi, India), S. ADIGA (National Remote Sensing Agency, Hyderabad, India), and K. KRISHNANUNNI (Department of Space and Space Commission, Bangalore, India) IAF, International Astronautical Congress, 39th, Bangalore, India, Oct. 8-15, 1988. 9 p. (IAF PAPER 88-131)

The acquisition and utilization of remote sensing data in India is reviewed. The use of Landsat data, the development and use of the Indian Remote Sensing Satellite, and the data management and distribution are discussed. Possibilities for future use of remote sensing technologies in India are considered. Suggestions are made for other countries considering the use of remote sensing for natural resource management. R.B.

A89-17690#**THE ERS-1 INSTRUMENT DATA HANDLING AND TRANSMISSION SUBSYSTEM (IDHT) AND ITS EVOLUTION**

A. BERETTA, F. DI TOLLE, and D. MASARO (ISC Laben, Vimodrone, Italy) IAF, International Astronautical Congress, 39th, Bangalore, India, Oct. 8-15, 1988. 5 p. (IAF PAPER 88-134)

This paper examines the development of the Instrument Data Handling and Transmission (IDHT) subsystem for collecting, processing, and transmitting data from payloads on the ERS-1 satellite. The formatting, recording, transmission, control, and management functions of the IDHT are discussed. The application requirements and architecture of the IDHT are presented. R.B.

A89-18073#**FAULT TOLERANT DESIGN OF ATTITUDE AND ORBIT CONTROL SUBSYSTEM FOR EARTH RESOURCES SATELLITE-1**

TAKASHI SUZUKI (National Space Development Agency of Japan, Tokyo), NAOYUKI NATORI, TOSHIKI UESUGI, and YASUNORI KAMOGUCHI (Mitsubishi Electric Corp., Kamakura Works, Japan) IN: AIAA/IEEE Digital Avionics Systems Conference, 8th, San Jose, CA, Oct. 17-20, 1988, Technical Papers. Part 1. Washington, DC, American Institute of Aeronautics and Astronautics, 1988, p. 156-162. refs (AIAA PAPER 88-3879)

This article describes a fault tolerant system for an attitude and orbit control subsystem (AOCS) of a three-axis stabilized earth observation satellite. The fault tolerant design includes both hardware and software methods to establish high availability and safety (survivability) of the AOCS. The fault tolerant system provides for continuous operation of the satellite mission and safety of the satellite, and it consists of three reconfiguration levels in the AOCS: subsystem, component and device. Autonomous reconfiguration to realize high performance on availability is mainly implemented by fault tolerant softwares. Non-autonomous reconfiguration to realize high performance on safety is mainly implemented by the OBC and discrete circuits. One of the critical issues for the fault tolerant design was the software errors due to single event upsets (SEU) of bipolar devices used in the onboard computer (OBS) of the AOCS. The extensions of fault tolerant design to the software errors were investigated and incorporated in the system. Author

A89-18710**ACCOUNTING FOR SELECTIVE ABSORPTION IN THE EVALUATION OF THE EARTH SURFACE TEMPERATURE BY AN ANGULAR METHOD [UCHET SELEKTIVNOGO POGLOSHCHENIIA V ZADACHE OPREDELENIYA TEMPERATURY ZEMNOI POVERKHNOSTI UGLOVYM METODOM]**

A. K. GORODETSKII and N. G. MAMEDOV (AN SSSR, Institut Kosmicheskikh Issledovaniy, Moscow, USSR) Issledovanie Zemli iz Kosmosa (ISSN 0205-9614), July-Aug. 1988, p. 66-76. In Russian. refs

This paper considers the error contributed by selective absorption by water vapor to the values of surface temperature

determined by an angular method. The method, based on a linear relation between the thickness of the air layer and the mass of air, makes it possible to estimate gas absorption in the IR atmospheric windows using line-by-line integration. Calculations are presented that take into account continuous and selective absorption by atmospheric gases. On the basis of these calculations, the spectral ranges of 10.2-11.15 and 10.5-11.5 microns are recommended for the determinations of angular distributions in radiation intensity. Using this method and absorption measurements in these wavelength ranges, surface temperatures were calculated with an estimated error of 0.5 K. I.S.

A89-18736#

EXPERIMENTAL PERSONAL SATELLITE COMMUNICATIONS SYSTEM USING MILLIMETER-WAVE FOR ASIA-OCEANIAN REGION

SHUNKICHI ISOBE, YOSHINORI ARIMOTO, YOSHIKI SUZUKI, SHIGETOSHI YOSHIMOTO, MASAZUMI NISHIDA (National Space Development Agency of Japan, Tokyo) et al. Communications Research Laboratory, Journal (ISSN 0914-9260), vol. 35, July 1988, p. 209-224. refs

The millimeter-wave satellite communication system for the Asia-Oceanian region is discussed. The concept of the personal satellite communication system is studied using inexpensive and simple small earth stations. The rain margin or link availability is calculated to determine the possibility of using the millimeter-wave in the Asia-Oceanian region. Transmission rates, channel capacity, and parameters of the on-board equipment and earth stations are examined and an example system configuration is presented. Plans for experiments using the Engineering Test Satellite-VI are given. R.B.

A89-19173

TECHNOLOGICAL CONSTRAINTS ON THE USE OF THERMAL IMAGERY FOR REMOTE SENSING

S. P. BRAIM (Royal Signals and Radar Establishment, Malvern, England) IN: Applications of infrared technology; Proceedings of the Meeting, London, England, June 9, 10, 1988. Bellingham, WA, Society of Photo-Optical Instrumentation Engineers, 1988, p. 110-121. refs

The application of the technological advances in terrestrial infrared systems and components to satellite remote sensing and the constraints involved are discussed. Particular attention is given to the future use of detector arrays made of cadmium mercury telluride. The discussion is illustrated by an example system based on a satellite operating at 800 km altitude in a circular orbit. V.L.

A89-19176

CONFERENCE ON NUMERICAL WEATHER PREDICTION, 8TH, BALTIMORE, MD, FEB. 22-26, 1988, PREPRINTS

Conference sponsored by the American Meteorological Society, Boston, MA, American Meteorological Society, 1988, 880 p. For individual items see A89-19177 to A89-19286.

Papers concerning numerical weather prediction are presented, including quality control and analysis considerations, the equations of motion and dynamic balance, physical processes and surface effects, the use of satellite observations, improvements to forecast models, the use of wind profiler data, data assimilation systems, diagnostic techniques, systematic errors in global forecast models, and forecast verification. Meteorological modeling topics include of the severe storm environment, hailstorms, clouds, severe convection, microbursts, thunderstorms, squall lines, mesoscale convection, tropical cyclones, and winter storm cyclogenesis. In addition, statistical and local forecasting, predictability and forecast error, data impact studies, extended-range forecasting, gravity wave drag, initialization, horizontal, vertical, and temporal considerations of numerical methods, and semi-Lagrangian applications of numerical methods are discussed. R.B.

A89-20101

EASCON '88; PROCEEDINGS OF THE TWENTY-FIRST ANNUAL ELECTRONICS AND AEROSPACE CONFERENCE, ARLINGTON, VA, NOV. 9-11, 1988

Conference sponsored by IEEE. New York, Institute of Electrical and Electronics Engineers, Inc., 1988, 268 p. For individual items see A89-20102 to 20110, A89-20112 to A89-20128.

The capabilities of present and future space and terrestrial communication systems are examined in reviews and reports. Topics addressed include competition between space and terrestrial technologies, remote sensing, carrier services in public switched telephone networks, surveillance and warning systems, telepresence and telerobotics, integrated networks and systems, and military communication systems. Consideration is given to navigation and geolocation services; high-definition TV broadcasting; technical, economic, marketing, and strategic aspects of VSATs; future technology drivers; and SDI technologies. T.K.

A89-20102

COMMERCIALIZED REMOTE SENSING - A COMPREHENSIVE VIEW FOR GLOBAL STUDIES

DAVID S. JULYAN (SPOT Image Corp., Reston, VA) IN: EASCON '88; Proceedings of the Twenty-first Annual Electronics and Aerospace Conference, Arlington, VA, Nov. 9-11, 1988. New York, Institute of Electrical and Electronics Engineers, Inc., 1988, p. 7-10.

SPOT's system and commercial background are discussed. SPOT commercial policies are considered as a model for global development. Issues discussed are initial commercialization, SPOT products and pricing, and satellite acquisitions. It is concluded that the SPOT commercial approach established the standards for not only data suppliers but also for other business components of the industry. Marketplace economics have replaced government policy as the single most significant component affecting the growth of the remote sensing industry. I.E.

A89-20105

ENVIROSAT - A VEHICLE FOR EXAMINING THE OPTIONS FOR EARTH OBSERVATIONS IN THE 1990'S

PAUL M. MAUGHAN and TIMOTHY M. ALEXANDER (Space Development Services, Fort Washington, MD) IN: EASCON '88; Proceedings of the Twenty-first Annual Electronics and Aerospace Conference, Arlington, VA, Nov. 9-11, 1988. New York, Institute of Electrical and Electronics Engineers, Inc., 1988, p. 25-34. refs

It is argued that, in considering the options for earth observations in the 1990s, the fundamental issue for the U.S. is whether there is a national interest in the supply of land remote-sensing data. It is further argued that, if there is a national interest, then Envirosat may be the most effective way to assure the supply of data. Finally, it is suggested that, if there is not a national interest in the supply of land remote-sensing data, then disengagement (i.e., leaving the field free for entrepreneurial entry, by rescinding Public Law 98-365) or tapping foreign supplies may be the most effective options. I.E.

A89-20711

THE CONTRIBUTION OF SATELLITE INFORMATION TO OPERATIONAL WEATHER FORECASTING - ACHIEVEMENTS AND OBJECTIVES IN THE 1990S

J. REIFF (Koninklijk Nederlands Meteorologisch Instituut, De Bilt, Netherlands) (European Association of Remote Sensing Laboratories, Annual Symposium on European Remote Sensing Needs in the 1990s, Noordwijkerhout, Netherlands, May 4-8, 1987) International Journal of Remote Sensing (ISSN 0143-1161), vol. 9, Oct.-Nov. 1988, p. 1675-1680.

The use of satellite information in nowcasting and short- and medium-range forecasting in the Netherlands is reviewed. Research concerning satellite weather forecasting is discussed, focusing on improvements in satellite data and data processing. It is suggested that the major objective in weather forecasting research should be the development of coupled retrieval methods in which satellite data, classical weather data, and guess fields of numerical weather forecast models are used together to obtain an optimum effect. R.B.

A89-20714

ANALYSIS OF LARGE FORMAT CAMERA PHOTOGRAPHS OF THE PO DELTA, ITALY, FOR TOPOGRAPHIC AND THEMATIC MAPPING

W. STOLZ (Muenchen, Universitaet, Munich, Federal Republic of Germany) (European Association of Remote Sensing Laboratories, Annual Symposium on European Remote Sensing Needs in the 1990s, Noordwijkerhout, Netherlands, May 4-8, 1987) International Journal of Remote Sensing (ISSN 0143-1161), vol. 9, Oct.-Nov. 1988, p. 1705-1714. refs
(Contract BMFT-FKZ-01-QS-85090)

A89-20715

EVALUATION OF SPACE PHOTOGRAPHS

K. JACOBSEN and W. MUELLER (Hannover, Universitaet, Hanover, Federal Republic of Germany) (European Association of Remote Sensing Laboratories, Annual Symposium on European Remote Sensing Needs in the 1990s, Noordwijkerhout, Netherlands, May 4-8, 1987) International Journal of Remote Sensing (ISSN 0143-1161), vol. 9, Oct.-Nov. 1988, p. 1715-1721.

Metric Camera photographs taken from the Space Shuttle in December 1983 and photographs from the Large Format Camera taken in October 1984 are evaluated. The procedure is described from the aerial triangulation up to mapping and orthophotographic production. The geometric conditions and the completeness of the achieved maps are discussed. It is suggested that the difference in quality between Metric Camera and Large Format Camera photographs demonstrates the necessity of forward motion compensation. R.B.

A89-20718

GEOMETRIC CORRECTION OF REMOTELY-SENSED IMAGERY USING GROUND CONTROL POINTS AND ORTHOGONAL POLYNOMIALS

A. J. DE LEEUW, L. M. M. VEUGEN, and H. T. C. VAN STOKKOM (Rijkswaterstaat, Delft, Netherlands) (European Association of Remote Sensing Laboratories, Annual Symposium on European Remote Sensing Needs in the 1990s, Noordwijkerhout, Netherlands, May 4-8, 1987) International Journal of Remote Sensing (ISSN 0143-1161), vol. 9, Oct.-Nov. 1988, p. 1751-1759.

A geometric correction function for remotely-sensed data from satellites and airplanes is evaluated. The function uses ground control points and orthogonal functions. The possibility of performing an accuracy analysis before processing the images is discussed. A case study using the correction function for thermal images of the Waal river in the Netherlands is presented. The advantages of using orthogonal functions are considered. It is found that the number of ground control points affects the accuracy of the transformed image, with more ground control points leading to a smaller residual sum of squares. R.B.

N89-10320# Rijkswaterstaat, Delft (Netherlands).

VALIDATION OF AN ATMOSPHERIC CORRECTION METHOD FOR SATELLITE BORNE IMAGERY

J. M. M. KOKKE, H. T. C. VANSTOKKOM, J. F. DEHAAN, and J. W. HOVENIER (Vrije Universiteit, Amsterdam, Netherlands) In ESA, Proceedings of the 4th International Colloquium on Spectral Signatures in Remote Sensing p 99-104 Apr. 1988
Avail: NTIS HC A23/MF A01; ESA Publications Division, ESTEC, Noordwijk, Netherlands 80 Dutch guilders

In order to evaluate an atmospheric correction method for multispectral satellite borne imagery in the visible, validation experiments were carried out for the applied simplified radiative transfer method (SMART-method). This was performed by comparing the computed results and obtained correction parameters for a number of theoretical situations with those of an exact method which provides high quality data. It is concluded that the SMART-method is sufficiently accurate under the circumstances commonly to be expected. The ground-based spectroradiometers used in the correction method were preliminary calibrated in an absolute sense by assessing the frequency characteristics of the spectral channels. ESA

N89-10330# Sherbrooke Univ. (Quebec).

ANALYSIS OF THE CONTRIBUTION OF THE ATMOSPHERE TO WATER REFLECTANCE IN THE FIRST TWO CHANNELS OF THE NOAA SATELLITES AVHRR [ANALYSE DE LA CONTRIBUTION DE L'ATMOSPHERE A LA REFLECTANCE DE L'EAU DANS LES DEUX PREMIERS CANAUX AVHRR DES SATELLITES NOAA]

A. ROYER, L. CHARTIER, and P. COTE In ESA, Proceedings of the 4th International Colloquium on Spectral Signatures in Remote Sensing p 151-156 Apr. 1988 In FRENCH
Avail: NTIS HC A23/MF A01; ESA Publications Division, ESTEC, Noordwijk, Netherlands 80 Dutch guilders

Optical thickness of aerosols was determined from water reflectance. The signal measured at the sensor is modeled according to four components: volumetric reflectance of water; diffuse specular reflectance; direct specular reflectance as a function of wind speed; and atmospheric reflectance. The contributions of these factors is analyzed in terms of view angle for different turbidity and wind conditions. It is shown that even outside critical zones, the relative terms of surface phenomena can be superior to other components. The amplitude of calculated variations compares well with those observed on three NOAA AVHRR image pairs for successive orbits. Model validation results using ground measurements, however, indicate an overestimation of optical thicknesses. ESA

N89-10335*# Scripps Institution of Oceanography, La Jolla, CA. California Space Inst.

SENSITIVITY OF SATELLITE-DERIVED NET SHORTWAVE IRRADIANCE AT THE EARTH'S SURFACE TO RADIOMETRIC CALIBRATION

C. GAUTIER and R. FROUIN In ESA, Proceedings of the 4th International Colloquium on Spectral Signatures in Remote Sensing p 179-184 Apr. 1988

(Contract NAS1-4195-C; NA86AA-D-AC051)

Avail: NTIS HC A23/MF A01; ESA Publications Division, ESTEC, Noordwijk, Netherlands 80 Dutch guilders CSCL 02F

The effect of radiometric calibration uncertainties on satellite-derived net shortwave irradiance at the Earth's surface was examined. Net shortwave irradiance sensitivity to calibration is expressed as a function of two basic components that depend on surface and cloud albedo sensitivities, respectively. The analysis of these sensitivities for a wide range of atmospheric and surface conditions, as well as radiation geometries, shows that a 10 percent uncertainty in the calibration induces up to 40 W/sqm errors in instantaneous net shortwave irradiance (negative when the calibration uncertainty is positive). The maximum relative errors are obtained in overcast conditions when cloud albedos are high. On a monthly time scale, the induced error becomes typically 13 W/sqm in the tropics and 16 W/sqm in higher latitude regions during summer. The error almost vanishes at high latitudes during winter. A 10 percent positive uncertainty in the calibration gives a net shortwave irradiance error similar to that induced by the 3 hr sampling of the ISCCP Project. ESA

N89-10345# Deutsche Forschungs- und Versuchsanstalt fuer Luft- und Raumfahrt, Oberpfaffenhofen (West Germany). Inst. for Optoelectronics.

THERMAL INFRARED LASER SPECTROSCOPY: THE POTENTIAL OF DUAL ACTIVE/PASSIVE THERMAL INFRARED SENSORS FOR EARTH OBSERVATION

F. LEHMANN and R. RICHTER In ESA, Proceedings of the 4th International Colloquium on Spectral Signatures in Remote Sensing p 229-232 Apr. 1988

Avail: NTIS HC A23/MF A01; ESA Publications Division, ESTEC, Noordwijk, Netherlands 80 Dutch guilders

Laboratory spectroscopic measurements and airborne campaigns to demonstrate the potential of CO2 laser systems for the discrimination and identification of natural and manmade materials are reviewed. The extremely high spectral resolution (0.1 nm) and multispectral reflectance measurement capability of CO2 laser spectrometers in the thermal infrared is a complementary, not competitive, method compared to passive thermal infrared

sensors. The combination of multispectral active and passive sensors is a step to advanced thermal infrared remote sensing systems for the analysis and interpretation of spectral signatures, ground temperature estimation, and atmospheric effects. ESA

N89-10346# Joint Research Centre of the European Communities, Ispra (Italy).

TIME-RESOLVED LASER FLUORESCENCING: TRENDS AND APPLICATIONS

G. BERTOLINI, P. CAMAGNI (Pavia Univ., Italy), C. KOEHLER, A. PEDRINI, and A. PRODOCIMI / In ESA, Proceedings of the 4th International Colloquium on Spectral Signatures in Remote Sensing p 233-238 Apr. 1988

Avail: NTIS HC A23/MF A01; ESA Publications Division, ESTEC, Noordwijk, Netherlands 80 Dutch guilders

Oil fluorosensing is reviewed. Fluorescent spectra from natural oil targets can be remotely sensed with available techniques of pulsed excitation and multispectral detection, so as to insure a consistent analysis of their time evolution, with sufficient sensitivity to follow simultaneously the time decay of separated spectral regions on the scale of nanoseconds. Therefore different classes of oils can be monitored in terms of specific signatures, linking decay times, wavelength, and emission efficiency of definite spectral components to the nature and composition of the oil in which they are contained. Criteria for fingerprinting can be derived on this basis. Monitoring of fluorescent and scattering phenomena in the water column are considered. ESA

N89-10347# Consiglio Nazionale delle Ricerche, Florence (Italy).

A NEW LIDAR SYSTEM FOR APPLICATIONS OVER LAND AND SEA

F. CASTAGNOLI, G. CECCHI, L. PANTANI, B. RADICATI, P. MAZZINGHI, A. BARBARO, and M. ROMOLI (Florence Univ., Italy) / In ESA, Proceedings of the 4th International Colloquium on Spectral Signatures in Remote Sensing p 239-243 Apr. 1988

Avail: NTIS HC A23/MF A01; ESA Publications Division, ESTEC, Noordwijk, Netherlands 80 Dutch guilders

The use of fluorescence lidars for environmental monitoring was studied. A sensor prototype was designed and built to operate as a fluorescence lidar and a passive spectrometer in the visible, in both cases with a high spectral resolution. Field experiments on sea and vegetation remote sensing show that the sensor can detect fluorescence and Raman spectra in different water conditions, and can be used to detect photosynthesis behavior. ESA

N89-10353# Institute of Ocean Sciences, Sidney (British Columbia).

THE FLUORESCENCE LINE IMAGER: HIGH-RESOLUTION IMAGING SPECTROSCOPY OVER WATER AND LAND

J. F. R. GOWER, G. A. BORSTAD, L. H. GRAY, and H. R. EDEL (Department of Fisheries and Environment, Ottawa, Ontario) / In ESA, Proceedings of the 4th International Colloquium on Spectral Signatures in Remote Sensing p 273-278 Apr. 1988

Avail: NTIS HC A23/MF A01; ESA Publications Division, ESTEC, Noordwijk, Netherlands 80 Dutch guilders

The FLI (Fluorescence Line Imager) airborne imaging spectrometer was designed and constructed as the first stage in developing an advanced satellite sensor based on CCD cameras. It was flown on a wide variety of airborne test flights to evaluate the applications of its higher resolution and sensitivity. The primary goal of the FLI was to image the spatial distribution of naturally stimulated fluorescence emission from chlorophyll A in phytoplankton in near surface sea and lake water. Sensitivity limit is 0.2 to 0.3 mg/cu m. Results also demonstrate other uses over a wide variety of targets on land and water. ESA

N89-10356# Iceland Univ., Reykjavik. Lab. for Information Technology and Signal Processing.

A NARROW-BAND THERMAL IMAGER BASED ON MULTILINE REAL-TIME AVERAGING

S. BJORNSSON, V. THORVALDSSON, and A. EIRIKSSON / In

ESA, Proceedings of the 4th International Colloquium on Spectral Signatures in Remote Sensing p 291-292 Apr. 1988

Avail: NTIS HC A23/MF A01; ESA Publications Division, ESTEC, Noordwijk, Netherlands 80 Dutch guilders

A multichannel thermal imager for low temperatures is described. It is capable of high sensitivity in narrow bands (selective search mode), high thermal resolution in case of known or constant emissivity (thermal mapping), material selectivity in case of known or constant temperature, and wavelength dependent emissivity (thematic mapping); as well as allowing the customary method of measuring the total emissive power with much increased sensitivity. It is intended for research on volcanoes and geothermal areas. ESA

N89-10357*# Jet Propulsion Lab., California Inst. of Tech., Pasadena.

AIRBORNE VISIBLE/INFRARED IMAGING SPECTROMETER (AVIRIS): INFLIGHT RADIOMETRIC CALIBRATION AND THE DETERMINATION OF SURFACE REFLECTANCE

J. E. CONEL, G. VANE, R. O. GREEN, R. E. ALLEY, V. CARERE, A. GABELL, and C. J. BRUEGGE / In ESA, Proceedings of the 4th International Colloquium on Spectral Signatures in Remote Sensing p 293-297 Apr. 1988

Avail: NTIS HC A23/MF A01; ESA Publications Division, ESTEC, Noordwijk, Netherlands 80 Dutch guilders CSDL 02F

The inflight radiometric performance of AVIRIS is presented together with a comparison of methods of recovering surface spectral reflectance from the data. Performance is evaluated by comparing radiance predicted from AVIRIS with radiance generated from the LOWIRAN 6 atmospheric model and measured surface reflectance. Comparisons show apparent agreement to within a few percent between 1800 and 2450 nm. Between 600 and 1800 nm the response of AVIRIS is systematically low by as much as 70 percent, and between 400 and 600 nm it is higher than expected. These problems are traced to thermal distortions of the instrument, and to detachment during flight of optical fibers connecting foreoptics to two of four spectrometers in the instrument. Of three methods studied, an empirical one involving calibration curves constructed from field reflectance measurements returns accurate predictions of the surface reflectance independent of the actual radiometric significance of the flight data. ESA

N89-10364*# National Aeronautics and Space Administration. Goddard Space Flight Center, Greenbelt, MD.

SPATIAL RESOLUTION REQUIREMENTS FOR MODIS-N

J. R. G. TOWNSHEND, C. O. JUSTICE, B. L. MARKHAM, and S. A. BRIGGS (Royal Aircraft Establishment, Farnborough, England) / In ESA, Proceedings of the 4th International Colloquium on Spectral Signatures in Remote Sensing p 329-331 Apr. 1988

(Contract NAGS-399; NERC-F60/G6/12; GFSC-PROJ-415)

Avail: NTIS HC A23/MF A01; ESA Publications Division, ESTEC, Noordwijk, Netherlands 80 Dutch guilders CSDL 02F

An empirical investigation of the required spatial resolution for MODIS-N is outlined. It is based on 5 LANDSAT multispectral scanner system images of the normalized difference vegetation index degraded to resolutions between 250 m and 4000 m. Pairs of images from different dates were registered and difference images were generated. Fourier analysis indicates that resolutions finer than 1 km are highly desirable for change detection. A sensor with a resolution of 500 m is recommended as providing the best compromise between detail of changes detected and the size of the resultant data volume, but other options are also suggested. ESA

N89-10379*# National Aeronautics and Space Administration. Goddard Space Flight Center, Greenbelt, MD.

COMPARATIVE POINT-SPREAD FUNCTION CALCULATIONS FOR THE MOMS-1, THEMATIC MAPPER AND SPOT-HRV INSTRUMENTS

V. V. SALOMONSON, J. E. NICKESON, J. BODECHTEL, and J. ZILGER (Technische Univ., Munich, West Germany) / In ESA, Proceedings of the 4th International Colloquium on Spectral

Signatures in Remote Sensing p 407-412 Apr. 1988
 Avail: NTIS HC A23/MF A01; ESA Publications Division, ESTEC, Noordwijk, Netherlands 80 Dutch guilders CSDL 02F

Point-spread functions (PSF) comparisons were made between the Modular Optoelectronic Multispectral Scanner (MOMS-01), the LANDSAT Thematic Mapper (TM) and the SPOT-HRV instruments, principally near Lake Nakuru, Kenya. The results, expressed in terms of the width of the point spread functions at the 50 percent power points as determined from the in-scene analysis show that the TM has a PSF equal to or narrower than the MOMS-01 instrument (50 to 55 for the TM versus 50 to 68 for the MOMS). The SPOT estimates of the PSF range from 36 to 40. When the MOMS results are adjusted for differences in edge scanning as compared to the TM and SPOT, they are nearer 40 in the 575 to 625 nm band. ESA

N89-10381# Karlsruhe Univ. (Germany, F.R.). Dept. of Photogrammetry and Remote Sensing.

DESIGN OF SPECTRAL BANDS FOR THE GERMAN MOMS-2 SENSOR

H. KAUFMANN, D. MEISSNER, J. BODECHTEL (Commission of the European Communities, Ispra, Italy), F. J. BEHR, R. GEERKEN, and K. JUNG In ESA, Proceedings of the 4th International Colloquium on Spectral Signatures in Remote Sensing p 425-430 Apr. 1988 Sponsored by the Bundesministerium fuer Forschung und Technologie, Bonn, Fed. Republic of Germany
 Avail: NTIS HC A23/MF A01; ESA Publications Division, ESTEC, Noordwijk, Netherlands 80 Dutch guilders

Spectral bands for the MOMS-02 instrument, designed as a pushbroom scanning device with on-track three channel stereo capability and four spectral bands in the visible and NIR range are discussed. For centering and defining the width of spectral bands in the 0.4 to 1 micron range, laboratory measurements, using spectrophotometer were performed. Various species of 3 yr old deciduous and coniferous trees as well as mineral standards, rocks, and soils containing Fe(2+/3+) ions were measured and analyzed. Band optimization is based on an iterative process including the spectral properties of distinct targets, atmospheric transmission (LOWTRAN 6), calibration standards and system parameters. The proposed spectral bands (435 to 510 nm; 530 to 575 nm; 655 to 685 nm; 830 to 890 nm) were calculated for 15.75 x 15.75 m ground pixel size (nominal altitude = 324 km at equator) and an internal dynamic range of 9-bit, whereby priority was given to vegetation targets. The wavelength range of the panchromatic nadir and off-nadir looking stereo modules is established at 625 nm + or - 125. ESA

N89-10664# Metocean Consultancy Ltd., Haslemere (England). REVIEW OF THE REQUIREMENTS FOR HIGHER LEVEL ERS-1 PRODUCTS WITHIN EUROPE

NORMAN H. BABEDGE and KEVIN R. DEEMING Paris, France ESA Sep. 1987 64 p
 (Contract ESA-6877/87-HGE-1(SC); P73/1987)
 (ESA-CR(P)-2586; ETN-88-93030) Avail: NTIS HC A04/MF A01

Potential users of ERS-1 ocean, ice, and land products were asked to define their needs. Low bit rate ocean products such as wind and wave data are proven products which should be available on a near operational basis. For these, users are able to be fairly specific about their requirements. For SAR products and most other land products, users are not yet in a position to specify formats for products because some are still experimental. For these products the attitude is much more one of wait and see. Nevertheless, considerable interest is expressed in their potential. Users are concerned that no details are available of the proposed costs of the data, and that no provisional mission plans are published. Recommendations are made for the production of marketing booklets to be distributed to the ERS-1 end user community in advance of the launch of the satellite; many potential users have either not heard of ERS-1, or have only vague ideas of its capabilities and potential. ESA

N89-11352# Instituto de Pesquisas Espaciais, Sao Jose dos Campos (Brazil).

DEVELOPMENT OF A SEMI-EMPIRICAL MODEL FOR ESTIMATING THE GLOBAL SOLAR RADIATION M.S. Thesis [DESENVOLVIMENTO DE UM MODELO SEMI-EMPIRICO PARA ESTIMATIVA DA RADIAÇÃO SOLAR GLOBAL]

PAULO ROBERTO PELUFOFOSTER Jul. 1988 107 p In PORTUGUESE; ENGLISH summary
 (INPE-4620-TDL/328) Avail: NTIS HC A06/MF A01

The large amount of energy which is continuously received from the sun has led more recently to increased efforts toward a better knowledge of its disposition to satisfy world wide energy demands. There is no unique solution for solar energy utilization, since the local requirements depend on climatological achievements and local availability of materials and technicians. For solving present and future problems strong efforts have to be initiated in collecting and estimating data for availability of solar radiation with high local and temporal resolution. Since the implementation of the Brazilian network of meteorological observing stations the sunshine duration was recorded, by the Campbell-Stokes recorder. The characteristics were analyzed for the 12 different cards, concerning: color, dimension, time of burning and overburning as well as the value of the minimum radiation flux necessary to start burning. At the same time the present study aims at providing a semi-empirical model for the estimation of daily global solar radiation and the components of direct and diffuse radiation. In the model methods of parameterization such as Rayleigh and Mie scattering, absorption due to water vapor, CO₂, O₃, and oxygen were used. The entries in the model were the meteorological variables observed in the met-station at the surface: atmospheric pressure, air temperature, air moisture, cloud types, and cloudiness. The model was tested for seven places and showed a relative error smaller than the one given by the pyranometer (5 percent). Author

N89-11364 Minnesota Univ., Minneapolis.

MICROWAVE RADIANCES FROM HORIZONTALLY FINITE, VERTICALLY STRUCTURED PRECIPITATING CLOUDS Ph.D. Thesis

CHRISTIAN DETLEF KUMMEROW 1987 162 p
 Avail: Univ. Microfilms Order No. DA8802405

A model for the transfer of microwave radiances through horizontally finite, vertically structured clouds was developed. Radiances that would be measured from satellite borne radiometers were computed as a function of rainfall rate for finite precipitating clouds that contain liquid as well as frozen hydrometeors. Ice at the top of the precipitating clouds depress brightness temperatures by reflecting radiances emitted by liquid at the lower elevations. Radiation leaking out through the faces of the cloud thus becomes an important finite cloud effect when ice concentrations are high. Recent observations at 37 GHz show a 10 to 15 K difference in the upwelling radiances of the two orthogonally polarized radiances at high rainfall rates. This may be due to the aspherical nature of the ice hydrometeors. The hydrometeors were therefore assumed to be flattened along the axis of fall. A simple regression scheme was used to test the retrievability of the rainfall rate if neither the horizontal size nor shape of the precipitating cloud is known. To simulate real observations, a synthetic data set generated by the aforementioned model with random errors comparable to radiometer noise added to it was used. Dissert. Abstr.

N89-11366 Washington Univ., Seattle.

A STUDY OF THE DYNAMICS OF MARITIME FRONTS USING REMOTELY SENSED WIND AND STRESS MEASUREMENTS Ph.D. Thesis

GAD LEVY 1987 173 p
 Avail: Univ. Microfilms Order No. DA8802285

The satellite scatterometer data open unprecedented opportunities to look at maritime storms and fronts. They are combined with observations, modeling efforts, and theory to study 5 cases. These provide the data to investigate frontal behavior in terms of its vorticity and divergence. The appropriate momentum, divergence and vorticity equations are derived and investigated

including the inertial and frictional terms. The analysis is used to study frontal dynamics. The results indicate that the large scale horizontal and vertical thermodynamic structure of the boundary layer significantly influence baroclinic waves and frontal structure. These effects promote more efficient mixing and transport of heat, moisture, and westerly momentum in midlatitude storms. Conclusions are presented and discussed. Dissert. Abstr.

N89-11645# Max-Planck-Inst. fuer Radioastronomie, Bonn (Germany, F.R.).

VERY LONG BASELINE INTERFEROMETRY (VLBI) FROM GROUND AND SPACE

E. PREUSS *In* ESA, Space Science and Fundamental Physics p 105-116 May 1988

Avail: NTIS HC A10/MF A01

Radio astronomy and very long base interferometry (VLBI) are introduced. Temporal and spatial coherence; VLBI imaging; high precision interferometry; areas of scientific impact (extragalactic radio sources, masers, continuum sources associated with stars, Earth rotation, crustal motion); and developments of VLBI are discussed. ESA

N89-11774*# Jet Propulsion Lab., California Inst. of Tech., Pasadena.

SENSORS RESEARCH AND TECHNOLOGY

JAMES A. CUTTS *In* NASA, Washington, Technology for Future NASA Missions: Civil Space Technology Initiative (CSTI) and Pathfinder p 283-304 Sep. 1988

Avail: NTIS HC A23/MF A01 CSCL 22A

Information on sensors research and technology is given in viewgraph form. Information is given on sensing techniques for space science, passive remote sensing techniques and applications, submillimeter coherent sensing, submillimeter mixers and local oscillator sources, non-coherent sensors, active remote sensing, solid state laser development, a low vibration cooler, separation of liquid helium and vapor phase in zero gravity, and future plans. R.J.F.

N89-12105# National Oceanic and Atmospheric Administration, Washington, DC. Office of Systems Development.

THE GVAR USERS COMPENDIUM, VOLUME 1

KEITH MCKENZIE, ed., RAYMOND J. KOMAJDA, ed. (Mitre Corp., Washington, D.C.), CAROLYN BRADLEY, EARL FEIGEL, JOHN FIORELLO, DEBORAH GARR, PATRICK GERDES, MICHAEL JAMIESON, DONALD MACK, JEFFREY SHAFFER et al. May 1988 205 p

(NOAA-NESDIS-21-VOL-1) Avail: NTIS HC A10/MF A01

The GEOS VARIable (GVAR) Users Compendium assumes reader familiarity with the GOES-I spacecraft and Ground Support Systems. Readers lacking this familiarity are advised to read NOAA Technical Report NESDIS 33, An Introduction to the GOES-IM Imager and Sounder Instruments and the GVAR Retransmission Format. Some sections assume an introductory knowledge of the GVAR format as well. It is the goal of this Compendium to cover a spectrum of issues of interest to the GOES direct readout user. While the editors have tried to convey a sense of cohesiveness, a totally cohesive document at the level of detail presented would take on encyclopedic proportions. The GOES I-M Ground System Project library contains over 1200 documents, ranging from 2-page memos to 300-page Interface Control Documents (ICDs) and grows at the rate of a dozen documents per week. This Compendium is a collection of excerpts from a variety of documents produced during the development of the GOES I-M spacecraft and ground systems. The information ranges from technical background material on the spacecraft instruments to current mission plans as GOES I becomes operational. Author

N89-12111*# Massachusetts Inst. of Tech., Cambridge. Research Lab. of Electronics.

REMOTE SENSING OF EARTH TERRAIN Semiannual Report, 1 Mar. - 31 Aug. 1988

J. A. KONG Aug. 1988 25 p

(Contract NAG5-270)

(NASA-CR-183347; NAS 1.26:183347) Avail: NTIS HC A03/MF A01 CSCL 08B

Two monographs and 85 journal and conference papers on remote sensing of earth terrain have been published, sponsored by NASA Contract NAG5-270. A multivariate K-distribution is proposed to model the statistics of fully polarimetric data from earth terrain with polarizations HH, HV, VH, and VV. In this approach, correlated polarizations of radar signals, as characterized by a covariance matrix, are treated as the sum of N n-dimensional random vectors; N obeys the negative binomial distribution with a parameter alpha and mean bar N. Subsequently, and n-dimensional K-distribution, with either zero or non-zero mean, is developed in the limit of infinite bar N or illuminated area. The probability density function (PDF) of the K-distributed vector normalized by its Euclidean norm is independent of the parameter alpha and is the same as that derived from a zero-mean Gaussian-distributed random vector. The above model is well supported by experimental data provided by MIT Lincoln Laboratory and the Jet Propulsion Laboratory in the form of polarimetric measurements. Author

N89-12114*# National Aeronautics and Space Administration. Goddard Space Flight Center, Greenbelt, MD.

LANDSAT-4 AND LANDSAT-5 MULTISPECTRAL SCANNER COHERENT NOISE CHARACTERIZATION AND REMOVAL

JAMES C. TILTON and WILLIAM L. ALFORD (Defense Mapping Agency, Washington, D.C.) Feb. 1988 46 p

(NASA-TP-2595-REV; NAS 1.60:2595-REV; REPT-86B0040)

Avail: NTIS HC A03/MF A01 CSCL 08B

A technique is described for characterizing the coherent noise found in LANDSAT-4 and LANDSAT-5 MSS data and a companion technique for filtering out the coherent noise. The techniques are demonstrated on LANDSAT-4 and LANDSAT-5 MSS data sets, and explanations of the noise pattern are suggested in Appendix C. A cookbook procedure for characterizing and filtering the coherent noise using special NASA/Goddard IDIMS functions is included. Also presented are analysis results from the retrofitted LANDSAT-5 MSS sensor, which shows that the coherent noise has been substantially reduced. Author

N89-12158*# National Aeronautics and Space Administration. Goddard Space Flight Center, Greenbelt, MD.

LAWS (LASER ATMOSPHERIC WIND SOUNDER) EARTH OBSERVING SYSTEM

1988 68 p Original document contains color illustrations (NASA-TM-101204; NAS 1.15:101204) Avail: NTIS HC A04/MF A01 CSCL 04B

Wind profiles can be measured from space using current technology. These wind profiles are essential for answering many of the interdisciplinary scientific questions to be addressed by EOS, the Earth Observing System. This report provides guidance for the development of a spaceborne wind sounder, the Laser Atmospheric Wind Sounder (LAWS), discussing the current state of the technology and reviewing the scientific rationale for the instrument. Whether obtained globally from the EOS polar platform or in the tropics and subtropics from the Space Station, wind profiles from space will provide essential information for advancing the skill of numerical weather prediction, furthering knowledge of large-scale atmospheric circulation and climate dynamics, and improving understanding of the global biogeochemical and hydrologic cycles. The LAWS Instrument Panel recommends that it be given high priority for new instrument development because of the pressing scientific need and the availability of the necessary technology. LAWS is to measure wind profiles with an accuracy of a few meters per second and to sample at intervals of 100 km horizontally for layers km thick. Author

N89-12936# European Space Agency, Paris (France).

PROCEEDINGS OF THE 1988 INTERNATIONAL GEOSCIENCE AND REMOTE SENSING SYMPOSIUM (IGARSS 1988) ON REMOTE SENSING: MOVING TOWARDS THE 21ST CENTURY, VOLUME 1

T. D. GUYENNE, ed. and J. J. HUNT, ed. Aug. 1988 673 p

Partly in ENGLISH and FRENCH Symposium held in Edinburgh, United Kingdom, 12-16 Sep. 1988; sponsored by the Remote Sensing Society, the Geoscience and Remote Sensing Society, IEEE, and IURS (ESA-SP-284-VOL-1; IEEE-88CH2497-6-VOL-1; ISSN-0379-6566; LC-87-83254; ETN-88-93242) Avail: NTIS HC A99/MF E03; ESA Publications Div., ESTEC, Noordwijk, Netherlands, 120 US dollars or 250 Dutch guilders

Radiometry; radar cross section data bases and modeling services; multipolarization SAR; geographic information systems; ocean waves; land ice; future space remote sensing systems; pattern recognition and feature extraction; rain; calibration and verification of ground-based measurements; backscatter modeling of volume scattering; multipolarization SAR systems; geology; sea ice (SAR); snow; SPOT; and wind measurement were discussed.

ESA

N89-12937# Cologne Univ. (Germany, F.R.). Inst. fuer Geophysik und Meteorologie.

THE AIRBORNE VERSION CONICAL SCAN RADIOMETER (AVCSR): AN AIRBORNE RADIOMETER AS A TOOL FOR SATELLITE DATA VALIDATION

J. WIRTH and M. PEETERS /In ESA, Proceedings of the 1988 International Geoscience and Remote Sensing Symposium (IGARSS 1988) on Remote Sensing: Moving Towards the 21st Century, Volume 1 p 11-12 Aug. 1988

Avail: NTIS HC A99/MF E03; ESA Publications Div., ESTEC, Noordwijk, Netherlands, 120 US dollars or 250 Dutch guilders

The airborne radiation budget radiometer AVCSR for satellite radiometer data validation by development of a special validation strategy to define a best estimate standard satellite instrument, to establish the AVCSR as a stable transfer standard for satellite data validation is described. The calibration strategy of the AVCSR is presented. Expected accuracies are 2 to 5 percent in the solar spectral range; 3 to 10 percent in the terrestrial. Campaigns are planned to validate the data of the Scanner for Radiation Budget (ScaRaB) on the USSR satellites METEOR and of the ATSR on ERS-1.

ESA

N89-12939# Deutsche Forschungs- und Versuchsanstalt fuer Luft- und Raumfahrt, Oberpfaffenhofen (West Germany).

THE AIRBORNE RADIOMETRY EXPERIMENT (ABREX) INSTRUMENT, AN EXPERIMENTAL TEST BED FOR THE SPECIFICATION OF SATELLITE-BORNE MICROWAVE RADIOMETER AT 90 GHZ

W. KEYDEL and H. GOESSL /In ESA, Proceedings of the 1988 International Geoscience and Remote Sensing Symposium (IGARSS 1988) on Remote Sensing: Moving Towards the 21st Century, Volume 1 p 15-16 Aug. 1988

Avail: NTIS HC A99/MF E03; ESA Publications Div., ESTEC, Noordwijk, Netherlands, 120 US dollars or 250 Dutch guilders

The AirBorne Radiometry Experiment (ABREX), a 90 GHz Hach-radiometer breadboard realization of a planned satellite radiometer is described. It was built following the Phase A study results of a satellite-borne radiometer experiment as a testbed for future satellite radiometers with respect to components, calibration, measurement possibilities, etc., and as an instrument for pre-experiments and accompanying measurements of similar 90 GHz satellite-borne radiometers as well. The goals of the experiment, the specifications, and the realized hardware are presented, as well as measurement results.

ESA

N89-12941# National Oceanic and Atmospheric Administration, Boulder, CO. Wave Propagation Lab.

VERIFICATION OF THE ACCURACY OF A NETWORK OF WATER-VAPOR RADIOMETERS

J. B. SNIDER /In ESA, Proceedings of the 1988 International Geoscience and Remote Sensing Symposium (IGARSS 1988) on Remote Sensing: Moving Towards the 21st Century, Volume 1 p 19-20 Aug. 1988

Avail: NTIS HC A99/MF E03; ESA Publications Div., ESTEC, Noordwijk, Netherlands, 120 US dollars or 250 Dutch guilders

Calibration of a network of water vapor radiometers by means

of a mobile radiometer used as a standard is described. Precipitable water vapor (PWV) calculated from radiosonde data is consistently lower than that measured by the radiometers by approximately 0.8 mm. The low bias of the radiometer measurement may be caused by inaccuracies in the radiosonde hygistor, deficiencies in microwave absorption theory, or undetected errors in the tipping curve calibration. Differences in PWV measured at 2 min intervals by the radiometric systems are less than 0.58 mm considering the network as a whole. The mobile radiometer indicates slightly lower PWV values than the network systems. A well calibrated radiometer can continuously monitor short and long-term variations in water vapor with accuracy comparable to or better than that of the radiosonde. Although questions remain in regard to absorption theory and the radiosonde moisture sensor, these uncertainties have a relatively small effect upon the radiometric vapor measurement. Therefore, deployment of vapor-liquid radiometers to complement the wind profiler network is feasible.

ESA

N89-12955# Karlsruhe Univ. (Germany, F.R.). Inst. fuer Hochfrequenztechnik und Elektronik.

POLARIZATION-DEPENDENT ATTENUATION OF DIELECTRIC CYLINDER ARRAYS

W. WIESBECK, D. KAEHNY, and S. RIEGGER /In ESA, Proceedings of the 1988 International Geoscience and Remote Sensing Symposium (IGARSS 1988) on Remote Sensing: Moving Towards the 21st Century, Volume 1 p 73-74 Aug. 1988

Avail: NTIS HC A99/MF E03; ESA Publications Div., ESTEC, Noordwijk, Netherlands, 120 US dollars or 250 Dutch guilders

Land use inventory by remote sensing is reviewed, and the characteristics of the transmitted signal, concerning the polarization dependency as a function of the dielectric properties and the size and orientation of cylinders, are studied. Measurements from 5 to 20 GHz on lossy dielectric cylinders show that transmitted power decreases continuously with frequency. This is due to the increasing reflected power and increasing losses. Transmission attenuation is considerably higher for vertical polarization than for horizontal polarization. Slant linear polarized signals are attenuated accordingly. The resonances, which occur at circumferences of multiples of half a wavelength for dielectric cylinders, are not significant.

ESA

N89-13000# Direction de la Meteorologie Nationale, Paris (France). Div. Prevision.

TOWARDS DIRECT VARIATIONAL ASSIMILATION OF SCATTEROMETER BACKSCATTER MEASUREMENTS INTO NUMERICAL WEATHER PREDICTION MODELS

H. ROQUET and A. RATIER (Centre National d'Etudes Spatiales, Toulouse, France) /In ESA, Proceedings of the 1988 International Geoscience and Remote Sensing Symposium (IGARSS 1988) on Remote Sensing: Moving Towards the 21st Century, Volume 1 p 257-260 Aug. 1988

Avail: NTIS HC A99/MF E03; ESA Publications Div., ESTEC, Noordwijk, Netherlands, 120 US dollars or 250 Dutch guilders

As a step towards variational assimilation of scatterometer backscatter measurements into numerical weather forecasting models, a variational surface wind analysis scheme was developed, whereby a field of unique surface wind vectors is directly retrieved from sigma naught triplets, through the minimization of a cost function involving observation error penalty and smoothness constraint terms. Realistic ERS1 simulations lead to promising wind retrieval performances as regards accuracy, implicit ambiguity removal, preservation of actual wind structures of dynamical significance, and cost efficiency. No sensitivity is found to the initial wind field, and smoothness constraints are shown to reduce the rms error induced by instrumental noise on wind divergence and key ocean forcing parameters.

ESA

N89-13004# National Space Development Agency, Ohashi (Japan). Earth Observation Center.

VERIFICATION RESULTS OF MOS-1 MULTISPECTRAL SELF SCANNING RADIOMETER (MESSR) DATA

K. MAEDA, H. WAKABAYASHI, K. TASAKI, M. SHIMADA, and H. SATO /In ESA, Proceedings of the 1988 International Geoscience

and Remote Sensing Symposium (IGARSS 1988) on Remote Sensing: Moving Towards the 21st Century, Volume 1 p 271-274 Aug. 1988

Avail: NTIS HC A99/MF E03; ESA Publications Div., ESTEC, Noordwijk, Netherlands, 120 US dollars or 250 Dutch guilders

The first MESSR imagery was obtained 4 days after the launch of MOS-1, and MESSR is found to be as expected during mission check period (3 months after the launch). Initial verification results of MESSR radiometric and geometric performance are presented.

ESA

N89-13007# National Space Development Agency, Ohashi (Japan). Earth Observation Center.

DATA COLLECTION SYSTEM OPERATING ON JAPAN'S FIRST MARINE OBSERVATION SATELLITE: INFLIGHT EVALUATION OF THE SYSTEM PERFORMANCE

M. SHIMADA, T. YAMAZAKI, M. TSUJI, and K. AYABE /in ESA, Proceedings of the 1988 International Geoscience and Remote Sensing Symposium (IGARSS 1988) on Remote Sensing: Moving Towards the 21st Century, Volume 1 p 283-286 Aug. 1988
Avail: NTIS HC A99/MF E03; ESA Publications Div., ESTEC, Noordwijk, Netherlands, 120 US dollars or 250 Dutch guilders

Location accuracy of the marine observation satellite (MOS) data collection system was assessed. The location determination algorithm and correction parameters are described. Analysis shows that location of data collection platforms (DCP) is accurate to within 500 m for DCP located between 100 and 2000 km from the MOS-1 subsatellite track.

ESA

N89-13017# Academia Sinica, Beijing (China). Inst. of Electronics.

A SYNTHETIC APERTURES RADAR WITH MULTICHANNEL AND MULTIPOLARISATION

CHENG BO ZHANG /in ESA, Proceedings of the 1988 International Geoscience and Remote Sensing Symposium (IGARSS 1988) on Remote Sensing: Moving Towards the 21st Century, Volume 1 p 331-333 Aug. 1988

Avail: NTIS HC A99/MF E03; ESA Publications Div., ESTEC, Noordwijk, Netherlands, 120 US dollars or 250 Dutch guilders

A SAR system, which has quadri-mapping channel and quadri-polarization was developed. The system, designed to provide capabilities for land use, includes an airborne radar installed in a small aircraft, a real-time down link subsystem, a ground based image processor, and a data film analyzer. The design concept, main features of the system, and its applications are described. The SAR imagery is presented.

ESA

N89-13059# Oslo Univ. (Norway). Dept. of Geography.

EFFECTS OF CHANGING SATELLITE SENSOR ATTRIBUTES

A. K. GJERTSEN /in ESA, Proceedings of the 1988 International Geoscience and Remote Sensing Symposium (IGARSS 1988) on Remote Sensing: Moving Towards the 21st Century, Volume 1 p 501-504 Aug. 1988

Avail: NTIS HC A99/MF E03; ESA Publications Div., ESTEC, Noordwijk, Netherlands, 120 US dollars or 250 Dutch guilders

A satellite scene is classified into a land cover/land use map, and the effects of changing sensor attributes like, e.g., the resolution cells are evaluated. To quantitatively evaluate the effects of the different attributes of the TM sensor a statistical method for analysis of variance was employed. A three factor, two level fixed effect model was adopted. Finer resolution cells (30 m) result in a reduction in total classification accuracy, but 30 m cells show better results than with 80 m cells to classify the forest into quality classes.

ESA

N89-13069# British Antarctic Survey, Cambridge (England).

CLOUD TRACK WINDS FROM POLAR ORBITING SATELLITES

D. WARREN and J. TURNER /in ESA, Proceedings of the 1988 International Geoscience and Remote Sensing Symposium (IGARSS 1988) on Remote Sensing: Moving Towards the 21st Century, Volume 1 p 549-550 Aug. 1988

Avail: NTIS HC A99/MF E03; ESA Publications Div., ESTEC, Noordwijk, Netherlands, 120 US dollars or 250 Dutch guilders

A means of estimating wind speed and direction at high latitudes from polar orbiting satellite data is described. The method is similar to that used to obtain cloud track winds from geostationary satellite imagery and takes advantage of the large overlap between successive AVHRR images at latitudes poleward of 70 deg. Sources of error inherent in the techniques are described along with the quality control criteria applied to eliminate inaccurate estimates.

ESA

N89-13071# GEC-Marconi Electronics Ltd., Chelmsford (England).

AN ANALYSIS OF DIRECTIONAL AMBIGUITIES IN WIND SCATTEROMETER MEASUREMENTS

J. LAYCOCK /in ESA, Proceedings of the 1988 International Geoscience and Remote Sensing Symposium (IGARSS 1988) on Remote Sensing: Moving Towards the 21st Century, Volume 1 p 557-560 Aug. 1988

Avail: NTIS HC A99/MF E03; ESA Publications Div., ESTEC, Noordwijk, Netherlands, 120 US dollars or 250 Dutch guilders

The dependence of the accuracy with which wind scatterometers are able to measure wind fields on solving the problem of directional ambiguities, is discussed. The results of a simulation to analyze the performance of systems of a similar configuration to the ERS-1 wind scatterometer are assessed. The results show that an initial skill of between 70 percent to 80 percent is expected. Most errors are caused by ambiguities, and although any ambiguous solution which is chosen as rank 1 is bound to be highly inaccurate, this does mean that substantially correct wind measurements are achievable, provided that the problem of ambiguities can be overcome. Ambiguity removal techniques are reviewed. Promising results are obtained using smoothing algorithms. Ways in which algorithm performance might be further improved are identified.

ESA

N89-13072# Marconi Space Systems Ltd., Portsmouth (England).

MULTISTATIC SCATTEROMETRY

C. D. HALL and R. A. CORDEY (GEC-Marconi Electronics Ltd., Chelmsford, England) /in ESA, Proceedings of the 1988 International Geoscience and Remote Sensing Symposium (IGARSS 1988) on Remote Sensing: Moving Towards the 21st Century, Volume 1 p 561-562 Aug. 1988

Avail: NTIS HC A99/MF E03; ESA Publications Div., ESTEC, Noordwijk, Netherlands, 120 US dollars or 250 Dutch guilders

The concept of a scatterometer based on multistatic principles is described. The performance of a system using GPSS transmitters and a radiometer style receiver is shown to be inadequate. It is shown that transmitters of much higher power and a longer code modulation than GPSS are required to realise a system with useful performance.

ESA

N89-13081# Deutsche Forschungs- und Versuchsanstalt fuer Luft- und Raumfahrt, Oberpfaffenhofen (West Germany). Inst. for Optoelectronics.

THE MEOSX EXPERIMENT: A TEST CASE FOR FUTURE CARTOGRAPHIC MISSIONS

F. LANZL, A. DRESCHER, K. HILLER, M. HAUCK, and D. BERAN /in ESA, Proceedings of the 1988 International Geoscience and Remote Sensing Symposium (IGARSS 1988) on Remote Sensing: Moving Towards the 21st Century, Volume 1 p 599-604 Aug. 1988

Avail: NTIS HC A99/MF E03; ESA Publications Div., ESTEC, Noordwijk, Netherlands, 120 US dollars or 250 Dutch guilders

The Indian/West German monocular electro optical stereo CCD line scanner planned to be launched in 1988 as a joint satellite experiment is presented. The camera system, the mission aspects, and the planned evaluation methods are summarized.

ESA

N89-13092# Naval Postgraduate School, Monterey, CA.

MULTISPECTRAL SATELLITE ANALYSIS OF MARINE STRATOCUMULUS CLOUD MICROPHYSICS M.S. Thesis

GARY M. MINEART Mar. 1988 149 p
(AD-A197316) Avail: NTIS HC A07/MF A01 CSCL 04A

Variations in marine stratocumulus cloud microphysics during FIRE IFO 1987 are observed and analyzed through the use of NOAA-9/10 AVHRR satellite data and aircraft in-cloud measurements. The relationships between channel 3 reflectance and cloud microphysical properties are examined through model reflectances based on Mie theory and the delta-Eddington approximation, and reveal a channel 3 reflectance dependence on cloud droplet size distribution. Satellite observations show significant regions of continental influence over the ocean through higher channel 3 reflectances resulting from the injection of continental aerosols and the associated modification of cloud droplet characteristics. Channel 3 reflectance gradients across individual cloud elements correspond to radially varying cloud droplet size distributions within the elements. Various mesoscale and microscale features such as ship stack effluent tracks and pollution sources are observed in the data. Correlations between reflectance values and aircraft measurements illustrate the potential of estimating cloud droplet size distribution and marine atmospheric boundary layer aerosol composition and concentration through use of satellite data. Such an estimation technique may prove useful in determining climatic implications of cloud reflectance changes due to the influence of natural and man-made aerosol sources, and provide a means to assess the performance of boundary layer electro-optic systems. GRA

N89-13094# National Oceanic and Atmospheric Administration, Washington, DC. National Environmental Satellite, Data and Information Service.

PRECIPITATION DETECTION WITH SATELLITE MICROWAVE DATA

Y. CHENGANG and A. TIMCHALK Jun. 1988 37 p Prepared in cooperation with Chinese Academy of Meteorological Sciences, Beijing (PB88-240239; NOAA-TR-NESDIS-32) Avail: NTIS HC A03/MF A01 CSCL 04B

When all four channels of the NOAA polar-orbiting satellite Microwave Sounding Unit (MSU) instrument were screened against a measure of rainrate, MSU Ch 2 (53.74 GHz) was found to be the most useful channel for detecting precipitation over land. The MFA2 values were found to be correlated with an Effective Rain Rate (ERR). In the winter cases, convection was relatively weak and rain rates were small. Results indicate that the MFA2 is marginally useful in detecting rain rates. Its operational use in the TIROS Operational Vertical Sounding (TOVS) algorithm, however, does serve well to prevent cold biased temperature retrievals from being calculated in areas where precipitation contamination is strong. GRA

N89-14189*# National Aeronautics and Space Administration, Lyndon B. Johnson Space Center, Houston, TX.

REMOTE SENSING IN POLARIZED LIGHT

VICTOR S. WHITEHEAD and KINSELL L. COULSON (California Univ., Davis.) Oct. 1988 40 p Proceedings of Workshop held in Houston, Tex., 3-5 Nov. 1987 (NASA-CP-3014; S-577; NAS 1.55:3014) Avail: NTIS HC A03/MF A01 CSCL 05B

Preliminary analysis of polarized images of earth collected by hand-held cameras on Shuttle Missions 51A, 51G, 51I, and 61A indicate that information of the earth's surface and atmosphere exists in those data. To ensure that follow-on research in polarization is focused upon and that the experiments are properly designed to address specific questions, 26 scientists with past experience and interest in polarization observations met at the Lyndon B. Johnson Space Center on November 3 to 5, 1987. This conference report summarizes the discussions and provides the recommendations of the group for follow-on research. Author

N89-14414# Air Force Geophysics Lab., Hanscom AFB, MA. **POSSIBLE MEASUREMENT ERRORS IN CALIBRATED AVHRR (ADVANCED VERY HIGH RESOLUTION RADIOMETER) DATA** *Environmental Research Papers, 1987 - 1988* ROBERT P. DENTREMONT and THOMAS J. KLEESPIES 1

Apr. 1988 27 p

(AD-A198342; AFGL-TR-88-0105; AFGL-ERP-1001) Avail: NTIS HC A03/MF A01 CSCL 04A

Visible and infrared meteorological satellite data are a primary source of global cloud observations. Such data are calibrated in order to provide its users with a method for converting from raw measurements, called counts, to physically sensible measurements such as albedo or brightness temperature. This report describes the procedure for converting National Oceanic and Atmospheric Administration Advanced Very High Resolution Radiometer (NOAA AVHRR) raw counts to albedos and brightness temperatures. This procedure involves the use of calibration coefficients that help define the relationship between the raw counts and the physical measurements they represent. Such relationships are referred to as look-up-tables. In theory, calibration coefficients (and therefore look-up tables) do not change noticeably from one scanline of satellite data to the next. This makes feasible the generation of a constant look-up table that can be used over long periods of time for all data. In practice, calibration coefficients can and often do change from one scan to the next. These changes imply accuracy errors in measured brightness temperatures that are significant for some satellite data analysis algorithms; others are less severely affected. This report addresses the potential errors that can be expected when using constant look-up tables, i.e., by assuming that sensor calibration does not change from one scanline to the next. GRA

N89-14482# Forest Service, Washington, DC. Engineering Staff.

SPACE SHUTTLE LARGE FORMAT CAMERA PHOTOGRAPHY CLOUD COVER INTERFERENCE DIAGRAMS Final Report

JERRY D. GREER Jul. 1988 24 p (PB88-244405; EM-7140-17) Avail: NTIS HC A03/MF A01 CSCL 14E

High-resolution photographs of the Earth's land features acquired by space vehicles can present information that is not obvious on other types of imagery. For investigators interested in resources, the land must be visible on the photograph. This is not generally the case with imagery acquired during the October 1984 flight of the Space Shuttle Challenger carrying the large format camera. The report reviews and compares various records concerning the cloud cover. The imagery of the United States is reviewed, and frame-by-frame sketch diagrams of cloud cover are presented. GRA

N89-14490# Technische Hogeschool, Delft (Netherlands). Faculty of Geodesy.

AUTOMATIC PROCEDURE TO FIND CORRESPONDING POINTS IN CCD AIRBORNE EXPERIMENTAL SCANNER FOR APPLICATIONS IN REMOTE SENSING (CAESAR) IMAGES Thesis [EEN AUTOMATISCHE PROCEDURE TER VERKRIJGING VAN CORRESPONDERENDE PUNTEN IN CAESAR-BEELDEN]

W. J. LOOYEN Feb. 1988 67 p In DUTCH; ENGLISH summary Original contains color illustrations (B8821609; ETN-89-93333) Avail: NTIS HC A04/MF A01

An automatic procedure for finding corresponding points in images of the multispectral scanner CAESAR is described. First, the CAESAR images are geometrically corrected using inertial systems data and a geometrical analysis. These images are then used in an automatic procedure to calculate the geometrical transformation model between the images in order to use the spectral information as well as possible. Correlation techniques are used. Using two images, in the first one interesting points are found applying the Moravec operator. The corresponding points in the second image are determined using a two-dimensional cross correlation. From the two point lists the geometrical transformation model can be calculated, after which a resampling takes place to match the images. ESA

N89-14522*# National Aeronautics and Space Administration. Ames Research Center, Moffett Field, CA.

COMPARISON OF IN SITU AEROSOL MEASUREMENTS WITH SAGE 2 AND SAM 2 AEROSOL MEASUREMENTS DURING THE AIRBORNE ANTARCTIC OZONE EXPERIMENT Abstract Only

G. V. FERRY, M. PATRICK MCCORMICK, R. F. PUESCHEL, and J. M. LIVINGSTON (SRI International Corp., Menlo Park, Calif.) /n NASA, Goddard Space Flight Center, Polar Ozone Workshop. Abstracts p 56 May 1988
Avail: NTIS HC A14/MF A01 CSCL 13B

Models indicate that stratospheric aerosols play a major role in the destruction of ozone during the Austral winter. Although many in situ measurements of stratospheric aerosols were made during the Airborne Antarctic Ozone Experiment, changes of aerosol concentration and size distributions across the polar vortex are important to understanding changes of chemical species taking place during this time. Therefore comparing the in situ measurements with measurements made by satellites scanning wider areas will give a clearer picture of the possible role played by aerosols during this period. The wire impactor size distributions are compared to those from the aerosol spectrometers and a best fit size distribution determined. Aerosol extinctions are calculated from the in situ measurements and compared to the extinctions measured by the satellites. Five comparisons are made with SAGE 2 and four with SAM 2. Extinctions agree as close as a factor of two. Author

N89-14635 Wisconsin Univ., Madison.

CLASSIFICATION AND ANALYSIS OF SURFACE AND CLOUDS AT HIGH LATITUDES FROM AVHRR

MULTISPECTRAL SATELLITE DATA Ph.D. Thesis

ELIZABETH EBY EBERT 1987 193 p

Avail: Univ. Microfilms Order No. DA8800706

Measurement of polar cloud cover is important because of its strong radiative influence on the energy balance of the snow and ice surface. However, conventional satellite cloud detection schemes often fail in the polar regions because of small visible and thermal contrasts. Some of these limitations were overcome by a pattern recognition algorithm which uses visible, near-infrared, and infrared Advanced Very High Resolution Radiometer (AVHRR) satellite data to identify regions of various surface and cloud types at high latitudes. For each of the four periods (Arctic summer, Arctic winter, Antarctic summer, Antarctic winter) approximately 1000 training samples were used to teach the algorithm the spectral and textural characteristics of 18 surface and cloud classes. The algorithm then combines the classification information with a hybrid histogram-spatial coherence analysis to estimate the fractional cloud cover, as well as clear and cloudy albedos and brightness temperatures. The hybrid histogram-spatial coherence method accurately analyzed sixty artificial scenes which had known values of cloud fraction and surface and cloud properties. Two days of polar AVHRR data from 6 January 1984 and 1 July 1984 were analyzed. Dissert. Abstr.

N89-14648*# National Aeronautics and Space Administration. Goddard Space Flight Center, Greenbelt, MD.

USER'S GUIDE FOR THE NIMBUS 7 SCANNING MULTICHANNEL MICROWAVE RADIOMETER (SMMR) CELL-ALL TAPE

C. C. CU, D. HAN, S. T. KIM (ST Systems Corp., Lanham, Md.), and P. GLOERSEN Oct. 1988 152 p
(Contract NAS5-29386)

(NASA-RP-1210; REPT-88-181; NAS 1.61:1210) Avail: NTIS HC A08/MF A01 CSCL 04B

The SMMR instrument onboard the Nimbus-7 satellite has been in operation since October 1978. It provided global coverage of passive microwave observations at 6.6, 10.7, 18, 21, and 37 GHz. The observed brightness temperature can be used to retrieve geophysical parameters, principally sea surface temperature, atmospheric water vapor and liquid water content over oceans, sea ice concentration, and snow cover over land. The SMME CELL-ALL Tape contains earth-located calibrated brightness

temperature data which have been appropriately binned into cells of various grid sizes, allowing intercomparisons of observations made at different frequencies (with corresponding different footprint sizes). This user's guide describes the operation of the instrument, the flow of the data processing the calibration procedure, and the characteristics of the calibrated brightness temperatures and how they are binned. Detailed tape specifications and lists of available data are also provided. Author

09

GENERAL

Includes economic analysis.

A89-12121#

PRINCIPLES RELATING TO REMOTE SENSING OF THE EARTH FROM SPACE - TERRITORIAL SPHERE OF APPLICATION

GENNADII M. DANILENKO (AN SSSR, Institut Gosudarstva i Prava, Moscow, USSR) IN: Colloquium on the Law of Outer Space, 30th, Brighton, England, Oct. 10-17, 1987, Proceedings. Washington, DC, American Institute of Aeronautics and Astronautics, 1988, p. 289-294. refs

This paper examines the problems concerning the territorial sphere of application of the UN Principles Relating to Remote Sensing of the Earth from Space (1986). The provisions of the Principles and the relevant preparatory documents are analyzed in order to determine the territorial scope of application of obligations concerning the nondiscriminatory access of sensed states to data and information obtained by remote sensing. It is concluded that the territorial sphere of application of these obligations is not clearly defined by the Principles. Author

A89-12125#

UNITED NATIONS ACTIVITY ON REMOTE SENSING - LEGAL AND POLITICAL IMPLICATIONS

DAVID S. MYERS (West Florida, University, Pensacola, FL) IN: Colloquium on the Law of Outer Space, 30th, Brighton, England, Oct. 10-17, 1987, Proceedings. Washington, DC, American Institute of Aeronautics and Astronautics, 1988, p. 361-365. refs

International regulation of terrestrial remote sensing from space is discussed, with a focus on UN activities. The Principles on Remote Sensing drafted by COPUOS and approved by the General Assembly in 1986 are summarized in detail. In essence, the Principles permit remote sensing and dissemination of remote-sensing data without prior consent of the states whose territory is being observed, while encouraging the satellite operators to cooperate with and provide data to those states, and requiring the states with jurisdiction over the operators to take some responsibility for the remote-sensing activities of their nationals. Although the Principles have been adopted, it appears unlikely that they will soon be formalized as a treaty to be signed by UN member nations. T.K.

A89-12126#

INTERNATIONAL SPACE LAW NORMS REGULATING REMOTE SENSING OF THE EARTH FROM OUTER SPACE

CHARLES CHUKWUMA OKOLIE (Okolie International Law Chambers, Chicago, IL) IN: Colloquium on the Law of Outer Space, 30th, Brighton, England, Oct. 10-17, 1987, Proceedings. Washington, DC, American Institute of Aeronautics and Astronautics, 1988, p. 366-370. refs

The applicability of international customary law and treaties to commercial satellite remote sensing of earth resources is examined. The history of space remote sensing is briefly traced, and the applicable UN legislation is characterized in detail. It is argued that currently valid international law, while permitting remote-sensing activities without the consent of the states whose territory is being observed, demands that the states with jurisdiction

over the remote-sensing operators encourage them to make the remote-sensing information available to the observed states.

T.K.

A89-17680*# Jet Propulsion Lab., California Inst. of Tech., Pasadena.

STANDARDS FOR EARTH OBSERVATIONS FROM SPACE

H. J. SHEETZ (AIAA, Washington, DC) and M. S. REID (California Institute of Technology, Jet Propulsion Laboratory, Pasadena) IAF, International Astronautical Congress, 39th, Bangalore, India, Oct. 8-15, 1988. 17 p. refs

(IAF PAPER 88-107)

The development of earth observation standards and the need for cooperation between national and international earth resource organizations are discussed. Possible solutions to the problem of developing a coordinated effort in the development of observational satellite systems are given. The activities of the AIAA Earth Observation Committee on Standards are reviewed. It is suggested that earth observation organizations must combine their resources and efforts and that computer programs of earth observation organizations, their work and products, and agreements between various organizations, should be developed. Charts of organizations addressing the problems in earth observations by satellite are presented, including descriptions of their activities.

R.B.

A89-19385

UN PRINCIPLES ON REMOTE SENSING - AN AGREEMENT ON ECONOMIC RELATIONS

N. JASENTULIYANA (UN, Outer Space Affairs Div., New York) Space Policy (ISSN 0265-9646), vol. 4, Nov. 1988, p. 281-284.

Consideration is given to the political and economic impact of the principles regarding the remote sensing of earth from space adopted as a resolution by the UN General Assembly in 1986. The fact that these principles were not formalized as a binding international treaty is stressed, and it is suggested that, although commercial relations between the providers of remote-sensing services and developing countries have improved, serious political problems are posed by the commercial availability of surveillance-quality remote-sensing images of military installations and other restricted areas. The need for a legal framework to reduce such international tensions is indicated.

T.K.

A89-20104

BUSINESS STRATEGIES AND LAND REMOTE SENSING CAPABILITIES

PITT G. THOME and STAN A. MORAIN (New Mexico, University, Albuquerque) IN: EASCON '88; Proceedings of the Twenty-first Annual Electronics and Aerospace Conference, Arlington, VA, Nov. 9-11, 1988. New York, Institute of Electrical and Electronics Engineers, Inc., 1988, p. 17-23.

It is suggested that land remote sensing in the U.S. is at a critical juncture while the government gives serious study to the direction it will take beyond the privatization of the current Landsats and its investment in Landsat 6. The issues revolve around questions of the relative roles of government and private industry and the attractiveness of future business opportunities. An attempt is made to clarify several aspects of the issues, especially from the marketing point of view of an entrepreneur. The current status of the U.S. remote-sensing industry is summarized; several scenarios for the future are suggested; some of the more critical capability and technology needs to support these scenarios are indicated; and the marketing challenges confronting the industry are set forth.

I.E.

A89-20701

EUROPEAN REMOTE SENSING NEEDS IN THE 1990S; PROCEEDINGS OF THE ANNUAL SYMPOSIUM OF EARSSEL, NOORDWIJKERHOUT, NETHERLANDS, MAY 4-8, 1987

R. VAN KONIJNENBURG, ED. Symposium sponsored by the European Association of Remote Sensing Laboratories. International Journal of Remote Sensing (ISSN 0143-1161), vol. 9, Oct.-Nov. 1988, 347 p. For individual items see A89-20702 to A89-20724.

Topics related to remote sensing are presented, including radiometric measurements and crop yield forecasting, the lowest order correction for solar zenith angle to the global vegetation index, regional land cover and agricultural area statistics and mapping, and the analysis of large format camera photographs for topographic and thematic mapping. In addition, the evaluation of space photographs, advances in computerized information retrieval, geometric correction of imagery using ground control points and orthogonal polynomials, regional hydrological systems analysis, and marine science applications of remote sensing are discussed. Other aspects include the use of TM data for forest classification, mineral exploration, and topographic mapping, processing SPOT data, the use of Landsat and Seasat data in kinematic analysis, the determination of ocean surface parameters from satellite data, aerial photography for biomass assessment, and the prospects for future developments in operational weather forecasting and wave studies.

R.B.

N89-10392# Centre National d'Etudes Spatiales, Paris (France). THE FRENCH SPACE PROGRAM FOR EARTH OBSERVATION [LE PROGRAMME SPATIAL FRANCAIS POUR L'OBSERVATION DE LA TERRE]

M. CHEVREL /In ESA, Proceedings of the 4th International Colloquium on Spectral Signatures in Remote Sensing p 483-486 Apr. 1988 In FRENCH

Avail: NTIS HC A23/MF A01; ESA Publications Division, ESTEC, Noordwijk, Netherlands 80 Dutch guilders

Earth observations from space (land, ocean, climate) are reviewed. The SPOT and TOPEX/POSEIDON programs are introduced. Instrumentation and systems of future space based programs, and an airplane for atmospheric research and remote sensing are mentioned.

ESA

N89-10393*# National Aeronautics and Space Administration, Washington, DC.

NASA'S FUTURE LAND REMOTE SENSING PROGRAM

R. E. MURPHY, M. BALTUCK, M. RUZEK, and D. E. WICKLAND /In ESA, Proceedings of the 4th International Colloquium on Spectral Signatures in Remote Sensing p 487-492 Apr. 1988

Avail: NTIS HC A23/MF A01; ESA Publications Division, ESTEC, Noordwijk, Netherlands 80 Dutch guilders CSDL 02F

The NASA remote sensing plans for the Land Processes Program are reviewed in the context of the science driven programs in ecology, hydrology, and geology. The instrumental capabilities in place on airborne platforms, and those available on the Earth Observing System in the mid 1990s, are considered. Coordinated field experiments which are evolutionary from the First ISLSCP Field Experiment are discussed.

ESA

N89-10905*# Technische Univ., Berlin (Germany, F.R.). Dept. of Satellite Design and Technology.

TUBSAT-1, SATELLITE TECHNOLOGY FOR EDUCATIONAL PURPOSES

A. GINATI /In NASA, Goddard Space Flight Center, The 1988 Get Away Special Experimenter's Symposium p 17-24 Sep. 1988

Avail: NTIS HC A07/MF A01 CSDL 22A

TUBSAT-1 (Technical University of Berlin Satellite) is an experimental low-cost satellite within the NASA Get Away Special (GAS) program. This project is being financed by the German BMFT (Federal Ministry for Research and Technology), mainly for student education. The dimensions and weight are determined by GAS requirements and the satellite will be ejected from the space shuttle into an approximately 300-km circular orbit. It is a sun/star oriented satellite with an additional spin stabilization mode. The first planned payload is to be used for observing flight paths of migratory birds from northern Europe to southern Africa and back.

Author

N89-11295# Instituto de Pesquisas Espaciais, Sao Jose dos Campos (Brazil).

TRAINING ACTIVITIES IN REMOTE SENSING AT THE INSTITUTO DE PESQUISAS ESPACIAIS-INPE/BRAZIL [AS ATIVIDADES DE TREINAMENTO EM SENSORIAMENTO REMOTO NO INSTITUTO DE PESQUISAS ESPACIAIS-INPE/BRASIL]

TANIA MARIA SAUSEN and ROBERTO PEREIRADACUNHA Aug. 1988 21 p In PORTUGUESE; ENGLISH summary Presented at the 2nd Latin American Symposium of Remote Perception, Bogota, Columbia, 16-23 Nov. 1987 (INPE-4686-PRE/1380) Avail: NTIS HC A03/MF A01

The Institute for Space Research (Instituto de Pesquisas Espaciais - INPE) began its research program in remote sensing in 1972, with the launching of the American LANDSAT satellites. Research was developed mainly in the field of natural resources, through the studies of geology, environmental analysis, agriculture and vegetation. In October 1985 the Technical Orientation in Remote Sensing (Coordenadoria de Orientacao Tecnica em Sensoriamento Remoto COT) was created; its main objective is to coordinate the transference of remote sensing technologies and methodologies developed by INPE, to external users. Under the responsibility of COT, there exists a Training Group (Coordenadoria Adjunta de Treinamento), responsible for the realization of national and international training courses for the job training in remote sensing and for the II International Training Course in Remote Sensing. The INPE's Remote Sensing Area has a group of researchers in academic titles of Master of Science in remote sensing and Doctorate in different fields of natural resources, in charge of giving training courses as well as developing researches. This paper explains the remote sensing activities in training courses, realized through the Training Group of COT in the years 1985, 1986 and 1987 and its training policy for the next years.

Author

are summarized. The projects are discussed in some detail.

B.G.

N89-13082# Indian Inst. of Tech., Bombay. Center of Studies in Resources Engineering.

IMPORTANT ASPECTS OF TECHNOLOGY TRANSFER: TRAINING OF INSERVICE ENGINEERS AND SCIENTISTS; SATELLITE REMOTE SENSING

T. V. PAVATE In ESA, Proceedings of the 1988 International Geoscience and Remote Sensing Symposium (IGARSS 1988) on Remote Sensing: Moving Towards the 21st Century, Volume 1 p 607-608 Aug. 1988

Avail: NTIS HC A99/MF E03; ESA Publications Div., ESTEC, Noordwijk, Netherlands, 120 US dollars or 250 Dutch guilders

Technology transfer, especially with respect to emerging areas such as satellite remote sensing, and operationalization in multidisciplinary user agencies is discussed. There is a certain amount of urgency being felt in this regard as the conventional method of university education has limited scope in training of large numbers of inservice engineers and scientists who are already working in different capacities. A new approach is mandatory in training of very large number of engineers and scientists towards operationalization of uses of satellite remote sensing to identify, quantify, and manage natural resources on the global scale.

ESA

N89-14481*# California Univ., Santa Barbara.

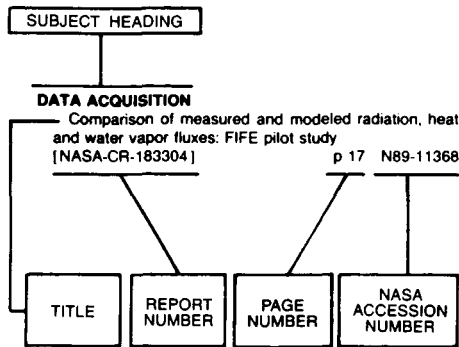
REMOTE SENSING INFORMATION SCIENCES RESEARCH GROUP Final Report, Year 5

JOHN E. ESTES, TERENCE SMITH, and JEFFREY L. STAR 1 Jun. 1988 61 p (Contract NAGW-455)

(NASA-CR-183374; NAS 1.26:183374) Avail: NTIS HC A04/MF A01 CSCL 05B

Research conducted under this grant was used to extend and expand existing remote sensing activities at the University of California, Santa Barbara in the areas of georeferenced information systems, matching assisted information extraction from image data and large spatial data bases, artificial intelligence, and vegetation analysis and modeling. The research thrusts during the past year

Typical Subject Index Listing



The subject heading is a key to the subject content of the document. The title is used to provide a description of the subject matter. When the title is insufficiently descriptive of document content, a title extension is added, separated from the title by three hyphens. The (NASA or AIAA) accession number and the page number are included in each entry to assist the user in locating the abstract in the abstract section. If applicable, a report number is also included as an aid in identifying the document. Under any one subject heading, the accession numbers are arranged in sequence with the AIAA accession numbers appearing first.

A

ABSORPTANCE

A simplified vegetation canopy reflectance and absorption model p 10 N89-10322

ABSORPTION SPECTRA

Reflectance characteristics of dry plant materials p 3 A89-10977

ABSORPTION SPECTROSCOPY

High-resolution spectroscopy for remote sensing of ocean and atmosphere p 48 N89-10352

ABSORPTIVITY

Development of a semi-empirical model for estimating the global solar radiation [INPE-4620-TDL/328] p 84 N89-11352

ABSTRACTS

Biogeochemical processes in sagebrush steppe: Interactions of terrain, vegetation and chemical cycles [NASA-CR-181486] p 21 N89-13088

ACCURACY

Continuous deformation monitoring with GPS [AD-A196447] p 27 N89-10886

A study of accuracy enhancement in satellite magnetic modeling p 28 N89-12102

Evaluation of GEOSAT (Geodetic Satellite) data and application to variability of the northeast Pacific Ocean [AD-A198950] p 53 N89-13863

ACOUSTIC PROPERTIES

Estimation of the variability of acoustic characteristics in the region of frontal zones and mesoscale vortices using remote sensing data p 47 A89-18843

ADVANCED VERY HIGH RESOLUTION RADIOMETER

Remote sensing of suspended sediments in estuaries using atmospheric and compositional corrections to AVHRR data p 57 A89-10940

Regional and global fire detection using AVHRR data p 2 A89-10956

Effect of spatial resolution of the statistical properties of satellite images - A case study p 66 A89-12221

Estimation of multiple reflection and lowest order adjacency effects on remotely-sensed data p 5 A89-12354

The navigation of AVHRR imagery p 66 A89-12357

Snow and low-cloud discrimination from multispectral satellite measurements p 78 A89-12850

Effects of data resolution on marine stratiform cloud detection using AVHRR and VISSR satellite data p 78 A89-12854

Evaluation of 3.7 micron split windows for estimating surface temperature p 43 A89-12855

EOF analysis of AVHRR and CZCS imagery p 43 A89-12856

Nimbus-7 SMMR derived sea-ice concentrations over Antarctica p 43 A89-12857

A simple method for estimating monthly mean albedo of land surfaces from AVHRR data p 6 A89-15493

Possible measurement errors in calibrated AVHRR (Advanced Very High Resolution Radiometer) data [AD-A198342] p 88 N89-14414

Classification and analysis of surface and clouds at high latitudes from AVHRR multispectral satellite data p 89 N89-14635

ADVECTION

Mass and heat balances in the upper ocean p 53 N89-13089

The role of horizontal processes in upper-ocean prediction: A forecast simulation in the Sea of Japan [AD-A198827] p 55 N89-14654

AERIAL PHOTOGRAPHY

The practice and understanding of using aerial remote sensing in the investigation of coastal zone p 37 A89-10995

Acreeage and yield determination - 1987 Kansas winter wheat p 4 A89-11007

Image analysis techniques for the interpretation of airphoto lineaments - Petroleum exploration, Eromanga Basin, Australia p 30 A89-14011

Simplified forest inventory using large-scale 70-mm photography and tariff tables p 6 A89-14090

Aerospace monitoring of ecosystem dynamics and ecological prognoses p 23 A89-15050

Shuttered camera - Aerial color video imaging in the visible and near infrared p 8 A89-20630

Aerial photography for biomass assessment in the intertidal zone p 9 A89-20724

Aircraft remote sensing in HAPEX --- hydrology p 59 N89-10388

CIR aerial photography applied to the evaluation of the air pollution impact in a tropical forest: The case of Cubatao, Brazil p 17 N89-11324

Small format air photo from ultrahigh aircraft as an aid for data collection of agricultural statistics in Sahelian countries p 19 N89-13003

Mapping the distribution and abundance of lithological units and surface mineralogies at Jabal Sa'id, Saudi Arabia: An application of spectral mixture modelling p 34 N89-13024

AERODYNAMIC DRAG

SAR image statistics related to atmospheric drag over sea ice p 52 N89-13034

AEROSOLS

Analysis of the contribution of the atmosphere to water reflectance in the first two channels of the NOAA satellites AVHRR p 82 N89-10330

Comparison of in situ aerosol measurements with SAGE 2 and SAM 2 aerosol measurements during the airborne Antarctic ozone experiment p 89 N89-14522

AEROSPACE ENVIRONMENTS

Fiber-optic sensor systems for aerospace applications p 74 A89-10359

AEROSPACE TECHNOLOGY TRANSFER

Important aspects of technology transfer: Training of inservice engineers and scientists; satellite remote sensing p 91 N89-13082

AFRICA

The use of MOMS-1 data for geological mapping of the Aswa lineament (East African rift) p 33 N89-10382

Small format air photo from ultrahigh aircraft as an aid for data collection of agricultural statistics in Sahelian countries p 19 N89-13003

AFRICAN RIFT SYSTEM

A regional tectonic study of NE and E Africa and its implication for mineral exploration: A synoptic view from satellite imagery p 34 N89-13023

AGRICULTURAL AIRCRAFT

Computational design and efficiency optimization of agricultural airplanes p 5 A89-13670

Small format air photo from ultrahigh aircraft as an aid for data collection of agricultural statistics in Sahelian countries p 19 N89-13003

AGRICULTURE

Remote sensing and geographic information systems for agricultural statistics-gathering and agricultural monitoring in Morocco p 2 A89-10960

Effect of soil roughness on SAR images of harvested agricultural fields p 4 A89-11004

Acreeage and yield determination - 1987 Kansas winter wheat p 4 A89-11007

Comparison of SPOT, TM and MSS data for agricultural land-use mapping in Gujarat (India) [IAF PAPER 88-139] p 7 A89-17692

Regional land cover and agricultural area statistics and mapping in The Departement Ardeche, France, by use of Thematic Mapper data p 8 A89-20705

AGRISAR'86: Contributing to signature research p 15 N89-10387

Technique for obtaining agricultural property boundaries through satellite imagery, certified to control and accompany agricultural activity p 16 N89-11294

Crop separation analysis through SPOT and TM digital data [INPE-4641-PRE/1351] p 18 N89-12110

An integrated remote sensing approach for regional agrostatistics and land monitoring p 24 N89-12960

Agroecological information content of SPOT data p 19 N89-13050

Evaluation of LANDSAT TM and SPOT imagery for agricultural land use planning in less developed countries p 19 N89-13051

The California Cooperative Remote Sensing Project [NASA-TM-100073] p 22 N89-13824

AGROMETEOROLOGY

The effect of agrometeorological conditions on the characteristics of space radar imagery of agricultural regions in winter p 8 A89-18709

AIR LAND INTERACTIONS

The effect of snow parameter variations on the thermal microwave emission of the soil-snow-atmosphere system p 59 A89-18712

AIR POLLUTION

Detection of forest damage on Whiteface Mountain, New York, using Landsat Thematic Mapper data p 3 A89-10987

Complex experiment on the investigation of the atmosphere pollution using space, aircraft and ground information [IAF PAPER 88-161] p 23 A89-17702

CIR aerial photography applied to the evaluation of the air pollution impact in a tropical forest: The case of Cubatao, Brazil p 17 N89-11324

Analysis of crop loss for alternative ozone exposure indices [PB88-214788] p 22 N89-14608

AIR SEA ICE INTERACTIONS

Mizex '87 - Overview of the Winter Marginal Ice Zone Experiment in the Greenland and Barents Seas p 36 A89-10931

The LIMEX 1987 pilot project, LIMEX 1989 and long-term objective for data collection on the Canadian East coast p 52 N89-13037

AIR WATER INTERACTIONS

Atmospheric absorption in the VAS split-window channels p 39 A89-11225

Wind and wind stress curl fields for the Northeast Pacific Ocean using satellite scatterometer data p 78 A89-12859

X-band scatterometer measurements at low winds in a wavetank p 78 A89-12867

The dependence of sea surface slope on atmospheric stability and swell conditions p 45 A89-16983

- Wind stress measurements during the Tower Ocean Wave and Radar Dependence experiment p 45 A89-16984
- Acoustic Doppler current profiling in the equatorial Pacific in 1984 p 45 A89-16986
- Coastally trapped waves in the presence of a shelf edge density front p 46 A89-16989
- A three degree-of-freedom description of the ocean surface for microwave remote sensing of wave height and wind friction velocity p 47 N89-10314
- A numerical model for the computation of radiance distributions in natural waters with wind-roughened surfaces [AD-A197207] p 53 N89-13128
- AIRBORNE EQUIPMENT**
- Imaging spectroscopy II; Proceedings of the Meeting, San Diego, CA, Aug. 20, 21, 1987 p 73 A89-10311
- [SPIE-834] p 73 A89-10324
- Imaging spectrometry as a tool for botanical mapping p 73 A89-10324
- Extracting spectral information from imaging spectrometer data - A case history from the northern Grapevine Mountains, Nevada/California p 29 A89-10326
- Advanced airborne electro-optical imager p 74 A89-10929
- Accuracy evaluation of airborne stereo line imager data p 75 A89-10936
- Radar applications in remote sensing - An airborne remote sensing case history presented at the Twenty-first International Symposium on Remote Sensing of Environment, Ann Arbor, Michigan, October 26-30, 1987 p 75 A89-10969
- Study of monitoring sea ice using an airborne microwave radiometer system p 37 A89-10972
- Airborne lidar detection of subsurface oceanic scattering layers p 41 A89-12260
- Corrections of surface particle probe measurements for the effects of aspiration p 58 A89-14022
- An airborne gamma ray snow survey of a forest covered area with a deep snowpack p 7 A89-12284
- Strengths and shortcomings in Airborne Thematic Mapper (ATM) technology as applied to volcanic and geothermal areas in Iceland p 32 A89-10337
- The fluorescence line imager: High-resolution imaging spectroscopy over water and land p 83 N89-10353
- Stress detection in mixed coniferous-broadleaved forests from Airborne Imaging Spectrometer (AIS) data p 13 N89-10355
- The airborne radiometry experiment (ABREX) instrument, an experimental test bed for the specification of satellite-borne microwave radiometer at 90 GHz p 86 N89-12939
- A synthetic apertures radar with multichannel and multipolarisation p 87 N89-13017
- Estimating aircraft SAR response characteristics and approximating ocean wave spectra in the Labrador Sea p 52 N89-13032
- AIRBORNE LASERS**
- Soil erosion study using an airborne laser profiler p 1 A89-10952
- Airborne and spaceborne lasers for terrestrial geophysical sensing; Proceedings of the Meeting, Los Angeles, CA, Jan. 14, 15, 1988 [SPIE-889] p 79 A89-15870
- AIRCRAFT DESIGN**
- Computational design and efficiency optimization of agricultural airplanes p 5 A89-13670
- AIRCRAFT WAKES**
- Computational design and efficiency optimization of agricultural airplanes p 5 A89-13670
- ALASKA**
- Development of Alaskan gas hydrate resources [DE88-010270] p 35 N89-13093
- ALFALFA**
- Estimation of the interception efficiency of an alfalfa canopy from a vegetative index p 11 N89-10332
- ALGORITHMS**
- Atmospheric effect removal from space imagery p 69 N89-10338
- A new method for estimating regional evaporation from thermal infrared surface temperature measurements p 60 N89-10390
- A new radar technique for satellite rainfall algorithm development [NASA-CR-183471] p 60 N89-11102
- Sea ice type classification of SAR imagery p 52 N89-13039
- Precipitation detection with satellite microwave data [PB88-240239] p 88 N89-13094
- ALTIMETERS**
- Evaluation of GEOSAT (Geodetic Satellite) data and application to variability of the northeast Pacific Ocean [AD-A198950] p 53 N89-13863

ALTIMETRY

Modeling of the dynamic sea surface with satellite altimeter signals p 38 A89-11158

AMBIGUITY

An analysis of directional ambiguities in wind scatterometer measurements p 87 N89-13071

ANDES MOUNTAINS (SOUTH AMERICA)

Landsat Thematic Mapper observations of debris avalanche deposits in the Central Andes p 31 A89-19838

ANNUAL VARIATIONS

Variations in the Arctic, Antarctic, and global sea ice covers during 1978-1987 as observed with the Nimbus 7 scanning multichannel microwave radiometer p 38 A89-11145

Influence of sea surface temperature on intra- and inter-annual variations of ITCZ --- InterTropical Convergent Zones p 43 A89-12871

Observing the seasonal variability in the tropical Atlantic from altimetry p 46 A89-16987

PRISM B (Prediction of the Indian Summer Monsoon - Bellevue) p 58 A89-17873

Monitoring seasonal variations of soil moisture and vegetation cover using satellite microwave radiometry p 15 N89-10378

Active modes of the Pacific Intertropical Convergence Zone (ITCZ) p 49 N89-11374

Detection of seasonal and long-term changes in land cover from multitemporal LANDSAT MSS data p 71 N89-12989

Investigation of radar backscattering from second-year sea ice [NASA-CR-180986] p 54 N89-14479

ANTARCTIC OCEAN

Phytoplankton standing crops within an Antarctic ice edge assessed by satellite remote sensing p 41 A89-12174

ANTARCTIC REGIONS

Nimbus-7 SMMR derived sea-ice concentrations over Antarctica p 43 A89-12857

Data report for the Siple Coast (Antarctica) project [NASA-TM-100708] p 49 N89-10403

Inference of radio scattering parameters of Antarctic ice sheet using 179 MHz airborne radio echo sounding data p 51 N89-12975

Comparison of in situ aerosol measurements with SAGE 2 and SAM 2 aerosol measurements during the airborne Antarctic ozone experiment p 89 N89-14522

Evolution of polar stratospheric clouds during the Antarctic winter p 55 N89-14534

ANTENNA ARRAYS

The electronically steered thinned array radiometer p 74 A89-10932

AQUATIC PLANTS

Aerial photography for biomass assessment in the intertidal zone p 9 A89-20724

AQUICULTURE

Remote measurements of diatoms chlorophyll-a in the Nori farm p 38 A89-11001

ARCHAEOLOGY

SPOT bathymetric image for archeological investigations p 37 A89-10990

ARCTIC REGIONS

Evolution of the helicopter-borne scatterometer p 37 A89-10971

Monitoring vegetation index and biomass production in Southern Greenland based on NOAA-AVHRR data p 3 A89-10993

Comparison of Nimbus 7 scanning multichannel microwave radiometer radiance and derived sea ice concentrations with Landsat imagery for the north water area of Baffin Bay p 38 A89-11150

An autonomous ocean instrument platform driven vertically by the current [AD-A198226] p 54 N89-13865

ARGOS SYSTEM

Enhancements to the ARGOS system - Presented at the Twenty-first International Symposium on Remote Sensing of Environment, Ann Arbor, Michigan, October 26-30, 1987 p 22 A89-10957

ARID LANDS

Improving the detection of human-induced change in west Africa's semi-arid zone using multitemporal Landsat MSS imagery p 64 A89-10983

Estimating the distribution of grazing and patterns of cattle movement in a large arid zone paddock p 5 A89-12356

Invertible canopy reflectance modeling of vegetation structure in semiarid woodland p 6 A89-15918

An enhanced classification approach to change detection in semi-arid environments p 68 A89-20627

Applications of LANDSAT (TM and MSS) data for an estimation of rangeland conditions in semiarid and arid areas of northern Kenya p 16 N89-10404

[DFVLR-FB-88-18] p 16 N89-10404

Remote sensing and hydrologic modeling of arid watersheds: A scale analysis [DE88-014625] p 60 N89-11293

ARTIFICIAL SATELLITES

The numerical simulation of infrared satellite measurements over the Greenland-Iceland-Norwegian Sea [AD-A198653] p 54 N89-14484

ATLANTIC OCEAN

Observing the seasonal variability in the tropical Atlantic from altimetry p 46 A89-16987

The numerical simulation of infrared satellite measurements over the Greenland-Iceland-Norwegian Sea [AD-A198653] p 54 N89-14484

ATMOSPHERIC BOUNDARY LAYER

Marine boundary layer depth and relative humidity estimates using multispectral satellite measurements [AD-A196525] p 49 N89-12112

ATMOSPHERIC CIRCULATION

The development of tropical cyclones in the north-west of Australia p 41 A89-12203

Evaporation over land surfaces - First results from HAPEX-MOBILHY Special Observing Period p 57 A89-12211

A pilot study to determine relationships between North Pacific precipitation from Nimbus-7 Scanning Multichannel Microwave Radiometer data and associated atmospheric conditions p 43 A89-12837

Orographic channeling of a cold front by the Pyrenees p 79 A89-14073

The role of horizontal processes in upper-ocean prediction: A forecast simulation in the Sea of Japan [AD-A198827] p 55 N89-14654

ATMOSPHERIC COMPOSITION

Observation of precipitation using GMS imagery [IAF PAPER 88-151] p 58 A89-17697

Complex experiment on the investigation of the atmosphere pollution using space, aircraft and ground information [IAF PAPER 88-161] p 23 A89-17702

Comparison of in situ aerosol measurements with SAGE 2 and SAM 2 aerosol measurements during the airborne Antarctic ozone experiment p 89 N89-14522

ATMOSPHERIC CORRECTION

Remote sensing of suspended sediments in estuaries using atmospheric and compositional corrections to AVHRR data p 57 A89-10940

Thematic Mapper data screening and external effects correction p 64 A89-10978

Atmospheric correction of NS-001 data and extraction of multiple angle reflectance data sets p 64 A89-10998

Algorithm for automatic atmospheric corrections to visible and near-IR satellite imagery p 66 A89-12224

Estimation of multiple reflection and lowest order adjacency effects on remotely-sensed data p 5 A89-12354

Accounting for selective absorption in the evaluation of the earth surface temperature by an angular method p 80 A89-18710

Validation of an atmospheric correction method for satellite borne imagery p 82 N89-10320

Atmospheric correction of thermal infrared data from LANDSAT-5 for surface temperature estimation p 70 N89-10339

ATMOSPHERIC DENSITY

Coastally trapped waves in the presence of a shelf edge density front p 46 A89-16989

ATMOSPHERIC EFFECTS

Analysis of the contribution of the atmosphere to water reflectance in the first two channels of the NOAA satellites AVHRR p 82 N89-10330

Atmospheric effect removal from space imagery p 69 N89-10338

ATMOSPHERIC HEATING

The use of polar orbiter data in tropical weather system analysis p 77 A89-12818

ATMOSPHERIC MODELS

Marine boundary layer depth and relative humidity estimates using multispectral satellite measurements [AD-A196525] p 49 N89-12112

Towards direct variational assimilation of scatterometer backscatter measurements into numerical weather prediction models p 86 N89-13000

Model-based estimation of wind fields over the ocean from wind scatterometer measurements p 53 N89-13070

Multispectral satellite analysis of marine stratocumulus cloud microphysics [AD-A197316] p 87 N89-13092

Development of a ground hydrology model suitable for global climate modeling using soil morphology and vegetation cover, and an evaluation of remotely sensed information
[NASA-CR-180463] p 21 N89-13821

ATMOSPHERIC MOISTURE

An example of estimates of precipitable water derived from Nimbus-7 SMMR satellite measurements and FGGE upper air data p 42 A89-12792

Remote sensing of surface air temperature and humidity over oceanic areas with application to climatology and weather prediction p 42 A89-12798

Analysis of the contribution of the atmosphere to water reflectance in the first two channels of the NOAA satellites AVHRR p 82 N89-10330

ATMOSPHERIC OPTICS

Analysis of the contribution of the atmosphere to water reflectance in the first two channels of the NOAA satellites AVHRR p 82 N89-10330

ATMOSPHERIC PHYSICS

A numerical study of mesoscale ocean eddy interaction with a marginal ice zone p 41 A89-12172

ATMOSPHERIC RADIATION

Retrieval of air surface temperatures over oceans from satellite radiance measurements using stratification techniques p 42 A89-12779

ATMOSPHERIC REFRACTION

Atmospheric effect removal from space imagery p 69 N89-10338

ATMOSPHERIC SOUNDING

Atmospheric absorption in the VAS split-window channels p 39 A89-11225

Airborne and spaceborne lasers for terrestrial geophysical sensing; Proceedings of the Meeting, Los Angeles, CA, Jan. 14, 15, 1988
[SPIE-889] p 79 A89-15870

Lidar atmospheric sounder and altimetry for the Earth Observing System (EOS) satellite p 79 A89-15873
Laser Atmospheric Wind Sounder (LAWS)
p 79 A89-15889

Satellite phasing problems for ocean and atmospheric studies
[IAF PAPER 88-152] p 46 A89-17698

High-resolution spectroscopy for remote sensing of ocean and atmosphere p 48 N89-10352

LAWS (Laser Atmospheric Wind Sounder) earth observing system
[NASA-TM-101204] p 85 N89-12158

ATMOSPHERIC TEMPERATURE

Retrieval of air surface temperatures over oceans from satellite radiance measurements using stratification techniques p 42 A89-12779

An extension of the split window technique for the retrieval of precipitable water - Experimental verification [AD-A199515] p 76 A89-12796

Remote sensing of surface air temperature and humidity over oceanic areas with application to climatology and weather prediction p 42 A89-12798

ATOLLS

SPOT bathymetric image for archeological investigations p 37 A89-10990

AUSTRALIA

Remote sensing of laterized Archaean greenstone terrain - Marshall Pool Area, Northeastern Yilgarn Block, Western Australia p 31 A89-20628

AUTOCORRELATION

Ocean wave number spectra and spatial autocorrelation functions from SAR images p 50 N89-12970

AUTOMATIC CONTROL

An autonomous ocean instrument platform driven vertically by the current p 54 N89-13865
[AD-A198226]

Automatic procedure to find corresponding points in CCD Airborne Experimental Scanner for Applications in Remote Sensing (CAESAR) images
[B8821609] p 88 N89-14490

AUTOMATIC WEATHER STATIONS

Comparison of measured and modeled radiation, heat and water vapor fluxes: FIFE pilot study
[NASA-CR-183304] p 17 N89-11368

AVALANCHES

Landsat Thematic Mapper observations of debris avalanche deposits in the Central Andes p 31 A89-19838

B**BACKSCATTERING**

Backscattering coefficient of rice crops and rice fields by an X-band scatterometer p 3 A89-10980

Modulation of radar backscatter from the ocean by a variable surface current p 39 A89-12158

Microwave backscatter from beets, peas and potatoes throughout the growing season p 9 N89-10309

Improvement and extension of a radar forest backscattering model
[NASA-CR-183259] p 16 N89-11292

Effect of curvature on the backscattering from leaves
[NASA-CR-183326] p 16 N89-11296

Constraints on two-scale descriptions of radar backscattering from the sea surface using scatterometer model functions p 49 N89-12945

Towards direct variational assimilation of scatterometer backscatter measurements into numerical weather prediction models p 86 N89-13000

Modulation of the radar backscatter from the ocean surface by a long gravity wave p 51 N89-13031

Snow cover to alter terrain signatures on radar images p 62 N89-13048

Investigation of radar backscattering from second-year sea ice
[NASA-CR-180986] p 54 N89-14479

BATHYMETERS

Bathymetry using SPOT imagery of the Casamance (Senegal). First results p 59 N89-10375
MOMS-1 data for bathymetric and geological studies p 33 N89-10383

BATHYTHERMOGRAPHS

The impact of satellite infrared sea surface temperatures on the FNOC (Fleet Numerical Oceanography Center) EOTS (Expanded Ocean Thermal Structure) regional gulf stream analysis
[AD-A198965] p 54 N89-13864

BAYES THEOREM

Binary image classification p 73 N89-13908

BEER LAW

Relative water content of Spruce needles determined by the leaf water content index p 4 A89-11012

BIDIRECTIONAL REFLECTANCE

Summary of along-track data from the earth radiation budget satellite for several representative ocean regions
[NASA-RP-1206] p 55 N89-14634

BIOCHEMISTRY

Prediction of leaf chemistry by the use of visible and near infrared reflectance spectroscopy p 7 A89-17283

BIOMASS

Monitoring vegetation index and biomass production in Southern Greenland based on NOAA-AVHRR data p 3 A89-10993

Optical modeling of the upper ocean in relation to its biogenous matter content (case 1 waters) p 38 A89-11149

Aerial photography for biomass assessment in the intertidal zone p 9 A89-20724

Spectral profile and biomass estimation p 10 N89-10319

BIRDS

Monitoring Wood Stork foraging habitat using remote sensing and geographic information systems p 7 A89-17399

BOLL WEEVILS

Cotton area mapping using multitemporal satellite data integrated within a geographical information system applied to a cotton boll weevil control programme in Paraguay p 20 N89-13077

BOUGUER LAW

Relative water content of Spruce needles determined by the leaf water content index p 4 A89-11012

BOUNDARIES

Technique for obtaining agricultural property boundaries through satellite imagery, certified to control and accompany agricultural activity
[INPE-4640-PRE/1351] p 16 N89-11294

BOUNDARY VALUE PROBLEMS

Multi-point matching along vertical lines in SPOT images p 69 A89-20713

BRAGG ANGLE

Shadows and wedges in scattering from the sea p 49 N89-12946

BRAZIL

Environmental impact of the urban growth on the Western Sao Paulo metropolitan area
[INPE-4670-PRE/1370] p 23 N89-10413

Training activities in remote sensing at the Instituto de Pesquisas Espaciais-INPE/Brazil
[INPE-4686-PRE/1380] p 91 N89-11295

BRIGHTNESS

The normalization of a soil brightness index for the study of changes in soil conditions p 14 N89-10370

BRIGHTNESS TEMPERATURE

Thunderstorm ice induced brightness temperature depressions at 18, 37, and 92 GHz during Cohex and their implications for satellite precipitation retrievals p 42 A89-12835

Microwave emission and reflection from the wind-roughened sea surface at 6.7 and 18.6 GHz p 44 A89-15923

An approximative model for the microwave brightness temperature scattered by a rough open ocean surface p 48 N89-10344

BUOYS

Comparison of wave parameters determined from SLAR images and a pitch and roll buoy p 47 A89-20721

Drifting buoy data from the Equatorial Pacific for the period January 1, 1984 through May 31, 1985
[PB88-212824] p 49 N89-10516

An intercomparison of SAR and buoy directional wave spectra from the Labrador Sea Extreme Waves Experiment (LEWEX) p 50 N89-12972

Estimation of sea surface temperature via NOAA-AVHRR sensor: Comparison with sea truth data by fixed buoys p 51 N89-13005

An autonomous ocean instrument platform driven vertically by the current
[AD-A198226] p 54 N89-13865

C**C BAND**

Complementary of microwave and optical range in the characterization of crops by remote sensing p 10 N89-10310

CALIBRATING

Sensitivity of satellite-derived net shortwave irradiance at the Earth's surface to radiometric calibration p 82 N89-10335

Airborne Visible/Infrared Imaging Spectrometer (AVIRIS): Inflight radiometric calibration and the determination of surface reflectance p 83 N89-10357

The Airborne Version Conical Scan Radiometer (AVCSR): An airborne radiometer as a tool for satellite data validation p 86 N89-12937

Verification of the accuracy of a network of water-vapor radiometers p 86 N89-12941

Possible measurement errors in calibrated AVHRR (Advanced Very High Resolution Radiometer) data
[AD-A198342] p 88 N89-14414

The numerical simulation of infrared satellite measurements over the Greenland-Iceland-Norwegian Sea
[AD-A198653] p 54 N89-14484

CALIFORNIA

Mass and heat balances in the upper ocean p 53 N89-13089

The California Cooperative Remote Sensing Project [NASA-TM-100073] p 22 N89-13824

CAMERAS

Shuttered camera - Aerial color video imaging in the visible and near infrared p 8 A89-20630

Analysis of large format camera photographs of the Po Delta, Italy, for topographic and thematic mapping p 82 A89-20714

Evaluation of space photographs ... mapping using Metric Camera and Large Format Camera p 82 A89-20715

Remote Sensing in Polarized Light
[NASA-CP-3014] p 88 N89-14189

CANADA

The LIMEX 1987 pilot project, LIMEX 1989 and long-term objective for data collection on the Canadian East coast p 52 N89-13037

CANOPIES (VEGETATION)

Estimation of forest canopy characteristics and nitrogen cycling using imaging spectrometry p 1 A89-10325

Invertible canopy reflectance modeling of vegetation structure in semiarid woodland p 6 A89-15918

A perspective on vegetation canopy reflectance models p 10 N89-10317

A simplified vegetation canopy reflectance and absorption model p 10 N89-10322

The angular reflectance signature of the canopy hot spot in the optical regime p 11 N89-10325

A model for radiative transfer in heterogeneous three-dimensional canopies p 11 N89-10326

A simplified reflectance model for shrub canopies p 11 N89-10329

Estimation of the interception efficiency of an alfalfa canopy from a vegetative index p 11 N89-10332

Developing a radiometric leaf area index p 12 N89-10334

Spectral reflectance of sugar beet and winter wheat canopies in the visible and infrared during growth p 12 N89-10342

Use of high spectral resolution to follow the state of vegetation canopies p 13 N89-10354

Environmental impact of the urban growth on the Western Sao Paulo metropolitan area
[INPE-4670-PRE/1370] p 23 N89-10413

Digital processing applied to vegetation
[INPE-4695-MD/036] p 17 N89-12107

Interaction of solar radiation with vegetation
[INPE-4697-MD/038] p 17 N89-12109

- The structure of red-infrared scattergrams of semivegetated landscapes [NASA-CR-183385] p 21 N89-13091
- Use of LANDSAT images of vegetation cover to estimate effective hydraulic properties of soils [NASA-CR-183384] p 21 N89-13823
- CATHODE RAY TUBES**
- CANVAS - An intelligent system for colour selection on CRT displays p 76 A89-12353
- CELESTIAL GEODESY**
- Beyond plate tectonics - Looking at plate deformation with space geodesy p 44 A89-13758
- CHANGE DETECTION**
- Evapotranspiration monitored from satellites as an indication of shift and impact of vegetation change p 2 A89-10975
- Land cover change detection with Thematic Mapper spectral textural data at the rural-urban fringe p 23 A89-10982
- Improving the detection of human-induced change in west Africa's semi-arid zone using multitemporal Landsat MSS imagery p 64 A89-10983
- An enhanced classification approach to change detection in semi-arid environments p 68 A89-20627
- Detection of seasonal and long-term changes in land cover from multitemporal LANDSAT MSS data p 71 N89-12989
- Monitoring playas using Thematic Mapper data p 60 N89-13028
- Monitoring of seasonal snow cover on glaciers p 61 N89-13044
- Monitoring urban change from LANDSAT TM and SPOT satellite imagery by image differencing p 25 N89-13058
- Change direction analysis using LANDSAT imagery: A review of methodology p 72 N89-13068
- Building a monitoring system based on satellite data to detect vegetation and land use changes in a subtropical region of Mexico p 20 N89-13079
- CHANNEL FLOW**
- Orographic channeling of a cold front by the Pyrenees p 79 A89-14073
- CHARACTERIZATION**
- Multispectral characterization of the spatial structure of remotely sensed scenes p 70 N89-10340
- CHARGE COUPLED DEVICES**
- The MEOS experiment: A test case for future cartographic missions p 87 N89-13081
- CHEMICAL COMPOSITION**
- Prediction of leaf chemistry by the use of visible and near infrared reflectance spectroscopy p 7 A89-17283
- Spectral studies of three oxisols and a Ultisol of Brazil [INPE-4644-PRE/1355] p 17 N89-11297
- CHEMICAL REACTIONS**
- Chemical variability in ocean frontal areas [AD-A198418] p 56 N89-14655
- CHLOROPHYLLS**
- Remote measurements of diatoms chlorophyll-a in the Nori farm p 38 A89-11001
- Optical modeling of the upper ocean in relation to its biogenous matter content (case I waters) p 38 A89-11149
- Changes in the chlorophyll fluorescence spectra during the Kautsky induction kinetics p 12 N89-10348
- Chlorophyll fluorescence spectra of leaves as induced by blue light and red laser light p 12 N89-10349
- Laser-induced fluorescence on in-vivo chlorophyll of a rice plant: A technique for the remote detection of plant growth p 12 N89-10350
- Techniques for remote sensing of life span and quantum yield of chlorophyll fluorescence in vivo p 13 N89-10351
- Estimation of leaf spectra from measurements in wide spectral bands p 14 N89-10368
- CITIES**
- A new tool - SPOT imagery for studying rapid movements p 64 A89-10996
- Multi-point matching along vertical lines in SPOT images p 69 A89-20713
- CITRUS TREES**
- Spectral signature of citrus fruits and its evolution: Identification of the vegetative index of least temporal variation p 14 N89-10373
- CLASSIFICATIONS**
- Evaluating Landsat classification accuracy from forest cover-type maps p 5 A89-12756
- Optimization for classification of forest damage classes p 13 N89-10359
- Use of remote sensing for land use policy formulation [NASA-CR-183148] p 15 N89-10395
- An international approach to GIS based on remote sensing and terrain classification --- geographic information system (GIS) p 24 N89-12966

- Large area TM land cover classification of Mittlerer Oberrhein County, southwest Germany, and its use for regional planning and crop surveys p 18 N89-12986
- Towards an urban land-use classification using textural and morphological criteria p 25 N89-12987
- Crop classification with multi-temporal X-band SAR data p 19 N89-12990
- Sea ice type classification of SAR imagery p 52 N89-13039
- Efficient classification of multispectral images by a best linear discriminant function p 72 N89-13060
- A new spatial classification algorithm for high ground resolution images p 72 N89-13061
- Classification decision rule modification on the basis of information extracted from training data --- satellite imagery p 72 N89-13062
- Accuracy of land cover classification of Thematic Mapper (TM) and SPOT data p 72 N89-13066
- The classification of semi-natural vegetation from LANDSAT Thematic Mapper imagery: A user's perspective p 21 N89-13084
- Classification and analysis of surface and clouds at high latitudes from AVHRR multispectral satellite data p 89 N89-14635
- CLASSIFIERS**
- Forest mapping accuracies are improved using a supervised nonparametric classifier with SPOT data p 6 A89-14089
- CLIMATE CHANGE**
- Climate tracking with remote sensing p 75 A89-10943
- CLIMATOLOGY**
- The French space oceanography program p 44 A89-15116
- Development of a semi-empirical model for estimating the global solar radiation [INPE-4620-TDL/328] p 84 N89-11352
- CLOUD COVER**
- Improvement of cloud cover assessment of Landsat Thematic Mapper data p 65 A89-11003
- Classification of cloud fields based on textural characteristics p 65 A89-11727
- An example of estimates of precipitable water derived from Nimbus-7 SMMR satellite measurements and FGGE upper air data p 42 A89-12792
- The addition of visible channel data to satellite infrared rain estimation schemes p 78 A89-12839
- The evaluation of simple approaches for the delineation of rain area from satellite imagery p 66 A89-12842
- Snow and low-cloud discrimination from multispectral satellite measurements p 78 A89-12850
- Resolution dependence in satellite imagery - Multifractal analysis p 67 A89-12852
- Effects of data resolution on marine stratiform cloud detection using AVHRR and VISSR satellite data p 78 A89-12854
- Space shuttle large format camera photography cloud cover interference diagrams [PB88-244405] p 88 N89-14482
- Classification and analysis of surface and clouds at high latitudes from AVHRR multispectral satellite data p 89 N89-14635
- CLOUD HEIGHT INDICATORS**
- Mid-latitude evaluation of some satellite rainfall estimation techniques p 78 A89-12844
- CLOUD PHOTOGRAPHS**
- Satellite cloud image standardization p 76 A89-11731
- CLOUD PHOTOGRAPHY**
- Improvement of cloud cover assessment of Landsat Thematic Mapper data p 65 A89-11003
- Cloud track winds from polar orbiting satellites p 87 N89-13069
- CLOUD PHYSICS**
- Multispectral satellite analysis of marine stratocumulus cloud microphysics [AD-A197316] p 87 N89-13092
- CLOUDS**
- Evolution of polar stratospheric clouds during the Antarctic winter p 55 N89-14534
- The design and protocol of a summertime rainfall enhancement program for West Texas p 63 N89-14636
- CLOUDS (METEOROLOGY)**
- A new tool - SPOT imagery for studying rapid movements p 64 A89-10996
- Microwave radiances from horizontally finite, vertically structured precipitating clouds p 84 N89-11364
- COASTAL CURRENTS**
- Prediction of mesoscale ocean circulation in the Norwegian coastal current p 37 A89-10994
- A three-dimensional coupled ice-ocean model of coastal circulation p 38 A89-11148
- COASTAL ECOLOGY**
- SAR and visible remote sensing of the Taoer River coastal zone at Bohai Bay p 38 A89-11005

- Application of satellite data for monitoring degradation of tidal wetlands of the Gulf of Kachchh, Western India [IAF PAPER 88-146] p 46 A89-17695
- The derivation of sub-canopy surface terrain models of coastal forests using synthetic aperture radar p 20 N89-13083
- Utilizing remote sensing of thematic mapper data to improve our understanding of estuarine processes and their influence on the productivity of estuarine-dependent fisheries [NASA-CR-183409] p 62 N89-13822
- COASTAL WATER**
- Remote sensing of estuaries - An overview p 56 A89-10939
- Passive microwave remote sensing of salinity in coastal zones p 36 A89-10942
- Analyses of marine shallow water-bottom features using the Landsat Thematic Mapper, SPOT, and the Large Format Camera p 37 A89-10981
- Application of satellite data for monitoring degradation of tidal wetlands of the Gulf of Kachchh, Western India [IAF PAPER 88-146] p 46 A89-17695
- Aerial photography for biomass assessment in the intertidal zone p 9 A89-20724
- COASTAL ZONE COLOR SCANNER**
- EOF analysis of AVHRR and CZCS imagery p 43 A89-12856
- COASTS**
- The practice and understanding of using aerial remote sensing in the investigation of coastal zone p 37 A89-10995
- Coastally trapped waves in the presence of a shelf edge density front p 46 A89-16989
- COHERENT ELECTROMAGNETIC RADIATION**
- LANDSAT-4 and LANDSAT-5 multispectral scanner coherent noise characterization and removal [NASA-TP-2595-REV] p 85 N89-12114
- COHERENT RADAR**
- A concept for measuring currents from geostationary satellites p 75 A89-10933
- Microwave scattering from internal wave modulated surface waves - A shipboard real aperture coherent radar study in the Georgia Strait Experiment p 39 A89-12157
- COLD FRONTS**
- Orographic channeling of a cold front by the Pyrenees p 79 A89-14073
- COLLECTION**
- The GVAR users compendium, volume 1 [NOAA-NESDIS-21-VOL-1] p 85 N89-12105
- COLLOCATION**
- A study on least-squares prediction and collocation --- geodesy [ETN-89-93336] p 29 N89-14492
- COLOR**
- Spectral studies of three oxisols and a Ultisol of Brazil [INPE-4644-PRE/1355] p 17 N89-11297
- COLOR CODING**
- Color enhancement of remote sensing imagery using IHS transformations and decorrelation stretch methods [INPE-4559-PRE/1300] p 70 N89-11418
- COLOR INFRARED PHOTOGRAPHY**
- CIR aerial photography applied to the evaluation of the air pollution impact in a tropical forest: The case of Cubatao, Brazil [INPE-4651-PRE/1358] p 17 N89-11324
- COLOR PHOTOGRAPHY**
- Shuttered camera - Aerial color video imaging in the visible and near infrared p 8 A89-20630
- Environmental impact of the urban growth on the Western Sao Paulo metropolitan area [INPE-4670-PRE/1370] p 23 N89-10413
- COLOR VISION**
- CANVAS - An intelligent system for colour selection on CRT displays p 76 A89-12353
- COLORADO**
- Sapping features of the Colorado Plateau: A comparative planetary geology field guide [NASA-SP-491] p 34 N89-10401
- COLORIMETRY**
- Modeling of soil color by remote sensing p 14 N89-10369
- COMMUNICATION NETWORKS**
- EASCON '88, Proceedings of the Twenty-first Annual Electronics and Aerospace Conference, Arlington, VA, Nov. 9-11, 1988 p 81 A89-20101
- COMPARISON**
- Sapping features of the Colorado Plateau: A comparative planetary geology field guide [NASA-SP-491] p 34 N89-10401
- COMPUTATION**
- A numerical model for the computation of radiance distributions in natural waters with wind-roughened surfaces [AD-A197207] p 53 N89-13128

COMPUTER AIDED DESIGN

Computational design and efficiency optimization of agricultural airplanes p 5 A89-13670

COMPUTER AIDED MAPPING

Combining spectral and structural analyses to select useful cartographic information from SPOT imagery p 71 N89-13052

Extraction of dense digital elevation models from SPOT stereo imagery p 71 N89-13053

Make-map and MEDMAP: Two programs for plotting maps of the Mediterranean Sea [AD-A198491] p 73 N89-14483

COMPUTER AIDED TOMOGRAPHY

Engineering evaluation of mountain topography exodynamics from remotely sensed data p 31 A89-18707

COMPUTER GRAPHICS

Meteorological surface analysis using perspective topographic maps p 65 A89-11740

A general data model for geographic information systems [INPE-4560-PRE/1301] p 24 N89-10676

Improvement in NOAA-AVHRR snowcover determination for runoff prediction p 61 N89-13040

Statistics and high resolution imaging of snowpack at 35 GHz using a microcomputer p 61 N89-13047

Microcomputers (PCs) for snow cover analyses using multisensor satellite data p 62 N89-13049

Make-map and MEDMAP: Two programs for plotting maps of the Mediterranean Sea [AD-A198491] p 73 N89-14483

COMPUTER PROGRAMMING

Improvement and extension of a radar forest backscattering model [NASA-CR-183259] p 16 N89-11292

COMPUTER PROGRAMS

The design and protocol of a summertime rainfall enhancement program for West Texas p 63 N89-14636

COMPUTER SYSTEMS DESIGN

Improving the accessibility of spatially referenced geological information p 35 N89-13026

Statistics and high resolution imaging of snowpack at 35 GHz using a microcomputer p 61 N89-13047

COMPUTER TECHNIQUES

Advances in computerized information retrieval in remote sensing p 69 A89-20717

COMPUTER VISION

Detection of circular geological features using the Hough transform p 30 A89-12358

COMPUTERIZED SIMULATION

Analysis of nonlinear internal waves in the New York Bight p 40 A89-12163

Numerical simulations of the profile properties of undeformed first-year sea ice during the growth season p 40 A89-12171

A numerical study of mesoscale ocean eddy interaction with a marginal ice zone p 41 A89-12172

Satellite microwave rainfall simulations with a three-dimensional dynamical cloud model p 77 A89-12833

Computational design and efficiency optimization of agricultural airplanes p 5 A89-13670

CONFERENCES

Photogrammetric Week, 41st, Universitaet Stuttgart, Federal Republic of Germany, Sept. 14-19, 1987, Proceedings p 63 A89-10611

International Symposium on Remote Sensing of Environment, 21st, University of Michigan, Ann Arbor, Oct. 26-30, 1987, Proceedings. Volumes 1 & 2 p 22 A89-10926

Digital image processing and visual communications technologies in meteorology; Proceedings of the Meeting, Cambridge, MA, Oct. 27, 28, 1987 [SPIE-846] p 65 A89-11726

Conference on Satellite Meteorology and Oceanography, 3rd, Anaheim, CA, Feb. 1-5, 1988, Preprints p 42 A89-12776

Airborne and spaceborne lasers for terrestrial geophysical sensing; Proceedings of the Meeting, Los Angeles, CA, Jan. 14, 15, 1988 [SPIE-889] p 79 A89-15870

Conference on Numerical Weather Prediction, 8th, Baltimore, MD, Feb. 22-26, 1988, Preprints p 81 A89-19176

EASCON '88; Proceedings of the Twenty-first Annual Electronics and Aerospace Conference, Arlington, VA, Nov. 9-11, 1988 p 81 A89-20101

European remote sensing needs in the 1990s; Proceedings of the Annual Symposium of EARSeL, Noordwijkerhout, Netherlands, May 4-8, 1987 p 90 A89-20701

Proceedings of the 1988 International Geoscience and Remote Sensing Symposium (IGARSS 1988) on Remote Sensing: Moving Towards the 21st Century, volume 1 [ESA-SP-284-VOL-1] p 85 N89-12936

CONIFERS

Evaluation of a multispectral linear array sensor for assessing juvenile stand conditions p 3 A89-11000

The effects of bark beetle stress on the foliar spectral reflectance of lodgepole pine p 5 A89-12355

Sensor band selection for detecting current defoliation caused by the spruce budworm p 6 A89-16062

Coherent polarimetric signatures of coniferous trees: A survey p 9 N89-10307

CONTINENTAL SHELVES

Coastally trapped waves in the presence of a shelf edge density front p 46 A89-16989

Mass and heat balances in the upper ocean p 53 N89-13089

CONVECTION

Active modes of the Pacific Intertropical Convergence Zone (ITCZ) [AD-A196406] p 49 N89-11374

CONVECTION CLOUDS

Using satellite data to aid in diagnosing and forecasting convective development and intensity along arc cloud lines p 76 A89-12810

CONVERGENCE

Determination of convergence rates across the Ventura Basin, Southern California, using GPS and historical triangulation [NASA-CR-183014] p 29 N89-14624

COORDINATE TRANSFORMATIONS

Detection of circular geological features using the Hough transform p 30 A89-12358

CORAL REEFS

Application of satellite data for monitoring degradation of tidal wetlands of the Gulf of Kachchh, Western India [IAF PAPER 88-146] p 46 A89-17695

CORRELATION

Correlation function study for sea ice p 46 A89-16990

COST ANALYSIS

Radar applications in remote sensing - An airborne remote sensing case history presented at the Twenty-first International Symposium on Remote Sensing of Environment, Ann Arbor, Michigan, October 26-30, 1987 p 75 A89-10969

COST EFFECTIVENESS

Satellite data analysis for inventorying crops grown in a complex, small-field environment p 1 A89-10951

COTTON

Cotton area mapping using multitemporal satellite data integrated within a geographical information system applied to a cotton boll weevil control programme in Paraguay p 20 N89-13077

COUPLED MODES

A three-dimensional coupled ice-ocean model of coastal circulation p 38 A89-11148

COVARIANCE

On the connection of geodetic point fields in Réseau European Trigonometrique (RETRIG) and related tests for model errors [ETN-89-93327] p 28 N89-14485

A study on least-squares prediction and collocation --- geodesy [ETN-89-93336] p 29 N89-14492

CROP GROWTH

Satellite data analysis for inventorying crops grown in a complex, small-field environment p 1 A89-10951

The character of reflective spectrum of winter wheat and the principle of its yield estimation with remote sensing method p 2 A89-10973

A study of estimation of winter wheat yield for large area using remote sensing method p 2 A89-10974

Acreeage and yield determination - 1987 Kansas winter wheat p 4 A89-11007

Radiometric measurements and crop yield forecasting - Some observations over millet and sorghum experimental plots in Mali p 8 A89-20702

Microwave backscatter from beets, peas and potatoes throughout the growing season p 9 N89-10309

Laser-induced fluorescence on in-vivo chlorophyll of a rice plant: A technique for the remote detection of plant growth p 12 N89-10350

High spectral resolution indices for monitoring crop growth and chlorosis p 13 N89-10358

An agricultural crop yield model by satellite: A simulation [INPE-4639-PRE/1350] p 17 N89-12106

CROP IDENTIFICATION

Backscattering coefficient of rice crops and rice fields by an X-band scatterometer p 3 A89-10980

Landsat TM and MSS digital data comparison - Imperial Valley --- crop classifications p 3 A89-10989

Crop separation analysis through SPOT and TM digital data [INPE-4641-PRE/1352] p 18 N89-12110

Crop classification with multi-temporal X-band SAR data p 19 N89-12990

CROP INVENTORIES

Satellite data analysis for inventorying crops grown in a complex, small-field environment p 1 A89-10951

Regional variation and crop separability in a Thematic Mapper based crop inventory of New York State p 4 A89-11002

The use of spectral reflectance characteristics for the estimation of the wheat crop state p 5 A89-12874

Complementary of microwave and optical range in the characterization of crops by remote sensing p 10 N89-10310

Potential number of winter wheat ears estimation using radiometry techniques at an early stage p 10 N89-10323

Analysis of potato crop distribution using remotely sensed and environmental data in a pilot geographical information system p 18 N89-12967

Large area TM land cover classification of Mittlerer Oberrhein County, southwest Germany, and its use for regional planning and crop surveys p 18 N89-12986

Crop classification with multi-temporal X-band SAR data p 19 N89-12990

Small format air photo from ultrahigh aircraft as an aid for data collection of agricultural statistics in Sahelian countries p 19 N89-13003

An evaluation of satellite imagery, LANDSAT Thematic Mapper and SPOT-1 HRV, for grassland inventory in the UK p 20 N89-13057

The California Cooperative Remote Sensing Project [NASA-TM-100073] p 22 N89-13824

Analysis of crop loss for alternative ozone exposure indices [PB88-214788] p 22 N89-14608

CROP VIGOR

Global land-surface primary productivity based upon Nimbus-7 37 GHz data [IAF PAPER 88-159] p 8 A89-17701

Spectral profile and biomass estimation p 10 N89-10319

Biomass and wheat crop yield estimation from SPOT vegetative indexes p 11 N89-10327

Relation between sugar beet crop yield and vegetative indexes calculated from LANDSAT MSS images p 11 N89-10333

Analysis of potato crop distribution using remotely sensed and environmental data in a pilot geographical information system p 18 N89-12967

Analysis of crop loss for alternative ozone exposure indices [PB88-214788] p 22 N89-14608

CROSSOVERS

Geost crossover analysis in the tropical Pacific. I - Constrained sinusoidal crossover adjustment p 38 A89-11143

CURVATURE

Effect of curvature on the backscattering from leaves [NASA-CR-183326] p 16 N89-11296

CYCLONES

The development of tropical cyclones in the north-west of Australia p 41 A89-12203

On the interpretation of integrated water vapor patterns in midlatitude cyclones derived from the Nimbus 7 scanning multichannel microwave radiometer p 76 A89-12790

Tropopause adjustment to tropical cyclones as inferred from satellite ozone observations p 77 A89-12816

Satellite diagnosis of tropical cyclones p 42 A89-12823

CYLINDRICAL ANTENNAS

Polarization-dependent attenuation of dielectric cylinder arrays p 86 N89-12955

D**DAMAGE ASSESSMENT**

Detection of forest damage on Whiteface Mountain, New York, using Landsat Thematic Mapper data p 3 A89-10987

Optimization for classification of forest damage classes p 13 N89-10359

Spectral characterization of forest damage in beech, oak and pine stands p 21 N89-13085

DAMS

Snowmelt runoff estimation using snow cover extent data and its application to optimum control of dam water level p 61 N89-13042

DATA ACQUISITION

Comparison of measured and modeled radiation, heat and water vapor fluxes: FIFE pilot study [NASA-CR-183304] p 17 N89-11368

Working group on studies of the lithosphere: Recommendations p 27 N89-12099

A study of accuracy enhancement in satellite magnetic modeling p 28 N89-12102

Small format air photo from ultrahigh aircraft as an aid for data collection of agricultural statistics in Sahelian countries p 19 N89-13003

DATA BASES

The development of a standardized grassland Landsat MSS information data base p 3 A89-10979
NASA/Crustal Dynamics Project geodetic data analysis p 25 A89-13760
A general data model for geographic information systems

[INPE-4560-PRE/1301] p 24 N89-10676
Integrated database approach for geodetic applications [DE88-012726] p 27 N89-11615

Development of a ground hydrology model suitable for global climate modeling using soil morphology and vegetation cover, and an evaluation of remotely sensed information [NASA-CR-180463] p 21 N89-13821

DOE/DOD environmental data bank [DE88-015262] p 25 N89-14942

DATA COLLECTION PLATFORMS

Data collection system operating on Japan's first marine observation satellite: Inflight evaluation of the system performance p 87 N89-13007

DATA CORRELATION

Resolution improvement by multi-temporal data merging p 63 A89-10937

DATA INTEGRATION

Integrating remotely sensed data into PC-based geographic information systems p 23 A89-10959

DATA PROCESSING

Applications of spatial postclassification models p 63 A89-10958

Using the VAS data utilization center (VDUC) for the analysis and forecasting of heavy rainfall producing mesoscale convective systems (MCSs) p 77 A89-12819

Integrated database approach for geodetic applications [DE88-012726] p 27 N89-11615

Method of visual analysis of remote sensing data-vegetation [INPE-4696-MD/037] p 17 N89-12108

The influence of grazing on land surface climatological variables [NASA-CR-183308] p 22 N89-14637

User's guide for the Nimbus 7 Scanning Multichannel Microwave Radiometer (SMMR) CELL-ALL tape [NASA-RP-1210] p 89 N89-14648

DATA PROCESSING EQUIPMENT

A satellite data processing and analysis software system for earth's atmosphere and surface research p 67 A89-12864

DATA REDUCTION

A comparison of reduction methods for satellite altimetry data p 39 A89-11424

Look-up tables to convert Landsat TM thermal IR data to water surface temperatures p 67 A89-14012

DATA RETRIEVAL

Retrieval of air surface temperatures over oceans from satellite radiance measurements using stratification techniques p 42 A89-12779

An extension of the split window technique for the retrieval of precipitable water - Experimental verification [AD-A199515] p 76 A89-12796

Advances in computerized information retrieval in remote sensing p 69 A89-20717

DATA SAMPLING

Simplified forest inventory using large-scale 70-mm photography and tariff tables p 6 A89-14090

DATA SIMULATION

Extraction of topography from side-looking satellite systems - A case study with SPOT simulation data p 68 A89-16063

DATA SMOOTHING

An analysis of directional ambiguities in wind scatterometer measurements p 87 N89-13071

DATA SYSTEMS

The ERS-1 Instrument Data Handling and Transmission subsystem (IDHT) and its evolution [IAF PAPER 88-134] p 80 A89-17690

Requirements for ongoing development of the Pilot Land Data System (PLDS) p 24 N89-12958

DATA TRANSMISSION

The navigation of AVHRR imagery p 66 A89-12357

The ERS-1 Instrument Data Handling and Transmission subsystem (IDHT) and its evolution [IAF PAPER 88-134] p 80 A89-17690

DECISION MAKING

Classification decision rule modification on the basis of information extracted from training data --- satellite imagery p 72 N89-13062

DEFOLIATION

Sensor band selection for detecting current defoliation caused by the spruce budworm p 6 A89-16062

DELTA

Mapping abandoned river channels in Mali through directional filtering of Thematic Mapper data p 58 A89-17285

The use of TM data for the study of a modern deltaic depositional system p 59 A89-20707

Analysis of large format camera photographs of the Po Delta, Italy, for topographic and thematic mapping p 82 A89-20714

DEPLOYMENT

An autonomous ocean instrument platform driven vertically by the current [AD-A198226] p 54 N89-13865

DEPTH MEASUREMENT

Marine boundary layer depth and relative humidity estimates using multispectral satellite measurements [AD-A198525] p 49 N89-12112

DESERTS

Desert varnish on volcanic rocks of the Basin and Range province - Composition, morphology, distribution, origin and influence on Landsat imagery p 30 A89-10988

DEVELOPING NATIONS

The application of remote sensing for drought early warning in Africa p 1 A89-10948

A typical case of integrated remote sensing center concept - The Nairobi multipurpose reception and processing center [IAF PAPER 88-106] p 80 A89-17679

Evaluation of LANDSAT TM and SPOT imagery for agricultural land use planning in less developed countries p 19 N89-13051

DIELECTRIC PROPERTIES

Microwave dielectric properties of low-salinity sea ice p 52 N89-13036

DIELECTRICS

Polarization-dependent attenuation of dielectric cylinder arrays p 86 N89-12955

DIGITAL DATA

Operational use of Landsat data for timber inventory p 2 A89-10970

Edge detection and processing of remotely sensed digital images p 64 A89-10984

Landsat TM and MSS digital data comparison - Imperia Valley --- crop classifications p 3 A89-10969

Terrain relief and pattern description using digital elevation and Landsat data p 65 A89-11010

The use of fractal geometry to identify ranges of scale-invariance in digital remotely sensed data p 4 A89-11011

A procedure for modeling the terrain relief by using digitized topographic maps p 67 A89-14005

On displaying multispectral imagery p 68 A89-20631

Crop separation analysis through SPOT and TM digital data [INPE-4641-PRE/1352] p 18 N89-12110

DIGITAL FILTERS

On the application of averaging median filters in remote sensing p 68 A89-15920

DIGITAL TECHNIQUES

Evaluation and digital processing of multispectral SPOT data p 68 A89-20708

Interpretation and geometrical aspects of Thematic Mapper data p 69 A89-20716

Digital processing applied to vegetation [INPE-4695-MD/036] p 17 N89-12107

Precision of line following in digital images [B8821610] p 73 N89-14486

DISCOLORATION

Relationship between discoloration and histological changes in leaves of trees affected by forest decline p 7 A89-17286

DISPLAY DEVICES

CANVAS - An intelligent system for colour selection on CRT displays p 76 A89-12353

DMSP SATELLITES

NASA Sea Ice and Snow Validation Program for the DMSP SSM/I: NASA DC-8 flight report [NASA-TM-100706] p 53 N89-13861

DOCUMENTS

Biogeochemical processes in sagebrush steppe: Interactions of terrain, vegetation and chemical cycles [NASA-CR-181486] p 21 N89-13088

DOPPLER EFFECT

Acoustic Doppler current profiling in the equatorial Pacific in 1984 p 45 A89-16986

DOPPLER RADAR

Doppler lidar wind measurements on the EOS - LAWS p 77 A89-12829

Observation of precipitation using GMS imagery [IAF PAPER 88-151] p 58 A89-17697

DRAINAGE PATTERNS

Sapping features of the Colorado Plateau: A comparative planetary geology field guide [NASA-SP-491] p 34 N89-10401

DROUGHT

The application of remote sensing for drought early warning in Africa p 1 A89-10948

E**EARLY WARNING SYSTEMS**

The application of remote sensing for drought early warning in Africa p 1 A89-10948

EARTH ALBEDO

A simple method for estimating monthly mean albedo of land surfaces from AVHRR data p 6 A89-15493

EARTH ATMOSPHERE

A satellite data processing and analysis software system for earth's atmosphere and surface research p 67 A89-12864

The numerical simulation of infrared satellite measurements over the Greenland-Iceland-Norwegian Sea [AD-A198653] p 54 N89-14484

EARTH CORE

Contributions to the GASP workshop proceedings (not presented orally) p 27 N89-12100

EARTH CRUST

Magnetic mineralogy in an archaic crustal cross section - Implications for crustal magnetization p 30 A89-12292

The Crustal Dynamics Project p 25 A89-13757

Geodesy by radio interferometry - Determination of vector motions for sites in the western United States p 25 A89-13759

NASA/Crustal Dynamics Project geodetic data analysis p 25 A89-13760

Geophysical interpretation of the magnetic anomalies of China derived from Magsat data p 26 A89-20200

Presentations by participants (edited and condensed) p 27 N89-12097

Working group on studies of the lithosphere: Recommendations p 27 N89-12099

Contributions to the GASP workshop proceedings (not presented orally) p 27 N89-12100

Heat flow and magnetization in the oceanic lithosphere [NASA-CR-183346] p 55 N89-14653

EARTH OBSERVATIONS (FROM SPACE)

On-board processing and national earth observations centers p 22 A89-10927

Principles Relating to Remote Sensing of the Earth from Space - Territorial sphere of application p 89 A89-12121

Algorithm for automatic atmospheric corrections to visible and near-IR satellite imagery p 66 A89-12224

NASA's Earth Science Geostationary Platform p 77 A89-12828

The addition of visible channel data to satellite infrared rain estimation schemes p 78 A89-12839

Airborne and spaceborne lasers for terrestrial geophysical sensing: Proceedings of the Meeting, Los Angeles, CA, Jan. 14, 15, 1988 [SPIE-889] p 79 A89-15870

Lidar atmospheric sounder and altimetry for the Earth Observing System (EOS) satellite p 79 A89-15873

Standards for earth observations from space [IAF PAPER 88-107] p 90 A89-17680

The Earth Observing System --- from space using platforms in conjunction with Space Station [IAF PAPER 88-114] p 80 A89-17682

New SPOT generation --- development of remote sensing satellites [IAF PAPER 88-117] p 7 A89-17683

Three-dimensional observation by means of tethered antennae --- for earth observation from space [IAF PAPER 88-118] p 80 A89-17684

Wide field high performance lenses --- for Indian remote sensing satellite [IAF PAPER 88-120] p 80 A89-17685

Indian experience in the dissemination and use of remote sensing data and future prospects [IAF PAPER 88-131] p 80 A89-17689

UN principles on remote sensing - An agreement on economic relations [IAF PAPER 88-134] p 80 A89-17690

Envirostat - A vehicle for examining the options for earth observations in the 1990's p 81 A89-20105

Solid earth mission study. Volume 2: Technical report [ESA-CR(P)-2626-VOL-2] p 26 N89-10303

Thermal infrared laser spectroscopy: The potential of dual active/passive thermal infrared sensors for Earth observation p 82 N89-10345

The French space program for Earth observation p 90 N89-10392

NASA's future land remote sensing program p 90 N89-10393

Solid Earth mission study. Volume 1: Executive summary [ESA-CR(P)-2626-VOL-1] p 26 N89-10397

Solid earth mission study. Volume 3: Program planning report
[ESA-CR(P)-2626-VOL-3] p 27 N89-10399

Very Long Baseline Interferometry (VLBI) from ground and space p 85 N89-11645

Sensors research and technology p 85 N89-11774

Working group reports submitted by group chairmen following workshop p 27 N89-12098

Proceedings of the 1988 International Geoscience and Remote Sensing Symposium (IGARSS 1988) on Remote Sensing: Moving Towards the 21st Century, volume 1 [ESA-SP-284-VOL-1] p 85 N89-12936

Geodynamics laser ranging system: Performance simulations and development of the EOS facility --- Earth Observing System (EOS) p 28 N89-12982

Data collection system operating on Japan's first marine observation satellite: Inflight evaluation of the system performance p 87 N89-13007

Remote Sensing in Polarized Light [NASA-CP-3014] p 88 N89-14189

EARTH OBSERVING SYSTEM (EOS)

Earth Observing System - A platform for imaging spectrometers p 74 A89-10332

MODIS - A global ocean facility for the Earth Observing System p 75 A89-10955

Doppler lidar wind measurements on the EOS - LAWS p 77 A89-12829

Applications of spaceborne laser ranger on EOS p 79 A89-15878

Laser Atmospheric Wind Sounder (LAWS) p 79 A89-15889

The Earth Observing System --- from space using platforms in conjunction with Space Station [IAF PAPER 88-114] p 80 A89-17682

Status and perspectives of vegetation monitoring by remote sensing p 8 A89-17693

LAWS (Laser Atmospheric Wind Sounder) earth observing system p 85 N89-12158

[NASA-TM-101204] p 85 N89-12158

Remote sensing information sciences research group [NASA-CR-183374] p 91 N89-14481

EARTH PLANETARY STRUCTURE

Remote sensing strategies for global resource exploration and environmental management [IAF PAPER 88-103] p 23 A89-17678

EARTH RADIATION BUDGET EXPERIMENT

Summary of along-track data from the earth radiation budget satellite for several representative ocean regions [NASA-RP-1206] p 55 N89-14634

EARTH RESOURCES

The potentials and challenges afforded by SPOT-1 data p 63 A89-10945

Remote sensing strategies for global resource exploration and environmental management [IAF PAPER 88-103] p 23 A89-17678

Fault tolerant design of attitude and orbit control subsystem for earth resources satellite-1 [AIAA PAPER 88-3879] p 80 A89-18073

Training activities in remote sensing at the Instituto de Pesquisas Espaciais-INPE/Brazil [INPE-4686-PRE/1380] p 91 N89-11295

Crop separation analysis through SPOT and TM digital data [INPE-4641-PRE/1352] p 18 N89-12110

Multitemporal resource complex analysis of Catania province, Italy from LANDSAT-TM data p 71 N89-12985

EARTH ROTATION

VLBI studies of the nutations of the earth p 26 A89-13764

EARTH SURFACE

Effect of soil roughness on SAR images of harvested agricultural fields p 4 A89-11004

Comparison of weather radar and satellite-based passive microwave observations of rainfall over land and oceans p 43 A89-12836

Surface identification using satellite microwave radiometers p 79 A89-15922

Accounting for selective absorption in the evaluation of the earth surface temperature by an angular method p 80 A89-18710

Sensitivity of satellite-derived net shortwave irradiance at the Earth's surface to radiometric calibration p 82 N89-10335

Airborne Visible/Infrared Imaging Spectrometer (AVIRIS): Inflight radiometric calibration and the determination of surface reflectance p 83 N89-10357

A new method for estimating regional evaporation from thermal infrared surface temperature measurements p 60 N89-10390

ECHO SOUNDING

Inference of radio scattering parameters of Antarctic ice sheet using 179 MHz airborne radio echo sounding data p 51 N89-12975

ECOLOGY

Complex experiment on the investigation of the atmosphere pollution using space, aircraft and ground information [IAF PAPER 88-161] p 23 A89-17702

Agroecological information content of SPOT data p 19 N89-13050

The influence of grazing on land surface climatological variables [NASA-CR-183308] p 22 N89-14637

ECONOMIC ANALYSIS

Development of Alaskan gas hydrate resources [DE88-010270] p 35 N89-13093

ECOSYSTEMS

Aerospace monitoring of ecosystem dynamics and ecological prognoses p 23 A89-15050

Use of remote sensing for land use policy formulation [NASA-CR-183148] p 15 N89-10395

EDGES

Edge detection and processing of remotely sensed digital images p 64 A89-10984

EDUCATION

TUBSAT-1, satellite technology for educational purposes p 90 N89-10905

Training activities in remote sensing at the Instituto de Pesquisas Espaciais-INPE/Brazil [INPE-4686-PRE/1380] p 91 N89-11295

EL NINO

Sea level variations in the tropical Pacific during 1985-87 derived from GEOSAT altimetry p 36 A89-10961

Active modes of the Pacific Intertropical Convergence Zone (ITCZ) [AD-A196406] p 49 N89-11374

ELECTRICAL RESISTIVITY

Satellite measurements required for deep-earth geophysics p 28 N89-12103

ELECTRO-OPTICAL PHOTOGRAPHY

The results of the Geosat MOMS subcommittee's data evaluation: Performance and applicability of the MOMS-1 sensor for exploration geology p 33 N89-10380

Design of spectral bands for the German MOMS-2 sensor p 84 N89-10381

The use of MOMS-1 data for geological mapping of the Aswa lineament (East African rift) p 33 N89-10382

MOMS-1 data for bathymetric and geological studies p 33 N89-10383

MOMS-1 used synergistically with LANDSAT TM p 33 N89-10384

Digital analysis of MOMS-1, LANDSAT TM, and SPOT data of the Nakuru area (Kenya) p 33 N89-10386

The MEOSX experiment: A test case for future cartographic missions p 87 N89-13081

ELECTRO-OPTICS

Advanced airborne electro-optical imager p 74 A89-10929

Multispectral satellite analysis of marine stratocumulus cloud microphysics [AD-A197316] p 87 N89-13092

ELECTROKINETICS

Changes in the chlorophyll fluorescence spectra during the Kautsky induction kinetics p 12 N89-10348

ELECTROMAGNETIC NOISE

LANDSAT-4 and LANDSAT-5 multispectral scanner coherent noise characterization and removal [NASA-TP-2595-REV] p 85 N89-12114

EMISSION SPECTRA

Attempt at absolute determination of spectral signatures of bare soils in the thermal infrared, in emission and reflection p 12 N89-10336

ENERGY CONSUMPTION

Development of a semi-empirical model for estimating the global solar radiation [INPE-4620-TDL/328] p 84 N89-11352

ENERGY TRANSFER

Surface energy flux measurements and reflectance factors using satellite-, aircraft-, and ground-based instrumentation p 1 A89-10950

ENVIRONMENT EFFECTS

Environmental impact of the urban growth on the Western Sao Paulo metropolitan area [INPE-4670-PRE/1370] p 23 N89-10413

Utilizing remote sensing of thematic mapper data to improve our understanding of estuarine processes and their influence on the productivity of estuarine-dependent fisheries [NASA-CR-183409] p 62 N89-13822

ENVIRONMENT MANAGEMENT

Remote sensing strategies for global resource exploration and environmental management [IAF PAPER 88-103] p 23 A89-17678

ENVIRONMENTAL MONITORING

International Symposium on Remote Sensing of Environment, 21st, University of Michigan, Ann Arbor, Oct. 26-30, 1987, Proceedings. Volumes 1 & 2 p 22 A89-10926

On-board processing and national earth observations centers p 22 A89-10927

Enhancements to the ARGOS system - Presented at the Twenty-first International Symposium on Remote Sensing of Environment, Ann Arbor, Michigan, October 26-30, 1987 p 22 A89-10957

Study of monitoring sea ice using an airborne microwave radiometer system p 37 A89-10972

Improving the detection of human-induced change in west Africa's semi-arid zone using multitemporal Landsat MSS imagery p 64 A89-10983

The practice and understanding of using aerial remote sensing in the investigation of coastal zone p 37 A89-10995

Real-time environment monitoring using data from Meteosat and NOAA imaging satellites p 23 A89-11730

Segmentation of remotely-sensed images by a split-and-merge process p 66 A89-12222

Aerospace monitoring of ecosystem dynamics and ecological prognoses p 23 A89-15050

A new lidar system for applications over land and sea p 83 N89-10347

Monitoring playas using Thematic Mapper data p 60 N89-13028

Change direction analysis using LANDSAT imagery: A review of methodology p 72 N89-13068

Building a monitoring system based on satellite data to detect vegetation and land use changes in a subtropical region of Mexico p 20 N89-13079

DOE/DOD environmental data bank [DE88-015262] p 25 N89-14942

EQUATORIAL REGIONS

Acoustic Doppler current profiling in the equatorial Pacific in 1984 p 45 A89-16986

Drifting buoy data from the Equatorial Pacific for the period January 1, 1984 through May 31, 1985 [PB88-212824] p 49 N89-10516

EROSION

Remote sensing and hydrologic modeling of arid watersheds: A scale analysis [DE88-014625] p 60 N89-11293

ERROR ANALYSIS

Geosat crossover analysis in the tropical Pacific. I - Constrained sinusoidal crossover adjustment p 38 A89-11143

A preliminary model for Geosat altimeter data errors p 44 A89-13958

ERRORS

Possible measurement errors in calibrated AVHRR (Advanced Very High Resolution Radiometer) data [AD-A198342] p 88 N89-14414

ERS-1 (ESA SATELLITE)

The ERS-1 Instrument Data Handling and Transmission subsystem (IDHT) and its evolution [IAF PAPER 88-134] p 80 A89-17690

Fault tolerant design of attitude and orbit control subsystem for earth resources satellite-1 [AIAA PAPER 88-3879] p 80 A89-18073

Review of the requirements for higher level ERS-1 products within Europe [ESA-CR(P)-2586] p 84 N89-10664

Complex SAR imagery and speckle filtering for ERS-1 wave mode p 71 N89-13029

ESTIMATES

Simulation of radar and surface measurements of rainfall p 62 N89-13924

ESTUARIES

Remote sensing of estuaries - An overview p 56 A89-10939

Remote sensing of suspended sediments in estuaries using atmospheric and compositional corrections to AVHRR data p 57 A89-10940

Aerial photography for biomass assessment in the intertidal zone p 9 A89-20724

EUROPE

European remote sensing needs in the 1990s; Proceedings of the Annual Symposium of EARS&L, Noordwijkerhout, Netherlands, May 4-8, 1987 p 90 A89-20701

Review of the requirements for higher level ERS-1 products within Europe [ESA-CR(P)-2586] p 84 N89-10664

EUROPEAN SPACE AGENCY

Operational environmental instrumentation proposed by NOAA and the international community for the NASA and ESA polar orbiting platforms p 36 A89-10964

EUROPEAN SPACE PROGRAMS

Solid earth mission study. Volume 2: Technical report [ESA-CR(P)-2626-VOL-2] p 26 N89-10303

Solid Earth mission study. Volume 1: Executive summary [ESA-CR(P)-2626-VOL-1] p 26 N89-10397

Solid earth mission study. Volume 3: Program planning report [ESA-CR(P)-2626-VOL-3] p 27 N89-10399

EVAPORATION

- Evaporation over land surfaces - First results from HAPEX-MOBILHY Special Observing Period p 57 A89-12211
- A new method for estimating regional evaporation from thermal infrared surface temperature measurements p 60 N89-10390
- Remote sensing technologies and spatial data applications [AD-A195809] p 62 N89-14480

EVAPOTRANSPIRATION

- Surface energy flux measurements and reflectance factors using satellite-, aircraft-, and ground-based instrumentation p 1 A89-10950
- Evapotranspiration monitored from satellites as an indication of shift and impact of vegetation change p 2 A89-10975

EXPERIMENT DESIGN

- The Labrador Sea Extreme Waves Experiment: Objectives, status and plans p 51 N89-12974
- The LIMEX 1987 pilot project, LIMEX 1989 and long-term objective for data collection on the Canadian East coast p 52 N89-13037

EXPERT SYSTEMS

- Model-based remotely-sensed imagery interpretation p 66 A89-12223
- Remote sensing information sciences research group [NASA-CR-183374] p 91 N89-14481

EXTREMELY HIGH FREQUENCIES

- The airborne radiometry experiment (ABREX) instrument, an experimental test bed for the specification of satellite-borne microwave radiometer at 90 GHz p 86 N89-12939

F

FARM CROPS

- Surface energy flux measurements and reflectance factors using satellite-, aircraft-, and ground-based instrumentation p 1 A89-10950
- Landsat TM and MSS digital data comparison - Imperial Valley --- crop classifications p 3 A89-10989
- Regional land cover and agricultural area statistics and mapping in The Departement Ardeche, France, by use of Thematic Mapper data p 8 A89-20705

FARMLANDS

- A theoretical model for interpreting remotely sensed thermal infrared measurements obtained over agricultural areas p 12 N89-10343
- Discrimination of zones of high water erosion risk using SPOT images p 15 N89-10376
- Technique for obtaining agricultural property boundaries through satellite imagery, certified to control and accompany agricultural activity [INPE-4640-PRE/1351] p 16 N89-11294

FAULT TOLERANCE

- Fault tolerant design of attitude and orbit control subsystem for earth resources satellite-1 [AIAA PAPER 88-3879] p 80 A89-18073

FEASIBILITY ANALYSIS

- Feasibility study for the development of a joint surge and wave model [PB88-230917] p 55 N89-14652

FIBER OPTICS

- Fiber-optic sensor systems for aerospace applications p 74 A89-10359

FIELD STRENGTH

- Satellite measurements required for deep-earth geophysics p 28 N89-12103

FIRES

- Regional and global fire detection using AVHRR data p 2 A89-10956

FISHERIES

- Utilizing remote sensing of thematic mapper data to improve our understanding of estuarine processes and their influence on the productivity of estuarine-dependent fisheries [NASA-CR-183409] p 62 N89-13822

FLOODS

- Validation of the on-site Flash Flood Potential System for Nexrad p 57 A89-10949
- Remote sensing technologies and spatial data applications [AD-A195809] p 62 N89-14480

FLUORESCENCE

- The fluorescence line imager - An imaging spectrometer for ocean and land remote sensing p 73 A89-10312
- Laser fluorosensing of water quality - A review p 57 A89-10941
- The fluorescence line imager: High-resolution imaging spectroscopy over water and land p 83 N89-10353

FLUX QUANTIZATION

- Surface energy flux measurements and reflectance factors using satellite-, aircraft-, and ground-based instrumentation p 1 A89-10950

FOCUSING

- Phase versus orbital velocity in SAR wave imaging: Paradox lost p 52 N89-13033

FORECASTING

- Remote sensing technologies and spatial data applications [AD-A195809] p 62 N89-14480

FOREST FIRE DETECTION

- Regional and global fire detection using AVHRR data p 2 A89-10956

FORESTS

- Estimation of forest canopy characteristics and nitrogen cycling using imaging spectrometry p 1 A89-10325
- Land and forest cover information from aerial video p 1 A89-10946
- Automatic control point determination for image registration using texture analysis methods p 3 A89-10985
- Detection of forest damage on Whiteface Mountain, New York, using Landsat Thematic Mapper data p 3 A89-10987
- Evaluation of a multispectral linear array sensor for assessing juvenile stand conditions p 3 A89-11000
- The use of fractal geometry to identify ranges of scale-invariance in digital remotely sensed data p 4 A89-11011
- Directional effects on scene complexity in oblique thermal imagery and photographs of a deciduous forest p 4 A89-12261
- Evaluating Landsat classification accuracy from forest cover-type maps p 5 A89-12756
- A comparative evaluation of use of Landsat MSS FCC and MKF-6M photographs for forest type delineation p 6 A89-14010
- Forest mapping accuracies are improved using a supervised nonparametric classifier with SPOT data p 6 A89-14089
- Simplified forest inventory using large-scale 70-mm photography and tariff tables p 6 A89-14090
- An airborne gamma ray snow survey of a forest covered area with a deep snowpack p 7 A89-17284
- Relationship between discoloration and histological changes in leaves of trees affected by forest decline p 7 A89-17286
- Shuttered camera - Aerial color video imaging in the visible and near infrared p 8 A89-20630
- Forest classification by principal component analyses of TM data p 8 A89-20706
- Spectral characterization of forest targets in mountainous zones on Thematic Mapper images p 11 N89-10328
- Stress detection in mixed coniferous-broadleaved forests from Airborne Imaging Spectrometer (AIS) data p 13 N89-10355
- Optimization for classification of forest damage classes p 13 N89-10359
- Texture analysis in forest areas: High spectral resolution synthetic aperture radar data p 14 N89-10367
- Use of remote sensing for land use policy formulation [NASA-CR-183148] p 15 N89-10395
- Identifying the reforested areas utilizing the SPOT satellite data [INPE-4624-PRE/1343] p 15 N89-10396
- Nation-wide forest mapping and timber volume estimation using LANDSAT-5 TM imagery [INPE-4643-PRE/1354] p 16 N89-10402
- Improvement and extension of a radar forest backscattering model p 16 N89-11292
- CIR aerial photography applied to the evaluation of the air pollution impact in a tropical forest: The case of Cubatao, Brazil [INPE-4651-PRE/1358] p 17 N89-11324
- Spatial resolution for remote sensing of forest plantations p 19 N89-12991
- The derivation of sub-canopy surface terrain models of coastal forests using synthetic aperture radar p 20 N89-13083
- Spectral characterization of forest damage in beech, oak and pine stands p 21 N89-13085
- The influence of grazing on land surface climatological variables [NASA-CR-183308] p 22 N89-14637
- FRACTALS**
- The use of fractal geometry to identify ranges of scale-invariance in digital remotely sensed data p 4 A89-11011
- Resolution dependence in satellite imagery - Multifractal analysis p 67 A89-12852
- FRENCH SPACE PROGRAMS**
- The French space oceanography program p 44 A89-15116
- The French space program for Earth observation p 90 N89-10392

FREQUENCY DIVISION MULTIPLEXING

- Study of the multiplexing of image telemetry data from SPOT 4 HRVIR and Vegetation sensors [CNES-87/229/CT/DRT/TIT/TR] p 70 N89-109

FRICTION FACTOR

- A three degree-of-freedom description of the ocean surface for microwave remote sensing of wave height and wind friction velocity p 47 N89-103

FRONTS (METEOROLOGY)

- A study of the dynamics of maritime fronts using remotely sensed wind and stress measurements p 84 N89-113

FROST

- Spectral signature of citrus fruits and its evolution: Identification of the vegetative index of least temporal variation p 14 N89-103

FUNCTIONAL DESIGN SPECIFICATIONS

- Spatial resolution requirements for MODIS-N --- Platform Moderate Resolution Imaging Spectrometer (MODIS) p 83 N89-103
- The airborne radiometry experiment (ABREX) instrument, an experimental test bed for the specification of satellite-borne microwave radiometer at 90 GHz p 86 N89-129
- Multistatic scatterometry p 87 N89-130

G

GAMMA RAYS

- An airborne gamma ray snow survey of a forest covered area with a deep snowpack p 7 A89-172

GEODESY

- Solid earth mission study. Volume 2: Technical report [ESA-CR(P)-2626-VOL-2] p 26 N89-103
- Solid Earth mission study. Volume 1: Executive summary [ESA-CR(P)-2626-VOL-1] p 26 N89-103
- Solid earth mission study. Volume 3: Program planning report [ESA-CR(P)-2626-VOL-3] p 27 N89-103
- Integrated database approach for geodesy applications [DE88-012726] p 27 N89-116
- On the connection of geodetic point fields in Rese European Trigonometrie (RETRI) and related tests model errors [ETN-89-93327] p 28 N89-144
- On the connection of digitized maps to a unified coordinate system. A special case of the geodesic connection problem [B8821602] p 28 N89-144
- A study on least-squares prediction and collocation geodesy [ETN-89-93336] p 29 N89-144
- Very Long Baseline Interferometry (VLBI): Relativity a geodesy [ETN-89-93337] p 29 N89-144
- GEODETIC ACCURACY**
- The differential rectification of SPOT HRV panchrome and multispectral imagery using a digital elevation model p 28 N89-130
- On the connection of geodetic point fields in Rese European Trigonometrie (RETRI) and related tests model errors [ETN-89-93327] p 28 N89-144

GEODETIC SATELLITES

- Evaluation of GEOSAT (Geodetic Satellite) data application to variability of the northeast Pacific Ocean [AD-A198950] p 53 N89-138

GEODETIC SURVEYS

- NASA/Crustal Dynamics Project geodesic data analysis p 25 A89-137
- VLBI geodesy - 2 parts-per-billion precision in length determinations for transcontinental baselines p 26 A89-137
- Time series of European baselines determined by Lageos p 26 A89-137
- Continuous deformation monitoring with GPS [AD-A196447] p 27 N89-106
- Integrated database approach for geodesy applications [DE88-012726] p 27 N89-111
- Determination of convergence rates across the Vent Basin, Southern California, using GPS and historical triangulation [NASA-CR-183014] p 29 N89-141

GEODYNAMICS

- The Crustal Dynamics Project p 25 A89-137
- Geodesy by radio interferometry - Determination of vector motions for sites in the western United States p 25 A89-137
- Distribution of relative plate motion along Pacific-North American plate boundary determined by mobile VLBI measurements p 26 A89-137

- Use of Landsat and Seasat data as a tool in kinematic analysis - The Tunisian Atlas p 31 A89-20710
- Solid earth mission study. Volume 2: Technical report [ESA-CR(P)-2626-VOL-2] p 26 N89-10303
- Solid Earth mission study. Volume 1: Executive summary [ESA-CR(P)-2626-VOL-1] p 26 N89-10397
- Solid earth mission study. Volume 3: Program planning report [ESA-CR(P)-2626-VOL-3] p 27 N89-10399
- Geodynamics laser ranging system: Performance simulations and development of the EOS facility --- Earth Observing System (EOS) p 28 N89-12982
- GEOGRAPHIC INFORMATION SYSTEMS**
- Integrating remotely sensed data into PC-based geographic information systems p 23 A89-10959
- Remote sensing and geographic information systems for agricultural statistics-gathering and agricultural monitoring in Morocco p 2 A89-10960
- The development of a standardized grassland Landsat MSS information data base p 3 A89-10979
- Utilization of Landsat data and a geographic information system (GIS) for improving watershed management in India p 57 A89-11014
- Model-based remotely-sensed imagery interpretation p 66 A89-12223
- Monitoring Wood Stork foraging habitat using remote sensing and geographic information systems p 7 A89-17399
- Project Vasundhara - Multi-theme integration of satellite remote sensing and geological data for regional level mineral prognostics [IAF PAPER 88-145] p 31 A89-17694
- Regional hydrological systems analysis using satellite remote sensing data and a geographical information system - Application to groundwater modelling of the Roermond area, The Netherlands p 59 A89-20720
- A general data model for geographic information systems [INPE-4560-PRE/1301] p 24 N89-10676
- Requirements for ongoing development of the Pilot Land Data System (PLDS) p 24 N89-12958
- The use of remote sensing in conjunction with geographic information systems for local planning p 24 N89-12959
- An integrated remote sensing approach for regional agrostatistics and land monitoring p 24 N89-12960
- Modelling land resources within a pilot geographical information system p 18 N89-12962
- Integrating remote sensing data into a geographical information system: A foundation for rural land use strategies: Nature Conservancy Council project p 24 N89-12964
- An international approach to GIS based on remote sensing and terrain classification --- geographic information system (GIS) p 24 N89-12966
- Analysis of potato crop distribution using remotely sensed and environmental data in a pilot geographical information system p 18 N89-12967
- Improving the accessibility of spatially referenced geological information p 35 N89-13026
- Cotton area mapping using multitemporal satellite data integrated within a geographical information system applied to a cotton boll weevil control programme in Paraguay p 20 N89-13077
- Remote sensing technologies and spatial data applications [AD-A195809] p 62 N89-14480
- Remote sensing information sciences research group [NASA-CR-183374] p 91 N89-14481
- GEOIDS**
- Somali Basin, Chain Ridge, and origin of the Northern Somali Basin gravity and geoid low p 30 A89-12290
- GEOLOGICAL FAULTS**
- Recognition of seismically hazardous fault dislocations in space images of the Dushanbe depression p 31 A89-18706
- The use of MOMS-1 data for geological mapping of the Aswa lineament (East African rift) p 33 N89-10382
- GEOLOGICAL SURVEYS**
- Sino-American cooperative studies on applications of remote sensing to surveying and mapping p 29 A89-10967
- SIR-B view of the Jabal Hadn lineament and its groundwater implications p 29 A89-10976
- Detection of circular geological features using the Hough transform p 30 A89-12358
- Geological mapping and mineral exploration in eastern Nova Scotia utilizing airborne and spaceborne multisensor data p 30 A89-14008
- Radar polarimetry - Analysis tools and applications p 30 A89-15915
- Mineral exploration along the Aqaba-Levant structure by use of TM-data - Concepts, processing and results p 31 A89-20709
- Evaluation of VARAN data in geology and geomorphology in the southeast of France p 32 N89-10313
- Usefulness of high spectral resolution radiometry for geological mapping in the Mediterranean region p 32 N89-10360
- The results of the Geosat MOMS subcommittee's data evaluation: Performance and applicability of the MOMS-1 sensor for exploration geology p 33 N89-10380
- The use of MOMS-1 data for geological mapping of the Aswa lineament (East African rift) p 33 N89-10382
- MOMS-1 data for bathymetric and geological studies p 33 N89-10383
- MOMS-1 used synergistically with LANDSAT TM p 33 N89-10384
- Comparative geological evolution of different remote sensing data of the Hoggar Mountains (Algeria) p 33 N89-10385
- Inference of geologic surface parameters from polarimetric radar observations and model inversion p 34 N89-12950
- The relativity utility of LANDSAT MSS and SIR-A imagery in reconnaissance geological mapping in Northern Sudan p 34 N89-13022
- Mapping the distribution and abundance of lithological units and surface mineralogies at Jabal Sa'id, Saudi Arabia: An application of spectral mixture modelling p 34 N89-13024
- LANDSAT Thematic Mapping (TM) and SPOT HRV for survey mapping of bedrock outcrops p 20 N89-13055
- Applications of remote sensing for geological mapping in eastern Egypt p 35 N89-13087
- Geologic mapping in the US Geological Survey [PB88-223870] p 35 N89-14477
- GEOLOGY**
- Extracting spectral information from imaging spectrometer data - A case history from the northern Grapevine Mountains, Nevada/California p 29 A89-10326
- Development of Alaskan gas hydrate resources [DE88-010270] p 35 N89-13093
- GEOMAGNETISM**
- Solid earth mission study. Volume 2: Technical report [ESA-CR(P)-2626-VOL-2] p 26 N89-10303
- Solid Earth mission study. Volume 1: Executive summary [ESA-CR(P)-2626-VOL-1] p 26 N89-10397
- Solid earth mission study. Volume 3: Program planning report [ESA-CR(P)-2626-VOL-3] p 27 N89-10399
- Presentations by participants (edited and condensed) p 27 N89-12097
- Working group reports submitted by group chairmen following workshop p 27 N89-12098
- Contributions to the GASP workshop proceedings (not presented orally) p 27 N89-12100
- Simulation of a spinning spacecraft magnetometer p 28 N89-12101
- A study of accuracy enhancement in satellite magnetic modeling p 28 N89-12102
- Satellite measurements required for deep-earth geophysics p 28 N89-12103
- GEOMETRIC RECTIFICATION (IMAGERY)**
- Geometric correction of satellite images using composite transformation functions p 64 A89-10986
- Geometric correction of remotely-sensed imagery using ground control points and orthogonal polynomials p 82 A89-20718
- The differential rectification of SPOT HRV panchromatic and multispectral imagery using a digital elevation model p 28 N89-13054
- GEOMETRICAL OPTICS**
- Shadows and wedges in scattering from the sea p 49 N89-12946
- GEOMETRY**
- Continuous deformation monitoring with GPS [AD-A196447] p 27 N89-10886
- GEOMORPHOLOGY**
- Desert varnish on volcanic rocks of the Basin and Range province - Composition, morphology, distribution, origin and influence on Landsat imagery p 30 A89-10988
- Terrain relief and pattern description using digital elevation and Landsat data p 65 A89-11010
- Evaluation of VARAN data in geology and geomorphology in the southeast of France p 32 N89-10313
- Sapping features of the Colorado Plateau: A comparative planetary geology field guide [NASA-SP-491] p 34 N89-10401
- The production of anaglyphs from SPOT-HRV panchromatic data for geomorphological mapping p 72 N89-13056
- GEOPHYSICS**
- Beyond plate tectonics - Looking at plate deformation with space geodesy p 44 A89-13758
- Satellite measurements required for deep-earth geophysics p 28 N89-12103
- Evaluation of GEOSAT (Geodetic Satellite) data and application to variability of the northeast Pacific Ocean [AD-A198950] p 53 N89-13863
- GEOPOTENTIAL**
- Solid earth mission study. Volume 2: Technical report [ESA-CR(P)-2626-VOL-2] p 26 N89-10303
- Solid Earth mission study. Volume 1: Executive summary [ESA-CR(P)-2626-VOL-1] p 26 N89-10397
- Solid earth mission study. Volume 3: Program planning report [ESA-CR(P)-2626-VOL-3] p 27 N89-10399
- GEOSAT SATELLITES**
- Improvements in the marine gravity field from Geosat/ERM p 36 A89-10962
- Geosat crossover analysis in the tropical Pacific. I - Constrained sinusoidal crossover adjustment p 38 A89-11143
- A preliminary model for Geosat altimeter data errors p 44 A89-13958
- Evaluation of GEOSAT (Geodetic Satellite) data and application to variability of the northeast Pacific Ocean [AD-A198950] p 53 N89-13863
- GEOTEMPERATURE**
- Strengths and shortcomings in Airborne Thematic Mapper (ATM) technology as applied to volcanic and geothermal areas in Iceland p 32 N89-10337
- GET AWAY SPECIALS (STS)**
- TUBSAT-1, satellite technology for educational purposes p 90 N89-10905
- GLACIERS**
- Monitoring of seasonal snow cover on glaciers p 61 N89-13044
- GLACIOLOGY**
- Nival-glacial systems and their mapping --- Russian book p 56 A89-10728
- Data report for the Siple Coast (Antarctica) project [NASA-TM-100708] p 49 N89-10403
- GLOBAL POSITIONING SYSTEM**
- Continuous deformation monitoring with GPS [AD-A196447] p 27 N89-10886
- Determination of convergence rates across the Ventura Basin, Southern California, using GPS and historical triangulation [NASA-CR-183014] p 29 N89-14624
- GOES SATELLITES**
- The GVAR users compendium, volume 1 [NOAA-NESDIS-21-VOL-1] p 85 N89-12105
- GOES 1**
- GOES I-M image navigation and registration system p 75 A89-10965
- GOVERNMENT/INDUSTRY RELATIONS**
- Business strategies and land remote sensing capabilities p 90 A89-20104
- GRAIN SIZE**
- Comparison between active and passive microwave measurements over Antarctica p 48 N89-10316
- Spectral studies of three oxisols and a Ultisol of Brazil [INPE-4644-PRE/1355] p 17 N89-11297
- GRASSES**
- Relationships between the nitrogen content of grass and reflectance p 19 N89-13002
- GRASSLANDS**
- The development of a standardized grassland Landsat MSS information data base p 3 A89-10979
- SPOT satellite data for pattern recognition on the North American tall-grass prairie Long-Term Ecological Research site p 5 A89-14009
- The Transformed Vegetation Index (TVI) for estimation of Brazilian cerrado's phytomass [INPE-4603-PRE/1326] p 15 N89-10400
- The detection of unimproved grassland in Berkshire using a binary decision tree approach p 18 N89-12988
- An evaluation of satellite imagery, LANDSAT Thematic Mapper and SPOT-1 HRV, for grassland inventory in the UK p 20 N89-13057
- The influence of grazing on land surface climatological variables [NASA-CR-183308] p 22 N89-14637
- GRAVITATIONAL FIELDS**
- Improvements in the marine gravity field from Geosat/ERM p 36 A89-10962
- GRAVITY ANOMALIES**
- Somali Basin, Chain Ridge, and origin of the Northern Somali Basin gravity and geoid low p 30 A89-12290
- GRAVITY WAVES**
- Modulation of the radar backscatter from the ocean surface by a long gravity wave p 51 N89-13031
- Phase versus orbital velocity in SAR wave imaging: Paradox lost p 52 N89-13033

GRAZING

- Estimating the distribution of grazing and patterns of cattle movement in a large arid zone paddock p 5 A89-12356

GREENLAND

- The numerical simulation of infrared satellite measurements over the Greenland-Iceland-Norwegian Sea [AD-A198653] p 54 N89-14484

GROUND OPERATIONAL SUPPORT SYSTEM

- GOES I-M image navigation and registration system p 75 A89-10965

GROUND SUPPORT SYSTEMS

- The GVAR users compendium, volume 1 [NOAA-NESDIS-21-VOL-1] p 85 N89-12105

GROUND TRUTH

- The Transformed Vegetation Index (TVI) for estimation of Brazilian cerrado's phytomass [INPE-4603-PRE/1326] p 15 N89-10400
Verification of the accuracy of a network of water-vapor radiometers p 86 N89-12941

GROUND WATER

- SIR-B view of the Jabal Hadn lineament and its groundwater implications p 29 A89-10976
Regional hydrological systems analysis using satellite remote sensing data and a geographical information system - Application to groundwater modelling of the Roermond area, The Netherlands p 59 A89-20720
Sapping features of the Colorado Plateau: A comparative planetary geology field guide [NASA-SP-491] p 34 N89-10401

GULF STREAM

- The impact of satellite infrared sea surface temperatures on the FNOG (Fleet Numerical Oceanography Center) EOTS (Expanded Ocean Thermal Structure) regional gulf stream analysis [AD-A198965] p 54 N89-13864

H

HABITATS

- Monitoring Wood Stork foraging habitat using remote sensing and geographic information systems p 7 A89-17399

HAZE

- Thematic Mapper data screening and external effects correction p 64 A89-10978

HEAT BALANCE

- Mass and heat balances in the upper ocean p 53 N89-13089

HEAT FLUX

- Comparison of measured and modeled radiation, heat and water vapor fluxes: FIFE pilot study [NASA-CR-183304] p 17 N89-11368
Heat flow and magnetization in the oceanic lithosphere [NASA-CR-183346] p 55 N89-14653

HELICOPTERS

- Evolution of the helicopter-borne scatterometer p 37 A89-10971

HIGH RESOLUTION

- High Resolution Imaging Spectrometer (HIRIS) p 74 A89-10334
HIRIS - EOS instrument with high spectral and spatial resolution p 74 A89-10928
Use of high spectral resolution to follow the state of vegetation canopies p 13 N89-10354
High spectral resolution indices for monitoring crop growth and chlorosis p 13 N89-10358
Usefulness of high spectral resolution radiometry for geological mapping in the Mediterranean region p 32 N89-10360
High resolution radiometric measurement of intertidal microphytobenthos p 48 N89-10365
Statistics and high resolution imaging of snowpack at 35 GHz using a microcomputer p 61 N89-13047
An autonomous ocean instrument platform driven vertically by the current [AD-A198226] p 54 N89-13865

HIGHWAYS

- Automatic road detection on Landsat 4 TM images p 23 A89-10997

HISTOLOGY

- Relationship between discoloration and histological changes in leaves of trees affected by forest decline p 7 A89-17286

HOT SURFACES

- The angular reflectance signature of the canopy hot spot in the optical regime p 11 N89-10325

HUMIDITY MEASUREMENT

- Marine boundary layer depth and relative humidity estimates using multispectral satellite measurements [AD-A196525] p 49 N89-12112

HURRICANES

- Comparison of satellite IR rain estimates with radar rain observations in hurricanes p 57 A89-12845

HYDRATES

- Development of Alaskan gas hydrate resources [DE88-010270] p 35 N89-13093

HYDRODYNAMICS

- An autonomous ocean instrument platform driven vertically by the current [AD-A198226] p 54 N89-13865

HYDROGEOLOGY

- The role of linear and ring features in hydrogeology p 31 A89-18705

HYDROGRAPHY

- Acoustic Doppler current profiling in the equatorial Pacific in 1984 p 45 A89-16986

HYDROLOGY

- Nival-glacial systems and their mapping --- Russian book p 56 A89-10728
Laser fluorosensing of water quality - A review p 57 A89-10941
The use of microwave radiometry in watershed hydrology p 57 A89-10992
Evaporation over land surfaces - First results from HAPEX-MOBILHY Special Observing Period p 57 A89-12211
Aircraft remote sensing in HAPEX --- hydrology p 59 N89-10388

- Development of a ground hydrology model suitable for global climate modeling using soil morphology and vegetation cover, and an evaluation of remotely sensed information [NASA-CR-180463] p 21 N89-13821

HYDROLOGY MODELS

- Regional hydrological systems analysis using satellite remote sensing data and a geographical information system - Application to groundwater modelling of the Roermond area, The Netherlands p 59 A89-20720
Remote sensing and hydrologic modeling of arid watersheds: A scale analysis [DE88-014625] p 60 N89-11293
Remote sensing technologies and spatial data applications [AD-A195809] p 62 N89-14480

HYDROMETEOROLOGY

- Cross-polar radar measurements in ice and rain p 60 N89-12993

I

ICE

- Cross-polar radar measurements in ice and rain p 60 N89-12993

ICE ENVIRONMENTS

- Variations in the Arctic, Antarctic, and global sea ice covers during 1978-1987 as observed with the Nimbus 7 scanning multichannel microwave radiometer p 38 A89-11145

- Comparison of Nimbus 7 scanning multichannel microwave radiometer radiance and derived sea ice concentrations with Landsat imagery for the north water area of Baffin Bay p 38 A89-11150

ICE FORMATION

- Numerical simulations of the profile properties of undeformed first-year sea ice during the growth season p 40 A89-12171
Evolution of polar stratospheric clouds during the Antarctic winter p 55 N89-14534

ICE MAPPING

- Mizex '87 - Overview of the Winter Marginal Ice Zone Experiment in the Greenland and Barents Seas p 36 A89-10931
Evolution of the helicopter-borne scatterometer p 37 A89-10971

ICE REPORTING

- Surveillance radar, a new tool for ice surveillance p 37 A89-10991
Satellite surveillance of ice and snow covered surfaces in the French Alps using visible and near infrared reflectance measurements from the SPOT and LANDSAT Thematic Mapper sensors p 59 N89-10372
The LIMEX 1987 pilot project, LIMEX 1989 and long-term objective for data collection on the Canadian East coast p 52 N89-13037

ICELAND

- The interpretation of Icelandic tundra features from LANDSAT-MSS data p 35 N89-13027
The numerical simulation of infrared satellite measurements over the Greenland-Iceland-Norwegian Sea [AD-A198653] p 54 N89-14484

IGNEOUS ROCKS

- The basis for the spectral behaviour of silicates in the thermal infrared and applications to remote sensing p 32 N89-10366

IMAGE ANALYSIS

- Imaging spectroscopy II; Proceedings of the Meeting, San Diego, CA, Aug. 20, 21, 1987 [SPIE-834] p 73 A89-10311
Extracting spectral information from imaging spectrometer data - A case history from the northern Grapevine Mountains, Nevada/California p 29 A89-10326
Automatic control point determination for image registration using texture analysis methods p 3 A89-10985

- An improved procedure for analysis of change in Thematic Mapper image-pairs p 65 A89-11013
Image analysis techniques for the interpretation of airphoto lineaments - Petroleum exploration, Eromanga Basin, Australia p 30 A89-14011
Combining Laplacian images of different spatial frequencies (scales) - Implications for remote sensing image analysis p 68 A89-15919
Automated segmentation of pseudoinvariant features from multispectral imagery p 68 A89-17906
Multispectral characterization of the spatial structure of remotely sensed scenes p 70 N89-10340
A study of the vegetation cover with AVHRR during HAPEX-MOBILHY p 15 N89-10389
Spectral analysis of ocean wave imagery using 2-D linear prediction p 50 N89-12968
On the use of speckle statistics for the extraction of ocean wave spectra from SAR imagery p 50 N89-12969

- Multitemporal resource complex analysis of Catania province, Italy from LANDSAT-TM data p 71 N89-12985

- The detection of unimproved grassland in Berkshire using a binary decision tree approach p 18 N89-12988

- Detection of seasonal and long-term changes in land cover from multitemporal LANDSAT MSS data p 71 N89-12989

- The interpretation of Icelandic tundra features from LANDSAT-MSS data p 35 N89-13027
Microcomputers (PCs) for snow cover analyses using multisensor satellite data p 62 N89-13049
Binary image classification p 73 N89-13908

IMAGE CONTRAST

- Snow and low-cloud discrimination from multispectral satellite measurements p 78 A89-12850

IMAGE ENHANCEMENT

- Region extraction in SPOT data p 67 A89-14007
Interpretation and geometrical aspects of Thematic Mapper data p 69 A89-20716
Photogrammetric model for correction of MSS-LANDSAT imagery [INPE-4652-PRE/1359] p 73 N89-13090

IMAGE FILTERS

- Complex SAR imagery and speckle filtering for ERS-1 wave mode p 71 N89-13029

IMAGE MOTION COMPENSATION

- GOES I-M image navigation and registration system p 75 A89-10965

IMAGE PROCESSING

- The fluorescence line imager - An imaging spectrometer for ocean and land remote sensing p 73 A89-10312
Imaging spectrometry for water applications p 56 A89-10327

- Edge detection and processing of remotely sensed digital images p 64 A89-10984
Digital image processing and visual communications technologies in meteorology; Proceedings of the Meeting, Cambridge, MA, Oct. 27, 28, 1987 [SPIE-846] p 65 A89-11726

- Applications of digital image processing to ongoing research in complex terrain meteorology p 65 A89-11743

- Segmentation of remotely-sensed images by a split-and-merge process p 66 A89-12222
CANVAS - An intelligent system for colour selection on CRT displays p 76 A89-12353

- The navigation of AVHRR imagery p 66 A89-12357
On the application of averaging median filters in remote sensing p 68 A89-15920

- Mapping abandoned river channels in Mali through directional filtering of Thematic Mapper data p 58 A89-17285

- Commercialized remote sensing - A comprehensive view for global studies p 81 A89-20102
On displaying multispectral imagery p 68 A89-20631

- Evaluation and digital processing of multispectral SPOT data p 68 A89-20708

- Mineral exploration along the Aqaba-Levant structure by use of TM-data - Concepts, processing and results p 31 A89-20709

- Multi-point matching along vertical lines in SPOT images p 69 A89-20713

- Analysis of directional effects on NOAA AVHRR
p 70 N89-10341
- Applications of LANDSAT (TM and MSS) data for an estimation of rangeland conditions in semiarid and arid areas of northern Kenya
[DFVLR-FB-88-18] p 16 N89-10404
- A general data model for geographic information systems
[INPE-4560-PRE/1301] p 24 N89-10676
- Study of the multiplexing of image telemetry data from SPOT 4 HRVIR and Vegetation sensors
[CNES-87/229/CT/DRT/TIT/TR] p 70 N89-10930
- Color enhancement of remote sensing imagery using IHS transformations and decorrelation stretch methods
[INPE-4559-PRE/1300] p 70 N89-11418
- Performance modeling and results for X-SAR
p 71 N89-13009
- Complex SAR imagery and speckle filtering for ERS-1 wave mode
p 71 N89-13029
- Extraction of dense digital elevation models from SPOT stereo imagery
p 71 N89-13053
- Binary image classification
p 73 N89-13908
- Remote sensing technologies and spatial data applications
[AD-A195809] p 62 N89-14480
- Remote sensing information sciences research group
[NASA-CR-183374] p 91 N89-14481
- Precision of line following in digital images
[B8821610] p 73 N89-14486
- Automatic procedure to find corresponding points in CCD Airborne Experimental Scanner for Applications in Remote sensing (CAESAR) images
[B8821609] p 88 N89-14490
- IMAGE RESOLUTION**
- Resolution improvement by multi-temporal data merging
p 63 A89-10937
- The effective resolution element of Landsat Thematic Mapper
p 65 A89-12220
- SPOT image quality - Twenty months of experience
p 66 A89-12352
- Resolution dependence in satellite imagery - Multifractal analysis
p 67 A89-12852
- Effects of data resolution on marine stratiform cloud detection using AVHRR and VISSR satellite data
p 78 A89-12854
- A procedure for modeling the terrain relief by using digitized topographic maps
p 67 A89-14005
- Effects of changing satellite sensor attributes
p 87 N89-13059
- IMAGES**
- Marine boundary layer depth and relative humidity estimates using multispectral satellite measurements
[AD-A196525] p 49 N89-12112
- IMAGING RADAR**
- An analytic representation of the synthetic aperture radar image spectrum for ocean waves
p 45 A89-16979
- IMAGING SPECTROMETERS**
- Imaging spectroscopy II; Proceedings of the Meeting, San Diego, CA, Aug. 20, 21, 1987
[SPIE-834] p 73 A89-10311
- The fluorescence line imager - An imaging spectrometer for ocean and land remote sensing
p 73 A89-10312
- Imaging spectrometry as a tool for botanical mapping
p 73 A89-10324
- Estimation of forest canopy characteristics and nitrogen cycling using imaging spectrometry
p 1 A89-10325
- Extracting spectral information from imaging spectrometer data - A case history from the northern Grapevine Mountains, Nevada/California
p 29 A89-10326
- Imaging spectrometry for water applications
p 56 A89-10327
- Earth Observing System - A platform for imaging spectrometers
p 74 A89-10332
- High Resolution Imaging Spectrometer (HIRIS)
p 74 A89-10334
- MODIS - A global ocean facility for the Earth Observing System
p 75 A89-10955
- IMAGING TECHNIQUES**
- Advanced airborne electro-optical imager
p 74 A89-10929
- Accuracy evaluation of airborne stereo line imager data
p 75 A89-10936
- Applications of multispectral video for natural resource assessment
p 63 A89-10968
- The fluorescence line imager: High-resolution imaging spectroscopy over water and land
p 83 N89-10353
- Improvement and extension of a radar forest backscattering model
[NASA-CR-183259] p 16 N89-11292
- The use of remote sensing in conjunction with geographic information systems for local planning
p 24 N89-12959
- Remote Sensing in Polarized Light
[NASA-CP-3014] p 88 N89-14189
- The influence of grazing on land surface climatological variables
[NASA-CR-183308] p 22 N89-14637
- INDEXES (DOCUMENTATION)**
- Analysis of crop loss for alternative ozone exposure indices
[PB88-214788] p 22 N89-14608
- INDIAN OCEAN**
- Role of absorbed solar radiation on Indian Ocean surface temperature - A case study using satellite data
[IAF PAPER 88-155] p 46 A89-17700
- INDIAN SPACECRAFT**
- Wide field high performance lenses --- for Indian remote sensing satellite
[IAF PAPER 88-120] p 80 A89-17685
- Indian experience in the dissemination and use of remote sensing data and future prospects
[IAF PAPER 88-131] p 80 A89-17689
- INFESTATION**
- Sensor band selection for detecting current defoliation caused by the spruce budworm
p 6 A89-16062
- INFORMATION DISSEMINATION**
- The navigation of AVHRR imagery
p 66 A89-12357
- INFORMATION RETRIEVAL**
- Improving the accessibility of spatially referenced geological information
p 35 N89-13026
- An autonomous ocean instrument platform driven vertically by the current
[AD-A198226] p 54 N89-13865
- DOE/DOD environmental data bank
[DE88-015262] p 25 N89-14942
- INFORMATION SYSTEMS**
- Use of remote sensing for land use policy formulation
[NASA-CR-183148] p 15 N89-10395
- The GVAR users compendium, volume 1
[NOAA-NESDIS-21-VOL-1] p 85 N89-12105
- DOE/DOD environmental data bank
[DE88-015262] p 25 N89-14942
- INFRARED ABSORPTION**
- Estimation of the interception efficiency of an alfalfa canopy from a vegetative index
p 11 N89-10332
- INFRARED DETECTORS**
- Estimation of forest canopy characteristics and nitrogen cycling using imaging spectrometry
p 1 A89-10325
- The numerical simulation of infrared satellite measurements over the Greenland-Iceland-Norwegian Sea
[AD-A198653] p 54 N89-14484
- INFRARED IMAGERY**
- Directional effects on scene complexity in oblique thermal imagery and photographs of a deciduous forest
p 4 A89-12261
- The evaluation of simple approaches for the delineation of rain area from satellite imagery
p 66 A89-12842
- Variation of satellite rain relationships in space and time
p 67 A89-12843
- Look-up tables to convert Landsat TM thermal IR data to water surface temperatures
p 67 A89-14012
- The image detection subassembly for the SPOT 4 'vegetation' instrument
[IAF PAPER 88-121] p 7 A89-17686
- Technological constraints on the use of thermal imagery for remote sensing
p 81 A89-19173
- Shuttered camera - Aerial color video imaging in the visible and near infrared
p 8 A89-20630
- A new method for estimating regional evaporation from thermal infrared surface temperature measurements
p 60 N89-10390
- The need for volcano monitoring and the ability to detect activity using emitted short wavelength infrared
p 34 N89-13025
- INFRARED PHOTOGRAPHY**
- Directional effects on scene complexity in oblique thermal imagery and photographs of a deciduous forest
p 4 A89-12261
- INFRARED RADIATION**
- Snow and low-cloud discrimination from multispectral satellite measurements
p 78 A89-12850
- The impact of satellite infrared sea surface temperatures on the FNOC (Fleet Numerical Oceanography Center) EOTS (Expanded Ocean Thermal Structure) regional gulf stream analysis
[AD-A198965] p 54 N89-13864
- The numerical simulation of infrared satellite measurements over the Greenland-Iceland-Norwegian Sea
[AD-A198653] p 54 N89-14484
- INFRARED RADIOMETERS**
- Infrared temperature measurements over bare soil and vegetation - A HAPEX perspective
p 2 A89-10953
- VISSR sensor introduced modifications in the presence of large temperature gradients
p 78 A89-12860
- Airborne Visible/Infrared Imaging Spectrometer (AVIRIS): Inflight radiometric calibration and the determination of surface reflectance
p 83 N89-10357
- Rock and soil discrimination in natural tropical conditions using a spot-calibrated radiometer
p 14 N89-10374
- The numerical simulation of infrared satellite measurements over the Greenland-Iceland-Norwegian Sea
[AD-A198653] p 54 N89-14484
- INFRARED SCANNERS**
- A narrow-band thermal imager based on multiline real-time averaging
p 83 N89-10356
- Emitted short wavelength infrared radiation for detection and monitoring of volcanic activity
p 32 N89-10377
- Aircraft remote sensing in HAPEX --- hydrology
p 59 N89-10388
- INFRARED SIGNATURES**
- Comparison of remote measurements of infrared surface temperatures and microwave soil moisture
p 4 A89-11009
- INFRARED SPECTRA**
- Complementary of microwave and optical range in the characterization of crops by remote sensing
p 10 N89-10310
- Attempt at absolute determination of spectral signatures of bare soils in the thermal infrared, in emission and reflection
p 12 N89-10336
- Atmospheric correction of thermal infrared data from LANDSAT-5 for surface temperature estimation
p 70 N89-10339
- A theoretical model for interpreting remotely sensed thermal infrared measurements obtained over agricultural areas
p 12 N89-10343
- The basis for the spectral behaviour of silicates in the thermal infrared and applications to remote sensing
p 32 N89-10366
- The numerical simulation of infrared satellite measurements over the Greenland-Iceland-Norwegian Sea
[AD-A198653] p 54 N89-14484
- INFRARED SPECTROMETERS**
- Thermal infrared laser spectroscopy: The potential of dual active/passive thermal infrared sensors for Earth observation
p 82 N89-10345
- Stress detection in mixed coniferous-broadleaved forests from Airborne Imaging Spectrometer (AIS) data
p 13 N89-10355
- Airborne Visible/Infrared Imaging Spectrometer (AVIRIS): Inflight radiometric calibration and the determination of surface reflectance
p 83 N89-10357
- Imaging spectrometry applied to the remote sensing of submerged seaweed
p 48 N89-10361
- Spatial resolution requirements for MODIS-N --- Polar Platform Moderate Resolution Imaging Spectrometer (MODIS)
p 83 N89-10364
- INFRARED SPECTROSCOPY**
- Prediction of leaf chemistry by the use of visible and near infrared reflectance spectroscopy
p 7 A89-17283
- Characterization of rocks by visible and infrared high spectral resolution terrain spectroscopy
p 32 N89-10362
- INLAND WATERS**
- The Remote Sensing Loosdrecht Lakes project
p 59 A89-20719
- INSOLATION**
- A comparison of satellite and empirical formula techniques for estimating insolation over the oceans
p 44 A89-15495
- INTERFACES**
- Qualitative aspects of seismograph/ocean bottom interaction
[AD-A198652] p 56 N89-14656
- INTERNAL WAVES**
- Joint Canada-U.S. Ocean Wave Investigation Project - An overview of the Georgia Strait Experiment
p 39 A89-12156
- Microwave scattering from internal wave modulated surface waves - A shipboard real aperture coherent radar study in the Georgia Strait Experiment
p 39 A89-12157
- An overview of the SAR Internal Wave Signature Experiment
p 40 A89-12162
- Analysis of nonlinear internal waves in the New York Bight
p 40 A89-12163
- Measurements of surface wave modulations from internal waves during the SAR Internal Wave Signature Experiment
p 40 A89-12164
- A comparison of measured surface wave spectral modulations with predictions from a wave-current interaction model
p 40 A89-12165
- Full-spectrum modeling of synthetic aperture radar internal wave signatures
p 40 A89-12166
- Contrast ratios of internal waves in synthetic aperture radar imagery - A comparison of SAR Internal Wave Signature Experiment observations with theory
p 40 A89-12167
- The registration of the surface effects of internal ocean waves using microwave radiometry
p 43 A89-13300

INTERNATIONAL COOPERATION

- United Nations activity on remote sensing - Legal and political implications p 89 A89-12125
Standards for earth observations from space [IAF PAPER 88-107] p 90 A89-17680
An international approach to GIS based on remote sensing and terrain classification --- geographic information system (GIS) p 24 N89-12966

INTERNATIONAL LAW

- Marine remote sensing and international law p 39 A89-12124

INTERNATIONAL RELATIONS

- Principles Relating to Remote Sensing of the Earth from Space - Territorial sphere of application p 89 A89-12121
UN principles on remote sensing - An agreement on economic relations p 90 A89-19385

INTERTROPICAL CONVERGENT ZONES

- Influence of sea surface temperature on intra- and inter-annual variations of ITCZ --- InterTropical Convergent Zones p 43 A89-12871
Active modes of the Pacific Intertropical Convergence Zone (ITCZ) [AD-A196406] p 49 N89-11374

IRRADIANCE

- Sensitivity of satellite-derived net shortwave irradiance at the Earth's surface to radiometric calibration p 82 N89-10335

J

JAPANESE SPACECRAFT

- Verification results of MOS-1 multispectral self scanning radiometer (MESSR) data p 86 N89-13004
Data collection system operating on Japan's first marine observation satellite: Inflight evaluation of the system performance p 87 N89-13007

K

KINEMATICS

- Use of Landsat and Seasat data as a tool in kinematic analysis - The Tunisian Atlas p 31 A89-20710

L

LAGEOS (SATELLITE)

- Time series of European baselines determined with Lageos p 26 A89-17945

LAKES

- Climate tracking with remote sensing p 75 A89-10943
The potential of using remotely sensed information for studying the contamination and eutrophication of lake systems p 58 A89-18708
Estimating concentrations of optically active components from the remotely sensed spectral radiance of a water surface p 58 A89-18711

LAND

- A new lidar system for applications over land and sea p 83 N89-10347
NASA's future land remote sensing program p 90 N89-10393

LAND ICE

- Nival-glacial systems and their mapping --- Russian book p 56 A89-10728
Data report for the Siple Coast (Antarctica) project [NASA-TM-100708] p 49 N89-10403
Inference of radio scattering parameters of Antarctic ice sheet using 179 MHz airborne radio echo sounding data p 51 N89-12975
Topographic effects on light scattering from snow p 71 N89-12976

LAND MANAGEMENT

- Modelling land resources within a pilot geographical information system p 18 N89-12962
The detection of unimproved grassland in Berkshire using a binary decision tree approach p 18 N89-12988
An evaluation of satellite imagery, LANDSAT Thematic Mapper and SPOT-1 HRV, for grassland inventory in the UK p 20 N89-13057

LAND USE

- Comparison of SPOT, TM and MSS data for agricultural land-use mapping in Gujarat (India) [IAF PAPER 88-139] p 7 A89-17692
Global land-surface primary productivity based upon Nimbus-7 37 GHz data [IAF PAPER 88-159] p 8 A89-17701
Business strategies and land remote sensing capabilities p 90 A89-20104
Envirostat - A vehicle for examining the options for earth observations in the 1990's p 81 A89-20105

Some results of microwave remote sensing research in The Netherlands with a view to land applications in the 1990s p 8 A89-20703

Regional land cover and agricultural area statistics and mapping in The Departement Ardeche, France, by use of Thematic Mapper data p 8 A89-20705

Polarization-dependent attenuation of dielectric cylinder arrays p 86 N89-12955

The use of remote sensing in conjunction with geographic information systems for local planning p 24 N89-12959

An integrated remote sensing approach for regional agrostistics and land monitoring p 24 N89-12960

Multitemporal resource complex analysis of Catina province, Italy from LANDSAT-TM data p 71 N89-12985

Large area TM land cover classification of Mittlerer Oberrhein County, southwest Germany, and its use for regional planning and crop surveys p 18 N89-12986

Towards an urban land-use classification using textural and morphological criteria p 25 N89-12987
Detection of seasonal and long-term changes in land cover from multitemporal LANDSAT MSS data p 71 N89-12989

A new spatial classification algorithm for high ground resolution images p 72 N89-13061

Accuracy of land cover classification of Thematic Mapper (TM) and SPOT data p 72 N89-13066

Building a monitoring system based on satellite data to detect vegetation and land use changes in a subtropical region of Mexico p 20 N89-13079

Development of a ground hydrology model suitable for global climate modeling using soil morphology and vegetation cover, and an evaluation of remotely sensed information [NASA-CR-180463] p 21 N89-13821

Geologic mapping in the US Geological Survey [PB88-223870] p 35 N89-14477

LANDSAT SATELLITES

HIRIS - EOS instrument with high spectral and spatial resolution p 74 A89-10928

Operational use of Landsat data for timber inventory p 2 A89-10970

The development of a standardized grassland Landsat MSS information data base p 3 A89-10979

Regional variation and crop separability in a Thematic Mapper based crop inventory of New York State p 4 A89-11002

Spectral and spatial characterisation of orchards in New York State using Thematic Mapper Imagery p 4 A89-11008

Terrain relief and pattern description using digital elevation and Landsat data p 65 A89-11010

An improved procedure for analysis of change in Thematic Mapper image-pairs p 65 A89-11013

Utilization of Landsat data and a geographic information system (GIS) for improving watershed management in India p 57 A89-11014

A useful model in mineral exploration with remotely sensed data p 30 A89-11017

Comparison of Nimbus 7 scanning multichannel microwave radiometer radiance and derived sea ice concentrations with Landsat imagery for the north water area of Baffin Bay p 38 A89-11150

A comparative evaluation of use of Landsat MSS FCC and MKF-6M photographs for forest type delineation p 6 A89-14010

Invertible canopy reflectance modeling of vegetation structure in semiarid woodland p 6 A89-15918

Combining Laplacian images of different spatial frequencies (scales) - Implications for remote sensing image analysis p 68 A89-15919

Business strategies and land remote sensing capabilities p 90 A89-20104

A study of the vegetation cover with AVHRR during HAPEX-MOBILHY p 15 N89-10389

Training activities in remote sensing at the Instituto de Pesquisas Espaciais-INPE/Brazil [INPE-4686-PRE/1380] p 91 N89-11295

The relative utility of LANDSAT MSS and SIR-A imagery in reconnaissance geological mapping in Northern Sudan p 34 N89-13022

The interpretation of Icelandic tundra features from LANDSAT-MSS data p 35 N89-13027

Change direction analysis using LANDSAT imagery: A review of methodology p 72 N89-13068

Photogrammetric model for correction of MSS-LANDSAT imagery [INPE-4652-PRE/1359] p 73 N89-13090

Use of LANDSAT images of vegetation cover to estimate effective hydraulic properties of soils [NASA-CR-183384] p 21 N89-13823

Binary image classification p 73 N89-13908

LANDSAT 4

LANDSAT-4 and LANDSAT-5 multispectral scanner coherent noise characterization and removal [NASA-TP-2595-REV] p 85 N89-12114

LANDSAT 5

LANDSAT-4 and LANDSAT-5 multispectral scanner coherent noise characterization and removal [NASA-TP-2595-REV] p 85 N89-12114

LASER ALTIMETERS

Geodynamics laser ranging system: Performance simulations and development of the EOS facility --- Earth Observing System (EOS) p 28 N89-12982

LASER APPLICATIONS

Laser fluorosensing of water quality - A review p 57 A89-10941

Measuring in-situ soil surface roughness using a laser profilometer p 9 N89-10308

LAWS (Laser Atmospheric Wind Sounder) earth observing system [NASA-TM-101204] p 85 N89-12158

LASER INDUCED FLUORESCENCE

Time-resolved laser fluorescence: Trends and applications p 83 N89-10346

A new lidar system for applications over land and sea p 83 N89-10347

Changes in the chlorophyll fluorescence spectra during the Kautsky induction kinetics p 12 N89-10348

Chlorophyll fluorescence spectra of leaves as induced by blue light and red laser light p 12 N89-10349

Laser-induced fluorescence on in-vivo chlorophyll of a rice plant: A technique for the remote detection of plant growth p 12 N89-10350

Techniques for remote sensing of life span and quantum yield of chlorophyll fluorescence in vivo p 13 N89-10351

LASER RANGE FINDERS

Time series of European baselines determined with Lageos p 26 A89-17945

Geodynamics laser ranging system: Performance simulations and development of the EOS facility --- Earth Observing System (EOS) p 28 N89-12982

LASER RANGER/TRACKER

Applications of spaceborne laser ranger on EOS p 79 A89-15878

LATENT HEAT

Comparison of measured and modeled radiation, heat and water vapor fluxes: FIFE pilot study [NASA-CR-183304] p 17 N89-11368

LEAF AREA INDEX

Developing a radiometric leaf area index p 12 N89-10334

Effect of curvature on the backscattering from leaves [NASA-CR-183326] p 16 N89-11296

LEAST SQUARES METHOD

A study on least-squares prediction and collocation --- geodesy [ETN-89-93336] p 29 N89-14492

LEAVES

Reflectance characteristics of dry plant materials p 3 A89-10977

Relative water content of Spruce needles determined by the leaf water content index p 4 A89-11012

Prediction of leaf chemistry by the use of visible and near infrared reflectance spectroscopy p 7 A89-17283

Relationship between discoloration and histological changes in leaves of trees affected by forest decline p 7 A89-17286

Chlorophyll fluorescence spectra of leaves as induced by blue light and red laser light p 12 N89-10349

Estimation of leaf spectra from measurements in wide spectral bands p 14 N89-10368

Relationships between the nitrogen content of grass and reflectance p 19 N89-13002

LENS DESIGN

Wide field high performance lenses --- for Indian remote sensing satellite [IAF PAPER 88-120] p 80 A89-17685

LIBRARIES

The GVAR users compendium, volume 1 [NOAA-NESDIS-21-VOL-1] p 85 N89-12105

LIGHT SCATTERING

Topographic effects on light scattering from snow p 71 N89-12976

LIMB DARKENING

Summary of along-track data from the earth radiation budget satellite for several representative ocean regions [NASA-RP-1206] p 55 N89-14634

LIMNOLOGY

The Remote Sensing Loosdrecht Lakes project p 59 A89-20719

LINE SPECTRA

The fluorescence line imager - An imaging spectrometer for ocean and land remote sensing p 73 A89-10312

LINEAR POLARIZATION

- Polarization-dependent attenuation of dielectric cylinder arrays p 86 N89-12955

LITHOLOGY

- Usefulness of high spectral resolution radiometry for geological mapping in the Mediterranean region p 32 N89-10360
- Characterization of rocks by visible and infrared high spectral resolution terrain spectroscopy p 32 N89-10362
- Mapping the distribution and abundance of lithological units and surface mineralogies at Jabal Sa'id, Saudi Arabia: An application of spectral mixture modelling p 34 N89-13024

LITHOSPHERE

- Heat flow and magnetization in the oceanic lithosphere [NASA-CR-183346] p 55 N89-14653

LONG TERM EFFECTS

- Climate tracking with remote sensing p 75 N89-10943
- Influence of sea surface temperature on intra- and inter-annual variations of ITCZ --- InterTropical Convergent Zones p 43 N89-12871
- The prospects for detecting spectral shifts due to satellite sensor aging p 6 N89-16061
- The influence of grazing on land surface climatological variables [NASA-CR-183308] p 22 N89-14637

LONG WAVE RADIATION

- Active modes of the Pacific Intertropical Convergence Zone (ITCZ) [AD-A196406] p 49 N89-11374

LOOK ANGLES (ELECTRONICS)

- Analysis of directional effects on NOAA AVHRR p 70 N89-10341

LOUISIANA

- Utilizing remote sensing of thematic mapper data to improve our understanding of estuarine processes and their influence on the productivity of estuarine-dependent fisheries [NASA-CR-183409] p 62 N89-13822

LOW COST

- SeaWiFS - An ocean-imaging sensor p 74 N89-10338

LOW TEMPERATURE ENVIRONMENTS

- A narrow-band thermal imager based on multiline real-time averaging p 83 N89-10356

M**MAGNETIC ANOMALIES**

- Geophysical interpretation of the magnetic anomalies of China derived from Magsat data p 26 N89-20200
- Presentations by participants (edited and condensed) p 27 N89-12097
- Working group on studies of the lithosphere: Recommendations p 27 N89-12099

MAGNETIC DISTURBANCES

- Contributions to the GASP workshop proceedings (not presented orally) p 27 N89-12100

MAGNETIC FLUX

- Working group reports submitted by group chairmen following workshop p 27 N89-12098

MAGNETIC SURVEYS

- Solid earth mission study. Volume 2: Technical report [ESA-CR(P)-2626-VOL-2] p 26 N89-10303
- Solid Earth mission study. Volume 1: Executive summary [ESA-CR(P)-2626-VOL-1] p 26 N89-10397
- Solid earth mission study. Volume 3: Program planning report [ESA-CR(P)-2626-VOL-3] p 27 N89-10399

MAGNETIC TAPES

- User's guide for the Nimbus 7 Scanning Multichannel Microwave Radiometer (SMMR) CELL-ALL tape [NASA-RP-1210] p 89 N89-14648

MAGNETITE

- Magnetic mineralogy in an archean crustal cross section - Implications for crustal magnetization p 30 N89-12292

MAGNETIZATION

- Heat flow and magnetization in the oceanic lithosphere [NASA-CR-183346] p 55 N89-14653

MAGNETOMETERS

- Working group reports submitted by group chairmen following workshop p 27 N89-12098
- Simulation of a spinning spacecraft magnetometer p 28 N89-12101

MAGNETOSPHERE-IONOSPHERE COUPLING

- Contributions to the GASP workshop proceedings (not presented orally) p 27 N89-12100

MAGSAT SATELLITES

- Geophysical interpretation of the magnetic anomalies of China derived from Magsat data p 26 N89-20200

MAN ENVIRONMENT INTERACTIONS

- Evapotranspiration monitored from satellites as an indication of shift and impact of vegetation change p 2 N89-10975
- Improving the detection of human-induced change in west Africa's semi-arid zone using multitemporal Landsat MSS imagery p 64 N89-10983
- The potential of using remotely sensed information for studying the contamination and eutrophication of lake systems p 58 N89-18708
- Use of remote sensing for land use policy formulation [NASA-CR-183148] p 15 N89-10395

MANNED SPACE FLIGHT

- NASA's Earth Science Geostationary Platform p 77 N89-12828

MAPPING

- Accuracy evaluation of airborne stereo line imager data p 75 N89-10936
- Sino-American cooperative studies on applications of remote sensing to surveying and mapping p 29 N89-10967
- Use of remote sensing for land use policy formulation [NASA-CR-183148] p 15 N89-10395
- A general data model for geographic information systems [INPE-4560-PRE/1301] p 24 N89-10676
- Technique for obtaining agricultural property boundaries through satellite imagery, certified to control and accompany agricultural activity [INPE-4640-PRE/1351] p 16 N89-11294
- The MEOSS experiment: A test case for future cartographic missions p 87 N89-13081
- Development of a ground hydrology model suitable for global climate modeling using soil morphology and vegetation cover, and an evaluation of remotely sensed information [NASA-CR-180463] p 21 N89-13821
- The California Cooperative Remote Sensing Project [NASA-TM-100073] p 22 N89-13824
- The impact of satellite infrared sea surface temperatures on the FNOC (Fleet Numerical Oceanography Center) EOTS (Expanded Ocean Thermal Structure) regional gulf stream analysis [AD-A198965] p 54 N89-13864
- Geologic mapping in the US Geological Survey [PB88-223870] p 35 N89-14477
- Heat flow and magnetization in the oceanic lithosphere [NASA-CR-183346] p 55 N89-14653

MARINE BIOLOGY

- Optical modeling of the upper ocean in relation to its biogenous matter content (case 1 waters) p 38 N89-11149
- Chemical variability in ocean frontal areas [AD-A198418] p 56 N89-14655

MARINE CHEMISTRY

- Chemical variability in ocean frontal areas [AD-A198418] p 56 N89-14655

MARINE ENVIRONMENTS

- Analyses of marine shallow water-bottom features using the Landsat Thematic Mapper, SPOT, and the Large Format Camera p 37 N89-10981
- Marine remote sensing and international law p 39 N89-12124
- A comparison of satellite and empirical formula techniques for estimating insolation over the oceans p 44 N89-15495
- Marine boundary layer depth and relative humidity estimates using multispectral satellite measurements [AD-A196525] p 49 N89-12112
- Multispectral satellite analysis of marine stratocumulus cloud microphysics [AD-A197316] p 87 N89-13092

MARINE METEOROLOGY

- Surface windspeed measurements over the ocean with a C-band microwave radiometer p 75 N89-11006
- The development of tropical cyclones in the north-west of Australia p 41 N89-12203
- Assimilation of satellite surface wind speed data using the GLA analysis/forecast system p 77 N89-12811
- Effects of data resolution on marine stratiform cloud detection using AVHRR and VISSR satellite data p 78 N89-12854
- The dependence of sea surface slope on atmospheric stability and swell conditions p 45 N89-16983
- Evaluation of preliminary experiments assimilating Seasat significant wave heights into a spectral wave model p 46 N89-16991
- Future measurements of rain from space [IAF PAPER 88-112] p 58 N89-17681
- A study of the dynamics of maritime fronts using remotely sensed wind and stress measurements p 84 N89-11366

- Multispectral satellite analysis of marine stratocumulus cloud microphysics [AD-A197316] p 87 N89-13092

MARINE RESOURCES

- Estimation of primary marine production using spaceborne data on ocean color p 48 N89-10371

MARKET RESEARCH

- Review of the requirements for higher level ERS-1 products within Europe [ESA-CR(P)-2586] p 84 N89-10664

MARS SURFACE

- Sapping features of the Colorado Plateau: A comparative planetary geology field guide [NASA-SP-491] p 34 N89-10401

MARSHLANDS

- Comparative analysis of spectral response in the optical domain of targets in a tropical swamp at various spectral and spatial resolutions p 13 N89-10363

- Utilizing remote sensing of thematic mapper data to improve our understanding of estuarine processes and their influence on the productivity of estuarine-dependent fisheries [NASA-CR-183409] p 62 N89-13822

MASS DISTRIBUTION

- Mass and heat balances in the upper ocean p 53 N89-13089

MATHEMATICAL MODELS

- A perspective on vegetation canopy reflectance models p 10 N89-10317
- A model for radiative transfer in heterogeneous three-dimensional canopies p 11 N89-10326
- A theoretical model for interpreting remotely sensed thermal infrared measurements obtained over agricultural areas p 12 N89-10343
- Development of a semi-empirical model for estimating the global solar radiation [INPE-4620-TDL/328] p 84 N89-11352
- Working group on studies of the lithosphere: Recommendations p 27 N89-12099
- An agricultural crop yield model by satellite: A simulation [INPE-4639-PRE/1350] p 17 N89-12106
- Constraints on two-scale descriptions of radar backscattering from the sea surface using scatterometer model functions p 49 N89-12945
- Modelling of SAR polarisation phase difference from trees p 18 N89-12951
- The derivation of sub-canopy surface terrain models of coastal forests using synthetic aperture radar p 20 N89-13083
- The structure of red-infrared scattergrams of semivegetated landscapes [NASA-CR-183385] p 21 N89-13091
- A numerical model for the computation of radiance distributions in natural waters with wind-roughened surfaces [AD-A197207] p 53 N89-13128
- Binary image classification p 73 N89-13908
- On the connection of digitized maps to a uniform coordinate system. A special case of the geodetic connection problem [B8821602] p 28 N89-14487

MEDITERRANEAN SEA

- Usefulness of high spectral resolution radiometry for geological mapping in the Mediterranean region p 32 N89-10360
- Make-map and MEDMAP: Two programs for plotting maps of the Mediterranean Sea [AD-A198491] p 73 N89-14483

MELTING

- Snowmelt runoff estimation using snow cover extent data and its application to optimum control of dam water level p 61 N89-13042

MESOMETEOROLOGY

- The contribution of satellite information to operational weather forecasting - Achievements and objectives in the 1990s p 81 N89-20711

MESOSCALE PHENOMENA

- Prediction of mesoscale ocean circulation in the Norwegian coastal current p 37 N89-10994
- Modeling of the dynamic sea surface with satellite altimeter signals p 38 N89-11158
- Using satellite data to aid in diagnosing and forecasting convective development and intensity along arc cloud lines p 76 N89-12810
- The use of polar orbiter data in tropical weather system analysis p 77 N89-12818
- Using the VAS data utilization center (VDUC) for the analysis and forecasting of heavy rainfall producing mesoscale convective systems (MCSs) p 77 N89-12819
- Estimation of the variability of acoustic characteristics in the region of frontal zones and mesoscale vortices using remote sensing data p 47 N89-18843

METEOROLOGICAL FLIGHT

Surface windspeed measurements over the ocean with a C-band microwave radiometer p 75 A89-11006

METEOROLOGICAL PARAMETERS

Meteorological surface analysis using perspective topographic maps p 65 A89-11740
Applications of digital image processing to ongoing research in complex terrain meteorology p 65 A89-11743

EOF analysis of AVHRR and CZCS imagery p 43 A89-12856

An agricultural crop yield model by satellite: A simulation [INPE-4639-PRE/1350] p 17 N89-12106

METEOROLOGICAL RADAR

Validation of the on-site Flash Flood Potential System for Nexrad p 57 A89-10949

Comparison of weather radar and satellite-based passive microwave observations of rainfall over land and oceans p 43 A89-12836

The evaluation of simple approaches for the delineation of rain area from satellite imagery p 66 A89-12842
Variation of satellite rain relationships in space and time p 67 A89-12843

Comparison of satellite IR rain estimates with radar rain observations in hurricanes p 57 A89-12845

Design of a spaceborne radar for tropical rain mapping at the climatological scale p 60 N89-12997

Simulation of radar and surface measurements of rainfall p 62 N89-13924

METEOROLOGICAL SATELLITES

Color-composite image processing for multispectral meteorological satellite data [AD-A199574] p 76 A89-11742

Conference on Satellite Meteorology and Oceanography, 3rd, Anaheim, CA, Feb. 1-5, 1988, Preprints p 42 A89-12776

Retrieval of air surface temperatures over oceans from satellite radiance measurements using stratification techniques p 42 A89-12779

Satellite microwave rainfall simulations with a three-dimensional dynamical cloud model p 77 A89-12833

Variation of satellite rain relationships in space and time p 67 A89-12843

Mid-latitude evaluation of some satellite rainfall estimation techniques p 78 A89-12844

Comparison of satellite IR rain estimates with radar rain observations in hurricanes p 57 A89-12845

Resolution dependence in satellite imagery - Multifractal analysis p 67 A89-12852

Observation of precipitation using GMS imagery [IAF PAPER 88-151] p 58 A89-17697

The contribution of satellite information to operational weather forecasting - Achievements and objectives in the 1990s p 81 A89-20711

Sea surface parameters inferred from meteorological satellite data at CMS, Lannion p 47 A89-20722

Possible measurement errors in calibrated AVHRR (Advanced Very High Resolution Radiometer) data [AD-A198342] p 88 N89-14414

METEOROLOGY

Digital image processing and visual communications technologies in meteorology; Proceedings of the Meeting, Cambridge, MA, Oct. 27, 28, 1987 [SPIE-846] p 65 A89-11726

METEOSAT SATELLITE

Use of satellite and radar images in operational precipitation nowcasting p 79 A89-13415

METRIC PHOTOGRAPHY

Evaluation of space photographs --- mapping using Metric Camera and Large Format Camera p 82 A89-20715

Comparative geological evolution of different remote sensing data of the Hoggar Mountains (Algeria) p 33 N89-10385

MICROORGANISMS

High resolution radiometric measurement of intertidal microphytobenthos p 48 N89-10365

MICROWAVE EMISSION

Microwave emission and reflection from the wind-roughened sea surface at 6.7 and 18.6 GHz p 44 A89-15923

Polarisation of passive microwave signals as indicator of snow water equivalent p 61 N89-13043

MICROWAVE FREQUENCIES

Satellite microwave rainfall simulations with a three-dimensional dynamical cloud model p 77 A89-12833

MICROWAVE IMAGERY

Phytoplankton standing crops within an Antarctic ice edge assessed by satellite remote sensing p 41 A89-12174

Comparison of weather radar and satellite-based passive microwave observations of rainfall over land and oceans p 43 A89-12836

MICROWAVE RADIOMETERS

The electronically steered thinned array radiometer p 74 A89-10932

Passive microwave remote sensing of salinity in coastal zones p 36 A89-10942

Study of monitoring sea ice using an airborne microwave radiometer system p 37 A89-10972

The use of microwave radiometry in watershed hydrology p 57 A89-10992

Surface windspeed measurements over the ocean with a C-band microwave radiometer p 75 A89-11006

Variations in the Arctic, Antarctic, and global sea ice covers during 1978-1987 as observed with the Nimbus 7 scanning multichannel microwave radiometer p 38 A89-11145

Comparison of Nimbus 7 scanning multichannel microwave radiometer radiance and derived sea ice concentrations with Landsat imagery for the north water area of Baffin Bay p 38 A89-11150

On the interpretation of integrated water vapor patterns in midlatitude cyclones derived from the Nimbus 7 scanning multichannel microwave radiometer p 76 A89-12790

An example of estimates of precipitable water derived from Nimbus-7 SMMR satellite measurements and FGGE upper air data p 42 A89-12792

Thunderstorm ice induced brightness temperature depressions at 18, 37, and 92 GHz during Comhex and their implications for satellite precipitation retrievals p 42 A89-12835

A pilot study to determine relationships between North Pacific precipitation from Nimbus-7 Scanning Multichannel Microwave Radiometer data and associated atmospheric conditions p 43 A89-12837

Surface identification using satellite microwave radiometers p 79 A89-15922

Correlation function study for sea ice p 46 A89-16990

Potential number of winter wheat ears estimation using radiometry techniques at an early stage p 10 N89-10323

Analysis of the contribution of the atmosphere to water reflectance in the first two channels of the NOAA satellites AVHRR p 82 N89-10330

Monitoring seasonal variations of soil moisture and vegetation cover using satellite microwave radiometry p 15 N89-10378

The airborne radiometry experiment (ABREX) instrument, an experimental test bed for the specification of satellite-borne microwave radiometer at 90 GHz p 86 N89-12939

Verification of the accuracy of a network of water-vapor radiometers p 86 N89-12941

Rainfall index over oceans derived from SSM/I data --- Special Sensor Microwave/Imager (SSM/I) p 51 N89-12998

Estimation of sea surface temperature via NOAA-AVHRR sensor: Comparison with sea truth data by fixed buoys p 51 N89-13005

Improvement in NOAA-AVHRR snowcover determination for runoff prediction p 61 N89-13040

Average areal water equivalent of snow in a mountain basin using microwave and visible satellite data p 61 N89-13045

User's guide for the Nimbus 7 Scanning Multichannel Microwave Radiometer (SMMR) CELL-ALL tape [NASA-RP-1210] p 89 N89-14648

MICROWAVE SCATTERING

Backscattering coefficient of rice crops and rice fields by an X-band scatterometer p 3 A89-10980

Microwave scattering from internal wave modulated surface waves - A shipboard real aperture coherent radar study in the Georgia Strait Experiment p 39 A89-12157

X-band scatterometer measurements at low winds in a wavetank p 78 A89-12867

An approximative model for the microwave brightness temperature scattered by a rough open ocean surface p 48 N89-10344

Shadows and wedges in scattering from the sea p 49 N89-12946

Some characteristics of short ocean waves as microwave scatterers p 51 N89-13030

Millimeter-wave backscatter measurements of various snow forms p 61 N89-13046

MICROWAVE SENSORS

Overview of oceanic microwave remote sensing from space p 35 A89-10930

Near surface soil moisture estimation from microwave measurements p 6 A89-17282

MICROWAVE SOUNDING

The effect of snow parameter variations on the thermal microwave emission of the soil-snow-atmosphere system p 59 A89-18712

Some results of microwave remote sensing research in The Netherlands with a view to land applications in the 1990s p 8 A89-20703

Precipitation detection with satellite microwave data [PB88-240239] p 88 N89-13094

MICROWAVES

Microwave radiances from horizontally finite, vertically structured precipitating clouds p 84 N89-11364

MIDLATITUDE ATMOSPHERE

Mid-latitude evaluation of some satellite rainfall estimation techniques p 78 A89-12844

MIE SCATTERING

Multispectral satellite analysis of marine stratocumulus cloud microphysics [AD-A197316] p 87 N89-13092

MILLET

Radiometric measurements and crop yield forecasting - Some observations over millet and sorghum experimental plots in Mali p 8 A89-20702

MILLIMETER WAVES

Experimental personal satellite communications system using millimeter-wave for Asia-Oceanian region p 81 A89-18736

MINERAL EXPLORATION

A useful model in mineral exploration with remotely sensed data p 30 A89-11017

Geological mapping and mineral exploration in eastern Nova Scotia utilizing airborne and spaceborne multisensor data p 30 A89-14008

Project Vasundhara - Multi-theme integration of satellite remote sensing and geological data for regional level mineral prognostics [IAF PAPER 88-145] p 31 A89-17694

Mineral exploration along the Aqaba-Levant structure by use of TM-data - Concepts, processing and results p 31 A89-20709

The results of the Geosat MOMS subcommittee's data evaluation: Performance and applicability of the MOMS-1 sensor for exploration geology p 33 N89-10380

A regional tectonic study of NE and E Africa and its implication for mineral exploration: A synoptic view from satellite imagery p 34 N89-13023

Geologic mapping in the US Geological Survey [PB88-223870] p 35 N89-14477

MINERALOGY

Extracting spectral information from imaging spectrometer data - A case history from the northern Grapevine Mountains, Nevada/California p 29 A89-10326

Magnetic mineralogy in an archean crustal cross section - Implications for crustal magnetization p 30 A89-12292

MISSION PLANNING

Orbit determination requirements for Topex [AAS PAPER 87-429] p 42 A89-12645

Solid earth mission study. Volume 3: Program planning report [ESA-CR(P)-2626-VOL-3] p 27 N89-10399

MOISTURE CONTENT

Relative water content of Spruce needles determined by the leaf water content index p 4 A89-11012

Evaluation of 3.7 micron split windows for estimating surface temperature p 43 A89-12855

Near surface soil moisture estimation from microwave measurements p 6 A89-17282

An airborne gamma ray snow survey of a forest covered area with a deep snowpack p 7 A89-17284

Polarisation of passive microwave signals as indicator of snow water equivalent p 61 N89-13043

Average areal water equivalent of snow in a mountain basin using microwave and visible satellite data p 61 N89-13045

MONSOONS

PRISM B (Prediction of the Indian Summer Monsoon - Bellevue) [IAF PAPER ST-88-02] p 58 A89-17873

MORPHOLOGY

Towards an urban land-use classification using textural and morphological criteria p 25 N89-12987

MOUNTAINS

Extracting spectral information from imaging spectrometer data - A case history from the northern Grapevine Mountains, Nevada/California p 29 A89-10326

Engineering evaluation of mountain topography exodynamics from remotely sensed data p 31 A89-18707

Spectral characterization of forest targets in mountainous zones on Thematic Mapper images p 11 N89-10328

MULTISENSOR APPLICATIONS

Geological mapping and mineral exploration in eastern Nova Scotia utilizing airborne and spaceborne multisensor data p 30 A89-14008

MULTISPECTRAL BAND SCANNERS

Imaging spectrometry as a tool for botanical mapping p 73 A89-10324

SeaWiFS - An ocean-imaging sensor p 74 A89-10338

- Advanced airborne electro-optical imager
p 74 A89-10929
- Land and forest cover information from aerial video
p 1 A89-10946
- A comparative evaluation of use of Landsat MSS FCC
and MKF-6M photographs for forest type delineation
p 6 A89-14010
- Combining Laplacian images of different spatial
frequencies (scales) - Implications for remote sensing
image analysis p 68 A89-15919
- Comparison of SPOT, TM and MSS data for agricultural
land-use mapping in Gujarat (India)
[IAF PAPER 88-139] p 7 A89-17692
- Comparison of the spectral information content of
Landsat Thematic Mapper and SPOT for three different
sites in the Phoenix, Arizona region p 68 A89-20626
- Applications of LANDSAT (TM and MSS) data for an
estimation of rangeland conditions in semiarid and arid
areas of northern Kenya
[DFVLR-FB-88-18] p 16 A89-10404
- The potential of combined use of satellite data with
topographic information
[NLR-MP-87061-U] p 70 A89-12113
- LANDSAT-4 and LANDSAT-5 multispectral scanner
coherent noise characterization and removal
[NASA-TP-2595-REV] p 85 A89-12114
- The relative utility of LANDSAT MSS and SIR-A imagery
in reconnaissance geological mapping in Northern
Sudan p 34 A89-13022
- The interpretation of Icelandic tundra features from
LANDSAT-MSS data p 35 A89-13027
- Photogrammetric model for correction of
MSS-LANDSAT imagery
[INPE-4652-PRE/1359] p 73 A89-13090
- Automatic procedure to find corresponding points in CCD
Airborne Experimental Scanner for Applications in Remote
sensing (CAESAR) images
[B8821609] p 88 A89-14490
- User's guide for the Nimbus 7 Scanning Multichannel
Microwave Radiometer (SMMR) CELL-ALL tape
[NASA-RP-1210] p 89 A89-14648
- MULTISPECTRAL LINEAR ARRAYS**
Evaluation of a multispectral linear array sensor for
assessing juvenile stand conditions p 3 A89-11000
- MULTISPECTRAL PHOTOGRAPHY**
Color-composite image processing for multispectral
meteorological satellite data p 76 A89-11742
- [AD-A199574]
Automated segmentation of pseudoinvariant features
from multispectral imagery p 68 A89-17906
- On displaying multispectral imagery
p 68 A89-20631
- Applications of LANDSAT (TM and MSS) data for an
estimation of rangeland conditions in semiarid and arid
areas of northern Kenya
[DFVLR-FB-88-18] p 16 A89-10404
- Efficient classification of multispectral images by a best
linear discriminant function p 72 A89-13060
- MULTISTATIC RADAR**
Multistatic scatterometry p 87 A89-13072
- MULTIVARIATE STATISTICAL ANALYSIS**
Remote sensing of earth terrain
[NASA-CR-183347] p 85 A89-12111

N

NASA SPACE PROGRAMS

- Operational environmental instrumentation proposed by
NOAA and the international community for the NASA and
ESA polar orbiting platforms p 36 A89-10964
- The Earth Observing System --- from space using
platforms in conjunction with Space Station
[IAF PAPER 88-114] p 80 A89-17682
- NASA's future land remote sensing program
p 90 A89-10393
- Geodynamics laser ranging system: Performance
simulations and development of the EOS facility --- Earth
Observing System (EOS) p 28 A89-12982

NATURAL GAS

- Development of Alaskan gas hydrate resources
[DE88-010270] p 35 A89-13093

NEARSHORE WATER

- Remote measurements of diatoms chlorophyll-a in the
Nori farm p 38 A89-11001
- Interpretation and geometrical aspects of Thematic
Mapper data p 69 A89-20716

NEPHANALYSIS

- Classification of cloud fields based on textural
characteristics p 65 A89-11727

NETWORK ANALYSIS

- On the connection of digitized maps to a uniform
coordinate system. A special case of the geodetic
connection problem
[B8821602] p 28 A89-14487

NIMBUS 7 SATELLITE

- Variations in the Arctic, Antarctic, and global sea ice
covers during 1978-1987 as observed with the Nimbus 7
scanning multichannel microwave radiometer
p 38 A89-11145

- Comparison of Nimbus 7 scanning multichannel
microwave radiometer radiance and derived sea ice
concentrations with Landsat imagery for the north water
area of Baffin Bay p 38 A89-11150

- A pilot study to determine relationships between North
Pacific precipitation from Nimbus-7 Scanning Multichannel
Microwave Radiometer data and associated atmospheric
conditions p 43 A89-12837

- Nimbus-7 SMMR derived sea-ice concentrations over
Antarctica p 43 A89-12857
- Monitoring seasonal variations of soil moisture and
vegetation cover using satellite microwave radiometry
p 15 A89-10378

- User's guide for the Nimbus 7 Scanning Multichannel
Microwave Radiometer (SMMR) CELL-ALL tape
[NASA-RP-1210] p 89 A89-14648

NITROGEN

- Relationships between the nitrogen content of grass and
reflectance p 19 A89-13002

NITROGENATION

- Estimation of forest canopy characteristics and nitrogen
cycling using imaging spectrometry p 1 A89-10325

NOAA SATELLITES

- Effect of spatial resolution of the statistical properties
of satellite images - A case study p 66 A89-12221
- A simple method for estimating monthly mean albedo
of land surfaces from AVHRR data p 6 A89-15493

- Analysis of the contribution of the atmosphere to water
reflectance in the first two channels of the NOAA satellites
AVHRR p 82 A89-10330
- Analysis of directional effects on NOAA AVHRR
p 70 A89-10341

- Estimation of sea surface temperature via
NOAA-AVHRR sensor: Comparison with sea truth data
by fixed buoys p 51 A89-13005
- Improvement in NOAA-AVHRR snowcover
determination for runoff prediction p 61 A89-13040

NOISE REDUCTION

- LANDSAT-4 and LANDSAT-5 multispectral scanner
coherent noise characterization and removal
[NASA-TP-2595-REV] p 85 A89-12114

NONLINEARITY

- SAR-seen multimode waves in ice: Evidence of imaging
nonlinearities p 50 A89-12971

NORMALIZING (STATISTICS)

- The normalization of a soil brightness index for the study
of changes in soil conditions p 14 A89-10370

NORWAY

- The numerical simulation of infrared satellite
measurements over the Greenland-Iceland-Norwegian
Sea
[AD-A198653] p 54 A89-14484

NOWCASTING

- Use of satellite and radar images in operational
precipitation nowcasting p 79 A89-13415

NUMERICAL ANALYSIS

- A numerical model for the computation of radiance
distributions in natural waters with wind-roughened
surfaces
[AD-A197207] p 53 A89-13128

NUMERICAL WEATHER FORECASTING

- Using the VAS data utilization center (VDUC) for the
analysis and forecasting of heavy rainfall producing
mesoscale convective systems (MCSs)
p 77 A89-12819

- Use of satellite and radar images in operational
precipitation nowcasting p 79 A89-13415

- Conference on Numerical Weather Prediction, 8th,
Baltimore, MD, Feb. 22-26, 1988, Preprints
p 81 A89-19176

- The contribution of satellite information to operational
weather forecasting - Achievements and objectives in the
1990s p 81 A89-20711

- Towards direct variational assimilation of scatterometer
backscatter measurements into numerical weather
prediction models p 86 A89-13000

NUTATION

- VLBI studies of the nutations of the earth
p 26 A89-13764

O

OCEAN BOTTOM

- Analyses of marine shallow water-bottom features using
the Landsat Thematic Mapper, SPOT, and the Large
Format Camera p 37 A89-10981

- Airborne lidar detection of subsurface oceanic scattering
layers p 41 A89-12260

- Somali Basin, Chain Ridge, and origin of the Northern
Somali Basin gravity and geoid low p 30 A89-12290

- Heat flow and magnetization in the oceanic
lithosphere
[NASA-CR-183346] p 55 A89-14653

- Qualitative aspects of seismograph/ocean bottom
interaction
[AD-A198652] p 56 A89-14656

OCEAN COLOR SCANNER

- SeaWiFS - An ocean-imaging sensor
p 74 A89-10338

- The SeaWiFS sensor for Landsat-6 p 36 A89-10954

OCEAN CURRENTS

- A concept for measuring currents from geostationary
satellites p 75 A89-10933

- Modulation of radar backscatter from the ocean by a
variable surface current p 39 A89-12158

- Comparison of Joint Canada-U.S. Ocean Wave
Investigation Project synthetic aperture radar data with
internal wave observations and modeling results
p 39 A89-12160

- Analysis of nonlinear internal waves in the New York
Bight p 40 A89-12163

- A comparison of measured surface wave spectral
modulations with predictions from a wave-current
interaction model p 40 A89-12165

- A numerical study of mesoscale ocean eddy interaction
with a marginal ice zone p 41 A89-12172

- Acoustic Doppler current profiling in the equatorial
Pacific in 1984 p 45 A89-16986

- The role of horizontal processes in upper-ocean
prediction: A forecast simulation in the Sea of Japan
[AD-A198827] p 55 A89-14654

- OCEAN DATA ACQUISITIONS SYSTEMS**
A new lidar system for applications over land and sea
p 83 A89-10347

- An intercomparison of SAR and buoy directional wave
spectra from the Labrador Sea Extreme Waves Experiment
(LEWEX) p 50 A89-12972

- Directional ocean wave spectra: Prospects for acquiring
a global data base from SIR-C p 50 A89-12973

- The Labrador Sea Extreme Waves Experiment:
Objectives, status and plans p 51 A89-12974

- OCEAN DYNAMICS**
Sea level variations in the tropical Pacific during 1985-87
derived from GEOSAT altimetry p 36 A89-10961

- A study of the dynamics of maritime fronts using remotely
sensed wind and stress measurements p 84 A89-11366

- OCEAN MODELS**
A three-dimensional coupled ice-ocean model of coastal
circulation p 38 A89-11148

- Optical modeling of the upper ocean in relation to its
biogenous matter content (case I waters)
p 38 A89-11149

- Altimetry for non-Gaussian oceans - Height biases and
estimation of parameters p 46 A89-16992

- Mass and heat balances in the upper ocean
p 53 A89-13089

- The role of horizontal processes in upper-ocean
prediction: A forecast simulation in the Sea of Japan
[AD-A198827] p 55 A89-14654

- OCEAN SURFACE**
Does a SAR respond to both phase speed and orbital
velocity in ocean sensing? p 36 A89-10947

- Improvements in the marine gravity field from
Geosat/ERM p 36 A89-10962

- Modeling of the dynamic sea surface with satellite
altimeter signals p 38 A89-11158

- Joint Canada-U.S. Ocean Wave Investigation Project -
An overview of the Georgia Strait Experiment
p 39 A89-12156

- Comparison of Joint Canada-U.S. Ocean Wave
Investigation Project synthetic aperture radar data with
internal wave observations and modeling results
p 39 A89-12160

- Synthetic aperture radar imaging of ocean waves from
an airborne platform - Focus and tracking issues
p 41 A89-12173

- An example of estimates of precipitable water derived
from Nimbus-7 SMMR satellite measurements and FGGE
upper air data p 42 A89-12792

- Assimilation of satellite surface wind speed data using
the GLA analysis/forecast system p 77 A89-12811

- Comparison of weather radar and satellite-based
passive microwave observations of rainfall over land and
oceans p 43 A89-12836

- Modelling of surface waves and sea state-dependent
wind stress for the Northeast Pacific Ocean using Seasat
scatterometer data p 43 A89-12858

- X-band scatterometer measurements at low winds in a
wavetank p 78 A89-12867

- The registration of the surface effects of internal ocean
waves using microwave radiometry p 43 A89-13300

- Microwave emission and reflection from the
wind-roughened sea surface at 6.7 and 18.6 GHz
p 44 A89-15923

- Tower Ocean Wave and Radar Dependence experiment
- An overview p 44 A89-16976
Theory for synthetic aperture radar imaging of the ocean surface - With application to the Tower Ocean Wave and Radar Dependence experiment on focus, resolution, and wave height spectra p 44 A89-16977
Multifocus processing of L band synthetic aperture radar images of ocean waves obtained during the Tower Ocean Wave and Radar Dependence experiment p 45 A89-16978
An analytic representation of the synthetic aperture radar image spectrum for ocean waves p 45 A89-16979
Comparison of measured and predicted sea surface spectra of short waves p 45 A89-16981
Directional measurement of short ocean waves with stereophotography p 45 A89-16982
The dependence of sea surface slope on atmospheric stability and swell conditions p 45 A89-16983
Wind stress measurements during the Tower Ocean Wave and Radar Dependence experiment p 45 A89-16984
Observing the seasonal variability in the tropical Atlantic from altimetry p 46 A89-16987
Altimetry for non-Gaussian oceans - Height biases and estimation of parameters p 46 A89-16992
Comparison of wave parameters determined from SLAR images and a pitch and roll buoy p 47 A89-20721
Sea surface parameters inferred from meteorological satellite data at CMS, Lannion p 47 A89-20722
A three degree-of-freedom description of the ocean surface for microwave remote sensing of wave height and wind friction velocity p 47 N89-10314
The use of the complex correlation function in the recovery of ocean wave spectra from SAR images p 47 N89-10315
An approximative model for the microwave brightness temperature scattered by a rough open ocean surface p 48 N89-10344
Marine boundary layer depth and relative humidity estimates using multispectral satellite measurements [AD-A196525] p 49 N89-12112
Constraints on two-scale descriptions of radar backscattering from the sea surface using scatterometer model functions p 49 N89-12945
Shadows and wedges in scattering from the sea p 49 N89-12946
Spectral analysis of ocean wave imagery using 2-D linear prediction p 50 N89-12968
On the use of speckle statistics for the extraction of ocean wave spectra from SAR imagery p 50 N89-12969
Ocean wave number spectra and spatial autocorrelation functions from SAR images p 50 N89-12970
Some characteristics of short ocean waves as microwave scatterers p 51 N89-13030
Modulation of the radar backscatter from the ocean surface by a long gravity wave p 51 N89-13031
Estimating aircraft SAR response characteristics and approximating ocean wave spectra in the Labrador Sea p 52 N89-13032
Evaluation of GEOSAT (Geodetic Satellite) data and application to variability of the northeast Pacific Ocean [AD-A198950] p 53 N89-13863
The impact of satellite infrared sea surface temperatures on the FNOG (Fleet Numerical Oceanography Center) EOTS (Expanded Ocean Thermal Structure) regional gulf stream analysis p 54 N89-13864
The numerical simulation of infrared satellite measurements over the Greenland-Iceland-Norwegian Sea [AD-A198653] p 54 N89-14484
Summary of along-track data from the earth radiation budget satellite for several representative ocean regions [NASA-RP-1206] p 55 N89-14634
- OCEANOGRAPHIC PARAMETERS**
A dual-satellite algorithm for deriving sea surface temperature p 41 A89-12209
Wind and wind stress curl fields for the Northeast Pacific Ocean using satellite scatterometer data p 78 A89-12859
Estimation of the variability of acoustic characteristics in the region of frontal zones and mesoscale vortices using remote sensing data p 47 A89-18843
Satellite remote sensing and wave studies into the 1990s p 47 A89-20723
The Labrador Sea Extreme Waves Experiment: Objectives, status and plans p 51 N89-12974
Model-based estimation of wind fields over the ocean from wind scatterometer measurements p 53 N89-13070
Performance of a scanning pencil-beam spaceborne scatterometer for ocean wind measurements p 53 N89-13073

OCEANOGRAPHY

- Overview of oceanic microwave remote sensing from space p 35 A89-10930
Airborne lidar detection of subsurface oceanic scattering layers p 41 A89-12260
Conference on Satellite Meteorology and Oceanography, 3rd, Anaheim, CA, Feb. 1-5, 1988, Preprints p 42 A89-12776
A preliminary model for Geosat altimeter data errors p 44 A89-13958
The French space oceanography program p 44 A89-15116
Satellite phasing problems for ocean and atmospheric studies [IAF PAPER 88-152] p 46 A89-17698
High-resolution spectroscopy for remote sensing of ocean and atmosphere p 48 N89-10352
Drifting buoy data from the Equatorial Pacific for the period January 1, 1984 through May 31, 1985 [PB88-212824] p 49 N89-10516
The impact of satellite infrared sea surface temperatures on the FNOG (Fleet Numerical Oceanography Center) EOTS (Expanded Ocean Thermal Structure) regional gulf stream analysis [AD-A198965] p 54 N89-13864
An autonomous ocean instrument platform driven vertically by the current [AD-A198226] p 54 N89-13865
The role of horizontal processes in upper-ocean prediction: A forecast simulation in the Sea of Japan [AD-A198827] p 55 N89-14654
- OCEANS**
Rainfall index over oceans derived from SSM/I data -- Special Sensor Microwave/Imager (SSM/I) p 51 N89-12998
The impact of satellite infrared sea surface temperatures on the FNOG (Fleet Numerical Oceanography Center) EOTS (Expanded Ocean Thermal Structure) regional gulf stream analysis [AD-A198965] p 54 N89-13864
Chemical variability in ocean frontal areas [AD-A198418] p 56 N89-14655
- OIL EXPLORATION**
Surveillance radar, a new tool for ice surveillance p 37 A89-10991
Image analysis techniques for the interpretation of airphoto lineaments - Petroleum exploration, Eromanga Basin, Australia p 30 A89-14011
- OIL POLLUTION**
Time-resolved laser fluorescing: Trends and applications p 83 N89-10346
- ONBOARD DATA PROCESSING**
On-board processing and national earth observations centers p 22 A89-10927
Study of the multiplexing of image telemetry data from SPOT 4 HRVIR and Vegetation sensors [CNES-87/229/CT/DRT/TIT/TR] p 70 N89-10930
- OPTICAL DATA PROCESSING**
Possible measurement errors in calibrated AVHRR (Advanced Very High Resolution Radiometer) data [AD-A198342] p 88 N89-14414
- OPTICAL EMISSION SPECTROSCOPY**
High-resolution spectroscopy for remote sensing of ocean and atmosphere p 48 N89-10352
- OPTICAL RADAR**
Airborne lidar detection of subsurface oceanic scattering layers p 41 A89-12260
Doppler lidar wind measurements on the EOS - LAWS p 77 A89-12829
Lidar atmospheric sounder and altimetry for the Earth Observing System (EOS) satellite p 79 A89-15873
A new lidar system for applications over land and sea p 83 N89-10347
- OPTICAL THICKNESS**
Analysis of the contribution of the atmosphere to water reflectance in the first two channels of the NOAA satellites AVHRR p 82 N89-10330
- OPTIMIZATION**
Computational design and efficiency optimization of agricultural airplanes p 5 A89-13670
- ORBIT CALCULATION**
Orbit determination requirements for Topex [AAS PAPER 87-429] p 42 A89-12645
- ORBITAL MECHANICS**
Geosat crossover analysis in the tropical Pacific. I - Constrained sinusoidal crossover adjustment p 38 A89-11143
- ORBITAL VELOCITY**
Does a SAR respond to both phase speed and orbital velocity in ocean sensing? p 36 A89-10947
- ORCHARDS**
Spectral and spatial characterisation of orchards in New York State using Thematic Mapper Imagery p 4 A89-11008

OROGRAPHY

- Orographic channeling of a cold front by the Pyrenees p 79 A89-14073
Use of Landsat and Seasat data as a tool in kinematic analysis - The Tunisian Atlas p 31 A89-20710
- ORTHOGONAL FUNCTIONS**
EOF analysis of AVHRR and CZCS imagery p 43 A89-12856
- OUTCROPS**
LANDSAT Thematic Mapping (TM) and SPOT HRV for survey mapping of bedrock outcrops p 20 N89-13055
- OZONE**
Comparison of in situ aerosol measurements with SAGE 2 and SAM 2 aerosol measurements during the airborne Antarctic ozone experiment p 89 N89-14522
Analysis of crop loss for alternative ozone exposure indices [PB88-214788] p 22 N89-14608
- OZONE DEPLETION**
Comparison of in situ aerosol measurements with SAGE 2 and SAM 2 aerosol measurements during the airborne Antarctic ozone experiment p 89 N89-14522
Evolution of polar stratospheric clouds during the Antarctic winter p 55 N89-14534

P**PACIFIC NORTHWEST (US)**

- Distribution of relative plate motion along the Pacific-North American plate boundary determined from mobile VLBI measurements p 26 A89-13761

PACIFIC OCEAN

- Sea level variations in the tropical Pacific during 1985-87 derived from GEOSAT altimetry p 36 A89-10961
Geosat crossover analysis in the tropical Pacific. I - Constrained sinusoidal crossover adjustment p 38 A89-11143
A pilot study to determine relationships between North Pacific precipitation from Nimbus-7 Scanning Multichannel Microwave Radiometer data and associated atmospheric conditions p 43 A89-12837
Acoustic Doppler current profiling in the equatorial Pacific in 1984 p 45 A89-16986
Drifting buoy data from the Equatorial Pacific for the period January 1, 1984 through May 31, 1985 [PB88-212824] p 49 N89-10516
Active modes of the Pacific Intertropical Convergence Zone (ITCZ) [AD-A196406] p 49 N89-11374
Evaluation of GEOSAT (Geodetic Satellite) data and application to variability of the northeast Pacific Ocean [AD-A198950] p 53 N89-13863
- PALEOMAGNETISM**
Magnetic mineralogy in an Archean crustal cross section - Implications for crustal magnetization p 30 A89-12292

PARAMETERIZATION

- Retrieving vegetation and soil parameters from radar measurements p 10 N89-10321

PARTICLE SIZE DISTRIBUTION

- Comparison of in situ aerosol measurements with SAGE 2 and SAM 2 aerosol measurements during the airborne Antarctic ozone experiment p 89 N89-14522

PARTICULATE SAMPLING

- Corrections of surface particle probe measurements for the effects of aspiration p 58 A89-14022

PATTERN RECOGNITION

- SPOT satellite data for pattern recognition on the North American tall-grass prairie Long-Term Ecological Research site p 5 A89-14009
Efficient classification of multispectral images by a best linear discriminant function p 72 N89-13060
Precision of line following in digital images [B8821610] p 73 N89-14486

PENCIL BEAMS

- Performance of a scanning pencil-beam spaceborne scatterometer for ocean wind measurements p 53 N89-13073

PERFORMANCE TESTS

- Qualitative aspects of seismograph/ocean bottom interaction [AD-A198652] p 56 N89-14656

PERSONAL COMPUTERS

- Integrating remotely sensed data into PC-based geographic information systems p 23 A89-10959

PERSONNEL DEVELOPMENT

- Important aspects of technology transfer: Training of inservice engineers and scientists; satellite remote sensing p 91 N89-13082

PESTICIDES

- Cotton area mapping using multitemporal satellite data integrated within a geographical information system applied to a cotton boll weevil control programme in Paraguay p 20 N89-13077

PETROLOGY

Desert varnish on volcanic rocks of the Basin and Range province - Composition, morphology, distribution, origin and influence on Landsat imagery p 30 A89-10988

PH

Spectral studies of three oxisols and a Ultisol of Brazil [INPE-4644-PRE/1355] p 17 N89-11297

PHASE SHIFT

A new radar technique for satellite rainfall algorithm development [NASA-CR-183471] p 60 N89-11102

PHASE VELOCITY

Does a SAR respond to both phase speed and orbital velocity in ocean sensing? p 36 A89-10947

PHOENIX (AZ)

Comparison of the spectral information content of Landsat Thematic Mapper and SPOT for three different sites in the Phoenix, Arizona region p 68 A89-20626

PHOTO GEOLOGY

A useful model in mineral exploration with remotely sensed data p 30 A89-11017

Image analysis techniques for the interpretation of airphoto lineaments - Petroleum exploration, Eromanga Basin, Australia p 30 A89-14011

Project Vasundhara - Multi-theme integration of satellite remote sensing and geological data for regional level mineral prognostics [IAF PAPER 88-145] p 31 A89-17694

Remote sensing of laterized Archaean greenstone terrain - Marshall Pool Area, Northeastern Yilgarn Block, Western Australia p 31 A89-20628

Evaluation and digital processing of multispectral SPOT data p 68 A89-20708

Mineral exploration along the Aqaba-Levant structure by use of TM-data - Concepts, processing and results p 31 A89-20709

Comparative geological evolution of different remote sensing data of the Hoggar Mountains (Algeria) p 33 N89-10385

Digital analysis of MOMS-1, LANDSAT TM, and SPOT data of the Nakuru area (Kenya) p 33 N89-10386

PHOTOGRAMMETRY

Photogrammetric Week, 41st, Universitaet Stuttgart, Federal Republic of Germany, Sept. 14-19, 1987, Proceedings p 63 A89-10611

Automatic control point determination for image registration using texture analysis methods p 3 A89-10985

Geometric correction of satellite images using composite transformation functions p 64 A89-10986

Geometric correction of remotely-sensed imagery using ground control points and orthogonal polynomials p 82 A89-20718

Photogrammetric model for correction of MSS-LANDSAT imagery [INPE-4652-PRE/1359] p 73 N89-13090

PHOTOINTERPRETATION

Model based remotely-sensed imagery interpretation p 66 A89-12223

Evaluation of space photographs --- mapping using Metric Camera and Large Format Camera p 82 A89-20715

Identifying the reforested areas utilizing the SPOT satellite data [INPE-4624-PRE/1343] p 15 N89-10396

CIR aerial photography applied to the evaluation of the air pollution impact in a tropical forest: The case of Cubatao, Brazil [INPE-4651-PRE/1358] p 17 N89-11324

Color enhancement of remote sensing imagery using IHS transformations and decorrelation stretch methods [INPE-4659-PRE/1309] p 70 N89-11418

PHOTOMAPPING

Sino-American cooperative studies on applications of remote sensing to surveying and mapping p 29 A89-10967

Evaluating Landsat classification accuracy from forest cover-type maps p 5 A89-12756

A comparative evaluation of use of Landsat MSS FCC and MKF-6M photographs for forest type delineation p 6 A89-14010

Topographic mapping from SPOT imagery p 67 A89-14088

Tests of topographic mapping with Thematic Mapper images p 69 A89-20712

Analysis of large format camera photographs of the Po Delta, Italy, for topographic and thematic mapping p 82 A89-20714

The potential of combined use of satellite data with topographic information [NLR-MP-87061-U] p 70 N89-12113

PHOTOMETERS

Comparison of in situ aerosol measurements with SAGE 2 and SAM 2 aerosol measurements during the airborne Antarctic ozone experiment p 89 N89-14522

PHYSICAL OPTICS

Shadows and wedges in scattering from the sea p 49 N89-12946

PLANAR STRUCTURES

Effect of curvature on the backscattering from leaves [NASA-CR-183326] p 16 N89-11296

PLANKTON

Phytoplankton standing crops within an Antarctic ice edge assessed by satellite remote sensing p 41 A89-12174

PLANT STRESS

Imaging spectrometry as a tool for botanical mapping p 73 A89-10324
The effects of bark beetle stress on the foliar spectral reflectance of lodgepole pine p 5 A89-12355
Stress detection in mixed coniferous-broadleaved forests from Airborne Imaging Spectrometer (AIS) data p 13 N89-10355

PLATEAUS

Sapping features of the Colorado Plateau: A comparative planetary geology field guide [NASA-SP-491] p 34 N89-10401

PLATES (TECTONICS)

The Crustal Dynamics Project p 25 A89-13757
Beyond plate tectonics - Looking at plate deformation with space geodesy p 44 A89-13758
Geodesy by radio interferometry - Determination of vector motions for sites in the western United States p 25 A89-13759

Distribution of relative plate motion along the Pacific-North American plate boundary determined from mobile VLBI measurements p 26 A89-13761

PLAYAS

Monitoring playas using Thematic Mapper data p 60 N89-13028

POINT SPREAD FUNCTIONS

Comparative point-spread function calculations for the MOMS-1, Thematic Mapper and SPOT-HRV instruments p 83 N89-10379

POLAR CAPS

Nimbus-7 SMMR derived sea-ice concentrations over Antarctica p 43 A89-12857

POLAR ORBITS

Snow and low-cloud discrimination from multispectral satellite measurements p 78 A89-12850
Cloud track winds from polar orbiting satellites p 87 N89-13069

POLAR REGIONS

Cloud track winds from polar orbiting satellites p 87 N89-13069

POLARIMETERS

Coherent polarimetric signatures of coniferous trees: A survey p 9 N89-10307

POLARIMETRY

Radar polarimetry - Analysis tools and applications p 30 A89-15915

Remote sensing of earth terrain [NASA-CR-183347] p 85 N89-12111

Cross-polar radar measurements in ice and rain p 60 N89-12993

POLARIZATION (WAVES)

A new radar technique for satellite rainfall algorithm development [NASA-CR-183471] p 60 N89-11102

Remote Sensing in Polarized Light [NASA-CP-3014] p 88 N89-14189

POLARIZATION CHARACTERISTICS

Modelling of SAR polarisation phase difference from trees p 18 N89-12951

POLLUTION MONITORING

Time-resolved laser fluorescing: Trends and applications p 83 N89-10346

POSITION (LOCATION)

Data collection system operating on Japan's first marine observation satellite: Inflight evaluation of the system performance p 87 N89-13007

POTATOES

Microwave backscatter from beets, peas and potatoes throughout the growing season p 9 N89-10309

Analysis of potato crop distribution using remotely sensed and environmental data in a pilot geographical information system p 18 N89-12967

PRECIPITATION (METEOROLOGY)

Atmospheric absorption in the VAS split-window channels p 39 A89-11225

An extension of the split window technique for the retrieval of precipitable water - Experimental verification [AD-A199515] p 76 A89-12796

Thunderstorm ice induced brightness temperature depressions at 18, 37, and 92 GHz during Cohmex and their implications for satellite precipitation retrievals p 42 A89-12835

A pilot study to determine relationships between North Pacific precipitation from Nimbus-7 Scanning Multichannel Microwave Radiometer data and associated atmospheric conditions p 43 A89-12837

Variation of satellite rain relationships in space and time p 67 A89-12843

Mid-latitude evaluation of some satellite rainfall estimation techniques p 78 A89-12844

Use of satellite and radar images in operational precipitation nowcasting p 79 A89-13415

Observation of precipitation using GMS imagery [IAF PAPER 88-151] p 58 A89-17697

Precipitation detection with satellite microwave data [PB88-240239] p 88 N89-13094

PRECIPITATION PARTICLE MEASUREMENT

Cross-polar radar measurements in ice and rain p 60 N89-12993

PRECISION

Precision of line following in digital images [B8821610] p 73 N89-14486

PREDICTION ANALYSIS TECHNIQUES

Introducing spectral data into a plant process model for improving its prediction ability p 10 N89-10324

Spectral analysis of ocean wave imagery using 2-D linear prediction p 50 N89-12968

Improvement in NOAA-AVHRR snowcover determination for runoff prediction p 61 N89-13040

The role of horizontal processes in upper-ocean prediction: A forecast simulation in the Sea of Japan [AD-A198827] p 55 N89-14654

PRIMITIVE EQUATIONS

A numerical study of mesoscale ocean eddy interaction with a marginal ice zone p 41 A89-12172

PRINCIPAL COMPONENTS ANALYSIS

Forest classification by principal component analyses of TM data p 8 A89-20706

PROBLEM SOLVING

On the connection of digitized maps to a uniform coordinate system. A special case of the geodetic connection problem [B8821602] p 28 N89-14487

PRODUCTIVITY

The influence of grazing on land surface climatological variables [NASA-CR-183308] p 22 N89-14637

PROFILOMETERS

Measuring in-situ soil surface roughness using a laser profilometer p 9 N89-10308

PROJECT MANAGEMENT

Geologic mapping in the US Geological Survey [PB88-223870] p 35 N89-14477

PROTOCOL (COMPUTERS)

The design and protocol of a summertime rainfall enhancement program for West Texas p 63 N89-14636

PULSE FREQUENCY MODULATION TELEMETRY

Study of the multiplexing of image telemetry data from SPOT 4 HRVIR and Vegetation sensors [CNES-87/229/CT/DR7/TIT/TR] p 70 N89-10930

PUSHBROOM SENSOR MODES

Design of spectral bands for the German MOMS-2 sensor p 84 N89-10381

PYRENEES MOUNTAINS (EUROPE)

Orographic channeling of a cold front by the Pyrenees p 79 A89-14073

Q

QUANTUM EFFICIENCY

Techniques for remote sensing of life span and quantum yield of chlorophyll fluorescence in vivo p 13 N89-10351

R

RADAR ANTENNAS

Three-dimensional observation by means of tethered antennae --- for earth observation from space [IAF PAPER 88-118] p 80 A89-17684

Experimental personal satellite communications system using millimeter-wave for Asia-Oceanian region p 81 A89-18736

RADAR ATTENUATION

Polarization-dependent attenuation of dielectric cylinder arrays p 86 N89-12955

RADAR CROSS SECTIONS

Constraints on two-scale descriptions of radar backscattering from the sea surface using scatterometer model functions p 49 N89-12945

RADAR DATA

The evaluation of simple approaches for the delineation of rain area from satellite imagery p 66 A89-12842

Resolution dependence in satellite imagery - Multifactor analysis p 67 A89-12852

Evaluation of VARAN data in geology and geomorphology in the southeast of France p 32 N89-10313

An intercomparison of SAR and buoy directional wave spectra from the Labrador Sea Extreme Waves Experiment (LEWEX) p 50 N89-12972

RADAR DETECTION

A new radar technique for satellite rainfall algorithm development [NASA-CR-183471] p 60 N89-11102

RADAR ECHOES

Investigation of radar backscattering from second-year sea ice [NASA-CR-180986] p 54 N89-14479

RADAR EQUIPMENT

Evolution of the helicopter-borne scatterometer p 37 N89-10971

RADAR IMAGERY

Does a SAR respond to both phase speed and orbital velocity in ocean sensing? p 36 N89-10947
SIR-B view of the Jabal Hadn lineament and its groundwater implications p 29 N89-10976
Surveillance radar, a new tool for ice surveillance p 37 N89-10991

Effect of soil roughness on SAR images of harvested agricultural fields p 4 N89-11004
Comparison of Joint Canada-U.S. Ocean Wave Investigation Project synthetic aperture radar data with internal wave observations and modeling results p 39 N89-12160

An overview of the SAR Internal Wave Signature Experiment p 40 N89-12162

Measurements of surface wave modulations from internal waves during the SAR Internal Wave Signature Experiment p 40 N89-12164

Full-spectrum modeling of synthetic aperture radar internal wave signatures p 40 N89-12166

Contrast ratios of internal waves in synthetic aperture radar imagery - A comparison of SAR Internal Wave Signature Experiment observations with theory p 40 N89-12167

Synthetic aperture radar imaging of ocean waves from an airborne platform - Focus and tracking issues p 41 N89-12173

Tower Ocean Wave and Radar Dependence experiment - An overview p 44 N89-16976

Theory for synthetic aperture radar imaging of the ocean surface - With application to the Tower Ocean Wave and Radar Dependence experiment on focus, resolution, and wave height spectra p 44 N89-16977

Multifocus processing of L band synthetic aperture radar images of ocean waves obtained during the Tower Ocean Wave and Radar Dependence experiment p 45 N89-16978

Comparison of measured and predicted sea surface spectra of short waves p 45 N89-16981

Wind stress measurements during the Tower Ocean Wave and Radar Dependence experiment p 45 N89-16984

The effect of agrometeorological conditions on the characteristics of space radar imagery of agricultural regions in winter p 8 N89-18709

Comparison of wave parameters determined from SLAR images and a pitch and roll buoy p 47 N89-20721

Texture analysis in forest areas: High spectral resolution synthetic aperture radar data p 14 N89-10367

On the use of speckle statistics for the extraction of ocean wave spectra from SAR imagery p 50 N89-12969

Ocean wave number spectra and spatial autocorrelation functions from SAR images p 50 N89-12970

SAR-seen multimode waves in ice: Evidence of imaging nonlinearities p 50 N89-12971

Crop classification with multi-temporal X-band SAR data p 19 N89-12990

A synthetic apertures radar with multichannel and multipolarisation p 87 N89-13017

The relative utility of LANDSAT MSS and SIR-A imagery in reconnaissance geological mapping in Northern Sudan p 34 N89-13022

Sea ice type classification of SAR imagery p 52 N89-13039

Statistics and high resolution imaging of snowpack at 35 GHz using a microcomputer p 61 N89-13047

Snow cover to alter terrain signatures on radar images p 62 N89-13048

The derivation of sub-canopy surface terrain models of coastal forests using synthetic aperture radar p 20 N89-13083

Development of a ground hydrology model suitable for global climate modeling using soil morphology and vegetation cover, and an evaluation of remotely sensed information [NASA-CR-180463] p 21 N89-13821

The design and protocol of a summertime rainfall enhancement program for West Texas p 63 N89-14636

RADAR MAPS

Use of satellite and radar images in operational precipitation nowcasting p 79 N89-13415

Design of a spaceborne rain mapping radar [IAF PAPER 88-124] p 58 N89-17688

SAR image statistics related to atmospheric drag over sea ice p 52 N89-13034

RADAR MEASUREMENT

Validation of the on-site Flash Flood Potential System for Nexrad p 57 N89-10949

Design of a spaceborne rain mapping radar [IAF PAPER 88-124] p 58 N89-17688

Retrieving vegetation and soil parameters from radar measurements p 10 N89-10321

Cross-polar radar measurements in ice and rain p 60 N89-12993

Phase versus orbital velocity in SAR wave imaging: Paradox lost p 52 N89-13033

Microwave dielectric properties of low-salinity sea ice p 52 N89-13036

RADAR SCATTERING

Modulation of radar backscatter from the ocean by a variable surface current p 39 N89-12158

Contrast ratios of internal waves in synthetic aperture radar imagery - A comparison of SAR Internal Wave Signature Experiment observations with theory p 40 N89-12167

Radar polarimetry - Analysis tools and applications p 30 N89-15915

Microwave backscatter from beets, peas and potatoes throughout the growing season p 9 N89-10309

Constraints on two-scale descriptions of radar backscattering from the sea surface using scatterometer model functions p 49 N89-12945

Inference of geologic surface parameters from polarimetric radar observations and model inversion p 34 N89-12950

Modeling of SAR polarisation phase difference from trees p 18 N89-12951

Modulation of the radar backscatter from the ocean surface by a long gravity wave p 51 N89-13031

RADAR SIGNATURES

Proceedings of the 4th International Colloquium on Spectral Signatures in Remote Sensing [ESA-SP-287] p 9 N89-10305

Evaluation of VARAN data in geology and geomorphology in the southeast of France p 32 N89-10313

AGRSAR'86: Contributing to signature research p 15 N89-10387

Snow cover to alter terrain signatures on radar images p 62 N89-13048

RADAR TRACKING

Synthetic aperture radar imaging of ocean waves from an airborne platform - Focus and tracking issues p 41 N89-12173

Comparison of satellite IR rain estimates with radar rain observations in hurricanes p 57 N89-12845

RADIANCE

Microwave radiances from horizontally finite, vertically structured precipitating clouds p 84 N89-11364

A numerical model for the computation of radiance distributions in natural waters with wind-roughened surfaces [AD-A197207] p 53 N89-13128

Summary of along-track data from the earth radiation budget satellite for several representative ocean regions [NASA-RP-1206] p 55 N89-14634

RADIATION MEASUREMENT

Comparison of measured and modeled radiation, heat and water vapor fluxes: FIFE pilot study [NASA-CR-183304] p 17 N89-11368

RADIATIVE TRANSFER

Satellite microwave rainfall simulations with a three-dimensional dynamical cloud model p 77 N89-12833

Estimating concentrations of optically active components from the remotely sensed spectral radiance of a water surface p 58 N89-18711

The spectral bidirectional reflectance of snow p 69 N89-10318

A model for radiative transfer in heterogeneous three-dimensional canopies p 11 N89-10326

Remote Sensing in Polarized Light [NASA-CP-3014] p 88 N89-14189

Very Long Baseline Interferometry (VLBI) from ground and space p 85 N89-11645

RADIO FREQUENCIES

Comparison of measured and modeled radiation, heat and water vapor fluxes: FIFE pilot study [NASA-CR-183304] p 17 N89-11368

RADIO INTERFEROMETERS

Geodesy by radio interferometry - Determination of vector motions for sites in the western United States p 25 N89-13759

RADIO SCATTERING

Inference of radio scattering parameters of Antarctic ice sheet using 179 MHz airborne radio echo sounding data p 51 N89-12975

RADIOMETERS

The Airborne Version Conical Scan Radiometer (AVCSR): An airborne radiometer as a tool for satellite data validation p 86 N89-12937

Verification results of MOS-1 multispectral self scanning radiometer (MESSR) data p 86 N89-13004

RADIOMETRIC CORRECTION

Lowest order correction for solar zenith angle to Global Vegetation Index (GVI) data p 8 N89-20704

Sensitivity of satellite-derived net shortwave irradiance at the Earth's surface to radiometric calibration p 82 N89-10335

RADIOMETRIC RESOLUTION

SPOT image quality - Twenty months of experience p 66 N89-12352

High resolution radiometric measurement of intertidal microphytobenthos p 48 N89-10365

RAIN

Using the VAS data utilization center (VDUC) for the analysis and forecasting of heavy rainfall producing mesoscale convective systems (MCSs) p 77 N89-12819

Thunderstorm ice induced brightness temperature depressions at 18, 37, and 92 GHz during Cohmet and their implications for satellite precipitation retrievals p 42 N89-12835

Comparison of weather radar and satellite-based passive microwave observations of rainfall over land and oceans p 43 N89-12836

The addition of visible channel data to satellite infrared rain estimation schemes p 78 N89-12839

The evaluation of simple approaches for the delineation of rain area from satellite imagery p 66 N89-12842

Variation of satellite rain relationships in space and time p 67 N89-12843

Mid-latitude evaluation of some satellite rainfall estimation techniques p 78 N89-12844

Comparison of satellite IR rain estimates with radar rain observations in hurricanes p 57 N89-12845

Future measurements of rain from space [IAF PAPER 88-112] p 58 N89-17681

Design of a spaceborne rain mapping radar [IAF PAPER 88-124] p 58 N89-17688

PRISM B (Prediction of the Indian Summer Monsoon - Bellevue) p 58 N89-17873

A new radar technique for satellite rainfall algorithm development [NASA-CR-183471] p 60 N89-11102

Microwave radiances from horizontally finite, vertically structured precipitating clouds p 84 N89-11364

An agricultural crop yield model by satellite: A simulation [INPE-4639-PRE/1350] p 17 N89-12106

Cross-polar radar measurements in ice and rain p 60 N89-12993

Design of a spaceborne radar for tropical rain mapping at the climatological scale p 60 N89-12997

Rainfall index over oceans derived from SSM/I data --- Special Sensor Microwave/Imager (SSM/I) p 51 N89-12998

Simulation of radar and surface measurements of rainfall p 62 N89-13924

The design and protocol of a summertime rainfall enhancement program for West Texas p 63 N89-14636

RAINDROPS

Satellite microwave rainfall simulations with a three-dimensional dynamical cloud model p 77 N89-12833

RANGELANDS

Applications of LANDSAT (TM and MSS) data for an estimation of rangeland conditions in semiarid and arid areas of northern Kenya [DFVLR-FB-88-18] p 16 N89-10404

REDUCED GRAVITY

Sensors research and technology p 85 N89-11774

REFLECTANCE

Invertible canopy reflectance modeling of vegetation structure in semiarid woodland p 6 N89-15918

A perspective on vegetation canopy reflectance models p 10 N89-10317

The spectral bidirectional reflectance of snow p 69 N89-10318

A simplified vegetation canopy reflectance and absorption model p 10 N89-10322

The angular reflectance signature of the canopy hot spot in the optical regime p 11 N89-10325

A simplified reflectance model for shrub canopies p 11 N89-10329

- Analysis of the contribution of the atmosphere to water reflectance in the first two channels of the NOAA satellites AVHRR p 82 N89-10330
- Developing a radiometric leaf area index p 12 N89-10334
- Spectral reflectance of sugar beet and winter wheat canopies in the visible and infrared during growth p 12 N89-10342
- Relationships between the nitrogen content of grass and reflectance p 19 N89-13002
- Snow cover to alter terrain signatures on radar images p 62 N89-13048
- A numerical model for the computation of radiance distributions in natural waters with wind-roughened surfaces [AD-A197207] p 53 N89-13128
- REFORESTATION**
- Identifying the reforested areas utilizing the SPOT satellite data [INPE-4624-PRE/1343] p 15 N89-10396
- REGIONAL PLANNING**
- Large area TM land cover classification of Mittlerer Oberrhein County, southwest Germany, and its use for regional planning and crop surveys p 18 N89-12986
- The detection of unimproved grassland in Berkshire using a binary decision tree approach p 18 N89-12988
- Evaluation of LANDSAT TM and SPOT imagery for agricultural land use planning in less developed countries p 19 N89-13051
- REGRESSION ANALYSIS**
- The Transformed Vegetation Index (TVI) for estimation of Brazilian cerrado's phytomass [INPE-4603-PRE/1326] p 15 N89-10400
- REGULATIONS**
- International space law norms regulating remote sensing of the earth from outer space p 89 A89-12126
- RELATIVISTIC EFFECTS**
- Very Long Baseline Interferometry (VLBI): Relativity and geodesy [ETN-89-93337] p 29 N89-14493
- RELIEF MAPS**
- A procedure for modeling the terrain relief by using digitized topographic maps p 67 A89-14005
- REMOTE SENSING**
- The fluorescence line imager - An imaging spectrometer for ocean and land remote sensing p 73 A89-10312
- Imaging spectrometry for water applications p 56 A89-10327
- High Resolution Imaging Spectrometer (HIRIS) p 74 A89-10334
- SeaWiFS - An ocean-imaging sensor p 74 A89-10338
- Photogrammetric Week, 41st, Universitat Stuttgart, Federal Republic of Germany, Sept. 14-19, 1987, Proceedings p 63 A89-10611
- International Symposium on Remote Sensing of Environment, 21st, University of Michigan, Ann Arbor, Oct. 26-30, 1987, Proceedings. Volumes 1 & 2 p 22 A89-10926
- Overview of oceanic microwave remote sensing from space p 35 A89-10930
- The electronically steered thinned array radiometer p 74 A89-10932
- Accuracy evaluation of airborne stereo line imager data p 75 A89-10936
- Resolution improvement by multi-temporal data merging p 63 A89-10937
- Remote sensing of estuaries - An overview p 56 A89-10939
- Laser fluorosensing of water quality - A review p 57 A89-10941
- Passive microwave remote sensing of salinity in coastal zones p 36 A89-10942
- Climate tracking with remote sensing p 75 A89-10943
- Land and forest cover information from aerial video p 1 A89-10946
- The application of remote sensing for drought early warning in Africa p 1 A89-10948
- Surface energy flux measurements and reflectance factors using satellite-, aircraft-, and ground-based instrumentation p 1 A89-10950
- Satellite data analysis for inventorying crops grown in a complex, small-field environment p 1 A89-10951
- Soil erosion study using an airborne laser profiler p 1 A89-10952
- Infrared temperature measurements over bare soil and vegetation - A HAPEX perspective p 2 A89-10953
- The Seawifs sensor for Landsat-6 p 36 A89-10954
- Enhancements to the ARGOS system - Presented at the Twenty-first International Symposium on Remote Sensing of Environment, Ann Arbor, Michigan, October 26-30, 1987 p 22 A89-10957
- Applications of spatial postclassification models p 63 A89-10958
- Integrating remotely sensed data into PC-based geographic information systems p 23 A89-10959
- Remote sensing and geographic information systems for agricultural statistics-gathering and agricultural monitoring in Morocco p 2 A89-10960
- Sino-American cooperative studies on applications of remote sensing to surveying and mapping p 29 A89-10967
- Applications of multispectral video for natural resource assessment p 63 A89-10968
- Radar applications in remote sensing - An airborne remote sensing case history presented at the Twenty-first International Symposium on Remote Sensing of Environment, Ann Arbor, Michigan, October 26-30, 1987 p 75 A89-10969
- Evolution of the helicopter-borne scatterometer p 37 A89-10971
- Study of monitoring sea ice using an airborne microwave radiometer system p 37 A89-10972
- The character of reflective spectrum of winter wheat and the principle of its yield estimation with remote sensing method p 2 A89-10973
- A study of estimation of winter wheat yield for large area using remote sensing method p 2 A89-10974
- Reflectance characteristics of dry plant materials p 3 A89-10977
- Backscattering coefficient of rice crops and rice fields by an X-band scatterometer p 3 A89-10980
- Analyses of marine shallow water-bottom features using the Landsat Thematic Mapper, SPOT, and the Large Format Camera p 37 A89-10981
- Land cover change detection with Thematic Mapper spectral textural data at the rural-urban fringe p 23 A89-10982
- Edge detection and processing of remotely sensed digital images p 64 A89-10984
- Automatic control point determination for image registration using texture analysis methods p 3 A89-10985
- Geometric correction of satellite images using composite transformation functions p 64 A89-10986
- Detection of forest damage on Whiteface Mountain, New York, using Landsat Thematic Mapper data p 3 A89-10987
- Surveillance radar, a new tool for ice surveillance p 37 A89-10991
- The use of microwave radiometry in watershed hydrology p 57 A89-10992
- The practice and understanding of using aerial remote sensing in the investigation of coastal zone p 37 A89-10995
- A new tool - SPOT imagery for studying rapid movements p 64 A89-10996
- Atmospheric correction of NS-001 data and extraction of multiple angle reflectance data sets p 64 A89-10998
- Evaluation of a multispectral linear array sensor for assessing juvenile stand conditions p 3 A89-11000
- Remote measurements of diatoms chlorophyll-a in the Nori farm p 38 A89-11001
- SAR and visible remote sensing of the Taor River coastal zone at Bohai Bay p 38 A89-11005
- Comparison of remote measurements of infrared surface temperatures and microwave soil moisture p 4 A89-11009
- The use of fractal geometry to identify ranges of scale-invariance in digital remotely sensed data p 4 A89-11011
- Relative water content of Spruce needles determined by the leaf water content index p 4 A89-11012
- Evaluation of technology in the detection and counting of seals p 76 A89-11016
- A useful model in mineral exploration with remotely sensed data p 30 A89-11017
- Principles Relating to Remote Sensing of the Earth from Space - Territorial sphere of application p 89 A89-12121
- Marine remote sensing and international law p 39 A89-12124
- United Nations activity on remote sensing - Legal and political implications p 89 A89-12125
- International space law norms regulating remote sensing of the earth from outer space p 89 A89-12126
- Joint Canada-U.S. Ocean Wave Investigation Project - An overview of the Georgia Strait Experiment p 39 A89-12156
- Phytoplankton standing crops within an Antarctic ice edge assessed by satellite remote sensing p 41 A89-12174
- Evaporation over land surfaces - First results from HAPEX-MOBILHY Special Observing Period p 57 A89-12211
- Segmentation of remotely-sensed images by a split-and-merge process p 66 A89-12222
- Model-based remotely-sensed imagery interpretation p 66 A89-12223
- Algorithm for automatic atmospheric corrections to visible and near-IR satellite imagery p 66 A89-12224
- Airborne lidar detection of subsurface oceanic scattering layers p 41 A89-12260
- Directional effects on scene complexity in oblique thermal imagery and photographs of a deciduous forest p 4 A89-12261
- SPOT image quality - Twenty months of experience p 66 A89-12352
- CANVAS - An intelligent system for colour selection on CRT displays p 76 A89-12353
- Estimation of multiple reflection and lowest order adjacency effects on remotely-sensed data p 5 A89-12354
- The effects of bark beetle stress on the foliar spectral reflectance of lodgepole pine p 5 A89-12355
- Estimating the distribution of grazing and patterns of cattle movement in a large arid zone paddock p 5 A89-12356
- Detection of circular geological features using the Hough transform p 30 A89-12358
- Remote sensing of surface air temperature and humidity over oceanic areas with application to climatology and weather prediction p 42 A89-12798
- NASA's Earth Science Geostationary Platform p 77 A89-12828
- The use of spectral reflectance characteristics for the estimation of the wheat crop state p 5 A89-12874
- A procedure for modeling the terrain relief by using digitized topographic maps p 67 A89-14005
- Geological mapping and mineral exploration in eastern Nova Scotia utilizing airborne and spaceborne multisensor data p 30 A89-14008
- Aerospace monitoring of ecosystem dynamics and ecological prognoses p 23 A89-15050
- Airborne and spaceborne lasers for terrestrial geophysical sensing: Proceedings of the Meeting, Los Angeles, CA, Jan. 14, 15, 1988 p 79 A89-15870
- Lidar atmospheric sounder and altimetry for the Earth Observing System (EOS) satellite p 79 A89-15873
- Radar polarimetry - Analysis tools and applications p 30 A89-15915
- Combining Laplacian images of different spatial frequencies (scales) - Implications for remote sensing image analysis p 68 A89-15919
- On the application of averaging median filters in remote sensing p 68 A89-15920
- Surface identification using satellite microwave radiometers p 79 A89-15922
- Comparison of measured and predicted sea surface spectra of short waves p 45 A89-16981
- Directional measurement of short ocean waves with stereophotography p 45 A89-16982
- Correlation function study for sea ice p 46 A89-16990
- Near surface soil moisture estimation from microwave measurements p 6 A89-17282
- Prediction of leaf chemistry by the use of visible and near infrared reflectance spectroscopy p 7 A89-17283
- An airborne gamma ray snow survey of a forest covered area with a deep snowpack p 7 A89-17284
- Mapping abandoned river channels in Mali through directional filtering of Thematic Mapper data p 58 A89-17285
- Relationship between discoloration and histological changes in leaves of trees affected by forest decline p 7 A89-17286
- Monitoring Wood Stork foraging habitat using remote sensing and geographic information systems p 7 A89-17399
- Remote sensing strategies for global resource exploration and environmental management [IAF PAPER 88-103] p 23 A89-17678
- A typical case of integrated remote sensing center concept - The Nairobi multipurpose reception and processing center [IAF PAPER 88-106] p 80 A89-17679
- Future measurements of rain from space [IAF PAPER 88-112] p 58 A89-17681
- New SPOT generation --- development of remote sensing satellites [IAF PAPER 88-117] p 7 A89-17683
- Wide field high performance lenses --- for Indian remote sensing satellite [IAF PAPER 88-120] p 80 A89-17685
- The image detection subassembly for the SPOT 4 'vegetation' instrument [IAF PAPER 88-121] p 7 A89-17686
- Indian experience in the dissemination and use of remote sensing data and future prospects [IAF PAPER 88-131] p 80 A89-17689
- Status and perspectives of vegetation monitoring by remote sensing [IAF PAPER 88-140] p 8 A89-17693

Project Vasundhara - Multi-theme integration of satellite remote sensing and geological data for regional level mineral prognostics p 31 A89-17694
[IAF PAPER 88-145]
Engineering evaluation of mountain topography exodynamics from remotely sensed data p 31 A89-18707
The potential of using remotely sensed information for studying the contamination and eutrophication of lake systems p 58 A89-18708
The effect of agrometeorological conditions on the characteristics of space radar imagery of agricultural regions in winter p 8 A89-18709
Accounting for selective absorption in the evaluation of the earth surface temperature by an angular method p 80 A89-18710
Estimating concentrations of optically active components from the remotely sensed spectral radiance of a water surface p 58 A89-18711
The effect of snow parameter variations on the thermal microwave emission of the soil-snow-atmosphere system p 59 A89-18712
Estimation of the variability of acoustic characteristics in the region of frontal zones and mesoscale vortices using remote sensing data p 47 A89-18843
Technological constraints on the use of thermal imagery for remote sensing p 81 A89-19173
UN principles on remote sensing - An agreement on economic relations p 90 A89-19385
Landsat Thematic Mapper observations of debris avalanche deposits in the Central Andes p 31 A89-19838
EASCON '88; Proceedings of the Twenty-first Annual Electronics and Aerospace Conference, Arlington, VA, Nov. 9-11, 1988 p 81 A89-20101
Commercialized remote sensing - A comprehensive view for global studies p 81 A89-20102
Business strategies and land remote sensing capabilities p 90 A89-20104
Envirosat - A vehicle for examining the options for earth observations in the 1990's p 81 A89-20105
An enhanced classification approach to change detection in semi-arid environments p 68 A89-20627
Remote sensing of laterized Archaean greenstone terrain - Marshall Pool Area, Northeastern Yilgarn Block, Western Australia p 31 A89-20628
Mapping dominant vegetation communities in the Colorado Rocky Mountain Front Range with Landsat Thematic Mapper and digital terrain data p 8 A89-20629
Shuttered camera - Aerial color video imaging in the visible and near infrared p 8 A89-20630
European remote sensing needs in the 1990s; Proceedings of the Annual Symposium of EARSeL, Noordwijkerhout, Netherlands, May 4-8, 1987 p 90 A89-20701
Radiometric measurements and crop yield forecasting - Some observations over millet and sorghum experimental plots in Mali p 8 A89-20702
Some results of microwave remote sensing research in The Netherlands with a view to land applications in the 1990s p 8 A89-20703
Lowest order correction for solar zenith angle to Global Vegetation Index (GVI) data p 8 A89-20704
Regional land cover and agricultural area statistics and mapping in The Departement Ardeche, France, by use of Thematic Mapper data p 8 A89-20705
Forest classification by principal component analyses of TM data p 8 A89-20706
The use of TM data for the study of a modern deltaic depositional system p 59 A89-20707
Evaluation and digital processing of multispectral SPOT data p 68 A89-20708
Use of Landsat and Seasat data as a tool in kinematic analysis - The Tunisian Atlas p 31 A89-20710
Analysis of large format camera photographs of the Po Delta, Italy, for topographic and thematic mapping p 82 A89-20714
Advances in computerized information retrieval in remote sensing p 69 A89-20717
Geometric correction of remotely-sensed imagery using ground control points and orthogonal polynomials p 82 A89-20718
The Remote Sensing Loosdrecht Lakes project p 59 A89-20719
Regional hydrological systems analysis using satellite remote sensing data and a geographical information system - Application to groundwater modelling of the Roermond area, The Netherlands p 59 A89-20720
Satellite remote sensing and wave studies into the 1990s p 47 A89-20723
Aerial photography for biomass assessment in the intertidal zone p 9 A89-20724
Proceedings of the 4th International Colloquium on Spectral Signatures in Remote Sensing [ESA-SP-287] p 9 A89-10305

Extracting soil and vegetation characteristics from microwave remote sensing data p 9 N89-10306
Coherent polarimetric signatures of coniferous trees: A survey p 9 N89-10307
Measuring in-situ soil surface roughness using a laser profilometer p 9 N89-10308
Microwave backscatter from beets, peas and potatoes throughout the growing season p 9 N89-10309
Complementary of microwave and optical range in the characterization of crops by remote sensing p 10 N89-10310
Evaluation of VARAN data in geology and geomorphology in the southeast of France p 32 N89-10313
A three degree-of-freedom description of the ocean surface for microwave remote sensing of wave height and wind friction velocity p 47 N89-10314
The use of the complex correlation function in the recovery of ocean wave spectra from SAR images p 47 N89-10315
Comparison between active and passive microwave measurements over Antarctica p 48 N89-10316
A perspective on vegetation canopy reflectance models p 10 N89-10317
The spectral bidirectional reflectance of snow p 69 N89-10318
Spectral profile and biomass estimation p 10 N89-10319
Validation of an atmospheric correction method for satellite borne imagery p 82 N89-10320
Retrieving vegetation and soil parameters from radar measurements p 10 N89-10321
A simplified vegetation canopy reflectance and absorption model p 10 N89-10322
Potential number of winter wheat ears estimation using radiometry techniques at an early stage p 10 N89-10323
Introducing spectral data into a plant process model for improving its prediction ability p 10 N89-10324
The angular reflectance signature of the canopy hot spot in the optical regime p 11 N89-10325
A model for radiative transfer in heterogeneous three-dimensional canopies p 11 N89-10326
A simplified reflectance model for shrub canopies p 11 N89-10329
Developing a radiometric leaf area index p 12 N89-10334
Attempt at absolute determination of spectral signatures of bare soils in the thermal infrared, in emission and reflection p 12 N89-10336
Strengths and shortcomings in Airborne Thematic Mapper (ATM) technology as applied to volcanic and geothermal areas in Iceland p 32 N89-10337
Atmospheric correction of thermal infrared data from LANDSAT-5 for surface temperature estimation p 70 N89-10339
Spectral reflectance of sugar beet and winter wheat canopies in the visible and infrared during growth p 12 N89-10342
A theoretical model for interpreting remotely sensed thermal infrared measurements obtained over agricultural areas p 12 N89-10343
An approximative model for the microwave brightness temperature scattered by a rough open ocean surface p 48 N89-10344
Thermal infrared laser spectroscopy: The potential of dual active/passive thermal infrared sensors for Earth observation p 82 N89-10345
Time-resolved laser fluorescence: Trends and applications p 83 N89-10346
A new lidar system for applications over land and sea p 83 N89-10347
Changes in the chlorophyll fluorescence spectra during the Kautsky induction kinetics p 12 N89-10348
Chlorophyll fluorescence spectra of leaves as induced by blue light and red laser light p 12 N89-10349
Laser-induced fluorescence on in-vivo chlorophyll of a rice plant: A technique for the remote detection of plant growth p 12 N89-10350
Techniques for remote sensing of life span and quantum yield of chlorophyll fluorescence in vivo p 13 N89-10351
High-resolution spectroscopy for remote sensing of ocean and atmosphere p 48 N89-10352
The fluorescence line imager: High-resolution imaging spectroscopy over water and land p 83 N89-10353
Use of high spectral resolution to follow the state of vegetation canopies p 13 N89-10354
Stress detection in mixed coniferous-broadleaved forests from Airborne Imaging Spectrometer (AIS) data p 13 N89-10355
A narrow-band thermal imager based on multiline real-time averaging p 83 N89-10356
High spectral resolution indices for monitoring crop growth and chlorosis p 13 N89-10358

Usefulness of high spectral resolution radiometry for geological mapping in the Mediterranean region p 32 N89-10360
Imaging spectrometry applied to the remote sensing of submerged seaweed p 48 N89-10361
Characterization of rocks by visible and infrared high spectral resolution terrain spectroscopy p 32 N89-10362
Comparative analysis of spectral response in the optical domain of targets in a tropical swamp at various spectral and spatial resolutions p 13 N89-10363
Spatial resolution requirements for MODIS-N --- Polar Platform Moderate Resolution Imaging Spectrometer (MODIS) p 83 N89-10364
High resolution radiometric measurement of intertidal microphytobenthos p 48 N89-10365
The basis for the spectral behaviour of silicates in the thermal infrared and applications to remote sensing p 32 N89-10366
Texture analysis in forest areas: High spectral resolution synthetic aperture radar data p 14 N89-10367
Estimation of leaf spectra from measurements in wide spectral bands p 14 N89-10368
Modeling of soil color by remote sensing p 14 N89-10369
The normalization of a soil brightness index for the study of changes in soil conditions p 14 N89-10370
Estimation of primary marine production using spaceborne data on ocean color p 48 N89-10371
Satellite surveillance of ice and snow covered surfaces in the French Alps using visible and near infrared reflectance measurements from the SPOT and LANDSAT Thematic Mapper sensors p 59 N89-10372
Spectral signature of citrus fruits and its evolution: Identification of the vegetative index of least temporal variation p 14 N89-10373
Rock and soil discrimination in natural tropical conditions using a spot-calibrated radiometer p 14 N89-10374
Bathymetry using SPOT imagery of the Casamance (Senegal). First results p 59 N89-10375
Discrimination of zones of high water erosion risk using SPOT images p 15 N89-10376
Emitted short wavelength infrared radiation for detection and monitoring of volcanic activity p 32 N89-10377
Monitoring seasonal variations of soil moisture and vegetation cover using satellite microwave radiometry p 15 N89-10378
Comparative point-spread function calculations for the MOMS-1, Thematic Mapper and SPOT-HRV instruments p 83 N89-10379
The results of the Geosat MOMS subcommittee's data evaluation: Performance and applicability of the MOMS-1 sensor for exploration geology p 33 N89-10380
Design of spectral bands for the German MOMS-2 sensor p 84 N89-10381
The use of MOMS-1 data for geological mapping of the Aswa lineament (East African rift) p 33 N89-10382
MOMS-1 data for bathymetric and geological studies p 33 N89-10383
MOMS-1 used synergistically with LANDSAT TM p 33 N89-10384
Comparative geological evolution of different remote sensing data of the Hoggar Mountains (Algeria) p 33 N89-10385
AGRSAR'86: Contributing to signature research p 15 N89-10387
Aircraft remote sensing in HAPEX --- hydrology p 59 N89-10388
A study of the vegetation cover with AVHRR during HAPEX-MOBILHY p 15 N89-10389
The French space program for Earth observation p 90 N89-10392
NASA's future land remote sensing program p 90 N89-10393
Use of remote sensing for land use policy formulation [NASA-CR-183148] p 15 N89-10395
Remote sensing and hydrologic modeling of arid watersheds: A scale analysis [DE88-014625] p 60 N89-11293
Training activities in remote sensing at the Instituto de Pesquisas Espaciais-INPE/Brazil [INPE-4686-PRE/1380] p 91 N89-11295
Sensors research and technology p 85 N89-11774
Digital processing applied to vegetation [INPE-4695-MD/036] p 17 N89-12107
Method of visual analysis of remote sensing data-vegetation [INPE-4696-MD/037] p 17 N89-12108
Crop separation analysis through SPOT and TM digital data [INPE-4641-PRE/1352] p 18 N89-12110
Remote sensing of earth terrain [NASA-CR-183347] p 85 N89-12111

- Proceedings of the 1988 International Geoscience and Remote Sensing Symposium (IGARSS 1988) on Remote Sensing: Moving Towards the 21st Century, volume 1 [ESA-SP-284-VOL-1] p 85 N89-12936
- Polarization-dependent attenuation of dielectric cylinder arrays p 86 N89-12955
- The use of remote sensing in conjunction with geographic information systems for local planning p 24 N89-12959
- An integrated remote sensing approach for regional agrostistics and land monitoring p 24 N89-12960
- Integrating remote sensing data into a geographical information system: A foundation for rural land use strategies: Nature Conservancy Council project p 24 N89-12964
- An international approach to GIS based on remote sensing and terrain classification --- geographic information system (GIS) p 24 N89-12966
- Analysis of potato crop distribution using remotely sensed and environmental data in a pilot geographical information system p 18 N89-12967
- Spatial resolution for remote sensing of forest plantations p 19 N89-12991
- Relationships between the nitrogen content of grass and reflectance p 19 N89-13002
- The LIMEX 1987 pilot project, LIMEX 1989 and long-term objective for data collection on the Canadian East coast p 52 N89-13037
- Average areal water equivalent of snow in a mountain basin using microwave and visible satellite data p 61 N89-13045
- Microwave remote sensing at the Institute for Space Research (INPE) Brazil: Concepts and future prospects of soil moisture studies p 20 N89-13080
- Important aspects of technology transfer: Training of inservice engineers and scientists; satellite remote sensing p 91 N89-13082
- Applications of remote sensing for geological mapping in eastern Egypt p 35 N89-13087
- Biogeochemical processes in sagebrush steppe: Interactions of terrain, vegetation and chemical cycles [NASA-CR-181486] p 21 N89-13088
- Use of LANDSAT images of vegetation cover to estimate effective hydraulic properties of soils [NASA-CR-183384] p 21 N89-13823
- The California Cooperative Remote Sensing Project [NASA-TM-100073] p 22 N89-13824
- NASA Sea Ice and Snow Validation Program for the DMSP SSM/I: NASA DC-8 flight report [NASA-TM-100706] p 53 N89-13861
- Simulation of radar and surface measurements of rainfall p 62 N89-13924
- Remote sensing information sciences research group [NASA-CR-183374] p 91 N89-14481
- REMOTE SENSORS**
- Advanced airborne electro-optical imager p 74 A89-10929
- The electronically steered thinned array radiometer p 74 A89-10932
- The prospects for detecting spectral shifts due to satellite sensor aging p 6 A89-16061
- Atmospheric effect removal from space imagery p 69 N89-10338
- Multispectral characterization of the spatial structure of remotely sensed scenes p 70 N89-10340
- Optimization for classification of forest damage classes p 13 N89-10359
- Sensors research and technology p 85 N89-11774
- Marine boundary layer depth and relative humidity estimates using multispectral satellite measurements [AD-A196525] p 49 N89-12112
- Effects of changing satellite sensor attributes p 87 N89-13059
- The impact of satellite infrared sea surface temperatures on the FNO (Fleet Numerical Oceanography Center) EOTS (Expanded Ocean Thermal Structure) regional gulf stream analysis [AD-A198965] p 54 N89-13864
- REPORTS**
- Biogeochemical processes in sagebrush steppe: Interactions of terrain, vegetation and chemical cycles [NASA-CR-181486] p 21 N89-13088
- REPRODUCTION (BIOLOGY)**
- Evaluation of technology in the detection and counting of seals p 76 A89-11016
- RESEARCH AIRCRAFT**
- NASA Sea Ice and Snow Validation Program for the DMSP SSM/I: NASA DC-8 flight report [NASA-TM-100706] p 53 N89-13861
- RESOURCES**
- Chemical variability in ocean frontal areas [AD-A198418] p 56 N89-14655
- RESOURCES MANAGEMENT**
- The potentials and challenges afforded by SPOT-1 data p 63 A89-10945
- Applications of multispectral video for natural resource assessment p 63 A89-10968
- Estimation of primary marine production using spaceborne data on ocean color p 48 N89-10371
- Utilizing remote sensing of thematic mapper data to improve our understanding of estuarine processes and their influence on the productivity of estuarine-dependent fisheries [NASA-CR-183409] p 62 N89-13822
- RICE**
- Backscattering coefficient of rice crops and rice fields by an X-band scatterometer p 3 A89-10980
- Laser-induced fluorescence on in-vivo chlorophyll of a rice plant: A technique for the remote detection of plant growth p 12 N89-10350
- RIDGES**
- Somali Basin, Chain Ridge, and origin of the Northern Somali Basin gravity and geoid low p 30 A89-12290
- RIO GRANDE (NORTH AMERICA)**
- Average areal water equivalent of snow in a mountain basin using microwave and visible satellite data p 61 N89-13045
- RIVERS**
- Mapping abandoned river channels in Mali through directional filtering of Thematic Mapper data p 58 A89-17285
- Bathymetry using SPOT imagery of the Casamance (Senegal): First results p 59 N89-10375
- Sapping features of the Colorado Plateau: A comparative planetary geology field guide [NASA-SP-491] p 34 N89-10401
- ROBOTICS**
- EASCON '88; Proceedings of the Twenty-first Annual Electronics and Aerospace Conference, Arlington, VA, Nov. 9-11, 1988 p 81 A89-20101
- ROCKS**
- Desert varnish on volcanic rocks of the Basin and Range province - Composition, morphology, distribution, origin and influence on Landsat imagery p 30 A89-10988
- Characterization of rocks by visible and infrared high spectral resolution terrain spectroscopy p 32 N89-10362
- Rock and soil discrimination in natural tropical conditions using a spot-calibrated radiometer p 14 N89-10374
- ROCKY MOUNTAINS (NORTH AMERICA)**
- Mapping dominant vegetation communities in the Colorado Rocky Mountain Front Range with Landsat Thematic Mapper and digital terrain data p 8 A89-20629
- Average areal water equivalent of snow in a mountain basin using microwave and visible satellite data p 61 N89-13045
- RULES**
- Classification decision rule modification on the basis of information extracted from training data --- satellite imagery p 72 N89-13062
- RURAL LAND USE**
- Integrating remote sensing data into a geographical information system: A foundation for rural land use strategies: Nature Conservancy Council project p 24 N89-12964
- The detection of unimproved grassland in Berkshire using a binary decision tree approach p 18 N89-12988
- Evaluation of LANDSAT TM and SPOT imagery for agricultural land use planning in less developed countries p 19 N89-13051
- S**
- SAHARA DESERT (AFRICA)**
- Applications of remote sensing for geological mapping in eastern Egypt p 35 N89-13087
- SALINITY**
- Passive microwave remote sensing of salinity in coastal zones p 36 A89-10942
- Numerical simulations of the profile properties of undeformed first-year sea ice during the growth season p 40 A89-12171
- SALYUT SPACE STATION**
- A comparative evaluation of use of Landsat MSS FCC and MKF-6M photographs for forest type delineation p 6 A89-14010
- SATELLITE ALTIMETRY**
- Sea level variations in the tropical Pacific during 1985-87 derived from GEOSAT altimetry p 36 A89-10961
- A comparison of reduction methods for satellite altimetry data p 39 A89-11424
- Orbit determination requirements for Topex [AAS PAPER 87-429] p 42 A89-12645
- A preliminary model for Geosat altimeter data errors p 44 A89-13958
- Lidar atmospheric sounder and altimetry for the Earth Observing System (EOS) satellite p 79 A89-15873
- Applications of spaceborne laser ranger on EOS p 79 A89-15878
- Observing the seasonal variability in the tropical Atlantic from altimetry p 46 A89-16987
- Altimetry for non-Gaussian oceans - Height biases and estimation of parameters p 46 A89-16992
- Geodynamics laser ranging system: Performance simulations and development of the EOS facility --- Earth Observing System (EOS) p 28 N89-12982
- SATELLITE ATTITUDE CONTROL**
- Fault tolerant design of attitude and orbit control subsystem for earth resources satellite-1 [AIAA PAPER 88-3879] p 80 A89-18073
- SATELLITE COMMUNICATION**
- Experimental personal satellite communications system using millimeter-wave for Asia-Oceanian region p 81 A89-18736
- EASCON '88; Proceedings of the Twenty-first Annual Electronics and Aerospace Conference, Arlington, VA, Nov. 9-11, 1988 p 81 A89-20101
- SATELLITE DESIGN**
- New SPOT generation --- development of remote sensing satellites [IAF PAPER 88-117] p 7 A89-17683
- TUBSAT-1, satellite technology for educational purposes p 90 N89-10905
- SATELLITE IMAGERY**
- Resolution improvement by multi-temporal data merging p 63 A89-10937
- Remote sensing of suspended sediments in estuaries using atmospheric and compositional corrections to AVHRR data p 57 A89-10940
- The potentials and challenges afforded by SPOT-1 data p 63 A89-10945
- Satellite data analysis for inventorying crops grown in a complex, small-field environment p 1 A89-10951
- GOES I-M image navigation and registration system p 75 A89-10965
- A study of estimation of winter wheat yield for large area using remote sensing method p 2 A89-10974
- Analyses of marine shallow water-bottom features using the Landsat Thematic Mapper, SPOT, and the Large Format Camera p 37 A89-10981
- Improving the detection of human-induced change in west Africa's semi-arid zone using multitemporal Landsat MSS imagery p 64 A89-10983
- Geometric correction of satellite images using composite transformation functions p 64 A89-10986
- Desert varnish on volcanic rocks of the Basin and Range province - Composition, morphology, distribution, origin and influence on Landsat imagery p 30 A89-10988
- Landsat TM and MSS digital data comparison - Imperial Valley --- crop classifications p 3 A89-10989
- SPOT bathymetric image for archeological investigations p 37 A89-10990
- Monitoring vegetation index and biomass production in Southern Greenland based on NOAA-AVHRR data p 3 A89-10993
- Prediction of mesoscale ocean circulation in the Norwegian coastal current p 37 A89-10994
- A new tool - SPOT imagery for studying rapid movements p 64 A89-10996
- Automatic road detection on Landsat 4 TM images p 23 A89-10997
- Improvement of cloud cover assessment of Landsat Thematic Mapper data p 65 A89-11003
- SAR and visible remote sensing of the Taoer River coastal zone at Bohai Bay p 38 A89-11005
- Spectral and spatial characterisation of orchards in New York State using Thematic Mapper Imagery p 4 A89-11008
- Terrain relief and pattern description using digital elevation and Landsat data p 65 A89-11010
- An improved procedure for analysis of change in Thematic Mapper image-pairs p 65 A89-11013
- Real-time environment monitoring using data from Meteosat and NOAA imaging satellites p 23 A89-11730
- Satellite cloud image standardization p 76 A89-11731
- Color-composite image processing for multispectral meteorological satellite data [AD-A199574] p 76 A89-11742
- Phytoplankton standing crops within an Antarctic ice edge assessed by satellite remote sensing p 41 A89-12174
- The effective resolution element of Landsat Thematic Mapper p 65 A89-12220
- Effect of spatial resolution of the statistical properties of satellite images - A case study p 66 A89-12221
- Algorithm for automatic atmospheric corrections to visible and near-IR satellite imagery p 66 A89-12224
- SPOT image quality - Twenty months of experience p 66 A89-12352

Estimating the distribution of grazing and patterns of cattle movement in a large arid zone paddock p 5 A89-12356

The navigation of AVHRR imagery p 66 A89-12357

Evaluating Landsat classification accuracy from forest cover-type maps p 5 A89-12756

The use of polar orbiter data in tropical weather system analysis p 77 A89-12818

The evaluation of simple approaches for the delineation of rain area from satellite imagery p 66 A89-12842

Resolution dependence in satellite imagery - Multifractal analysis p 67 A89-12852

Effects of data resolution on marine stratiform cloud detection using AVHRR and VISSR satellite data p 78 A89-12854

EOF analysis of AVHRR and CZCS imagery p 43 A89-12856

Nimbus-7 SMMR derived sea-ice concentrations over Antarctica p 43 A89-12857

A satellite data processing and analysis software system for earth's atmosphere and surface research p 67 A89-12864

Use of satellite and radar images in operational precipitation nowcasting p 79 A89-13415

Region extraction in SPOT data p 67 A89-14007

SPOT satellite data for pattern recognition on the North American tall-grass prairie Long-Term Ecological Research site p 5 A89-14009

Topographic mapping from SPOT imagery p 67 A89-14088

Combining Laplacian images of different spatial frequencies (scales) - Implications for remote sensing image analysis p 68 A89-15919

On the application of averaging median filters in remote sensing p 68 A89-15920

Extraction of topography from side-looking satellite systems - A case study with SPOT simulation data p 68 A89-16063

The image detection subassembly for the SPOT 4 'vegetation' instrument [IAF PAPER 88-121] p 7 A89-17686

Comparison of SPOT, TM and MSS data for agricultural land-use mapping in Gujarat (India) [IAF PAPER 88-139] p 7 A89-17692

Project Vasundhara - Multi-theme integration of satellite remote sensing and geological data for regional level mineral prognostics [IAF PAPER 88-145] p 31 A89-17694

Application of satellite data for monitoring degradation of tidal wetlands of the Gulf of Kachchh, Western India [IAF PAPER 88-146] p 46 A89-17695

Observation of precipitation using GMS imagery [IAF PAPER 88-151] p 58 A89-17697

Complex experiment on the investigation of the atmosphere pollution using space, aircraft and ground information [IAF PAPER 88-161] p 23 A89-17702

Automated segmentation of pseudoinvariant features from multispectral imagery p 68 A89-17906

Estimating concentrations of optically active components from the remotely sensed spectral radiance of a water surface p 58 A89-18711

Comparison of the spectral information content of Landsat Thematic Mapper and SPOT for three different sites in the Phoenix, Arizona region p 68 A89-20626

An enhanced classification approach to change detection in semi-arid environments p 68 A89-20627

Lowest order correction for solar zenith angle to Global Vegetation Index (GVI) data p 8 A89-20704

Use of Landsat and Seasat data as a tool in kinematic analysis - The Tunisian Atlas p 31 A89-20710

Multi-point matching along vertical lines in SPOT images p 69 A89-20713

Geometric correction of remotely-sensed imagery using ground control points and orthogonal polynomials p 82 A89-20718

Regional hydrological systems analysis using satellite remote sensing data and a geographical information system - Application to groundwater modelling of the Roermond area, The Netherlands p 59 A89-20720

Satellite remote sensing and wave studies into the 1990s p 47 A89-20723

Validation of an atmospheric correction method for satellite borne imagery p 82 A89-10320

Relation between sugar beet crop yield and vegetative indexes calculated from LANDSAT MSS images p 11 A89-10333

Atmospheric effect removal from space imagery p 69 A89-10338

Analysis of directional effects on NOAA AVHRR p 70 A89-10341

Estimation of primary marine production using spaceborne data on ocean color p 48 A89-10371

Satellite surveillance of ice and snow covered surfaces in the French Alps using visible and near infrared reflectance measurements from the SPOT and LANDSAT Thematic Mapper sensors p 59 A89-10372

A study of the vegetation cover with AVHRR during HAPEX-MOBILHY p 15 A89-10389

Use of remote sensing for land use policy formulation [NASA-CR-183148] p 15 A89-10395

Identifying the reforested areas utilizing the SPOT satellite data [INPE-4624-PRE/1343] p 15 A89-10396

Nation-wide forest, mapping and timber volume estimation using LANDSAT-5 TM imagery [INPE-4643-PRE/1354] p 16 A89-10402

Applications of LANDSAT (TM and MSS) data for an estimation of rangeland conditions in semiarid and arid areas of northern Kenya [DFVLR-FB-88-18] p 16 A89-10404

A general data model for geographic information systems [INPE-4560-PRE/1301] p 24 A89-10676

A new radar technique for satellite rainfall algorithm development [NASA-CR-183471] p 60 A89-11102

Technique for obtaining agricultural property boundaries through satellite imagery, certified to control and accompany agricultural activity p 16 A89-11294

Color enhancement of remote sensing imagery using IHS transformations and decorrelation stretch methods [INPE-4559-PRE/1300] p 70 A89-11418

An agricultural crop yield model by satellite: A simulation [INPE-4639-PRE/1350] p 17 A89-12106

The potential of combined use of satellite data with topographic information [NLR-MP-87061-U] p 70 A89-12113

An integrated remote sensing approach for regional agrostistics and land monitoring p 24 A89-12960

Spectral analysis of ocean wave imagery using 2-D linear prediction p 50 A89-12968

Topographic effects on light scattering from snow p 71 A89-12976

Multitemporal resource complex analysis of Catina province, Italy from LANDSAT-TM data p 71 A89-12985

Large area TM land cover classification of Mittlerer Oberrhein County, southwest Germany, and its use for regional planning and crop surveys p 18 A89-12986

Towards an urban land-use classification using textural and morphological criteria p 25 A89-12987

The detection of unimproved grassland in Berkshire using a binary decision tree approach p 18 A89-12988

Detection of seasonal and long-term changes in land cover from multitemporal LANDSAT MSS data p 71 A89-12989

Verification results of MOS-1 multispectral self scanning radiometer (MESSR) data p 86 A89-13004

Performance modeling and results for X-SAR p 71 A89-13009

A regional tectonic study of NE and E Africa and its implication for mineral exploration: A synoptic view from satellite imagery p 34 A89-13023

The interpretation of Icelandic tundra features from LANDSAT-MSS data p 35 A89-13027

Complex SAR imagery and speckle filtering for ERS-1 wave mode p 71 A89-13029

Analysis of Seasat SAR sea-ice data from the Beaufort Sea p 52 A89-13035

Improvement in NOAA-AVHRR snowcover determination for runoff prediction p 61 A89-13040

Snowmelt runoff estimation using snow cover extent data and its application to optimum control of dam water level p 61 A89-13042

Monitoring of seasonal snow cover on glaciers p 61 A89-13044

Microcomputers (PCs) for snow cover analyses using multisensor satellite data p 62 A89-13049

Evaluation of LANDSAT TM and SPOT imagery for agricultural land use planning in less developed countries p 19 A89-13051

Combining spectral and structural analyses to select useful cartographic information from SPOT imagery p 71 A89-13052

Extraction of dense digital elevation models from SPOT stereo imagery p 71 A89-13053

The differential rectification of SPOT HRV panchromatic and multispectral imagery using a digital elevation model p 28 A89-13054

LANDSAT Thematic Mapping (TM) and SPOT HRV for survey mapping of bedrock outcrops p 20 A89-13055

The production of anaglyphs from SPOT-HRV panchromatic data for geomorphological mapping p 72 A89-13056

An evaluation of satellite imagery, LANDSAT Thematic Mapper and SPOT-1 HRV, for grassland inventory in the UK p 20 A89-13057

Monitoring urban change from LANDSAT TM and SPOT satellite imagery by image differencing p 25 A89-13058

Effects of changing satellite sensor attributes p 87 A89-13059

Efficient classification of multispectral images by a best linear discriminant function p 72 A89-13060

A new spatial classification algorithm for high ground resolution images p 72 A89-13061

Classification decision rule modification on the basis of information extracted from training data --- satellite imagery p 72 A89-13062

Accuracy of land cover classification of Thematic Mapper (TM) and SPOT data p 72 A89-13066

The extrapolation of spectral signatures illustrates LANDSAT's potential to detect wetlands p 62 A89-13067

Change direction analysis using LANDSAT imagery: A review of methodology p 72 A89-13068

Building a monitoring system based on satellite data to detect vegetation and land use changes in a subtropical region of Mexico p 20 A89-13079

Important aspects of technology transfer: Training of inservice engineers and scientists; satellite remote sensing p 91 A89-13082

Development of a ground hydrology model suitable for global climate modeling using soil morphology and vegetation cover, and an evaluation of remotely sensed information [NASA-CR-180463] p 21 A89-13821

Use of LANDSAT images of vegetation cover to estimate effective hydraulic properties of soils [NASA-CR-183384] p 21 A89-13823

Binary image classification p 73 A89-13908

Remote sensing technologies and spatial data applications [AD-A195809] p 62 A89-14480

Space shuttle large format camera photography cloud cover interference diagrams [PB88-244405] p 88 A89-14482

Classification and analysis of surface and clouds at high latitudes from AVHRR multispectral satellite data p 89 A89-14635

The design and protocol of a summertime rainfall enhancement program for West Texas p 63 A89-14636

SATELLITE INSTRUMENTS

Operational environmental instrumentation proposed by NOAA and the international community for the NASA and ESA polar orbiting platforms p 36 A89-10964

SATELLITE NETWORKS

An autonomous ocean instrument platform driven vertically by the current [AD-A198226] p 54 A89-13865

SATELLITE OBSERVATION

SeaWiFS - An ocean-imaging sensor p 74 A89-10338

Marine remote sensing and international law p 39 A89-12124

International space law norms regulating remote sensing of the earth from outer space p 89 A89-12126

Using satellite data to aid in diagnosing and forecasting convective development and intensity along arc cloud lines p 76 A89-12810

Assimilation of satellite surface wind speed data using the GLA analysis/forecast system p 77 A89-12811

Tropopause adjustment to tropical cyclones as inferred from satellite ozone observations p 77 A89-12816

Comparison of weather radar and satellite-based passive microwave observations of rainfall over land and oceans p 43 A89-12836

The French space oceanography program p 44 A89-15116

A comparison of satellite and empirical formula techniques for estimating insolation over the oceans p 44 A89-15495

Remote sensing strategies for global resource exploration and environmental management [IAF PAPER 88-103] p 23 A89-17678

Role of absorbed solar radiation on Indian Ocean surface temperature - A case study using satellite data [IAF PAPER 88-155] p 46 A89-17700

Global land-surface primary productivity based upon Nimbus-7 37 GHz data [IAF PAPER 88-159] p 8 A89-17701

The role of linear and ring features in hydrogeology p 31 A89-18705

Working group reports submitted by group chairmen following workshop p 27 A89-12098

Contributions to the GASP workshop proceedings (not presented orally) p 27 A89-12100

A study of accuracy enhancement in satellite magnetic modeling p 28 A89-12102

- Marine boundary layer depth and relative humidity estimates using multispectral satellite measurements [AD-A196525] p 49 N89-12112
- SATELLITE ROTATION**
Simulation of a spinning spacecraft magnetometer p 28 N89-12101
- SATELLITE SOUNDING**
On-board processing and national earth observations centers p 22 A89-10927
A concept for measuring currents from geostationary satellites p 75 A89-10933
Better understanding of intense and tornadic thunderstorms through research using geostationary satellite data p 56 A89-10934
Evapotranspiration monitored from satellites as an indication of shift and impact of vegetation change p 2 A89-10975
Modeling of the dynamic sea surface with satellite altimeter signals p 38 A89-11158
Atmospheric absorption in the VAS split-window channels p 39 A89-11225
A dual-satellite algorithm for deriving sea surface temperature p 41 A89-12209
Using the VAS data utilization center (VDUC) for the analysis and forecasting of heavy rainfall producing mesoscale convective systems (MCSs) p 77 A89-12819
Satellite diagnosis of tropical cyclones p 42 A89-12823
A simple method for estimating monthly mean albedo of land surfaces from AVHRR data p 6 A89-15493
Satellite phasing problems for ocean and atmospheric studies [IAF PAPER 88-152] p 46 A89-17698
The potential of using remotely sensed information for studying the contamination and eutrophication of lake systems p 58 A89-18708
Accounting for selective absorption in the evaluation of the earth surface temperature by an angular method p 80 A89-18710
Sea surface parameters inferred from meteorological satellite data at CMS, Lannion p 47 A89-20722
Satellite remote sensing and wave studies into the 1990s p 47 A89-20723
Marine boundary layer depth and relative humidity estimates using multispectral satellite measurements [AD-A196525] p 49 N89-12112
Rainfall index over oceans derived from SSM/I data --- Special Sensor Microwave/Imager (SSM/I) p 51 N89-12998
Cloud track winds from polar orbiting satellites p 87 N89-13069
Precipitation detection with satellite microwave data [PB88-240239] p 88 N89-13094
- SATELLITE-BORNE INSTRUMENTS**
HIRIS - EOS instrument with high spectral and spatial resolution p 74 A89-10928
Overview of oceanic microwave remote sensing from space p 35 A89-10930
Evaluation of 3.7 micron split windows for estimating surface temperature p 43 A89-12855
VISSR sensor introduced modifications in the presence of large temperature gradients p 78 A89-12860
Surface identification using satellite microwave radiometers p 79 A89-15922
The prospects for detecting spectral shifts due to satellite sensor aging p 6 A89-16061
The image detection subassembly for the SPOT 4 'vegetation' instrument [IAF PAPER 88-121] p 7 A89-17686
The ERS-1 Instrument Data Handling and Transmission subsystem (IDHT) and its evolution [IAF PAPER 88-134] p 80 A89-17690
Technological constraints on the use of thermal imagery for remote sensing p 81 A89-19173
Commercialized remote sensing - A comprehensive view for global studies p 81 A89-20102
Presentations by participants (edited and condensed) p 27 N89-12097
LAWS (Laser Atmospheric Wind Sounder) earth observing system [NASA-TM-101204] p 85 N89-12158
The Airborne Version Conical Scan Radiometer (AVCSR): An airborne radiometer as a tool for satellite data validation p 86 N89-12937
The airborne radiometry experiment (ABREX) instrument, an experimental test bed for the specification of satellite-borne microwave radiometer at 90 GHz p 86 N89-12939
Verification results of MOS-1 multispectral self scanning radiometer (MESSR) data p 86 N89-13004
Performance of a scanning pencil-beam spaceborne scatterometer for ocean wind measurements p 53 N89-13073
The MEOSS experiment: A test case for future cartographic missions p 87 N89-13081

- SATELLITE-BORNE PHOTOGRAPHY**
Acreage and yield determination - 1987 Kansas winter wheat p 4 A89-11007
Recognition of seismically hazardous fault dislocations in space images of the Dushanbe depression p 31 A89-18706
Evaluation of space photographs --- mapping using Metric Camera and Large Format Camera p 82 A89-20715
- SATELLITE-BORNE RADAR**
Design of a spaceborne radar for tropical rain mapping at the climatological scale p 60 N89-12997
- SAUDI ARABIA**
Mapping the distribution and abundance of lithological units and surface mineralogies at Jabal Sa'id, Saudi Arabia: An application of spectral mixture modelling p 34 N89-13024
- SCANNERS**
On the interpretation of integrated water vapor patterns in midlatitude cyclones derived from the Nimbus 7 scanning multichannel microwave radiometer p 76 A89-12790
A pilot study to determine relationships between North Pacific precipitation from Nimbus-7 Scanning Multichannel Microwave Radiometer data and associated atmospheric conditions p 43 A89-12837
- SCANNING**
Possible measurement errors in calibrated AVHRR (Advanced Very High Resolution Radiometer) data [AD-A198342] p 88 N89-14414
- SCATTERING**
Development of a semi-empirical model for estimating the global solar radiation [INPE-4620-TDL/328] p 84 N89-11352
- SCATTERING COEFFICIENTS**
Thunderstorm ice induced brightness temperature depressions at 18, 37, and 92 GHz during Cohmex and their implications for satellite precipitation retrievals p 42 A89-12835
- SCATTERING CROSS SECTIONS**
Constraints on two-scale descriptions of radar backscattering from the sea surface using scatterometer model functions p 49 N89-12945
Millimeter-wave backscatter measurements of various snow forms p 61 N89-13046
- SCATTEROMETERS**
Evolution of the helicopter-borne scatterometer p 37 A89-10971
Wind and wind stress curl fields for the Northeast Pacific Ocean using satellite scatterometer data p 78 A89-12859
X-band scatterometer measurements at low winds in a wavetank p 78 A89-12867
Constraints on two-scale descriptions of radar backscattering from the sea surface using scatterometer model functions p 49 N89-12945
Towards direct variational assimilation of scatterometer backscatter measurements into numerical weather prediction models p 86 N89-13000
Model-based estimation of wind fields over the ocean from wind scatterometer measurements p 53 N89-13070
An analysis of directional ambiguities in wind scatterometer measurements p 87 N89-13071
Multistatic scatterometry p 87 N89-13072
Performance of a scanning pencil-beam spaceborne scatterometer for ocean wind measurements p 53 N89-13073
- SCENE ANALYSIS**
Directional effects on scene complexity in oblique thermal imagery and photographs of a deciduous forest p 4 A89-12261
Multispectral characterization of the spatial structure of remotely sensed scenes p 70 N89-10340
The structure of red-infrared scattergrams of semivegetated landscapes [NASA-CR-183385] p 21 N89-13091
- SCIENTIFIC SATELLITES**
TUBSAT-1, satellite technology for educational purposes p 90 N89-10905
- SEA BREEZE**
Surface windspeed measurements over the ocean with a C-band microwave radiometer p 75 A89-11006
- SEA ICE**
Overview of oceanic microwave remote sensing from space p 35 A89-10930
Mizex '87 - Overview of the Winter Marginal Ice Zone Experiment in the Greenland and Barents Seas p 36 A89-10931
Study of monitoring sea ice using an airborne microwave radiometer system p 37 A89-10972
Variations in the Arctic, Antarctic, and global sea ice covers during 1978-1987 as observed with the Nimbus 7 scanning multichannel microwave radiometer p 38 A89-11145
A three-dimensional coupled ice-ocean model of coastal circulation p 38 A89-11148

- Comparison of Nimbus 7 scanning multichannel microwave radiometer radiance and derived sea ice concentrations with Landsat imagery for the north water area of Baffin Bay p 38 A89-11150
Numerical simulations of the profile properties of undeformed first-year sea ice during the growth season p 40 A89-12171
A numerical study of mesoscale ocean eddy interaction with a marginal ice zone p 41 A89-12172
Phytoplankton standing crops within an Antarctic ice edge assessed by satellite remote sensing p 41 A89-12174
Nimbus-7 SMMR derived sea-ice concentrations over Antarctica p 43 A89-12857
Correlation function study for sea ice p 46 A89-16990
Data report for the Siple Coast (Antarctica) project [NASA-TM-100708] p 49 N89-10403
SAR-seen multimode waves in ice: Evidence of imaging nonlinearities p 50 N89-12971
SAR image statistics related to atmospheric drag over sea ice p 52 N89-13034
Analysis of Seasat SAR sea-ice data from the Beaufort Sea p 52 N89-13035
Microwave dielectric properties of low-salinity sea ice p 52 N89-13036
The LIMEX 1987 pilot project, LIMEX 1989 and long-term objective for data collection on the Canadian East coast p 52 N89-13037
Sea ice type classification of SAR imagery p 52 N89-13039
NASA Sea Ice and Snow Validation Program for the DMSP SSM/I: NASA DC-8 flight report [NASA-TM-100706] p 53 N89-13861
Investigation of radar backscattering from second-year sea ice [NASA-CR-180986] p 54 N89-14479
- SEA LEVEL**
Sea level variations in the tropical Pacific during 1985-87 derived from GEOSAT altimetry p 36 A89-10961
- SEA ROUGHNESS**
The dependence of sea surface slope on atmospheric stability and swell conditions p 45 A89-16983
- SEA STATES**
Modelling of surface waves and sea state-dependent wind stress for the Northeast Pacific Ocean using Seasat scatterometer data p 43 A89-12858
The registration of the surface effects of internal ocean waves using microwave radiometry p 43 A89-13300
- SEA SURFACE TEMPERATURE**
The SeaWiFS sensor for Landsat-6 p 36 A89-10954
Atmospheric absorption in the VAS split-window channels p 39 A89-11225
A dual-satellite algorithm for deriving sea surface temperature p 41 A89-12209
Retrieval of air surface temperatures over oceans from satellite radiance measurements using stratification techniques p 42 A89-12779
An extension of the split window technique for the retrieval of precipitable water - Experimental verification [AD-A199515] p 76 A89-12796
Remote sensing of surface air temperature and humidity over oceanic areas with application to climatology and weather prediction p 42 A89-12798
Evaluation of 3.7 micron split windows for estimating surface temperature p 43 A89-12855
EOF analysis of AVHRR and CZCS imagery p 43 A89-12856
Influence of sea surface temperature on intra- and inter-annual variations of ITCZ --- InterTropical Convergent Zones p 43 A89-12871
Role of absorbed solar radiation on Indian Ocean surface temperature - A case study using satellite data [IAF PAPER 88-155] p 46 A89-17700
Estimation of sea surface temperature via NOAA-AVHRR sensor: Comparison with sea truth data by fixed buoys p 51 N89-13005
The impact of satellite infrared sea surface temperatures on the FNOC (Fleet Numerical Oceanography Center) EOTS (Expanded Ocean Thermal Structure) regional gulf stream analysis [AD-A198965] p 54 N89-13864
- SEA TRUTH**
Estimation of sea surface temperature via NOAA-AVHRR sensor: Comparison with sea truth data by fixed buoys p 51 N89-13005
- SEA WATER**
Numerical simulations of the profile properties of undeformed first-year sea ice during the growth season p 40 A89-12171
- SEALS (ANIMALS)**
Evaluation of technology in the detection and counting of seals p 76 A89-11016

SEAS

The role of horizontal processes in upper-ocean prediction: A forecast simulation in the Sea of Japan
[AD-A198827] p 55 N89-14654

SEASAT SATELLITES

Modelling of surface waves and sea state-dependent wind stress for the Northeast Pacific Ocean using Seasat scatterometer data p 43 N89-12858
Wind and wind stress curl fields for the Northeast Pacific Ocean using satellite scatterometer data p 78 N89-12859

Evaluation of preliminary experiments assimilating Seasat significant wave heights into a spectral wave model p 46 N89-16991
Analysis of Seasat SAR sea-ice data from the Beaufort Sea p 52 N89-13035

SEAWEEDES

Imaging spectrometry applied to the remote sensing of submerged seaweed p 48 N89-10361

SEDIMENT TRANSPORT

Remote sensing and hydrologic modeling of arid watersheds: A scale analysis p 60 N89-11293
[DE88-014625]
Monitoring playas using Thematic Mapper data p 60 N89-13028

SEDIMENTS

Remote sensing of suspended sediments in estuaries using atmospheric and compositional corrections to AVHRR data p 57 N89-10940
High resolution radiometric measurement of intertidal microphytobenthos p 48 N89-10365

SEEPAGE

Sapping features of the Colorado Plateau: A comparative planetary geology field guide
[NASA-SP-491] p 34 N89-10401

SEISMOGRAPHS

Qualitative aspects of seismograph/ocean bottom interaction
[AD-A198652] p 56 N89-14656

SEISMOLOGY

Recognition of seismically hazardous fault dislocations in space images of the Dushanbe depression p 31 N89-18706

SENEGAL

Bathymetry using SPOT imagery of the Casamance (Senegal): First results p 59 N89-10375

SENSITIVITY

Analysis of crop loss for alternative ozone exposure indices
[PB88-214788] p 22 N89-14608

SENSORS

Fiber-optic sensor systems for aerospace applications p 74 N89-10359

SERVICE LIFE

The prospects for detecting spectral shifts due to satellite sensor aging p 6 N89-16061

SHADOWS

Shadows and wedges in scattering from the sea p 49 N89-12946

SHALLOW WATER

Analyses of marine shallow water-bottom features using the Landsat Thematic Mapper, SPOT, and the Large Format Camera p 37 N89-10981

SHORT WAVE RADIATION

Comparison of measured and predicted sea surface spectra of short waves p 45 N89-16981
Sensitivity of satellite-derived net shortwave irradiance at the Earth's surface to radiometric calibration p 82 N89-10335

SHUTTLE IMAGING RADAR

SIR-B view of the Jabal Hadn lineament and its groundwater implications p 29 N89-10976
Comparative geological evolution of different remote sensing data of the Hoggar Mountains (Algeria) p 33 N89-10385
Directional ocean wave spectra: Prospects for acquiring a global data base from SIR-C p 50 N89-12973
The relative utility of LANDSAT MSS and SIR-A imagery in reconnaissance geological mapping in Northern Sudan p 34 N89-13022
The derivation of sub-canopy surface terrain models of coastal forests using synthetic aperture radar p 20 N89-13083

SIDE-LOOKING RADAR

Comparison of wave parameters determined from SLAR images and a pitch and roll buoy p 47 N89-20721

SIGNAL ANALYSIS

The use of the complex correlation function in the recovery of ocean wave spectra from SAR images p 47 N89-10315

SIGNATURE ANALYSIS

An overview of the SAR Internal Wave Signature Experiment p 40 N89-12162
Measurements of surface wave modulations from internal waves during the SAR Internal Wave Signature Experiment p 40 N89-12164

Contrast ratios of internal waves in synthetic aperture radar imagery - A comparison of SAR Internal Wave Signature Experiment observations with theory p 40 N89-12167

The extrapolation of spectral signatures illustrates LANDSATs' potential to detect wetlands p 62 N89-13067

Spectral characterization of forest damage in beech, oak and pine stands p 21 N89-13085

SILICATES

The basis for the spectral behaviour of silicates in the thermal infrared and applications to remote sensing p 32 N89-10366

SIMULATION

Simulation of a spinning spacecraft magnetometer p 28 N89-12101
Simulation of radar and surface measurements of rainfall p 62 N89-13924

SKY RADIATION

Microwave emission and reflection from the wind-roughened sea surface at 6.7 and 18.6 GHz p 44 N89-15923

SNOW

Corrections of surface particle probe measurements for the effects of aspiration p 58 N89-14022
Comparison between active and passive microwave measurements over Antarctica p 48 N89-10316
The spectral bidirectional reflectance of snow p 69 N89-10318
Topographic effects on light scattering from snow p 71 N89-12976
Polarisation of passive microwave signals as indicator of snow water equivalent p 61 N89-13043
Millimeter-wave backscatter measurements of various snow forms p 61 N89-13046

SNOW COVER

Nival-glacial systems and their mapping --- Russian book p 56 N89-10728
Snow and low-cloud discrimination from multispectral satellite measurements p 78 N89-12850
An airborne gamma ray snow survey of a forest covered area with a deep snowpack p 7 N89-17284
The effect of snow parameter variations on the thermal microwave emission of the soil-snow-atmosphere system p 59 N89-18712
Satellite surveillance of ice and snow covered surfaces in the French Alps using visible and near infrared reflectance measurements from the SPOT and LANDSAT Thematic Mapper sensors p 59 N89-10372
Improvement in NOAA-AVHRR snowcover determination for runoff prediction p 61 N89-13040
Snowmelt runoff estimation using snow cover extent data and its application to optimum control of dam water level p 61 N89-13042
Monitoring of seasonal snow cover on glaciers p 61 N89-13044
Average areal water equivalent of snow in a mountain basin using microwave and visible satellite data p 61 N89-13045

Statistics and high resolution imaging of snowpack at 35 GHz using a microcomputer p 61 N89-13047
Snow cover to alter terrain signatures on radar images p 62 N89-13048

Microcomputers (PCs) for snow cover analyses using multisensor satellite data p 62 N89-13049
NASA Sea Ice and Snow Validation Program for the DMSP SSM/I: NASA DC-8 flight report p 53 N89-13861

Remote sensing technologies and spatial data applications
[AD-A195809] p 62 N89-14480

SOFTWARE TOOLS

A satellite data processing and analysis software system for earth's atmosphere and surface research p 67 N89-12864

SOIL EROSION

Soil erosion study using an airborne laser profiler p 1 N89-10952

SOIL MOISTURE

Infrared temperature measurements over bare soil and vegetation - A HAPEX perspective p 2 N89-10953
The use of microwave radiometry in watershed hydrology p 57 N89-10992
Comparison of remote measurements of infrared surface temperatures and microwave soil moisture p 4 N89-11009

Near surface soil moisture estimation from microwave measurements p 6 N89-17282
Monitoring seasonal variations of soil moisture and vegetation cover using satellite microwave radiometry p 15 N89-10378

Microwave remote sensing at the Institute for Space Research (INPE) Brazil: Concepts and future prospects of soil moisture studies p 20 N89-13080

The structure of red-infrared scattergrams of semivegetated landscapes
[NASA-CR-183385] p 21 N89-13091
Remote sensing technologies and spatial data applications
[AD-A195809] p 62 N89-14480

SOIL SCIENCE

Extracting soil and vegetation characteristics from microwave remote sensing data p 9 N89-10306
Modeling of soil color by remote sensing p 14 N89-10369

SOILS

Measuring in-situ soil surface roughness using a laser profilometer p 9 N89-10308
Retrieving vegetation and soil parameters from radar measurements p 10 N89-10321
Attempt at absolute determination of spectral signatures of bare soils in the thermal infrared, in emission and reflection p 12 N89-10336
The normalization of a soil brightness index for the study of changes in soil conditions p 14 N89-10370
Rock and soil discrimination in natural tropical conditions using a spot-calibrated radiometer p 14 N89-10374
Spectral studies of three oxisols and a Ultisol of Brazil [INPE-4644-PRE/1355] p 17 N89-11297
Development of a ground hydrology model suitable for global climate modeling using soil morphology and vegetation cover, and an evaluation of remotely sensed information
[NASA-CR-180463] p 21 N89-13821

SOLAR ENERGY

Development of a semi-empirical model for estimating the global solar radiation
[INPE-4620-TDL/328] p 84 N89-11352

SOLAR POSITION

Lowest order correction for solar zenith angle to Global Vegetation Index (GVI) data p 8 N89-20704

SOLAR RADIATION

A comparison of satellite and empirical formula techniques for estimating insolation over the oceans p 44 N89-15495
Role of absorbed solar radiation on Indian Ocean surface temperature - A case study using satellite data [IAF PAPER 88-155] p 46 N89-17700
Interaction of solar radiation with vegetation [INPE-4697-MD/038] p 17 N89-12109

SOLID PHASES

Chemical variability in ocean frontal areas
[AD-A198418] p 56 N89-14655

SOLITARY WAVES

Analysis of nonlinear internal waves in the New York Bight p 40 N89-12163

SORGHUM

Radiometric measurements and crop yield forecasting - Some observations over millet and sorghum experimental plots in Mali p 8 N89-20702

SPACE BASED RADAR

Design of a spaceborne rain mapping radar [IAF PAPER 88-124] p 58 N89-17688
The effect of agrometeorological conditions on the characteristics of space radar imagery of agricultural regions in winter p 8 N89-18709
Comparison of wave parameters determined from SLAR images and a pitch and roll buoy p 47 N89-20721

SPACE COMMERCIALIZATION

Commercialized remote sensing - A comprehensive view for global studies p 81 N89-20102
Business strategies and land remote sensing capabilities p 90 N89-20104
Review of the requirements for higher level ERS-1 products within Europe [ESA-CR(P)-2586] p 84 N89-10664

SPACE LAW

Principles Relating to Remote Sensing of the Earth from Space - Territorial sphere of application p 89 N89-12121
Marine remote sensing and international law p 39 N89-12124

United Nations activity on remote sensing - Legal and political implications p 89 N89-12125

International space law norms regulating remote sensing of the earth from outer space p 89 N89-12126

UN principles on remote sensing - An agreement on economic relations p 90 N89-19385

SPACE OBSERVATIONS (FROM EARTH)

Very Long Baseline Interferometry (VLBI) from ground and space p 85 N89-11645

SPACE PLATFORMS

Operational environmental instrumentation proposed by NOAA and the international community for the NASA and ESA polar orbiting platforms p 36 N89-10964

SPACE SHUTTLE MISSION 41-B

The results of the Geosat MOMS subcommittee's data evaluation: Performance and applicability of the MOMS-1 sensor for exploration geology p 33 N89-10380

SPACE SHUTTLE PAYLOADS

Comparative point-spread function calculations for the MOMS-1, Thematic Mapper and SPOT-HRV instruments p 83 N89-10379

Design of spectral bands for the German MOMS-2 sensor p 84 N89-10381
MOMS-1 data for bathymetric and geological studies p 33 N89-10383

MOMS-1 used synergistically with LANDSAT TM p 33 N89-10384

Remote Sensing in Polarized Light [NASA-CP-3014] p 88 N89-14189
Space shuttle large format camera photography cloud cover interference diagrams [PB88-244405] p 88 N89-14482

SPACE STATION POLAR PLATFORMS

Earth Observing System - A platform for imaging spectrometers p 74 A89-10332

High Resolution Imaging Spectrometer (HIRIS) p 74 A89-10334
Doppler lidar wind measurements on the EOS - LAWS p 77 A89-12829

The Earth Observing System --- from space using platforms in conjunction with Space Station [IAF PAPER 88-114] p 80 A89-17682

Spatial resolution requirements for MODIS-N --- Polar Platform Moderate Resolution Imaging Spectrometer (MODIS) p 83 N89-10364

SPACE STATIONS

Three-dimensional observation by means of tethered antennae --- for earth observation from space [IAF PAPER 88-118] p 80 A89-17684

SPACEBORNE ASTRONOMY

Very Long Baseline Interferometry (VLBI) from ground and space p 85 N89-11645

SPACEBORNE LASERS

Airborne and spaceborne lasers for terrestrial geophysical sensing; Proceedings of the Meeting, Los Angeles, CA, Jan. 14, 15, 1988 [SPIE-889] p 79 A89-15870

Applications of spaceborne laser ranger on EOS p 79 A89-15878

Laser Atmospheric Wind Sounder (LAWS) p 79 A89-15889

SPACEBORNE PHOTOGRAPHY

The use of MOMS-1 data for geological mapping of the Aswa lineament (East African rift) p 33 N89-10382
MOMS-1 data for bathymetric and geological studies p 33 N89-10383

Comparative geological evolution of different remote sensing data of the Hoggar Mountains (Algeria) p 33 N89-10385

Digital analysis of MOMS-1, LANDSAT TM, and SPOT data of the Nakuru area (Kenya) p 33 N89-10386
Space shuttle large format camera photography cloud cover interference diagrams [PB88-244405] p 88 N89-14482

SPACECRAFT INSTRUMENTS

Imaging spectroscopy II; Proceedings of the Meeting, San Diego, CA, Aug. 20, 21, 1987 [SPIE-834] p 73 A89-10311

Fiber-optic sensor systems for aerospace applications p 74 A89-10359

SPATIAL DISTRIBUTION

A new spatial classification algorithm for high ground resolution images p 72 N89-13061

SPATIAL FILTERING

Applications of spatial postclassification models p 63 A89-10958

SPATIAL RESOLUTION

MODIS - A global ocean facility for the Earth Observing System p 75 A89-10955

The effective resolution element of Landsat Thematic Mapper p 65 A89-12220

Effect of spatial resolution of the statistical properties of satellite images - A case study p 66 A89-12221

Spatial resolution requirements for MODIS-N --- Polar Platform Moderate Resolution Imaging Spectrometer (MODIS) p 83 N89-10364

Spatial resolution for remote sensing of forest plantations p 19 N89-12991

SPECKLE PATTERNS

On the use of speckle statistics for the extraction of ocean wave spectra from SAR imagery p 50 N89-12969

Complex SAR imagery and speckle filtering for ERS-1 wave mode p 71 N89-13029

SPECTRAL BANDS

Design of spectral bands for the German MOMS-2 sensor p 84 N89-10381

SPECTRAL METHODS

Sensor band selection for detecting current defoliation caused by the spruce budworm p 6 A89-16062

Evaluation of preliminary experiments assimilating Seasat significant wave heights into a spectral wave model p 46 A89-16991

SPECTRAL REFLECTANCE

Applications of multispectral video for natural resource assessment p 63 A89-10968

The character of reflective spectrum of winter wheat and the principle of its yield estimation with remote sensing method p 2 A89-10973

Reflectance characteristics of dry plant materials p 3 A89-10977

Atmospheric correction of NS-001 data and extraction of multiple angle reflectance data sets p 64 A89-10998

Estimation of multiple reflection and lowest order adjacency effects on remotely-sensed data p 5 A89-12354

The effects of bark beetle stress on the foliar spectral reflectance of lodgepole pine p 5 A89-12355

The use of spectral reflectance characteristics for the estimation of the wheat crop state p 5 A89-12874

An analytic representation of the synthetic aperture radar image spectrum for ocean waves p 45 A89-16979

Prediction of leaf chemistry by the use of visible and near infrared reflectance spectroscopy p 7 A89-17283

Estimating concentrations of optically active components from the remotely sensed spectral radiance of a water surface p 58 A89-18711

Proceedings of the 4th International Colloquium on Spectral Signatures in Remote Sensing [ESA-SP-287] p 9 N89-10305

Airborne Visible/Infrared Imaging Spectrometer (AVIRIS): Inflight radiometric calibration and the determination of surface reflectance p 83 N89-10357

Comparative analysis of spectral response in the optical domain of targets in a tropical swamp at various spectral and spatial resolutions p 13 N89-10363

Estimation of leaf spectra from measurements in wide spectral bands p 14 N89-10368

Satellite surveillance of ice and snow covered surfaces in the French Alps using visible and near infrared reflectance measurements from the SPOT and LANDSAT Thematic Mapper sensors p 59 N89-10372

Interaction of solar radiation with vegetation [INPE-4697-MD/038] p 17 N89-12109

The structure of red-infrared scattergrams of semivegetated landscapes [NASA-CR-183385] p 21 N89-13091

SPECTRAL RESOLUTION

Imaging spectrometry for water applications p 56 A89-10327

Use of high spectral resolution to follow the state of vegetation canopies p 13 N89-10354

High spectral resolution indices for monitoring crop growth and chlorosis p 13 N89-10358

Usefulness of high spectral resolution radiometry for geological mapping in the Mediterranean region p 32 N89-10360

Color enhancement of remote sensing imagery using IHS transformations and decorrelation stretch methods [INPE-4559-PRE/1300] p 70 N89-11418

SPECTRAL SIGNATURES

Applications of spatial postclassification models p 63 A89-10958

Full-spectrum modeling of synthetic aperture radar internal wave signatures p 40 A89-12166

The prospects for detecting spectral shifts due to satellite sensor aging p 6 A89-16061

Proceedings of the 4th International Colloquium on Spectral Signatures in Remote Sensing [ESA-SP-287] p 9 N89-10305

Extracting soil and vegetation characteristics from microwave remote sensing data p 9 N89-10306

Coherent polarimetric signatures of coniferous trees: A survey p 9 N89-10307

Measuring in-situ soil surface roughness using a laser profilometer p 9 N89-10308

Complementary of microwave and optical range in the characterization of crops by remote sensing p 10 N89-10310

Evaluation of VARAN data in geology and geomorphology in the southeast of France p 32 N89-10313

A three degree-of-freedom description of the ocean surface for microwave remote sensing of wave height and wind friction velocity p 47 N89-10314

The use of the complex correlation function in the recovery of ocean wave spectra from SAR images p 47 N89-10315

Comparison between active and passive microwave measurements over Antarctica p 48 N89-10316

A perspective on vegetation canopy reflectance models p 10 N89-10317

The spectral bidirectional reflectance of snow p 69 N89-10318

Spectral profile and biomass estimation p 10 N89-10319

Validation of an atmospheric correction method for satellite borne imagery p 82 N89-10320

Retrieving vegetation and soil parameters from radar measurements p 10 N89-10321

Potential number of winter wheat ears estimation using radiometry techniques at an early stage p 10 N89-10323

Introducing spectral data into a plant process model for improving its prediction ability p 10 N89-10324

The angular reflectance signature of the canopy hot spot in the optical regime p 11 N89-10325

A model for radiative transfer in heterogeneous three-dimensional canopies p 11 N89-10326

Spectral characterization of forest targets in mountainous zones on Thematic Mapper images p 11 N89-10328

A simplified reflectance model for shrub canopies p 11 N89-10329

Developing a radiometric leaf area index p 12 N89-10334

Attempt at absolute determination of spectral signatures of bare soils in the thermal infrared, in emission and reflection p 12 N89-10336

Strengths and shortcomings in Airborne Thematic Mapper (ATM) technology as applied to volcanic and geothermal areas in Iceland p 32 N89-10337

Atmospheric effect removal from space imagery p 69 N89-10338

Atmospheric correction of thermal infrared data from LANDSAT-5 for surface temperature estimation p 70 N89-10339

Analysis of directional effects on NOAA AVHRR p 70 N89-10341

Spectral reflectance of sugar beet and winter wheat canopies in the visible and infrared during growth p 12 N89-10342

A theoretical model for interpreting remotely sensed thermal infrared measurements obtained over agricultural areas p 12 N89-10343

An approximative model for the microwave brightness temperature scattered by a rough open ocean surface p 48 N89-10344

Thermal infrared laser spectroscopy: The potential of dual active/passive thermal infrared sensors for Earth observation p 82 N89-10345

Time-resolved laser fluorescence: Trends and applications p 83 N89-10346

A new lidar system for applications over land and sea p 83 N89-10347

Changes in the chlorophyll fluorescence spectra during the Kautsky induction kinetics p 12 N89-10348

Chlorophyll fluorescence spectra of leaves as induced by blue light and red laser light p 12 N89-10349

Techniques for remote sensing of life span and quantum yield of chlorophyll fluorescence in vivo p 13 N89-10351

High-resolution spectroscopy for remote sensing of ocean and atmosphere p 48 N89-10352

The fluorescence line imager: High-resolution imaging spectroscopy over water and land p 83 N89-10353

Use of high spectral resolution to follow the state of vegetation canopies p 13 N89-10354

Stress detection in mixed coniferous-broadleaved forests from Airborne Imaging Spectrometer (AIS) data p 13 N89-10355

A narrow-band thermal imager based on multilayer real-time averaging p 83 N89-10356

Airborne Visible/Infrared Imaging Spectrometer (AVIRIS): Inflight radiometric calibration and the determination of surface reflectance p 83 N89-10357

High spectral resolution indices for monitoring crop growth and chlorosis p 13 N89-10358

Optimization for classification of forest damage classes p 13 N89-10359

Usefulness of high spectral resolution radiometry for geological mapping in the Mediterranean region p 32 N89-10360

Imaging spectrometry applied to the remote sensing of submerged seaweed p 48 N89-10361

Characterization of rocks by visible and infrared high spectral resolution terrain spectroscopy p 32 N89-10362

Comparative analysis of spectral response in the optical domain of targets in a tropical swamp at various spectral and spatial resolutions p 13 N89-10363

Spatial resolution requirements for MODIS-N --- Polar Platform Moderate Resolution Imaging Spectrometer (MODIS) p 83 N89-10364

High resolution radiometric measurement of intertidal microphytobenthos p 48 N89-10365

The basis for the spectral behaviour of silicates in the thermal infrared and applications to remote sensing p 32 N89-10366

Texture analysis in forest areas: High spectral resolution synthetic aperture radar data p 14 N89-10367

- Estimation of leaf spectra from measurements in wide spectral bands p 14 N89-10368
Modeling of soil color by remote sensing p 14 N89-10369
- The normalization of a soil brightness index for the study of changes in soil conditions p 14 N89-10370
Estimation of primary marine production using spaceborne data on ocean color p 48 N89-10371
Satellite surveillance of ice and snow covered surfaces in the French Alps using visible and near infrared reflectance measurements from the SPOT and LANDSAT Thematic Mapper sensors p 59 N89-10372
Spectral signature of citrus fruits and its evolution: Identification of the vegetative index of least temporal variation p 14 N89-10373
Rock and soil discrimination in natural tropical conditions using a spot-calibrated radiometer p 14 N89-10374
Bathymetry using SPOT imagery of the Casamance (Senegal). First results p 59 N89-10375
Discrimination of zones of high water erosion risk using SPOT images p 15 N89-10376
Emitted short wavelength infrared radiation for detection and monitoring of volcanic activity p 32 N89-10377
Monitoring seasonal variations of soil moisture and vegetation cover using satellite microwave radiometry p 15 N89-10378
Comparative point-spread function calculations for the MOMS-1, Thematic Mapper and SPOT-HRV instruments p 83 N89-10379
The results of the Geosat MOMS subcommittee's data evaluation: Performance and applicability of the MOMS-1 sensor for exploration geology p 33 N89-10380
MOMS-1 used synergistically with LANDSAT TM p 33 N89-10384
Comparative geological evolution of different remote sensing data of the Hoggar Mountains (Algeria) p 33 N89-10385
AGRISAR'86: Contributing to signature research p 15 N89-10387
Aircraft remote sensing in HAPEX --- hydrology p 59 N89-10388
A study of the vegetation cover with AVHRR during HAPEX-MOBILHY p 15 N89-10389
The French space program for Earth observation p 90 N89-10392
The extrapolation of spectral signatures illustrates LANDSAT's potential to detect wetlands p 62 N89-10367
Spectral characterization of forest damage in beech, oak and pine stands p 21 N89-10385
- SPECTROMETERS**
HIRIS - EOS instrument with high spectral and spatial resolution p 74 N89-10928
- SPECTRUM ANALYSIS**
On the application of averaging median filters in remote sensing p 68 N89-15920
The use of the complex correlation function in the recovery of ocean wave spectra from SAR images p 47 N89-10315
Spectral studies of three oxisols and a Ultisol of Brazil [INPE-4644-PRE/1355] p 17 N89-11297
Spectral analysis of ocean wave imagery using 2-D linear prediction p 50 N89-12968
An intercomparison of SAR and buoy directional wave spectra from the Labrador Sea Extreme Waves Experiment (LEWEX) p 50 N89-12972
Estimating aircraft SAR response characteristics and approximating ocean wave spectra in the Labrador Sea p 52 N89-13032
Combining spectral and structural analyses to select useful cartographic information from SPOT imagery p 71 N89-13052
- SPECULAR REFLECTION**
Comparison of Joint Canada-U.S. Ocean Wave Investigation Project synthetic aperture radar data with internal wave observations and modeling results p 39 N89-12160
- SPIN**
Simulation of a spinning spacecraft magnetometer p 28 N89-12101
- SPOT (FRENCH SATELLITE)**
The potentials and challenges afforded by SPOT-1 data p 63 N89-10945
SPOT bathymetric image for archeological investigations p 37 N89-10990
A new tool - SPOT imagery for studying rapid movements p 64 N89-10996
SPOT image quality - Twenty months of experience p 66 N89-12352
Region extraction in SPOT data p 67 N89-14007
SPOT satellite data for pattern recognition on the North American tall-grass prairie Long-Term Ecological Research site p 5 N89-14009
Topographic mapping from SPOT imagery p 67 N89-14088

- Forest mapping accuracies are improved using a supervised nonparametric classifier with SPOT data p 6 N89-14089
- A typical case of integrated remote sensing center concept - The Nairobi multipurpose reception and processing center p 80 N89-17679
[IAF PAPER 88-106]
New SPOT generation --- development of remote sensing satellites p 7 N89-17683
[IAF PAPER 88-117]
The image detection subassembly for the SPOT 4 'vegetation' instrument p 7 N89-17686
[IAF PAPER 88-121]
Comparison of SPOT, TM and MSS data for agricultural land-use mapping in Gujarat (India) p 7 N89-17692
[IAF PAPER 88-139]
Commercialized remote sensing - A comprehensive view for global studies p 81 N89-20102
Comparison of the spectral information content of Landsat Thematic Mapper and SPOT for three different sites in the Phoenix, Arizona region p 68 N89-20626
Evaluation and digital processing of multispectral SPOT data p 68 N89-20708
Multi-point matching along vertical lines in SPOT images p 69 N89-20713
Complementary of microwave and optical range in the characterization of crops by remote sensing p 10 N89-10310
Biomass and wheat crop yield estimation from SPOT vegetative indexes p 11 N89-10327
Rock and soil discrimination in natural tropical conditions using a spot-calibrated radiometer p 14 N89-10374
Bathymetry using SPOT imagery of the Casamance (Senegal). First results p 59 N89-10375
Discrimination of zones of high water erosion risk using SPOT images p 15 N89-10376
Comparative point-spread function calculations for the MOMS-1, Thematic Mapper and SPOT-HRV instruments p 83 N89-10379
Digital analysis of MOMS-1, LANDSAT TM, and SPOT data of the Nakuru area (Kenya) p 33 N89-10386
Study of the multiplexing of image telemetry data from SPOT 4 HRVIR and Vegetation sensors p 70 N89-10930
[CNES-87/229/CT/DRT/TIT/TR]
Crop separation analysis through SPOT and TM digital data p 18 N89-12110
[INPE-4641-PRE/1352]
The potential of combined use of satellite data with topographic information p 70 N89-12113
[NLR-MP-87061-U]
Agroecological information content of SPOT data p 19 N89-13050
Evaluation of LANDSAT TM and SPOT imagery for agricultural land use planning in less developed countries p 19 N89-13051
Combining spectral and structural analyses to select useful cartographic information from SPOT imagery p 71 N89-13052
Extraction of dense digital elevation models from SPOT stereo imagery p 71 N89-13053
The differential rectification of SPOT HRV panchromatic and multispectral imagery using a digital elevation model p 28 N89-13054
LANDSAT Thematic Mapping (TM) and SPOT HRV for survey mapping of bedrock outcrops p 20 N89-13055
The production of anaglyphs from SPOT-HRV panchromatic data for geomorphological mapping p 72 N89-13056
An evaluation of satellite imagery, LANDSAT Thematic Mapper and SPOT-1 HRV, for grassland inventory in the UK p 20 N89-13057
Monitoring urban change from LANDSAT TM and SPOT satellite imagery by image differencing p 25 N89-13058
Accuracy of land cover classification of Thematic Mapper (TM) and SPOT data p 72 N89-13066
- STATISTICAL ANALYSIS**
Remote sensing and geographic information systems for agricultural statistics-gathering and agricultural monitoring in Morocco p 2 N89-10960
Multispectral characterization of the spatial structure of remotely sensed scenes p 70 N89-10340
Simulation of radar and surface measurements of rainfall p 62 N89-13924
- STATISTICAL DISTRIBUTIONS**
Active modes of the Pacific Intertropical Convergence Zone (ITCZ) p 49 N89-11374
[AD-A196406]
- STATISTICAL TESTS**
On the connection of geodetic point fields in Reseau European Trigonometrique (RETRIG) and related tests for model errors p 28 N89-14485
[ETN-89-93327]
- STEREOPHOTOGRAPHY**
Topographic mapping from SPOT imagery p 67 N89-14088

- Directional measurement of short ocean waves with stereophotography p 45 N89-16982
Extraction of dense digital elevation models from SPOT stereo imagery p 71 N89-13053
- STEREOSCOPY**
Accuracy evaluation of airborne stereo line imager data p 75 N89-10936
- STORMS**
A study of the dynamics of maritime fronts using remotely sensed wind and stress measurements p 84 N89-11366
- STORMS (METEOROLOGY)**
Validation of the on-site Flash Flood Potential System for Nexrad p 57 N89-10949
Using satellite data to aid in diagnosing and forecasting convective development and intensity along arc cloud lines p 76 N89-12810
- STRATIFICATION**
Retrieval of air surface temperatures over oceans from satellite radiance measurements using stratification techniques p 42 N89-12779
- STRATOCUMULUS CLOUDS**
Multispectral satellite analysis of marine stratocumulus cloud microphysics [AD-A197316] p 87 N89-13092
- STRATOSPHERE**
Evolution of polar stratospheric clouds during the Antarctic winter p 55 N89-14534
- STRUCTURAL ANALYSIS**
Multispectral characterization of the spatial structure of remotely sensed scenes p 70 N89-10340
Continuous deformation monitoring with GPS [AD-A196447] p 27 N89-10886
Combining spectral and structural analyses to select useful cartographic information from SPOT imagery p 71 N89-13052
- STRUCTURAL BASINS**
Somali Basin, Chain Ridge, and origin of the Northern Somali Basin gravity and geoid low p 30 N89-12290
Image analysis techniques for the interpretation of airphoto lineaments - Petroleum exploration, Eromanga Basin, Australia p 30 N89-14011
- STRUCTURAL ENGINEERING**
Continuous deformation monitoring with GPS [AD-A196447] p 27 N89-10886
- STRUCTURAL PROPERTIES (GEOLOGY)**
SIR-B view of the Jabal Hadn lineament and its groundwater implications p 29 N89-10976
The role of linear and ring features in hydrogeology p 31 N89-18705
Remote sensing of laterized Archean greenstone terrain - Marshall Pool Area, Northeastern Yilgarn Block, Western Australia p 31 N89-20628
Use of Landsat and Seasat data as a tool in kinematic analysis - The Tunisian Atlas p 31 N89-20710
- SUBURBAN AREAS**
Land cover change detection with Thematic Mapper spectral textural data at the rural-urban fringe p 23 N89-10982
- SUGAR BEETS**
Microwave backscatter from beets, peas and potatoes throughout the growing season p 9 N89-10309
Relation between sugar beet crop yield and vegetative indexes calculated from LANDSAT MSS images p 11 N89-10333
Spectral reflectance of sugar beet and winter wheat canopies in the visible and infrared during growth p 12 N89-10342
- SUNLIGHT**
An agricultural crop yield model by satellite: A simulation [INPE-4639-PRE/1350] p 17 N89-12106
- SUPERHIGH FREQUENCIES**
Complementary of microwave and optical range in the characterization of crops by remote sensing p 10 N89-10310
Performance modeling and results for X-SAR p 71 N89-13009
Polarisation of passive microwave signals as indicator of snow water equivalent p 61 N89-13043
- SURFACE ROUGHNESS**
Measuring in-situ soil surface roughness using a laser profilometer p 9 N89-10308
A numerical model for the computation of radiance distributions in natural waters with wind-roughened surfaces [AD-A197207] p 53 N89-13128
- SURFACE ROUGHNESS EFFECTS**
Effect of soil roughness on SAR images of harvested agricultural fields p 4 N89-11004
X-band scatterometer measurements at low winds in a wavetank p 78 N89-12867
Microwave emission and reflection from the wind-roughened sea surface at 6.7 and 18.6 GHz p 44 N89-15923

- An approximative model for the microwave brightness temperature scattered by a rough open ocean surface p 48 N89-10344
- Inference of geologic surface parameters from polarimetric radar observations and model inversion p 34 N89-12950
- Topographic effects on light scattering from snow p 71 N89-12976

SURFACE TEMPERATURE

- Comparison of remote measurements of infrared surface temperatures and microwave soil moisture p 4 A89-11009
- Look-up tables to convert Landsat TM thermal IR data to water surface temperatures p 67 A89-14012
- Accounting for selective absorption in the evaluation of the earth surface temperature by an angular method p 80 A89-18710
- Atmospheric correction of thermal infrared data from LANDSAT-5 for surface temperature estimation p 70 N89-10339
- A new method for estimating regional evaporation from thermal infrared surface temperature measurements p 60 N89-10390
- The numerical simulation of infrared satellite measurements over the Greenland-Iceland-Norwegian Sea [AD-A198653] p 54 N89-14484

SURFACE VEHICLES

- A new tool - SPOT imagery for studying rapid movements p 64 A89-10996

SURFACE WAVES

- Joint Canada-U.S. Ocean Wave Investigation Project - An overview of the Georgia Strait Experiment p 39 A89-12156
- Microwave scattering from internal wave modulated surface waves - A shipboard real aperture coherent radar study in the Georgia Strait Experiment p 39 A89-12157
- Modulation of radar backscatter from the ocean by a variable surface current p 39 A89-12158
- An overview of the SAR Internal Wave Signature Experiment p 40 A89-12162
- Measurements of surface wave modulations from internal waves during the SAR Internal Wave Signature Experiment p 40 A89-12164
- A comparison of measured surface wave spectral modulations with predictions from a wave-current interaction model p 40 A89-12165
- Directional measurement of short ocean waves with stereophotography p 45 A89-16982
- Feasibility study for the development of a joint surge and wave model [PB88-230917] p 55 N89-14652

SURGES

- Feasibility study for the development of a joint surge and wave model [PB88-230917] p 55 N89-14652

SURVEILLANCE RADAR

- Surveillance radar, a new tool for ice surveillance p 37 A89-10991

SYNCHRONOUS PLATFORMS

- NASA's Earth Science Geostationary Platform p 77 A89-12828

SYNCHRONOUS SATELLITES

- A concept for measuring currents from geostationary satellites p 75 A89-10933
- Better understanding of intense and tornadic thunderstorms through research using geostationary satellite data p 56 A89-10934
- Mid-latitude evaluation of some satellite rainfall estimation techniques p 78 A89-12844
- VISSR sensor introduced modifications in the presence of large temperature gradients p 78 A89-12860
- Observation of precipitation using GMS imagery [IAF PAPER 88-151] p 58 A89-17697

SYNTHETIC APERTURE RADAR

- Does a SAR respond to both phase speed and orbital velocity in ocean sensing? p 36 A89-10947
- Radar applications in remote sensing - An airborne remote sensing case history presented at the Twenty-first International Symposium on Remote Sensing of Environment, Ann Arbor, Michigan, October 26-30, 1987 p 75 A89-10969
- Effect of soil roughness on SAR images of harvested agricultural fields p 4 A89-11004
- Joint Canada-U.S. Ocean Wave Investigation Project - An overview of the Georgia Strait Experiment p 39 A89-12156
- Microwave scattering from internal wave modulated surface waves - A shipboard real aperture coherent radar study in the Georgia Strait Experiment p 39 A89-12157
- Modulation of radar backscatter from the ocean by a variable surface current p 39 A89-12158

- Comparison of Joint Canada-U.S. Ocean Wave Investigation Project synthetic aperture radar data with internal wave observations and modeling results p 39 A89-12160

- An overview of the SAR Internal Wave Signature Experiment p 40 A89-12162
- Analysis of nonlinear internal waves in the New York Bight p 40 A89-12163

- Measurements of surface wave modulations from internal waves during the SAR Internal Wave Signature Experiment p 40 A89-12164

- A comparison of measured surface wave spectral modulations with predictions from a wave-current interaction model p 40 A89-12165

- Full-spectrum modeling of synthetic aperture radar internal wave signatures p 40 A89-12166

- Contrast ratios of internal waves in synthetic aperture radar imagery - A comparison of SAR Internal Wave Signature Experiment observations with theory p 40 A89-12167

- Synthetic aperture radar imaging of ocean waves from an airborne platform - Focus and tracking issues p 41 A89-12173

- Radar polarimetry - Analysis tools and applications p 30 A89-15915

- Tower Ocean Wave and Radar Dependence experiment - An overview p 44 A89-16976

- Theory for synthetic aperture radar imaging of the ocean surface - With application to the Tower Ocean Wave and Radar Dependence experiment on focus, resolution, and wave height spectra p 44 A89-16977

- Multifocus processing of L band synthetic aperture radar images of ocean waves obtained during the Tower Ocean Wave and Radar Dependence experiment p 45 A89-16978

- An analytic representation of the synthetic aperture radar image spectrum for ocean waves p 45 A89-16979

- Three-dimensional observation by means of tethered antennae --- for earth observation from space [IAF PAPER 88-118] p 80 A89-17684

- The use of the complex correlation function in the recovery of ocean wave spectra from SAR images p 47 N89-10315

- Texture analysis in forest areas: High spectral resolution synthetic aperture radar data p 14 N89-10367

- AGRISAR 86: Contributing to signature research p 15 N89-10387

- Modelling of SAR polarisation phase difference from trees p 18 N89-12951

- On the use of speckle statistics for the extraction of ocean wave spectra from SAR imagery p 50 N89-12969

- Ocean wave number spectra and spatial autocorrelation functions from SAR images p 50 N89-12970

- SAR seen multimode waves in ice: Evidence of imaging nonlinearities p 50 N89-12971

- An intercomparison of SAR and buoy directional wave spectra from the Labrador Sea Extreme Waves Experiment (LEWEX) p 50 N89-12972

- Crop classification with multi-temporal X-band SAR data p 19 N89-12990

- Performance modeling and results for X-SAR p 71 N89-13009

- A synthetic apertures radar with multichannel and multipolarisation p 87 N89-13017

- Complex SAR imagery and speckle filtering for ERS-1 wave mode p 71 N89-13029

- Estimating aircraft SAR response characteristics and approximating ocean wave spectra in the Labrador Sea p 52 N89-13032

- Phase versus orbital velocity in SAR wave imaging: Paradox lost p 52 N89-13033

- SAR image statistics related to atmospheric drag over sea ice p 52 N89-13034

- Analysis of Seasat SAR sea-ice data from the Beaufort Sea p 52 N89-13035

- Sea ice type classification of SAR imagery p 52 N89-13039

- The derivation of sub-canopy surface terrain models of coastal forests using synthetic aperture radar p 20 N89-13083

SYSTEMS SIMULATION

- Geodynamics laser ranging system: Performance simulations and development of the EOS facility --- Earth Observing System (EOS) p 28 N89-12982

T

TECHNOLOGICAL FORECASTING

- European remote sensing needs in the 1990s; Proceedings of the Annual Symposium of EARSeL, Noordwijkerhout, Netherlands, May 4-8, 1987 p 90 A89-20701

- Some results of microwave remote sensing research in The Netherlands with a view to land applications in the 1990s p 8 A89-20703

TECHNOLOGY ASSESSMENT

- Large area TM land cover classification of Mittlerer Oberrhein County, southwest Germany, and its use for regional planning and crop surveys p 18 N89-12986
- Verification results of MOS-1 multispectral self scanning radiometer (MESSR) data p 86 N89-13004
- The reliability utility of LANDSAT MSS and SIR-A imagery in reconnaissance geological mapping in Northern Sudan p 34 N89-13022

TECHNOLOGY UTILIZATION

- Technological constraints on the use of thermal imagery for remote sensing p 81 A89-19173

TECTONICS

- Determination of convergence rates across the Ventura Basin, Southern California, using GPS and historical triangulation [NASA-CR-183014] p 29 N89-14624

TELEMETRY

- Multispectral satellite analysis of marine stratocumulus cloud microphysics [AD-A197316] p 87 N89-13092

- The impact of satellite infrared sea surface temperatures on the FNOC (Fleet Numerical Oceanography Center) EOTS (Expanded Ocean Thermal Structure) regional gulf stream analysis [AD-A198965] p 54 N89-13864

- Possible measurement errors in calibrated AVHRR (Advanced Very High Resolution Radiometer) data [AD-A198342] p 88 N89-14414

TELEPHONY

- EASCON '88; Proceedings of the Twenty-first Annual Electronics and Aerospace Conference, Arlington, VA, Nov. 9-11, 1988 p 81 A89-20101

TEMPERATE REGIONS

- On the interpretation of integrated water vapor patterns in midlatitude cyclones derived from the Nimbus 7 scanning multichannel microwave radiometer p 76 A89-12790
- Building a monitoring system based on satellite data to detect vegetation and land use changes in a subtropical region of Mexico p 20 N89-13079

TEMPERATURE DISTRIBUTION

- The impact of satellite infrared sea surface temperatures on the FNOC (Fleet Numerical Oceanography Center) EOTS (Expanded Ocean Thermal Structure) regional gulf stream analysis [AD-A198965] p 54 N89-13864

TEMPERATURE GRADIENTS

- The impact of satellite infrared sea surface temperatures on the FNOC (Fleet Numerical Oceanography Center) EOTS (Expanded Ocean Thermal Structure) regional gulf stream analysis [AD-A198965] p 54 N89-13864

TEMPERATURE MEASUREMENT

- Infrared temperature measurements over bare soil and vegetation - A HAPEX perspective p 2 A89-10953
- Comparison of remote measurements of infrared surface temperatures and microwave soil moisture p 4 A89-11009

- A dual-satellite algorithm for deriving sea surface temperature p 41 A89-12209

- Atmospheric correction of thermal infrared data from LANDSAT-5 for surface temperature estimation p 70 N89-10339

- Emitted short wavelength infrared radiation for detection and monitoring of volcanic activity p 32 N89-10377

- A new method for estimating regional evaporation from thermal infrared surface temperature measurements p 60 N89-10390

- Estimation of sea surface temperature via NOAA-AVHRR sensor: Comparison with sea truth data by fixed buoys p 51 N89-13005

TERRAIN

- An international approach to GIS based on remote sensing and terrain classification --- geographic information system (GIS) p 24 N89-12966

- Snow cover to alter terrain signatures on radar images p 62 N89-13048

- Extraction of dense digital elevation models from SPOT stereo imagery p 71 N89-13053

- The derivation of sub-canopy surface terrain models of coastal forests using synthetic aperture radar p 20 N89-13083

- Terrain relief and pattern description using digital elevation and Landsat data p 65 A89-11010

- Applications of digital image processing to ongoing research in complex terrain meteorology p 65 A89-11743

- Segmentation of remotely-sensed images by a split-and-merge process p 66 A89-12222

- A procedure for modeling the terrain relief by using digitized topographic maps p 67 A89-14005

- Remote sensing of earth terrain
[NASA-CR-183347] p 85 N89-12111
- TERRESTRIAL RADIATION**
Summary of along-track data from the earth radiation budget satellite for several representative ocean regions [NASA-RP-1206] p 55 N89-14634
- TETHERED SATELLITES**
Three-dimensional observation by means of tethered antennae --- for earth observation from space [IAF PAPER 88-118] p 80 A89-17684
- TEXAS**
The design and protocol of a summertime rainfall enhancement program for West Texas p 63 N89-14636
- TEXTURES**
Automatic control point determination for image registration using texture analysis methods p 3 A89-10985
Texture analysis in forest areas: High spectral resolution synthetic aperture radar data p 14 N89-10367
Towards an urban land-use classification using textural and morphological criteria p 25 N89-12987
- THEMATIC MAPPERS (LANDSAT)**
Thematic Mapper data screening and external effects correction p 64 A89-10978
Land cover change detection with Thematic Mapper spectral textural data at the rural-urban fringe p 23 A89-10982
Detection of forest damage on Whiteface Mountain, New York, using Landsat Thematic Mapper data p 3 A89-10987
Automatic road detection on Landsat 4 TM images p 23 A89-10997
Improvement of cloud cover assessment of Landsat Thematic Mapper data p 65 A89-11003
The effective resolution element of Landsat Thematic Mapper p 65 A89-12220
Look-up tables to convert Landsat TM thermal IR data to water surface temperatures p 67 A89-14012
Mapping abandoned river channels in Mali through directional filtering of Thematic Mapper data p 58 A89-17285
Monitoring Wood Stork foraging habitat using remote sensing and geographic information systems p 7 A89-17399
Landsat Thematic Mapper observations of debris avalanche deposits in the Central Andes p 31 A89-19838
Comparison of the spectral information content of Landsat Thematic Mapper and SPOT for three different sites in the Phoenix, Arizona region p 68 A89-20626
Mapping dominant vegetation communities in the Colorado Rocky Mountain Front Range with Landsat Thematic Mapper and digital terrain data p 8 A89-20629
Regional land cover and agricultural area statistics and mapping in The Departement Ardeche, France, by use of Thematic Mapper data p 8 A89-20705
Forest classification by principal component analyses of TM data p 8 A89-20706
The use of TM data for the study of a modern deltaic depositional system p 59 A89-20707
Mineral exploration along the Aqaba-Levant structure by use of TM-data - Concepts, processing and results p 31 A89-20709
Tests of topographic mapping with Thematic Mapper images p 69 A89-20712
Interpretation and geometrical aspects of Thematic Mapper data p 69 A89-20716
Spectral characterization of forest targets in mountainous zones on Thematic Mapper images p 11 N89-10328
Atmospheric correction of thermal infrared data from LANDSAT-5 for surface temperature estimation p 70 N89-10339
Comparative point-spread function calculations for the MOMS-1, Thematic Mapper and SPOT-HRV instruments p 83 N89-10379
MOMS-1 used synergistically with LANDSAT TM p 33 N89-10384
Comparative geological evolution of different remote sensing data of the Hoggar Mountains (Algeria) p 33 N89-10385
Digital analysis of MOMS-1, LANDSAT TM, and SPOT data of the Nakuru area (Kenya) p 33 N89-10386
Applications of LANDSAT (TM and MSS) data for an estimation of rangeland conditions in semiarid and arid areas of northern Kenya [DFVLR-FB-88-18] p 16 N89-10404
Multitemporal resource complex analysis of Catania province, Italy from LANDSAT-TM data p 71 N89-12985
Mapping the distribution and abundance of lithological units and surface mineralogies at Jabal Sa'id, Saudi Arabia: An application of spectral mixture modelling p 34 N89-13024

- The need for volcano monitoring and the ability to detect activity using emitted short wavelength infrared p 34 N89-13025
- Monitoring playas using Thematic Mapper data p 60 N89-13028
- Evaluation of LANDSAT TM and SPOT imagery for agricultural land use planning in less developed countries p 19 N89-13051
- LANDSAT Thematic Mapping (TM) and SPOT HRV for survey mapping of bedrock outcrops p 20 N89-13055
- An evaluation of satellite imagery, LANDSAT Thematic Mapper and SPOT-1 HRV, for grassland inventory in the UK p 20 N89-13057
- Monitoring urban change from LANDSAT TM and SPOT satellite imagery by image differencing p 25 N89-13058
- The classification of semi-natural vegetation from LANDSAT Thematic Mapper imagery: A user's perspective p 21 N89-13084
- Biogeochemical processes in sagebrush steppe: Interactions of terrain, vegetation and chemical cycles [NASA-CR-181486] p 21 N89-13088
- THEMATIC MAPPING**
Imaging spectrometry as a tool for botanical mapping p 73 A89-10324
Photogrammetric Week, 41st, Universitaet Stuttgart, Federal Republic of Germany, Sept. 14-19, 1987, Proceedings p 63 A89-10611
Nival-glacial systems and their mapping --- Russian book p 56 A89-10728
Spectral and spatial characterisation of orchards in New York State using Thematic Mapper Imagery p 4 A89-11008
An improved procedure for analysis of change in Thematic Mapper image-pairs p 65 A89-11013
Geological mapping and mineral exploration in eastern Nova Scotia utilizing airborne and spaceborne multisensor data p 30 A89-14008
Forest mapping accuracies are improved using a supervised nonparametric classifier with SPOT data p 6 A89-14089
Invertible canopy reflectance modeling of vegetation structure in semiarid woodland p 6 A89-15918
Comparison of SPOT, TM and MSS data for agricultural land-use mapping in Gujarat (India) [IAF PAPER 88-139] p 7 A89-17692
Engineering evaluation of mountain topography exodynamics from remotely sensed data p 31 A89-18707
Mapping dominant vegetation communities in the Colorado Rocky Mountain Front Range with Landsat Thematic Mapper and digital terrain data p 8 A89-20629
Analysis of large format camera photographs of the Po Delta, Italy, for topographic and thematic mapping p 82 A89-20714
Strengths and shortcomings in Airborne Thematic Mapper (ATM) technology as applied to volcanic and geothermal areas in Iceland p 32 N89-10337
Nation-wide forest mapping and timber volume estimation using LANDSAT-5 TM imagery [INPE-4643-PRE/1354] p 16 N89-10402
Working group reports submitted by group chairmen following workshop p 27 N89-12098
Working group on studies of the lithosphere: Recommendations p 27 N89-12099
Crop separation analysis through SPOT and TM digital data [INPE-4641-PRE/1352] p 18 N89-12110
The potential of combined use of satellite data with topographic information p 70 N89-12113
Large area TM land cover classification of Mittlerer Oberrhein County, southwest Germany, and its use for regional planning and crop surveys p 18 N89-12986
Mapping the distribution and abundance of lithological units and surface mineralogies at Jabal Sa'id, Saudi Arabia: An application of spectral mixture modelling p 34 N89-13024
Agroecological information content of SPOT data p 19 N89-13050
LANDSAT Thematic Mapping (TM) and SPOT HRV for survey mapping of bedrock outcrops p 20 N89-13055
The production of anaglyphs from SPOT-HRV panchromatic data for geomorphological mapping p 72 N89-13056
Effects of changing satellite sensor attributes p 87 N89-13059
Cotton area mapping using multitemporal satellite data integrated within a geographical information system applied to a cotton boll weevil control programme in Paraguay p 20 N89-13077
Applications of remote sensing for geological mapping in eastern Egypt p 35 N89-13087

THERMAL ANALYSIS

- The impact of satellite infrared sea surface temperatures on the FNOC (Fleet Numerical Oceanography Center) EOTS (Expanded Ocean Thermal Structure) regional gulf stream analysis [AD-A198965] p 54 N89-13864

THERMAL EMISSION

- The effect of snow parameter variations on the thermal microwave emission of the soil-snow-atmosphere system p 59 A89-18712

THERMAL MAPPING

- Comparison of remote measurements of infrared surface temperatures and microwave soil moisture p 4 A89-11009
Surface identification using satellite microwave radiometers p 79 A89-15922
Geometric correction of remotely-sensed imagery using ground control points and orthogonal polynomials p 82 A89-20718

THREE AXIS STABILIZATION

- Fault tolerant design of attitude and orbit control subsystem for earth resources satellite-1 [AIAA PAPER 88-3679] p 80 A89-18073

THREE DIMENSIONAL MODELS

- A three-dimensional coupled ice-ocean model of coastal circulation p 38 A89-11148
Satellite microwave rainfall simulations with a three-dimensional dynamical cloud model p 77 A89-12833

THUNDERSTORMS

- Better understanding of intense and tornadic thunderstorms through research using geostationary satellite data p 56 A89-10934
Thunderstorm ice induced brightness temperature depressions at 18, 37, and 92 GHz during Cohmex and their implications for satellite precipitation retrievals p 42 A89-12835

TIDAL FLATS

- Application of satellite data for monitoring degradation of tidal wetlands of the Gulf of Kachchh, Western India [IAF PAPER 88-146] p 46 A89-17695

TIDES

- Evaluation of GEOSAT (Geodetic Satellite) data and application to variability of the northeast Pacific Ocean [AD-A198950] p 53 N89-13863
Feasibility study for the development of a joint surge and wave model [PB88-230917] p 55 N89-14652

TIMBER IDENTIFICATION

- Forest classification by principal component analyses of TM data p 8 A89-20706

TIMBER INVENTORY

- Operational use of Landsat data for timber inventory p 2 A89-10970
Simplified forest inventory using large-scale 70-mm photography and tariff tables p 6 A89-14090
Nation-wide forest mapping and timber volume estimation using LANDSAT-5 TM imagery [INPE-4643-PRE/1354] p 16 N89-10402
- TIMBER VIGOR**
Imaging spectrometry as a tool for botanical mapping p 73 A89-10324
Detection of forest damage on Whiteface Mountain, New York, using Landsat Thematic Mapper data p 3 A89-10987
Evaluation of a multispectral linear array sensor for assessing juvenile stand conditions p 3 A89-11000
Sensor band selection for detecting current defoliation caused by the spruce budworm p 6 A89-16062
Relationship between discoloration and histological changes in leaves of trees affected by forest decline p 7 A89-17286

TIME LAG

- Phase versus orbital velocity in SAR wave imaging: Paradox lost p 52 N89-13033

TIME SERIES ANALYSIS

- Time series of European baselines determined with Lageos p 26 A89-17945
Active modes of the Pacific Intertropical Convergence Zone (ITCZ) [AD-A196406] p 49 N89-11374

TOPEX

- Orbit determination requirements for Topex [AAS PAPER 87-429] p 42 A89-12645

TOPOGRAPHY

- A procedure for modeling the terrain relief by using digitized topographic maps p 67 A89-14005
Topographic mapping from SPOT imagery p 67 A89-14088
Extraction of topography from side-looking satellite systems - A case study with SPOT simulation data p 68 A89-16063
Tests of topographic mapping with Thematic Mapper images p 69 A89-20712

U

- Analysis of large format camera photographs of the Po Delta, Italy, for topographic and thematic mapping p 82 A89-20714
- The potential of combined use of satellite data with topographic information [NLR-MP-87061-U] p 70 A89-12113
- Topographic effects on light scattering from snow p 71 A89-12976
- TORNADOES**
- Better understanding of intense and tornadic thunderstorms through research using geostationary satellite data p 56 A89-10934
- TOTAL OZONE MAPPING SPECTROMETER**
- Tropopause adjustment to tropical cyclones as inferred from satellite ozone observations p 77 A89-12816
- TRANSMISSION**
- An autonomous ocean instrument platform driven vertically by the current [AD-A198226] p 54 A89-13865
- TRANSMITTANCE**
- A numerical model for the computation of radiance distributions in natural waters with wind-roughened surfaces [AD-A197207] p 53 A89-13128
- TREES (MATHEMATICS)**
- The detection of unimproved grassland in Berkshire using a binary decision tree approach p 18 A89-12988
- TREES (PLANTS)**
- Reflectance characteristics of dry plant materials p 3 A89-10977
- Modelling of SAR polarisation phase difference from trees p 18 A89-12951
- Spectral characterization of forest damage in beech, oak and pine stands p 21 A89-13085
- TRENDS**
- Climate tracking with remote sensing p 75 A89-10943
- TRIANGULATION**
- On the connection of geodetic point fields in Réseau European Trigonometrique (RETRIG) and related tests for model errors [ETN-89-93327] p 28 A89-14485
- Determination of convergence rates across the Ventura Basin, Southern California, using GPS and historical triangulation [NASA-CR-183014] p 29 A89-14624
- TROPICAL METEOROLOGY**
- The development of tropical cyclones in the north-west of Australia p 41 A89-12203
- Tropopause adjustment to tropical cyclones as inferred from satellite ozone observations p 77 A89-12816
- The use of polar orbiter data in tropical weather system analysis p 77 A89-12818
- Satellite diagnosis of tropical cyclones p 42 A89-12823
- Evaluation of 3.7 micron split windows for estimating surface temperature p 43 A89-12855
- Future measurements of rain from space [IAF PAPER 88-112] p 58 A89-17681
- Design of a spaceborne rain mapping radar [IAF PAPER 88-124] p 58 A89-17688
- Design of a spaceborne radar for tropical rain mapping at the climatological scale p 60 A89-12997
- TROPICAL REGIONS**
- Sea level variations in the tropical Pacific during 1985-87 derived from GEOSAT altimetry p 36 A89-10961
- Geosat crossover analysis in the tropical Pacific. I - Constrained sinusoidal crossover adjustment p 38 A89-11143
- Observing the seasonal variability in the tropical Atlantic from altimetry p 46 A89-16987
- Comparative analysis of spectral response in the optical domain of targets in a tropical swamp at various spectral and spatial resolutions p 13 A89-10363
- Rock and soil discrimination in natural tropical conditions using a spot-calibrated radiometer p 14 A89-10374
- Building a monitoring system based on satellite data to detect vegetation and land use changes in a subtropical region of Mexico p 20 A89-13079
- TROPOPAUSE**
- Tropopause adjustment to tropical cyclones as inferred from satellite ozone observations p 77 A89-12816
- TROPOSPHERE**
- Atmospheric absorption in the VAS split-window channels p 39 A89-11225
- TUNDRA**
- The interpretation of Icelandic tundra features from LANDSAT-MSS data p 35 A89-13027
- TURBULENT MIXING**
- Mass and heat balances in the upper ocean p 53 A89-13089

ULTRAHIGH FREQUENCIES

- Multifocus processing of L band synthetic aperture radar images of ocean waves obtained during the Tower Ocean Wave and Radar Dependence experiment p 45 A89-16978

ULTRALIGHT AIRCRAFT

- Small format air photo from ultrahigh aircraft as an aid for data collection of agricultural statistics in Sahelian countries p 19 A89-13003

ULTRAVIOLET PHOTOGRAPHY

- Evaluation of technology in the detection and counting of seals p 76 A89-11016

UNDERWATER ACOUSTICS

- Qualitative aspects of seismograph/ocean bottom interaction [AD-A198652] p 56 A89-14656

UNDERWATER RESOURCES

- Imaging spectrometry applied to the remote sensing of submerged seaweed p 48 A89-10361

UNITED NATIONS

- UN principles on remote sensing - An agreement on economic relations p 90 A89-19385

UNIX (OPERATING SYSTEM)

- Improvement and extension of a radar forest backscattering model [NASA-CR-183259] p 16 A89-11292

URBAN DEVELOPMENT

- Environmental impact of the urban growth on the Western Sao Paulo metropolitan area [INPE-4670-PRE/1370] p 23 A89-10413

URBAN PLANNING

- The use of remote sensing in conjunction with geographic information systems for local planning p 24 A89-12959
- Towards an urban land-use classification using textural and morphological criteria p 25 A89-12987

URBAN RESEARCH

- Monitoring urban change from LANDSAT TM and SPOT satellite imagery by image differencing p 25 A89-13058

USER MANUALS (COMPUTER PROGRAMS)

- User's guide for the Nimbus 7 Scanning Multichannel Microwave Radiometer (SMMR) CELL-ALL tape [NASA-RP-1210] p 89 A89-14648

USER REQUIREMENTS

- European remote sensing needs in the 1990s; Proceedings of the Annual Symposium of EARSeL, Noordwijkerhout, Netherlands, May 4-8, 1987 p 90 A89-20701
- Review of the requirements for higher level ERS-1 products within Europe [ESA-CR(P)-2586] p 84 A89-10664
- Requirements for ongoing development of the Pilot Land Data System (PLDS) p 24 A89-12958

V

VEGETATION

- Infrared temperature measurements over bare soil and vegetation - A HAPEX perspective p 2 A89-10953
- Evapotranspiration monitored from satellites as an indication of shift and impact of vegetation change p 2 A89-10975
- Land cover change detection with Thematic Mapper spectral textural data at the rural-urban fringe p 23 A89-10982
- The use of microwave radiometry in watershed hydrology p 57 A89-10992
- Estimating the distribution of grazing and patterns of cattle movement in a large arid zone paddock p 5 A89-12356
- Radar polarimetry - Analysis tools and applications p 30 A89-15915
- New SPOT generation --- development of remote sensing satellites [IAF PAPER 88-117] p 7 A89-17683
- Status and perspectives of vegetation monitoring by remote sensing [IAF PAPER 88-140] p 8 A89-17693
- Mapping dominant vegetation communities in the Colorado Rocky Mountain Front Range with Landsat Thematic Mapper and digital terrain data p 8 A89-20629
- Extracting soil and vegetation characteristics from microwave remote sensing data p 9 A89-10306
- Retrieving vegetation and soil parameters from radar measurements p 10 A89-10321
- Monitoring seasonal variations of soil moisture and vegetation cover using satellite microwave radiometry p 15 A89-10378
- Method of visual analysis of remote sensing data-vegetation [INPE-4696-MD/037] p 17 A89-12108

- Modelling land resources within a pilot geographical information system p 18 A89-12962
- Building a monitoring system based on satellite data to detect vegetation and land use changes in a subtropical region of Mexico p 20 A89-13079
- The classification of semi-natural vegetation from LANDSAT Thematic Mapper imagery: A user's perspective p 21 A89-13084

VEGETATIVE INDEX

- Monitoring vegetation index and biomass production in Southern Greenland based on NOAA-AVHRR data p 3 A89-10993
- Relative water content of Spruce needles determined by the leaf water content index p 4 A89-11012
- Lowest order correction for solar zenith angle to Global Vegetation Index (GVI) data p 8 A89-20704
- Introducing spectral data into a plant process model for improving its prediction ability p 10 A89-10324
- Biomass and wheat crop yield estimation from SPOT vegetative indexes p 11 A89-10327
- Estimation of the interception efficiency of an alfalfa canopy from a vegetative index p 11 A89-10332
- Relation between sugar beet crop yield and vegetative indexes calculated from LANDSAT MSS images p 11 A89-10333

- Spectral signature of citrus fruits and its evolution: Identification of the vegetative index of least temporal variation p 14 A89-10373

- A study of the vegetation cover with AVHRR during HAPEX-MOBILHY p 15 A89-10389

- The Transformed Vegetation Index (TVI) for estimation of Brazilian cerrado's phytomass [INPE-4603-PRE/1326] p 15 A89-10400

- The structure of red-infrared scattergrams of semivegetated landscapes [NASA-CR-183385] p 21 A89-13091

- Development of a ground hydrology model suitable for global climate modeling using soil morphology and vegetation cover, and an evaluation of remotely sensed information [NASA-CR-180463] p 21 A89-13821

- Use of LANDSAT images of vegetation cover to estimate effective hydraulic properties of soils [NASA-CR-183384] p 21 A89-13823

VELOCITY MEASUREMENT

- Phase versus orbital velocity in SAR wave imaging: Paradox lost p 52 A89-13033

VERTICAL MOTION

- An autonomous ocean instrument platform driven vertically by the current [AD-A198226] p 54 A89-13865

VERY LONG BASE INTERFEROMETRY

- The Crustal Dynamics Project p 25 A89-13757
- Geodesy by radio interferometry - Determination of vector motions for sites in the western United States p 25 A89-13759

- NASA/Crustal Dynamics Project geodetic data analysis p 25 A89-13760

- Distribution of relative plate motion along the Pacific-North American plate boundary determined from mobile VLBI measurements p 26 A89-13761

- VLBI geodesy - 2 parts-per-billion precision in length determinations for transcontinental baselines p 26 A89-13762

- VLBI studies of the nutations of the earth p 26 A89-13764

- Very Long Baseline Interferometry (VLBI) from ground and space p 85 A89-11645

- Very Long Baseline Interferometry (VLBI): Relativity and geodesy [ETN-89-93337] p 29 A89-14493

VIDEO DATA

- Land and forest cover information from aerial video p 1 A89-10946

- Shuttered camera - Aerial color video imaging in the visible and near infrared p 8 A89-20630

VIDEO EQUIPMENT

- Applications of multispectral video for natural resource assessment p 63 A89-10968

VISIBLE INFRARED SPIN SCAN RADIOMETER

- Using the VAS data utilization center (VDUC) for the analysis and forecasting of heavy rainfall producing mesoscale convective systems (MCSs) p 77 A89-12819

- The addition of visible channel data to satellite infrared rain estimation schemes p 78 A89-12839

- Variation of satellite rain relationships in space and time p 67 A89-12843

- Comparison of satellite IR rain estimates with radar rain observations in hurricanes p 57 A89-12845

- Effects of data resolution on marine stratiform cloud detection using AVHRR and VISSR satellite data p 78 A89-12854

VISUAL OBSERVATION

Digital image processing and visual communications technologies in meteorology; Proceedings of the Meeting, Cambridge, MA, Oct. 27, 28, 1987
[SPIE-846] p 65 A89-11726

VISUAL PERCEPTION

Method of visual analysis of remote sensing data-vegetation
[INPE-4696-MD/037] p 17 N89-12108
A numerical model for the computation of radiance distributions in natural waters with wind-roughened surfaces
[AD-A197207] p 53 N89-13128

VOLCANOES

Desert varnish on volcanic rocks of the Basin and Range province - Composition, morphology, distribution, origin and influence on Landsat imagery p 30 A89-10988
Landsat Thematic Mapper observations of debris avalanche deposits in the Central Andes p 31 A89-19838

VOLCANOLOGY

Strengths and shortcomings in Airborne Thematic Mapper (ATM) technology as applied to volcanic and geothermal areas in Iceland p 32 N89-10337
Emitted short wavelength infrared radiation for detection and monitoring of volcanic activity p 32 N89-10377
The need for volcano monitoring and the ability to detect activity using emitted short wavelength infrared p 34 N89-13025

VORTICES

A numerical study of mesoscale ocean eddy interaction with a marginal ice zone p 41 A89-12172
Estimation of the variability of acoustic characteristics in the region of frontal zones and mesoscale vortices using remote sensing data p 47 A89-18843

W**WATER CIRCULATION**

Prediction of mesoscale ocean circulation in the Norwegian coastal current p 37 A89-10994
Estimation of the variability of acoustic characteristics in the region of frontal zones and mesoscale vortices using remote sensing data p 47 A89-18843

WATER COLOR

Estimation of primary marine production using spaceborne data on ocean color p 48 N89-10371

WATER DEPTH

SPOT bathymetric image for archeological investigations p 37 A89-10990

WATER EROSION

Discrimination of zones of high water erosion risk using SPOT images p 15 N89-10376

WATER MANAGEMENT

Utilization of Landsat data and a geographic information system (GIS) for improving watershed management in India p 57 A89-11014
Snowmelt runoff estimation using snow cover extent data and its application to optimum control of dam water level p 61 N89-13042

WATER POLLUTION

The potential of using remotely sensed information for studying the contamination and eutrophication of lake systems p 58 A89-18708

WATER QUALITY

Imaging spectrometry for water applications p 56 A89-10327
Laser fluorosensing of water quality - A review p 57 A89-10941
The Remote Sensing Loosdrecht Lakes project p 59 A89-20719

WATER RUNOFF

Improvement in NOAA-AVHRR snowcover determination for runoff prediction p 61 N89-13040
Snowmelt runoff estimation using snow cover extent data and its application to optimum control of dam water level p 61 N89-13042

WATER TEMPERATURE

Look-up tables to convert Landsat TM thermal IR data to water surface temperatures p 67 A89-14012

WATER VAPOR

On the interpretation of integrated water vapor patterns in midlatitude cyclones derived from the Nimbus 7 scanning multichannel microwave radiometer p 76 A89-12790
An example of estimates of precipitable water derived from Nimbus-7 SMMR satellite measurements and FGGE upper air data p 42 A89-12792
An extension of the split window technique for the retrieval of precipitable water - Experimental verification [AD-A199515] p 76 A89-12796
Verification of the accuracy of a network of water-vapor radiometers p 86 N89-12941

WATER WAVES

Joint Canada-U.S. Ocean Wave Investigation Project - An overview of the Georgia Strait Experiment p 39 A89-12156

Microwave scattering from internal wave modulated surface waves - A shipboard real aperture coherent radar study in the Georgia Strait Experiment p 39 A89-12157

Modulation of radar backscatter from the ocean by a variable surface current p 39 A89-12158
Comparison of Joint Canada-U.S. Ocean Wave Investigation Project synthetic aperture radar data with internal wave observations and modeling results p 39 A89-12160

An overview of the SAR Internal Wave Signature Experiment p 40 A89-12162
Analysis of nonlinear internal waves in the New York Bight p 40 A89-12163

Measurements of surface wave modulations from internal waves during the SAR Internal Wave Signature Experiment p 40 A89-12164
Full-spectrum modeling of synthetic aperture radar internal wave signatures p 40 A89-12166
Contrast ratios of internal waves in synthetic aperture radar imagery - A comparison of SAR Internal Wave Signature Experiment observations with theory p 40 A89-12167

Synthetic aperture radar imaging of ocean waves from an airborne platform - Focus and tracking issues p 41 A89-12173
Modelling of surface waves and sea state-dependent wind stress for the Northeast Pacific Ocean using Seasat scatterometer data p 43 A89-12858

The registration of the surface effects of internal ocean waves using microwave radiometry p 43 A89-13300
Tower Ocean Wave and Radar Dependence experiment - An overview p 44 A89-16976
Theory for synthetic aperture radar imaging of the ocean surface - With application to the Tower Ocean Wave and Radar Dependence experiment on focus, resolution, and wave height spectra p 44 A89-16977

Multifocus processing of L band synthetic aperture radar images of ocean waves obtained during the Tower Ocean Wave and Radar Dependence experiment p 45 A89-16978
An analytic representation of the synthetic aperture radar image spectrum for ocean waves p 45 A89-16979
Comparison of measured and predicted sea surface spectra of short waves p 45 A89-16981

Directional measurement of short ocean waves with stereophotography p 45 A89-16982
Wind stress measurements during the Tower Ocean Wave and Radar Dependence experiment p 45 A89-16984
Coastally trapped waves in the presence of a shelf edge density front p 46 A89-16989
Evaluation of preliminary experiments assimilating Seasat significant wave heights into a spectral wave model p 46 A89-16991

Altimetry for non-Gaussian oceans - Height biases and estimation of parameters p 46 A89-16992
Comparison of wave parameters determined from SLAR images and a pitch and roll buoy p 47 A89-20721
Satellite remote sensing and wave studies into the 1990s p 47 A89-20723
A three degree-of-freedom description of the ocean surface for microwave remote sensing of wave height and wind friction velocity p 47 N89-10314

The use of the complex correlation function in the recovery of ocean wave spectra from SAR images p 47 N89-10315
Spectral analysis of ocean wave imagery using 2-D linear prediction p 50 N89-12968
On the use of speckle statistics for the extraction of ocean wave spectra from SAR imagery p 50 N89-12969

Ocean wave number spectra and spatial autocorrelation functions from SAR images p 50 N89-12970
SAR-seen multimode waves in ice: Evidence of imaging nonlinearities p 50 N89-12971
An intercomparison of SAR and buoy directional wave spectra from the Labrador Sea Extreme Waves Experiment (LEWEX) p 50 N89-12972

Directional ocean wave spectra: Prospects for acquiring a global data base from SIR-C p 50 N89-12973
The Labrador Sea Extreme Waves Experiment: Objectives, status and plans p 51 N89-12974
Complex SAR imagery and speckle filtering for ERS-1 wave mode p 71 N89-13029
Some characteristics of short ocean waves as microwave scatterers p 51 N89-13030
Modulation of the radar backscatter from the ocean surface by a long gravity wave p 51 N89-13031

Estimating aircraft SAR response characteristics and approximating ocean wave spectra in the Labrador Sea p 52 N89-13032
Phase versus orbital velocity in SAR wave imaging: Paradox lost p 52 N89-13033
Feasibility study for the development of a joint surge and wave model [PB88-230917] p 55 N89-14652

WATERSHEDS

The use of microwave radiometry in watershed hydrology p 57 A89-10992
Utilization of Landsat data and a geographic information system (GIS) for improving watershed management in India p 57 A89-11014
Remote sensing and hydrologic modeling of arid watersheds: A scale analysis [DE88-014625] p 60 N89-11293

WAVE INTERACTION

Joint Canada-U.S. Ocean Wave Investigation Project - An overview of the Georgia Strait Experiment p 39 A89-12156
A comparison of measured surface wave spectral modulations with predictions from a wave-current interaction model p 40 A89-12165
Feasibility study for the development of a joint surge and wave model [PB88-230917] p 55 N89-14652

WAVE REFLECTION

Microwave emission and reflection from the wind-roughened sea surface at 6.7 and 18.6 GHz p 44 A89-15923

WEATHER FORECASTING

Validation of the on-site Flash Flood Potential System for Nexrad p 57 A89-10949
Remote sensing of surface air temperature and humidity over oceanic areas with application to climatology and weather prediction p 42 A89-12798
Using satellite data to aid in diagnosing and forecasting convective development and intensity along arc cloud lines p 76 A89-12810
Assimilation of satellite surface wind speed data using the GLA analysis/forecast system p 77 A89-12811
PRISM B (Prediction of the Indian Summer Monsoon - Bellevue) [IAF PAPER ST-88-02] p 58 A89-17873

WEDGES

Shadows and wedges in scattering from the sea p 49 N89-12946

WELLS

Development of Alaskan gas hydrate resources [DE88-010270] p 35 N89-13093

WETLANDS

Remote sensing of estuaries - An overview p 56 A89-10939
Application of satellite data for monitoring degradation of tidal wetlands of the Gulf of Kachchh, Western India [IAF PAPER 88-146] p 46 A89-17695
The extrapolation of spectral signatures illustrates LANDSATs' potential to detect wetlands p 62 N89-13067

WHEAT

The character of reflective spectrum of winter wheat and the principle of its yield estimation with remote sensing method p 2 A89-10973
A study of estimation of winter wheat yield for large area using remote sensing method p 2 A89-10974
Acreage and yield determination - 1987 Kansas winter wheat p 4 A89-11007
The use of spectral reflectance characteristics for the estimation of the wheat crop state p 5 A89-12874
Potential number of winter wheat ears estimation using radiometry techniques at an early stage p 10 N89-10323
Biomass and wheat crop yield estimation from SPOT vegetative indexes p 11 N89-10327
Spectral reflectance of sugar beet and winter wheat canopies in the visible and infrared during growth p 12 N89-10342

WIDE ANGLE LENSES

Wide field high performance lenses --- for Indian remote sensing satellite [IAF PAPER 88-120] p 80 A89-17685

WIND DIRECTION

An analysis of directional ambiguities in wind scatterometer measurements p 87 N89-13071

WIND EFFECTS

Modelling of surface waves and sea state-dependent wind stress for the Northeast Pacific Ocean using Seasat scatterometer data p 43 A89-12858
Wind and wind stress curl fields for the Northeast Pacific Ocean using satellite scatterometer data p 78 A89-12859

Comparison between active and passive microwave measurements over Antarctica p 48 N89-10316
The Labrador Sea Extreme Waves Experiment: Objectives, status and plans p 51 N89-12974

WIND MEASUREMENT

Doppler lidar wind measurements on the EOS - LAWS p 77 A89-12829

SUBJECT INDEX

X RAY IMAGERY

A three degree-of-freedom description of the ocean surface for microwave remote sensing of wave height and wind friction velocity p 47 N89-10314
A study of the dynamics of maritime fronts using remotely sensed wind and stress measurements p 84 N89-11366
Cloud track winds from polar orbiting satellites p 87 N89-13069
Model-based estimation of wind fields over the ocean from wind scatterometer measurements p 53 N89-13070
An analysis of directional ambiguities in wind scatterometer measurements p 87 N89-13071
Performance of a scanning pencil-beam spaceborne scatterometer for ocean wind measurements p 53 N89-13073

WIND PROFILES

Assimilation of satellite surface wind speed data using the GLA analysis/forecast system p 77 A89-12811
Doppler lidar wind measurements on the EOS - LAWS p 77 A89-12829
Laser Atmospheric Wind Sounder (LAWS) p 79 A89-15889
LAWS (Laser Atmospheric Wind Sounder) earth observing system [NASA-TM-101204] p 85 N89-12158

WIND VARIATIONS

The role of horizontal processes in upper-ocean prediction: A forecast simulation in the Sea of Japan [AD-A198827] p 55 N89-14654

WIND VELOCITY

A comparison of measured surface wave spectral modulations with predictions from a wave-current interaction model p 40 A89-12165
Full-spectrum modeling of synthetic aperture radar internal wave signatures p 40 A89-12166
Assimilation of satellite surface wind speed data using the GLA analysis/forecast system p 77 A89-12811

WIND VELOCITY MEASUREMENT

Surface windspeed measurements over the ocean with a C-band microwave radiometer p 75 A89-11006

WINTER

Mizex '87 - Overview of the Winter Marginal Ice Zone Experiment in the Greenland and Barents Seas p 36 A89-10931
Evolution of polar stratospheric clouds during the Antarctic winter p 55 N89-14534

WOOD

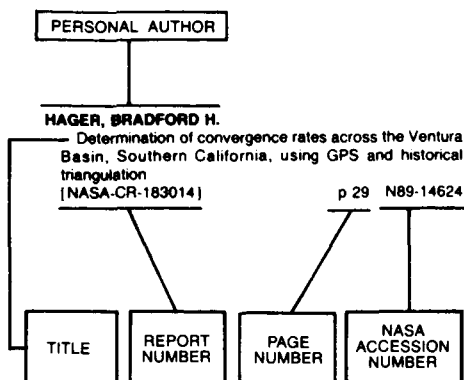
Invertible canopy reflectance modeling of vegetation structure in semiarid woodland p 6 A89-15918

X

X RAY IMAGERY

Backscattering coefficient of rice crops and rice fields by an X-band scatterometer p 3 A89-10980

Typical Personal Author Index Listing



Listings in this index are arranged alphabetically by personal author. The title of the document provides the user with a brief description of the subject matter. The report number helps to indicate the type of document listed (e.g., NASA report, translation, NASA contractor report). The page and accession numbers are located beneath and to the right of the title. Under any one author's name the accession numbers are arranged in sequence with the AIAA accession numbers appearing first.

A

- ABEDNEGO, B.**
The normalization of a soil brightness index for the study of changes in soil conditions p 14 N89-10370
- ABER, JOHN D.**
Estimation of forest canopy characteristics and nitrogen cycling using imaging spectrometry p 1 A89-10325
Prediction of leaf chemistry by the use of visible and near infrared reflectance spectroscopy p 7 A89-17283
- ADENIYI, PETER O.**
Improving the detection of human-induced change in west Africa's semi-arid zone using multitemporal Landsat MSS imagery p 64 A89-10983
An enhanced classification approach to change detection in semi-arid environments p 68 A89-20627
- ADIGA, S.**
Indian experience in the dissemination and use of remote sensing data and future prospects [IAF PAPER 88-131] p 80 A89-17689
- ADLER, ROBERT F.**
Satellite microwave rainfall simulations with a three-dimensional dynamical cloud model p 77 A89-12833
The addition of visible channel data to satellite infrared rain estimation schemes p 78 A89-12839
Comparison of satellite IR rain estimates with radar rain observations in hurricanes p 57 A89-12845
- AHEARN, SEAN C.**
Combining Laplacian images of different spatial frequencies (scales) - Implications for remote sensing image analysis p 68 A89-15919
- AHERN, F. J.**
Evaluation of a multispectral linear array sensor for assessing juvenile stand conditions p 3 A89-11000
The effects of bark beetle stress on the foliar spectral reflectance of lodgepole pine p 5 A89-12355
- AKHAVI, M. S.**
Geological mapping and mineral exploration in eastern Nova Scotia utilizing airborne and spaceborne multisensor data p 30 A89-14008
- AL-NASER, ABDULLAH H.**
SIR-B view of the Jabal Hadn lineament and its groundwater implications p 29 A89-10976

- AL-SARI, A.**
Mapping the distribution and abundance of lithological units and surface mineralogies at Jabal Sa'id, Saudi Arabia: An application of spectral mixture modelling p 34 N89-13024
- ALEM, E. M.**
Characterization of rocks by visible and infrared high spectral resolution terrain spectroscopy p 32 N89-10362
- ALEXANDER, TIMOTHY M.**
Envirostat - A vehicle for examining the options for earth observations in the 1990's p 81 A89-20105
- ALFORD, WILLIAM L.**
LANDSAT-4 and LANDSAT-5 multispectral scanner coherent noise characterization and removal [NASA-TP-2595-REV] p 85 N89-12114
- ALI, M. M.**
Role of absorbed solar radiation on Indian Ocean surface temperature - A case study using satellite data [IAF PAPER 88-155] p 46 A89-17700
- ALI, SHARAFAT**
Utilization of Landsat data and a geographic information system (GIS) for improving watershed management in India p 57 A89-11014
- ALISHOUSE, JOHN C.**
Comparison of weather radar and satellite-based passive microwave observations of rainfall over land and oceans p 43 A89-12836
Evaluation of 3.7 micron split windows for estimating surface temperature p 43 A89-12855
- ALLAN, T. D.**
A comparison of reduction methods for satellite altimetry data p 39 A89-11424
- ALLARIO, FRANK**
Airborne and spaceborne lasers for terrestrial geophysical sensing; Proceedings of the Meeting, Los Angeles, CA, Jan. 14, 15, 1988 [SPIE-889] p 79 A89-15870
- ALLEN, ROBERT C.**
Snow and low-cloud discrimination from multispectral satellite measurements p 78 A89-12850
- ALLEWIJN, R.**
Regional hydrological systems analysis using satellite remote sensing data and a geographical information system - Application to groundwater modelling of the Roermond area, The Netherlands p 59 A89-20720
- ALLEY, R. E.**
Airborne Visible/Infrared Imaging Spectrometer (AVIRIS): Inflight radiometric calibration and the determination of surface reflectance p 83 N89-10357
- ALLIRAND, J. M.**
Estimation of the interception efficiency of an alfalfa canopy from a vegetative index p 11 N89-10332
- AMAYENC, P.**
Design of a spaceborne rain mapping radar [IAF PAPER 88-124] p 58 A89-17688
Design of a spaceborne radar for tropical rain mapping at the climatological scale p 60 N89-12997
- AMILHAT, ISABELLE**
PRISM B (Prediction of the Indian Summer Monsoon - Bellevue) [IAF PAPER ST-88-02] p 58 A89-17873
- AMIRKHANOVA, F. SH.**
The role of linear and ring features in hydrogeology p 31 A89-18705
- ANDERE, D. K.**
A typical case of integrated remote sensing center concept - The Nairobi multipurpose reception and processing center [IAF PAPER 88-106] p 80 A89-17679
- ANDERSON, M.**
Comparison between active and passive microwave measurements over Antarctica p 48 N89-10316
- ANDERSON, MARK R.**
A pilot study to determine relationships between North Pacific precipitation from Nimbus-7 Scanning Multichannel Microwave Radiometer data and associated atmospheric conditions p 43 A89-12837
- ANDRE, JEAN-CLAUDE**
Evaporation over land surfaces - First results from HAPEX-MOBILHY Special Observing Period p 57 A89-12211

- ANDRIEU, B.**
Relation between sugar beet crop yield and vegetative indexes calculated from LANDSAT MSS images p 11 N89-10333
Estimation of leaf spectra from measurements in wide spectral bands p 14 N89-10368
- ANTIKIDIS, J.-P.**
A typical case of integrated remote sensing center concept - The Nairobi multipurpose reception and processing center [IAF PAPER 88-106] p 80 A89-17679
- APEL, J. R.**
An overview of the SAR Internal Wave Signature Experiment p 40 A89-12162
- ARCONE, S. A.**
Correlation function study for sea ice p 46 A89-16990
- ARIMOTO, YOSHINORI**
Experimental personal satellite communications system using millimeter-wave for Asia-Oceanian region p 81 A89-18736
- ARKANI-HAMED, J.**
Geophysical interpretation of the magnetic anomalies of China derived from Magsat data p 26 A89-20200
- ARNASON, K.**
Strengths and shortcomings in Airborne Thematic Mapper (ATM) technology as applied to volcanic and geothermal areas in Iceland p 32 N89-10337
- ARNAUD, M.**
New SPOT generation [IAF PAPER 88-117] p 7 A89-17683
- ASANUMA, ICHIO**
Microwave emission and reflection from the wind-roughened sea surface at 6.7 and 18.6 GHz p 44 A89-15923
- ATKINSON, P. M.**
Spatial resolution for remote sensing of forest plantations p 19 N89-12991
- ATLAS, R.**
Assimilation of satellite surface wind speed data using the GLA analysis/forecast system p 77 A89-12811
- AUSTIN, G. L.**
VISSR sensor introduced modifications in the presence of large temperature gradients p 78 A89-12860
- AXELSSON, S.**
Atmospheric correction of thermal infrared data from LANDSAT-5 for surface temperature estimation p 70 N89-10339
- AYABE, K.**
Data collection system operating on Japan's first marine observation satellite: Inflight evaluation of the system performance p 87 N89-13007

B

- BABBEDGE, NORMAN H.**
Review of the requirements for higher level ERS-1 products within Europe [ESA-CR(P)-2586] p 84 N89-10664
- BACKHAUS, R.**
Status and perspectives of vegetation monitoring by remote sensing [IAF PAPER 88-140] p 8 A89-17693
- BAKER, MICHAEL**
Integrating remotely sensed data into PC-based geographic information systems p 23 A89-10959
- BALICK, LEE K.**
Directional effects on scene complexity in oblique thermal imagery and photographs of a deciduous forest p 4 A89-12261
- BALLEW, G. I.**
The results of the Geosat MOMS subcommittee's data evaluation: Performance and applicability of the MOMS-1 sensor for exploration geology p 33 N89-10380
- BALTUCK, M.**
NASA's future land remote sensing program p 90 N89-10393
- BANNINGER, C.**
Stress detection in mixed coniferous-broadleaved forests from Airborne Imaging Spectrometer (AIS) data p 13 N89-10355

BARBARO, A.

A new lidar system for applications over land and sea p 83 N89-10347

BARET, F.

Complementary of microwave and optical range in the characterization of crops by remote sensing p 10 N89-10310

Spectral profile and biomass estimation p 10 N89-10319

A simplified vegetation canopy reflectance and absorption model p 10 N89-10322

Use of high spectral resolution to follow the state of vegetation canopies p 13 N89-10354

Estimation of leaf spectra from measurements in wide spectral bands p 14 N89-10368

BARIL, D.

Discrimination of zones of high water erosion risk using SPOT images p 15 N89-10376

BARNES, W. L.

MODIS - A global ocean facility for the Earth Observing System p 75 A89-10955

BARTHOLOME, E.

Evapotranspiration monitored from satellites as an indication of shift and impact of vegetation change p 2 A89-10975

BARTHOLOME, E.

Small format air photo from ultrahigh aircraft as an aid for data collection of agricultural statistics in Sahelian countries p 19 N89-13003

BARTHOLOME, ETIENNE

Radiometric measurements and crop yield forecasting - Some observations over millet and sorghum experimental plots in Mali p 8 A89-20702

BARTOLUCCI, LUIS A.

Look-up tables to convert Landsat TM thermal IR data to water surface temperatures p 67 A89-14012

BARTON, IAN J.

Atmospheric absorption in the VAS split-window channels p 39 A89-11225

BATES, J.

A satellite data processing and analysis software system for earth's atmosphere and surface research p 67 A89-12864

BAUDOT, Y.

Towards an urban land-use classification using textural and morphological criteria p 25 N89-12987

BAUFAYS, C.

A three degree-of-freedom description of the ocean surface for microwave remote sensing of wave height and wind friction velocity p 47 N89-10314

An approximative model for the microwave brightness temperature scattered by a rough open ocean surface p 48 N89-10344

BAUMANN, ROBERT H.

Utilizing remote sensing of thematic mapper data to improve our understanding of estuarine processes and their influence on the productivity of estuarine-dependent fisheries [NASA-CR-183409] p 62 N89-13822

BAUMGARTNER, M. F.

Microcomputers (PCs) for snow cover analyses using multisensor satellite data p 62 N89-13049

BEAL, R. C.

Directional ocean wave spectra: Prospects for acquiring a global data base from SIR-C p 50 N89-12973

The Labrador Sea Extreme Waves Experiment: Objectives, status and plans p 51 N89-12974

BEARDSLEY, R. C.

Modelling of surface waves and sea state-dependent wind stress for the Northeast Pacific Ocean using Seasat scatterometer data p 43 A89-12858

Wind and wind stress curl fields for the Northeast Pacific Ocean using satellite scatterometer data p 78 A89-12859

BEAUMONT, T. E.

Cotton area mapping using multitemporal satellite data integrated within a geographical information system applied to a cotton boll weevil control programme in Paraguay p 20 N89-13077

BECKER, F.

A theoretical model for interpreting remotely sensed thermal infrared measurements obtained over agricultural areas p 12 N89-10343

BECKER, FRANCOIS

Evaporation over land surfaces - First results from HAPEX-MOBILHY Special Observing Period p 57 A89-12211

BEGNI, GERARD

SPOT image quality - Twenty months of experience p 66 A89-12352

BEGUE, A.

Analysis of directional effects on NOAA AVHRR p 70 N89-10341

BEHR, F. J.

Design of spectral bands for the German MOMS-2 sensor p 84 N89-10381

BEHRE, S. M.

A regional tectonic study of NE and E Africa and its implication for mineral exploration: A synoptic view from satellite imagery p 34 N89-13023

BELLON, A.

VISSR sensor introduced modifications in the presence of large temperature gradients p 78 A89-12860

BELWARD, A. S.

The classification of semi-natural vegetation from LANDSAT Thematic Mapper imagery: A user's perspective p 21 N89-13084

BENNETT, JOHN R.

Full-spectrum modeling of synthetic aperture radar internal wave signatures p 40 A89-12166

BENTON, EDWARD R.

Satellite measurements required for deep-earth geophysics p 28 N89-12103

BENZ, R.

Solid earth mission study. Volume 2: Technical report [ESA-CR(P)-2626-VOL-2] p 26 N89-10303

Solid Earth mission study. Volume 1: Executive summary [ESA-CR(P)-2626-VOL-1] p 26 N89-10397

Solid earth mission study. Volume 3: Program planning report [ESA-CR(P)-2626-VOL-3] p 27 N89-10399

BERAN, D.

The MEOS experiment: A test case for future cartographic missions p 87 N89-13081

BERANEK, R.

Laser Atmospheric Wind Sounder (LAWS) p 79 A89-15889

BERETTA, A.

The ERS-1 Instrument Data Handling and Transmission subsystem (IDHT) and its evolution [IAF PAPER 88-134] p 80 A89-17690

BERLIN, GRAYDON LENNIS

SIR-B view of the Jabal Hadn lineament and its groundwater implications p 29 A89-10976

BERNARD, A.

Solid earth mission study. Volume 2: Technical report [ESA-CR(P)-2626-VOL-2] p 26 N89-10303

Solid Earth mission study. Volume 1: Executive summary [ESA-CR(P)-2626-VOL-1] p 26 N89-10397

Solid earth mission study. Volume 3: Program planning report [ESA-CR(P)-2626-VOL-3] p 27 N89-10399

BERRY, J. A. M.

A comparison of reduction methods for satellite altimetry data p 39 A89-11424

BERTHELOT, B.

Estimation of primary marine production using spaceborne data on ocean color p 48 N89-10371

BERTOLINI, G.

Time-resolved laser fluorescence: Trends and applications p 83 N89-10346

BERTUZZI, P.

Measuring in-situ soil surface roughness using a laser profilometer p 9 N89-10308

BESSEMOULIN, PIERRE

Evaporation over land surfaces - First results from HAPEX-MOBILHY Special Observing Period p 57 A89-12211

BGATOV, A. P.

Engineering evaluation of mountain topography exodynamics from remotely sensed data p 31 A89-18707

BHAT, M. K. P.

GOES I-M image navigation and registration system p 75 A89-10965

BIGNAL, E.

The classification of semi-natural vegetation from LANDSAT Thematic Mapper imagery: A user's perspective p 21 N89-13084

BILBRO, J. W.

Laser Atmospheric Wind Sounder (LAWS) p 79 A89-15889

BINDSCHADLER, R. A.

Data report for the Siple Coast (Antarctica) project [NASA-TM-100708] p 49 N89-10403

BIRD, ARLENE A.

A numerical study of mesoscale ocean eddy interaction with a marginal ice zone p 41 A89-12172

BJORNSSON, S.

Strengths and shortcomings in Airborne Thematic Mapper (ATM) technology as applied to volcanic and geothermal areas in Iceland p 32 N89-10337

A narrow-band thermal imager based on multiline real-time averaging p 83 N89-10356

BLACK, P. G.

Surface windspeed measurements over the ocean with a C-band microwave radiometer p 75 A89-11006

BLACK, S. M.

Improving the accessibility of spatially referenced geological information p 35 N89-13026

BLAD, BLAINE L.

Comparison of measured and modeled radiation, heat and water vapor fluxes: FIFE pilot study [NASA-CR-183304] p 17 N89-11368

BLAIS, J. A. R.

On the application of averaging median filters in remote sensing p 68 A89-15920

BLOOM, S. C.

Assimilation of satellite surface wind speed data using the GLA analysis/forecast system p 77 A89-12811

BLUME, HANS-JUERGEN C.

Passive microwave remote sensing of salinity in coastal zones p 36 A89-10942

BODECHTEL, J.

Comparative point-spread function calculations for the MOMS-1, Thematic Mapper and SPOT-HRV instruments p 83 N89-10379

Design of spectral bands for the German MOMS-2 sensor p 84 N89-10381

BOER, LEENDERT

Very Long Baseline Interferometry (VLBI): Relativity and geodesy [ETN-89-93337] p 29 N89-14493

BOGDANOV, A. I.

Engineering evaluation of mountain topography exodynamics from remotely sensed data p 31 A89-18707

BOGDANOV, A. M.

Engineering evaluation of mountain topography exodynamics from remotely sensed data p 31 A89-18707

BOISSARD, P.

Potential number of winter wheat ears estimation using radiometry techniques at an early stage p 10 N89-10323

BONN, F.

Discrimination of zones of high water erosion risk using SPOT images p 15 N89-10376

BORSTAD, G. A.

Imaging spectrometry for water applications p 56 A89-10327

The fluorescence line imager: High-resolution imaging spectroscopy over water and land p 83 N89-10353

BOUCHER, J.-M.

Spectral analysis of ocean wave imagery using 2-D linear prediction p 50 N89-12968

BOULIANNE, M.

On the application of averaging median filters in remote sensing p 68 A89-15920

BOUMAN, B. A. M.

Microwave backscatter from beets, peas and potatoes throughout the growing season p 9 N89-10309

BOWELL, JO ANN

Comparison of the spectral information content of Landsat Thematic Mapper and SPOT for three different sites in the Phoenix, Arizona region p 68 A89-20626

BOWLIN, HARRY L.

Operational use of Landsat data for timber inventory p 2 A89-10970

BRADLEY, CAROLYN

The GVAR users compendium, volume 1 [NOAA-NESDIS-21-VOL-1] p 85 N89-12105

BRAIM, S. P.

Technological constraints on the use of thermal imagery for remote sensing p 81 A89-19173

BRIANTIS, J. M.

Techniques for remote sensing of life span and quantum yield of chlorophyll fluorescence in vivo p 13 N89-10351

BRIGGS, JOHN M.

SPOT satellite data for pattern recognition on the North American tall-grass prairie Long-Term Ecological Research site p 5 A89-14009

BRIGGS, S. A.

Spatial resolution requirements for MODIS-N p 83 N89-10364

BRINGI, V. N.

Simulation of radar and surface measurements of rainfall p 62 N89-13924

BROCKHAUS, J.

Multitemporal resource complex analysis of Catania province, Italy from LANDSAT-TM data p 71 N89-12985

BROOKS, DAVID R.

Summary of along-track data from the earth radiation budget satellite for several representative ocean regions [NASA-RP-1206] p 55 N89-14634

BRONER, WILLIAM G.

Remote sensing technologies and spatial data applications [AD-A195809] p 62 N89-14480

- BROWDER, JOAN A.**
Utilizing remote sensing of thematic mapper data to improve our understanding of estuarine processes and their influence on the productivity of estuarine-dependent fisheries
[NASA-CR-183409] p 62 N89-13822
- BROWN, K.**
The spectral bidirectional reflectance of snow
p 69 N89-10318
- BRUCKLER, L.**
Near surface soil moisture estimation from microwave measurements p 6 A89-17282
- BRUEGGE, C. J.**
Airborne Visible/Infrared Imaging Spectrometer (AVIRIS): Inflight radiometric calibration and the determination of surface reflectance p 83 N89-10357
- BRUEL, ERIK**
Precision of line following in digital images
[B8821610] p 73 N89-14486
- BRUK, V. V.**
The potential of using remotely sensed information for studying the contamination and eutrophication of lake systems p 58 A89-18708
- BRUNET, Y.**
A new method for estimating regional evaporation from thermal infrared surface temperature measurements
p 60 N89-10390
- BRUSH, R. J. H.**
The navigation of AVHRR imagery p 66 A89-12357
- BRYANT, JACK**
On displaying multispectral imagery p 68 A89-20631
- BUDGE, THOMAS**
Remote sensing and geographic information systems for agricultural statistics-gathering and agricultural monitoring in Morocco p 2 A89-10960
- BUDGELL, W. PAUL**
A numerical study of mesoscale ocean eddy interaction with a marginal ice zone p 41 A89-12172
- BUECHEL, S. W.**
Satellite data analysis for inventorying crops grown in a complex, small-field environment p 1 A89-10951
Regional variation and crop separability in a Thematic Mapper based crop inventory of New York State p 4 A89-11002
- BUISSON, O.**
Potential number of winter wheat ears estimation using radiometry techniques at an early stage p 10 N89-10323
- BULLOCK, BRIAN L.**
Radar applications in remote sensing - An airborne remote sensing case history presented at the Twenty-first International Symposium on Remote Sensing of Environment, Ann Arbor, Michigan, October 26-30, 1987 p 75 A89-10969
- BULLOCK, RONALD A.**
An enhanced classification approach to change detection in semi-arid environments p 68 A89-20627
- BUNTING, JAMES T.**
Color-composite image processing for multispectral meteorological satellite data
[AD-A199574] p 76 A89-11742
- BUNTZEN, RODNEY R.**
Airborne lidar detection of subsurface oceanic scattering layers p 41 A89-12260
- BURNS, B. A.**
SAR image statistics related to atmospheric drag over sea ice p 52 N89-13034
- BUSCHMANN, C.**
Changes in the chlorophyll fluorescence spectra during the Kautsky induction kinetics p 12 N89-10348
- BUTLER, DIXON M.**
NASA's Earth Science Geostationary Platform p 77 A89-12828
- BUTTNER, G.**
Agroecological information content of SPOT data p 19 N89-13050
- BYCHKOV, D. M.**
The effect of agrometeorological conditions on the characteristics of space radar imagery of agricultural regions in winter p 8 A89-18709
- CAI, DENG-LIN**
Model-based remotely-sensed imagery interpretation p 66 A89-12223
- CAIN, J. C.**
Simulation of a spinning spacecraft magnetometer p 28 N89-12101
A study of accuracy enhancement in satellite magnetic modeling p 28 N89-12102
- CALLIS, SUSAN L.**
The application of remote sensing for drought early warning in Africa p 1 A89-10948
- CALOZ, R.**
The normalization of a soil brightness index for the study of changes in soil conditions p 14 N89-10370
- CAMAGNI, P.**
Time-resolved laser fluorescence: Trends and applications p 83 N89-10346
- CAMARANETO, GILBERTO**
A general data model for geographic information systems
[INPE-4560-PRE/1301] p 24 N89-10676
- CAMPBELL, JEFFREY WILLIAM**
Evaluation of GEOSAT (Geodetic Satellite) data and application to variability of the northeast Pacific Ocean
[AD-A198950] p 53 N89-13863
- CAMPBELL, WILLIAM J.**
Variations in the Arctic, Antarctic, and global sea ice covers during 1978-1987 as observed with the Nimbus 7 scanning multichannel microwave radiometer p 38 A89-11145
- CAMPION, D. G.**
Cotton area mapping using multitemporal satellite data integrated within a geographical information system applied to a cotton boll weevil control programme in Paraguay p 20 N89-13077
- CAMPOS-MARQUETTI, RAUL**
Remote sensing and geographic information systems for agricultural statistics-gathering and agricultural monitoring in Morocco p 2 A89-10960
- CANEILL, J.**
Relation between sugar beet crop yield and vegetative indexes calculated from LANDSAT MSS images p 11 N89-10333
- CAPONI, E. A.**
Modulation of radar backscatter from the ocean by a variable surface current p 39 A89-12158
- CAPOREALI, A.**
Time series of European baselines determined with Lageos p 26 A89-17945
- CARD, DON H.**
Prediction of leaf chemistry by the use of visible and near infrared reflectance spectroscopy p 7 A89-17283
- CARERE, V.**
Airborne Visible/Infrared Imaging Spectrometer (AVIRIS): Inflight radiometric calibration and the determination of surface reflectance p 83 N89-10357
- CARIOU, C.**
Spectral analysis of ocean wave imagery using 2-D linear prediction p 50 N89-12968
- CARLOSDEALMEIDA, FAUSTO**
An agricultural crop yield model by satellite: A simulation
[INPE-4639-PRE/1350] p 17 N89-12106
- CARLSON, TOBY N.**
Infrared temperature measurements over bare soil and vegetation - A HAPEX perspective p 2 A89-10953
Comparison of remote measurements of infrared surface temperatures and microwave soil moisture p 4 A89-11009
- CARROLL, T. R.**
An airborne gamma ray snow survey of a forest covered area with a deep snowpack p 7 A89-17284
- CARTER, D. J. T.**
Satellite remote sensing and wave studies into the 1990s p 47 A89-20723
- CASELLES, V.**
A theoretical model for interpreting remotely sensed thermal infrared measurements obtained over agricultural areas p 12 N89-10343
- CASTAGNOLI, F.**
A new lidar system for applications over land and sea p 83 N89-10347
- CAUSSIGNAC, J. M.**
Measuring in-situ soil surface roughness using a laser profilometer p 9 N89-10308
- CAVALIERI, D. J.**
NASA Sea Ice and Snow Validation Program for the DMSP SSM/I: NASA DC-8 flight report
[NASA-TM-100706] p 53 N89-13861
- CECCHI, G.**
A new lidar system for applications over land and sea p 83 N89-10347
- CELSODECARVALHO, VITOR**
Digital processing applied to vegetation
[INPE-4695-MD/036] p 17 N89-12107
- CENCI, A.**
Time series of European baselines determined with Lageos p 26 A89-17945
- CERVILLE, B.**
Evaluation of VARAN data in geology and geomorphology in the southeast of France p 32 N89-10313
Usefulness of high spectral resolution radiometry for geological mapping in the Mediterranean region p 32 N89-10360
- Characterization of rocks by visible and infrared high spectral resolution terrain spectroscopy p 32 N89-10362
- CHAKRABORTY, M.**
Comparison of SPOT, TM and MSS data for agricultural land-use mapping in Gujarat (India)
[IAF PAPER 88-139] p 7 A89-17692
- CHALLENGER, P. G.**
Satellite remote sensing and wave studies into the 1990s p 47 A89-20723
- CHAMPION, I.**
Extracting soil and vegetation characteristics from microwave remote sensing data p 9 N89-10306
Complementary of microwave and optical range in the characterization of crops by remote sensing p 10 N89-10310
- CHANDRASEKAR, V.**
Simulation of radar and surface measurements of rainfall p 62 N89-13924
- CHANG, A. T. C.**
The spectral bidirectional reflectance of snow p 69 N89-10318
Rainfall index over oceans derived from SSM/I data p 51 N89-12998
Average areal water equivalent of snow in a mountain basin using microwave and visible satellite data p 61 N89-13045
- CHANG, MAO**
Look-up tables to convert Landsat TM thermal IR data to water surface temperatures p 67 A89-14012
- CHANG, SIMON**
Tropopause adjustment to tropical cyclones as inferred from satellite ozone observations p 77 A89-12816
- CHAPMAN, M. A.**
Accuracy evaluation of airborne stereo line imager data p 75 A89-10936
- CHARTIER, L.**
Analysis of the contribution of the atmosphere to water reflectance in the first two channels of the NOAA satellites AVHRR p 82 N89-10330
- CHARTIER, M.**
Estimation of the interception efficiency of an alfalfa canopy from a vegetative index p 11 N89-10332
- CHAVEZ, PAT S., JR.**
Comparison of the spectral information content of Landsat Thematic Mapper and SPOT for three different sites in the Phoenix, Arizona region p 68 A89-20626
- CHEN, D. W.**
Classification of cloud fields based on textural characteristics p 65 A89-11727
- CHEN, GAN-CHENG**
The practice and understanding of using aerial remote sensing in the investigation of coastal zone p 37 A89-10995
- CHEN, SHERRY CHOU**
Crop separation analysis through SPOT and TM digital data
[INPE-4641-PRE/1352] p 18 N89-12110
- CHENEY, ROBERT E.**
Sea level variations in the tropical Pacific during 1985-87 derived from GEOSAT altimetry p 36 A89-10961
- CHENG, DOU-SHEN**
Model-based remotely-sensed imagery interpretation p 66 A89-12223
- CHENG, JICHENG**
The character of reflective spectrum of winter wheat and the principle of its yield estimation with remote sensing method p 2 A89-10973
A study of estimation of winter wheat yield for large area using remote sensing method p 2 A89-10974
- CHENGANG, Y.**
Precipitation detection with satellite microwave data
[PB88-240239] p 88 N89-13094
- CHERNA, E. V.**
VISSR sensor introduced modifications in the presence of large temperature gradients p 78 A89-12860
- CHERRY, S. M.**
Cross-polar radar measurements in ice and rain p 60 N89-12993
- CHEVREL, M.**
The French space program for Earth observation p 90 N89-10392
- CHEWINGS, V. H.**
Estimating the distribution of grazing and patterns of cattle movement in a large arid zone paddock p 5 A89-12356
- CHIARANTINI, L.**
The use of microwave radiometry in watershed hydrology p 57 A89-10992
- CHIEN, LAI-CHEN**
Observation of precipitation using GMS imagery
[IAF PAPER 88-151] p 58 A89-17697
- CHOROWICZ, J.**
Evaluation of VARAN data in geology and geomorphology in the southeast of France p 32 N89-10313

- Usefulness of high spectral resolution radiometry for geological mapping in the Mediterranean region p 32 N89-10360
- Characterization of rocks by visible and infrared high spectral resolution terrain spectroscopy p 32 N89-10362
- The use of MOMS-1 data for geological mapping of the Aswa lineament (East African rift) p 33 N89-10382
- CHOUDHARY, R. K.**
Project Vasundhara - Multi-theme integration of satellite remote sensing and geological data for regional level mineral prognostics [IAF PAPER 88-145] p 31 A89-17694
- CHOUDHURY, B. J.**
Global land-surface primary productivity based upon Nimbus-7 37 GHz data [IAF PAPER 88-159] p 8 A89-17701
- CHU, LIANGCAI**
Sino-American cooperative studies on applications of remote sensing to surveying and mapping p 29 A89-10967
- CIAMPOLINI, A.**
Solid earth mission study. Volume 2: Technical report [ESA-CR(P)-2626-VOL-2] p 26 N89-10303
Solid Earth mission study. Volume 1: Executive summary [ESA-CR(P)-2626-VOL-1] p 26 N89-10397
Solid earth mission study. Volume 3: Program planning report [ESA-CR(P)-2626-VOL-3] p 27 N89-10399
- CIHLAR, JOSEF**
Effect of soil roughness on SAR images of harvested agricultural fields p 4 A89-11004
- CITEAU, J.**
Bathymetry using SPOT imagery of the Casamance (Senegal). First results p 59 N89-10375
- CLARK, DAVID D.**
Enhancements to the ARGOS system - Presented at the Twenty-first International Symposium on Remote Sensing of Environment, Ann Arbor, Michigan, October 26-30, 1987 p 22 A89-10957
- CLARKE, GAR**
Remote sensing and geographic information systems for agricultural statistics-gathering and agricultural monitoring in Morocco p 2 A89-10960
- COATES, ROBERT J.**
The Crustal Dynamics Project p 25 A89-13757
- COCHRAN, JAMES R.**
Somali Basin, Chain Ridge, and origin of the Northern Somali Basin gravity and geoid low p 30 A89-12290
- COHEN, S. C.**
Geodynamics laser ranging system: Performance simulations and development of the EOS facility p 28 N89-12982
- COHEN, STEVEN C.**
Applications of spaceborne laser ranger on EOS p 79 A89-15878
- COLLET, C.**
The normalization of a soil brightness index for the study of changes in soil conditions p 14 N89-10370
- COLLINS, W. G.**
Advances in computerized information retrieval in remote sensing p 69 A89-20717
An evaluation of satellite imagery, LANDSAT Thematic Mapper and SPOT-1 HRV, for grassland inventory in the UK p 20 N89-13057
- COLWELL, J. E.**
An improved procedure for analysis of change in Thematic Mapper image-pairs p 65 A89-11013
- COLWELL, JOHN**
Utilization of Landsat data and a geographic information system (GIS) for improving watershed management in India p 57 A89-11014
- COMISO, J. C.**
Phytoplankton standing crops within an Antarctic ice edge assessed by satellite remote sensing p 41 A89-12174
- CONEL, J. E.**
Airborne Visible/Infrared Imaging Spectrometer (AVIRIS): Inflight radiometric calibration and the determination of surface reflectance p 83 N89-10357
- CONESE, C.**
Forest classification by principal component analyses of TM data p 8 A89-20706
- CONLEY, JOSEPH M.**
High Resolution Imaging Spectrometer (HIRIS) p 74 A89-10334
- CONWAY, J. A.**
Constraints on two-scale descriptions of radar backscattering from the sea surface using scatterometer model functions p 49 N89-12945
- CORDEY, R. A.**
The use of the complex correlation function in the recovery of ocean wave spectra from SAR images p 47 N89-10315

- Constraints on two-scale descriptions of radar backscattering from the sea surface using scatterometer model functions p 49 N89-12945
Complex SAR imagery and speckle filtering for ERS-1 wave mode p 71 N89-13029
Multistatic scatterometry p 87 N89-13072
- COTE, P.**
Analysis of the contribution of the atmosphere to water reflectance in the first two channels of the NOAA satellites AVHRR p 82 N89-10330
- COULSON, KINSELL L.**
Remote Sensing in Polarized Light [NASA-CP-3014] p 88 N89-14189
- COULTER, MALCOLM C.**
Monitoring Wood Stork foraging habitat using remote sensing and geographic information systems p 7 A89-17399
- COURAULT, D.**
Modeling of soil color by remote sensing p 14 N89-10369
- COUSSOT, M.**
Wide field high performance lenses [IAF PAPER 88-120] p 80 A89-17685
- COX, G. F. N.**
Numerical simulations of the profile properties of undeformed first-year sea ice during the growth season p 40 A89-12171
- COX, J. J.**
Advances in computerized information retrieval in remote sensing p 69 A89-20717
- CRACKNELL, A. P.**
MOMS-1 data for bathymetric and geological studies p 33 N89-10363
- CRAWFORD, D. R.**
Modulation of radar backscatter from the ocean by a variable surface current p 39 A89-12158
- CRITCHLEY, B. R.**
Cotton area mapping using multitemporal satellite data integrated within a geographical information system applied to a cotton boll weevil control programme in Paraguay p 20 N89-13077
- CROSBY, DAVID S.**
Evaluation of 3.7 micron split windows for estimating surface temperature p 43 A89-12855
- CROSS, A. M.**
Segmentation of remotely-sensed images by a split-and-merge process p 66 A89-12222
Detection of circular geological features using the Hough transform p 30 A89-12358
- CSILLAG, F.**
Agroecological information content of SPOT data p 19 N89-13050
- CU, C. C.**
User's guide for the Nimbus 7 Scanning Multichannel Microwave Radiometer (SMMR) CELL-ALL tape [NASA-RP-1210] p 89 N89-14648
- CURRAN, P. J.**
Developing a radiometric leaf area index p 12 N89-10334
Crop classification with multi-temporal X-band SAR data p 19 N89-12990
- CURRAN, ROBERT J.**
NASA's Earth Science Geostationary Platform p 77 A89-12828
- CURTIS, D.**
The classification of semi-natural vegetation from LANDSAT Thematic Mapper imagery: A user's perspective p 21 N89-13084
- CUSHNIE, J. L.**
The use of remote sensing in conjunction with geographic information systems for local planning p 24 N89-12959
- CUTTS, JAMES A.**
Sensors research and technology p 85 N89-11774

D

- D'AGUANNO, JANE**
Nimbus-7 SMMR derived sea-ice concentrations over Antarctica p 43 A89-12857
- D'ENTREMONT, ROBERT P.**
Color-composite image processing for multispectral meteorological satellite data [AD-A199574] p 76 A89-11742
- DACOSTAFREITASYANASSE, CORINA**
An agricultural crop yield model by satellite: A simulation [INPE-4639-PRE/1350] p 17 N89-12106
- DADHWAL, V. K.**
Comparison of SPOT, TM and MSS data for agricultural land-use mapping in Gujarat (India) [IAF PAPER 88-139] p 7 A89-17692

- DAILLET-ROCHETTE, SYLVIANE**
Satellite phasing problems for ocean and atmospheric studies [IAF PAPER 88-152] p 46 A89-17698
- DALLEMAND, JEAN FRANCOIS**
Crop separation analysis through SPOT and TM digital data [INPE-4641-PRE/1352] p 18 N89-12110
- DANES, P. L. R.**
Polarisation of passive microwave signals as indicator of snow water equivalent p 61 N89-13043
- DANES, Z. F.**
Polarisation of passive microwave signals as indicator of snow water equivalent p 61 N89-13043
- DANIELS, JAIME M.**
Influence of sea surface temperature on intra- and inter-annual variations of ITCZ p 43 A89-12871
- DANILENKO, GENNADI M.**
Principles Relating to Remote Sensing of the Earth from Space - Territorial sphere of application p 89 A89-12121
- DANSON, F. M.**
Spatial resolution for remote sensing of forest plantations p 19 N89-12991
- DARWISH, LAYLA**
PRISM B (Prediction of the Indian Summer Monsoon - Bellevue) [IAF PAPER ST-88-02] p 58 A89-17873
- DAVIDSON, C. A.**
DOE/DOD environmental data bank [DE88-015262] p 25 N89-14942
- DAVIDSON, J. M.**
Distribution of relative plate motion along the Pacific-North American plate boundary determined from mobile VLBI measurements p 26 A89-13761
- DAVIDSON, K. L.**
Wind stress measurements during the Tower Ocean Wave and Radar Dependence experiment p 45 A89-16984
- DAVIS, J. L.**
VLBI geodesy - 2 parts-per-billion precision in length determinations for transcontinental baselines p 26 A89-13762
- DAVIS, R. E.**
The spectral bidirectional reflectance of snow p 69 N89-10318
- DAWE, B.**
Evaluation of technology in the detection and counting of seals p 76 A89-11016
- DAWSON, T. W.**
Joint Canada-U.S. Ocean Wave Investigation Project - An overview of the Georgia Strait Experiment p 39 A89-12156
- DE LEEUW, A. J.**
Geometric correction of remotely-sensed imagery using ground control points and orthogonal polynomials p 82 A89-20718
- DEALY, B.**
A satellite data processing and analysis software system for earth's atmosphere and surface research p 67 A89-12864
- DEARAUJO, ANTONIO JOSE**
The Transformed Vegetation Index (TVI) for estimation of Brazilian cerrado's phytomass [INPE-4603-PRE/1326] p 15 N89-10400
- DEDIEU, J.-P.**
Satellite surveillance of ice and snow covered surfaces in the French Alps using visible and near infrared reflectance measurements from the SPOT and LANDSAT Thematic Mapper sensors p 59 N89-10372
- DEEMING, KEVIN R.**
Review of the requirements for higher level ERS-1 products within Europe [ESA-CR(P)-2586] p 84 N89-10664
- DEFEO, NANCY J.**
Detection of forest damage on Whiteface Mountain, New York, using Landsat Thematic Mapper data p 3 A89-10987
- DEGNAN, JOHN J.**
Applications of spaceborne laser ranger on EOS p 79 A89-15878
- DEHAAN, J. F.**
Validation of an atmospheric correction method for satellite borne imagery p 82 N89-10320
- DEKKER, A. G.**
The Remote Sensing Loosdrecht Lakes project p 59 A89-20719
- DELECOLLE, R.**
Introducing spectral data into a plant process model for improving its prediction ability p 10 N89-10324
Biomass and wheat crop yield estimation from SPOT vegetative indexes p 11 N89-10327
- DELOACH, STEPHEN R.**
Continuous deformation monitoring with GPS [AD-A196447] p 27 N89-10886

- DEMARCO, H.**
Bathymetry using SPOT imagery of the Casamance (Senegal). First results p 59 N89-10375
- DEMETRIADES-SHAH, T. H.**
High spectral resolution indices for monitoring crop growth and chlorosis p 13 N89-10358
- DEMORISSONVALERIANO, DALTON**
CIR aerial photography applied to the evaluation of the air pollution impact in a tropical forest: The case of Cubatao, Brazil
[INPE-4651-PRE/1358] p 17 N89-11324
- DENORE, B. J.**
Cotton area mapping using multitemporal satellite data integrated within a geographical information system applied to a cotton boll weevil control programme in Paraguay p 20 N89-13077
- DENSKAT, U.**
Solid earth mission study. Volume 2: Technical report [ESA-CR(P)-2626-VOL-2] p 26 N89-10303
Solid Earth mission study. Volume 1: Executive summary [ESA-CR(P)-2626-VOL-1] p 26 N89-10397
Solid earth mission study. Volume 3: Program planning report [ESA-CR(P)-2626-VOL-3] p 27 N89-10399
- DENTREMENT, ROBERT P.**
Possible measurement errors in calibrated AVHRR (Advanced Very High Resolution Radiometer) data [AD-A198342] p 88 N89-14414
- DESCHAMPS, P. Y.**
Analysis of directional effects on NOAA AVHRR p 70 N89-10341
- DESCHAMPS, P.-Y.**
Estimation of primary marine production using spaceborne data on ocean color p 48 N89-10371
- DESHLER, TERRY**
Corrections of surface particle probe measurements for the effects of aspiration p 58 N89-14022
- DEUTSCH, MORRIS**
Remote sensing technologies and spatial data applications [AD-A195809] p 62 N89-14480
- DEVOS, W.**
An integrated remote sensing approach for regional agrostistics and land monitoring p 24 N89-12960
- DI TOLLE, F.**
The ERS-1 Instrument Data Handling and Transmission subsystem (IDHT) and its evolution [IAF PAPER 88-134] p 80 N89-17690
- DISPERATI, ATTILIO ANTONIO**
The Transformed Vegetation Index (TVI) for estimation of Brazilian cerrado's phytomass [INPE-4603-PRE/1326] p 15 N89-10400
- DOAK, EDWIN L.**
Directional effects on scene complexity in oblique thermal imagery and photographs of a deciduous forest p 4 N89-12261
- DOCKTER, K.**
Spectral reflectance of sugar beet and winter wheat canopies in the visible and infrared during growth p 12 N89-10342
- DOEFFER, R.**
High-resolution spectroscopy for remote sensing of ocean and atmosphere p 48 N89-10352
- DOHARE, DIN DAYAL**
Utilization of Landsat data and a geographic information system (GIS) for improving watershed management in India p 57 N89-11014
- DONNAY, J.-P.**
Towards an urban land-use classification using textural and morphological criteria p 25 N89-12987
- DONNELLAN, ANDREA**
Determination of convergence rates across the Ventura Basin, Southern California, using GPS and historical triangulation [NASA-CR-183014] p 29 N89-14624
- DOSSANTOS, JOAO ROBERTO**
The Transformed Vegetation Index (TVI) for estimation of Brazilian cerrado's phytomass [INPE-4603-PRE/1326] p 15 N89-10400
- DOWDESWELL, J. A.**
Topographic effects on light scattering from snow p 71 N89-12976
- DOWIE, P.**
Integrating remote sensing data into a geographical information system: A foundation for rural land use strategies: Nature Conservancy Council project p 24 N89-12964
- DOWMAN, I. J.**
Topographic mapping from SPOT imagery p 67 N89-14088
- DOZIER, J.**
The spectral bidirectional reflectance of snow p 69 N89-10318
- DOZIER, JEFF**
HIRIS - EOS instrument with high spectral and spatial resolution p 74 N89-10928
- DRAKE, N.**
Mapping the distribution and abundance of lithological units and surface mineralogies at Jabal Sa'id, Saudi Arabia: An application of spectral mixture modelling p 34 N89-13024
Monitoring playas using Thematic Mapper data p 60 N89-13028
- DREISER, CHRISTOPH**
Applications of LANDSAT (TM and MSS) data for an estimation of rangeland conditions in semiarid and arid areas of northern Kenya [DFVLR-FB-88-18] p 16 N89-10404
- DRESCHER, A.**
The MEOSX experiment: A test case for future cartographic missions p 87 N89-13081
- DRURY, S. A.**
Remote sensing of laterized Archaean greenstone terrain - Marshall Pool Area, Northeastern Yilgarn Block, Western Australia p 31 N89-20628
- DRUZHININ, G. V.**
The potential of using remotely sensed information for studying the contamination and eutrophication of lake systems p 58 N89-18708
- DUARTE, VALDETE**
Technique for obtaining agricultural property boundaries through satellite imagery, certified to control and accompany agricultural activity [INPE-4640-PRE/1351] p 16 N89-11294
- DUBOIS, J. M. M.**
Imaging spectrometry applied to the remote sensing of submerged seaweed p 48 N89-10361
- DUBOIS, P. C.**
Inference of geologic surface parameters from polarimetric radar observations and model inversion p 34 N89-12950
- DUDHIA, ANU**
A dual-satellite algorithm for deriving sea surface temperature p 41 N89-12209
- DURAND, J.-M.**
Spectral characterization of forest targets in mountainous zones on Thematic Mapper images p 11 N89-10328
- DURAND, P.**
Evaluation of VARAN data in geology and geomorphology in the southeast of France p 32 N89-10313
- DURKEE, PHILIP A.**
Snow and low-cloud discrimination from multispectral satellite measurements p 78 N89-12850
- DURPAIRE, J. P.**
The image detection subassembly for the SPOT 4 'vegetation' instrument [IAF PAPER 88-121] p 7 N89-17686
- DURY, S. J.**
Segmentation of remotely-sensed images by a split-and-merge process p 66 N89-12222
- DUTTO, VALERIE**
PRISM B (Prediction of the Indian Summer Monsoon - Bellevue) [IAF PAPER ST-88-02] p 58 N89-17873
- DYE, ROBERT**
Resolution improvement by multi-temporal data merging p 63 N89-10937
- DYER, M. I.**
The influence of grazing on land surface climatological variables [NASA-CR-183308] p 22 N89-14637
- E**
- EAGLESON, PETER S.**
The structure of red-infrared scattergrams of semivegetated landscapes [NASA-CR-183385] p 21 N89-13091
Use of LANDSAT images of vegetation cover to estimate effective hydraulic properties of soils [NASA-CR-183384] p 21 N89-13823
- EBERT, ELIZABETH EBY**
Classification and analysis of surface and clouds at high latitudes from AVHRR multispectral satellite data p 89 N89-14635
- ECHERT, D. C.**
An autonomous ocean instrument platform driven vertically by the current [AD-A198226] p 54 N89-13865
- EDEL, H.**
Imaging spectrometry for water applications p 56 N89-10327
Imaging spectrometry applied to the remote sensing of submerged seaweed p 48 N89-10361
- EDEL, H. R.**
The fluorescence line imager - An imaging spectrometer for ocean and land remote sensing p 73 N89-10312
The fluorescence line imager: High-resolution imaging spectroscopy over water and land p 83 N89-10353
- EDWARDS, G.**
Texture analysis in forest areas: High spectral resolution synthetic aperture radar data p 14 N89-10367
- EERENS, H.**
An integrated remote sensing approach for regional agrostistics and land monitoring p 24 N89-12960
- EGAN, WALTER G.**
Climate tracking with remote sensing p 75 N89-10943
- EGAWA, HIROICHI**
Region extraction in SPOT data p 67 N89-14007
- EGOROV, L. K.**
The potential of using remotely sensed information for studying the contamination and eutrophication of lake systems p 58 N89-18708
- EIRIKSSON, A.**
A narrow-band thermal imager based on multilane real-time averaging p 83 N89-10356
- ELIZECHEA, E.**
Satellite surveillance of ice and snow covered surfaces in the French Alps using visible and near infrared reflectance measurements from the SPOT and LANDSAT Thematic Mapper sensors p 59 N89-10372
- ELTOFT, T.**
Ocean wave number spectra and spatial autocorrelation functions from SAR images p 50 N89-12970
- ELVIDGE, CHRISTOPHER D.**
Reflectance characteristics of dry plant materials p 3 N89-10977
- EMORI, Y.**
Laser-induced fluorescence on in-vivo chlorophyll of a rice plant: A technique for the remote detection of plant growth p 12 N89-10350
- ENSLIN, WILLIAM R.**
Automatic road detection on Landsat 4 TM images p 23 N89-10997
- ERASTOVA, N. B.**
The effect of snow parameter variations on the thermal microwave emission of the soil-snow-atmosphere system p 59 N89-18712
- ERTHAL, GUARACI JOSE**
A general data model for geographic information systems [INPE-4560-PRE/1301] p 24 N89-10676
- ESCADAFAL, R.**
Modeling of soil color by remote sensing p 14 N89-10369
- ESCOBAR, D. E.**
Applications of multispectral video for natural resource assessment p 63 N89-10968
- ESSAJI, ABDELKADER**
Remote sensing and geographic information systems for agricultural statistics-gathering and agricultural monitoring in Morocco p 2 N89-10960
- ESTES, JOHN E.**
Remote sensing information sciences research group [NASA-CR-183374] p 91 N89-14481
- ESTEVA, DINORAH C.**
Evaluation of preliminary experiments assimilating Seasat significant wave heights into a spectral wave model p 46 N89-16991
- ETIENNE, C.**
Solid earth mission study. Volume 2: Technical report [ESA-CR(P)-2626-VOL-2] p 26 N89-10303
Solid Earth mission study. Volume 1: Executive summary [ESA-CR(P)-2626-VOL-1] p 26 N89-10397
Solid earth mission study. Volume 3: Program planning report [ESA-CR(P)-2626-VOL-3] p 27 N89-10399
- EVANS, DIANE L.**
Radar polarimetry - Analysis tools and applications p 30 N89-15915
- EVERITT, J. H.**
Applications of multispectral video for natural resource assessment p 63 N89-10968
- F**
- FARAGO, T.**
Estimating concentrations of optically active components from the remotely sensed spectral radiance of a water surface p 58 N89-18711
- FARR, T. G.**
Inference of geologic surface parameters from polarimetric radar observations and model inversion p 34 N89-12950
- FARR, TOM G.**
Radar polarimetry - Analysis tools and applications p 30 N89-15915

FAULK, H.

- Solid earth mission study. Volume 2: Technical report [ESA-CR(P)-2626-VOL-2] p 26 N89-10303
- Solid Earth mission study. Volume 1: Executive summary [ESA-CR(P)-2626-VOL-1] p 26 N89-10397
- Solid earth mission study. Volume 3: Program planning report [ESA-CR(P)-2626-VOL-3] p 27 N89-10399
- FEDOSEJEVS, G.**
Sensor band selection for detecting current defoliation caused by the spruce budworm p 6 A89-16062
- FEIGEL, EARL**
The GVAR users compendium, volume 1 [NOAA-NESDIS-21-VOL-1] p 85 N89-12105
- FELLOUS, J.-L.**
The French space oceanography program p 44 A89-15116
- FENN, MARTA A.**
Summary of along-track data from the earth radiation budget satellite for several representative ocean regions [NASA-RP-1206] p 55 N89-14634
- FERGUSON, KENNETH P.**
SPOT bathymetric image for archeological investigations p 37 A89-10990
- FERMI, M.**
Time series of European baselines determined with Lagos p 26 A89-17945
- FERRARI, C.**
The use of TM data for the study of a modern deltaic depositional system p 59 A89-20707
- FERRARO, RALPH R.**
Comparison of weather radar and satellite-based passive microwave observations of rainfall over land and oceans p 43 A89-12836
- Nimbus-7 SMMR derived sea-ice concentrations over Antarctica p 43 A89-12857
- FERRY, G. V.**
Comparison of in situ aerosol measurements with SAGE 2 and SAM 2 aerosol measurements during the airborne Antarctic ozone experiment p 89 N89-14522
- FIGORE, JOSEPH V.**
Comparison of weather radar and satellite-based passive microwave observations of rainfall over land and oceans p 43 A89-12836
- FIGIELLO, JOHN**
The GVAR users compendium, volume 1 [NOAA-NESDIS-21-VOL-1] p 85 N89-12105
- FISCHER, J.**
High-resolution spectroscopy for remote sensing of ocean and atmosphere p 48 N89-10352
- FITZJARRALD, D.**
Laser Atmospheric Wind Sounder (LAWS) p 79 A89-15889
- FITZJARRALD, DANIEL E.**
Doppler lidar wind measurements on the EOS - LAWS p 77 A89-12829
- FLATHER, R. A.**
Feasibility study for the development of a joint surge and wave model [PB88-230917] p 55 N89-14652
- FOODY, G. M.**
Crop classification with multi-temporal X-band SAR data p 19 N89-12990
- Classification decision rule modification on the basis of information extracted from training data p 72 N89-13062
- FOOTE, HARLAN P.**
Applications of digital image processing to ongoing research in complex terrain meteorology p 65 A89-11743
- FORESTI, CELINA**
Environmental impact of the urban growth on the Western Sao Paulo metropolitan area [INPE-4670-PRE/1370] p 23 N89-10413
- FORMAGGIO, ANTONIO ROBERTO**
Spectral studies of three oxisols and a Ultisol of Brazil [INPE-4644-PRE/1355] p 17 N89-11297
- FOSNIGHT, EUGENE A.**
Applications of spatial postclassification models p 63 A89-10958
- FOSTER, I. J.**
The development of tropical cyclones in the north-west of Australia p 41 A89-12203
- FOSTER, J. L.**
Average areal water equivalent of snow in a mountain basin using microwave and visible satellite data p 61 N89-13045
- FOUNTAIN, DAVID M.**
Magnetic mineralogy in an archaic crustal cross section - Implications for crustal magnetization p 30 A89-12292
- FRANCIS, P. W.**
Landsat Thematic Mapper observations of debris avalanche deposits in the Central Andes p 31 A89-19838

Emitted short wavelength infrared radiation for detection and monitoring of volcanic activity p 32 N89-10377

FRANK, C.

Improvement in NOAA-AVHRR snowcover determination for runoff prediction p 61 N89-13040

FRANK, THOMAS D.

Mapping dominant vegetation communities in the Colorado Rocky Mountain Front Range with Landsat Thematic Mapper and digital terrain data p 8 A89-20629

FRANKLIN, JANET

Invertible canopy reflectance modeling of vegetation structure in semiarid woodland p 6 A89-15918

FRANKLIN, STEVEN E.

Terrain relief and pattern description using digital elevation and Landsat data p 65 A89-11010

FROUIN, R.

A satellite data processing and analysis software system for earth's atmosphere and surface research p 67 A89-12864

Sensitivity of satellite-derived net shortwave irradiance at the Earth's surface to radiometric calibration p 82 N89-10335

FROUIN, ROBERT

A comparison of satellite and empirical formula techniques for estimating insolation over the oceans p 44 A89-15495

FUK, K.

Performance of a scanning pencil-beam spaceborne scatterometer for ocean wind measurements p 53 N89-13073

FUKUE, K.

A new spatial classification algorithm for high ground resolution images p 72 N89-13061

Accuracy of land cover classification of Thematic Mapper (TM) and SPOT data p 72 N89-13066

FUNG, TUNG

Land cover change detection with Thematic Mapper spectral textural data at the rural-urban fringe p 23 A89-10982

G

GABELL, A.

Airborne Visible/Infrared imaging Spectrometer (AVIRIS): Inflight radiometric calibration and the determination of surface reflectance p 83 N89-10357

GABRIEL, P.

Resolution dependence in satellite imagery - Multifractal analysis p 67 A89-12852

GADOMSKI, FREDERICK J.

Meteorological surface analysis using perspective topographic maps p 65 A89-11740

GAIAZOVA, A. K.

Recognition of seismically hazardous fault dislocations in space images of the Dushanbe depression p 31 A89-18706

GAIDANSKII, S. I.

The registration of the surface effects of internal ocean waves using microwave radiometry p 43 A89-13300

GAISER, P. W.

Millimeter-wave backscatter measurements of various snow forms p 61 N89-13046

GANDIA, S.

Spectral signature of citrus fruits and its evolution: Identification of the vegetative index of least temporal variation p 14 N89-10373

GARAND, LOUIS

Remote sensing of surface air temperature and humidity over oceanic areas with application to climatology and weather prediction p 42 A89-12798

GARR, DEBORAH

The GVAR users compendium, volume 1 [NOAA-NESDIS-21-VOL-1] p 85 N89-12105

GASPAROVIC, R. F.

An overview of the SAR Internal Wave Signature Experiment p 40 A89-12162

GAUTHIER, Y.

Imaging spectrometry applied to the remote sensing of submerged seaweed p 48 N89-10361

GAUTIER, C.

A satellite data processing and analysis software system for earth's atmosphere and surface research p 67 A89-12864

Sensitivity of satellite-derived net shortwave irradiance at the Earth's surface to radiometric calibration p 82 N89-10335

GAUTIER, CATHERINE

A comparison of satellite and empirical formula techniques for estimating insolation over the oceans p 44 A89-15495

GEERKEN, R.

Design of spectral bands for the German MOMS-2 sensor p 84 N89-10381

GEERNAERT, G. L.

Wind stress measurements during the Tower Ocean Wave and Radar Dependence experiment p 45 A89-16984

GEILE, W.

Snow cover to alter terrain signatures on radar images p 62 N89-13048

GELLER, E. W.

An autonomous ocean instrument platform driven vertically by the current [AD-A198226] p 54 N89-13865

GENTEN, P.

High resolution radiometric measurement of intertidal microphytobenthos p 48 N89-10365

GERACHI, A.

Multitemporal resource complex analysis of Catania province, Italy from LANDSAT-TM data p 71 N89-12985

GERDES, PATRICK

The GVAR users compendium, volume 1 [NOAA-NESDIS-21-VOL-1] p 85 N89-12105

GERLING, T. W.

The Labrador Sea Extreme Waves Experiment: Objectives, status and plans p 51 N89-12974

GERSHENSON, V. E.

The registration of the surface effects of internal ocean waves using microwave radiometry p 43 A89-13300

The effect of snow parameter variations on the thermal microwave emission of the soil-snow-atmosphere system p 59 A89-18712

GERSTL, S. A. W.

The angular reflectance signature of the canopy hot spot in the optical regime p 11 N89-10325

GESCH, D. B.

The derivation of sub-canopy surface terrain models of coastal forests using synthetic aperture radar p 20 N89-13083

GIBSON, J. R.

Accuracy evaluation of airborne stereo line imager data p 75 A89-10936

GILBERT, A.

Spectral signature of citrus fruits and its evolution: Identification of the vegetative index of least temporal variation p 14 N89-10373

GILBERT, GARY D.

Airborne lidar detection of subsurface oceanic scattering layers p 41 A89-12260

GILBERT, P.

Texture analysis in forest areas: High spectral resolution synthetic aperture radar data p 14 N89-10367

GILL, GRAHAM A.

CANVAS - An intelligent system for colour selection on CRT displays p 76 A89-12353

GINATI, A.

TUBSAT-1, satellite technology for educational purposes p 90 N89-10905

GIRARD, M.-C.

Modeling of soil color by remote sensing p 14 N89-10369

GJERTSEN, A. K.

Effects of changing satellite sensor attributes p 87 N89-13059

GLOERSEN, P.

User's guide for the Nimbus 7 Scanning Multichannel Microwave Radiometer (SMMR) CELL-ALL tape [NASA-RP-1210] p 89 N89-14648

GLOERSEN, PER

Variations in the Arctic, Antarctic, and global sea ice covers during 1978-1987 as observed with the Nimbus 7 scanning multichannel microwave radiometer p 38 A89-11145

GLOTOV, A. A.

The effect of snow parameter variations on the thermal microwave emission of the soil-snow-atmosphere system p 59 A89-18712

GLUKH, A. K.

The role of linear and ring features in hydrogeology p 31 A89-18705

GLYNN, J. E.

An airborne gamma ray snow survey of a forest covered area with a deep snowpack p 7 A89-17284

GODBOLE, S. P.

Development of Alaskan gas hydrate resources [DE88-010270] p 35 N89-13093

GODDARD, J. F. W.

Cross-polar radar measurements in ice and rain p 60 N89-12993

GOEL, N. S.

A perspective on vegetation canopy reflectance models p 10 N89-10317

A model for radiative transfer in heterogeneous three-dimensional canopies p 11 N89-10326

GOESSL, H.
The airborne radiometry experiment (ABREX) instrument, an experimental test bed for the specification of satellite-borne microwave radiometer at 90 GHz p 86 N89-12939

GOETZ, ALEXANDER F. H.
HIRIS - EOS instrument with high spectral and spatial resolution p 74 A89-10928

GOETZ, S. J.
Atmospheric correction of NS-001 data and extraction of multiple angle reflectance data sets p 64 A89-10998

GOGINENI, S. P.
Modulation of the radar backscatter from the ocean surface by a long gravity wave p 51 N89-13031
Investigation of radar backscattering from second-year sea ice [NASA-CR-180986] p 54 N89-14479

GOMBEER, P.
An integrated remote sensing approach for regional agrostistics and land monitoring p 24 N89-12960

GORDON, DAVID
Geodesy by radio interferometry - Determination of vector motions for sites in the western United States p 25 A89-13759

GORODETSKII, A. K.
Accounting for selective absorption in the evaluation of the earth surface temperature by an angular method p 80 A89-18710

GOSHTASBY, ARDESHIR
Geometric correction of satellite images using composite transformation functions p 64 A89-10986

GOSSE, G.
Estimation of the interception efficiency of an alfalfa canopy from a vegetative index p 11 N89-10332

GOSSELINK, JAMES G.
Utilizing remote sensing of thematic mapper data to improve our understanding of estuarine processes and their influence on the productivity of estuarine-dependent fisheries [NASA-CR-183409] p 62 N89-13822

GOTWOLS, B. L.
Measurements of surface wave modulations from internal waves during the SAR Internal Wave Signature Experiment p 40 A89-12164
A comparison of measured surface wave spectral modulations with predictions from a wave-current interaction model p 40 A89-12165

GOULAS, Y.
Techniques for remote sensing of life span and quantum yield of chlorophyll fluorescence in vivo p 13 N89-10351

GOUTORBE, JEAN-PAUL
Evaporation over land surfaces - First results from HAPEX-MOBILHY Special Observing Period p 57 A89-12211

GOW, A. J.
Correlation function study for sea ice p 46 A89-16990

GOWER, J. F.
Imaging spectrometry for water applications p 56 A89-10327

GOWER, J. F. R.
The fluorescence line imager - An imaging spectrometer for ocean and land remote sensing p 73 A89-10312
The fluorescence line imager: High-resolution imaging spectroscopy over water and land p 83 N89-10353

GRABER, H. C.
Modelling of surface waves and sea state-dependent wind stress for the Northeast Pacific Ocean using Seasat scatterometer data p 43 A89-12858
Wind and wind stress curl fields for the Northeast Pacific Ocean using satellite scatterometer data p 78 A89-12859

GRASSL, H.
High-resolution spectroscopy for remote sensing of ocean and atmosphere p 48 N89-10352

GRASTY, R. L.
An airborne gamma ray snow survey of a forest covered area with a deep snowpack p 7 A89-17284

GRAY, L. H.
The fluorescence line imager - An imaging spectrometer for ocean and land remote sensing p 73 A89-10312
The fluorescence line imager: High-resolution imaging spectroscopy over water and land p 83 N89-10353

GREEN, R. O.
Airborne Visible/Infrared Imaging Spectrometer (AVIRIS): Inflight radiometric calibration and the determination of surface reflectance p 83 N89-10357

GREER, JERRY D.
Space shuttle large format camera photography cloud cover interference diagrams [PB88-244405] p 88 N89-14482

GREGOIRE, J.-M.
Small format air photo from ultrahigh aircraft as an aid for data collection of agricultural statistics in Sahelian countries p 19 N89-13003

GRIER, T.
A model for radiative transfer in heterogeneous three-dimensional canopies p 11 N89-10326

GRIFFITHS, G. H.
Monitoring urban change from LANDSAT TM and SPOT satellite imagery by image differencing p 25 N89-13058

GRIFFITHS, P. S.
The relativity utility of LANDSAT MSS and SIR-A imagery in reconnaissance geological mapping in Northern Sudan p 34 N89-13022

GRODY, NORMAN C.
Surface identification using satellite microwave radiometers p 79 A89-15922

GROMOV, V. K.
The registration of the surface effects of internal ocean waves using microwave radiometry p 43 A89-13300

GRONDIN, M.
Study of the multiplexing of image telemetry data from SPOT 4 HRVIR and Vegetation sensors [CNES-87/229/CT/DRT/TIT/TR] p 70 N89-10930

GROOM, G. B.
Crop classification with multi-temporal X-band SAR data p 19 N89-12990

GU, X.
Biomass and wheat crop yield estimation from SPOT vegetative indexes p 11 N89-10327

GUERIF, M.
Introducing spectral data into a plant process model for improving its prediction ability p 10 N89-10324
Biomass and wheat crop yield estimation from SPOT vegetative indexes p 11 N89-10327

GUEZLANE, M.
The use of MOMS-1 data for geological mapping of the Aswa lineament (East African rift) p 33 N89-10382

GUGAN, D. J.
Topographic mapping from SPOT imagery p 67 A89-14088

GUILLAUMONT, B.
High resolution radiometric measurement of intertidal microphytobenthos p 48 N89-10365

GUINOT, J. P.
Biomass and wheat crop yield estimation from SPOT vegetative indexes p 11 N89-10327

GUISSARD, A.
A three degree-of-freedom description of the ocean surface for microwave remote sensing of wave height and wind friction velocity p 47 N89-10314
An approximative model for the microwave brightness temperature scattered by a rough open ocean surface p 48 N89-10344

GUPTA, M. C.
Application of satellite data for monitoring degradation of tidal wetlands of the Gulf of Kachchh, Western India [IAF PAPER 88-146] p 46 A89-17695

GUTMAN, GEORGE
A simple method for estimating monthly mean albedo of land surfaces from AVHRR data p 6 A89-15493

GUTTMANN, S.
Spectral characterization of forest damage in beech, oak and pine stands p 21 N89-13085

GUYENNE, T. D.
Proceedings of the 4th International Colloquium on Spectral Signatures in Remote Sensing [ESA-SP-287] p 9 N89-10305
Proceedings of the 1988 International Geoscience and Remote Sensing Symposium (IGARSS 1988) on Remote Sensing: Moving Towards the 21st Century, volume 1 [ESA-SP-284-VOL-1] p 85 N89-12936

GUYOT, G.
Extracting soil and vegetation characteristics from microwave remote sensing data p 9 N89-10306
Complementary of microwave and optical range in the characterization of crops by remote sensing p 10 N89-10310
Spectral profile and biomass estimation p 10 N89-10319
Use of high spectral resolution to follow the state of vegetation canopies p 13 N89-10354

H

HAACK, BARRY
Landsat TM and MSS digital data comparison - Imperial Valley p 3 A89-10989

HAEFNER, H.
Monitoring of seasonal snow cover on glaciers p 61 N89-13044

HAGER, BRADFORD H.
Determination of convergence rates across the Ventura Basin, Southern California, using GPS and historical triangulation [NASA-CR-183014] p 29 N89-14624

HAJA, S. R.
Extraction of dense digital elevation models from SPOT stereo imagery p 71 N89-13053

HALL, C. D.
Multistatic scatterometry p 87 N89-13072

HALL, F. G.
Atmospheric correction of NS-001 data and extraction of multiple angle reflectance data sets p 64 A89-10998

HALLIKAINEN, M. T.
Microwave dielectric properties of low-salinity sea ice p 52 N89-13036

HAME, TUOMAS
Shuttered camera - Aerial color video imaging in the visible and near infrared p 8 A89-20630

HAN, D.
User's guide for the Nimbus 7 Scanning Multichannel Microwave Radiometer (SMMR) CELL-ALL tape [NASA-RP-1210] p 89 N89-14648

HANSEN, BIRGER
Monitoring vegetation index and biomass production in Southern Greenland based on NOAA-AVHRR data p 3 A89-10993

HANSSEN, A. J.
Mid-latitude evaluation of some satellite rainfall estimation techniques p 78 A89-12844

HARDING, JOHN M., JR.
The role of horizontal processes in upper-ocean prediction: A forecast simulation in the Sea of Japan [AD-A198827] p 55 N89-14654

HARDISKY, M. A.
Remote sensing of estuaries - An overview p 56 A89-10939

HARDTKE, P. G.
Solid earth mission study. Volume 2: Technical report [ESA-CR(P)-2626-VOL-2] p 26 N89-10303
Solid Earth mission study. Volume 1: Executive summary [ESA-CR(P)-2626-VOL-1] p 26 N89-10397
Solid earth mission study. Volume 3: Program planning report [ESA-CR(P)-2626-VOL-3] p 27 N89-10399

HARE, E. W.
Imaging spectrometry as a tool for botanical mapping p 73 A89-10324

HASELMANN, S.
Modelling of surface waves and sea state-dependent wind stress for the Northeast Pacific Ocean using Seasat scatterometer data p 43 A89-12858

HASTINGS, DAVID
Working group on studies of the lithosphere: Recommendations p 27 N89-12099

HAUCK, M.
The MEOSS experiment: A test case for future cartographic missions p 87 N89-13081

HAUDECOEUR, BENEDICTE
PRISM B (Prediction of the Indian Summer Monsoon - Bellevue) [IAF PAPER ST-88-02] p 58 A89-17873

HAWKINS, JEFFREY D.
The impact of satellite infrared sea surface temperatures on the FNOG (Fleet Numerical Oceanography Center) EOTS (Expanded Ocean Thermal Structure) regional gulf stream analysis [AD-A198965] p 54 N89-13864

HAYAKAWA, SEIJIRO
Remote measurements of diatoms chlorophyll-a in the Nori farm p 38 A89-11001

HAYAKAWA, TATSUO
Remote measurements of diatoms chlorophyll-a in the Nori farm p 38 A89-11001

HAYES, PATRICK M.
Active modes of the Pacific Intertropical Convergence Zone (ITCZ) [AD-A196406] p 49 N89-11374

HAYLING, KJELL LENNART
Heat flow and magnetization in the oceanic lithosphere [NASA-CR-183304] p 55 N89-14653

HAYS, CYNTHIA
Comparison of measured and modeled radiation, heat and water vapor fluxes: FIFE pilot study [NASA-CR-183304] p 17 N89-11368

HE, CHANSHENG
Evapotranspiration monitored from satellites as an indication of shift and impact of vegetation change p 2 A89-10975

HEALEY, R

Integrating remote sensing data into a geographical information system: A foundation for rural land use strategies: Nature Conservancy Council project p 24 N89-12964

HEIMANN, DIETRICH

Orographic channeling of a cold front by the Pyrenees p 79 A89-14073

HENDERSON, F. B., III

The results of the Geosat MOMS subcommittee's data evaluation: Performance and applicability of the MOMS-1 sensor for exploration geology p 33 N89-10380

HENDERSON, FREDERICK B., III

Remote sensing strategies for global resource exploration and environmental management [IAF PAPER 88-103] p 23 A89-17678

HENKEL, J.

Evaluation and digital processing of multispectral SPOT data p 68 A89-20708
Digital analysis of MOMS-1, LANDSAT TM, and SPOT data of the Nakuru area (Kenya) p 33 N89-10386

HERBER, R.

Qualitative aspects of seismograph/ocean bottom interaction [AD-A198652] p 56 N89-14656

HERIC, MATTHEW

Analyses of marine shallow water-bottom features using the Landsat Thematic Mapper, SPOT, and the Large Format Camera p 37 A89-10981

HERMANCE, JOHN F.

Contributions to the GASP workshop proceedings (not presented orally) p 27 N89-12100

HERNANDEZFILHO, PEDRO

Identifying the reforested areas utilizing the SPOT satellite data [INPE-4624-PRE/1343] p 15 N89-10396
Nation-wide forest mapping and timber volume estimation using LANDSAT-5 TM imagery [INPE-4643-PRE/1354] p 16 N89-10402
Method of visual analysis of remote sensing data-vegetation [INPE-4696-MD/037] p 17 N89-12108

HERRING, MARK

High Resolution Imaging Spectrometer (HIRIS) p 74 A89-10334

HERRING, T. A.

VLBI geodesy - 2 parts-per-billion precision in length determinations for transcontinental baselines p 26 A89-13762
VLBI studies of the nutations of the earth p 26 A89-13764

HIGLEY, S. E.

Fiber-optic sensor systems for aerospace applications p 74 A89-10359

HILL, JOACHIM

Regional land cover and agricultural area statistics and mapping in The Departement Ardeche, France, by use of Thematic Mapper data p 8 A89-20705

HILLER, K.

The MOESS experiment: A test case for future cartographic missions p 87 N89-13081

HIMWICH, W. E.

NASA/Crustal Dynamics Project geodetic data analysis p 25 A89-13760

HIRONO, KIICHI

Remote measurements of diatoms chlorophyll-a in the Nori farm p 38 A89-11001

HLAVKA, CHRISTINE A.

The California Cooperative Remote Sensing Project [NASA-TM-100073] p 22 N89-13824

HODGSON, MICHAEL E.

Monitoring Wood Stork foraging habitat using remote sensing and geographic information systems p 7 A89-17399

HOGE, FRANK E.

Airborne lidar detection of subsurface oceanic scattering layers p 41 A89-12260

HOGG, J.

Modelling land resources within a pilot geographical information system p 18 N89-12962
Analysis of potato crop distribution using remotely sensed and environmental data in a pilot geographical information system p 18 N89-12967

HOGG, W. D.

Mid-latitude evaluation of some satellite rainfall estimation techniques p 78 A89-12844

HOGSETT, WILLIAM E.

Analysis of crop loss for alternative ozone exposure indices [PB88-214788] p 22 N89-14608

HOINKA, KLAUS P.

Orographic channeling of a cold front by the Pyrenees p 79 A89-14073

HOLBROOK, J.

Integrating remote sensing data into a geographical information system: A foundation for rural land use strategies: Nature Conservancy Council project p 24 N89-12964

HOLLINGER, A. B.

The fluorescence line imager - An imaging spectrometer for ocean and land remote sensing p 73 A89-10312
Imaging spectrometry as a tool for botanical mapping p 73 A89-10324

HOLLOWAY, K.

Cross-polar radar measurements in ice and rain p 60 N89-12993

HOLMAN, P. B.

An airborne gamma ray snow survey of a forest covered area with a deep snowpack p 7 A89-17284

HOLT, HENRY E.

Sapping features of the Colorado Plateau: A comparative planetary geology field guide [NASA-SP-491] p 34 N89-10401

HOLTZMAN, J. C.

Modulation of the radar backscatter from the ocean surface by a long gravity wave p 51 N89-13031

HOOD, ROBBIE E.

Thunderstorm ice induced brightness temperature depressions at 18, 37, and 92 GHz during Cohnex and their implications for satellite precipitation retrievals p 42 A89-12835

HOOGBOOM, P.

Comparison of wave parameters determined from SLAR images and a pitch and roll buoy p 47 A89-20721

HOQUE, ENAMUL

Relationship between discoloration and histological changes in leaves of trees affected by forest decline p 7 A89-17286

HOSAKAWA, ROBERTO TUYOSHI

The Transformed Vegetation Index (TVI) for estimation of Brazilian cerrado's phytomass [INPE-4603-PRE/1326] p 15 N89-10400

HOVENIER, J. W.

Validation of an atmospheric correction method for satellite borne imagery p 82 N89-10320

HOWARD, ALAN D.

Sapping features of the Colorado Plateau: A comparative planetary geology field guide [NASA-SP-491] p 34 N89-10401

HOWARTH, P. J.

The use of fractal geometry to identify ranges of scale-invariance in digital remotely sensed data p 4 A89-11011

HOWARTH, PHILIP J.

Improving the detection of human-induced change in west Africa's semi-arid zone using multitemporal Landsat MSS imagery p 64 A89-10983
An enhanced classification approach to change detection in semi-arid environments p 68 A89-20627

HOWES, S.

Use of satellite and radar images in operational precipitation nowcasting p 79 A89-13415

HOWMAN, A.

The extrapolation of spectral signatures illustrates LANDSAT's potential to detect wetlands p 62 N89-13067

HSU, L. C.

Desert varnish on volcanic rocks of the Basin and Range province - Composition, morphology, distribution, origin and influence on Landsat imagery p 30 A89-10988

HUBBARD, KENNETH G.

Comparison of measured and modeled radiation, heat and water vapor fluxes: FIFE pilot study [NASA-CR-183304] p 17 N89-11368

HUBBE, JOHN M.

Applications of digital image processing to ongoing research in complex terrain meteorology p 65 A89-11743

HUBBERT, K. P.

Feasibility study for the development of a joint surge and wave model [PB88-230917] p 55 N89-14652

HUBERT, L.

Imaging spectrometry applied to the remote sensing of submerged seaweed p 48 N89-10361

HUDSON, W. D.

Evaluating Landsat classification accuracy from forest cover-type maps p 5 A89-12756

HUDSON, WILLIAM D.

Automatic road detection on Landsat 4 TM images p 23 A89-10997

HUGHES, B. A.

Joint Canada-U.S. Ocean Wave Investigation Project - An overview of the Georgia Strait Experiment p 39 A89-12156

Comparison of Joint Canada-U.S. Ocean Wave Investigation Project synthetic aperture radar data with internal wave observations and modeling results p 39 A89-12160

HUNT, E. RAYMOND, JR.

Relative water content of Spruce needles determined by the leaf water content index p 4 A89-11011

HUNT, G. A.

Remote sensing of laterized Archaean greenstone terrain - Marshall Pool Area, Northeastern Yilgarn Block Western Australia p 31 A89-20622

HUNT, J. J.

Proceedings of the 4th International Colloquium on Spectral Signatures in Remote Sensing [ESA-SP-287] p 9 N89-10300

Proceedings of the 1988 International Geoscience and Remote Sensing Symposium (IGARSS 1988) on Remote Sensing: Moving Towards the 21st Century, volume 1 [ESA-SP-284-VOL-1] p 85 N89-12933

HUTZLER, PETER J. S.

Relationship between discoloration and histological changes in leaves of trees affected by forest decline p 7 A89-17286

HWANG, P. A.

Comparison of measured and predicted sea surface spectra of short waves p 45 A89-16988

HWANG, PAUL A.

The dependence of sea surface slope on atmospheric stability and swell conditions p 45 A89-16988

HYATT, E. C.

Advances in computerized information retrieval in remote sensing p 69 A89-20711

HYPPA, J. M.

Microwave dielectric properties of low-salinity sea ice p 52 N89-13033

I

IBRAHIM, M.

MOMS-1 data for bathymetric and geological studies p 33 N89-10386

IIKURA, Y.

Efficient classification of multispectral images by a best linear discriminant function p 72 N89-13066

IKEDA, MOTO

Prediction of mesoscale ocean circulation in the Norwegian coastal current p 37 A89-10999

IKEDA, MOTOYOSHI

A three-dimensional coupled ice-ocean model of coastal circulation p 38 A89-11144

IL'ICHEV, V. I.

Estimation of the variability of acoustic characteristics in the region of frontal zones and mesoscale vortices using remote sensing data p 47 A89-18844

IMHOFF, M. L.

The derivation of sub-canopy surface terrain models of coastal forests using synthetic aperture radar p 20 N89-13088

IRISH, RICHARD

Extraction of topography from side-looking satellite systems - A case study with SPOT simulation data p 68 A89-16066

ISAACS, RONALD G.

Satellite cloud image standardization p 76 A89-11733

ISOBE, SHUNKICHI

Experimental personal satellite communications system using millimeter-wave for Asia-Oceanian region p 81 A89-18733

ITTEN, K. I.

Improvement in NOAA-AVHRR snowcover determination for runoff prediction p 61 N89-13046

J

JACKSON, T. J.

Soil erosion study using an airborne laser profiler p 1 A89-10959

JACOBBERGER, P. A.

Mapping abandoned river channels in Mali through directional filtering of Thematic Mapper data p 58 A89-17288

JACOBSEN, K.

Evaluation of space photographs p 82 A89-20711

JACOBSEN, S.

Ocean wave number spectra and spatial autocorrelation functions from SAR images p 50 N89-12977

JAIN, ANIL K.

Automatic road detection on Landsat 4 TM images p 23 A89-10997

JAMESON, ARTHUR R.

A new radar technique for satellite rainfall algorithm development [NASA-CR-183471] p 60 N89-11100

JAMIESON, MICHAEL

The GVAR users compendium, volume 1 [NOAA-NESDI-S-21-VOL-1] p 85 N89-12100

K

- JAMPOLER, SUSAN**
Landsat TM and MSS digital data comparison - Imperial Valley p 3 A89-10989
- JANOTA, PAUL**
Digital image processing and visual communications technologies in meteorology; Proceedings of the Meeting, Cambridge, MA, Oct. 27, 28, 1987 [SPIE-846] p 65 A89-11726
- JANSSEN, L.**
Aircraft remote sensing in HAPEX p 59 N89-10388
- JAPPIOT, M.**
Biomass and wheat crop yield estimation from SPOT vegetative indexes p 11 N89-10327
- JARVIS, C.**
Evaluation of LANDSAT TM and SPOT imagery for agricultural land use planning in less developed countries p 19 N89-13051
- JASENTULIYANA, N.**
UN principles on remote sensing - An agreement on economic relations p 90 A89-19385
- JASINSKI, MICHAEL F.**
The structure of red-infrared scattergrams of semivegetated landscapes [NASA-CR-183385] p 21 N89-13091
Use of LANDSAT images of vegetation cover to estimate effective hydraulic properties of soils [NASA-CR-183384] p 21 N89-13823
- JASKOLLA, F.**
Evaluation and digital processing of multispectral SPOT data p 68 A89-20708
Comparative geological evolution of different remote sensing data of the Hoggar Mountains (Algeria) p 33 N89-10385
- JAYASINGHE, DON**
Automatic control point determination for image registration using texture analysis methods p 3 A89-10985
- JENSEN, JOHN R.**
Monitoring Wood Stork foraging habitat using remote sensing and geographic information systems p 7 A89-17399
- JENTZ, R. R.**
Sea ice type classification of SAR imagery p 52 N89-13039
- JOHANNESEN, JOHNNY A.**
Mizex '87 - Overview of the Winter Marginal Ice Zone Experiment in the Greenland and Barents Seas p 36 A89-10931
- JOHANNESEN, JOHNNY ANDRE**
Prediction of mesoscale ocean circulation in the Norwegian coastal current p 37 A89-10994
- JOHANNESEN, OLA M.**
Mizex '87 - Overview of the Winter Marginal Ice Zone Experiment in the Greenland and Barents Seas p 36 A89-10931
- JOHNSEN, H.**
Ocean wave number spectra and spatial autocorrelation functions from SAR images p 50 N89-12970
- JOHNSON, D.**
Some characteristics of short ocean waves as microwave scatterers p 51 N89-13030
- JOHNSON, EDWARD R.**
Validation of the on-site Flash Flood Potential System for Nexrad p 57 A89-10949
- JOHNSON, GARY E.**
The application of remote sensing for drought early warning in Africa p 1 A89-10948
- JONES, W. P.**
Geological mapping and mineral exploration in eastern Nova Scotia utilizing airborne and spaceborne multisensor data p 30 A89-14008
- JORDAN, THOMAS H.**
Beyond plate tectonics - Looking at plate deformation with space geodesy p 44 A89-13758
- JOUAN, JACKY**
Wide field high performance lenses [IAF PAPER 88-120] p 80 A89-17685
- JUHASZ, I.**
Agroecological information content of SPOT data p 19 N89-13050
- JULLIEN, J. P.**
A study of the vegetation cover with AVHRR during HAPEX-MOBILHY p 15 N89-10389
- JULYAN, DAVID S.**
Commercialized remote sensing - A comprehensive view for global studies p 81 A89-20102
- JUNG, K.**
Design of spectral bands for the German MOMS-2 sensor p 84 N89-10381
- JUSTICE, C. O.**
Spatial resolution requirements for MODIS-N p 83 N89-10364
- JUVIGNY, A.**
The image detection subassembly for the SPOT 4 'vegetation' instrument [IAF PAPER 88-121] p 7 A89-17686
- KAEHNY, D.**
Coherent polarimetric signatures of coniferous trees: A survey p 9 N89-10307
Polarization-dependent attenuation of dielectric cylinder arrays p 86 N89-12955
- KALINAUSKAS, A. R.**
Imaging spectrometry for water applications p 56 A89-10327
- KAMATH, V. A.**
Development of Alaskan gas hydrate resources [DE88-010270] p 35 N89-13093
- KAMEL, A. A.**
GOES I-M image navigation and registration system p 75 A89-10965
- KAMOCHI, YASUNORI**
Fault tolerant design of attitude and orbit control subsystem for earth resources satellite-1 [AIAA PAPER 88-3879] p 80 A89-18073
- KAMOUN, P.**
Evaluation of VARAN data in geology and geomorphology in the southeast of France p 32 N89-10313
- KANGEYAM, S. K.**
A comparative evaluation of use of Landsat MSS FCC and MKF-6M photographs for forest type delineation p 6 A89-14010
- KANTCHEVA, R.**
The use of spectral reflectance characteristics for the estimation of the wheat crop state p 5 A89-12874
- KAROUICHE, N.**
Design of a spaceborne rain mapping radar [IAF PAPER 88-124] p 58 A89-17688
Design of a spaceborne radar for tropical rain mapping at the climatological scale p 60 N89-12997
- KASILINGAM, DAYALAN P.**
Theory for synthetic aperture radar imaging of the ocean surface - With application to the Tower Ocean Wave and Radar Dependence experiment on focus, resolution, and wave height spectra p 44 A89-16977
- KASISCHKE, E. S.**
Comparison of Joint Canada-U.S. Ocean Wave Investigation Project synthetic aperture radar data with internal wave observations and modeling results p 39 A89-12160
An overview of the SAR Internal Wave Signature Experiment p 40 A89-12162
- KASISCHKE, ERIC S.**
Contrast ratios of internal waves in synthetic aperture radar imagery - A comparison of SAR Internal Wave Signature Experiment observations with theory p 40 A89-12167
- KATSAROS, KRISTINA B.**
On the interpretation of integrated water vapor patterns in midlatitude cyclones derived from the Nimbus 7 scanning multichannel microwave radiometer p 76 A89-12790
A comparison of satellite and empirical formula techniques for estimating insolation over the oceans p 44 A89-15495
- KAUFFMAN, D. S.**
Extraction of dense digital elevation models from SPOT stereo imagery p 71 N89-13053
- KAUFMAN, YORAM J.**
Algorithm for automatic atmospheric corrections to visible and near-IR satellite imagery p 66 A89-12224
- KAUFMANN, H.**
Mineral exploration along the Aqaba-Levant structure by use of TM-data - Concepts, processing and results p 31 A89-20709
Design of spectral bands for the German MOMS-2 sensor p 84 N89-10381
- KAWATA, Y.**
Snowmelt runoff estimation using snow cover extent data and its application to optimum control of dam water level p 61 N89-13042
- KAY, S.**
The differential rectification of SPOT HRV panchromatic and multispectral imagery using a digital elevation model p 28 N89-13054
- KELLER, MARY R.**
X-band scatterometer measurements at low winds in a wavetank p 78 A89-12867
- KELLER, V.**
Laser Atmospheric Wind Sounder (LAWS) p 79 A89-15889
- KELLEY, JOHN G. W.**
Meteorological surface analysis using perspective topographic maps p 65 A89-11740
- KELLY, K. A.**
Modelling of surface waves and sea state-dependent wind stress for the Northeast Pacific Ocean using Seasat scatterometer data p 43 A89-12858
Wind and wind stress curl fields for the Northeast Pacific Ocean using satellite scatterometer data p 78 A89-12859
- KENDALL, BRUCE M.**
Passive microwave remote sensing of salinity in coastal zones p 36 A89-10942
- KENNETT, R. G.**
Performance of a scanning pencil-beam spaceborne scatterometer for ocean wind measurements p 53 N89-13073
- KENSELAAR, FRANK**
On the connection of digitized maps to a uniform coordinate system. A special case of the geodetic connection problem [B8821602] p 28 N89-14487
- KERR, Y. H.**
Monitoring seasonal variations of soil moisture and vegetation cover using satellite microwave radiometry p 15 N89-10378
- KESHAVAMURTHY, A. C.**
A comparative evaluation of use of Landsat MSS FCC and MKF-6M photographs for forest type delineation p 6 A89-14010
- KESTER, DANA A.**
Chemical variability in ocean frontal areas [AD-A198418] p 56 N89-14655
- KEYDEL, W.**
The airborne radiometry experiment (ABREX) instrument, an experimental test bed for the specification of satellite-borne microwave radiometer at 90 GHz p 86 N89-12939
- KHORRAM, S.**
Multitemporal resource complex analysis of Catina province, Italy from LANDSAT-TM data p 71 N89-12985
- KILAMBI, A.**
VISSR sensor introduced modifications in the presence of large temperature gradients p 78 A89-12860
- KIM, HONGSUK H.**
Atmospheric effect removal from space imagery p 69 N89-10338
- KIM, S. T.**
User's guide for the Nimbus 7 Scanning Multichannel Microwave Radiometer (SMMR) CELL-ALL tape [NASA-RP-1210] p 89 N89-14648
- KIMURA, A.**
Laser-induced fluorescence on in-vivo chlorophyll of a rice plant: A technique for the remote detection of plant growth p 12 N89-10350
- KING, D.**
Land and forest cover information from aerial video p 1 A89-10946
- KING, PATRICK**
Variation of satellite rain relationships in space and time p 67 A89-12843
- KING, R. B.**
Evaluation of LANDSAT TM and SPOT imagery for agricultural land use planning in less developed countries p 19 N89-13051
- KIRCHHOFF, W.**
Spectral characterization of forest damage in beech, oak and pine stands p 21 N89-13085
- KITTLESOM, KYLE**
Evapotranspiration monitored from satellites as an indication of shift and impact of vegetation change p 2 A89-10975
- KLEESPIES, THOMAS J.**
An extension of the split window technique for the retrieval of precipitable water - Experimental verification [AD-A199515] p 76 A89-12796
Possible measurement errors in calibrated AVHRR (Advanced Very High Resolution Radiometer) data [AD-A198342] p 88 N89-14414
- KLEIN, R.**
Solid earth mission study. Volume 2: Technical report [ESA-CR(P)-2626-VOL-2] p 26 N89-10303
Solid Earth mission study. Volume 1: Executive summary [ESA-CR(P)-2626-VOL-1] p 26 N89-10397
Solid earth mission study. Volume 3: Program planning report [ESA-CR(P)-2626-VOL-3] p 27 N89-10399
- KLEMAS, V.**
Remote sensing of estuaries - An overview p 56 A89-10939
- KNEPPECK, I. D.**
Evaluation of a multispectral linear array sensor for assessing juvenile stand conditions p 3 A89-11000
- KNIGHT, PAUL G.**
Meteorological surface analysis using perspective topographic maps p 65 A89-11740
- KOCHEL, R. CRAIG**
Sapping features of the Colorado Plateau: A comparative planetary geology field guide [NASA-SP-491] p 34 N89-10401
- KOECHLER, C.**
Time-resolved laser fluorescing: Trends and applications p 83 N89-10346

L

- KOKKE, J. M. M.**
Validation of an atmospheric correction method for satellite borne imagery p 82 N89-10320
- KOMAJDA, RAYMOND J.**
The GVAR users compendium, volume 1 [NOAA-NESDIS-21-VOL-1] p 85 N89-12105
- KONDRATEV, K. IA.**
The potential of using remotely sensed information for studying the contamination and eutrophication of lake systems p 58 A89-18708
- KONG, J. A.**
Correlation function study for sea ice p 46 A89-16990
- Remote sensing of earth terrain [NASA-CR-183347] p 85 N89-12111
- KONG, XIANG NING**
Effect of spatial resolution of the statistical properties of satellite images - A case study p 66 A89-12221
- KOSTERS, ANTON J. M.**
On the connection of geodetic point fields in Réseau European Trigonometrique (RETRIG) and related tests for model errors [ETN-89-93327] p 28 N89-14485
- KOZU, TOSHIAKI**
Backscattering coefficient of rice crops and rice fields by an X-band scatterometer p 3 A89-10980
- KRABILL, WILLIAM B.**
Airborne lidar detection of subsurface oceanic scattering layers p 41 A89-12260
- KRISHNANUNNI, K.**
Indian experience in the dissemination and use of remote sensing data and future prospects [IAF PAPER 88-131] p 80 A89-17689
- KRITIKOS, G.**
Optimization for classification of forest damage classes p 13 N89-10359
- KROGER, P. M.**
Distribution of relative plate motion along the Pacific-North American plate boundary determined from mobile VLB measurements p 26 A89-13761
- KROGSTAD, H. E.**
An intercomparison of SAR and buoy directional wave spectra from the Labrador Sea Extreme Waves Experiment (LEWEX) p 50 N89-12972
- KRUG, THELMA**
An agricultural crop yield model by satellite: A simulation [INPE-4639-PRE/1350] p 17 N89-12106
- KRUL, L.**
Some results of microwave remote sensing research in The Netherlands with a view to land applications in the 1990s p 8 A89-20703
- KRUSE, FRED A.**
Extracting spectral information from imaging spectrometer data - A case history from the northern Grapevine Mountains, Nevada/California p 29 A89-10326
- KUEHBAUCH, W.**
Spectral reflectance of sugar beet and winter wheat canopies in the visible and infrared during growth p 12 N89-10342
- KUMAR, R.**
Improvement of cloud cover assessment of Landsat Thematic Mapper data p 65 A89-11003
- KUMMEROW, CHRISTIAN DETLEF**
Microwave radiances from horizontally finite, vertically structured precipitating clouds p 84 A89-11364
- KUPFER, G.**
Spectral reflectance of sugar beet and winter wheat canopies in the visible and infrared during growth p 12 N89-10342
- KUROSU, TAKASHI**
Backscattering coefficient of rice crops and rice fields by an X-band scatterometer p 3 A89-10980
- KUSAKA, T.**
Snowmelt runoff estimation using snow cover extent data and its application to optimum control of dam water level p 61 N89-13042
- KUSAKA, TAKASHI**
Region extraction in SPOT data p 67 A89-14007
- KUSHWAHA, S. P. S.**
A comparative evaluation of use of Landsat MSS FCC and MKF-6M photographs for forest type delineation p 6 A89-14010
- KUX, H. J. H.**
Microwave remote sensing at the Institute for Space Research (INPE) Brazil: Concepts and future prospects of soil moisture studies p 20 N89-13080
- KWOH, D. S. W.**
Microwave scattering from internal wave modulated surface waves - A shipboard real aperture coherent radar study in the Georgia Strait Experiment p 39 A89-12157

- LAAGER, P.**
Monitoring of seasonal snow cover on glaciers p 61 N89-13044
- LABEL, J.**
Attempt at absolute determination of spectral signatures of bare soils in the thermal infrared, in emission and reflection p 12 N89-10336
- LAGERLOEF, GARY S. E.**
EOF analysis of AVHRR and CZCS imagery p 43 A89-12856
- LAGOUARDE, J. P.**
A new method for estimating regional evaporation from thermal infrared surface temperature measurements p 60 N89-10390
- LAKE, B. M.**
Microwave scattering from internal wave modulated surface waves - A shipboard real aperture coherent radar study in the Georgia Strait Experiment p 39 A89-12157
- Comparison of Joint Canada-U.S. Ocean Wave Investigation Project synthetic aperture radar data with internal wave observations and modeling results p 39 A89-12160
- LAMBERT, E.**
Imaging spectrometry applied to the remote sensing of submerged seaweed p 48 N89-10361
- LAMBERTY, M.**
Spectral characterization of forest damage in beech, oak and pine stands p 21 N89-13085
- LANDRY, R.**
Texture analysis in forest areas: High spectral resolution synthetic aperture radar data p 14 N89-10367
- LANGEMANN, M.**
Solid earth mission study. Volume 2: Technical report [ESA-CR(P)-2626-VOL-2] p 26 N89-10303
- Solid Earth mission study. Volume 1: Executive summary [ESA-CR(P)-2626-VOL-1] p 26 N89-10397
- Solid earth mission study. Volume 3: Program planning report [ESA-CR(P)-2626-VOL-3] p 27 N89-10399
- LANGLOIS, P. M.**
Millimeter-wave backscatter measurements of various snow forms p 61 N89-13046
- LANZL, F.**
The MEOSS experiment: A test case for future cartographic missions p 87 N89-13081
- LAROCHE, P.**
Spectral analysis of ocean wave imagery using 2-D linear prediction p 50 N89-12968
- LARSEN, S. E.**
Wind stress measurements during the Tower Ocean Wave and Radar Dependence experiment p 45 A89-16984
- LARSEN, SHAWN**
Determination of convergence rates across the Ventura Basin, Southern California, using GPS and historical triangulation [NASA-CR-183014] p 29 N89-14624
- LAUER, DONALD T.**
Sino-American cooperative studies on applications of remote sensing to surveying and mapping p 29 A89-10967
- LAURIN, RAYMOND**
Utilization of Landsat data and a geographic information system (GIS) for improving watershed management in India p 57 A89-11014
- LAVREAU, J.**
Rock and soil discrimination in natural tropical conditions using a spot-calibrated radiometer p 14 N89-10374
- LAYCOCK, J.**
An analysis of directional ambiguities in wind scatterometer measurements p 87 N89-13071
- LE BOURLOUT, L.**
The image detection subassembly for the SPOT 4 'vegetation' instrument [IAF PAPER 88-121] p 7 A89-17686
- LE VOURCH, J.**
Sea surface parameters inferred from meteorological satellite data at CMS, Lannion p 47 A89-20722
- LEBORGNE, P.**
Sea surface parameters inferred from meteorological satellite data at CMS, Lannion p 47 A89-20722
- LECHI, G.**
Tests of topographic mapping with Thematic Mapper images p 69 A89-20712
- LECKIE, D. G.**
Advanced airborne electro-optical imager p 74 A89-10929
- Sensor band selection for detecting current defoliation caused by the spruce budworm p 6 A89-16062
- LECONG, P.**
Fiber-optic sensor systems for aerospace applications p 74 A89-10359

- LEDREW, ELLSWORTH**
Land cover change detection with Thematic Mapper spectral textural data at the rural-urban fringe p 23 A89-10982
- LEDUC, SHARON K.**
The application of remote sensing for drought early warning in Africa p 1 A89-10948
- LEE, DAVID CHUNG LIANG**
Nation-wide forest mapping and timber volume estimation using LANDSAT-5 TM imagery [INPE-4643-PRE/1354] p 16 N89-10402
- LEE, E. HENRY**
Analysis of crop loss for alternative ozone exposure indices [PB88-214788] p 22 N89-14608
- LEETMAA, ANTS**
Acoustic Doppler current profiling in the equatorial Pacific in 1984 p 45 A89-16986
- LEHMANN, F.**
Thermal infrared laser spectroscopy: The potential of dual active/passive thermal infrared sensors for Earth observation p 82 N89-10345
- LEI, GUANG-TSAI**
Investigation of radar backscattering from second-year sea ice [NASA-CR-180986] p 54 N89-14479
- LEMASON, C.**
Comparative analysis of spectral response in the optical domain of targets in a tropical swamp at various spectral and spatial resolutions p 13 N89-10363
- LEPPERT, NORMAN D.**
Acreage and yield determination - 1987 Kansas winter wheat p 4 A89-11007
- LEPRIEUR, C.**
Spectral characterization of forest targets in mountainous zones on Thematic Mapper images p 11 N89-10328
- LESCHACK, A. RICHARD**
A preliminary model for Geosat altimeter data errors p 44 A89-13958
- LESCHACK, L.**
Soil erosion study using an airborne laser profiler p 1 A89-10952
- LETERME, P.**
Potential number of winter wheat ears estimation using radiometry techniques at an early stage p 10 N89-10323
- LETOAN, ALPHONSE**
Retrieving vegetation and soil parameters from radar measurements p 10 N89-10321
- LETOAN, T.**
Retrieving vegetation and soil parameters from radar measurements p 10 N89-10321
- LEVINE, D. M.**
The electronically steered thinned array radiometer p 74 A89-10932
- LEVY, GAD**
A study of the dynamics of maritime fronts using remotely sensed wind and stress measurements p 84 N89-11366
- LEWES, FRANK J.**
Working group reports submitted by group chairmen following workshop p 27 N89-12098
- LEWIS, R.**
Development of a ground hydrology model suitable for global climate modeling using soil morphology and vegetation cover, and an evaluation of remotely sensed information [NASA-CR-180463] p 21 N89-13821
- LICHTENTHALER, H. K.**
Changes in the chlorophyll fluorescence spectra during the Kautsky induction kinetics p 12 N89-10348
- Chlorophyll fluorescence spectra of leaves as induced by blue light and red laser light p 12 N89-10349
- LILLESAND, THOMAS M.**
The potentials and challenges afforded by SPOT-1 data p 63 A89-10945
- LIN, F. C.**
Correlation function study for sea ice p 46 A89-16990
- LIND, RICHARD J.**
A comparison of satellite and empirical formula techniques for estimating insolation over the oceans p 44 A89-15495
- LINDSTROM, D. R.**
Data report for the Siple Coast (Antarctica) project [NASA-TM-100708] p 49 N89-10403
- LINGNER, D.**
A satellite data processing and analysis software system for earth's atmosphere and surface research p 67 A89-12864
- LIU, ANTONY K.**
Analysis of nonlinear internal waves in the New York Bight p 40 A89-12163

- LIVINGSTON, J. M.**
Comparison of in situ aerosol measurements with SAGE 2 and SAM 2 aerosol measurements during the airborne Antarctic ozone experiment p 89 N89-14522
- LOBANOV, V. B.**
Estimation of the variability of acoustic characteristics in the region of frontal zones and mesoscale vortices using remote sensing data p 47 A89-18843
- LODWICK, G. D.**
Edge detection and processing of remotely sensed digital images p 64 A89-10984
- LONG, D. G.**
Model-based estimation of wind fields over the ocean from wind scatterometer measurements p 53 N89-13070
- LOOYEN, W. J.**
Automatic procedure to find corresponding points in CCD Airborne Experimental Scanner for Applications in Remote sensing (CAESAR) images [B8821609] p 88 N89-14490
- LOUAHALA, S.**
Evaluation of VARAN data in geology and geomorphology in the southeast of France p 32 N89-10313
Usefulness of high spectral resolution radiometry for geological mapping in the Mediterranean region p 32 N89-10360
- LOUBERSAC, L.**
Comparative analysis of spectral response in the optical domain of targets in a tropical swamp at various spectral and spatial resolutions p 13 N89-10363
- LOVEJOY, S.**
Resolution dependence in satellite imagery - Multifractal analysis p 67 A89-12852
- LUBICH, DEBRA A.**
The use of polar orbiter data in tropical weather system analysis p 77 A89-12818
- LUDWIG, R.**
Improvement of cloud cover assessment of Landsat Thematic Mapper data p 65 A89-11003
- LUNDEN, B.**
Atmospheric correction of thermal infrared data from LANDSAT-5 for surface temperature estimation p 70 N89-10339
LANDSAT Thematic Mapping (TM) and SPOT HRV for survey mapping of bedrock outcrops p 20 N89-13055
- LYONS, T. J.**
The development of tropical cyclones in the north-west of Australia p 41 A89-12203
- LYZENGA, D. R.**
Comparison of Joint Canada-U.S. Ocean Wave Investigation Project synthetic aperture radar data with internal wave observations and modeling results p 39 A89-12160
- LYZENGA, DAVID R.**
Full-spectrum modeling of synthetic aperture radar internal wave signatures p 40 A89-12166
Contrast ratios of internal waves in synthetic aperture radar imagery - A comparison of SAR Internal Wave Signature Experiment observations with theory p 40 A89-12167
An analytic representation of the synthetic aperture radar image spectrum for ocean waves p 45 A89-16979
- LYZENGA, G. A.**
Distribution of relative plate motion along the Pacific-North American plate boundary determined from mobile VLBI measurements p 26 A89-13761
- M**
- MACARTHUR, J. L.**
Directional ocean wave spectra: Prospects for acquiring a global data base from SIR-C p 50 N89-12973
- MACAYEAL, D. R.**
Data report for the Siple Coast (Antarctica) project [NASA-TM-100708] p 49 N89-10403
- MACHADOESILVA, ANTONIO JOSE F.**
Photogrammetric model for correction of MSS-LANDSAT imagery [INPE-4652-PRE/1359] p 73 N89-13090
- MACK, DONALD**
The GVAR users compendium, volume 1 [NOAA-NESDIS-21-VOL-1] p 85 N89-12105
- MACEY, HALKARD E., JR.**
Monitoring Wood Stork foraging habitat using remote sensing and geographic information systems p 7 A89-17399
- MACKIE, M.**
Improvement of cloud cover assessment of Landsat Thematic Mapper data p 65 A89-11003
- MACKIN, S.**
Mapping the distribution and abundance of lithological units and surface mineralogies at Jabal Sa'id, Saudi Arabia: An application of spectral mixture modelling p 34 N89-13024
- MACKLIN, J. T.**
The use of the complex correlation function in the recovery of ocean wave spectra from SAR images p 47 N89-10315
Constraints on two-scale descriptions of radar backscattering from the sea surface using scatterometer model functions p 49 N89-12945
Complex SAR imagery and speckle filtering for ERS-1 wave mode p 71 N89-13029
- MACLENNAN, M. J.**
The use of fractal geometry to identify ranges of scale-invariance in digital remotely sensed data p 4 A89-11011
- MADHAVAN UNNI, N. V.**
A comparative evaluation of use of Landsat MSS FCC and MKF-6M photographs for forest type delineation p 6 A89-14010
- MAE, S.**
Inference of radio scattering parameters of Antarctic ice sheet using 179 MHz airborne radio echo sounding data p 51 N89-12975
- MAEDA, K.**
Verification results of MOS-1 multispectral self scanning radiometer (MESSR) data p 86 N89-13004
- MAJOR, EUGENE R.**
Nimbus-7 SMMR derived sea-ice concentrations over Antarctica p 43 A89-12857
- MAKI, LESLIE W.**
Integrating remotely sensed data into PC-based geographic information systems p 23 A89-10959
- MALILA, W.**
The prospects for detecting spectral shifts due to satellite sensor aging p 6 A89-16061
- MALLINGE, N.**
Wide field high performance lenses [IAF PAPER 88-120] p 80 A89-17685
- MALYKHINA, I. I.**
The potential of using remotely sensed information for studying the contamination and eutrophication of lake systems p 58 A89-18708
- MAMEDOV, N. G.**
Accounting for selective absorption in the evaluation of the earth surface temperature by an angular method p 80 A89-18710
- MARACCHI, G.**
Forest classification by principal component analyses of TM data p 8 A89-20706
- MARCHAND, CAROLINE**
PRISM B (Prediction of the Indian Summer Monsoon - Bellevue) [IAF PAPER ST-88-02] p 58 A89-17873
- MARENGO, L. R. M.**
Cotton area mapping using multitemporal satellite data integrated within a geographical information system applied to a cotton boll weevil control programme in Paraguay p 20 N89-13077
- MARINO, C. M.**
Use of Landsat and Seasat data as a tool in kinematic analysis - The Tunisian Atlas p 31 A89-20710
- MARKHAM, B. L.**
Spatial resolution requirements for MODIS-N p 83 N89-10364
- MARSOUIN, A.**
Sea surface parameters inferred from meteorological satellite data at CMS, Lannion p 47 A89-20722
- MARTINEC, J.**
Average areal water equivalent of snow in a mountain basin using microwave and visible satellite data p 61 N89-13045
- MARTINUZZI, MICHEL**
Wide field high performance lenses [IAF PAPER 88-120] p 80 A89-17685
- MARZOUG, M.**
Design of a spaceborne rain mapping radar [IAF PAPER 88-124] p 58 A89-17688
Design of a spaceborne radar for tropical rain mapping at the climatological scale p 60 N89-12997
- MASARO, D.**
The ERS-1 Instrument Data Handling and Transmission subsystem (IDHT) and its evolution [IAF PAPER 88-134] p 80 A89-17690
- MASELLI, F.**
Forest classification by principal component analyses of TM data p 8 A89-20706
- MASLANIK, JAMES A.**
Comparison of Nimbus 7 scanning multichannel microwave radiometer radiance and derived sea ice concentrations with Landsat imagery for the north water area of Baffin Bay p 38 A89-11150
- MASON, D. C.**
Segmentation of remotely-sensed images by a split-and-merge process p 66 A89-12222
- MATHEWS, J.**
The classification of semi-natural vegetation from LANDSAT Thematic Mapper imagery: A user's perspective p 21 N89-13084
- MATSON, MICHAEL**
Regional and global fire detection using AVHRR data p 2 A89-10956
- MATSON, PAMELA A.**
Prediction of leaf chemistry by the use of visible and near infrared reflectance spectroscopy p 7 A89-17283
- MATSUMOTO, Y.**
Detection of seasonal and long-term changes in land cover from multitemporal LANDSAT MSS data p 71 N89-12989
- MAUGHAN, PAUL M.**
Envirosat - A vehicle for examining the options for earth observations in the 1990's p 81 A89-20105
- MAY, DOUGLAS A.**
The impact of satellite infrared sea surface temperatures on the FNOG (Fleet Numerical Oceanography Center) EOTS (Expanded Ocean Thermal Structure) regional gulf stream analysis [AD-A198965] p 54 N89-13864
- MAY, L. NELSON, JR.**
Utilizing remote sensing of thematic mapper data to improve our understanding of estuarine processes and their influence on the productivity of estuarine-dependent fisheries [NASA-CR-183409] p 62 N89-13822
- MAZZINGHI, P.**
A new lidar system for applications over land and sea p 83 N89-10347
- MCADOO, DAVID C.**
Improvements in the marine gravity field from Geosat/ERM p 36 A89-10962
- MCCADDEN, RICHARD J.**
Simplified forest inventory using large-scale 70-mm photography and tariff tables p 6 A89-14090
- MCCLAIN, C. R.**
Phytoplankton standing crops within an Antarctic ice edge assessed by satellite remote sensing p 41 A89-12174
- MCCORMICK, M. PATRICK**
Comparison of in situ aerosol measurements with SAGE 2 and SAM 2 aerosol measurements during the airborne Antarctic ozone experiment p 89 N89-14522
- MCDONALD, A. J. W.**
Applications of remote sensing for geological mapping in eastern Egypt p 35 N89-13087
- MCELROY, JOHN H.**
On-board processing and national earth observations centers p 22 A89-10927
- MCQUIRE, J.**
An evaluation of satellite imagery, LANDSAT Thematic Mapper and SPOT-1 HRV, for grassland inventory in the UK p 20 N89-13057
- MCINTOSH, R. E.**
A concept for measuring currents from geostationary satellites p 75 A89-10933
Millimeter-wave backscatter measurements of various snow forms p 61 N89-13046
- MCKENZIE, KEITH**
The GVAR users compendium, volume 1 [NOAA-NESDIS-21-VOL-1] p 85 N89-12105
- MCKIM, HARLAN L.**
Extraction of topography from side-looking satellite systems - A case study with SPOT simulation data p 68 A89-16063
- MCMILLIN, LARRY M.**
Retrieval of air surface temperatures over oceans from satellite radiance measurements using stratification techniques p 42 A89-12779
An extension of the split window technique for the retrieval of precipitable water - Experimental verification [AD-A199515] p 76 A89-12796
Evaluation of 3.7 micron split windows for estimating surface temperature p 43 A89-12855
- MCMURDIE, LYNN A.**
On the interpretation of integrated water vapor patterns in midlatitude cyclones derived from the Nimbus 7 scanning multichannel microwave radiometer p 76 A89-12790
- MCNUTT, L.**
The LIMEX 1987 pilot project, LIMEX 1989 and long-term objective for data collection on the Canadian East coast p 52 N89-13037
- MCWETHY, L. GUY**
Applications of digital image processing to ongoing research in complex terrain meteorology p 65 A89-11743
- MEADOWS, A. J.**
A comparison of reduction methods for satellite altimetry data p 39 A89-11424
- MEGIER, JACQUES**
Regional land cover and agricultural area statistics and mapping in The Departement Ardeche, France, by use of Thematic Mapper data p 8 A89-20705
- MEISSNER, D.**
Design of spectral bands for the German MOMS-2 sensor p 84 N89-10381

MELIA, J.

Spectral signature of citrus fruits and its evolution: Identification of the vegetative index of least temporal variation p 14 N89-10373

MENARD, YVES

Observing the seasonal variability in the tropical Atlantic from altimetry p 46 A89-16987

MENDEL, J. M.

Model-based estimation of wind fields over the ocean from wind scatterometer measurements p 53 N89-13070

MENESES, PAULO ROBERTO

Color enhancement of remote sensing imagery using IHS transformations and decorrelation stretch methods [INPE-4559-PRE/1300] p 70 N89-11418

MERRITT, EARL S.

Remote sensing technologies and spatial data applications [AD-A195809] p 62 N89-14480

MERRY, CAROLYN J.

Extraction of topography from side-looking satellite systems - A case study with SPOT simulation data p 68 A89-16063

MEULSTEE, C.

Aerial photography for biomass assessment in the intertidal zone p 9 A89-20724

MICHAELIS, M.

Interpretation and geometrical aspects of Thematic Mapper data p 69 A89-20716

MICHAL, R. J.

Fiber-optic sensor systems for aerospace applications p 74 A89-10359

MIGLIETTA, F.

Forest classification by principal component analyses of TM data p 8 A89-20706

MIKKELSEN, T.

Wind stress measurements during the Tower Ocean Wave and Radar Dependence experiment p 45 A89-16984

MILLER, D.

Performance modeling and results for X-SAR p 71 N89-13009

MILLER, DOUGLAS K.

An example of estimates of precipitable water derived from Nimbus-7 SMMR satellite measurements and FGGE upper air data p 42 A89-12792

MILLER, J. R.

Imaging spectrometry as a tool for botanical mapping p 73 A89-10324

MILLER, LAURY

Sea level variations in the tropical Pacific during 1985-87 derived from GEOSAT altimetry p 36 A89-10961

MILLER, MICHAEL S.

Extraction of topography from side-looking satellite systems - A case study with SPOT simulation data p 68 A89-16063

MILLINGTON, A. C.

Monitoring playas using Thematic Mapper data p 60 N89-13028

MILNE, A. K.

Change direction analysis using LANDSAT imagery: A review of methodology p 72 N89-13068

MILTON, E. J.

A simplified reflectance model for shrub canopies p 11 N89-10329

MINEART, GARY M.

Multispectral satellite analysis of marine stratocumulus cloud microphysics [AD-A197316] p 87 N89-13092

MINNETT, P. J.

The numerical simulation of infrared satellite measurements over the Greenland-Iceland-Norwegian Sea [AD-A198653] p 54 N89-14484

MINSTER, J. BERNARD

Beyond plate tectonics - Looking at plate deformation with space geodesy p 44 A89-13758

MINSTER, J. F.

Comparison between active and passive microwave measurements over Antarctica p 48 N89-10316

MIROVSKII, V. G.

The effect of snow parameter variations on the thermal microwave emission of the soil-snow-atmosphere system p 59 A89-18712

MITCHELL, A. J. B.

Evaluation of LANDSAT TM and SPOT imagery for agricultural land use planning in less developed countries p 19 N89-13051

MITCHELL, C. W.

An international approach to GIS based on remote sensing and terrain classification p 24 N89-12966

MITNIK, L. M.

Estimation of the variability of acoustic characteristics in the region of frontal zones and mesoscale vortices using remote sensing data p 47 A89-18843

MIZOGUCHI, T.

Efficient classification of multispectral images by a best linear discriminant function p 72 N89-13060

MO, TSAN

Modelling of SAR polarisation phase difference from trees p 18 N89-12951

MOBLEY, CURTIS D.

A numerical model for the computation of radiance distributions in natural waters with wind-roughened surfaces [AD-A197207] p 53 N89-13128

MOCCIA, A.

Three-dimensional observation by means of tethered antennae [IAF PAPER 88-118] p 80 A89-17684

MOCCIA, ANTONIO

A procedure for modeling the terrain relief by using digitized topographic maps p 67 A89-14005

MONALDO, F. M.

On the use of speckle statistics for the extraction of ocean wave spectra from SAR imagery p 50 N89-12969

Directional ocean wave spectra: Prospects for acquiring a global data base from SIR-C p 50 N89-12973

MOORE, R. K.

Modulation of the radar backscatter from the ocean surface by a long gravity wave p 51 N89-13031
Performance of a scanning pencil-beam spaceborne scatterometer for ocean wind measurements p 53 N89-13073

MOORE, RICHARD K.

Investigation of radar backscattering from second-year sea ice [NASA-CR-180986] p 54 N89-14479

MORAIN, STAN A.

Business strategies and land remote sensing capabilities p 90 A89-20104

MOREL, ANDRE

Optical modeling of the upper ocean in relation to its biogenous matter content (case I waters) p 38 A89-11149

MORIANDO, A.

Tests of topographic mapping with Thematic Mapper images p 69 A89-20712

MORISON, J. H.

An autonomous ocean instrument platform driven vertically by the current [AD-A198226] p 54 N89-13865

MORISSONVALERIANO, DALTON

Interaction of solar radiation with vegetation [INPE-4697-MD/038] p 17 N89-12109

MORRICE, J. G.

Analysis of potato crop distribution using remotely sensed and environmental data in a pilot geographical information system p 18 N89-12967

MORRIS, CARL N.

Binary image classification p 73 N89-13908

MORRIS, K. ROBERT

Comparison of satellite IR rain estimates with radar rain observations in hurricanes p 57 A89-12845

MORTON, A. J.

The detection of unimproved grassland in Berkshire using a binary decision tree approach p 18 N89-12988

MOUNTS, WILLIAM E.

Marine remote sensing and international law p 39 A89-12124

MOWLE, A.

Integrating remote sensing data into a geographical information system: A foundation for rural land use strategies: Nature Conservancy Council project p 24 N89-12964

MOYA, I.

Techniques for remote sensing of life span and quantum yield of chlorophyll fluorescence in vivo p 13 N89-10351

MUELLER, R.

Optimization for classification of forest damage classes p 13 N89-10359

MUELLER, W.

Evaluation of space photographs p 82 A89-20715

MUNDAY, T. J.

Mapping the distribution and abundance of lithological units and surface mineralogies at Jabal Sa'id, Saudi Arabia: An application of spectral mixture modelling p 34 N89-13024

MUNEYAMA, KEI

Microwave emission and reflection from the wind-roughened sea surface at 6.7 and 18.6 GHz p 44 A89-15923

MUNRO, D. C.

Crop classification with multi-temporal X-band SAR data p 19 N89-12990

MURPHY, R. E.

NASA's future land remote sensing program p 90 N89-10393

MUTALIK, PRALHAD

Development of Alaskan gas hydrate resources [DE88-010270] p 35 N89-13093

MYERS, DAVID S.

United Nations activity on remote sensing - Legal and political implications p 89 A89-12125

N

NADASDI, I.

Towards an urban land-use classification using textural and morphological criteria p 25 N89-12987

NADEM, MEHRDAD

Development of Alaskan gas hydrate resources [DE88-010270] p 35 N89-13093

NAITO, GEN'ICHI

Microwave emission and reflection from the wind-roughened sea surface at 6.7 and 18.6 GHz p 44 A89-15923

NAKAMURA, T.

Laser-induced fluorescence on in-vivo chlorophyll of a rice plant: A technique for the remote detection of plant growth p 12 N89-10350

NARAYANAN, R. M.

Millimeter-wave backscatter measurements of various snow forms p 61 N89-13046

NARAYANAN, SAVITHRI

Coastally trapped waves in the presence of a shelf edge density front p 46 A89-16989

NATORI, NAUYUKI

Fault tolerant design of attitude and orbit control subsystem for earth resources satellite-1 [AIAA PAPER 88-3879] p 80 A89-18073

NAYAK, SHAILESH

Application of satellite data for monitoring degradation of tidal wetlands of the Gulf of Kachchh, Western India [IAF PAPER 88-146] p 46 A89-17695

NEEDHAM, BRUCE H.

Operational environmental instrumentation proposed by NOAA and the international community for the NASA and ESA polar orbiting platforms p 36 A89-10964

NEGRI, ANDREW J.

The addition of visible channel data to satellite infrared rain estimation schemes p 78 A89-12839
Comparison of satellite IR rain estimates with radar rain observations in hurricanes p 57 A89-12845

NELLIS, M. DUANE

SPOT satellite data for pattern recognition on the North American tall-grass prairie Long-Term Ecological Research site p 5 A89-14009

NERRY, F.

Attempt at absolute determination of spectral signatures of bare soils in the thermal infrared, in emission and reflection p 12 N89-10336

NEVESEPIPHANIO, JOSE CARLOS

Spectral studies of three oxisols and a Ultisol of Brazil [INPE-4644-PRE/1355] p 17 N89-11297

NEVILLE, R. A.

Advanced airborne electro-optical imager p 74 A89-10929

NEWCOMER, J. A.

Requirements for ongoing development of the Pilot Land Data System (PLDS) p 24 N89-12958

NI, I. H.

Evaluation of technology in the detection and counting of seals p 76 A89-11016

NICKESON, J. E.

Comparative point-spread function calculations for the MOMS-1, Thematic Mapper and SPOT-HRV instruments p 83 N89-10379

NIENHUIS, P. H.

Aerial photography for biomass assessment in the intertidal zone p 9 A89-20724

NIITSOO, A.

Mid-latitude evaluation of some satellite rainfall estimation techniques p 78 A89-12844

NIKITIN, V. V.

The effect of snow parameter variations on the thermal microwave emission of the soil-snow-atmosphere system p 59 A89-18712

NISHIDA, MASAZUMI

Experimental personal satellite communications system using millimeter-wave for Asia-Oceanian region p 81 A89-18736

NISHIO, F.

Inference of radio scattering parameters of Antarctic ice sheet using 179 MHz airborne radio echo sounding data p 51 N89-12975

NIXON, P. R.

Applications of multispectral video for natural resource assessment p 63 A89-10968

NJOKU, E. G.

Monitoring seasonal variations of soil moisture and vegetation cover using satellite microwave radiometry p 15 N89-10378

NORMAN, JOHN M.

Comparison of measured and modeled radiation, heat and water vapor fluxes: FIFE pilot study
[NASA-CR-183304] p 17 N89-11368

NORRIS, DAVID D.

High Resolution Imaging Spectrometer (HIRIS)
p 74 A89-10334

NORTH, GERALD R.

Future measurements of rain from space
[IAF PAPER 88-112] p 58 A89-17681

NOVAES, RENE ANTONIO

Nation-wide forest mapping and timber volume estimation using LANDSAT-5 TM imagery
[INPE-4643-PRE/1354] p 16 N89-10402

NOVIKOV, IU.

Complex experiment on the investigation of the atmosphere pollution using space, aircraft and ground information
[IAF PAPER 88-161] p 23 A89-17702

NUNEZ, M.

A new method for estimating regional evaporation from thermal infrared surface temperature measurements
p 60 N89-10390

O**O'NEILL, N. T.**

Imaging spectrometry for water applications
p 56 A89-10327

OCONNOR, E. A.

Applications of remote sensing for geological mapping in eastern Egypt
p 35 N89-13087

ODEN, S. F.

Directional ocean wave spectra: Prospects for acquiring a global data base from SIR-C
p 50 N89-12973

ODENWELLER, JULIE B.

Thematic Mapper data screening and external effects correction
p 64 A89-10978

OHMAE, H.

Inference of radio scattering parameters of Antarctic ice sheet using 179 MHz airborne radio echo sounding data
p 51 N89-12975

OKOLIE, CHARLES CHUKWUMA

International space law norms regulating remote sensing of the earth from outer space
p 89 A89-12126

OLAUSSEN, TOR I.

Mizex '87 - Overview of the Winter Marginal Ice Zone Experiment in the Greenland and Barents Seas
p 36 A89-10931

OLLIVER, J. G.

A comparison of reduction methods for satellite altimetry data
p 39 A89-11424

OLSEN, R. B.

An intercomparison of SAR and buoy directional wave spectra from the Labrador Sea Extreme Waves Experiment (LEWEX)
p 50 N89-12972

ONEILL, N. T.

Imaging spectrometry applied to the remote sensing of submerged seaweed
p 48 N89-10361

ONSTOTT, ROBERT G.

Evolution of the helicopter-borne scatterometer
p 37 A89-10971

OSOKIN, N. I.

Nival-glacial systems and their mapping
p 56 A89-10728

OSTAFF, D. P.

Sensor band selection for detecting current defoliation caused by the spruce budworm
p 6 A89-16062

P**PACHECODOSSANTOS, ARMANDO**

Nation-wide forest mapping and timber volume estimation using LANDSAT-5 TM imagery
[INPE-4643-PRE/1354] p 16 N89-10402

PAGANO, THOMAS S.

SeaWiFS - An ocean-imaging sensor
p 74 A89-10338

PAGES, J.

Bathymetry using SPOT imagery of the Casamance (Senegal). First results
p 59 N89-10375

PAINE, DAVID P.

Simplified forest inventory using large-scale 70-mm photography and tariff tables
p 6 A89-14090

PAINE, S. H.

Edge detection and processing of remotely sensed digital images
p 64 A89-10984

PALOSCIA, S.

The use of microwave radiometry in watershed hydrology
p 57 A89-10992

PALUTAN, F.

Time series of European baselines determined with Lageos
p 26 A89-17945

PAMPALONI, P.

The use of microwave radiometry in watershed hydrology
p 57 A89-10992

PANDEYA, ANJALI

Application of satellite data for monitoring degradation of tidal wetlands of the Gulf of Kachchh, Western India
[IAF PAPER 88-146] p 46 A89-17695

PANI, ERIC ANDREW

The design and protocol of a summertime rainfall enhancement program for West Texas
p 63 N89-14636

PANTANI, L.

A new lidar system for applications over land and sea
p 83 N89-10347

PARADELLA, WALDIR R.

Color enhancement of remote sensing imagery using IHS transformations and decorrelation stretch methods
[INPE-4559-PRE/1300] p 70 N89-11418

PARAMJE, SURESH G.

Development of Alaskan gas hydrate resources
[DE88-010270] p 35 N89-13093

PARSON, CHARLES

Integrating remotely sensed data into PC-based geographic information systems
p 23 A89-10959

PARTINGTON, K. C.

Analysis of Seasat SAR sea-ice data from the Beaufort Sea
p 52 N89-13035

PATIL, S. L.

Development of Alaskan gas hydrate resources
[DE88-010270] p 35 N89-13093

PAVATE, T. V.

Important aspects of technology transfer: Training of inservice engineers and scientists; satellite remote sensing
p 91 N89-13082

PAZOS, MAYRA C.

Drifting buoy data from the Equatorial Pacific for the period January 1, 1984 through May 31, 1985
[PB88-212824] p 49 N89-10516

PEDRINI, A.

Time-resolved laser fluorescence: Trends and applications
p 83 N89-10346

PEETERS, H.

An integrated remote sensing approach for regional agrostatistics and land monitoring
p 24 N89-12960

PEETERS, M.

The Airborne Version Conical Scan Radiometer (AVCSR): An airborne radiometer as a tool for satellite data validation
p 86 N89-12937

PELUFFOSTER, PAULO ROBERTO

Development of a semi-empirical model for estimating the global solar radiation
[INPE-4620-TDL/328] p 84 N89-11352

PENDER, J.

Cotton area mapping using multitemporal satellite data integrated within a geographical information system applied to a cotton boll weevil control programme in Paraguay
p 20 N89-13077

PEREIRADACUNHA, ROBERTO

Training activities in remote sensing at the Instituto de Pesquisas Espaciais-INPE/Brazil
[INPE-4686-PRE/1380] p 91 N89-11295

PERRAS, S.

Discrimination of zones of high water erosion risk using SPOT images
p 15 N89-10376

PERRIER, ALAIN

Evaporation over land surfaces - First results from HAPEX-MOBILHY Special Observing Period
p 57 A89-12211

PERRY, EILEEN M.

Infrared temperature measurements over bare soil and vegetation - A HAPEX perspective
p 2 A89-10953
Comparison of remote measurements of infrared surface temperatures and microwave soil moisture
p 4 A89-11009

PESANT, A.

Discrimination of zones of high water erosion risk using SPOT images
p 15 N89-10376

PETERS, H. C.

Comparison of wave parameters determined from SLAR images and a pitch and roll buoy
p 47 A89-20721

PETERSON, DAVID L.

Estimation of forest canopy characteristics and nitrogen cycling using imaging spectrometry
p 1 A89-10325
Prediction of leaf chemistry by the use of visible and near infrared reflectance spectroscopy
p 7 A89-17283

PEYRON, J.-L.

Spectral characterization of forest targets in mountainous zones on Thematic Mapper images
p 11 N89-10328

PEYROT, P.

Solid earth mission study. Volume 2: Technical report
[ESA-CR(P)-2626-VOL-2] p 26 N89-10303

Solid Earth mission study. Volume 1: Executive summary
[ESA-CR(P)-2626-VOL-1] p 26 N89-10397

Solid earth mission study. Volume 3: Program planning report
[ESA-CR(P)-2626-VOL-3] p 27 N89-10399

PHILIPSON, W. R.

Satellite data analysis for inventorying crops grown in a complex, small-field environment
p 1 A89-10951
Regional variation and crop separability in a Thematic Mapper based crop inventory of New York State
p 4 A89-11002

Spectral and spatial characterisation of orchards in New York State using Thematic Mapper Imagery
p 4 A89-11008

PHILPOT, W. D.

Satellite data analysis for inventorying crops grown in a complex, small-field environment
p 1 A89-10951
Regional variation and crop separability in a Thematic Mapper based crop inventory of New York State
p 4 A89-11002

Spectral and spatial characterisation of orchards in New York State using Thematic Mapper Imagery
p 4 A89-11008

PHILPOT, WILLIAM D.

Laser fluorosensing of water quality - A review
p 57 A89-10941

PHULPIN, T.

A study of the vegetation cover with AVHRR during HAPEX-MOBILHY
p 15 N89-10389

PICHUGIN, A. P.

The effect of agrometeorological conditions on the characteristics of space radar imagery of agricultural regions in winter
p 8 A89-18709

PICKUP, G.

Estimating the distribution of grazing and patterns of cattle movement in a large arid zone paddock
p 5 A89-12356

PIL'GUI, IU. N.

Recognition of seismically hazardous fault dislocations in space images of the Dushanbe depression
p 31 A89-18706

PILON, PAUL G.

Improving the detection of human-induced change in west Africa's semi-arid zone using multitemporal Landsat MSS imagery
p 64 A89-10983

An enhanced classification approach to change detection in semi-arid environments
p 68 A89-20627

PLACE, MICHAEL

Remote sensing technologies and spatial data applications
[AD-A195809] p 62 N89-14480

PLANT, WILLIAM J.

X-band scatterometer measurements at low winds in a wavetank
p 78 A89-12867

PLUMMER, S. E.

Relationships between the nitrogen content of grass and reflectance
p 19 N89-13002

PODAIRE, A.

Analysis of directional effects on NOAA AVHRR
p 70 N89-10341

POINTEL, J.-G.

Potential number of winter wheat ears estimation using radiometry techniques at an early stage
p 10 N89-10323

POLAVARAPU, V. L.

Mid-latitude evaluation of some satellite rainfall estimation techniques
p 78 A89-12844

POLIDORI, L.

Evaluation of VARAN data in geology and geomorphology in the southeast of France
p 32 N89-10313

PONNUSWAMY, M.

Project Vasundhara - Multi-theme integration of satellite remote sensing and geological data for regional level mineral prognostics
[IAF PAPER 88-145] p 31 A89-17694

PONZONI, FLAVIO JORGE

Nation-wide forest mapping and timber volume estimation using LANDSAT-5 TM imagery
[INPE-4643-PRE/1354] p 16 N89-10402

CIR aerial photography applied to the evaluation of the air pollution impact in a tropical forest: The case of Cubatao, Brazil
[INPE-4651-PRE/1358] p 17 N89-11324

Digital processing applied to vegetation
[INPE-4695-MD/036] p 17 N89-12107

POPSTEFANILJA, I.

A concept for measuring currents from geostationary satellites
p 75 A89-10933

POUWELS, H.

Comparison of wave parameters determined from SLAR images and a pitch and roll buoy
p 47 A89-20721

PRASAD, K. N.

Application of satellite data for monitoring degradation of tidal wetlands of the Gulf of Kachchh, Western India
[IAF PAPER 88-146] p 46 A89-17695

PRASAD, N.

Satellite microwave rainfall simulations with a three-dimensional dynamical cloud model p 77 A89-12833

PREISENDORFER, RUDOLPH W.

A numerical model for the computation of radiance distributions in natural waters with wind-roughened surfaces [AD-A197207] p 53 N89-13128

PREUSS, E.

Very Long Baseline Interferometry (VLBI) from ground and space p 85 N89-11645

PREVOT, L.

Extracting soil and vegetation characteristics from microwave remote sensing data p 9 N89-10306
Complementary of microwave and optical range in the characterization of crops by remote sensing p 10 N89-10310

PRICE, CURTIS V.

Operational use of Landsat data for timber inventory p 2 A89-10970

PROSDOCIMI, A.

Time-resolved laser fluorescing: Trends and applications p 83 N89-10346

PUESCHEL, R. F.

Comparison of in situ aerosol measurements with SAGE 2 and SAM 2 aerosol measurements during the airborne Antarctic ozone experiment p 89 N89-14522

PURDOM, JAMES F. W.

Better understanding of intense and tornadic thunderstorms through research using geostationary satellite data p 56 A89-10934
Using satellite data to aid in diagnosing and forecasting convective development and intensity along arc cloud lines p 76 A89-12810

Q**QUARMBY, N. A.**

The use of remote sensing in conjunction with geographic information systems for local planning p 24 N89-12959
Monitoring playas using Thematic Mapper data p 60 N89-13028

R**RADICATI, B.**

A new lidar system for applications over land and sea p 83 N89-10347

RAFFY, M.

Multispectral characterization of the spatial structure of remotely sensed scenes p 70 N89-10340

RAGAN, ROBERT M.

Remote sensing technologies and spatial data applications [AD-A195809] p 62 N89-14480

RAJAN, Y. S.

Indian experience in the dissemination and use of remote sensing data and future prospects [IAF PAPER 88-131] p 80 A89-17689

RAMACHANDRAN, T. V.

Project Vasundhara - Multi-theme integration of satellite remote sensing and geological data for regional level mineral prognostics [IAF PAPER 88-145] p 31 A89-17694

RAMASWAMY, V.

Evolution of polar stratospheric clouds during the Antarctic winter p 55 N89-14534

RAMSTEIN, G.

Multispectral characterization of the spatial structure of remotely sensed scenes p 70 N89-10340

RANEY, R. K.

Does a SAR respond to both phase speed and orbital velocity in ocean sensing? p 36 A89-10947
Synthetic aperture radar imaging of ocean waves from an airborne platform - Focus and tracking issues p 41 A89-12173
SAR-seen multimode waves in ice: Evidence of imaging nonlinearities p 50 N89-12971
Phase versus orbital velocity in SAR wave imaging: Paradox lost p 52 N89-13033
The LIMEX 1987 pilot project, LIMEX 1989 and long-term objective for data collection on the Canadian East coast p 52 N89-13037

RANGO, A.

Average areal water equivalent of snow in a mountain basin using microwave and visible satellite data p 61 N89-13045

Microcomputers (PCs) for snow cover analyses using multisensor satellite data p 62 N89-13049

RANTASUO, MARKKU

Shuttered camera - Aerial color video imaging in the visible and near infrared p 8 A89-20630

RAST, M.

Comparative geological evolution of different remote sensing data of the Hoggar Mountains (Algeria) p 33 N89-10385

RATIER, A.

Towards direct variational assimilation of scatterometer backscatter measurements into numerical weather prediction models p 86 N89-13000

READING, A. J.

Monitoring playas using Thematic Mapper data p 60 N89-13028

REES, W. G.

Topographic effects on light scattering from snow p 71 N89-12976

REGINATO, ROBERT J.

Surface energy flux measurements and reflectance factors using satellite-, aircraft-, and ground-based instrumentation p 1 A89-10950

REID, M. S.

Standards for earth observations from space [IAF PAPER 88-107] p 90 A89-17680

REIFF, J.

The contribution of satellite information to operational weather forecasting - Achievements and objectives in the 1990s p 81 A89-20711

REINARTZ, P.

Optimization for classification of forest damage classes p 13 N89-10359

REINERS, WILLIAM A.

Biogeochemical processes in sagebrush steppe: Interactions of terrain, vegetation and chemical cycles [NASA-CR-181486] p 21 N89-13088

REMY, F.

Comparison between active and passive microwave measurements over Antarctica p 48 N89-10316

REVZON, A. L.

Engineering evaluation of mountain topography exodynamics from remotely sensed data p 31 A89-18707

RIAZANOFF, S.

Evaluation of VARAN data in geology and geomorphology in the southeast of France p 32 N89-10313

RICE, DANIEL P.

Thematic Mapper data screening and external effects correction p 64 A89-10978

RICHTER, R.

Thermal infrared laser spectroscopy: The potential of dual active/passive thermal infrared sensors for Earth observation p 82 N89-10345

RIEGGER, S.

Coherent polarimetric signatures of coniferous trees: A survey p 9 N89-10307
Polarization-dependent attenuation of dielectric cylinder arrays p 86 N89-12955

RIES, J. C.

Orbit determination requirements for Topex [AAS PAPER 87-429] p 42 A89-12645

RIGAL, D.

Spectral profile and biomass estimation p 10 N89-10319

RINDERLE, U.

Chlorophyll fluorescence spectra of leaves as induced by blue light and red laser light p 12 N89-10349
Estimation of leaf spectra from measurements in wide spectral bands p 14 N89-10368

RIPLEY, H. T.

Surveillance radar, a new tool for ice surveillance p 37 A89-10991
Evaluation of technology in the detection and counting of seals p 76 A89-11016

RITCHIE, JERRY C.

Soil erosion study using an airborne laser profiler p 1 A89-10952

ROADS, JOHN O.

A pilot study to determine relationships between North Pacific precipitation from Nimbus-7 Scanning Multichannel Microwave Radiometer data and associated atmospheric conditions p 43 A89-12837

ROBERTS, E. P.

Data report for the Siple Coast (Antarctica) project [NASA-TM-100708] p 49 N89-10403

ROCK, BARRETT N.

Detection of forest damage on Whiteface Mountain, New York, using Landsat Thematic Mapper data p 3 A89-10987

Relative water content of Spruce needles determined by the leaf water content index p 4 A89-11012

ROCKAERTS, M.

An integrated remote sensing approach for regional agrostatistics and land monitoring p 24 N89-12960

RODGERS, EDWARD B.

Tropopause adjustment to tropical cyclones as inferred from satellite ozone observations p 77 A89-12816

RODRIGUEZ, ERNESTO

Altimetry for non-Gaussian oceans - Height biases and estimation of parameters p 46 A89-16992

ROLLIN, E. M.

A simplified reflectance model for shrub canopies p 11 N89-10329

ROMOLI, M.

A new lidar system for applications over land and sea p 83 N89-10347

RONDEAUX, G.

Complementary of microwave and optical range in the characterization of crops by remote sensing p 10 N89-10310

ROQUET, H.

Towards direct variational assimilation of scatterometer backscatter measurements into numerical weather prediction models p 86 N89-13000

ROSENHOLM, DAN

Multi-point matching along vertical lines in SPOT images p 69 A89-20713

ROSENTHAL, ALAN

Utilizing remote sensing of thematic mapper data to improve our understanding of estuarine processes and their influence on the productivity of estuarine-dependent fisheries [NASA-CR-183409] p 62 N89-13822

ROTHERY, D. A.

Emitted short wavelength infrared radiation for detection and monitoring of volcanic activity p 32 N89-10377
MOMS-1 used synergistically with LANDSAT TM p 33 N89-10384
The need for volcano monitoring and the ability to detect activity using emitted short wavelength infrared p 34 N89-13025

ROUX, C.

Spectral analysis of ocean wave imagery using 2-D linear prediction p 50 N89-12968

ROYER, A.

Analysis of the contribution of the atmosphere to water reflectance in the first two channels of the NOAA satellites AVHRR p 82 N89-10330

RUDANT, J. P.

Evaluation of VARAN data in geology and geomorphology in the southeast of France p 32 N89-10313

Rock and soil discrimination in natural tropical conditions using a spot-calibrated radiometer p 14 N89-10374

RUDANT, J.-P.

Usefulness of high spectral resolution radiometry for geological mapping in the Mediterranean region p 32 N89-10360

Characterization of rocks by visible and infrared high spectral resolution terrain spectroscopy p 32 N89-10362

The use of MOMS-1 data for geological mapping of the Aswa lineament (East African rift) p 33 N89-10382

RUDDIN, P.

Surveillance radar, a new tool for ice surveillance p 37 A89-10991

RUDNICK, DANIEL LARS

Mass and heat balances in the upper ocean p 53 N89-13089

RUF, C. S.

The electronically steered thinned array radiometer p 74 A89-10932

RULAND, DETLEV

Integrated database approach for geodetic applications [DE88-012726] p 27 N89-11615

RULAND, ROBERT

Integrated database approach for geodetic applications [DE88-012726] p 27 N89-11615

RUNGALDIER, H.

Microwave scattering from internal wave modulated surface waves - A shipboard real aperture coherent radar study in the Georgia Strait Experiment p 39 A89-12157

RUSSO, JOSEPH M.

Meteorological surface analysis using perspective topographic maps p 65 A89-11740

RUZEK, M.

NASA's future land remote sensing program p 90 N89-10393

S**SACCO, V. M.**

Forest classification by principal component analyses of TM data p 8 A89-20706

SAFFMAN, P. G.

Modulation of radar backscatter from the ocean by a variable surface current p 39 A89-12158

- SAHAI, BALDEV**
Comparison of SPOT, TM and MSS data for agricultural land-use mapping in Gujarat (India)
[IAF PAPER 88-139] p 7 A89-17692
- SAILOR, RICHARD V.**
A preliminary model for Geosat altimeter data errors p 44 A89-13958
- SAITO, KAZUYA**
Remote measurements of diatoms chlorophyll-a in the Nori farm p 38 A89-11001
- SAKAMOTO, CLARENCE M.**
The application of remote sensing for drought early warning in Africa p 1 A89-10948
- SAKATA, T.**
A new spatial classification algorithm for high ground resolution images p 72 N89-13061
Accuracy of land cover classification of Thematic Mapper (TM) and SPOT data p 72 N89-13066
- SALASALVES, DIOGENES**
A general data model for geographic information systems
[INPE-4560-PRE/1301] p 24 N89-10676
- SALISBURY, J. W.**
The basis for the spectral behaviour of silicates in the thermal infrared and applications to remote sensing p 32 N89-10366
- SALOMONSON, V. V.**
Comparative point-spread function calculations for the MOMS-1, Thematic Mapper and SPOT-HRV instruments p 83 N89-10379
- SALVAGGIO, CARL**
Automated segmentation of pseudoinvariant features from multispectral imagery p 68 A89-17906
- SANDVEN, STEIN**
Mizex '87 - Overview of the Winter Marginal Ice Zone Experiment in the Greenland and Barents Seas p 36 A89-10931
- SANDWELL, DAVID T.**
Improvements in the marine gravity field from Geosat/ERM p 36 A89-10962
- SARABANDI, K.**
Effect of curvature on the backscattering from leaves [NASA-CR-183326] p 16 N89-11296
- SARAF, A. K.**
MOMS-1 data for bathymetric and geological studies p 33 N89-10383
- SASAKI, YASUNORI**
Microwave emission and reflection from the wind-roughened sea surface at 6.7 and 18.6 GHz p 44 A89-15923
- SATO, H.**
Verification results of MOS-1 multispectral self scanning radiometer (MESSR) data p 86 N89-13004
- SAUSEN, TANIA MARIA**
Training activities in remote sensing at the Instituto de Pesquisas Espaciais-INPE/Brazil
[INPE-4686-PRE/1380] p 91 N89-11295
- SAX, H.**
Status and perspectives of vegetation monitoring by remote sensing
[IAF PAPER 88-140] p 8 A89-17693
- SCANVIC, J.-Y.**
Usefulness of high spectral resolution radiometry for geological mapping in the Mediterranean region p 32 N89-10360
- SCHELLBERG, J.**
Spectral reflectance of sugar beet and winter wheat canopies in the visible and infrared during growth p 12 N89-10342
Estimation of leaf spectra from measurements in wide spectral bands p 14 N89-10368
- SCHERER, THOMAS**
Computational design and efficiency optimization of agricultural airplanes p 5 A89-13670
- SCHERTZER, D.**
Resolution dependence in satellite imagery - Multifractal analysis p 67 A89-12852
- SCHMUGGE, T.**
Aircraft remote sensing in HAPEX p 59 N89-10388
- SCHMULLIUS, C.**
Large area TM land cover classification of Mittlerer Oberrhein County, southwest Germany, and its use for regional planning and crop surveys p 18 N89-12986
- SCHNURR, J.**
Building a monitoring system based on satellite data to detect vegetation and land use changes in a subtropical region of Mexico p 20 N89-13079
- SCHOENE, G.**
Coherent polarimetric signatures of coniferous trees: A survey p 9 N89-10307
- SCHOTT, JOHN R.**
Automated segmentation of pseudoinvariant features from multispectral imagery p 68 A89-17906
- SCHRAMM, M.**
Spectral characterization of forest damage in beech, oak and pine stands p 21 N89-13085
- SCHULTZ, HOWARD J.**
Satellite cloud image standardization p 76 A89-11731
- SCHWIDERSKI, ERNST W.**
Modeling of the dynamic sea surface with satellite altimeter signals p 38 A89-11158
- SCOFIELD, RODERICK A.**
Using the VAS data utilization center (VDUC) for the analysis and forecasting of heavy rainfall producing mesoscale convective systems (MCSs) p 77 A89-12819
- SCRIMGER, P.**
Make-map and MEDMAP: Two programs for plotting maps of the Mediterranean Sea
[AD-A198491] p 73 N89-14483
- SEASTEDT, T. R.**
The influence of grazing on land surface climatological variables
[NASA-CR-183308] p 22 N89-14637
- SEGARRA, D.**
Spectral signature of citrus fruits and its evolution: Identification of the vegetative index of least temporal variation p 14 N89-10373
- SEIDLITZ, HARALD K.**
Relationship between discoloration and histological changes in leaves of trees affected by forest decline p 7 A89-17286
- SENDRA, CLAUDIA**
Algorithm for automatic atmospheric corrections to visible and near-IR satellite imagery p 66 A89-12224
- SENGUPTA, S. K.**
Classification of cloud fields based on textural characteristics p 65 A89-11727
- SENIOR, T. B. A.**
Effect of curvature on the backscattering from leaves
[NASA-CR-183326] p 16 N89-11296
- SERRADEIL, R.**
The image detection subassembly for the SPOT 4 'vegetation' instrument
[IAF PAPER 88-121] p 7 A89-17686
- SESHADRI, T. S.**
Project Vasundhara - Multi-theme integration of satellite remote sensing and geological data for regional level mineral prognostics
[IAF PAPER 88-145] p 31 A89-17694
- SETTLE, J.**
Mapping the distribution and abundance of lithological units and surface mineralogies at Jabal Sa'id, Saudi Arabia: An application of spectral mixture modelling p 34 N89-13024
- SEYHAN, E.**
The Remote Sensing Loosdrecht Lakes project p 59 A89-20719
- SGAVETTI, M.**
The use of TM data for the study of a modern deltaic depositional system p 59 A89-20707
- SHA, KINGWEI**
SAR and visible remote sensing of the Tacer River coastal zone at Bohai Bay p 38 A89-11005
- SHAFFER, JEFFREY**
The GVAR users compendium, volume 1
[NOAA-NESDIS-21-VOL-1] p 85 N89-12105
- SHAPIRO, I. I.**
VLBI geodesy - 2 parts-per-billion precision in length determinations for transcontinental baselines p 26 A89-13762
- SHARMA, G. D.**
Development of Alaskan gas hydrate resources
[DE88-010270] p 35 N89-13093
- SHEDD, ROBERT C.**
Validation of the on-site Flash Flood Potential System for Nexrad p 57 A89-10949
- SHEETZ, H. J.**
Standards for earth observations from space
[IAF PAPER 88-107] p 90 A89-17680
- SHEFFNER, EDWIN J.**
The California Cooperative Remote Sensing Project
[NASA-TM-100073] p 22 N89-13824
- SHEIKHO, KAMEL M.**
SIR-B view of the Jabal Hadn lineament and its groundwater implications p 29 A89-10976
- SHEMDIN, O. H.**
Tower Ocean Wave and Radar Dependence experiment - An overview p 44 A89-16976
Comparison of measured and predicted sea surface spectra of short waves p 45 A89-16981
- SHEMDIN, OMAR H.**
Theory for synthetic aperture radar imaging of the ocean surface - With application to the Tower Ocean Wave and Radar Dependence experiment on focus, resolution, and wave height spectra p 44 A89-16977
Directional measurement of short ocean waves with stereophotography p 45 A89-16982
The dependence of sea surface slope on atmospheric stability and swell conditions p 45 A89-16983
- SHIH, CHI-FAN**
Effects of data resolution on marine stratiform cloud detection using AVHRR and VISSR satellite data p 78 A89-12854
- SHIMADA, M.**
Verification results of MOS-1 multispectral self scanning radiometer (MESSR) data p 86 N89-13004
Data collection system operating on Japan's first marine observation satellite: Inflight evaluation of the system performance p 87 N89-13007
- SHIMODA, H.**
A new spatial classification algorithm for high ground resolution images p 72 N89-13061
Accuracy of land cover classification of Thematic Mapper (TM) and SPOT data p 72 N89-13066
- SHIN, R. T.**
Correlation function study for sea ice p 46 A89-16990
- SHIVE, PETER N.**
Magnetic mineralogy in an archean crustal cross section - Implications for crustal magnetization p 30 A89-12292
- SHUCHMAN, R. A.**
Comparison of Joint Canada-U.S. Ocean Wave Investigation Project synthetic aperture radar data with internal wave observations and modeling results p 39 A89-12160
Sea ice type classification of SAR imagery p 52 N89-13039
- SHUCHMAN, ROBERT A.**
Mizex '87 - Overview of the Winter Marginal Ice Zone Experiment in the Greenland and Barents Seas p 36 A89-10931
Evolution of the helicopter-borne scatterometer p 37 A89-10971
Contrast ratios of internal waves in synthetic aperture radar imagery - A comparison of SAR Internal Wave Signature Experiment observations with theory p 40 A89-12167
- SIEBER, A. J.**
AGRISAR '86: Contributing to signature research p 15 N89-10387
- SIMONETT, DAVID S.**
Improvement and extension of a radar forest backscattering model
[NASA-CR-183259] p 16 N89-11292
- SIMONIN, A.**
Evaluation of VARAN data in geology and geomorphology in the southeast of France p 32 N89-10313
- SIMPSON, JOANNE**
Satellite microwave rainfall simulations with a three-dimensional dynamical cloud model p 77 A89-12833
- SINCLAIR, PETER C.**
Using satellite data to aid in diagnosing and forecasting convective development and intensity along arc cloud lines p 76 A89-12810
- SINGH, S. M.**
Estimation of multiple reflection and lowest order adjacency effects on remotely-sensed data p 5 A89-12354
Lowest order correction for solar zenith angle to Global Vegetation Index (GVI) data p 8 A89-20704
- SKIDMORE, ANDREW K.**
Forest mapping accuracies are improved using a supervised nonparametric classifier with SPOT data p 6 A89-14089
- SMILEY, DANIEL**
Climate tracking with remote sensing p 75 A89-10943
- SMITH, DAVID C., IV**
A numerical study of mesoscale ocean eddy interaction with a marginal ice zone p 41 A89-12172
- SMITH, J.**
The use of remote sensing in conjunction with geographic information systems for local planning p 24 N89-12959
- SMITH, P.**
Some characteristics of short ocean waves as microwave scatterers p 51 N89-13030
- SMITH, TERENCE**
Remote sensing information sciences research group
[NASA-CR-183374] p 91 N89-14481
- SMITH, W. O., JR.**
Phytoplankton standing crops within an Antarctic ice edge assessed by satellite remote sensing p 41 A89-12174
- SMOLINSKI, STEVEN P.**
Marine boundary layer depth and relative humidity estimates using multispectral satellite measurements
[AD-A196525] p 49 N89-12112
- SNIDER, J. B.**
Verification of the accuracy of a network of water-vapor radiometers p 86 N89-12941

- SNOEK, M.**
Qualitative aspects of seismograph/ocean bottom interaction
[AD-A198652] p 56 N89-14656
- SOARES, J. V.**
Microwave remote sensing at the Institute for Space Research (INPE) Brazil: Concepts and future prospects of soil moisture studies p 20 N89-13080
- SOBIESKI, P.**
A three degree-of-freedom description of the ocean surface for microwave remote sensing of wave height and wind friction velocity p 47 N89-10314
An approximative model for the microwave brightness temperature scattered by a rough open ocean surface p 48 N89-10344
- SOBISHEK, B.**
Complex experiment on the investigation of the atmosphere pollution using space, aircraft and ground information
[IAF PAPER 88-161] p 23 A89-17702
- SOBRINO, J. A.**
A theoretical model for interpreting remotely sensed thermal infrared measurements obtained over agricultural areas p 12 N89-10343
- SOEGAARD, HENRIK**
Monitoring vegetation index and biomass production in Southern Greenland based on NOAA-AVHRR data p 3 A89-10993
- SOFFEN, GERALD A.**
The Earth Observing System
[IAF PAPER 88-114] p 80 A89-17682
- SPATZ, D. M.**
Desert varnish on volcanic rocks of the Basin and Range province - Composition, morphology, distribution, origin and influence on Landsat imagery p 30 A89-10988
- SPENCER, ROY W.**
Thunderstorm ice induced brightness temperature depressions at 18, 37, and 92 GHz during Cohnex and their implications for satellite precipitation retrievals p 42 A89-12835
- SROKOSZ, M. A.**
Satellite remote sensing and wave studies into the 1990s p 47 A89-20723
- STAENZ, K.**
Improvement in NOAA-AVHRR snowcover determination for runoff prediction p 61 N89-13040
- STAR, JEFFREY L.**
Remote sensing information sciences research group
[NASA-CR-183374] p 91 N89-14481
- STARKS, PATRICK**
Comparison of measured and modeled radiation, heat and water vapor fluxes: FIFE pilot study
[NASA-CR-183304] p 17 N89-11368
- STAUFENBIEL, ROLF**
Computational design and efficiency optimization of agricultural airplanes p 5 A89-13670
- STEFFEN, KONRAD**
Comparison of Nimbus 7 scanning multichannel microwave radiometer radiance and derived sea ice concentrations with Landsat imagery for the north water area of Baffin Bay p 38 A89-11150
- STEIGER, ISTVAN**
Computational design and efficiency optimization of agricultural airplanes p 5 A89-13670
- STEINMETZ, S.**
Biomass and wheat crop yield estimation from SPOT vegetative indexes p 11 N89-10327
- STENGEL, P.**
Near surface soil moisture estimation from microwave measurements p 6 A89-17282
- STEPHENS, GEORGE**
Regional and global fire detection using AVHRR data p 2 A89-10956
- STEPHENSON, S. N.**
Data report for the Siple Coast (Antarctica) project
[NASA-TM-100708] p 49 N89-10403
- STERANKA, JOSEPH**
Tropopause adjustment to tropical cyclones as inferred from satellite ozone observations p 77 A89-12816
- STERN, M.**
A new tool - SPOT imagery for studying rapid movements p 64 A89-10996
- STERNER, R. E., II**
Measurements of surface wave modulations from internal waves during the SAR Internal Wave Signature Experiment p 40 A89-12164
A comparison of measured surface wave spectral modulations with predictions from a wave-current interaction model p 40 A89-12165
- STEVEN, M. D.**
High spectral resolution indices for monitoring crop growth and chlorosis p 13 N89-10358
- STOLL, M. P.**
Attempt at absolute determination of spectral signatures of bare soils in the thermal infrared, in emission and reflection p 12 N89-10336
- STOLZ, W.**
Analysis of large format camera photographs of the Po Delta, Italy, for topographic and thematic mapping p 82 A89-20714
- STOUT, JOHN**
Tropopause adjustment to tropical cyclones as inferred from satellite ozone observations p 77 A89-12816
- STRAHLER, ALAN H.**
Invertible canopy reflectance modeling of vegetation structure in semiarid woodland p 6 A89-15918
- STRANGWAY, D. W.**
Geophysical interpretation of the magnetic anomalies of China derived from Magsat data p 26 A89-20200
- STREBEL, D. E.**
Atmospheric correction of NS-001 data and extraction of multiple angle reflectance data sets p 64 A89-10998
- STROME, W. M.**
Advanced airborne electro-optical imager p 74 A89-10929
- STUART, N.**
Analysis of potato crop distribution using remotely sensed and environmental data in a pilot geographical information system p 18 N89-12967
- STUMPF, RICHARD P.**
Remote sensing of suspended sediments in estuaries using atmospheric and compositional corrections to AVHRR data p 57 A89-10940
- STURGEON, D. R.**
Imaging spectrometry as a tool for botanical mapping p 73 A89-10324
- STUTTARD, M. J.**
The classification of semi-natural vegetation from LANDSAT Thematic Mapper imagery: A user's perspective p 21 N89-13084
- STYLES, P. J.**
The production of anaglyphs from SPOT-HRV panchromatic data for geomorphological mapping p 72 N89-13056
- SUBRAHMANYAM, V.**
Project Vasundhara - Multi-theme integration of satellite remote sensing and geological data for regional level mineral prognostics
[IAF PAPER 88-145] p 31 A89-17694
- SUITS, G.**
The prospects for detecting spectral shifts due to satellite sensor aging p 6 A89-16061
- SUITZ, TAKESHI**
Backscattering coefficient of rice crops and rice fields by an X-band scatterometer p 3 A89-10980
- SULLIVAN, C. W.**
Phytoplankton standing crops within an Antarctic ice edge assessed by satellite remote sensing p 41 A89-12174
- SUZUKI, TAKASHI**
Fault tolerant design of attitude and orbit control subsystem for earth resources satellite-1
[AIAA PAPER 88-3879] p 80 A89-18073
- SUZUKI, TSUTOMU**
Microwave emission and reflection from the wind-roughened sea surface at 6.7 and 18.6 GHz p 44 A89-15923
- SUZUKI, YOSHIKI**
Experimental personal satellite communications system using millimeter-wave for Asia-Oceanian region p 81 A89-18736
- SWEARINGEN, WILL D.**
Remote sensing and geographic information systems for agricultural statistics-gathering and agricultural monitoring in Morocco p 2 A89-10960
- SWIFT, C. T.**
Surface windspeed measurements over the ocean with a C-band microwave radiometer p 75 A89-11006
- SWIFT, CALVIN T.**
Overview of oceanic microwave remote sensing from space p 35 A89-10930
Passive microwave remote sensing of salinity in coastal zones p 36 A89-10942
- T**
- TABERNER, M.**
Satellite data analysis for inventorying crops grown in a complex, small-field environment p 1 A89-10951
- TABERNER, M. J.**
Spectral and spatial characterisation of orchards in New York State using Thematic Mapper imagery p 4 A89-11008
- TACONET, ODILE**
Infrared temperature measurements over bare soil and vegetation - A HAPEX perspective p 2 A89-10953
- TAI, CHANG-KOU**
Geosat crossover analysis in the tropical Pacific. I - Constrained sinusoidal crossover adjustment p 38 A89-11143
- TAJIRIAN, E. K.**
Multifocus processing of L band synthetic aperture radar images of ocean waves obtained during the Tower Ocean Wave and Radar Dependence experiment p 45 A89-16978
- TAKAHASHI, K.**
Laser-induced fluorescence on in-vivo chlorophyll of a rice plant: A technique for the remote detection of plant growth p 12 N89-10350
- TAMAIN, G.**
Characterization of rocks by visible and infrared high spectral resolution terrain spectroscopy p 32 N89-10362
- TANBA, SUMIO**
Estimation of sea surface temperature via NOAA-AVHRR sensor: Comparison with sea truth data by fixed buoys p 51 N89-13005
- TANIS, FRED J.**
SPOT bathymetric image for archeological investigations p 37 A89-10990
- TANNER, A. B.**
The electronically steered thinned array radiometer p 74 A89-10932
Surface windspeed measurements over the ocean with a C-band microwave radiometer p 75 A89-11006
- TANNOUS, I.**
Evaluation of VARAN data in geology and geomorphology in the southeast of France p 32 N89-10313
- TANRE, D.**
Analysis of directional effects on NOAA AVHRR p 70 N89-10341
- TAO, WEI-KUO**
Satellite microwave rainfall simulations with a three-dimensional dynamical cloud model p 77 A89-12833
- TAPLEY, B. D.**
Orbit determination requirements for Topex
[AAS PAPER 87-429] p 42 A89-12645
- TARANIK, J. V.**
Desert varnish on volcanic rocks of the Basin and Range province - Composition, morphology, distribution, origin and influence on Landsat imagery p 30 A89-10988
- TARPLEY, J. D.**
Nimbus-7 SMMR derived sea-ice concentrations over Antarctica p 43 A89-12857
- TASAKI, K.**
Verification results of MOS-1 multispectral self scanning radiometer (MESSR) data p 86 A89-13004
- TAYLOR, GEOFFREY R.**
Image analysis techniques for the interpretation of airphoto lineaments - Petroleum exploration, Eromanga Basin, Australia p 30 A89-14011
- TAYLOR, J. C.**
The classification of semi-natural vegetation from LANDSAT Thematic Mapper imagery: A user's perspective p 21 N89-13084
- TEBALDITARDIN, ANTONIO**
Crop separation analysis through SPOT and TM digital data
[INPE-4641-PRE/1352] p 18 N89-12110
- TEILLET, P. M.**
Sensor band selection for detecting current defoliation caused by the spruce budworm p 6 A89-16062
- TEIXEIRABATISTA, GETULIO**
Crop separation analysis through SPOT and TM digital data
[INPE-4641-PRE/1352] p 18 N89-12110
- TEMPELMANN, U.**
Spectral reflectance of sugar beet and winter wheat canopies in the visible and infrared during growth p 12 N89-10342
- TENG, XUYAN**
Study of monitoring sea ice using an airborne microwave radiometer system p 37 A89-10972
- TERES, J. M.**
Spectral profile and biomass estimation p 10 N89-10319
- TERHALLE, U.**
Digital analysis of MOMS-1, LANDSAT TM, and SPOT data of the Nakuru area (Kenya) p 33 N89-10386
- TESSAR, PAUL A.**
Integrating remotely sensed data into PC-based geographic information systems p 23 A89-10959
- THERIAULT, J. P.**
Fiber-optic sensor systems for aerospace applications p 74 A89-10359
- THOMASON, LARRY W.**
Color-composite image processing for multispectral meteorological satellite data
[AD-A199574] p 76 A89-11742
- THOME, PITT G.**
Business strategies and land remote sensing capabilities p 90 A89-20104

U

- THOMPSON, D. R.**
A comparison of measured surface wave spectral modulations with predictions from a wave-current interaction model p 40 A89-12165
- THOMSON, K. P. B.**
Texture analysis in forest areas: High spectral resolution synthetic aperture radar data p 14 A89-10367
- THORVALDSSON, V.**
A narrow-band thermal imager based on multilane real-time averaging p 83 A89-10356
- TIBALDI, A.**
Use of Landsat and Seasat data as a tool in kinematic analysis - The Tunisian Atlas p 31 A89-20710
- TILL, S. M.**
Advanced airborne electro-optical imager p 74 A89-10929
- TILLEY, D. G.**
Estimating aircraft SAR response characteristics and approximating ocean wave spectra in the Labrador Sea p 52 A89-13032
- TILTON, JAMES C.**
LANDSAT-4 and LANDSAT-5 multispectral scanner coherent noise characterization and removal [NASA-TP-2595-REV] p 85 A89-12114
- TIMCHALK, A.**
Precipitation detection with satellite microwave data [PB88-240239] p 88 A89-13094
- TINGEY, DAVID T.**
Analysis of crop loss for alternative ozone exposure indices [PB88-214788] p 22 A89-14608
- TOGLIATTI, G.**
Tests of topographic mapping with Thematic Mapper images p 69 A89-20712
- TOIKKA, M. V. O.**
Microwave dielectric properties of low-salinity sea ice p 52 A89-13036
- TON, JEZCHING**
Automatic road detection on Landsat 4 TM images p 23 A89-10997
- TOWNSHEND, J. R. G.**
Spatial resolution requirements for MODIS-N p 83 A89-10364
Monitoring playas using Thematic Mapper data p 60 A89-13028
- TRAN, H. MINH**
Directional measurement of short ocean waves with stereophotography p 45 A89-16982
- TRANGELED, A.**
Make-map and MEDMAP: Two programs for plotting maps of the Mediterranean Sea [AD-A198491] p 73 A89-14483
- TREFOIS, PHILIPPE**
Rock and soil discrimination in natural tropical conditions using a spot-calibrated radiometer p 14 A89-10374
- TRIGG, ANDREW D.**
CANVAS - An intelligent system for colour selection on CRT displays p 76 A89-12353
- TRIVEDI, C. R.**
Application of satellite data for monitoring degradation of tidal wetlands of the Gulf of Kachchh, Western India [IAF PAPER 88-146] p 46 A89-17695
- TRODD, N. M.**
The detection of unimproved grassland in Berkshire using a binary decision tree approach p 18 A89-12988
Classification decision rule modification on the basis of information extracted from training data p 72 A89-13062
- TROSTEL, J. M.**
Statistics and high resolution imaging of snowpack at 35 GHz using a microcomputer p 61 A89-13047
- TSONIS, ANASTASIOS A.**
The evaluation of simple approaches for the delineation of rain area from satellite imagery p 66 A89-12842
- TSUJI, M.**
Data collection system operating on Japan's first marine observation satellite: Inflight evaluation of the system performance p 87 A89-13007
- TURNER, B.**
The development of a standardized grassland Landsat MSS information data base p 3 A89-10979
- TURNER, BRIAN J.**
Forest mapping accuracies are improved using a supervised nonparametric classifier with SPOT data p 6 A89-14089
- TURNER, J.**
Cloud track winds from polar orbiting satellites p 87 A89-13069
- TYLER, WILLIAM A.**
SPOT bathymetric image for archeological investigations p 37 A89-10990

UDD, E.

- Fiber-optic sensor systems for aerospace applications p 74 A89-10359

UENO, S.

- Snowmelt runoff estimation using snow cover extent data and its application to optimum control of dam water level p 61 A89-13042

UESUGI, TOSHIKAKI

- Fault tolerant design of attitude and orbit control subsystem for earth resources satellite-1 [AIAA PAPER 88-3879] p 80 A89-18073

ULABY, F. T.

- Effect of curvature on the backscattering from leaves [NASA-CR-183326] p 16 A89-11296

UMEHARA, TOSHIHIKO

- Backscattering coefficient of rice crops and rice fields by an X-band scatterometer p 3 A89-10980

UNGAR, STEPHEN G.

- Extraction of topography from side-looking satellite systems - A case study with SPOT simulation data p 68 A89-16063

URATSUKA, S.

- Inference of radio scattering parameters of Antarctic ice sheet using 179 MHz airborne radio echo sounding data p 51 A89-12975

V

VACHON, P. W.

- Does a SAR respond to both phase speed and orbital velocity in ocean sensing? p 36 A89-10947
Synthetic aperture radar imaging of ocean waves from an airborne platform - Focus and tracking issues p 41 A89-12173

- SAR-seen multimode waves in ice: Evidence of imaging nonlinearities p 50 A89-12971

- Phase versus orbital velocity in SAR wave imaging: Paradox lost p 52 A89-13033

VAN INGEN SCHENAU, H. A.

- Real-time environment monitoring using data from Meteosat and NOAA imaging satellites p 23 A89-11730

VAN KONIJNENBURG, R.

- European remote sensing needs in the 1990s; Proceedings of the Annual Symposium of EARSeL, Noordwijkerhout, Netherlands, May 4-8, 1987 p 90 A89-20701

VAN STOKKOM, H. T. C.

- Geometric correction of remotely-sensed imagery using ground control points and orthogonal polynomials p 82 A89-20718

- Aerial photography for biomass assessment in the intertidal zone p 9 A89-20724

VAN ZYL, JAKOB J.

- Radar polarimetry - Analysis tools and applications p 30 A89-15915

VANDERLAAN, F. B.

- The potential of combined use of satellite data with topographic information [NLR-MP-87061-U] p 70 A89-12113

VANE, DEBORAH

- Earth Observing System - A platform for imaging spectrometers p 74 A89-10332

VANE, G.

- Airborne Visible/Infrared Imaging Spectrometer (AVIRIS): Inflight radiometric calibration and the determination of surface reflectance p 83 A89-10357

VANE, GREGG

- Imaging spectroscopy II; Proceedings of the Meeting, San Diego, CA, Aug. 20, 21, 1987 [SPIE-834] p 73 A89-10311

VANETTEN, R. P.

- A study on least-squares prediction and collocation [ETN-89-93336] p 29 A89-14492

VANKATWIJK, V.

- Average areal water equivalent of snow in a mountain basin using microwave and visible satellite data p 61 A89-13045

VANSTOKKOM, H. T. C.

- Validation of an atmospheric correction method for satellite borne imagery p 82 A89-10320

VANZYL, JAKOB J.

- Inference of geologic surface parameters from polarimetric radar observations and model inversion p 34 A89-12950

VASSILOU, A. A.

- On the application of averaging median filters in remote sensing p 68 A89-15920

VAUGHAN, P. O.

- The interpretation of Icelandic tundra features from LANDSAT-MSS data p 35 A89-13027

VAUGHAN, R. A.

- The interpretation of Icelandic tundra features from LANDSAT-MSS data p 35 A89-13027

VENEMA, J. C.

- Real-time environment monitoring using data from Meteosat and NOAA imaging satellites p 23 A89-11730

VERMA, SHASHI B.

- Comparison of measured and modeled radiation, heat and water vapor fluxes: FIFE pilot study [NASA-CR-183304] p 17 A89-11368

VERNEKAR, ANANDU D.

- Influence of sea surface temperature on intra- and inter-annual variations of ITCZ p 43 A89-12871

VETRELLA, S.

- Three-dimensional observation by means of tethered antennae [IAF PAPER 88-118] p 80 A89-17684

VETRELLA, SERGIO

- A procedure for modeling the terrain relief by using digitized topographic maps p 67 A89-14005

VEUGEN, L. M. M.

- Geometric correction of remotely-sensed imagery using ground control points and orthogonal polynomials p 82 A89-20718

VIDAL-MADJAR, DANIEL

- Effect of spatial resolution of the statistical properties of satellite images - A case study p 66 A89-12221

VIDAL, G.

- The use of MOMS-1 data for geological mapping of the Aswa lineament (East African rift) p 33 A89-10382

VIEIRADUTRA, LUCIANO

- Color enhancement of remote sensing imagery using IHS transformations and decorrelation stretch methods [INPE-4559-PRE/1300] p 70 A89-11418

VINCENT, DAYTON G.

- An example of estimates of precipitable water derived from Nimbus-7 SMMR satellite measurements and FGGE upper air data p 42 A89-12792

VINOGRADOV, B. V.

- Aerospace monitoring of ecosystem dynamics and ecological prognoses p 23 A89-15050

VIOLLIER, M.

- Comparative analysis of spectral response in the optical domain of targets in a tropical swamp at various spectral and spatial resolutions p 13 A89-10363
High resolution radiometric measurement of intertidal microphytobenthos p 48 A89-10365

VIRAG, L. A.

- An improved procedure for analysis of change in Thematic Mapper image-pairs p 65 A89-11013

VLCEK, J.

- Land and forest cover information from aerial video p 1 A89-10946

VODACEK, ANTHONY

- Laser fluorosensing of water quality - A review p 57 A89-10941

VOGELMANN, JAMES E.

- Detection of forest damage on Whiteface Mountain, New York, using Landsat Thematic Mapper data p 3 A89-10987

VOITURIEZ, B.

- The French space oceanography program p 44 A89-15116

VONDER HAAR, THOMAS H.

- Effects of data resolution on marine stratiform cloud detection using AVHRR and VISSR satellite data p 78 A89-12854

VONFRESE, R. R. B.

- Presentations by participants (edited and condensed) p 27 A89-12097

VONRUESTEN, C.

- Spectral reflectance of sugar beet and winter wheat canopies in the visible and infrared during growth p 12 A89-10342

W

WACKERMAN, C. C.

- Sea ice type classification of SAR imagery p 52 A89-13039

WACKERMAN, CHRISTOPHER C.

- Contrast ratios of internal waves in synthetic aperture radar imagery - A comparison of SAR Internal Wave Signature Experiment observations with theory p 40 A89-12167

WAKABAYASHI, H.

- Verification results of MOS-1 multispectral self scanning radiometer (MESSR) data p 86 A89-13004

WALLACE, K. S.

- Distribution of relative plate motion along the Pacific-North American plate boundary determined from mobile VLBI measurements p 26 A89-13761

WALTER, L. S.

The basis for the spectral behaviour of silicates in the thermal infrared and applications to remote sensing p 32 N89-10366

WALTERSHEA, ELIZABETH

Comparison of measured and modeled radiation, heat and water vapor fluxes: FIFE pilot study [NASA-CR-183304] p 17 N89-11368

WALTON, MARK L.

Validation of the on-site Flash Flood Potential System for Nexrad p 57 A89-10949

WANDERS, K.

Status and perspectives of vegetation monitoring by remote sensing [IAF PAPER 88-140] p 8 A89-17693

WANG, J. R.

Modeling of SAR polarisation phase difference from trees p 18 N89-12951

WANG, PIN QING

A useful model in mineral exploration with remotely sensed data p 30 A89-11017

WANG, WEN-TAO

Model-based remotely-sensed imagery interpretation p 66 A89-12223

WANG, YONG

Improvement and extension of a radar forest backscattering model [NASA-CR-183259] p 16 N89-11292

WANG, Z.

Simulation of a spinning spacecraft magnetometer p 28 N89-12101
A study of accuracy enhancement in satellite magnetic modeling p 28 N89-12102

WANG, ZHENG

A study of estimation of winter wheat yield for large area using remote sensing method p 2 A89-10974

WARDLEY, N. W.

Developing a radiometric leaf area index p 12 N89-10334

WARREN, D.

Cloud track winds from polar orbiting satellites p 87 N89-13069

WASH, CARLYLE H.

Snow and low-cloud discrimination from multispectral satellite measurements p 78 A89-12850

WEBSTER, IAN

Coastally trapped waves in the presence of a shelf edge density front p 46 A89-16989

WEEKS, W. F.

Numerical simulations of the profile properties of undeformed first-year sea ice during the growth season p 40 A89-12171

WEGENER, A.

SAR image statistics related to atmospheric drag over sea ice p 52 N89-13034

WELCH, R. M.

Classification of cloud fields based on textural characteristics p 65 A89-11727

WELLER, T.

The prospects for detecting spectral shifts due to satellite sensor aging p 6 A89-16061

WELLS, G. L.

Landsat Thematic Mapper observations of debris avalanche deposits in the Central Andes p 31 A89-19838

WESSMAN, CAROL A.

Estimation of forest canopy characteristics and nitrogen cycling using imaging spectrometry p 1 A89-10325

WEST, J. C.

Modulation of the radar backscatter from the ocean surface by a long gravity wave p 51 N89-13031

WESTER, K.

LANDSAT Thematic Mapping (TM) and SPOT HRV for survey mapping of bedrock outcrops p 20 N89-13055

WETZEL, L. B.

Shadows and wedges in scattering from the sea p 49 N89-12946

WETZEL, MELANIE

Effects of data resolution on marine stratiform cloud detection using AVHRR and VISSR satellite data p 78 A89-12854

WHARTON, S. W.

Requirements for ongoing development of the Pilot Land Data System (PLDS) p 24 N89-12958

WHEELER, J. R.

Evaluation of LANDSAT TM and SPOT imagery for agricultural land use planning in less developed countries p 19 N89-13051

WHITE, G. B.

An autonomous ocean instrument platform driven vertically by the current [AD-A198226] p 54 N89-13865

WHITE, J.

Soil erosion study using an airborne laser profiler p 1 A89-10952

WHITE, R. J.

Evaluation of LANDSAT TM and SPOT imagery for agricultural land use planning in less developed countries p 19 N89-13051

WHITEHEAD, VICTOR S.

Remote Sensing in Polarized Light [NASA-CP-3014] p 88 N89-14189

WHITEMAN, C. DAVID

Applications of digital image processing to ongoing research in complex terrain meteorology p 65 A89-11743

WICKLAND, D. E.

NASA's future land remote sensing program p 90 N89-10393

WIESBECK, W.

Coherent polarimetric signatures of coniferous trees: A survey p 9 N89-10307
Polarization-dependent attenuation of dielectric cylinder arrays p 86 N89-12955

WIESENBERG, DENIS A.

Chemical variability in ocean frontal areas [AD-A198418] p 56 N89-14655

WIESNET, DONALD

Remote sensing technologies and spatial data applications [AD-A195809] p 62 N89-14480

WILHEIT, T. T.

Rainfall index over oceans derived from SSM/I data p 51 N89-12998

WILLESEN, H.

Combining spectral and structural analyses to select useful cartographic information from SPOT imagery p 71 N89-13052

WILSON, ANDREW K.

The effective resolution element of Landsat Thematic Mapper p 65 A89-12220

WILSON, DOUG

Acoustic Doppler current profiling in the equatorial Pacific in 1984 p 45 A89-16986

WILSON, GREGORY S.

NASA's Earth Science Geostationary Platform p 77 A89-12828

WIRTH, J.

The Airborne Version Conical Scan Radiometer (AVCSR): An airborne radiometer as a tool for satellite data validation p 86 N89-12937

WITONO, H.

Near surface soil moisture estimation from microwave measurements p 6 A89-17282

WOERNER, CHARLES V.

Lidar atmospheric sounder and altimetry for the Earth Observing System (EOS) satellite p 79 A89-15873

WOLF, J.

Feasibility study for the development of a joint surge and wave model [PB88-230917] p 55 N89-14652

WONG, SAM K. S.

Relative water content of Spruce needles determined by the leaf water content index p 4 A89-11012

WOOD, C. A.

Emitted short wavelength infrared radiation for detection and monitoring of volcanic activity p 32 N89-10377

WOOD, LYNNETTE

Resolution improvement by multi-temporal data merging p 63 A89-10937

WOOD, T. F.

Classification decision rule modification on the basis of information extracted from training data p 72 N89-13062

WOODY, LOREN M.

SeaWiFS - An ocean-imaging sensor p 74 A89-10338

WRIGHT, C. WAYNE

The Seawifs sensor for Landsat-6 p 36 A89-10954

WRIGHT, G. G.

Airborne lidar detection of subsurface oceanic scattering layers p 41 A89-12260

WRIGHT, G. G.

Analysis of potato crop distribution using remotely sensed and environmental data in a pilot geographical information system p 18 N89-12967

WU, JIAN-KANG

Model-based remotely-sensed imagery interpretation p 66 A89-12223

WU, S. C.

Directional measurement of short ocean waves with stereophotography p 45 A89-16982

X

XIE, KUNQING

The character of reflective spectrum of winter wheat and the principle of its yield estimation with remote sensing method p 2 A89-10973

A study of estimation of winter wheat yield for large area using remote sensing method p 2 A89-10974

XU, BAIDE

SAR and visible remote sensing of the Taoer River coastal zone at Bohai Bay p 38 A89-11005

XU, XIRU

The character of reflective spectrum of winter wheat and the principle of its yield estimation with remote sensing method p 2 A89-10973

A study of estimation of winter wheat yield for large area using remote sensing method p 2 A89-10974

Y

YAMAGUCHI, R.

Accuracy of land cover classification of Thematic Mapper (TM) and SPOT data p 72 N89-13066

YAMAZAKI, T.

Data collection system operating on Japan's first marine observation satellite: Inflight evaluation of the system performance p 87 N89-13007

YASUOKA, Y.

Efficient classification of multispectral images by a best linear discriminant function p 72 N89-13060

YEH, HWA-YOUNG

Satellite microwave rainfall simulations with a three-dimensional dynamical cloud model p 77 A89-12833

YIP, TSOI-CHING

Variation of satellite rain relationships in space and time p 67 A89-12843

YOKOTA, T.

Detection of seasonal and long-term changes in land cover from multitemporal LANDSAT MSS data p 71 N89-12989

YOKOYAMA, R.

Estimation of sea surface temperature via NOAA-AVHRR sensor: Comparison with sea truth data by fixed buoys p 51 N89-13005

YOSHIKADO, SHIN

Backscattering coefficient of rice crops and rice fields by an X-band scatterometer p 3 A89-10980

YOSHIMOTO, SHIGETOSHI

Experimental personal satellite communications system using millimeter-wave for Asia-Oceanian region p 81 A89-18736

YUAN, X.

Land and forest cover information from aerial video p 1 A89-10946

YUAN, XIAOPING

Automatic control point determination for image registration using texture analysis methods p 3 A89-10985

YUEN, H. C.

Modulation of radar backscatter from the ocean by a variable surface current p 39 A89-12158

Z

ZEBKER, H. A.

Inference of geologic surface parameters from polarimetric radar observations and model inversion p 34 N89-12950

ZEBKER, HOWARD A.

Radar polarimetry - Analysis tools and applications p 30 A89-15915

ZEHR, RAYMOND M.

The use of polar orbiter data in tropical weather system analysis p 77 A89-12818

Satellite diagnosis of tropical cyclones p 42 A89-12823

ZEYEN, R.

Small format air photo from ultrahigh aircraft as an aid for data collection of agricultural statistics in Sahelian countries p 19 N89-13003

ZHANG, CHENG BO

A synthetic apertures radar with multichannel and multipolarisation p 87 N89-13017

ZHANG, DIANCHEN

Study of monitoring sea ice using an airborne microwave radiometer system p 37 A89-10972

ZHANG, JUNRONG

Study of monitoring sea ice using an airborne microwave radiometer system p 37 A89-10972

ZHANG, ZI-JUE

A new spatial classification algorithm for high ground resolution images p 72 N89-13061

Accuracy of land cover classification of Thematic Mapper (TM) and SPOT data p 72 N89-13066

ZHAO, RENVU

Study of monitoring sea ice using an airborne microwave radiometer system p 37 A89-10972

ZHAO, S. K.

Geophysical interpretation of the magnetic anomalies of China derived from Magsat data p 26 A89-20200

ZHU, XIACHONG

The character of reflective spectrum of winter wheat
and the principle of its yield estimation with remote sensing
method p 2 A89-10973

ZHU, XIAOHONG

A study of estimation of winter wheat yield for large
area using remote sensing method p 2 A89-10974

ZHURAVEL', N. E.

The effect of agrometeorological conditions on the
characteristics of space radar imagery of agricultural
regions in winter p 8 A89-18709

ZILGER, J.

Comparative point-spread function calculations for the
MOMS-1, Thematic Mapper and SPOT-HRV instruments
p 83 N89-10379

Digital analysis of MOMS-1, LANDSAT TM, and SPOT
data of the Nakuru area (Kenya) p 33 N89-10386

ZOBLER, L.

Development of a ground hydrology model suitable for
global climate modeling using soil morphology and
vegetation cover, and an evaluation of remotely sensed
information

[NASA-CR-180463] p 21 N89-13821

ZWENGER, I.

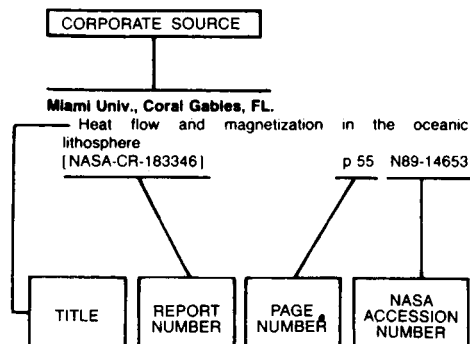
Spectral characterization of forest damage in beech, oak
and pine stands p 21 N89-13085

CORPORATE SOURCE INDEX

EARTH RESOURCES / A Continuing Bibliography (Issue 61)

APRIL 1989

Typical Corporate Source Index Listing



Listings in this index are arranged alphabetically by corporate source. The title of the document is used to provide a brief description of the subject matter. The page number and the accession number are included in each entry to assist the user in locating the abstract in the abstract section. If applicable, a report number is also included as an aid in identifying the document.

A

Academia Sinica, Beijing (China).

A synthetic apertures radar with multichannel and multipolarisation p 87 N89-13017

Aeritalia S.p.A., Turin (Italy).

Solid earth mission study. Volume 2: Technical report [ESA-CR(P)-2626-VOL-2] p 26 N89-10303

Solid Earth mission study. Volume 1: Executive summary [ESA-CR(P)-2626-VOL-1] p 26 N89-10397

Solid earth mission study. Volume 3: Program planning report [ESA-CR(P)-2626-VOL-3] p 27 N89-10399

Air Force Geophysics Lab., Hanscom AFB, MA.

Possible measurement errors in calibrated AVHRR (Advanced Very High Resolution Radiometer) data [AD-A198342] p 88 N89-14414

Air Force Inst. of Tech., Wright-Patterson AFB, OH.

Active modes of the Pacific Intertropical Convergence Zone (ITCZ) [AD-A196406] p 49 N89-11374

Alaska Univ., Fairbanks.

Development of Alaskan gas hydrate resources [DE88-010270] p 35 N89-13093

American Inst. of Aeronautics and Astronautics, New York, NY.

Standards for earth observations from space [IAF PAPER 88-107] p 90 N89-17680

American Inst. of Aeronautics and Astronautics, Washington, DC.

Standards for earth observations from space [IAF PAPER 88-107] p 90 N89-17680

Applied Research Corp., Landover, MD.

A new radar technique for satellite rainfall algorithm development [NASA-CR-183471] p 60 N89-11102

Army Cold Regions Research and Engineering Lab., Hanover, NH.

Numerical simulations of the profile properties of undeformed first-year sea ice during the growth season p 40 A89-12171

Extraction of topography from side-looking satellite systems - A case study with SPOT simulation data p 68 A89-16063

Correlation function study for sea ice p 46 A89-16990

Army Engineer Topographic Labs., Fort Belvoir, VA.

Continuous deformation monitoring with GPS [AD-A196447] p 27 N89-10886

Aston Univ., Birmingham (England).

An evaluation of satellite imagery, LANDSAT Thematic Mapper and SPOT-1 HRV, for grassland inventory in the UK p 20 N89-13057

B

Bergen Univ. (Norway).

Mizex '87 - Overview of the Winter Marginal Ice Zone Experiment in the Greenland and Barents Seas p 36 A89-10931

Bonn Univ. (Germany, F.R.).

Spectral reflectance of sugar beet and winter wheat canopies in the visible and infrared during growth p 12 N89-10342

British Aerospace Public Ltd. Co., Bristol (England).

Solid earth mission study. Volume 2: Technical report [ESA-CR(P)-2626-VOL-2] p 26 N89-10303

Solid Earth mission study. Volume 1: Executive summary [ESA-CR(P)-2626-VOL-1] p 26 N89-10397

Solid earth mission study. Volume 3: Program planning report [ESA-CR(P)-2626-VOL-3] p 27 N89-10399

British Antarctic Survey, Cambridge (England).

Cloud track winds from polar orbiting satellites p 87 N89-13069

Brown Univ., Providence, RI.

Contributions to the GASP workshop proceedings (not presented orally) p 27 N89-12100

C

Caelum Research Corp., Silver Spring, MD.

Satellite microwave rainfall simulations with a three-dimensional dynamical cloud model p 77 A89-12833

California Inst. of Tech., Pasadena.

Determination of convergence rates across the Ventura Basin, Southern California, using GPS and historical triangulation [NASA-CR-183014] p 29 N89-14624

California Univ., La Jolla.

Geosat crossover analysis in the tropical Pacific. I - Constrained sinusoidal crossover adjustment p 38 A89-11143

A pilot study to determine relationships between North Pacific precipitation from Nimbus-7 Scanning Multichannel Microwave Radiometer data and associated atmospheric conditions p 43 A89-12837

A satellite data processing and analysis software system for earth's atmosphere and surface research p 67 A89-12864

Beyond plate tectonics - Looking at plate deformation with space geodesy p 44 A89-13758

California Univ., San Diego.

Mass and heat balances in the upper ocean p 53 N89-13089

California Univ., Santa Barbara.

Invertible canopy reflectance modeling of vegetation structure in semiarid woodland p 6 A89-15918

The spectral bidirectional reflectance of snow p 69 N89-10318

Improvement and extension of a radar forest backscattering model [NASA-CR-183259] p 16 N89-11292

Remote sensing information sciences research group [NASA-CR-183374] p 91 N89-14481

Canada Centre for Remote Sensing, Ottawa (Ontario).

SAR-seen multimode waves in ice: Evidence of imaging nonlinearities p 50 N89-12971

Phase versus orbital velocity in SAR wave imaging: Paradox lost p 52 N89-13033

The LIMEX 1987 pilot project, LIMEX 1989 and long-term objective for data collection on the Canadian East coast p 52 N89-13037

Centre d'Etude Spatiale des Rayonnements, Toulouse (France).

Retrieving vegetation and soil parameters from radar measurements p 10 N89-10321

Centre de Recherches en Physique de l'Environnement, Issy-les-Moulineaux (France).

Infrared temperature measurements over bare soil and vegetation - A HAPEX perspective p 2 A89-10953

Design of a spaceborne radar for tropical rain mapping at the climatological scale p 60 N89-12997

Centre for Agrobiological Research, Wageningen (Netherlands).

Microwave backscatter from beets, peas and potatoes throughout the growing season p 9 N89-10309

Centre National d'Etudes Spatiales, Paris (France).

The French space program for Earth observation p 90 N89-10392

Centre National d'Etudes Spatiales, Toulouse (France).

Comparison between active and passive microwave measurements over Antarctica p 48 N89-10316

Spectral characterization of forest targets in mountainous zones on Thematic Mapper images p 11 N89-10328

Analysis of directional effects on NOAA AVHRR p 70 N89-10341

Estimation of primary marine production using spaceborne data on ocean color p 48 N89-10371

Study of the multiplexing of image telemetry data from SPOT 4 HRVIR and Vegetation sensors [CNES-87/229/CT/DRT/TIT/TR] p 70 N89-10930

Centre National de Recherches Meteorologiques, Toulouse (France).

Evaporation over land surfaces - First results from HAPEX-MOBILHY Special Observing Period p 57 A89-12211

A study of the vegetation cover with AVHRR during HAPEX-MOBILHY p 15 N89-10389

Chinese Academy of Meteorological Sciences, Beijing.

Precipitation detection with satellite microwave data [PB88-240239] p 88 N89-13094

Cologne Univ. (Germany, F.R.).

The Airborne Version Conical Scan Radiometer (AVCSR): An airborne radiometer as a tool for satellite data validation p 86 N89-12937

Colorado State Univ., Fort Collins.

Better understanding of intense and tornadic thunderstorms through research using geostationary satellite data p 56 A89-10934

Using satellite data to aid in diagnosing and forecasting convective development and intensity along arc cloud lines p 76 A89-12810

Simulation of radar and surface measurements of rainfall p 62 N89-13924

Colorado Univ., Boulder.

Satellite measurements required for deep-earth geophysics p 28 N89-12103

Columbia Univ., New York, NY.

Development of a ground hydrology model suitable for global climate modeling using soil morphology and vegetation cover, and an evaluation of remotely sensed information [NASA-CR-180463] p 21 N89-13821

Consiglio Nazionale delle Ricerche, Florence (Italy).

A new lidar system for applications over land and sea p 83 N89-10347

Cooperative Inst. for Research in the Atmosphere, Fort Collins, CO.

Using satellite data to aid in diagnosing and forecasting convective development and intensity along arc cloud lines p 76 A89-12810

SOURCE

D

- Department of Agriculture, Beltsville, MD.**
Aircraft remote sensing in HAPEX p 59 N89-10388
Microcomputers (PCs) for snow cover analyses using multisensor satellite data p 62 N89-13049
- Deutsche Forschungs- und Versuchsanstalt fuer Luft- und Raumfahrt, Oberpfaffenhofen (West Germany).**
Thermal infrared laser spectroscopy: The potential of dual active/passive thermal infrared sensors for Earth observation p 82 N89-10345
Optimization for classification of forest damage classes p 13 N89-10359
Applications of LANDSAT (TM and MSS) data for an estimation of rangeland conditions in semiarid and arid areas of northern Kenya p 16 N89-10404
[DFVLR-FB-88-18]
The airborne radiometry experiment (ABREX) instrument, an experimental test bed for the specification of satellite-borne microwave radiometer at 90 GHz p 86 N89-12939
The MEOSSE experiment: A test case for future cartographic missions p 87 N89-13081
Spectral characterization of forest damage in beech, oak and pine stands p 21 N89-13085
- Direction de la Meteorologie Nationale, Paris (France).**
Towards direct variational assimilation of scatterometer backscatter measurements into numerical weather prediction models p 86 N89-13000
- Dornier-Werke G.m.b.H., Friedrichshafen (Germany, F.R.).**
Solid earth mission study. Volume 2: Technical report [ESA-CR(P)-2626-VOL-2] p 26 N89-10303
Solid Earth mission study. Volume 1: Executive summary [ESA-CR(P)-2626-VOL-1] p 26 N89-10397
Solid earth mission study. Volume 3: Program planning report [ESA-CR(P)-2626-VOL-3] p 27 N89-10399
Performance modeling and results for X-SAR p 71 N89-13009
- Dundee Univ. (Scotland).**
MOMS-1 data for bathymetric and geological studies p 33 N89-10383
The interpretation of Icelandic tundra features from LANDSAT-MSS data p 35 N89-13027

E

- Earth Satellite Corp., Chevy Chase, MD.**
Remote sensing technologies and spatial data applications [AD-A195809] p 62 N89-14480
- Ecole Nationale Supérieure des Telecommunications, Brest (France).**
Spectral analysis of ocean wave imagery using 2-D linear prediction p 50 N89-12968
- Ecole Polytechnique Federale de Lausanne (Switzerland).**
The normalization of a soil brightness index for the study of changes in soil conditions p 14 N89-10370
- Edinburgh Univ. (Scotland).**
Integrating remote sensing data into a geographical information system: A foundation for rural land use strategies: Nature Conservancy Council project p 24 N89-12964
Evaluation of LANDSAT TM and SPOT imagery for agricultural land use planning in less developed countries p 19 N89-13051
- Environmental Protection Agency, Corvallis, OR.**
Analysis of crop loss for alternative ozone exposure indices [PB88-214788] p 22 N89-14608
- Environmental Research Inst. of Michigan, Ann Arbor.**
Mizex '87 - Overview of the Winter Marginal Ice Zone Experiment in the Greenland and Barents Seas p 36 N89-10931
The prospects for detecting spectral shifts due to satellite sensor aging p 6 N89-16061
SAR image statistics related to atmospheric drag over sea ice p 52 N89-13034
Sea ice type classification of SAR imagery p 52 N89-13039
- European Space Agency, Paris (France).**
Proceedings of the 4th International Colloquium on Spectral Signatures in Remote Sensing [ESA-SP-287] p 9 N89-10305
Proceedings of the 1988 International Geoscience and Remote Sensing Symposium (IGARSS 1988) on Remote Sensing: Moving Towards the 21st Century, volume 1 [ESA-SP-284-VOL-1] p 85 N89-12936

F

- Flow Research, Inc., Kent, WA.**
An autonomous ocean instrument platform driven vertically by the current [AD-A198226] p 54 N89-13865
- Fokker B.V., Amsterdam (Netherlands).**
Solid earth mission study. Volume 2: Technical report [ESA-CR(P)-2626-VOL-2] p 26 N89-10303
Solid Earth mission study. Volume 1: Executive summary [ESA-CR(P)-2626-VOL-1] p 26 N89-10397
Solid earth mission study. Volume 3: Program planning report [ESA-CR(P)-2626-VOL-3] p 27 N89-10399
- Forest Service, San Francisco, CA.**
Operational use of Landsat data for timber inventory p 2 N89-10970
- Forest Service, Washington, DC.**
Space shuttle large format camera photography cloud cover interference diagrams [PB88-244405] p 88 N89-14482
- Forut, Tromsø (Norway).**
Ocean wave number spectra and spatial autocorrelation functions from SAR images p 50 N89-12970

G

- GEC-Marconi Electronics Ltd., Chelmsford (England).**
Constraints on two-scale descriptions of radar backscattering from the sea surface using scatterometer model functions p 49 N89-12945
Complex SAR imagery and speckle filtering for ERS-1 wave mode p 71 N89-13029
Analysis of Seasat SAR sea-ice data from the Beaufort Sea p 52 N89-13035
An analysis of directional ambiguities in wind scatterometer measurements p 87 N89-13071
- General Sciences Corp., Laurel, MD.**
Tropopause adjustment to tropical cyclones as inferred from satellite ozone observations p 77 N89-12816
Satellite microwave rainfall simulations with a three-dimensional dynamical cloud model p 77 N89-12833
Comparison of satellite IR rain estimates with radar rain observations in hurricanes p 57 N89-12845
- Geological Survey, Dover, DE.**
Simulation of a spinning spacecraft magnetometer p 28 N89-12101
A study of accuracy enhancement in satellite magnetic modeling p 28 N89-12102
- Geological Survey, Flagstaff, AZ.**
Directional measurement of short ocean waves with stereophotography p 45 N89-16982
- Geological Survey, Tacoma, WA.**
Variations in the Arctic, Antarctic, and global sea ice covers during 1978-1987 as observed with the Nimbus 7 scanning multichannel microwave radiometer p 38 N89-11145
- Geological Survey of Britain, Nottingham.**
Applications of remote sensing for geological mapping in eastern Egypt p 35 N89-13087
- Georgia Inst. of Tech., Atlanta.**
Statistics and high resolution imaging of snowpack at 35 GHz using a microcomputer p 61 N89-13047
- GKSS-Forschungszentrum Geesthacht (Germany, F.R.).**
High-resolution spectroscopy for remote sensing of ocean and atmosphere p 48 N89-10352
- Goettingen Univ. (Germany, F.R.).**
Building a monitoring system based on satellite data to detect vegetation and land use changes in a subtropical region of Mexico p 20 N89-13079
- Grenoble-1 Univ. (France).**
Satellite surveillance of ice and snow covered surfaces in the French Alps using visible and near infrared reflectance measurements from the SPOT and LANDSAT Thematic Mapper sensors p 59 N89-10372
- Griffiths Remote Sensing, London (England).**
The relative utility of LANDSAT MSS and SIR-A imagery in reconnaissance geological mapping in Northern Sudan p 34 N89-13022
- Groupe Scientifique de Teledetection de Strasbourg (France).**
Attempt at absolute determination of spectral signatures of bare soils in the thermal infrared, in emission and reflection p 12 N89-10336
Multispectral characterization of the spatial structure of remotely sensed scenes p 70 N89-10340
- Groupe Scientifique de Teledetection Spatiale de Toulouse (France).**
Evaporation over land surfaces - First results from HAPEX-MOBILHY Special Observing Period p 57 N89-12211

H

- Harvard-Smithsonian Center for Astrophysics, Cambridge, MA.**
VLBI geodesy - 2 parts-per-billion precision in length determinations for transcontinental baselines p 26 N89-13762
VLBI studies of the nutations of the earth p 26 N89-13764
- Helsinki Univ. of Technology, Espoo (Finland).**
Microwave dielectric properties of low-salinity sea ice p 52 N89-13036
- Hunter Coll., New York.**
Invertible canopy reflectance modeling of vegetation structure in semiarid woodland p 6 N89-15918
- Hydrological Research Inst., Pretoria (South Africa).**
The extrapolation of spectral signatures illustrates LANDSATs' potential to detect wetlands p 62 N89-13067
- Iceland Univ., Reykjavik.**
Strengths and shortcomings in Airborne Thematic Mapper (ATM) technology as applied to volcanic and geothermal areas in Iceland p 32 N89-10337
A narrow-band thermal imager based on multilayer real-time averaging p 83 N89-10356
- Illinois Univ., Urbana.**
Mapping dominant vegetation communities in the Colorado Rocky Mountain Front Range with Landsat Thematic Mapper and digital terrain data p 8 N89-20629
- Indian Inst. of Tech., Bombay.**
Important aspects of technology transfer: Training of inservice engineers and scientists; satellite remote sensing p 91 N89-13082
- Institut Français de Recherche pour l'Exploitation de la Mer, Brest (France).**
Comparative analysis of spectral response in the optical domain of targets in a tropical swamp at various spectral and spatial resolutions p 13 N89-10363
High resolution radiometric measurement of intertidal microphytobenthos p 48 N89-10365
- Institut National de la Recherche Agronomique, Avignon (France).**
Extracting soil and vegetation characteristics from microwave remote sensing data p 9 N89-10306
- Institut National de la Recherche Agronomique, Montfavet (France).**
Measuring in-situ soil surface roughness using a laser profilometer p 9 N89-10308
Complementary of microwave and optical range in the characterization of crops by remote sensing p 10 N89-10310
Spectral profile and biomass estimation p 10 N89-10319
A simplified vegetation canopy reflectance and absorption model p 10 N89-10322
Introducing spectral data into a plant process model for improving its prediction ability p 10 N89-10324
Biomass and wheat crop yield estimation from SPOT vegetative indexes p 11 N89-10327
Use of high spectral resolution to follow the state of vegetation canopies p 13 N89-10354
- Institut National de la Recherche Agronomique, Thiverval-Grignon (France).**
Evaporation over land surfaces - First results from HAPEX-MOBILHY Special Observing Period p 57 N89-12211
Potential number of winter wheat ears estimation using radiometry techniques at an early stage p 10 N89-10323
Estimation of the interception efficiency of an alfalfa canopy from a vegetative index p 11 N89-10332
Relation between sugar beet crop yield and vegetative indexes calculated from LANDSAT MSS images p 11 N89-10333
Estimation of leaf spectra from measurements in wide spectral bands p 14 N89-10368
Modeling of soil color by remote sensing p 14 N89-10369
A new method for estimating regional evaporation from thermal infrared surface temperature measurements p 60 N89-10390
- Institute for Image Processing Computer Mapping, Graz (Austria).**
Stress detection in mixed coniferous-broadleaved forests from Airborne Imaging Spectrometer (AIS) data p 13 N89-10355
- Institute of Ocean Sciences, Sidney (British Columbia).**
The fluorescence line imager: High-resolution imaging spectroscopy over water and land p 83 N89-10353

Instituto de Pesquisas Espaciais, Cachoeira Paulista (Brazil).

Photogrammetric model for correction of MSS-LANDSAT imagery
[INPE-4652-PRE/1359] p 73 N89-13090

Instituto de Pesquisas Espaciais, Sao Jose dos Campos (Brazil).

Identifying the reforested areas utilizing the SPOT satellite data
[INPE-4624-PRE/1343] p 15 N89-10396

The Transformed Vegetation Index (TVI) for estimation of Brazilian cerrado's phytomass
[INPE-4603-PRE/1326] p 15 N89-10400

Nation-wide forest mapping and timber volume estimation using LANDSAT-5 TM imagery
[INPE-4643-PRE/1354] p 16 N89-10402

Environmental impact of the urban growth on the Western Sao Paulo metropolitan area
[INPE-4670-PRE/1370] p 23 N89-10413

A general data model for geographic information systems
[INPE-4560-PRE/1301] p 24 N89-10676

Technique for obtaining agricultural property boundaries through satellite imagery, certified to control and accompany agricultural activity
[INPE-4640-PRE/1351] p 16 N89-11294

Training activities in remote sensing at the Instituto de Pesquisas Espaciais-INPE/Brazil
[INPE-4686-PRE/1380] p 91 N89-11295

Spectral studies of three oxisols and a Ultisol of Brazil
[INPE-4644-PRE/1355] p 17 N89-11297

CIR aerial photography applied to the evaluation of the air pollution impact in a tropical forest: The case of Cubatão, Brazil
[INPE-4651-PRE/1358] p 17 N89-11324

Development of a semi-empirical model for estimating the global solar radiation
[INPE-4620-TDL/328] p 84 N89-11352

Color enhancement of remote sensing imagery using IHS transformations and decorrelation stretch methods
[INPE-4559-PRE/1300] p 70 N89-11418

An agricultural crop yield model by satellite: A simulation
[INPE-4639-PRE/1350] p 17 N89-12106

Digital processing applied to vegetation
[INPE-4695-MD/036] p 17 N89-12107

Method of visual analysis of remote sensing data-vegetation
[INPE-4696-MD/037] p 17 N89-12108

Interaction of solar radiation with vegetation
[INPE-4697-MD/038] p 17 N89-12109

Crop separation analysis through SPOT and TM digital data
[INPE-4641-PRE/1352] p 18 N89-12110

Microwave remote sensing at the Institute for Space Research (INPE) Brazil: Concepts and future prospects of soil moisture studies p 20 N89-13080

Iwate Univ., Morioka (Japan).

Estimation of sea surface temperature via NOAA-AVHRR sensor: Comparison with sea truth data by fixed buoys p 51 N89-13005

J**Jet Propulsion Lab., California Inst. of Tech., Pasadena.**

Imaging spectroscopy II: Proceedings of the Meeting, San Diego, CA, Aug. 20, 21, 1987
[SPIE-834] p 73 A89-10311

Earth Observing System - A platform for imaging spectrometers p 74 A89-10332

High Resolution Imaging Spectrometer (HIRIS)
p 74 A89-10334

Reflectance characteristics of dry plant materials
p 3 A89-10977

Relative water content of Spruce needles determined by the leaf water content index p 4 A89-11012

Distribution of relative plate motion along the Pacific-North American plate boundary determined from mobile VLBI measurements p 26 A89-13761

Radar polarimetry - Analysis tools and applications
p 30 A89-15915

Tower Ocean Wave and Radar Dependence experiment - An overview p 44 A89-16976

Theory for synthetic aperture radar imaging of the ocean surface - With application to the Tower Ocean Wave and Radar Dependence experiment on focus, resolution, and wave height spectra p 44 A89-16977

Comparison of measured and predicted sea surface spectra of short waves p 45 A89-16981

Directional measurement of short ocean waves with stereophotography p 45 A89-16982

The dependence of sea surface slope on atmospheric stability and swell conditions p 45 A89-16983

Altimetry for non-Gaussian oceans - Height biases and estimation of parameters p 46 A89-16992

Standards for earth observations from space
[IAF PAPER 88-107] p 90 A89-17680

The spectral bidirectional reflectance of snow
p 69 N89-10318

Airborne Visible/Infrared Imaging Spectrometer (AVIRIS): Inflight radiometric calibration and the determination of surface reflectance p 83 N89-10357

Monitoring seasonal variations of soil moisture and vegetation cover using satellite microwave radiometry
p 15 N89-10378

Sensors research and technology p 85 N89-11774

Inference of geologic surface parameters from polarimetric radar observations and model inversion
p 34 N89-12950

Performance of a scanning pencil-beam spaceborne scatterometer for ocean wind measurements
p 53 N89-13073

Johns Hopkins Univ., Laurel, MD.

On the use of speckle statistics for the extraction of ocean wave spectra from SAR imagery
p 50 N89-12969

Directional ocean wave spectra: Prospects for acquiring a global data base from SIR-C p 50 N89-12973

The Labrador Sea Extreme Waves Experiment: Objectives, status and plans p 51 N89-12974

Estimating aircraft SAR response characteristics and approximating ocean wave spectra in the Labrador Sea
p 52 N89-13032

Joint Research Centre of the European Communities, Ispra (Italy).

Time-resolved laser fluorescence: Trends and applications p 83 N89-10346

AGRISAR '86: Contributing to signature research
p 15 N89-10387

Small format air photo from ultrahigh aircraft as an aid for data collection of agricultural statistics in Sahelian countries p 19 N89-13003

The classification of semi-natural vegetation from LANDSAT Thematic Mapper imagery: A user's perspective p 21 N89-13084

K**Kanazawa Univ. (Japan).**

Snowmelt runoff estimation using snow cover extent data and its application to optimum control of dam water level p 61 N89-13042

Kansas State Univ., Manhattan.

The influence of grazing on land surface climatological variables
[NASA-CR-183308] p 22 N89-14637

Kansas Univ., Lawrence.

Modulation of the radar backscatter from the ocean surface by a long gravity wave p 51 N89-13031

Kansas Univ. Center for Research, Inc., Lawrence.

Investigation of radar backscattering from second-year sea ice
[NASA-CR-180986] p 54 N89-14479

Karlsruhe Univ. (Germany, F.R.).

Coherent polarimetric signatures of coniferous trees: A survey p 9 N89-10307

Changes in the chlorophyll fluorescence spectra during the Kautsky induction kinetics p 12 N89-10348

Chlorophyll fluorescence spectra of leaves as induced by blue light and red laser light p 12 N89-10349

Design of spectral bands for the German MOMS-2 sensor p 84 N89-10381

Polarization-dependent attenuation of dielectric cylinder arrays p 86 N89-12955

Large area TM land cover classification of Mittlerer Oberrhein County, southwest Germany, and its use for regional planning and crop surveys p 18 N89-12986

Katholieke Universiteit te Leuven (Belgium).

An integrated remote sensing approach for regional agrostatistics and land monitoring p 24 N89-12960

Kingston Polytechnic, Kingston-Upon-Thames (England).

The detection of unimproved grassland in Berkshire using a binary decision tree approach
p 18 N89-12988

Crop classification with multi-temporal X-band SAR data p 19 N89-12990

Classification decision rule modification on the basis of information extracted from training data
p 72 N89-13062

Kisarazu National Coll. of Technology (Japan).

Laser-induced fluorescence on in-vivo chlorophyll of a rice plant: A technique for the remote detection of plant growth p 12 N89-10350

L**LABEN Space Instrumentation and Systems, Milan (Italy).**

Solid earth mission study. Volume 2: Technical report [ESA-CR(P)-2626-VOL-2] p 26 N89-10303

Solid Earth mission study. Volume 1: Executive summary
[ESA-CR(P)-2626-VOL-1] p 26 N89-10397

Solid earth mission study. Volume 3: Program planning report
[ESA-CR(P)-2626-VOL-3] p 27 N89-10399

Laboratoire Central des Ponts et Chaussees, Paris (France).

Measuring in-situ soil surface roughness using a laser profilometer p 9 N89-10308

Lamont-Doherty Geological Observatory, Palisades, NY.

Somali Basin, Chain Ridge, and origin of the Northern Somali Basin gravity and geoid low p 30 A89-12290

Laval Univ. (Quebec).

Texture analysis in forest areas: High spectral resolution synthetic aperture radar data p 14 N89-10367

Leeds Univ. (England).

Modelling land resources within a pilot geographical information system p 18 N89-12962

Analysis of potato crop distribution using remotely sensed and environmental data in a pilot geographical information system p 18 N89-12967

Liege Univ. (Belgium).

Towards an urban land-use classification using textural and morphological criteria p 25 N89-12987

Linköping Univ. (Sweden).

Atmospheric correction of thermal infrared data from LANDSAT-5 for surface temperature estimation
p 70 N89-10339

Los Alamos National Lab., NM.

The angular reflectance signature of the canopy hot spot in the optical regime p 11 N89-10325

Lunar and Planetary Inst., Houston, TX.

Landsat Thematic Mapper observations of debris avalanche deposits in the Central Andes
p 31 A89-19838

M**MacDonald, Dettwiler and Associates Ltd., Richmond (British Columbia).**

Extraction of dense digital elevation models from SPOT stereo imagery p 71 N89-13053

Marconi Co. Ltd., Great Baddow (England).

The use of the complex correlation function in the recovery of ocean wave spectra from SAR images
p 47 N89-10315

Marconi Space Systems Ltd., Portsmouth (England).

Multistatic scatterometry p 87 N89-13072

Massachusetts Inst. of Tech., Cambridge.

Beyond plate tectonics - Looking at plate deformation with space geodesy p 44 A89-13758

Correlation function study for sea ice
p 46 A89-16990

Remote sensing of earth terrain
[NASA-CR-183347] p 85 N89-12111

The structure of red-infrared scattergrams of semivegetated landscapes
[NASA-CR-183385] p 21 N89-13091

Use of LANDSAT images of vegetation cover to estimate effective hydraulic properties of soils
[NASA-CR-183384] p 21 N89-13823

Evaluation of GEOSAT (Geodetic Satellite) data and application to variability of the northeast Pacific Ocean
[AD-A198950] p 53 N89-13863

Massachusetts Univ., Amherst.

The electronically steered thinned array radiometer
p 74 A89-10932

Passive microwave remote sensing of salinity in coastal zones p 36 A89-10942

Millimeter-wave backscatter measurements of various snow forms p 61 N89-13046

MATRA Espace, Toulouse (France).

Solid earth mission study. Volume 2: Technical report [ESA-CR(P)-2626-VOL-2] p 26 N89-10303

Solid Earth mission study. Volume 1: Executive summary
[ESA-CR(P)-2626-VOL-1] p 26 N89-10397

Solid earth mission study. Volume 3: Program planning report
[ESA-CR(P)-2626-VOL-3] p 27 N89-10399

Max-Planck-Inst. fuer Radioastronomie, Bonn (Germany, F.R.).

Very Long Baseline Interferometry (VLBI) from ground and space p 85 N89-11645

- Metocean Consultancy Ltd., Haslemere (England).**
Review of the requirements for higher level ERS-1 products within Europe
[ESA-CR(P)-2586] p 84 N89-10664
- Miami Univ., Coral Gables, FL.**
Heat flow and magnetization in the oceanic lithosphere
[NASA-CR-183346] p 55 N89-14653
- Michigan State Univ., East Lansing.**
Evaluating Landsat classification accuracy from forest cover-type maps p 5 A89-12756
Use of remote sensing for land use policy formulation
[NASA-CR-183148] p 15 N89-10395
- Michigan Univ., Ann Arbor.**
Effect of curvature on the backscattering from leaves
[NASA-CR-183326] p 16 N89-11296
- Ministry of Posts and Telecommunications, Tokyo (Japan).**
Inference of radio scattering parameters of Antarctic ice sheet using 179 MHz airborne radio echo sounding data
p 51 N89-12975
- Minnesota Univ., Minneapolis.**
Microwave radiances from horizontally finite, vertically structured precipitating clouds p 84 N89-11364
- Musee Royal de l'Afrique Centrale, Tervuren (Belgium).**
Rock and soil discrimination in natural tropical conditions using a spot-calibrated radiometer p 14 N89-10374

N

- Nansen Remote Sensing Center, Bergen (Norway).**
Mixex '87 - Overview of the Winter Marginal Ice Zone Experiment in the Greenland and Barents Seas
p 36 N89-10931
- National Academy of Sciences - National Research Council, Washington, DC.**
Geologic mapping in the US Geological Survey
[PB88-223870] p 35 N89-14477
- National Aeronautics and Space Administration, Washington, DC.**
NASA's Earth Science Geostationary Platform
p 77 A89-12828
NASA's future land remote sensing program
p 90 N89-10393
Sapping features of the Colorado Plateau: A comparative planetary geology field guide
[NASA-SP-491] p 34 N89-10401
Summary of along-track data from the earth radiation budget satellite for several representative ocean regions
[NASA-RP-1206] p 55 N89-14634
- National Aeronautics and Space Administration, Ames Research Center, Moffett Field, CA.**
Estimation of forest canopy characteristics and nitrogen cycling using imaging spectrometry p 1 A89-10325
Operational use of Landsat data for timber inventory
p 2 A89-10970
Prediction of leaf chemistry by the use of visible and near infrared reflectance spectroscopy
p 7 A89-12783
The California Cooperative Remote Sensing Project
[NASA-TM-100073] p 22 N89-13824
Comparison of in situ aerosol measurements with SAGE 2 and SAM 2 aerosol measurements during the airborne Antarctic ozone experiment p 89 N89-14522
- National Aeronautics and Space Administration, Goddard Inst. for Space Studies, New York, NY.**
Extraction of topography from side-looking satellite systems - A case study with SPOT simulation data
p 68 A89-16063
- National Aeronautics and Space Administration, Goddard Space Flight Center, Greenbelt, MD.**
The electronically steered thinned array radiometer
p 74 A89-10932
MODIS - A global ocean facility for the Earth Observing System
p 75 A89-10955
Atmospheric correction of NS-001 data and extraction of multiple angle reflectance data sets
p 64 A89-10998
Variations in the Arctic, Antarctic, and global sea ice covers during 1978-1987 as observed with the Nimbus 7 scanning multichannel microwave radiometer
p 38 A89-11145
Analysis of nonlinear internal waves in the New York Bight
p 40 A89-12163
Phytoplankton standing crops within an Antarctic ice edge assessed by satellite remote sensing
p 41 A89-12174
Evaporation over land surfaces - First results from HAPEX-MOBILHY Special Observing Period
p 57 A89-12211
Algorithm for automatic atmospheric corrections to visible and near-IR satellite imagery p 66 A89-12224
Assimilation of satellite surface wind speed data using the GLA analysis/forecast system p 77 A89-12811
- Tropopause adjustment to tropical cyclones as inferred from satellite ozone observations p 77 A89-12816
Satellite microwave rainfall simulations with a three-dimensional dynamical cloud model
p 77 A89-12833
The addition of visible channel data to satellite infrared rain estimation schemes p 78 A89-12839
Comparison of satellite IR rain estimates with radar rain observations in hurricanes p 57 A89-12845
The Crustal Dynamics Project p 25 A89-13757
Geodesy by radio interferometry - Determination of vector motions for sites in the western United States
p 25 A89-13759
Applications of spaceborne laser ranger on EOS
p 79 A89-15878
Extraction of topography from side-looking satellite systems - A case study with SPOT simulation data
p 68 A89-16063
The Earth Observing System
[IAF PAPER 88-114] p 80 A89-17682
Global land-surface primary productivity based upon Nimbus-7 37 GHz data
[IAF PAPER 88-159] p 8 A89-17701
The spectral bidirectional reflectance of snow
p 69 N89-10318
Atmospheric effect removal from space imagery
p 69 N89-10338
Spatial resolution requirements for MODIS-N
p 83 N89-10364
The basis for the spectral behaviour of silicates in the thermal infrared and applications to remote sensing
p 32 N89-10366
Comparative point-spread function calculations for the MOMS-1, Thematic Mapper and SPOT-HRV instruments
p 83 N89-10379
LANDSAT-4 and LANDSAT-5 multispectral scanner coherent noise characterization and removal
[NASA-TP-2595-REV] p 85 N89-12114
LAWS (Laser Atmospheric Wind Sounder) earth observing system
[NASA-TM-101204] p 85 N89-12158
Modelling of SAR polarisation phase difference from trees
p 18 N89-12951
Requirements for ongoing development of the Pilot Land Data System (PLDS) p 24 N89-12958
Geodynamics laser ranging system: Performance simulations and development of the EOS facility
p 28 N89-12982
Rainfall index over oceans derived from SSM/I data
p 51 N89-12998
Average areal water equivalent of snow in a mountain basin using microwave and visible satellite data
p 61 N89-13045
The derivation of sub-canopy surface terrain models of coastal forests using synthetic aperture radar
p 20 N89-13083
NASA Sea Ice and Snow Validation Program for the DMSP SSM/I: NASA DC-8 flight report
[NASA-TM-100706] p 53 N89-13861
User's guide for the Nimbus 7 Scanning Multichannel Microwave Radiometer (SMMR) CELL-ALL tape
[NASA-RP-1210] p 89 N89-14648
- National Aeronautics and Space Administration, Lyndon B. Johnson Space Center, Houston, TX.**
Emitted short wavelength infrared radiation for detection and monitoring of volcanic activity p 32 N89-10377
Remote Sensing in Polarized Light
[NASA-CP-3014] p 88 N89-14189
- National Aeronautics and Space Administration, Langley Research Center, Hampton, VA.**
Passive microwave remote sensing of salinity in coastal zones p 36 A89-10942
Airborne and spaceborne lasers for terrestrial geophysical sensing; Proceedings of the Meeting, Los Angeles, CA, Jan. 14, 15, 1988
[SPIE-889] p 79 A89-15870
Lidar atmospheric sounder and altimetry for the Earth Observing System (EOS) satellite p 79 A89-15873
- National Aeronautics and Space Administration, Lewis Research Center, Cleveland, OH.**
Data report for the Siple Coast (Antarctica) project
[NASA-TM-100708] p 49 N89-10403
- National Aeronautics and Space Administration, Marshall Space Flight Center, Huntsville, AL.**
NASA's Earth Science Geostationary Platform
p 77 A89-12828
Doppler lidar wind measurements on the EOS - LAWS
p 77 A89-12829
Thunderstorm ice induced brightness temperature depressions at 18, 37, and 92 GHz during Coihex and their implications for satellite precipitation retrievals
p 42 A89-12835
Laser Atmospheric Wind Sounder (LAWS)
p 79 A89-15889

- National Aeronautics and Space Administration, Wallops Flight Facility, Wallops Island, VA.**
Airborne lidar detection of subsurface oceanic scattering layers p 41 A89-12260
- National Aerospace Lab., Amsterdam (Netherlands).**
The potential of combined use of satellite data with topographic information
[NLR-MP-87061-U] p 70 N89-12113
- National Air and Space Museum, Washington, DC.**
Mapping abandoned river channels in Mali through directional filtering of Thematic Mapper data
p 58 A89-12785
- National Geophysical Data Center, Boulder, CO.**
Working group on studies of the lithosphere: Recommendations p 27 N89-12099
- National Inst. for Environment, Ibaraki (Japan).**
Efficient classification of multispectral images by a best linear discriminant function p 72 N89-13060
- National Inst. for Environmental Studies, Tsukuba (Japan).**
Detection of seasonal and long-term changes in land cover from multitemporal LANDSAT MSS data
p 71 N89-12989
- National Marine Fisheries Service, Miami, FL.**
Utilizing remote sensing of thematic mapper data to improve our understanding of estuarine processes and their influence on the productivity of estuarine-dependent fisheries
[NASA-CR-183409] p 62 N89-13822
- National Oceanic and Atmospheric Administration, Boulder, CO.**
Verification of the accuracy of a network of water-vapor radiometers p 86 N89-12941
- National Oceanic and Atmospheric Administration, Fort Collins, CO.**
Better understanding of intense and tornadic thunderstorms through research using geostationary satellite data p 56 A89-10934
Using satellite data to aid in diagnosing and forecasting convective development and intensity along arc cloud lines p 76 A89-12810
- National Oceanic and Atmospheric Administration, Miami, FL.**
Drifting buoy data from the Equatorial Pacific for the period January 1, 1984 through May 31, 1985
[PB88-212824] p 49 N89-10516
- National Oceanic and Atmospheric Administration, Washington, DC.**
The GVAR users compendium, volume 1
[NOAA-NESDIS-21-VOL-1] p 85 N89-12105
Precipitation detection with satellite microwave data
[PB88-240239] p 88 N89-13094
- National Remote Sensing Centre, Farnborough (England).**
Monitoring urban change from LANDSAT TM and SPOT satellite imagery by image differencing
p 25 N89-13058
- National Space Development Agency, Ohashi (Japan).**
Verification results of MOS-1 multispectral self scanning radiometer (MESSR) data p 86 N89-13004
Data collection system operating on Japan's first marine observation satellite: Inflight evaluation of the system performance p 87 N89-13007
- Naval Ocean Research and Development Activity, Bay St. Louis, MS.**
Some characteristics of short ocean waves as microwave scatterers p 51 N89-13030
The impact of satellite infrared sea surface temperatures on the FNOG (Fleet Numerical Oceanography Center) EOTS (Expanded Ocean Thermal Structure) regional gulf stream analysis
[AD-A198965] p 54 N89-13864
The role of horizontal processes in upper-ocean prediction: A forecast simulation in the Sea of Japan
[AD-A198827] p 55 N89-14654
Chemical variability in ocean frontal areas
[AD-A198418] p 56 N89-14655
- Naval Ocean Systems Center, San Diego, CA.**
Airborne lidar detection of subsurface oceanic scattering layers p 41 A89-12260
- Naval Postgraduate School, Monterey, CA.**
Marine boundary layer depth and relative humidity estimates using multispectral satellite measurements
[AD-A196525] p 49 N89-12112
Multispectral satellite analysis of marine stratocumulus cloud microphysics
[AD-A197316] p 87 N89-13092
- Naval Research Lab., Washington, DC.**
Tropopause adjustment to tropical cyclones as inferred from satellite ozone observations p 77 A89-12816
Shadows and wedges in scattering from the sea
p 49 N89-12946

Nebraska Univ., Lincoln.

A pilot study to determine relationships between North Pacific precipitation from Nimbus-7 Scanning Multichannel Microwave Radiometer data and associated atmospheric conditions p 43 A89-12837
Comparison of measured and modeled radiation, heat and water vapor fluxes: FIFE pilot study [NASA-CR-183304] p 17 N89-11368

New Hampshire Univ., Durham.

Prediction of leaf chemistry by the use of visible and near infrared reflectance spectroscopy p 7 A89-17283

New South Wales Univ., Kensington (Australia).

Change direction analysis using LANDSAT imagery: A review of methodology p 72 N89-13068

New York Dept. of City Planning, NY.

Extraction of topography from side-looking satellite systems - A case study with SPOT simulation data p 68 A89-16063

Newcastle Univ. (England).

Working group reports submitted by group chairmen following workshop p 27 N89-12098

North Carolina Univ., Raleigh.

Multitemporal resource complex analysis of Catania province, Italy from LANDSAT-TM data p 71 N89-12985

Nottingham Univ. (England).

High spectral resolution indices for monitoring crop growth and chlorosis p 13 N89-10358

O**Ocean Research and Engineering, Pasadena, CA.**

Theory for synthetic aperture radar imaging of the ocean surface - With application to the Tower Ocean Wave and Radar Dependence experiment on focus, resolution, and wave height spectra p 44 A89-16977

Oceanor, Trondheim (Norway).

An intercomparison of SAR and buoy directional wave spectra from the Labrador Sea Extreme Waves Experiment (LEWEX) p 50 N89-12972

Office de la Recherche Scientifique et Technique

Outre-Mer, Dakar (Senegal).
Bathymetry using SPOT imagery of the Casamance (Senegal). First results p 59 N89-10375

Office National d'Etudes et de Recherches

Aerospaciales, Paris (France).
Solid earth mission study. Volume 2: Technical report [ESA-CR(P)-2626-VOL-2] p 26 N89-10303
Solid Earth mission study. Volume 1: Executive summary [ESA-CR(P)-2626-VOL-1] p 26 N89-10397
Solid earth mission study. Volume 3: Program planning report [ESA-CR(P)-2626-VOL-3] p 27 N89-10399

Ohio State Univ., Columbus.

Presentations by participants (edited and condensed) p 27 N89-12097

Open Univ., Milton (England).

MOMS-1 used synergistically with LANDSAT TM p 33 N89-10384
A regional tectonic study of NE and E Africa and its implication for mineral exploration: A synoptic view from satellite imagery p 34 N89-13023
The need for volcano monitoring and the ability to detect activity using emitted short wavelength infrared p 34 N89-13025

Oslo Univ. (Norway).

Effects of changing satellite sensor attributes p 87 N89-13059

P**Paris VI Univ. (France).**

Evaluation of VARAN data in geology and geomorphology in the southeast of France p 32 N89-10313
Usefulness of high spectral resolution radiometry for geological mapping in the Mediterranean region p 32 N89-10360
Characterization of rocks by visible and infrared high spectral resolution terrain spectroscopy p 32 N89-10362
The use of MOMS-1 data for geological mapping of the Aswa lineament (East African rift) p 33 N89-10382

Paris XI Univ., Orsay (France).

Techniques for remote sensing of life span and quantum yield of chlorophyll fluorescence in vivo p 13 N89-10351

Pennsylvania State Univ., University Park.

Infrared temperature measurements over bare soil and vegetation - A HAPEX perspective p 2 A89-10953

Comparison of remote measurements of infrared surface temperatures and microwave soil moisture p 4 A89-11009

Remote sensing and hydrologic modeling of arid watersheds: A scale analysis [DE88-014625] p 60 N89-11293

Phillips Petroleum Co., Bartlesville, OK.

The results of the Geosat MOMS subcommittee's data evaluation: Performance and applicability of the MOMS-1 sensor for exploration geology p 33 N89-10380

Princeton Univ., NJ.

Evolution of polar stratospheric clouds during the Antarctic winter p 55 N89-14534

Proudman Oceanographic Lab., Birkenhead (England).

Feasibility study for the development of a joint surge and wave model [PB88-230917] p 55 N89-14652

Puget Sound Univ., Tacoma, WA.

Variations in the Arctic, Antarctic, and global sea ice covers during 1978-1987 as observed with the Nimbus 7 scanning multichannel microwave radiometer p 38 A89-11145

Polarisation of passive microwave signals as indicator of snow water equivalent p 61 N89-13043

Purdue Univ., West Lafayette, IN.

An example of estimates of precipitable water derived from Nimbus-7 SMMR satellite measurements and FGGE upper air data p 42 A89-12792

R**Reading Univ. (England).**

The use of remote sensing in conjunction with geographic information systems for local planning p 24 N89-12959

An international approach to GIS based on remote sensing and terrain classification p 24 N89-12966

Mapping the distribution and abundance of lithological units and surface mineralogies at Jabal Sa'id, Saudi Arabia: An application of spectral mixture modelling p 34 N89-13024

Monitoring playas using Thematic Mapper data p 60 N89-13028

The production of anaglyphs from SPOT-HRV panchromatic data for geomorphological mapping p 72 N89-13056

Research Inst. for Soil Science and Agricultural

Chemistry, Budapest (Turkey).
Agroecological information content of SPOT data p 19 N89-13050

Rijkswaterstaat, Delft (Netherlands).

Validation of an atmospheric correction method for satellite borne imagery p 82 N89-10320

Rothamsted Experimental Station, Harpenden

(England).
Spatial resolution for remote sensing of forest plantations p 19 N89-12991

Rutherford High Energy Lab., Chilton (England).

Cross-polar radar measurements in ice and rain p 60 N89-12993

S**SACLANT ASW Research Center, La Spezia (Italy).**

Make-map and MEDMAP: Two programs for plotting maps of the Mediterranean Sea [AD-A198491] p 73 N89-14483

The numerical simulation of infrared satellite measurements over the Greenland-Iceland-Norwegian Sea [AD-A198653] p 54 N89-14484

Qualitative aspects of seismograph/ocean bottom interaction [AD-A198652] p 56 N89-14656

Sandia National Labs., Albuquerque, NM.

DOE/DOD environmental data bank [DE88-015262] p 25 N89-14942

Satellite International Ltd., Didcot (England).

Solid earth mission study. Volume 2: Technical report [ESA-CR(P)-2626-VOL-2] p 26 N89-10303

Solid Earth mission study. Volume 1: Executive summary [ESA-CR(P)-2626-VOL-1] p 26 N89-10397

Solid earth mission study. Volume 3: Program planning report [ESA-CR(P)-2626-VOL-3] p 27 N89-10399

Science Applications Research, Greenbelt, MD.

Geodesy by radio interferometry - Determination of vector motions for sites in the western United States p 25 A89-13759

Extraction of topography from side-looking satellite systems - A case study with SPOT simulation data p 68 A89-16063

Science Applications Research, Lanham, MD.

Atmospheric correction of NS-001 data and extraction of multiple angle reflectance data sets p 64 A89-10998

Improvement of cloud cover assessment of Landsat Thematic Mapper data p 65 A89-11003

Scott, Wilson, Kirkpatrick and Partners, Basingstoke

(England).
Cotton area mapping using multitemporal satellite data integrated within a geographical information system applied to a cotton boll weevil control programme in Paraguay p 20 N89-13077

Scott Polar Research Inst., Cambridge (England).

Topographic effects on light scattering from snow p 71 N89-12976

Scripps Institution of Oceanography, La Jolla, CA.

Sensitivity of satellite-derived net shortwave irradiance at the Earth's surface to radiometric calibration p 82 N89-10335

Sheffield Univ. (England).

Developing a radiometric leaf area index p 12 N89-10334

Relationships between the nitrogen content of grass and reflectance p 19 N89-13002

Improving the accessibility of spatially referenced geological information p 35 N89-13026

Sherbrooke Univ. (Quebec).

Analysis of the contribution of the atmosphere to water reflectance in the first two channels of the NOAA satellites AVHRR p 82 N89-10330

Imaging spectrometry applied to the remote sensing of submerged seaweed p 48 N89-10361

Discrimination of zones of high water erosion risk using SPOT images p 15 N89-10376

South Dakota School of Mines and Technology, Rapid

City.
Classification of cloud fields based on textural characteristics p 65 A89-11727

Southampton Univ. (England).

A simplified reflectance model for shrub canopies p 11 N89-10329

Stanford Linear Accelerator Center, CA.

Integrated database approach for geodetic applications [DE88-012726] p 27 N89-11615

State Univ. of New York, Binghamton.

A perspective on vegetation canopy reflectance models p 10 N89-10317

A model for radiative transfer in heterogeneous three-dimensional canopies p 11 N89-10326

Stockholm Univ. (Sweden).

LANDSAT Thematic Mapping (TM) and SPOT HRV for survey mapping of bedrock outcrops p 20 N89-13055

T**Technion - Israel Inst. of Tech., Haifa.**

Algorithm for automatic atmospheric corrections to visible and near-IR satellite imagery p 66 A89-12224

Technische Hogeschool, Delft (Netherlands).

On the connection of geodetic point fields in Réseau European Trigonometrique (RETRIG) and related tests for model errors [ETN-89-93327] p 28 N89-14485

Precision of line following in digital images [B8821610] p 73 N89-14486

On the connection of digitized maps to a uniform coordinate system. A special case of the geodetic connection problem [B8821602] p 28 N89-14487

Automatic procedure to find corresponding points in CCD Airborne Experimental Scanner for Applications in Remote sensing (CAESAR) images [B8821609] p 88 N89-14490

A study on least-squares prediction and collocation [ETN-89-93336] p 29 N89-14492

Very Long Baseline Interferometry (VLBI): Relativity and geodesy [ETN-89-93337] p 29 N89-14493

Technische Univ., Berlin (Germany, F.R.).

TUBSAT-1, satellite technology for educational purposes p 90 N89-10905

Technische Univ., Munich (Germany, F.R.).

Comparative geological evolution of different remote sensing data of the Hoggar Mountains (Algeria) p 33 N89-10385

Digital analysis of MOMS-1, LANDSAT TM, and SPOT data of the Nakuru area (Kenya) p 33 N89-10386

Tennessee Univ., Knoxville.

Phytoplankton standing crops within an Antarctic ice edge assessed by satellite remote sensing p 41 A89-12174

Texas Technological Univ., Lubbock.

The design and protocol of a summertime rainfall enhancement program for West Texas

p 63 N89-14636

Texas Univ., Austin.

Orbit determination requirements for Topex

[AAS PAPER 87-429] p 42 A89-12645

Binary image classification p 73 N89-13908

TGS Technology, Inc., Moffett Field, CA.

Operational use of Landsat data for timber inventory

p 2 A89-10970

Tokai Univ., Kanagawa (Japan).

A new spatial classification algorithm for high ground resolution images

p 72 N89-13061

Accuracy of land cover classification of Thematic

Mapper (TM) and SPOT data p 72 N89-13066

Trier Univ., Trier-Tarforst (Germany, F.R.).

Snow cover to alter terrain signatures on radar images

p 62 N89-13048

U

Universite Catholique de Louvain (Belgium).

A three degree-of-freedom description of the ocean surface for microwave remote sensing of wave height and wind friction velocity

p 47 N89-10314

An approximative model for the microwave brightness temperature scattered by a rough open ocean surface

p 48 N89-10344

Combining spectral and structural analyses to select useful cartographic information from SPOT imagery

p 71 N89-13052

University Coll., London (England).

The differential rectification of SPOT HRV panchromatic and multispectral imagery using a digital elevation model

p 28 N89-13054

University of Southern California, Los Angeles.

Phytoplankton standing crops within an Antarctic ice edge assessed by satellite remote sensing

p 41 A89-12174

Model-based estimation of wind fields over the ocean from wind scatterometer measurements

p 53 N89-13070

V

Valencia Univ. (Spain).

A theoretical model for interpreting remotely sensed thermal infrared measurements obtained over agricultural areas

p 12 N89-10343

Spectral signature of citrus fruits and its evolution: Identification of the vegetative index of least temporal variation

p 14 N89-10373

W

Washington Univ., Seattle.

On the interpretation of integrated water vapor patterns in midlatitude cyclones derived from the Nimbus 7 scanning multichannel microwave radiometer

p 76 A89-12790

An example of estimates of precipitable water derived from Nimbus-7 SMMR satellite measurements and FGGE upper air data

p 42 A89-12792

A study of the dynamics of maritime fronts using remotely sensed wind and stress measurements

p 84 N89-11366

A numerical model for the computation of radiance distributions in natural waters with wind-roughened surfaces

[AD-A197207] p 53 N89-13128

Wisconsin Univ., Madison.

Estimation of forest canopy characteristics and nitrogen cycling using imaging spectrometry

p 1 A89-10325

Classification and analysis of surface and clouds at high latitudes from AVHRR multispectral satellite data

p 89 N89-14635

Woods Hole Oceanographic Institution, MA.

Evaluation of GEOSAT (Geodetic Satellite) data and application to variability of the northeast Pacific Ocean

[AD-A198950] p 53 N89-13863

Wyoming Univ., Laramie.

Biogeochemical processes in sagebrush steppe: Interactions of terrain, vegetation and chemical cycles

[NASA-CR-181486] p 21 N89-13088

Z

Zurich Univ. (Switzerland).

Improvement in NOAA-AVHRR snowcover determination for runoff prediction

p 61 N89-13040

Monitoring of seasonal snow cover on glaciers

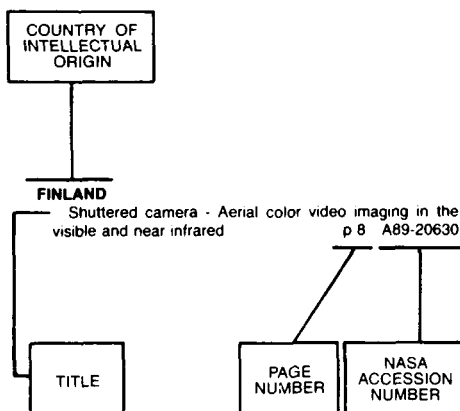
p 61 N89-13044

FOREIGN TECHNOLOGY INDEX

EARTH RESOURCES / A Continuing Bibliography (Issue 61)

APRIL 1989

Typical Foreign Technology Index Listing



Listings in this index are arranged alphabetically by country of intellectual origin. The title of the document is used to provide a brief description of the subject matter. The page number and the accession number are included in each entry to assist the user in locating the citation in the abstract section. If applicable, a report number is also included as an aid in identifying the document.

A

AUSTRALIA

- Atmospheric absorption in the VAS split-window channels p 39 A89-11225
- The development of tropical cyclones in the north-west of Australia p 41 A89-12203
- Estimating the distribution of grazing and patterns of cattle movement in a large arid zone paddock p 5 A89-12356
- Image analysis techniques for the interpretation of airphoto lineaments - Petroleum exploration, Eromanga Basin, Australia p 30 A89-14011
- Forest mapping accuracies are improved using a supervised nonparametric classifier with SPOT data p 6 A89-14089
- Change direction analysis using LANDSAT imagery: A review of methodology p 72 A89-13068

AUSTRIA

- Stress detection in mixed coniferous-broadleaved forests from Airborne Imaging Spectrometer (AIS) data p 13 A89-10355

B

BELGIUM

- A three degree-of-freedom description of the ocean surface for microwave remote sensing of wave height and wind friction velocity p 47 A89-10314
- An approximative model for the microwave brightness temperature scattered by a rough open ocean surface p 48 A89-10344
- An integrated remote sensing approach for regional agrostatistics and land monitoring p 24 A89-12960
- Towards an urban land-use classification using textural and morphological criteria p 25 A89-12987
- Combining spectral and structural analyses to select useful cartographic information from SPOT imagery p 71 A89-13052

BRAZIL

- Identifying the reforested areas utilizing the SPOT satellite data [INPE-4624-PRE/1343] p 15 A89-10396
- The Transformed Vegetation Index (TVI) for estimation of Brazilian cerrado's phytomass [INPE-4603-PRE/1326] p 15 A89-10400
- Nation-wide forest mapping and timber volume estimation using LANDSAT-5 TM imagery [INPE-4643-PRE/1354] p 16 A89-10402
- Environmental impact of the urban growth on the Western Sao Paulo metropolitan area [INPE-4670-PRE/1370] p 23 A89-10413
- A general data model for geographic information systems [INPE-4560-PRE/1301] p 24 A89-10676
- Technique for obtaining agricultural property boundaries through satellite imagery, certified to control and accompany agricultural activity [INPE-4640-PRE/1351] p 16 A89-11294
- Training activities in remote sensing at the Instituto de Pesquisas Espaciais-INPE/Brazil [INPE-4686-PRE/1380] p 91 A89-11295
- Spectral studies of three oxisols and a Ultisol of Brazil [INPE-4644-PRE/1355] p 17 A89-11297
- CIR aerial photography applied to the evaluation of the air pollution impact in a tropical forest: The case of Cubatao, Brazil [INPE-4651-PRE/1358] p 17 A89-11324
- Development of a semi-empirical model for estimating the global solar radiation [INPE-4620-TDL/328] p 84 A89-11352
- Color enhancement of remote sensing imagery using IHS transformations and decorrelation stretch methods [INPE-4559-PRE/1300] p 70 A89-11418
- An agricultural crop yield model by satellite: A simulation [INPE-4639-PRE/1350] p 17 A89-12106
- Digital processing applied to vegetation [INPE-4695-MD/036] p 17 A89-12107
- Method of visual analysis of remote sensing data-vegetation [INPE-4696-MD/037] p 17 A89-12108
- Interaction of solar radiation with vegetation [INPE-4697-MD/038] p 17 A89-12109
- Crop separation analysis through SPOT and TM digital data [INPE-4641-PRE/1352] p 18 A89-12110
- Microwave remote sensing at the Institute for Space Research (INPE) Brazil: Concepts and future prospects of soil moisture studies p 20 A89-13080
- Photogrammetric model for correction of MSS-LANDSAT imagery [INPE-4652-PRE/1359] p 73 A89-13090

BULGARIA

- The use of spectral reflectance characteristics for the estimation of the wheat crop state p 5 A89-12874

C

CANADA

- The fluorescence line imager - An imaging spectrometer for ocean and land remote sensing p 73 A89-10312
- Imaging spectrometry as a tool for botanical mapping p 73 A89-10324
- Imaging spectrometry for water applications p 56 A89-10327
- Advanced airborne electro-optical imager p 74 A89-10929
- Accuracy evaluation of airborne stereo line imager data p 75 A89-10936
- Does a SAR respond to both phase speed and orbital velocity in ocean sensing? p 36 A89-10947
- Radar applications in remote sensing - An airborne remote sensing case history presented at the Twenty-first International Symposium on Remote Sensing of Environment, Ann Arbor, Michigan, October 26-30, 1987 p 75 A89-10969
- Land cover change detection with Thematic Mapper spectral textural data at the rural-urban fringe p 23 A89-10982

- Improving the detection of human-induced change in west Africa's semi-arid zone using multitemporal Landsat MSS imagery p 64 A89-10983
- Edge detection and processing of remotely sensed digital images p 64 A89-10984
- Automatic control point determination for image registration using texture analysis methods p 3 A89-10985
- Surveillance radar, a new tool for ice surveillance p 37 A89-10991
- Evaluation of a multispectral linear array sensor for assessing juvenile stand conditions p 3 A89-11000
- Effect of soil roughness on SAR images of harvested agricultural fields p 4 A89-11004
- Terrain relief and pattern description using digital elevation and Landsat data p 65 A89-11010
- The use of fractal geometry to identify ranges of scale-invariance in digital remotely sensed data p 4 A89-11011
- Evaluation of technology in the detection and counting of seals p 76 A89-11016
- A three-dimensional coupled ice-ocean model of coastal circulation p 38 A89-11148
- Joint Canada-U.S. Ocean Wave Investigation Project - An overview of the Georgia Strait Experiment p 39 A89-12156
- Synthetic aperture radar imaging of ocean waves from an airborne platform - Focus and tracking issues p 41 A89-12173
- The effects of bark beetle stress on the foliar spectral reflectance of lodgepole pine p 5 A89-12355
- Remote sensing of surface air temperature and humidity over oceanic areas with application to climatology and weather prediction p 42 A89-12798
- Variation of satellite rain relationships in space and time p 67 A89-12843
- Mid-latitude evaluation of some satellite rainfall estimation techniques p 78 A89-12844
- Resolution dependence in satellite imagery - Multifractal analysis p 67 A89-12852
- VISSR sensor introduced modifications in the presence of large temperature gradients p 78 A89-12860
- Geological mapping and mineral exploration in eastern Nova Scotia utilizing airborne and spaceborne multisensor data p 30 A89-14008
- Sensor band selection for detecting current defoliation caused by the spruce budworm p 6 A89-16062
- Coastally trapped waves in the presence of a shelf edge density front p 46 A89-16989
- An airborne gamma ray snow survey of a forest covered area with a deep snowpack p 7 A89-17284
- Geophysical interpretation of the magnetic anomalies of China derived from Magsat data p 26 A89-20200
- An enhanced classification approach to change detection in semi-arid environments p 68 A89-20627
- Analysis of the contribution of the atmosphere to water reflectance in the first two channels of the NOAA satellites AVHRR p 82 A89-10330
- The fluorescence line imager: High-resolution imaging spectroscopy over water and land p 83 A89-10353
- Imaging spectrometry applied to the remote sensing of submerged seaweed p 48 A89-10361
- Texture analysis in forest areas: High spectral resolution synthetic aperture radar data p 14 A89-10367
- Discrimination of zones of high water erosion risk using SPOT images p 15 A89-10376
- SAR-seen multimode waves in ice: Evidence of imaging nonlinearities p 50 A89-12971
- Phase versus orbital velocity in SAR wave imaging: Paradox lost p 52 A89-13033
- The LIMEX 1987 pilot project, LIMEX 1989 and long-term objective for data collection on the Canadian East coast p 52 A89-13037
- Extraction of dense digital elevation models from SPOT stereo imagery p 71 A89-13053

CHINA, PEOPLE'S REPUBLIC OF

- Study of monitoring sea ice using an airborne microwave radiometer system p 37 A89-10972
- The character of reflective spectrum of winter wheat and the principle of its yield estimation with remote sensing method p 2 A89-10973

- A study of estimation of winter wheat yield for large area using remote sensing method p 2 A89-10974
- The practice and understanding of using aerial remote sensing in the investigation of coastal zone p 37 A89-10995
- SAR and visible remote sensing of the Taore River coastal zone at Bohai Bay p 38 A89-11005
- A useful model in mineral exploration with remotely sensed data p 30 A89-11017
- Model-based remotely-sensed imagery interpretation p 66 A89-12223
- A synthetic apertures radar with multichannel and multipolarisation p 87 A89-13017

D

DENMARK

- Monitoring vegetation index and biomass production in Southern Greenland based on NOAA-AVHRR data p 3 A89-10993

F

FINLAND

- Shuttered camera - Aerial color video imaging in the visible and near infrared p 8 A89-20630
- Microwave dielectric properties of low-salinity sea ice p 52 A89-13036

FRANCE

- Optical modeling of the upper ocean in relation to its biogenous matter content (case I waters) p 38 A89-11149
- Evaporation over land surfaces - First results from HAPEX-MOBILHY Special Observing Period p 57 A89-12211
- Effect of spatial resolution of the statistical properties of satellite images - A case study p 66 A89-12221
- SPOT image quality - Twenty months of experience p 66 A89-12352
- The French space oceanography program p 44 A89-15116
- Observing the seasonal variability in the tropical Atlantic from altimetry p 46 A89-16987
- Near surface soil moisture estimation from microwave measurements p 6 A89-17282
- New SPOT generation [IAF PAPER 88-117] p 7 A89-17683
- Wide field high performance lenses [IAF PAPER 88-120] p 80 A89-17685
- The image detection subassembly for the SPOT 4 'vegetation' instrument [IAF PAPER 88-121] p 7 A89-17686
- Design of a spaceborne rain mapping radar [IAF PAPER 88-124] p 58 A89-17688
- Satellite phasing problems for ocean and atmospheric studies [IAF PAPER 88-152] p 46 A89-17698
- PRISM B (Prediction of the Indian Summer Monsoon - Bellevue) [IAF PAPER ST-88-02] p 58 A89-17873
- Sea surface parameters inferred from meteorological satellite data at CMS, Lannion p 47 A89-20722
- Proceedings of the 4th International Colloquium on Spectral Signatures in Remote Sensing [ESA-SP-287] p 9 A89-10305
- Extracting soil and vegetation characteristics from microwave remote sensing data p 9 A89-10306
- Measuring in-situ soil surface roughness using a laser profilometer p 9 A89-10308
- Complementary of microwave and optical range in the characterization of crops by remote sensing p 10 A89-10310
- Evaluation of VARAN data in geology and geomorphology in the southeast of France p 32 A89-10313
- Comparison between active and passive microwave measurements over Antarctica p 48 A89-10316
- Spectral profile and biomass estimation p 10 A89-10319
- Retrieving vegetation and soil parameters from radar measurements p 10 A89-10321
- A simplified vegetation canopy reflectance and absorption model p 10 A89-10322
- Potential number of winter wheat ears estimation using radiometry techniques at an early stage p 10 A89-10323
- Introducing spectral data into a plant process model for improving its prediction ability p 10 A89-10324
- Biomass and wheat crop yield estimation from SPOT vegetative indexes p 11 A89-10327
- Spectral characterization of forest targets in mountainous zones on Thematic Mapper images p 11 A89-10328

- Estimation of the interception efficiency of an alfalfa canopy from a vegetative index p 11 A89-10332
- Relation between sugar beet crop yield and vegetative indexes calculated from LANDSAT MSS images p 11 A89-10333
- Attempt at absolute determination of spectral signatures of bare soils in the thermal infrared, in emission and reflection p 12 A89-10336
- Multispectral characterization of the spatial structure of remotely sensed scenes p 70 A89-10340
- Analysis of directional effects on NOAA AVHRR p 70 A89-10341
- Techniques for remote sensing of life span and quantum yield of chlorophyll fluorescence in vivo p 13 A89-10351
- Use of high spectral resolution to follow the state of vegetation canopies p 13 A89-10354
- Usefulness of high spectral resolution radiometry for geological mapping in the Mediterranean region p 32 A89-10360
- Characterization of rocks by visible and infrared high spectral resolution terrain spectroscopy p 32 A89-10362
- Comparative analysis of spectral response in the optical domain of targets in a tropical swamp at various spectral and spatial resolutions p 13 A89-10363
- High resolution radiometric measurement of intertidal microphytobenthos p 48 A89-10365
- Estimation of leaf spectra from measurements in wide spectral bands p 14 A89-10368
- Modeling of soil color by remote sensing p 14 A89-10369
- Estimation of primary marine production using spaceborne data on ocean color p 48 A89-10371
- Satellite surveillance of ice and snow covered surfaces in the French Alps using visible and near infrared reflectance measurements from the SPOT and LANDSAT Thematic Mapper sensors p 59 A89-10372
- Rock and soil discrimination in natural tropical conditions using a spot-calibrated radiometer p 14 A89-10374
- The use of MOMS-1 data for geological mapping of the Aswa lineament (East African rift) p 33 A89-10382
- A study of the vegetation cover with AVHRR during HAPEX-MOBILHY p 15 A89-10389
- A new method for estimating regional evaporation from thermal infrared surface temperature measurements p 60 A89-10390
- The French space program for Earth observation p 90 A89-10392
- Study of the multiplexing of image telemetry data from SPOT 4 HRVIR and Vegetation sensors [CNES-87/229/CT/DRT/TIT/TR] p 70 A89-10930
- Proceedings of the 1988 International Geoscience and Remote Sensing Symposium (IGARSS 1988) on Remote Sensing: Moving Towards the 21st Century, volume 1 [ESA-SP-284-VOL-1] p 85 A89-12936
- Spectral analysis of ocean wave imagery using 2-D linear prediction p 50 A89-12968
- Design of a spaceborne radar for tropical rain mapping at the climatological scale p 60 A89-12997
- Towards direct variational assimilation of scatterometer backscatter measurements into numerical weather prediction models p 86 A89-13000

G

GERMANY, FEDERAL REPUBLIC OF

- Photogrammetric Week, 41st, Universitaet Stuttgart, Federal Republic of Germany, Sept. 14-19, 1987, Proceedings p 63 A89-10611
- Computational design and efficiency optimization of agricultural airplanes p 5 A89-13670
- Orographic channeling of a cold front by the Pyrenees p 79 A89-14073
- Relationship between discoloration and histological changes in leaves of trees affected by forest decline p 7 A89-17286
- Status and perspectives of vegetation monitoring by remote sensing [IAF PAPER 88-140] p 8 A89-17693
- Evaluation and digital processing of multispectral SPOT data p 68 A89-20708
- Mineral exploration along the Aqaba-Levant structure by use of TM-data - Concepts, processing and results p 31 A89-20709
- Analysis of large format camera photographs of the Po Delta, Italy, for topographic and thematic mapping p 82 A89-20714
- Evaluation of space photographs p 82 A89-20715
- Interpretation and geometrical aspects of Thematic Mapper data p 69 A89-20716
- Solid earth mission study. Volume 2: Technical report [ESA-CR(P)-2626-VOL-2] p 26 A89-10303
- Coherent polarimetric signatures of coniferous trees: A survey p 9 A89-10307

- Spectral reflectance of sugar beet and winter wheat canopies in the visible and infrared during growth p 12 A89-10342
- Thermal infrared laser spectroscopy: The potential of dual active/passive thermal infrared sensors for Earth observation p 82 A89-10345
- Changes in the chlorophyll fluorescence spectra during the Kautsky induction kinetics p 12 A89-10348
- Chlorophyll fluorescence spectra of leaves as induced by blue light and red laser light p 12 A89-10349
- High-resolution spectroscopy for remote sensing of ocean and atmosphere p 48 A89-10352
- Optimization for classification of forest damage classes p 13 A89-10359
- Design of spectral bands for the German MOMS-2 sensor p 84 A89-10391
- Comparative geological evolution of different remote sensing data of the Hoggar Mountains (Algeria) p 33 A89-10385
- Digital analysis of MOMS-1, LANDSAT TM, and SPOT data of the Nakuru area (Kenya) p 33 A89-10386
- Solid Earth mission study. Volume 1: Executive summary [ESA-CR(P)-2626-VOL-1] p 26 A89-10397
- Solid earth mission study. Volume 3: Program planning report [ESA-CR(P)-2626-VOL-3] p 27 A89-10399
- Applications of LANDSAT (TM and MSS) data for an estimation of rangeland conditions in semiarid and arid areas of northern Kenya [DFVLR-FB-88-18] p 16 A89-10404
- TUBSAT-1, satellite technology for educational purposes p 90 A89-10905
- Very Long Baseline Interferometry (VLBI) from ground and space p 85 A89-11645
- The Airborne Version Conical Scan Radiometer (AVCSR): An airborne radiometer as a tool for satellite data validation p 86 A89-12937
- The airborne radiometry experiment (ABREX) instrument, an experimental test bed for the specification of satellite-borne microwave radiometer at 90 GHz p 86 A89-12939
- Polarization-dependent attenuation of dielectric cylinder arrays p 86 A89-12955
- Large area TM land cover classification of Mittlerer Oberrhein County, southwest Germany, and its use for regional planning and crop surveys p 18 A89-12986
- Performance modeling and results for X-SAR p 71 A89-13009
- Snow cover to alter terrain signatures on radar images p 82 A89-13048
- Building a monitoring system based on satellite data to detect vegetation and land use changes in a subtropical region of Mexico p 20 A89-13079
- The MEOS experiment: A test case for future cartographic missions p 87 A89-13081
- Spectral characterization of forest damage in beech, oak and pine stands p 21 A89-13085

H

HUNGARY

- Estimating concentrations of optically active components from the remotely sensed spectral radiance of a water surface p 58 A89-18711
- Agroecological information content of SPOT data p 19 A89-13050

I

ICELAND

- Strengths and shortcomings in Airborne Thematic Mapper (ATM) technology as applied to volcanic and geothermal areas in Iceland p 32 A89-10337
- A narrow-band thermal imager based on multiline real-time averaging p 83 A89-10356

INDIA

- A comparative evaluation of use of Landsat MSS FCC and MKF-6M photographs for forest type delineation p 6 A89-14010
- Indian experience in the dissemination and use of remote sensing data and future prospects [IAF PAPER 88-131] p 80 A89-17689
- Comparison of SPOT, TM and MSS data for agricultural land-use mapping in Gujarat (India) [IAF PAPER 88-139] p 7 A89-17692
- Project Vasundhara - Multi-theme integration of satellite remote sensing and geological data for regional level mineral prognostics [IAF PAPER 88-145] p 31 A89-17694
- Application of satellite data for monitoring degradation of tidal wetlands of the Gulf of Kachchh, Western India [IAF PAPER 88-146] p 46 A89-17695

- Role of absorbed solar radiation on Indian Ocean surface temperature - A case study using satellite data [IAF PAPER 88-155] p 46 A89-17700
- Important aspects of technology transfer: Training of inservice engineers and scientists: satellite remote sensing p 91 N89-13082

INTERNATIONAL ORGANIZATION

- UN principles on remote sensing - An agreement on economic relations p 90 A89-19385
- Radiometric measurements and crop yield forecasting - Some observations over millet and sorghum experimental plots in Mali p 8 A89-20702
- Regional land cover and agricultural area statistics and mapping in The Departement Ardeche, France, by use of Thematic Mapper data p 8 A89-20705

ITALY

- The use of microwave radiometry in watershed hydrology p 57 A89-10992
- A procedure for modeling the terrain relief by using digitized topographic maps p 67 A89-14005
- Three-dimensional observation by means of tethered antennae [IAF PAPER 88-118] p 80 A89-17684
- The ERS-1 Instrument Data Handling and Transmission subsystem (IDHT) and its evolution [IAF PAPER 88-134] p 80 A89-17690
- Time series of European baselines determined with Lageos p 26 A89-17945
- Forest classification by principal component analyses of TM data p 8 A89-20706
- The use of TM data for the study of a modern deltaic depositional system p 59 A89-20707
- Use of Landsat and Seasat data as a tool in kinematic analysis - The Tunisian Atlas p 31 A89-20710
- Tests of topographic mapping with Thematic Mapper images p 69 A89-20712
- Time-resolved laser fluorescing: Trends and applications p 83 N89-10346
- A new lidar system for applications over land and sea p 83 N89-10347
- AGRISAR'86: Contributing to signature research p 15 N89-10387
- Small format air photo from ultrahigh aircraft as an aid for data collection of agricultural statistics in Sahelian countries p 19 N89-13003
- The classification of semi-natural vegetation from LANDSAT Thematic Mapper imagery: A user's perspective p 21 N89-13084
- Make-map and MEDMAP: Two programs for plotting maps of the Mediterranean Sea [AD-A198491] p 73 N89-14483
- The numerical simulation of infrared satellite measurements over the Greenland-Iceland-Norwegian Sea [AD-A198653] p 54 N89-14484
- Qualitative aspects of seismograph/ocean bottom interaction [AD-A198652] p 56 N89-14656

J**JAPAN**

- Backscattering coefficient of rice crops and rice fields by an X-band scatterometer p 3 A89-10980
- Remote measurements of diatoms chlorophyll-a in the Nori farm p 38 A89-11001
- Region extraction in SPOT data p 67 A89-14007
- Microwave emission and reflection from the wind-roughened sea surface at 6.7 and 18.6 GHz p 44 A89-15923
- Fault tolerant design of attitude and orbit control subsystem for earth resources satellite-1 [AIAA PAPER 88-3879] p 80 A89-18073
- Experimental personal satellite communications system using millimeter-wave for Asia-Oceanian region p 81 A89-18736
- Laser-induced fluorescence on in-vivo chlorophyll of a rice plant: A technique for the remote detection of plant growth p 12 N89-10350
- Inference of radio scattering parameters of Antarctic ice sheet using 179 MHz airborne radio echo sounding data p 51 N89-12975
- Detection of seasonal and long-term changes in land cover from multitemporal LANDSAT MSS data p 71 N89-12989
- Verification results of MOS-1 multispectral self scanning radiometer (MESSR) data p 86 N89-13004
- Estimation of sea surface temperature via NOAA-AVHRR sensor: Comparison with sea truth data by fixed buoys p 51 N89-13005
- Data collection system operating on Japan's first marine observation satellite: Inflight evaluation of the system performance p 87 N89-13007

- Snowmelt runoff estimation using snow cover extent data and its application to optimum control of dam water level p 61 N89-13042
- Efficient classification of multispectral images by a best linear discriminant function p 72 N89-13060
- A new spatial classification algorithm for high ground resolution images p 72 N89-13061
- Accuracy of land cover classification of Thematic Mapper (TM) and SPOT data p 72 N89-13066

K**KENYA**

- A typical case of integrated remote sensing center concept - The Nairobi multipurpose reception and processing center [IAF PAPER 88-106] p 80 A89-17679

N**NETHERLANDS**

- Real-time environment monitoring using data from Meteosat and NOAA imaging satellites p 23 A89-11730
- European remote sensing needs in the 1990s: Proceedings of the Annual Symposium of EARSeL, Noordwijkerhout, Netherlands, May 4-8, 1987 p 90 A89-20701
- Some results of microwave remote sensing research in The Netherlands with a view to land applications in the 1990s p 8 A89-20703
- The contribution of satellite information to operational weather forecasting - Achievements and objectives in the 1990s p 81 A89-20711
- Geometric correction of remotely-sensed imagery using ground control points and orthogonal polynomials p 82 A89-20718
- The Remote Sensing Loosdrecht Lakes project p 59 A89-20719
- Regional hydrological systems analysis using satellite remote sensing data and a geographical information system - Application to groundwater modelling of the Roermond area, The Netherlands p 59 A89-20720
- Comparison of wave parameters determined from SLAR images and a pitch and roll buoy p 47 A89-20721
- Aerial photography for biomass assessment in the intertidal zone p 9 A89-20724
- Microwave backscatter from beets, peas and potatoes throughout the growing season p 9 N89-10309
- Validation of an atmospheric correction method for satellite borne imagery p 82 N89-10320
- The potential of combined use of satellite data with topographic information [NLR-MP-87061-U] p 70 N89-12113
- On the connection of geodetic point fields in Reseau European Trigonometrique (RETRIG) and related tests for model errors [ETN-89-93327] p 28 N89-14485
- Precision of line following in digital images [B8821610] p 73 N89-14486
- On the connection of digitized maps to a uniform coordinate system. A special case of the geodetic connection problem [B8821602] p 28 N89-14487
- Automatic procedure to find corresponding points in CCD Airborne Experimental Scanner for Applications in Remote sensing (CAESAR) images [B8821609] p 88 N89-14490
- A study on least-squares prediction and collocation [ETN-89-93336] p 29 N89-14492
- Very Long Baseline Interferometry (VLBI): Relativity and geodesy [ETN-89-93337] p 29 N89-14493

NORWAY

- Mizex '87 - Overview of the Winter Marginal Ice Zone Experiment in the Greenland and Barents Seas p 36 A89-10931
- Prediction of mesoscale ocean circulation in the Norwegian coastal current p 37 A89-10994
- Ocean wave number spectra and spatial autocorrelation functions from SAR images p 50 N89-12970
- An intercomparison of SAR and buoy directional wave spectra from the Labrador Sea Extreme Waves Experiment (LEWEX) p 50 N89-12972
- Effects of changing satellite sensor attributes p 87 N89-13059

S**SENEGAL**

- Bathymetry using SPOT imagery of the Casamance (Senegal). First results p 59 N89-10375

SOUTH AFRICA, REPUBLIC OF

- The development of a standardized grassland Landsat MSS information data base p 3 A89-10979
- The extrapolation of spectral signatures illustrates LANDSATs' potential to detect wetlands p 62 N89-13067

SPAIN

- A theoretical model for interpreting remotely sensed thermal infrared measurements obtained over agricultural areas p 12 N89-10343
- Spectral signature of citrus fruits and its evolution: Identification of the vegetative index of least temporal variation p 14 N89-10373

SWEDEN

- A new tool - SPOT imagery for studying rapid movements p 64 A89-10996
- Multi-point matching along vertical lines in SPOT images p 69 A89-20713
- Atmospheric correction of thermal infrared data from LANDSAT-5 for surface temperature estimation p 70 N89-10339
- LANDSAT Thematic Mapping (TM) and SPOT HRV for survey mapping of bedrock outcrops p 20 N89-13055

SWITZERLAND

- The normalization of a soil brightness index for the study of changes in soil conditions p 14 N89-10370
- Improvement in NOAA-AVHRR snowcover determination for runoff prediction p 61 N89-13040

T**TAIWAN**

- Observation of precipitation using GMS imagery [IAF PAPER 88-151] p 58 A89-17697

U**U.S.S.R.**

- Nival-glacial systems and their mapping p 56 A89-10728
- Principles Relating to Remote Sensing of the Earth from Space - Territorial sphere of application p 89 A89-12121
- The registration of the surface effects of internal ocean waves using microwave radiometry p 43 A89-13300
- Aerospace monitoring of ecosystem dynamics and ecological prognoses p 23 A89-15050
- Complex experiment on the investigation of the atmosphere pollution using space, aircraft and ground information [IAF PAPER 88-161] p 23 A89-17702
- The role of linear and ring features in hydrogeology p 31 A89-18705
- Recognition of seismically hazardous fault dislocations in space images of the Dushanbe depression p 31 A89-18706
- Engineering evaluation of mountain topography exodynamics from remotely sensed data p 31 A89-18707
- The potential of using remotely sensed information for studying the contamination and eutrophication of lake systems p 58 A89-18708
- The effect of agrometeorological conditions on the characteristics of space radar imagery of agricultural regions in winter p 8 A89-18709
- Accounting for selective absorption in the evaluation of the earth surface temperature by an angular method p 80 A89-18710
- The effect of snow parameter variations on the thermal microwave emission of the soil-snow-atmosphere system p 59 A89-18712
- Estimation of the variability of acoustic characteristics in the region of frontal zones and mesoscale vortices using remote sensing data p 47 A89-18843

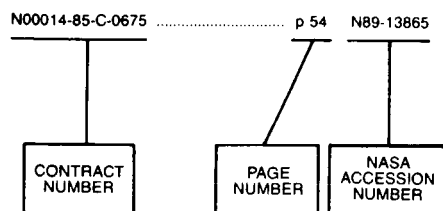
UNITED KINGDOM

- A comparison of reduction methods for satellite altimetry data p 39 A89-11424
- A dual-satellite algorithm for deriving sea surface temperature p 41 A89-12209
- The effective resolution element of Landsat Thematic Mapper p 65 A89-12220
- Segmentation of remotely-sensed images by a split-and-merge process p 66 A89-12222
- CANVAS - An intelligent system for colour selection on CRT displays p 76 A89-12353
- Estimation of multiple reflection and lowest order adjacency effects on remotely-sensed data p 5 A89-12354
- The navigation of AVHRR imagery p 66 A89-12357
- Detection of circular geological features using the Hough transform p 30 A89-12358
- Use of satellite and radar images in operational precipitation nowcasting p 79 A89-13415

- Topographic mapping from SPOT imagery
p 67 A89-14088
- Technological constraints on the use of thermal imagery
for remote sensing p 81 A89-19173
- Remote sensing of laterized Archean greenstone
terrain - Marshall Pool Area, Northeastern Yilgarn Block,
Western Australia p 31 A89-20628
- Lowest order correction for solar zenith angle to Global
Vegetation Index (GVI) data p 8 A89-20704
- Advances in computerized information retrieval in
remote sensing p 69 A89-20717
- Satellite remote sensing and wave studies into the
1990s p 47 A89-20723
- The use of the complex correlation function in the
recovery of ocean wave spectra from SAR images
p 47 N89-10315
- A simplified reflectance model for shrub canopies
p 11 N89-10329
- Developing a radiometric leaf area index
p 12 N89-10334
- High spectral resolution indices for monitoring crop
growth and chlorosis p 13 N89-10358
- MOMS-1 data for bathymetric and geological studies
p 33 N89-10383
- MOMS-1 used synergistically with LANDSAT TM
p 33 N89-10384
- Review of the requirements for higher level ERS-1
products within Europe p 84 N89-10664
[ESA-CR(P)-2586]
- Working group reports submitted by group chairmen
following workshop p 27 N89-12098
- Constraints on two-scale descriptions of radar
backscattering from the sea surface using scatterometer
model functions p 49 N89-12945
- The use of remote sensing in conjunction with
geographic information systems for local planning
p 24 N89-12959
- Modelling land resources within a pilot geographical
information system p 18 N89-12962
- Integrating remote sensing data into a geographical
information system: A foundation for rural land use
strategies: Nature Conservancy Council project
p 24 N89-12964
- An international approach to GIS based on remote
sensing and terrain classification p 24 N89-12966
- Analysis of potato crop distribution using remotely
sensed and environmental data in a pilot geographical
information system p 18 N89-12967
- Topographic effects on light scattering from snow
p 71 N89-12976
- The detection of unimproved grassland in Berkshire
using a binary decision tree approach p 18 N89-12988
- Crop classification with multi-temporal X-band SAR
data p 19 N89-12990
- Spatial resolution for remote sensing of forest
plantations p 19 N89-12991
- Cross-polar radar measurements in ice and rain
p 60 N89-12993
- Relationships between the nitrogen content of grass and
reflectance p 19 N89-13002
- A regional tectonic study of NE and E Africa and its
implication for mineral exploration: A synoptic view from
satellite imagery p 34 N89-13023
- Mapping the distribution and abundance of lithological
units and surface mineralogies at Jabal Sa'id, Saudi Arabia:
An application of spectral mixture modelling
p 34 N89-13024
- The need for volcano monitoring and the ability to detect
activity using emitted short wavelength infrared
p 34 N89-13025
- Improving the accessibility of spatially referenced
geological information p 35 N89-13026
- The interpretation of Icelandic tundra features from
LANDSAT-MSS data p 35 N89-13027
- Monitoring playas using Thematic Mapper data
p 60 N89-13028
- Complex SAR imagery and speckle filtering for ERS-1
wave mode p 71 N89-13029
- Analysis of Seasat SAR sea-ice data from the Beaufort
Sea p 52 N89-13035
- Evaluation of LANDSAT TM and SPOT imagery for
agricultural land use planning in less developed
countries p 19 N89-13051
- The differential rectification of SPOT HRV panchromatic
and multispectral imagery using a digital elevation model
p 28 N89-13054
- The production of anaglyphs from SPOT-HRV
panchromatic data for geomorphological mapping
p 72 N89-13056
- An evaluation of satellite imagery, LANDSAT Thematic
Mapper and SPOT-1 HRV, for grassland inventory in the
UK p 20 N89-13057
- Monitoring urban change from LANDSAT TM and SPOT
satellite imagery by image differencing p 25 N89-13058
- Classification decision rule modification on the basis of
information extracted from training data p 72 N89-13062
- Cloud track winds from polar orbiting satellites
p 87 N89-13069
- An analysis of directional ambiguities in wind
scatterometer measurements p 87 N89-13071
- Multistatic scatterometry p 87 N89-13072
- Cotton area mapping using multitemporal satellite data
integrated within a geographical information system
applied to a cotton boll weevil control programme in
Paraguay p 20 N89-13077
- Applications of remote sensing for geological mapping
in eastern Egypt p 35 N89-13087
- Feasibility study for the development of a joint surge
and wave model [PB88-230917] p 55 N89-14652

CONTRACT NUMBER INDEX

Typical Contract Number Index Listing



Listings in this index are arranged alphanumerically by contract number. Under each contract number, the accession numbers denoting documents that have been produced as a result of research done under the contract are arranged in ascending order with the AIAA accession numbers appearing first. The accession number denotes the number by which the citation is identified in the abstract section. Preceding the accession number is the page number on which the citation may be found.

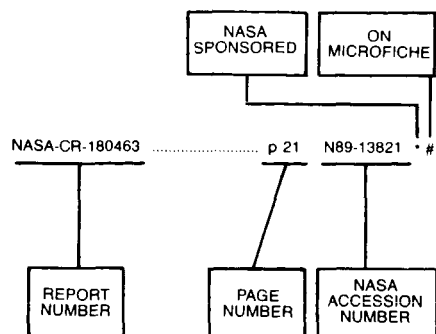
N00014-85-C-0675	p 54	N89-13865	
CONTRACT NUMBER	PAGE NUMBER	NASA ACCESSION NUMBER	
BMFT-FKZ-01-QS-85090	p 82	A89-20714	
CAICYT-A-172/85	p 12	N89-10343	
CEC-ST2J-0049-1-F	p 57	N89-10373	
CEC-ST2J-0049-2-UK	p 57	N89-12211	
CNES-86-1285	p 57	N89-12211	
CNRS-DRCI-86-920118	p 57	N89-12211	
DACW05-87-C-0012	p 62	N89-14480	
DE-AC03-76SF-00515	p 27	N89-11615	
DE-AC04-76DP-00789	p 25	N89-14942	
DE-AC06-76RL-01830	p 65	N89-11743	
DE-AC08-83NV-10282	p 4	N89-12261	
DE-AC09-76SR-00001	p 7	N89-17399	
DE-AC09-76SR-00819	p 7	N89-17399	
DE-FG02-86ER-60472	p 60	N89-11293	
DE-FG21-86FE-61114	p 35	N89-13093	
DI-14-08-0001-A-0468	p 35	N89-14477	
DOSSIER-3B1-68400260-002	p 15	N89-10376	
ESA-6877/87-HGE-1(SC)	p 84	N89-10664	
ESA-6878/87-HGE-1(SC)	p 47	N89-10315	
ESTEC-7149/87-NL-JS	p 26	N89-10303	
F19628-85-C-0102	p 26	N89-10397	
F19628-86-K-0025	p 27	N89-10399	
GFSC-PROJ-415	p 76	N89-11731	
GS-14-08-0001-A-0353	p 26	N89-13762	
JPL-956689	p 26	N89-13764	
JRC-3106-86-12-ED-ISP-D	p 83	N89-10364	
NAGS-399	p 61	N89-13043	
NAGW-1051	p 42	N89-12645	
NAGW-1141	p 9	N89-10307	
NAGW-1167	p 83	N89-10364	
NAGW-455	p 40	N89-12171	
NAGW-735	p 67	N89-12864	
NAGW-736	p 31	N89-19838	
NAGW-788	p 91	N89-14481	
NAGW-808	p 6	N89-15918	
NAG1-542	p 27	N89-12097	
NAG2-355	p 6	N89-15918	
NAG2-36	p 38	N89-11143	
NAG5-1010	p 65	N89-11727	
NAG5-270	p 21	N89-13088	
NAG5-414	p 43	N89-12837	
NAG5-459	p 16	N89-11292	
NAG5-480	p 46	N89-16990	
NAG5-510	p 85	N89-12111	
NAG5-538	p 55	N89-14653	
NAG5-561	p 44	N89-13758	
NAG5-842	p 16	N89-11296	
NAG5-881	p 21	N89-13091	
NAG5-897	p 21	N89-13823	
NAG5-919	p 26	N89-13762	
NASA ORDER W-16712			
NASW-4066			
NAS1-4195-C			
NAS2-12494			
NAS5-28200			
NAS5-28572			
NAS5-28759			
NAS5-28774			
NAS5-28781			
NAS5-29356			
NAS5-29386			
NAS5-30041			
NAS7-918			
NAS8-35187			
NAS8-36472			
NAS8-36473			
NAS8-37127			
NAS8AA-D-AC051			
NCA2-28			
NCC5-32			
NERC-CASE-GT4/86/GS/90			
NERC-F60/G6/03			
NERC-F60/G6/12			
NERC-GS/T/02/125			
NERC-GST/02/124			
NERC-GT4/85/GS/85			
NGI-23-004-083			
NGT-05-010-804			
NOAA-NA-84AAD00017			
NOAA-NA-84AAH00020			
NOAA-NA-85RAH05045			
NOAA-NA-87AAHRA076			
NSERC-A-0766			
NSERC-A-2037			
NSF ATM-84-20980			
NSF ATM-85-07918			
NSF ATM-85-11196			
NSF ATM-85-12535			
NSF ATM-86-01115			
NSF BSR-83-17531			
NSF BSR-85-14327			
NSF DMS-84-07876			
NSF DPP-82-18752			
NSF DPP-82-18758			
NSF DPP-83-13071			
NSF DPP-84-20213			
NSF DPP-85-20883			
NSF DPP-87-13916			
NSF EAR-83-06380			
NSF EAR-84-18350			
NSF EAR-85-07061			
NSF EAR-86-18989			
NSF ECS-85-04381			
NSF INT-85-14251			
NSF OCE-86-07962			
NSG-7572			
N00014-80-C-0440			
N00014-81-C-0195			
N00014-81-C-0295			
N00014-81-C-0692			
N00014-83-C-0724			
N00014-83-K-0258			
N00014-84-C-0111			
N00014-85-C-0055			
N00014-85-C-0675			
N00014-85-K-0200			
N00014-86-C-0303			
N00014-86-C-0459			
N00014-86-C-0816			
N00014-86-K-0752			
N00014-87-C-0418			
N00014-87-K-0525			
N00014-87-M-0057			
P73/1987			
SERC-SG/D/08464			
USGS-14-08-0001-22521			
146-66-01			
665-45-30-01			
A89-12160			
A89-12166			
A89-12167			
A89-12163			
A89-16990			
A89-15495			
A89-12172			
N89-13865			
N89-14479			
A89-16983			
A89-12854			
N89-13865			
A89-11143			
N89-13039			
N89-13128			
A89-12856			
A89-10664			
A89-11424			
A89-10958			
N89-13824			
N89-14634			

REPORT NUMBER INDEX

EARTH RESOURCES / A Continuing Bibliography (Issue 61)

APRIL 1989

Typical Report Number Index Listing



Listings in this index are arranged alphanumerically by report number. The page number indicates the page on which the citation is located. The accession number denotes the number by which the citation is identified. An asterisk (*) indicates that the item is a NASA report. A pound sign (#) indicates that the item is available on microfiche.

NASA-CR-180463	p 21	N89-13821 *	DFVLR-FB-88-18	p 16	N89-10404 #	ISSN-0379-6566	p 9	N89-10305 #
			DOE/ER-60472/02	p 60	N89-11293 #	ISSN-0379-6566	p 85	N89-12936 #
			DOE/FE-61114/2608	p 35	N89-13093 #	L-16449	p 55	N89-14634 *
			EM-7140-17	p 88	N89-14482 #	LC-87-15305	p 34	N89-10401 *
			EPA-600/D-88-118	p 22	N89-14608 #	LC-87-83254	p 85	N89-12936 #
			ESA-CR(P)-2586	p 84	N89-10664 #	NAS 1.15:100073	p 22	N89-13824 *
			ESA-CR(P)-2626-VOL-1	p 26	N89-10397 #	NAS 1.15:100706	p 53	N89-13861 *
			ESA-CR(P)-2626-VOL-2	p 26	N89-10303 #	NAS 1.15:100708	p 49	N89-10403 *
			ESA-CR(P)-2626-VOL-3	p 27	N89-10399 #	NAS 1.15:101204	p 85	N89-12158 *
						NAS 1.21:491	p 34	N89-10401 *
						NAS 1.26:180463	p 21	N89-13821 *
						NAS 1.26:180986	p 54	N89-14479 *
						NAS 1.26:181486	p 21	N89-13088 *
						NAS 1.26:183014	p 29	N89-14624 *
						NAS 1.26:183148	p 15	N89-10395 *
						NAS 1.26:183259	p 16	N89-11292 *
						NAS 1.26:183304	p 17	N89-11368 *
						NAS 1.26:183308	p 22	N89-14637 *
						NAS 1.26:183326	p 16	N89-11296 *
						NAS 1.26:183346	p 55	N89-14653 *
						NAS 1.26:183347	p 85	N89-12111 *
						NAS 1.26:183374	p 91	N89-14481 *
						NAS 1.26:183384	p 21	N89-13823 *
						NAS 1.26:183385	p 21	N89-13091 *
						NAS 1.26:183409	p 62	N89-13822 *
						NAS 1.26:183471	p 60	N89-11102 *
						NAS 1.55:3014	p 88	N89-14189 *
						NAS 1.60:2595-REV	p 85	N89-12114 *
						NAS 1.61:1206	p 55	N89-14634 *
						NAS 1.61:1210	p 89	N89-14648 *
						NASA-CP-3014	p 88	N89-14189 *
						NASA-CR-180463	p 21	N89-13821 *
						NASA-CR-180986	p 54	N89-14479 *
						NASA-CR-181486	p 21	N89-13088 *
						NASA-CR-183014	p 29	N89-14624 *
						NASA-CR-183148	p 15	N89-10395 *
						NASA-CR-183259	p 16	N89-11292 *
						NASA-CR-183304	p 17	N89-11368 *
						NASA-CR-183308	p 22	N89-14637 *
						NASA-CR-183326	p 16	N89-11296 *
						NASA-CR-183346	p 55	N89-14653 *
						NASA-CR-183347	p 85	N89-12111 *
						NASA-CR-183374	p 91	N89-14481 *
						NASA-CR-183384	p 21	N89-13823 *
						NASA-CR-183385	p 21	N89-13091 *
						NASA-CR-183409	p 62	N89-13822 *
						NASA-CR-183471	p 60	N89-11102 *
						NASA-RP-1206	p 55	N89-14634 *
						NASA-RP-1210	p 89	N89-14648 *
						NASA-SP-491	p 34	N89-10401 *
						NASA-TM-100073	p 22	N89-13824 *
						NASA-TM-100706	p 53	N89-13861 *
						NASA-TM-100708	p 49	N89-10403 *
						NASA-TM-101204	p 85	N89-12158 *
						NASA-TP-2595-REV	p 85	N89-12114 *
						NLR-MP-87061-U	p 70	N89-12113 #
						NOAA-DR-ERL-AOML-11	p 49	N89-10516 #
						NOAA-NESDIS-21-VOL-1	p 85	N89-12105 #
						NOAA-TR-NESDIS-32	p 88	N89-13094 #
						NOAA-PMEL-CONTRIB-813	p 53	N89-13128 #
						NOAA-PMEL-TM-75	p 53	N89-13128 #
						NORDA-SP-035	p 56	N89-14655 #
						NORDA-183	p 54	N89-13864 #
						NORDA-190	p 55	N89-14654 #
						PB88-212824	p 49	N89-10516 #
A-88105	p 22	N89-13824 *	ETN-88-93030	p 84	N89-10664 #			
AAS PAPER 87-429	p 42	A89-12645 *	ETN-88-93044	p 9	N89-10305 #			
AD-A195809	p 62	N89-14480 #	ETN-88-93091	p 70	N89-10930 #			
AD-A196406	p 49	N89-11374 #	ETN-88-93152	p 26	N89-10397 #			
AD-A196447	p 27	N89-10886 #	ETN-88-93153	p 26	N89-10303 #			
AD-A196525	p 49	N89-12112 #	ETN-88-93154	p 27	N89-10399 #			
AD-A197207	p 53	N89-13128 #	ETN-88-93185	p 16	N89-10404 #			
AD-A197316	p 87	N89-13092 #	ETN-88-93242	p 85	N89-12936 #			
AD-A198226	p 54	N89-13865 #	ETN-88-93402	p 70	N89-12113 #			
AD-A198342	p 88	N89-14414 #	ETN-88-93327	p 28	N89-14485 #			
AD-A198418	p 56	N89-14655 #	ETN-89-93329	p 73	N89-14486 #			
AD-A198491	p 73	N89-14483 #	ETN-89-93330	p 28	N89-14487 #			
AD-A198652	p 56	N89-14656 #	ETN-89-93333	p 88	N89-14490 #			
AD-A198653	p 54	N89-14484 #	ETN-89-93336	p 29	N89-14492 #			
AD-A198827	p 55	N89-14654 #	ETN-89-93337	p 29	N89-14493 #			
AD-A198950	p 53	N89-13863 #						
AD-A198965	p 54	N89-13864 #	FLOW-TR-448	p 54	N89-13865 #			
AD-A199515	p 76	N89-12796 #	IAF PAPER ST-88-02	p 58	A89-17873 #			
AD-A199574	p 76	A89-11742	IAF PAPER 88-103	p 23	A89-17678 #			
			IAF PAPER 88-106	p 80	A89-17679 #			
AD-B126126L	p 16	N89-10404 #	IAF PAPER 88-107	p 90	A89-17680 #			
AFGL-ERP-1001	p 88	N89-14414 #	IAF PAPER 88-112	p 58	A89-17681 #			
AFGL-TR-88-0105	p 88	N89-14414 #	IAF PAPER 88-114	p 80	A89-17682 #			
AFGL-TR-88-0207	p 76	A89-11742	IAF PAPER 88-117	p 7	A89-17683 #			
AFGL-TR-88-0237	p 76	A89-12796	IAF PAPER 88-118	p 80	A89-17684 #			
AFIT/CI/NR-88-29	p 49	N89-11374 #	IAF PAPER 88-120	p 80	A89-17685 #			
AIAA PAPER 88-3879	p 80	A89-18073 #	IAF PAPER 88-121	p 7	A89-17686 #			
ARC-R87-157	p 60	N89-11102 *	IAF PAPER 88-124	p 58	A89-17688 #			
B8815927	p 70	N89-12113 #	IAF PAPER 88-131	p 80	A89-17689 #			
B8821602	p 28	N89-14487 #	IAF PAPER 88-134	p 80	A89-17690 #			
B8821609	p 88	N89-14490 #	IAF PAPER 88-139	p 7	A89-17692 #			
B8821610	p 73	N89-14486 #	IAF PAPER 88-140	p 8	A89-17693 #			
CAMAC-PR-87-7	p 17	N89-11368 *	IAF PAPER 88-145	p 31	A89-17694 #			
CNES-87/229/CT/DRT/TIT/TR	p 70	N89-10930 #	IAF PAPER 88-146	p 46	A89-17695 #			
CONF-8806166-2	p 27	N89-11615 #	IAF PAPER 88-151	p 58	A89-17697 #			
CONF-881076-5	p 25	N89-14942 #	IAF PAPER 88-152	p 46	A89-17698 #			
CONTRIB-40	p 53	N89-13128 #	IAF PAPER 88-155	p 46	A89-17700 #			
DE88-010270	p 35	N89-13093 #	IAF PAPER 88-159	p 8	A89-17701 #			
DE88-012726	p 27	N89-11615 #	IAF PAPER 88-161	p 23	A89-17702 #			
DE88-014625	p 60	N89-11293 #	IEEE-88CH2497-6-VOL-1	p 85	N89-12936 #			
DE88-015262	p 25	N89-14942 #	INPE-4559-PRE/1300	p 70	N89-11418 #			
			INPE-4560-PRE/1301	p 24	N89-10676 #			
			INPE-4603-PRE/1326	p 15	N89-10400 #			
			INPE-4620-TDL/328	p 84	N89-11352 #			
			INPE-4624-PRE/1343	p 15	N89-10396 #			
			INPE-4639-PRE/1350	p 17	N89-12106 #			
			INPE-4640-PRE/1351	p 16	N89-11294 #			
			INPE-4641-PRE/1352	p 18	N89-12110 #			
			INPE-4643-PRE/1354	p 16	N89-10402 #			
			INPE-4644-PRE/1355	p 17	N89-11297 #			
			INPE-4651-PRE/1358	p 17	N89-11324 #			
			INPE-4652-PRE/1359	p 73	N89-13090 #			
			INPE-4670-PRE/1370	p 23	N89-10413 #			
			INPE-4686-PRE/1380	p 91	N89-11295 #			
			INPE-4695-MD/036	p 17	N89-12107 #			
			INPE-4696-MD/037	p 17	N89-12108 #			
			INPE-4697-MD/038	p 17	N89-12109 #			
			ISSN-0171-1342	p 16	N89-10404 #			

REPORT

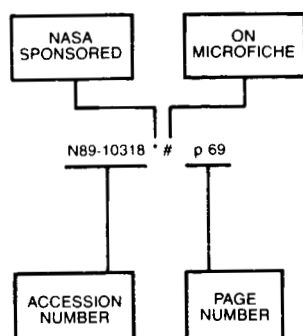
PB88-214788	p 22	N89-14608 #
PB88-223870	p 35	N89-14477 #
PB88-230917	p 55	N89-14652 #
PB88-240239	p 88	N89-13094 #
PB88-244405	p 88	N89-14482 #
RD-29	p 62	N89-14480 #
REPT-1	p 55	N89-14652 #
REPT-333	p 56	N89-14655 #
REPT-86B0040	p 85	N89-12114 * #
REPT-88-181	p 89	N89-14648 * #
REPT-88B-0214	p 49	N89-10403 * #
REPT-88B0262	p 53	N89-13861 * #
REPT-88	p 56	N89-14655 #
RSL-TR-3311-7	p 54	N89-14479 * #
S-577	p 88	N89-14189 * #
SACLANTCEN-SM-206	p 56	N89-14656 #
SACLANTCEN-SM-207	p 73	N89-14483 #
SACLANTCEN-SR-137	p 54	N89-14484 #
SAND-88-1429C	p 25	N89-14942 #
SPIE-834	p 73	A89-10311 *
SPIE-846	p 65	A89-11726 *
SPIE-889	p 79	A89-15870 *
SU-SLAC-PUB-4474	p 27	N89-11615 #

ACCESSION NUMBER INDEX

EARTH RESOURCES / A Continuing Bibliography (Issue 61)

APRIL 1989

Typical Accession Number Index Listing



Listings in this index are arranged alphabetically by accession number. The page number listed to the right indicates the page on which the citation is located. An asterisk (*) indicates that the item is a NASA report. A pound sign (#) indicates that the item is available on microfiche.

A89-10311 *	p 73	A89-10974 #	p 2	A89-13760	p 25	A89-18709	p 8
A89-10312	p 73	A89-10975 #	p 2	A89-13761 *	p 26	A89-18710	p 80
A89-10324	p 73	A89-10976 #	p 29	A89-13762 *	p 26	A89-18711	p 58
A89-10325 *	p 1	A89-10977 *	p 3	A89-13764 *	p 26	A89-18712	p 59
A89-10326	p 29	A89-10978 #	p 64	A89-13958	p 44	A89-18736 #	p 81
A89-10327	p 56	A89-10979 #	p 3	A89-14005	p 67	A89-18843	p 47
A89-10332 *	p 74	A89-10980 #	p 3	A89-14007	p 67	A89-19173	p 81
A89-10334 *	p 74	A89-10981 #	p 37	A89-14008	p 30	A89-19176	p 81
A89-10338	p 74	A89-10982 #	p 23	A89-14009	p 5	A89-19385	p 90
A89-10359	p 74	A89-10983 #	p 64	A89-14010	p 6	A89-19638 *	p 31
A89-10611	p 63	A89-10984 #	p 64	A89-14011	p 30	A89-20101	p 81
A89-10728	p 56	A89-10985 #	p 3	A89-14012	p 67	A89-20102	p 81
A89-10926	p 22	A89-10986 #	p 64	A89-14022 #	p 58	A89-20104	p 90
A89-10927 #	p 22	A89-10987 #	p 3	A89-14073	p 79	A89-20105	p 81
A89-10928 #	p 74	A89-10988 #	p 30	A89-14088	p 67	A89-20200	p 26
A89-10929 #	p 74	A89-10989 #	p 3	A89-14089	p 6	A89-20626	p 68
A89-10930 #	p 35	A89-10990 #	p 37	A89-14090	p 6	A89-20627	p 68
A89-10931 #	p 36	A89-10991 #	p 37	A89-15050	p 23	A89-20628	p 31
A89-10932 *	p 74	A89-10992 #	p 57	A89-15116	p 44	A89-20629 *	p 8
A89-10933 #	p 75	A89-10993 #	p 3	A89-15493	p 6	A89-20630	p 8
A89-10934 *	p 56	A89-10994 #	p 37	A89-15495	p 44	A89-20631	p 68
A89-10936 #	p 75	A89-10995 #	p 37	A89-15870 *	p 79	A89-20701	p 90
A89-10937 #	p 63	A89-10996 #	p 64	A89-15873 *	p 79	A89-20702	p 8
A89-10939 #	p 56	A89-10997 #	p 23	A89-15878 *	p 79	A89-20703	p 8
A89-10940 #	p 57	A89-10998 #	p 64	A89-15889 *	p 79	A89-20704	p 8
A89-10941 #	p 57	A89-11000 #	p 3	A89-15915 *	p 30	A89-20705	p 8
A89-10942 *	p 36	A89-11001 #	p 38	A89-15918 *	p 6	A89-20706	p 8
A89-10943 #	p 75	A89-11002 #	p 4	A89-15919	p 68	A89-20707	p 59
A89-10945 #	p 63	A89-11003 *	p 65	A89-15920	p 68	A89-20708	p 68
A89-10946 #	p 1	A89-11004 #	p 4	A89-15922 #	p 79	A89-20709	p 31
A89-10947 #	p 36	A89-11005 #	p 38	A89-15923	p 44	A89-20710	p 31
A89-10948 #	p 1	A89-11006 #	p 75	A89-16061 *	p 6	A89-20711	p 81
A89-10949 #	p 57	A89-11007 #	p 4	A89-16062	p 6	A89-20712	p 69
A89-10950 #	p 1	A89-11008 #	p 4	A89-16063 *	p 68	A89-20713	p 69
A89-10951 #	p 1	A89-11009 *	p 4	A89-16067 *	p 44	A89-20714	p 82
A89-10952 #	p 1	A89-11010 #	p 65	A89-16977 *	p 44	A89-20715	p 82
A89-10953 *	p 2	A89-11011 #	p 4	A89-16978	p 45	A89-20716	p 69
A89-10954 #	p 36	A89-11012 *	p 4	A89-16979	p 45	A89-20717	p 69
A89-10955 *	p 75	A89-11013 #	p 65	A89-16981 *	p 45	A89-20718	p 82
A89-10956 #	p 2	A89-11014 #	p 57	A89-16982 *	p 45	A89-20719	p 59
A89-10957 #	p 22	A89-11016 #	p 76	A89-16983 *	p 45	A89-20720	p 59
A89-10958 #	p 63	A89-11017 #	p 30	A89-16984	p 45	A89-20721	p 47
A89-10959 #	p 23	A89-11143 *	p 38	A89-16986 #	p 45	A89-20722	p 47
A89-10960 #	p 2	A89-11145 *	p 38	A89-16987	p 46	A89-20723	p 47
A89-10961 #	p 36	A89-11148	p 38	A89-16989	p 46	A89-20724	p 9
A89-10962 #	p 36	A89-11149	p 38	A89-16990 *	p 46		
A89-10964 #	p 36	A89-11150	p 38	A89-16991 #	p 46	N89-10303 #	p 26
A89-10965 #	p 75	A89-11158	p 38	A89-16992 *	p 46	N89-10305 #	p 9
A89-10967 #	p 29	A89-11225	p 39	A89-17282	p 6	N89-10306 #	p 9
A89-10968 #	p 63	A89-11424	p 39	A89-17283 *	p 7	N89-10307 #	p 9
A89-10969 #	p 75	A89-11726	p 65	A89-17284 *	p 7	N89-10308 #	p 9
A89-10970 *	p 2	A89-11727 *	p 65	A89-17285 *	p 58	N89-10309 #	p 9
A89-10971 #	p 37	A89-11730	p 23	A89-17286 *	p 7	N89-10310 #	p 10
A89-10972 #	p 37	A89-11731	p 76	A89-17287	p 7	N89-10313 #	p 32
A89-10973 #	p 2	A89-11740	p 65	A89-17399	p 7	N89-10314 #	p 47
				A89-17678 #	p 23	N89-10315 #	p 47
				A89-17679 #	p 80	N89-10316 #	p 48
				A89-17680 *	p 90	N89-10317 #	p 10
				A89-17681 #	p 58	N89-10318 *	p 69
				A89-17682 *	p 80	N89-10319 #	p 10
				A89-17683 #	p 7	N89-10320 #	p 82
				A89-17684 #	p 80	N89-10321 #	p 10
				A89-17685 #	p 80	N89-10322 #	p 10
				A89-17686 #	p 7	N89-10323 #	p 10
				A89-17688 #	p 58	N89-10324 #	p 10
				A89-17689 #	p 80	N89-10325 #	p 11
				A89-17690 #	p 80	N89-10326 *	p 11
				A89-17692 #	p 7	N89-10327 #	p 11
				A89-17693 #	p 8	N89-10328 #	p 11
				A89-17694 #	p 31	N89-10329 #	p 11
				A89-17695 #	p 46	N89-10330 #	p 82
				A89-17697 #	p 58	N89-10332 #	p 11
				A89-17698 #	p 46	N89-10333 #	p 11
				A89-17700 #	p 46	N89-10334 #	p 12
				A89-17701 *	p 8	N89-10335 *	p 82
				A89-17702 #	p 23	N89-10336 #	p 12
				A89-17873 #	p 58	N89-10337 #	p 32
				A89-17906	p 68	N89-10338 *	p 69
				A89-17945	p 26	N89-10339 #	p 70
				A89-18073 #	p 80	N89-10340 #	p 70
				A89-18075	p 31	N89-10341 #	p 70
				A89-18706	p 31	N89-10342 #	p 12
				A89-18707	p 31	N89-10343 #	p 12
				A89-18708	p 58		

N89-10344

N89-10344 # p 48
 N89-10345 # p 82
 N89-10346 # p 83
 N89-10347 # p 83
 N89-10348 # p 12
 N89-10349 # p 12
 N89-10350 # p 12
 N89-10351 # p 13
 N89-10352 # p 48
 N89-10353 # p 83
 N89-10354 # p 13
 N89-10355 # p 13
 N89-10356 # p 83
 N89-10357 * # p 83
 N89-10358 # p 13
 N89-10359 # p 13
 N89-10360 # p 32
 N89-10361 # p 48
 N89-10362 # p 32
 N89-10363 # p 13
 N89-10364 * # p 83
 N89-10365 # p 48
 N89-10366 * # p 32
 N89-10367 # p 14
 N89-10368 # p 14
 N89-10369 # p 14
 N89-10370 # p 14
 N89-10371 # p 48
 N89-10372 # p 59
 N89-10373 # p 14
 N89-10374 # p 14
 N89-10375 # p 59
 N89-10376 # p 15
 N89-10377 * # p 32
 N89-10378 * # p 15
 N89-10379 * # p 83
 N89-10380 # p 33
 N89-10381 # p 84
 N89-10382 # p 33
 N89-10383 # p 33
 N89-10384 # p 33
 N89-10385 # p 33
 N89-10386 # p 33
 N89-10387 # p 15
 N89-10388 # p 59
 N89-10389 # p 15
 N89-10390 # p 60
 N89-10392 # p 90
 N89-10393 * # p 90
 N89-10395 * # p 15
 N89-10396 # p 15
 N89-10397 # p 26
 N89-10399 # p 27
 N89-10400 # p 15
 N89-10401 * # p 34
 N89-10402 # p 16
 N89-10403 * # p 49
 N89-10404 # p 16
 N89-10413 # p 23
 N89-10516 # p 49
 N89-10664 # p 84
 N89-10676 # p 24
 N89-10886 # p 27
 N89-10905 * # p 90
 N89-10930 # p 70
 N89-11102 * # p 60
 N89-11292 * # p 16
 N89-11293 # p 60
 N89-11294 # p 16
 N89-11295 # p 91
 N89-11296 * # p 16
 N89-11297 # p 17
 N89-11324 # p 17
 N89-11352 # p 84
 N89-11364 # p 84
 N89-11366 # p 84
 N89-11368 * # p 17
 N89-11374 # p 49
 N89-11418 # p 70
 N89-11615 # p 27
 N89-11645 # p 85
 N89-11774 * # p 85
 N89-12097 * # p 27
 N89-12098 # p 27
 N89-12099 # p 27
 N89-12100 # p 27
 N89-12101 # p 28
 N89-12102 # p 28
 N89-12103 # p 28
 N89-12105 # p 85
 N89-12106 # p 17
 N89-12107 # p 17
 N89-12108 # p 17
 N89-12109 # p 17
 N89-12110 # p 18
 N89-12111 * # p 85

N89-12112 # p 49
 N89-12113 # p 70
 N89-12114 * # p 85
 N89-12158 * # p 85
 N89-12936 # p 85
 N89-12937 # p 86
 N89-12939 # p 86
 N89-12941 # p 86
 N89-12945 # p 49
 N89-12946 # p 49
 N89-12950 * # p 34
 N89-12951 * # p 18
 N89-12955 # p 86
 N89-12958 * # p 24
 N89-12959 # p 24
 N89-12960 # p 24
 N89-12962 # p 18
 N89-12964 # p 24
 N89-12966 # p 24
 N89-12967 # p 18
 N89-12968 # p 50
 N89-12969 # p 50
 N89-12970 # p 50
 N89-12971 # p 50
 N89-12972 # p 50
 N89-12973 # p 50
 N89-12974 # p 51
 N89-12975 # p 51
 N89-12976 # p 71
 N89-12982 * # p 28
 N89-12985 # p 71
 N89-12986 # p 18
 N89-12987 # p 25
 N89-12988 # p 18
 N89-12989 # p 71
 N89-12990 # p 19
 N89-12991 # p 19
 N89-12993 # p 60
 N89-12997 # p 60
 N89-12998 * # p 51
 N89-13000 # p 86
 N89-13002 # p 19
 N89-13003 # p 19
 N89-13004 # p 86
 N89-13005 # p 51
 N89-13007 # p 87
 N89-13009 # p 71
 N89-13017 # p 87
 N89-13022 # p 34
 N89-13023 # p 34
 N89-13024 # p 34
 N89-13025 # p 34
 N89-13026 # p 35
 N89-13027 # p 35
 N89-13028 # p 60
 N89-13029 # p 71
 N89-13030 # p 51
 N89-13031 # p 51
 N89-13032 * # p 52
 N89-13033 # p 52
 N89-13034 # p 52
 N89-13035 # p 52
 N89-13036 # p 52
 N89-13037 # p 52
 N89-13039 # p 52
 N89-13040 # p 61
 N89-13042 # p 61
 N89-13043 # p 61
 N89-13044 # p 61
 N89-13045 * # p 61
 N89-13046 # p 61
 N89-13047 # p 61
 N89-13048 # p 62
 N89-13049 # p 62
 N89-13050 # p 19
 N89-13051 # p 19
 N89-13052 # p 71
 N89-13053 # p 71
 N89-13054 # p 28
 N89-13055 # p 20
 N89-13056 # p 72
 N89-13057 # p 20
 N89-13058 # p 25
 N89-13059 # p 87
 N89-13060 # p 72
 N89-13061 # p 72
 N89-13062 # p 72
 N89-13066 # p 72
 N89-13067 # p 62
 N89-13068 # p 72
 N89-13069 # p 87
 N89-13070 # p 53
 N89-13071 # p 87
 N89-13072 # p 87
 N89-13073 * # p 53
 N89-13077 # p 20

N89-13079 # p 20
 N89-13080 # p 20
 N89-13081 # p 87
 N89-13082 # p 91
 N89-13083 * # p 20
 N89-13084 # p 21
 N89-13085 # p 21
 N89-13087 # p 35
 N89-13088 * # p 21
 N89-13089 # p 53
 N89-13090 # p 73
 N89-13091 * # p 21
 N89-13092 # p 87
 N89-13093 # p 35
 N89-13094 # p 88
 N89-13128 # p 53
 N89-13821 * # p 21
 N89-13822 * # p 62
 N89-13823 * # p 21
 N89-13824 * # p 22
 N89-13861 * # p 53
 N89-13863 # p 53
 N89-13864 # p 54
 N89-13865 # p 54
 N89-13908 * # p 73
 N89-13924 # p 62
 N89-14189 * # p 88
 N89-14414 # p 88
 N89-14477 # p 35
 N89-14479 * # p 54
 N89-14480 # p 62
 N89-14481 * # p 91
 N89-14482 # p 88
 N89-14483 # p 73
 N89-14484 # p 54
 N89-14485 # p 28
 N89-14486 # p 73
 N89-14487 # p 28
 N89-14490 # p 88
 N89-14492 # p 29
 N89-14493 # p 29
 N89-14522 * # p 89
 N89-14534 * # p 55
 N89-14608 # p 22
 N89-14624 * # p 29
 N89-14634 * # p 55
 N89-14635 # p 89
 N89-14636 # p 63
 N89-14637 * # p 22
 N89-14648 * # p 89
 N89-14652 # p 55
 N89-14653 * # p 55
 N89-14654 # p 55
 N89-14655 # p 56
 N89-14656 # p 56
 N89-14942 # p 25

AVAILABILITY OF CITED PUBLICATIONS

IAA ENTRIES (A89-10000 Series)

Publications announced in *IAA* are available from the AIAA Technical Information Service as follows: Paper copies of accessions are available at \$10.00 per document (up to 50 pages), additional pages \$0.25 each. Microfiche⁽¹⁾ of documents announced in *IAA* are available at the rate of \$4.00 per microfiche on demand. Standing order microfiche are available at the rate of \$1.45 per microfiche for *IAA* source documents and \$1.75 per microfiche for AIAA meeting papers.

Minimum air-mail postage to foreign countries is \$2.50. All foreign orders are shipped on payment of pro-forma invoices.

All inquiries and requests should be addressed to: Technical Information Service, American Institute of Aeronautics and Astronautics, 555 West 57th Street, New York, NY 10019. Please refer to the accession number when requesting publications.

STAR ENTRIES (N89-10000 Series)

One or more sources from which a document announced in *STAR* is available to the public is ordinarily given on the last line of the citation. The most commonly indicated sources and their acronyms or abbreviations are listed below. If the publication is available from a source other than those listed, the publisher and his address will be displayed on the availability line or in combination with the corporate source line.

Avail: NTIS. Sold by the National Technical Information Service. Prices for hard copy (HC) and microfiche (MF) are indicated by a price code preceded by the letters HC or MF in the *STAR* citation. Current values for the price codes are given in the tables on NTIS PRICE SCHEDULES.

Documents on microfiche are designated by a pound sign (#) following the accession number. The pound sign is used without regard to the source or quality of the microfiche.

Initially distributed microfiche under the NTIS SRIM (Selected Research in Microfiche) is available at greatly reduced unit prices. For this service and for information concerning subscription to NASA printed reports, consult the NTIS Subscription Section, Springfield, Va. 22161.

NOTE ON ORDERING DOCUMENTS: When ordering NASA publications (those followed by the * symbol), use the N accession number. NASA patent applications (only the specifications are offered) should be ordered by the US-Patent-Appl-SN number. Non-NASA publications (no asterisk) should be ordered by the AD, PB, or other *report number* shown on the last line of the citation, not by the N accession number. It is also advisable to cite the title and other bibliographic identification.

Avail: SOD (or GPO). Sold by the Superintendent of Documents, U.S. Government Printing Office, in hard copy. The current price and order number are given following the availability line. (NTIS will fill microfiche requests, as indicated above, for those documents identified by a # symbol.)

(1) A microfiche is a transparent sheet of film, 105 by 148 mm in size containing as many as 60 to 98 pages of information reduced to micro images (not to exceed 26.1 reduction).

- Avail: BLL (formerly NLL): British Library Lending Division, Boston Spa, Wetherby, Yorkshire, England. Photocopies available from this organization at the price shown. (If none is given, inquiry should be addressed to the BLL.)
- Avail: DOE Depository Libraries. Organizations in U.S. cities and abroad that maintain collections of Department of Energy reports, usually in microfiche form, are listed in *Energy Research Abstracts*. Services available from the DOE and its depositories are described in a booklet, *DOE Technical Information Center - Its Functions and Services* (TID-4660), which may be obtained without charge from the DOE Technical Information Center.
- Avail: ESDU. Pricing information on specific data, computer programs, and details on ESDU topic categories can be obtained from ESDU International Ltd. Requesters in North America should use the Virginia address while all other requesters should use the London address, both of which are on the page titled ADDRESSES OF ORGANIZATIONS.
- Avail: Fachinformationszentrum, Karlsruhe. Sold by the Fachinformationszentrum Energie, Physik, Mathematik GMBH, Eggenstein Leopoldshafen, Federal Republic of Germany, at the price shown in deutschmarks (DM).
- Avail: HMSO. Publications of Her Majesty's Stationery Office are sold in the U.S. by Pendragon House, Inc. (PHI), Redwood City, California. The U.S. price (including a service and mailing charge) is given, or a conversion table may be obtained from PHI.
- Avail: NASA Public Document Rooms. Documents so indicated may be examined at or purchased from the National Aeronautics and Space Administration, Public Documents Room (Room 126), 600 Independence Ave., S.W., Washington, D.C. 20546, or public document rooms located at each of the NASA research centers, the NASA Space Technology Laboratories, and the NASA Pasadena Office at the Jet Propulsion Laboratory.
- Avail: Univ. Microfilms. Documents so indicated are dissertations selected from *Dissertation Abstracts* and are sold by University Microfilms as xerographic copy (HC) and microfilm. All requests should cite the author and the Order Number as they appear in the citation.
- Avail: US Patent and Trademark Office. Sold by Commissioner of Patents and Trademarks, U.S. Patent and Trademark Office, at the standard price of \$1.50 each, postage free. (See discussion of NASA patents and patent applications below.)
- Avail: (US Sales Only). These foreign documents are available to users within the United States from the National Technical Information Service (NTIS). They are available to users outside the United States through the International Nuclear Information Service (INIS) representative in their country, or by applying directly to the issuing organization.
- Avail: USGS. Originals of many reports from the U.S. Geological Survey, which may contain color illustrations, or otherwise may not have the quality of illustrations preserved in the microfiche or facsimile reproduction, may be examined by the public at the libraries of the USGS field offices whose addresses are listed in this Introduction. The libraries may be queried concerning the availability of specific documents and the possible utilization of local copying services, such as color reproduction.
- Avail: Issuing Activity, or Corporate Author, or no indication of availability. Inquiries as to the availability of these documents should be addressed to the organization shown in the citation as the corporate author of the document.

PUBLIC COLLECTIONS OF NASA DOCUMENTS

DOMESTIC: NASA and NASA-sponsored documents and a large number of aerospace publications are available to the public for reference purposes at the library maintained by the American Institute of Aeronautics and Astronautics, Technical Information Service, 555 West 57th Street, 12th Floor, New York, New York 10019.

EUROPEAN: An extensive collection of NASA and NASA-sponsored publications is maintained by the British Library Lending Division, Boston Spa, Wetherby, Yorkshire, England for public access. The British Library Lending Division also has available many of the non-NASA publications cited in *STAR*. European requesters may purchase facsimile copy or microfiche of NASA and NASA-sponsored documents, those identified by both the symbols # and * from ESA — Information Retrieval Service European Space Agency, 8-10 rue Mario-Nikis, 75738 CEDEX 15, France.

FEDERAL DEPOSITORY LIBRARY PROGRAM

In order to provide the general public with greater access to U.S. Government publications, Congress established the Federal Depository Library Program under the Government Printing Office (GPO), with 50 regional depositories responsible for permanent retention of material, inter-library loan, and reference services. At least one copy of nearly every NASA and NASA-sponsored publication, either in printed or microfiche format, is received and retained by the 50 regional depositories. A list of the regional GPO libraries, arranged alphabetically by state, appears on the inside back cover. These libraries are *not* sales outlets. A local library can contact a Regional Depository to help locate specific reports, or direct contact may be made by an individual.

STANDING ORDER SUBSCRIPTIONS

NASA SP-7041 and its supplements are available from the National Technical Information Service (NTIS) on standing order subscription as PB 89-903800 at the price of \$15.50 domestic and \$31.00 foreign. Standing order subscriptions do not terminate at the end of a year, as do regular subscriptions, but continue indefinitely unless specifically terminated by the subscriber.

ADDRESSES OF ORGANIZATIONS

American Institute of Aeronautics and
Astronautics
Technical Information Service
555 West 57th Street, 12th Floor
New York, New York 10019

British Library Lending Division,
Boston Spa, Wetherby, Yorkshire,
England

Commissioner of Patents and
Trademarks
U.S. Patent and Trademark Office
Washington, D.C. 20231

Department of Energy
Technical Information Center
P.O. Box 62
Oak Ridge, Tennessee 37830

ESA-Information Retrieval Service
ESRIN
Via Galileo Galilei
00044 Frascati (Rome) Italy

ESDU International
P.O. Box 1633
Manassas, Virginia 22110

ESDU International, Ltd.
251-259 Regent Street
London, W1R 7AD, England

Fachinformationszentrum Energie, Physik,
Mathematik GMBH
7514 Eggenstein Leopoldshafen
Federal Republic of Germany

Her Majesty's Stationery Office
P.O. Box 569; S.E. 1
London, England

NASA Scientific and Technical Information
Facility
P.O. Box 8757
B.W.I. Airport, Maryland 21240

National Aeronautics and Space
Administration
Scientific and Technical Information
Division (NTT)
Washington, D.C. 20546

National Technical Information Service
5285 Port Royal Road
Springfield, Virginia 22161

Pendragon House, Inc.
899 Broadway Avenue
Redwood City, California 94063

Superintendent of Documents
U.S. Government Printing Office
Washington, D.C. 20402

University Microfilms
A Xerox Company
300 North Zeeb Road
Ann Arbor, Michigan 48106

University Microfilms, Ltd.
Tylers Green
London, England

U.S. Geological Survey Library
National Center - MS 950
12201 Sunrise Valley Drive
Reston, Virginia 22092

U.S. Geological Survey Library
2255 North Gemini Drive
Flagstaff, Arizona 86001

U.S. Geological Survey
345 Middlefield Road
Menlo Park, California 94025

U.S. Geological Survey Library
Box 25046
Denver Federal Center, MS914
Denver, Colorado 80225

NTIS PRICE SCHEDULES

(Effective January 1, 1989)

Schedule A STANDARD PRICE DOCUMENTS AND MICROFICHE

PRICE CODE	NORTH AMERICAN PRICE	FOREIGN PRICE
A01	\$ 6.95	\$13.90
A02	10.95	21.90
A03	13.95	27.90
A04-A05	15.95	31.90
A06-A09	21.95	43.90
A10-A13	28.95	57.90
A14-A17	36.95	73.90
A18-A21	42.95	85.90
A22-A25	49.95	99.90
A99	.	.
NO1	55.00	70.00
NO2	55.00	80.00

Schedule E EXCEPTION PRICE DOCUMENTS AND MICROFICHE

PRICE CODE	NORTH AMERICAN PRICE	FOREIGN PRICE
E01	\$ 9.00	18.00
E02	11.50	23.00
E03	13.00	26.00
E04	15.50	31.00
E05	17.50	35.00
E06	20.50	41.00
E07	23.00	46.00
E08	25.50	51.00
E09	28.00	56.00
E10	31.00	62.00
E11	33.50	67.00
E12	36.50	73.00
E13	39.00	78.00
E14	42.50	85.00
E15	46.00	92.00
E16	50.50	101.00
E17	54.50	109.00
E18	59.00	118.00
E19	65.50	131.00
E20	76.00	152.00
E99	.	.

*Contact NTIS for price quote.

IMPORTANT NOTICE

NTIS Shipping and Handling Charges

U.S., Canada, Mexico — ADD \$3.00 per TOTAL ORDER

All Other Countries — ADD \$4.00 per TOTAL ORDER

Exceptions — Does NOT apply to:

ORDERS REQUESTING NTIS RUSH HANDLING
ORDERS FOR SUBSCRIPTION OR STANDING ORDER PRODUCTS ONLY

NOTE: Each additional delivery address on an order
requires a separate shipping and handling charge.

1. Report No. NASA SP-7041 (61)		2. Government Accession No.		3. Recipient's Catalog No.	
4. Title and Subtitle EARTH RESOURCES A Continuing Bibliography with Indexes (Issue 61)				5. Report Date April, 1989	
				6. Performing Organization Code	
7. Author(s)				8. Performing Organization Report No.	
9. Performing Organization Name and Address National Aeronautics and Space Administration Washington, DC 20546				10. Work Unit No.	
				11. Contract or Grant No.	
12. Sponsoring Agency Name and Address				13. Type of Report and Period Covered	
				14. Sponsoring Agency Code	
15. Supplementary Notes					
16. Abstract <p>This bibliography lists 606 reports, articles and other documents introduced into the NASA scientific and technical information system between January 1 and March 31, 1989. Emphasis is placed on the use of remote sensing and geophysical instrumentation in spacecraft and aircraft to survey and inventory natural resources and urban areas. Subject matter is grouped according to agriculture and forestry, environmental changes and cultural resources, geodesy and cartography, geology and mineral resources, hydrology and water management, data processing and distribution systems, instrumentation and sensors, and economic analysis.</p>					
17. Key Words (Suggested by Authors(s)) Bibliographies Earth Resources Remote Sensors			18. Distribution Statement Unclassified - Unlimited		
19. Security Classif. (of this report) Unclassified		20. Security Classif. (of this page) Unclassified		21. No. of Pages 172	
				22. Price * A08/HC	

*For sale by the National Technical Information Service, Springfield, Virginia 22161

FEDERAL REGIONAL DEPOSITORY LIBRARIES

ALABAMA

AUBURN UNIV. AT MONTGOMERY LIBRARY

Documents Department
Montgomery, AL 36193
(205) 271-9650

UNIV. OF ALABAMA LIBRARY

Documents Dept.-Box S
University, AL 35486
(205) 348-6046

ARIZONA

DEPT. OF LIBRARY, ARCHIVES AND PUBLIC RECORDS

Third Floor—State Cap.
1700 West Washington
Phoenix, AZ 85007
(602) 255-4121

UNIVERSITY OF ARIZONA LIB.

Government Documents Dept.
Tucson, AZ 85721
(602) 621-6433

ARKANSAS

ARKANSAS STATE LIBRARY

One Capitol Mall
Little Rock, AR 72201
(501) 371-2326

CALIFORNIA

CALIFORNIA STATE LIBRARY

Govt. Publications Section
P.O. Box 2037
Sacramento, CA 95809
(916) 324-4863

COLORADO

UNIV. OF COLORADO LIB.

Government Pub. Division
Campus Box 184
Boulder, CO 80309
(303) 492-8834

DENVER PUBLIC LIBRARY

Govt. Pub. Department
1357 Broadway
Denver, CO 80203
(303) 571-2131

CONNECTICUT

CONNECTICUT STATE LIBRARY

Government Documents Unit
231 Capitol Avenue
Hartford, CT 06106
(203) 566-7029

FLORIDA

UNIV. OF FLORIDA LIBRARIES

Library West
Documents Department
Gainesville, FL 32611
(904) 392-0367

GEORGIA

UNIV. OF GEORGIA LIBRARIES

Government Reference Dept.
Athens, GA 30602
(404) 542-8949

HAWAII

UNIV. OF HAWAII LIBRARY

Govt. Documents Collection
2550 The Mall
Honolulu, HI 96822
(808) 948-8230

IDAHO

UNIV. OF IDAHO LIBRARY

Documents Section
Moscow, ID 83843
(208) 885-6344

ILLINOIS

ILLINOIS STATE LIBRARY

Information Services Branch
Centennial Building
Springfield, IL 62756
(217) 782-5185

INDIANA

INDIANA STATE LIBRARY

Serials Documents Section
140 North Senate Avenue
Indianapolis, IN 46204
(317) 232-3686

IOWA

UNIV. OF IOWA LIBRARIES

Govt. Documents Department
Iowa City, IA 52242
(319) 353-3318

KANSAS

UNIVERSITY OF KANSAS

Doc. Collect—Spencer Lib.
Lawrence, KS 66045-2800
(913) 864-4662

KENTUCKY

UNIV. OF KENTUCKY LIBRARIES

Govt. Pub. Department
Lexington, KY 40506-0039
(606) 257-3139

LOUISIANA

LOUISIANA STATE UNIVERSITY

Middleton Library
Govt. Docs. Dept.
Baton Rouge, LA 70803
(504) 388-2570

LOUISIANA TECHNICAL UNIV. LIBRARY

Documents Department
Ruston, LA 71272-0046
(318) 257-4962

MAINE

UNIVERSITY OF MAINE

Raymond H. Fogler Library
Tri-State Regional Documents
Depository
Orono, ME 04469
(207) 581-1680

MARYLAND

UNIVERSITY OF MARYLAND

McKeldin Lib.—Doc. Div.
College Park, MD 20742
(301) 454-3034

MASSACHUSETTS

BOSTON PUBLIC LIBRARY

Government Docs. Dept.
Boston, MA 02117
(617) 536-5400 ext. 226

MICHIGAN

DETROIT PUBLIC LIBRARY

Sociology Department
5201 Woodward Avenue
Detroit, MI 48202-4093
(313) 833-1409

MICHIGAN STATE LIBRARY

P.O. Box 30007
Lansing, MI 48909
(517) 373-1593

MINNESOTA

UNIVERSITY OF MINNESOTA

Government Pubs. Division
409 Wilson Library
309 19th Avenue South
Minneapolis, MN 55455
(612) 373-7870

MISSISSIPPI

UNIV. OF MISSISSIPPI LIB.

Documents Department
University, MS 38677
(601) 232-5857

MONTANA

UNIV. OF MONTANA

Mansfield Library
Documents Division
Missoula, MT 59812
(406) 243-6700

NEBRASKA

UNIVERSITY OF NEBRASKA - LINCOLN

Love Library
Documents Department
Lincoln, NE 68588-0410
(402) 472-2562

NEVADA

UNIVERSITY OF NEVADA LIB.

Govt. Pub. Department
Reno, NV 89557-0044
(702) 784-6579

NEW JERSEY

NEWARK PUBLIC LIBRARY

5 Washington Street
Newark, NJ 07101-0630
(201) 733-7812

NEW MEXICO

UNIVERSITY OF NEW MEXICO

Zimmerman Library
Government Pub. Dept.
Albuquerque, NM 87131
(505) 277-5441

NEW MEXICO STATE LIBRARY

Reference Department
325 Don Gaspar Avenue
Santa Fe, NM 87503
(505) 827-3826

NEW YORK

NEW YORK STATE LIBRARY

Empire State Plaza
Albany, NY 12230
(518) 474-5563

NORTH CAROLINA

UNIVERSITY OF NORTH CAROLINA AT CHAPEL HILL

Davis Library
BA/SS Documents Division
Chapel Hill, NC 27515
(919) 962-1151

NORTH DAKOTA

UNIVERSITY OF NORTH DAKOTA

Chester Fritz Library
Documents Department
Grand Forks, ND 58202
(701) 777-4629
In cooperation with North
Dakota State Univ. Library

OHIO

STATE LIBRARY OF OHIO

Documents Department
65 South Front Street
Columbus, OH 43266-0334
(614) 462-7051

OKLAHOMA

OKLAHOMA DEPT. OF LIB.

Government Documents
200 NE 18th Street
Oklahoma City, OK 73105
(405) 521-2502, ext. 252

OKLAHOMA STATE UNIV. LIB.

Documents Department
Stillwater, OK 74078
(405) 624-6546

OREGON

PORTLAND STATE UNIV. LIB.

Documents Department
P.O. Box 1151
Portland, OR 97207
(503) 229-3673

PENNSYLVANIA

STATE LIBRARY OF PENN.

Government Pub. Section
P.O. Box 1601
Harrisburg, PA 17105
(717) 787-3752

TEXAS

TEXAS STATE LIBRARY

Public Services Department
P.O. Box 12927—Cap. Sta.
Austin, TX 78711
(512) 475-2996

TEXAS TECH. UNIV. LIBRARY

Govt. Documents Department
Lubbock, TX 79409
(806) 742-2268

UTAH

UTAH STATE UNIVERSITY

Merrill Library, U.M.C. 30
Logan, UT 84322
(801) 750-2682

VIRGINIA

UNIVERSITY OF VIRGINIA

Alderman Lib.—Public Doc.
Charlottesville, VA 22903-2498
(804) 924-3133

WASHINGTON

WASHINGTON STATE LIBRARY

Documents Section
Olympia, WA 98504
(206) 753-4027

WEST VIRGINIA

WEST VIRGINIA UNIV. LIB.

Documents Department
Morgantown, WV 26506-6069
(304) 293-3640

WISCONSIN

MILWAUKEE PUBLIC LIBRARY

814 West Wisconsin Avenue
Milwaukee, WI 53233
(414) 278-3065

ST. HIST. LIB. OF WISCONSIN

Government Pub. Section
816 State Street
Madison, WI 53706
(608) 262-4347

WYOMING

WYOMING STATE LIBRARY

Supreme Ct. & Library Bld.
Cheyenne, WY 82002
(307) 777-5919

National Aeronautics and
Space Administration
Code NTT-4

Washington, D.C.
20546-0001

Official Business
Penalty for Private Use, \$300

SPECIAL FOURTH-CLASS RATE
POSTAGE & FEES PAID
NASA
Permit No. G-27

NASA

POSTMASTER: If Undeliverable (Section 158
Postal Manual) Do Not Return
